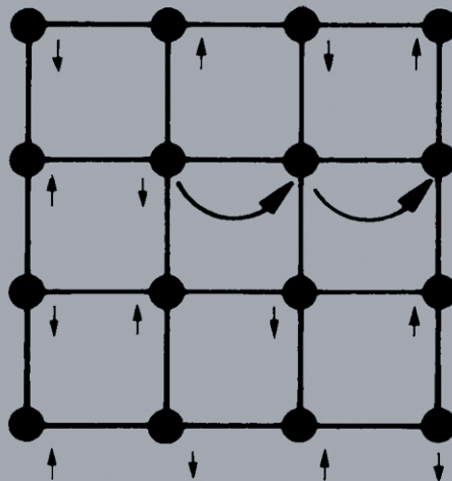


MODERN PROBLEMS IN CONDENSED MATTER SCIENCES

General Editors:
V.M. AGRANOVICH and A.A. MARADUDIN

VOLUME 32

ELECTRONIC PHASE TRANSITIONS



Volume Editors:
W. HANKE and Yu.V. KOPAEV

ELECTRONIC PHASE TRANSITIONS

MODERN PROBLEMS IN CONDENSED MATTER SCIENCES

Volume 32

Series editors

V.M. AGRANOVICH

Moscow, USSR

A.A. MARADUDIN

Irvine, California, USA

Advisory editorial board

F. Abelès, Paris, France

F. Bassani, Pisa, Italy

N. Bloembergen, Cambridge, MA, USA

E. Burstein, Philadelphia, PA, USA

I.L. Fabelinskii, Moscow, USSR

P. Fulde, Stuttgart, FRG

M.D. Galanin, Moscow, USSR

V.L. Ginzburg, Moscow, USSR

H. Haken, Stuttgart, FRG

R.M. Hochstrasser, Philadelphia, PA, USA

I.P. Ipatova, Leningrad, USSR

A.A. Kaplyanskii, Leningrad, USSR

L.V. Keldysh, Moscow, USSR

R. Kubo, Tokyo, Japan

R. Loudon, Colchester, UK

Yu.A. Ossipyan, Moscow, USSR

L.P. Pitaevskii, Moscow, USSR

A.M. Prokhorov, Moscow, USSR

K.K. Rebane, Tallinn, USSR

J.M. Rowell, Red Bank, NJ, USA



NORTH-HOLLAND

AMSTERDAM · LONDON · NEW YORK · TOKYO

ELECTRONIC PHASE TRANSITIONS

Volume editors

W. HANKE

Würzburg, Germany

Yu.V. KOPAEV

Moscow, USSR



1992

NORTH-HOLLAND
AMSTERDAM · LONDON · NEW YORK · TOKYO

© Elsevier Science Publishers B.V., 1992

All rights reserved. No part of this publication may be reproduced, stored in a retrieval system, or transmitted, in any form or by any means, electronic, mechanical, photocopying, recording or otherwise, without the written permission of the publisher, Elsevier Science Publishers B.V., Copyright and Permissions Department, P.O. Box 521, 1000 AM Amsterdam, The Netherlands.

Special regulations for readers in the USA: This publication has been registered with the Copyright Clearance Center Inc. (CCC), Salem, Massachusetts. Information can be obtained from the CCC about conditions under which photocopies of parts of this publication may be made in the USA.

All other copyright questions, including photocopying outside of the USA, should be referred to the publisher.

No responsibility is assumed by the Publisher for any injury and/or damage to persons or property as a matter of products liability, negligence or otherwise, or from any use or operation of any methods, products, instructions or ideas contained in the material herein.

ISBN: 0 444 88885 3

North-Holland

*Elsevier Science Publishers B.V.
P.O. Box 211
1000 AE Amsterdam
The Netherlands*

Sole distributors for the USA and Canada:
*Elsevier Science Publishing Company, Inc.
655 Avenue of the Americas
New York, NY 10010
USA*

Library of Congress Cataloging-in-Publication Data

Electronic phase transitions/volume editors, W. Hanke, Yu. V. Kopaev.
p. cm. – (Modern problems in condensed matter sciences,
vol 32).

Includes bibliographical references and index.

ISBN 0-444-88885-3

1. Electronic structure. 2. Anderson model. 3. Energy band theory
of solids. I. Hanke, W. II. Kopaev, Yu. V. III. Series.

QC 176.8.E4E36 1992

530.4' 1 – dc20

91-43063

CIP

Printed on acid-free paper
Printed in The Netherlands

MODERN PROBLEMS IN CONDENSED MATTER SCIENCES

Vol. 1. SURFACE POLARITONS

V.M. Agranovich and D.L. Mills, *editors*

Vol. 2. EXCITONS

E.I. Rashba and M.D. Sturge, *editors*

Vol. 3. ELECTRONIC EXCITATION ENERGY TRANSFER IN CONDENSED MATTER

V.M. Agranovich and M.D. Galanin

Vol. 4. SPECTROSCOPY AND EXCITATION DYNAMICS OF CONDENSED MOLECULAR SYSTEMS

V.M. Agranovich and R.M. Hochstrasser, *editors*

Vol. 5. LIGHT SCATTERING NEAR PHASE TRANSITIONS

H.Z. Cummins and A.P. Levanyuk, *editors*

Vol. 6. ELECTRON–HOLE DROPLETS IN SEMICONDUCTORS

C.D. Jeffries and L.V. Keldysh, *editors*

Vol. 7. THE DYNAMICAL JAHN–TELLER EFFECT IN LOCALIZED SYSTEMS

Yu.E. Perlin and M. Wagner, *editors*

Vol. 8. OPTICAL ORIENTATION

F. Meier and B.P. Zakharchenya, *editors*

Vol. 9. SURFACE EXCITATIONS

V.M. Agranovich and R. Loudon, *editors*

Vol. 10. ELECTRON–ELECTRON INTERACTIONS IN DISORDERED SYSTEMS

A.L. Efros and M. Pollak, *editors*

Vol. 11. MEDIUM-ENERGY ION REFLECTION FROM SOLIDS

E.S. Mashkova and V.A. Molchanov

Vol. 12. NONEQUILIBRIUM SUPERCONDUCTIVITY

D.N. Langenberg and A.I. Larkin, *editors*

MODERN PROBLEMS IN CONDENSED MATTER SCIENCES

Vol. 13. PHYSICS OF RADIATION EFFECTS IN CRYSTALS
R.A. Johnson and A.N. Orlov, *editors*

Vol. 14. INCOMMENSURATE PHASES IN DIELECTRICS
(Two volumes)
R. Blinc and A.P. Levanyuk, *editors*

Vol. 15. UNITARY TRANSFORMATIONS IN SOLID STATE
PHYSICS
M. Wagner

Vol. 16. NONEQUILIBRIUM PHONONS IN NONMETALLIC
CRYSTALS
W. Eisenmenger and A.A. Kaplyanskii, *editors*

Vol. 17. SOLITONS
S.E. Trullinger, V.E. Zakharov and V.L. Pokrovskii, *editors*

Vol. 18. TRANSPORT IN PHONON SYSTEMS
V.L. Gurevich

Vol. 19. CARRIER SCATTERING IN METALS AND
SEMICONDUCTORS
V.F. Gantmakher and I.B. Levinson

Vol. 20. SEMIMETALS – 1. GRAPHITE AND ITS COMPOUNDS
N.B. Brandt, S.M. Chudinov and Ya.G. Ponomarev

Vol. 21. SPECTROSCOPY OF SOLIDS CONTAINING RARE EARTH
IONS
A.A. Kaplyanskii and R.M. Macfarlane, *editors*

Vol. 22. SPIN WAVES AND MAGNETIC EXCITATIONS
(Two volumes)
A.S. Borovik-Romanov and S.K. Sinha, *editors*

Vol. 23. OPTICAL PROPERTIES OF MIXED CRYSTALS
R.J. Elliott and I.P. Ipatova, *editors*

MODERN PROBLEMS IN CONDENSED MATTER SCIENCES

Vol. 24. THE DIELECTRIC FUNCTION OF CONDENSED SYSTEMS
L.V. Keldysh, D.A. Kirzhnitz and A.A. Maradudin, *editors*

Vol. 25. CHARGE DENSITY WAVES IN SOLIDS
L.P. Gor'kov and G. Grüner, *editors*

Vol. 26. HELIUM THREE
W.P. Halperin and L.P. Pitaevskii, *editors*

Vol. 27. LANDAU LEVEL SPECTROSCOPY
(Two volumes)
G. Landwehr and E.I. Rashba, *editors*

Vol. 28. HOPPING TRANSPORT IN SOLIDS
M. Pollak and B. Shklovskii, *editors*

Vol. 29. NONLINEAR SURFACE ELECTROMAGNETIC PHENOMENA
H.-E. Ponath and G.I. Stegeman, *editors*

Vol. 30. MESOSCOPIC PHENOMENA IN SOLIDS
B.L. Altshuler, P.A. Lee and R.A. Webb, *editors*

Vol. 31. ELECTRIC STRAIN FIELDS AND DISLOCATION MOBILITY
V.L. Indenbom and J. Lothe, *editors*

Vol. 32. ELECTRONIC PHASE TRANSITIONS
W. Hanke and Yu.V. Kopaev, *editors*

This page intentionally left blank

*Oh, how many of them there
are in the fields!
But each flowers in its
own way –
In this is the highest achievement
of a flower!*

*Matsuo Bashó
1644–1694*

PREFACE TO THE SERIES

Our understanding of condensed matter is developing rapidly at the present time, and the numerous new insights gained in this field define to a significant degree the face of contemporary science. Furthermore, discoveries made in this area are shaping present and future technology. This being so, it is clear that the most important results and directions for future developments can only be covered by an international group of authors working in cooperation.

“Modern Problems in Condensed Matter Sciences” is a series of contributed volumes and monographs on condensed matter science that is published by Elsevier Science Publishers under the imprint of North-Holland. With the support of a distinguished Advisory Editorial Board, areas of current interest that have reached a maturity to be reviewed, are selected for the series. Both Soviet and Western scholars are contributing to the series, and each contributed volume has, accordingly, two editors. Monographs, written by either Western or Soviet authors, are also included. The complete series will provide the most comprehensive coverage available of condensed matter science.

Another important outcome of the foundation of this series is the emergence of a rather interesting and fruitful form of collaboration among scholars from different countries. We are deeply convinced that such international collaboration in the spheres of science and art, as well as other socially useful spheres of human activity, will assist in the establishment of a climate of confidence and peace.

The publishing house ‘Nauka’ publishes the volumes in the Russian language. This way the broadest possible readership is ensured.

The General Editors of the Series,

V.M. Agranovich

A.A. Maradudin

This page intentionally left blank

PREFACE

The volume on *Electronic Phase Transitions* deals with topics, which are presently in the center of scientific thrust in modern solid-state theory. *Anderson localization*, which has fundamental implications in many areas of solid-state physics as well as *spin glasses*, with its influence on quite different research activities such as neural networks, are two examples that are reviewed in this book. The *ab initio statistical mechanics of structural phase transitions* is another prime example, where the interplay and connection of two over decades unrelated disciplines of solid-state theory – first-principle electronic structure calculations and critical phenomena – has given rise to impressive new insights. Clearly, there is more and more need for accurate, stable *numerical simulations of models of interacting electrons*, presently discussed with great vigor in connection with high- T_c superconductors. In these last systems the superconducting transition is close to a magnetic transition, i.e. an *antiferromagnetic spin structure*.

All these topics are discussed and reviewed in the present volume by leading experts.

The theory of Anderson localization, as considered in the first chapter by Vollhardt and Wölfle, is an example for an electronic phase transition, which has received great attention in the last decade. Here, the nature of the electronic states can change drastically from extended to localized, triggered by disorder. A prime example is the so-called *weak localization*, a new quantum-mechanical interference phenomenon in condensed-matter physics.

Until the famous work by Anderson it was thought that the effect of disorder on the state of electrons in solids could be described in terms of low-order perturbation theory. Field-theoretic formulations of the Anderson localization problem provided the necessary framework for the discussion of the critical properties, close to the localization transition. However, many of the features obtained in the field-theoretic treatment can also be obtained from the self-consistent theory, as formulated and reviewed in Chapter 1 by Vollhardt and Wölfle. It can be made quantitative, in the sense, that the noncritical quantities in the theory may be renormalized; it has a simple physical interpretation and is, therefore, applicable to a wide variety of localization phenomena. After setting up in detail the self-consistent theory in various sections, this last point is

discussed in detail in Vollhardt's and Wölfle's review. It contains also a thorough and critical assessment of the available theories of Anderson localization.

A different type of electronic phase transition which, however, is also related to some kind of disorder, i.e. the non-periodic "freezing" of the spins in magnetic alloys, takes place in spin-glasses. The present state-of-the-art of this topic is discussed and reviewed by Sherrington in Chapter 2. Attempts to explain the random freezing in spin glasses as a function of temperature have opened a "Pandora's box" of new concepts and techniques far beyond magnetism: it started with the theory of Edwards and Anderson in 1975, an attempt to describe this "freezing" transition, and had, and still has, many implications in other areas of solid-state theory (for example, the replica theory). In addition, the theory of spin glasses has also influenced quite different research activities, such as the treatment of hard optimization problems and neural-network studies, which are both discussed in the present context. Sherrington successfully conveys the idea that spin-glass theory is a fascinating example of a situation, in which the attempt to understand the unusual physical properties of systems without obvious practical applications has led to a wealth of novel concepts on a wide scale and with far-reaching consequences.

A truly remarkable example of what the interplay of state-of-the-art computational techniques with modern theories of critical phenomena can achieve for describing phase transitions in *real rather than model* systems is provided in Chapter 3 by Rabe and Joannopoulos. Their approach is based on combining successful ab initio calculations of structural properties of solids, employing density-functional theory for total-energy calculations, with the analysis of the phase transition through powerful techniques of critical phenomena. The "ab initio statistical mechanics" treatment incorporates the microscopic physics, in particular, the electronic degrees of freedom (i.e. orbitals) and their interactions (within the frame of density-functional theory). This part focuses on the microscopic origin of the character of the bonding that results in models that describe the energies of low-lying configurations in a unified way. On the other hand, in a purely statistical mechanics treatment, a large number of systems with different types of order parameters are classified and their phase diagram is generated within mean-field as well as renormalization-group approaches. The establishment of the final links through ab initio total-energy calculations yields, as discussed by Rabe and Joannopoulos, useful insight into structural phase transitions.

Strongly correlated electronic systems that are close to a metal-insulator transition have been the subject of renewed interest lately. Prime examples are the heavy-fermion systems and most recently the high-temperature superconductors. Close to the transition to the antiferromagnetic insulating state the latter systems are simultaneously close to the metal-superconductor transition. Therefore, it is clearly of importance to get reliable handle on the electronic properties in the vicinity of a Mott-Hubbard type of transition. These electronic

phase transitions are usually discussed in terms of one or the other version of the Hubbard model. The aim of the review of Loh and Gubernatis in Chapter 4 is to discuss recent advances in numerical simulation techniques of Hubbard-type models for fermions with short-range interactions. In these models the competition between the kinetic and short-range Coulomb energies gives rise to the possible Mott–Hubbard or charge-transfer-induced (for the high- T_c superconductors) metal–insulator transition. In spite of a variety of perturbative, variational, and numerical calculations, the physical consequences that arise from this competition are not yet fully understood. Loh and Gubernatis address, in particular, the powerful Quantum-Monte-Carlo simulation technique, its technical advantages (size of simulated lattices), but also limitations (such as the “minus sign” problem). They discuss both repulsive and attractive Hubbard models, with the latter being prime examples for studying superconducting properties.

The last chapter of the book is a review of spin-density waves in itinerant antiferromagnets by Tugushev, a topic which nicely contrasts the more localized picture described in the previous chapter. Tugushev is concerned with the band theory of magnetism in three-dimensional (transition or rare-earth) metals and alloys, where there exists significant Fermi-surface “nesting”. Classical examples are chromium and its dilute alloys and some quasi-one-dimensional conductors. Also in this last chapter, the high- T_c superconducting metal-oxides are touched upon, however, now from the itinerant magnetism point of view.

W. Hanke
Yu.V. Kopaev

This page intentionally left blank

CONTENTS

Preface to the series	ix
Preface	xi
Contents	xv
1. Self-consistent theory of Anderson localization	1
<i>D. Vollhardt and P. Wölfle</i>	
2. Spin glasses	79
<i>D. Sherrington</i>	
3. Ab initio statistical mechanics of structural phase transitions	135
<i>K.M. Rabe and J.D. Joannopoulos</i>	
4. Stable numerical simulations of models of interacting electrons in condensed-matter physics	177
<i>E.Y. Loh Jr and J.E. Gubernatis</i>	
5. Modulated and localized structures of spin density waves in itinerant antiferromagnets	237
<i>V.V. Tugushev</i>	
Author index	307
Subject index	317
Cumulative index	323

This page intentionally left blank

CHAPTER 1

Self-Consistent Theory of Anderson Localization

DIETER VOLLHARDT

*Institut für Theoretische Physik C
Technische Hochschule Aachen
W-5100 Aachen, Federal Republic of Germany*

and

PETER WÖLFLE*

*Institut für Theorie der Kondensierten Materie, Universität Karlsruhe
Postfach 6980, W-7500 Karlsruhe, Federal Republic of Germany*

* Work partially performed at: Department of Physics, University of Florida
Gainesville, FL 32611, USA

© Elsevier Science Publishers B.V., 1992

*Electronic Phase Transitions
Edited by
W. Hanke and Yu.V. Kopaev*

Contents

1. Introduction	3
2. Models of disorder	8
3. Weak localization	11
3.1. Diffusion of classical and quantum-mechanical particles	12
3.2. Systematic calculation of the corrections to the Boltzmann conductivity	18
4. Density response theory	19
4.1. Infrared divergences of the irreducible vertex	27
5. Beyond perturbation theory: the self-consistent equation for $D(\omega)$	31
5.1. Method I	32
5.2. Method II	32
5.3. Anisotropic systems and general angle-dependent scattering	35
6. Solution of the self-consistent equation: scaling behavior of the dynamical conductivity	38
6.1. Solution in dimensions $d \leq 2$	39
6.2. Solution in dimensions $d > 2$	40
7. Length dependence of the conductance in finite samples	42
8. Alternative derivations and extensions of the self-consistent theory	49
9. Application of the self-consistent theory of localization to electronic systems and classical waves	54
9.1. Electrons in disordered systems with a specific geometry	54
9.2. Localization of classical waves and other wave-like entities moving in a random medium	55
10. Self-consistent theory of the tight-binding model with site-diagonal disorder	57
10.1. Locator expansion	59
10.2. Derivation of the self-consistent equation for the diffusion coefficient	64
10.3. Results of a numerical evaluation of the self-consistent equation	68
11. Conclusion	72
References	73

1. Introduction

The problem of localization of quantum particles in a disordered system has attracted great attention during the last decade, triggered by the discovery of a new quantum phenomenon in solid state physics, the so-called *weak localization* (Abrahams et al. 1979). After the first formulation of the modern theory of solids in the 1930s it was thought for a long time that the effect of disorder on the state of electrons in solids could be described, on a semiclassical level, in terms of low-order perturbation theory. Indeed, the quantum-mechanical adaptation of Boltzmann transport theory appeared to work perfectly well, except for certain inexplicable observations like negative magnetoresistance of doped semiconductors in a weak magnetic field.

It was only in 1958 that Anderson proposed the now famous concept of localization of electrons by disorder. Anderson argued that in a tight-binding model of electrons on a lattice with randomly varying site energies V_i , electrons of given energy E would become localized if the spread of the energies V_i (i.e. the disorder) was sufficiently large. In other words, the nature of the electronic states would change drastically from extended to localized. In the former case the disorder manifests itself mainly through a decay of phase coherence in the averaged single-particle propagator, while in the latter case a probability amplitude decreases exponentially as one moves away from the center of localization. This is not unexpected, since even in a classical system disorder may cause localization of particles. The corresponding problem of percolation of particles through a random medium has been widely investigated. Although the two problems of quantum localization and classical percolation, at first sight, seem to have much in common, the development of the two fields over the years appears to have set them more and more apart. Roughly speaking, the quantum nature of particles makes it harder for them to overcome narrow passages and channels, despite the fact that quantum particles may tunnel through classically forbidden regions. Hence, quantum particles tend to be localized more easily than classical particles.

The first qualitative consequence of the quantum nature of particles for transport in strongly disordered systems, is reflected in the fact that the mean free path l , e.g., of electrons scattering off imperfections in the crystal lattice, cannot become shorter than the wavelength of the particles, i.e. the Fermi

wavelength λ_F at low temperatures (Ioffe and Regel 1960). For electrons in the center of the band λ_F is of the order of the lattice spacing a , but for energies near the band edge λ_F may be much larger than a . In a classical system, the shortest possible mean free path is always given by the average distance between the scattering centers, irrespective of the particle energy. If the disorder is increased beyond the point where $l \approx \lambda_F$, or else if the energy of the electrons (and hence $1/\lambda_F$) is decreased for a fixed disorder, the nature of the electronic states is expected to change from extended to localized. Consequently, the electrical conductivity of the system (or mobility of the carriers) is expected to go to zero. The latter scenario, where a change in the electron energy induces a metal-insulator transition, was explored early on by Mott (see Mott 1966, 1967, 1968, 1970 and the books by Mott (1974) and by Mott and Davis (1979)). He coined the term *mobility edge* for the critical energy separating extended and localized states. These two types of states are not likely to coexist at a given energy, since any small change in the potential would cause admixtures of extended states with a localized state, and would thus delocalize it (a possible exception is a symmetry-induced orthogonality of states). On the basis of qualitative considerations and experimental data, Mott concluded that the Anderson transition in a three-dimensional system ($d = 3$) should be *discontinuous*, the conductivity jumping from a finite value, the so-called *minimum metallic conductivity* σ_{\min} , to zero. A minimal metallic conductivity was generally expected to exist also in two dimensions ($d = 2$). On the other hand, it was known that for $d = 1$ states are *always* localized, irrespective of the strength of the disorder, with the localization length being of the order of the mean free path (Mott and Twose 1961, Borland 1963, Berezinskii 1973, Abrikosov and Ryskin 1978, see also Landauer 1957, 1970). In fact, the situation for $d = 1$ is somewhat special and has its own long history (Erdős and Herndon 1982). The advent of the computer, which made the exact diagonalization of finite-size systems possible, and the advances in transport measurements near the metal-insulator transition at low temperatures changed this picture altogether. It seems to be well established now that there is no minimal metallic conductivity and that the transition is continuous, much like a continuous phase transition in a usual thermodynamical system. A continuous phase transition is necessarily associated with a characteristic length ξ (or possibly a set of such lengths), which tends to infinity as the transition is approached. At the transition, where the length ξ is infinite, a natural unit of length does not exist anymore and the system is therefore scale-invariant. The ensuing scaling behavior was discovered by Thouless and coworkers (for a review, see Thouless 1974) who noticed that the conductance of a finite-size block scales with the size in a universal way. Wegner (1976) applied concepts of the theory of critical phenomena to this problem and proposed scaling laws for the correlation functions and relations between the critical exponents.

The scaling hypothesis was given concrete physical meaning when Abrahams et al. (1979) discovered a scale-invariant contribution to the conductance in

lowest-order perturbation theory, and when Gorkov et al. (1979) showed the consistency of the scaling assumption in the next order in the expansion. The former group postulated a one-parameter scaling theory of localization with strong (and verifiable) predictions, such as the absence of diffusion, i.e. the absence of extended states in a two-dimensional disordered system at zero temperature. The concept of weak localization originating from this discovery has given rise to an extremely fruitful exploration and exploitation of quantum interference effects in low-dimensional systems (see Bergmann 1984, Chakravarty and Schmid 1986, Washburn and Webb 1986). Meanwhile, on the theoretical side the idea of a continuous phase transition characterized by an order parameter and a spontaneously broken symmetry was formalized by Wegner and coworkers (Wegner 1979, 1982, Schäfer and Wegner 1980), who were able to map the problem onto a nonlinear σ -model of n interacting matrix fields in the limit $n \rightarrow 0$. The one-parameter scaling hypothesis was put on a firmer basis when the lower critical dimension was identified as $d = 2$ (Wegner 1979, 1982, Hikami 1981, 1982) and an expansion around $d = 2$ confirmed and extended the results of Abrahams et al. (1979). An alternative field-theoretic formulation for the localization problem was discussed by Efetov et al. (1980) and Efetov (1983, 1984a, b, 1987a, b, 1988). Furthermore, Shapiro (1982a) and Zirnbauer (1988) presented a Migdal–Kadanoff renormalization group treatment for the localization problem, the latter author focussing on the critical exponent of the localization length in three dimensions for systems with broken time-reversal invariance.

It should be noted that Efetov (1984a, b, 1987a, b; see also Zirnbauer 1986a, b) obtained the exact solution of a nonlinear σ -model for the localization transition on a Bethe lattice. This lattice is usually expected to simulate a space of infinite dimensions ($d = \infty$), i.e. it is thought to yield the mean-field behavior. Efetov's results agree with ordinary perturbation theory for weak coupling and with earlier results obtained by Kunz and Souillard (1983) for the behavior of the localization length at the transition. However, the result for the critical behavior of the diffusion coefficient differs significantly from the mean-field result obtained by any other approach (see section 6), the diffusion coefficient according to Efetov's approach decreasing *exponentially* at the transition (see also Suslov 1986). Efetov (1987a) attributed this to the noncompactness of the symmetry group of his field theory, for which he obtained an exact solution in closed form. It is not self-evident, however, that a Bethe lattice, which has several artificial features (e.g., has no loops), really provides the mean-field solution for the localization problem in the same way as it does for localization spin models. Indeed, for quantum-mechanical problems involving itinerant degrees of freedom the limit $d \rightarrow \infty$ is in general nontrivial even for regular lattices (Metzner and Vollhardt 1989, van Dongen and Vollhardt 1990). Most recently, Chalker and Siak (1990) pointed out that the localized phase is insulating if the exponential decay of eigenstate amplitudes, with distance from an origin, is faster than

the corresponding exponential growth in number of sites. Otherwise eigenfunctions are not square-integrable and the phase is conducting. Thus, the localization transition is split into three stages on a (finite) Bethe lattice.

The above-mentioned field-theoretic formulations of the Anderson localization problem provide the necessary framework for a discussion of the critical properties, but are somewhat cumbersome when actual quantitative calculations are required. For the case of pure potential scattering it is actually possible to derive a self-consistent theory of Anderson localization, which incorporates many of the features obtained in the field-theoretic treatment (Vollhardt and Wölfle 1980a, b). This theory has a simple physical interpretation and is therefore adaptable to a wide variety of related localization phenomena. It can also be made quantitative in the sense that the noncritical quantities in the theory may be renormalized, e.g. within a self-consistent single-site approximation or coherent-potential approximation (Kroha et al. 1990, Kroha 1990). Comparison of the self-consistent theory with results of exact diagonalization of finite-size systems shows that the theory appears to capture the main features well, except possibly for the critical regime very close to the transition point in dimensions $d = 3$. However, extensions of the self-consistent theory to systems with broken time-reversal symmetry or with spin-orbit scattering have met with only limited success (see the discussion in section 8). In the case of time-reversal invariance the self-consistent theory of localization has been applied to a variety of problems, such as electrons in various geometries and localization of phonons, photons and other wave-like entities in a random medium.

More recently, the validity of the one-parameter scaling theory has been called into question (Altshuler et al. 1986a, b, Shapiro 1986, Henrichs 1988, see also Muttalib et al. 1987). In general, an ensemble of disordered systems is characterized by the probability distribution $P(g)$ for, say, the conductance g , rather than just the average (or the median) conductance. It is unclear at present whether the scaling behavior of $P(g)$ is controlled by a single parameter, or by two or more parameters. Whereas studies of higher-order correlation functions near the mobility edge seem to show a breakdown of one-parameter scaling theory – in the sense that the higher cumulants of the conductance scale with the length of the system in a totally unrelated way (Altshuler et al. 1986a, b) –, renormalization group studies of the probability distribution $P(R)$ of the resistances R indicate that $P(R)$ shifts towards a limiting universal distribution characterized by two parameters (Cohen et al. 1988). In fact, most recently Shapiro (1990) showed that in $d = 2 + \varepsilon$ dimensions the probability distribution $P(g)$ may well scale to a universal function as the mobility edge is approached, in spite of the fact that its higher moments are nonuniversal. This problem merits further investigation until a final judgement can be made.

It has turned out that comparison of the theory with experiments on electrons in disordered semiconductors or metals is complicated by the fact that, in contrast to earlier expectations, the electron interaction processes contribute

very significantly, i.e. lead to singularities near the Fermi surface. The scaling behavior is thereby changed even at the level of weak localization (Altshuler and Aronov 1979a, b). A scaling theory of the interacting disordered system has been developed for the case where the quantum-interference contribution responsible for weak localization is suppressed by a magnetic field (Finkelstein 1983, Castellani et al. 1984a). In principle, such a perturbation theory, in conjunction with a renormalization group treatment, may describe the disordered interacting system up to the metal-insulator transition (MIT). In particular, Finkelstein (1983, 1984a, b, c) was the first to identify the relevant scaling variables within a mapping of the problem to a nonlinear σ -model. Thereby it became clear that the results obtained from his theory for thermodynamic quantities, such as the compressibility (Finkelstein 1983), spin susceptibility (Finkelstein 1984a, Castellani et al. 1984a, b, 1986), and the specific heat (Castellani and DiCastro 1986), exhibit a detailed analogy with those obtained from Fermi liquid theory. This connection has been made precise by Castellani et al. (1987), who also gave a general description of the possible scaling scenarios. Probably, the most important result of the perturbative renormalization group approach is, that in a system with spin-*independent* scattering the static spin susceptibility of the metal is strongly enhanced at zero temperature and, in fact, diverges at the MIT itself. This instability indicates the appearance of local magnetic moments as the MIT is approached. The mechanism of formation of such local-moment states has recently been investigated within an effective-field theory (Milovanovic et al. 1989) and by a renormalization group treatment (Kirkpatrick and Belitz 1990). In this chapter we will not discuss interaction effects; they will only be mentioned in section 8 in connection with the theory of Sadovskii (1986), who incorporated the first-order correction term due to the interaction into the self-consistent theory of localization developed by the present authors. An exhaustive discussion of the theory of the MIT can be found in the review by Lee and Ramakrishnan (1985) and the proceedings volume "Anderson Localization" edited by Ando and Fukuyama (1988).

The scope of this chapter is as follows. In section 2, the most common models of disorder are introduced. Weak localization as a quantum-mechanical interference phenomenon is discussed in section 3. The formal density-response theory based on disorder-averaged Green's functions is presented in section 4, where also the weak localization results are rederived in a systematic way. Section 5 is devoted to the detailed derivation of the self-consistent theory of localization, the solutions of which are discussed in section 6. Finite-size scaling, or the length-dependence of the conductance, is considered in section 7. A review of alternative derivations or extensions of the self-consistent theory is given in section 8. Applications of the self-consistent theory to other systems are reviewed in section 9. In section 10, a quantitative version of the self-consistent theory as applied to the tight-binding model with site-diagonal disorder is presented and compared with results of exact diagonalization of finite-size

systems. Section 11 contains a summary and a critical assessment of the available theories of Anderson localization.

There exist a number of excellent review articles on the subject. Bergmann (1984) has provided a detailed discussion of the theory of weak localization and of related experiments. Altshuler and Aronov (1985) give a comprehensive discussion of weak localization with particular emphasis on the effect of time-reversal invariance breaking fields and Coulomb interaction. A path integral formulation of weak localization which stresses the aspect of quantum interference, has been considered by Chakravarty and Schmid (1986). The review article by Sadovkii (1986) covers many aspects of the theory, e.g. weak localization, general structure of response functions in the metallic and insulating state, self-consistent theory and field-theoretic treatments. The most complete and concise review article to date is the one by Lee and Ramakrishnan (1985), who present a critical assessment of virtually all aspects of Anderson localization, including experimental results. There have been numerous conferences on Anderson localization over the years. Several of them have resulted in books, in which the conference proceedings are published. Their publication details can be found in the beginning of the reference list at the end of this chapter. In other cases the proceedings were published in scientific journals. All of them provide a fine and more or less representative overview of the field at a given time.

2. Models of disorder

In the model originally introduced and discussed by Anderson (1958), a single electron moves on a regular lattice, e.g. a hypercubic lattice, where each lattice point carries a random on-site potential V_i (see fig. 1). Hence, in this model the disorder of the system is due to the *energy* states of the lattice sites encountered by the electron. The Hamiltonian for such a system may be written in position space as

$$H = \sum_{ij,\sigma} t_{ij} c_{i\sigma}^+ c_{j\sigma} + \sum_{i,\sigma} V_i n_{i\sigma}, \quad (2.1)$$

where $c_{i\sigma}^+$ and $c_{i\sigma}$ create and annihilate, respectively, a particle with spin σ on site

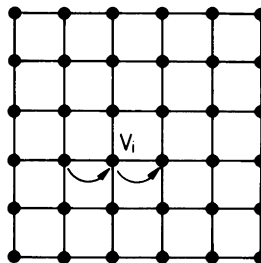


Fig. 1. Model of disorder with random on-site potential V_i (after Anderson 1958).

t_{ij} is the hopping matrix element between sites i and j , $n_{i\sigma} = c_{i\sigma}^\dagger c_{i\sigma}$ is the number operator and V_i are random (spin-independent) on-site energies. The energies V_i are characterized by their distribution $P(V_i)$, which may, e.g. be assumed to be constant (see fig. 2) within some interval of width W given by (Anderson 1958)

$$P(V_i) = \begin{cases} \frac{1}{W}, & |V_i| < \frac{1}{2}W, \\ 0, & \text{elsewhere,} \end{cases} \quad (2.2)$$

or to be Gaussian:

$$P(V_i) = \frac{1}{\sqrt{2\pi}} \frac{1}{W} \exp(-V_i^2/2W^2). \quad (2.3)$$

In momentum space eq. (2.1) takes the form (hereafter the spin indices will be suppressed)

$$H = \sum_k \varepsilon_k n_k + \sum_k V_k \rho_k, \quad (2.4)$$

where

$$V_k = \frac{1}{\sqrt{L}} \sum_i V_i \exp(i\mathbf{k} \cdot \mathbf{R}_i) \quad (2.5)$$

is the Fourier transform of the random energies V_i , with L as the number of lattice sites, $n_k = a_k^\dagger a_k$ is the momentum distribution operator and

$$\rho_k = \frac{1}{\sqrt{L}} \sum_q a_q^\dagger a_{q+k} \quad (2.6)$$

is the Fourier component of the local density-operator. The operators a_k^\dagger and a_k act as creation and annihilation operators for a particle with momentum $\hbar k$. In eq.(2.4), the disorder of the system is therefore contained in the random field V_k .

An alternative model of disorder is credited to Edwards (1958). In this model a particle is scattered by randomly distributed, static scattering centers (the

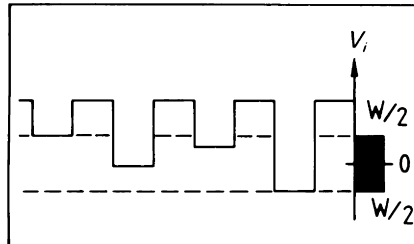


Fig. 2. Example of the on-site energies along a row of lattice sites for a rectangular energy distribution.

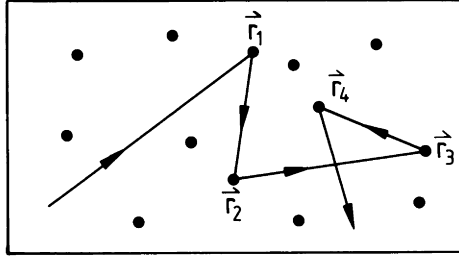


Fig. 3. Model of disorder with randomly distributed scatterers (after Edwards 1958).

impurities) of equal potential (fig. 3). In this case the disorder is due to the statistical *spatial* distribution of the scatterers. The Hamiltonian for this situation is given by

$$H = \int d\mathbf{r} \psi^+(\mathbf{r}) \left[-\frac{\hbar^2 \nabla^2}{2m} + \sum_i V(\mathbf{r} - \mathbf{r}_i) \right] \psi(\mathbf{r}), \quad (2.7)$$

where the field operators $\psi^+(\mathbf{r})$ and $\psi(\mathbf{r})$ create and annihilate, respectively, a particle at position \mathbf{r} , and $V(\mathbf{r} - \mathbf{r}_i)$ is the potential of an impurity at random position \mathbf{r}_i as felt by an electron at \mathbf{r} . In momentum representation eq. (2.7) takes the form

$$H = \sum_k \varepsilon_k n_k + \sum_i \sum_k V_k \exp(i\mathbf{k} \cdot \mathbf{r}_i) \rho_k, \quad (2.8)$$

where $\varepsilon_k = (\hbar k)^2 / 2m$ is the dispersion relation for free particles. In eq. (2.8) the disorder of the system is given by the randomness of the *positions* \mathbf{r}_i . While the former model, eq. (2.1), usually starts out from the localized regime, the starting point of the latter model is the regime of extended states with weak scattering. Indeed, the Edwards model is particularly suited for the formulation of a systematic perturbation theory which starts from the undisturbed, metallic regime and then includes a small concentration of impurities, i.e. considers weak disorder.

The investigations described in this paper make use of both formulations. However, we start out with the Edwards model assuming independent electrons, which are scattered by point-like, static, randomly distributed impurities of equal scattering strength. To describe the physics of a disordered system we are particularly interested in its conductivity σ or the diffusion coefficient D . The two quantities are, in fact, related by the Einstein relation

$$\sigma = e^2 N_F D, \quad (2.9)$$

where e is the electronic charge and N_F is the density of states at the Fermi surface. Indeed, scattering of the particles in a (weakly) disordered medium leads

to diffusion, i.e. to a diffusive motion of the particles. The concept of diffusion is of central importance in the theory of localization. In a three-dimensional system which is only weakly disturbed by impurities, the scattering of the particles at zero temperature may be described by a finite mean free path l . This in turn defines a *collision time* τ by

$$l = v\tau, \quad (2.10)$$

where v is the characteristic velocity, e.g. the Fermi velocity v_F in the case of electrons. The conductivity σ in eq. (2.9) generally depends on the frequency ω of the applied electric field. The DC-conductivity $\sigma(\omega = 0)$ is found from Drude or Boltzmann theory as

$$\sigma(0) \equiv \sigma_0 = \frac{e^2 n}{m} \tau, \quad (2.11)$$

where m is the mass of an electron and n is the total electron density. The quantity σ_0 is often referred to as *Drude* or *Boltzmann conductivity*, since eq.(2.11) is a direct consequence of the elementary transport theory.

3. Weak localization

We will first consider the case of very weak disorder. This is done for two reasons: first, the underlying physics is very simple and easy to understand, and second, the results already contain essential information about the behavior of the conductivity for stronger disorder. Our starting point is the metallic regime. We want to understand how a small concentration of impurities affects the metallic behavior. Since we are far from the actual Anderson transition itself, these effects can be treated in perturbation theory. Weak disorder means that the mean free path l is much greater than the quantum-mechanical wavelength k_F^{-1} of the particle, i.e. $k_F l \gg 1$ or, equivalently, $E_F \tau \gg 1$, where k_F and E_F are the Fermi wave number and the Fermi energy, respectively. We will therefore choose

$$\lambda = \frac{1}{2\pi E_F \tau} \quad (3.1)$$

as our small disorder parameter. Starting from the metallic regime we want to consider the precursor effects of localization, i.e. the corrections $\delta\sigma$ to the metallic conductivity

$$\sigma = \sigma_0 + \delta\sigma, \quad |\delta\sigma| \ll \sigma_0. \quad (3.2)$$

These perturbational effects are commonly called *weak localization*. Our aim is to calculate $\delta\sigma = f(L, \omega, T, H)$ as a function of several external parameters like the system size L , the frequency ω , the temperature T and the magnetic field H .

3.1. Diffusion of classical and quantum-mechanical particles

The DC-conductivity σ_0 [eq.(2.11)] is given in terms of the small disorder parameter λ as

$$\sigma_0 \propto \frac{1}{\lambda}. \quad (3.3)$$

This is a result of the conventional Boltzmann transport theory. In this theory consecutive collisions of particles are assumed to be independent of each other, i.e. collisions are assumed to be uncorrelated. This implies that multiple scattering of a particle from a particular scattering center is not taken into account. Consequently, if there is a finite probability for the repeated occurrence of such multiple scatterings, the basic assumption of the independence of scattering events breaks down and the validity of eq. (2.11) for σ_0 becomes questionable, at least.

To investigate this fundamental point we consider the diffusive behavior of a particle in a d -dimensional disordered system. Let the particle be located at \mathbf{r}_0 at time $t = 0$ (fig. 4a). Due to its diffusive motion the particle moves away from \mathbf{r}_0 . At some later time $t > \tau$ we will only be able to make a probabilistic statement about its position: that it will be located within some compact volume (fig. 4b) whose size is determined by the probability distribution $P(\mathbf{r}, t)$, which is the solution of the diffusion equation

$$\frac{\partial P}{\partial t} - D_0 \nabla^2 P = 0, \quad (3.4)$$

with suitable initial conditions. The diffusion constant D_0 is given by $D_0 = v_F^2 \tau / d$, where v_F is the characteristic velocity of the particles. The explicit solution of eq. (3.4) has the form

$$P(\mathbf{r}, t) = \frac{\exp(-|\mathbf{r} - \mathbf{r}_0|^2 / 4 D_0 t)}{(4\pi D_0 t)^{d/2}}. \quad (3.5)$$

The probability $P(\mathbf{r}, t)$ is sizeable only within a volume V_{diff} defined by

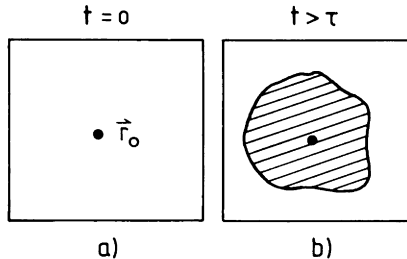


Fig. 4. Probability distribution for the location of a diffusing particle (a) $t = 0$. (b) $t > \tau$.

$|\mathbf{r} - \mathbf{r}_0|^2 \lesssim 4D_0 t$, into which the particle has diffused in time t , i.e. $V_{\text{diff}} \approx (D_0 t)^{d/2}$. Within the volume V_{diff} the probability is given by

$$P(\mathbf{r}, t) \propto \frac{1}{V_{\text{diff}}} = \frac{1}{(D_0 t)^{d/2}}. \quad (3.6)$$

These considerations are purely classical. To understand the difference in the diffusive behavior of classical and quantum-mechanical particles, we take a look at the path of a particle diffusing from some point A to some point B in the sample (fig. 5).* This transport can take place along different trajectories (in fig. 5 four examples are shown). The trajectories, or “tubes”, have a typical width given by the Fermi wavelength

$$\lambda_F = \frac{\hbar}{v_F m}. \quad (3.7)$$

In the classical case ($\hbar = 0$) these “Feynman paths” are arbitrarily sharp ($\lambda_F = 0$). In the quantum-mechanical case, however, one has $\lambda_F = 2\pi k_F^{-1}$, i.e. the tubes have a finite diameter. We now assume that (i) the disorder λ is very small ($\lambda_F/\lambda \ll 1$) and (ii) the temperature is low enough, so that inelastic processes, characterized by an inelastic scattering time τ_{in} , occur only very rarely ($\tau_{\text{in}} \gg \tau$).

Since the transport from A to B may take place along different trajectories, there is a probability amplitude A_i connected to every path i . In accordance with Feynman’s formulation of quantum mechanics, the total probability W to reach point B from A is then given by the square of the magnitude of the sum of all amplitudes:

$$W = \left| \sum_i A_i \right|^2 \quad (3.8a)$$

$$= \sum_i |A_i|^2 + \sum_{i \neq j} A_i A_j^*. \quad (3.8b)$$

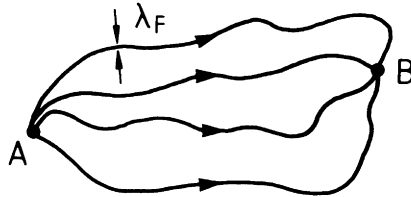


Fig. 5. Four typical paths of an electron diffusing from A to B.

* Here we follow the original discussion by Altshuler et al. (1983), Khmelnitskii (1984) and Altshuler and Aronov (1985); an equivalent explanation, using the behavior in k -space, has been given by Bergmann (1983, 1984).

The first term in eq. (3.8b) describes separate (i.e. noninterfering) paths – this is the classical case, in which the tubes are infinitely sharp. On the other hand, the second term represents the contribution due to interference of the paths, which is therefore an exclusively quantum-mechanical effect. In the conventional Boltzmann theory these interference terms had been neglected. In most cases this is indeed justified: since the trajectories have different lengths, the amplitudes A_i carry different phases. On the average, this leads to destructive interference. Hence, the quantum-mechanical interferences suggested in fig. 5 are generally unimportant.

There is, however, one particular exception to this conclusion: namely, if the points A and B coincide (fig. 6), i.e. if the path crosses itself. In this case the starting point and the endpoint are identical, so that the path in between can be traversed in two opposite directions: forward and backward. The probability W to go from A to B is thus the *return* probability to the starting point. Since paths 1 and 2 in fig. 6 are identical, the amplitudes A_1 and A_2 have a coherent phase relation. This leads to constructive interference, so that the quantum-mechanical contribution to W becomes very important. Equation (3.8b) then tells us that for $A_1 = A_2 \equiv A$, the classical return probability (due to the neglect of the interference terms) is given by $W_{\text{class}} = 2|A|^2$, while the quantum-mechanical case yields $W_{\text{qm}} = 2|A|^2 + 2A_1 A_2^* = 4|A|^2$. Thus, one obtains that

$$W_{\text{qm}} = 2W_{\text{class}}. \quad (3.9)$$

The probability for a quantum-mechanical particle to return to some starting point is thus seen to be twice that of a classical particle. One may therefore say that “quantum diffusion” is slower than classical diffusion due to the existence of a more effective backscattering effect in the former case. In other words: quantum-mechanical particles in a disordered medium are (at low temperatures) less mobile than classical particles. This in turn leads to a correspondingly lower conductivity σ .

It should be stressed that the factor of 2 in eq. (3.9) is simply a consequence of constructive wave interference of the two time-reversed paths in fig. 6. In the case of electrons its origin is quantum-mechanical, only because the wave nature of electrons is an inherently quantum-mechanical effect. In general, any wave propagation in a disordered medium will lead to a qualitatively identical result.

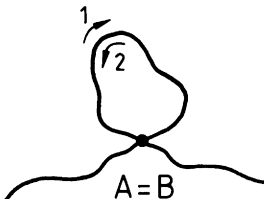


Fig. 6. Self-crossing path of a diffusing electron.

Any wave will do. For example, shouting into a forest (we assume a naturally grown forest, where trees are irregularly spaced) will lead to the same kind of enhancement (*echo*) along the backward direction as shining light into white paint will. Localization involving classical wave propagation has been discussed by Anderson (1985), who also gave a number of examples for related electromagnetic and acoustic phenomena.

Indeed, inspired by the weak-localization effects known from disordered electronic systems, it was convincingly shown that coherent backscattering applies equally to the propagation of light in a disordered medium (van Albada and Lagendijk 1985, Wolf and Maret 1985). Localization effects involving electromagnetic waves, sound and other wave-like entities in disordered media have since then been studied in detail. These effects will be discussed in section 9; for an earlier survey which includes some historical notes, see Vollhardt (1987).

To estimate the size of the effect of interference on σ , we consider the change $\delta\sigma$ relative to the metallic conductivity σ_0 , i.e. $\delta\sigma/\sigma_0$. Because of the expected decrease in σ , the sign of $\delta\sigma/\sigma_0$ must be negative. Furthermore, this change is expected to be proportional to the probability of occurrence of a closed path (as in fig. 6) during diffusion. (This is the probability to find a particle in a closed tube, i.e. the probability for the trajectory to intersect itself during diffusion.) Let us therefore have a look at a d -dimensional tube (fig. 7) with diameter λ_F , i.e. cross section λ_F^{d-1} . During the time interval dt the particle moves a distance $dl = v_F dt$, so that the corresponding volume element of the tube is given by $dV = v_F dt \lambda_F^{d-1}$. On the other hand, the maximum possible volume for the diffusing particle is given by V_{diff} (eq. (3.6)). The above-mentioned probability for a particle to be in a closed tube is therefore given by the integral over the ratio of these two volumes:

$$W = \int_{\tau}^{\tau_{\text{in}}} \frac{dV}{V_{\text{diff}}} = v_F \lambda_F^{d-1} \int_{\tau}^{\tau_{\text{in}}} \frac{dt}{(D_0 t)^{d/2}}. \quad (3.10)$$

Here we have integrated over all times $\tau \leq t \leq \tau_{\text{in}}$, where τ is the time for a single elastic collision and τ_{in} is the shortest inelastic relaxation time in the system. It

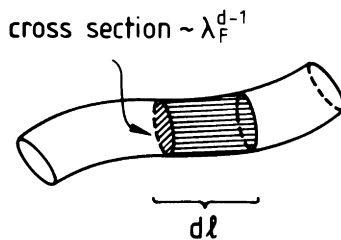


Fig. 7. Enlarged section of a d -dimensional quantum-mechanical trajectory of diameter $\lambda_F = h/mv_F$.

determines the maximal time during which coherent interference of the path amplitudes is possible. Because of $D_0 \propto 1/\lambda$ we obtain

$$\frac{\delta\sigma}{\sigma_0} \propto -\lambda \times \begin{cases} \left(\frac{\tau_{in}}{\tau}\right)^{1/2}, & d = 1, \\ \hbar \ln \frac{\tau_{in}}{\tau}, & d = 2, \\ \hbar^2 \left(\frac{\tau_{in}}{\tau}\right)^{-1/2}, & d = 3. \end{cases} \quad (3.11)$$

If we assume that for $T \rightarrow 0$ the inelastic relaxation rate vanishes with some power of T , i.e. $1/\tau_{in} \propto T^p$, where p is a constant, then eq. (3.11) becomes

$$\frac{\delta\sigma}{\sigma_0} \propto -\lambda \times \begin{cases} T^{-p/2}, & d = 1, \\ \hbar p \ln \frac{1}{T} + \text{constant}, & d = 2, \\ \hbar^2 T^{p/2}, & d = 3. \end{cases} \quad (3.12)$$

We thus find that (i) the conductivity decreases for decreasing temperature, (ii) the relative correction $\delta\sigma/\sigma_0$ is linear in the disorder parameter $\lambda \ll 1$ (lowest order in λ), (iii) except for $d = 1$, these corrections are of quantum-mechanical origin, i.e. they disappear for $\hbar \rightarrow 0$. (In the case $d = 1$, the “tube” in fig. 7 has no finite diameter, just as in the classical situation; furthermore, since for $d = 1$ there is only forward and backward scattering, all paths are trivially “closed”.)

In the case $d = 2$, therefore, one obtains a *logarithmic* temperature dependence of the conductivity correction $\delta\sigma$. We note that the elastic scattering due to the disorder, in principle, leads to a divergent temperature behavior of $\delta\sigma$ for $d \leq 2$. For the initial assumption $|\delta\sigma| \ll \sigma_0$ to remain valid, the results in eq. (3.12) for $d \leq 2$ may not, therefore, be used at too low a temperature. In particular, eq. (3.12) does not allow one to draw conclusions about $\delta\sigma$ at $T = 0$ exactly. We should like to stress once more that eqs. (3.11) and (3.12) are based on the explicit consideration of backscattering effects, i.e. multiple scattering and the correlation of consecutive collisions. Hence, these equations cannot be obtained within the framework of the conventional Boltzmann transport theory.*

Finally, it should be pointed out that the results in eq. (3.12) have been derived with a tacit assumption: namely, that the path amplitudes A_1 and A_2 in fig. 6 are perfectly coherent ($A_1 = A_2$). So, we actually took for granted that particle states with momentum \mathbf{k} and $-\mathbf{k}$ are equivalent. Such a *time-reversal symmetry*

* It should be noted that this theory *can* nevertheless be generalized to include the coherent backscattering associated with weak localization (Hershfield and Ambegaokar 1986). In fact, a quantum-kinetic equation, which includes weak localization effects and thereby leads to such a generalized Boltzmann equation, has been derived by use of the Keldysh-technique (Rammer and Smith 1986).

of single particle states is valid only in the absence of external magnetic fields and only if the impurities are nonmagnetic. In the presence of a magnetic field H , time-reversal invariance no longer holds and the amplitudes for the two paths in fig. 6 acquire field-dependent phases of opposite signs:

$$A_1 \rightarrow A \exp(i\varphi), \quad A_2 \rightarrow A \exp(-i\varphi). \quad (3.13)$$

Here

$$\varphi = \frac{e}{\hbar c} \oint dl \cdot A \quad (3.14a)$$

$$= 2\pi \frac{\Phi}{hc/e} \quad (3.14b)$$

is determined by the contour integral over the vector potential A , i.e. by the magnetic flux $\Phi = HS$ through the area S of the closed loop. Since the motion of the particles is diffusive, S is given by $S = D_0 t$, so that $\Phi = HD_0 t$. The return probability W_H of a particle to its starting point in the presence of a magnetic field is again given by eq. (3.8). One therefore obtains

$$W_H = 2|A|^2 \left[1 + \cos\left(2\pi \frac{\Phi}{\Phi_0}\right) \right], \quad (3.15)$$

where $\Phi_0 = ch/2e$ is the well-known *flux quantum* in superconductivity. (Here the charge $2e$ enters, since – as in superconductivity – the interference involves two momentum states, \mathbf{k} and $-\mathbf{k}$, of the electron.) If $H = 0$, we find the earlier obtained result (see text preceding eq. (3.9)) $W_{H=0} = 4|A|^2$. The conductivity correction in the presence of a magnetic field, $\delta\sigma(H)$, is again determined by the return probability W_H . The total change in the conductivity due to a magnetic field, $\Delta\sigma(H) = \delta\sigma(H) - \delta\sigma(0)$, therefore depends on the probability difference $\Delta W = W_H - W_{H=0}$. Hence,

$$\Delta\sigma(H) \propto \int_{\tau}^{\tau_{in}} v_F \lambda_F^{d-1} \frac{dt}{(D_0 t)^{d/2}} [1 - \cos(2\pi\Phi/\Phi_0)] > 0, \quad (3.16)$$

which shows that $\Delta\sigma(H)$ is a function of the parameter $HD_0\tau_{in}/\Phi_0$. In particular, $\Delta\sigma$ is always positive, implying that $\Delta R < 0$; so, the *resistance decreases* with increasing magnetic field (*anomalous magnetoresistance*) (Hikami et al. 1980). The reason lies in the disturbance of the phase coherence by the magnetic field, which leads to a weakening of the localization effects. The “critical” field H_c , above which localization is suppressed, is determined by the relation $2\pi H_c D_0 \tau_{in}/\Phi_0 = 1$ and depends on τ_{in} , and hence also on temperature. For typical values of D_0 and τ_{in} realized in experiments, H_c is of the order of 100–500 G. This should be contrasted with the classical result $\Delta\sigma(H)/\sigma_0 \approx -(\omega_L \tau)^2$ (here ω_L is the Larmor frequency), which is not only many orders of magnitude smaller, but also has a different sign. We, thus, see that even weak magnetic fields have a drastic influence on localization, and may easily suppress it.

Based on this phase sensitivity, Altshuler et al. (1981) predicted a novel kind of quantum oscillation in the magnetoresistance of a multiply connected geometry, e.g. a torus made by wrapping up a thin, disordered metallic film. These oscillations with magnetic flux periodicity Φ_0 (rather than $2\Phi_0$, as known from the Aharonov–Bohm effect) have indeed been measured (Sharvin and Sharvin 1981). This phenomenon is reminiscent of Parks–Little oscillations in a superconducting geometry (Parks and Little 1964). A short discussion of oscillation effects with periodicity Φ_0 , as in networks, and periodicity $2\Phi_0$, as in mesoscopic rings, has been given by Vollhardt (1987); for a detailed account of these effects see Imry (1986) and the proceedings volume “Anderson Localization”, edited by Ando and Fukuyama (1988).

3.2. Systematic calculation of corrections to the Boltzmann conductivity

The arguments leading to eq. (3.12) already contain the essential physics. They enable us to understand the temperature dependence of $\delta\sigma$. On the other hand, the precise prefactors in eq. (3.11) can thereby not be determined. Furthermore, the perturbation theory cannot be extended beyond first order in λ . For this we need a systematic approach. Such a method must take into account that, in spite of all quantum-mechanical effects, the functional form of the results expressed in eq. (3.12) is due to diffusive behavior of particles. Their probability distribution $P(\mathbf{r}, t)$ [eq. (3.5)] is determined by the diffusion equation (3.4). Fourier-transforming eq. (3.4), or $P(\mathbf{r}, t)$, leads to $P(\mathbf{q}, \omega)$ given by

$$P(\mathbf{q}, \omega) \propto \frac{1}{-\mathrm{i}\omega + D_0 q^2}. \quad (3.17)$$

This is called a *diffusion pole*, because $P(\mathbf{q}, \omega)$ diverges for $|\mathbf{q}|, \omega \rightarrow 0$. Its origin is exclusively due to particle conservation during diffusion.

The knowledge of $P(\mathbf{r}, t)$ or of $P(\mathbf{q}, \omega)$ is not sufficient if we want to calculate a dynamical quantity like the conductivity σ or the diffusion coefficient D . For this, one needs a more general function, e.g. the so-called *density-density correlation function* $\chi(\mathbf{r}, t)$. It describes the dependence of a density distribution at one point in space and time on that at some other point in space and time. Its Fourier transform has the general structure (see, e.g. Forster 1975)

$$\chi(\mathbf{q}, \omega) = \frac{D(\mathbf{q}, \omega) q^2}{-\mathrm{i}\omega + D(\mathbf{q}, \omega) q^2} N_F, \quad (3.18)$$

implying that it also has a diffusion pole. Here $D(\mathbf{q}, \omega)$ is a \mathbf{q} - and ω -dependent, generalized diffusion coefficient. Once we know $\chi(\mathbf{q}, \omega)$, we obviously know $D(\mathbf{q}, \omega)$, too. The quantity $\chi(\mathbf{q}, \omega)$ is therefore of fundamental importance for a systematic calculation of corrections $\delta\sigma$ and δD (to σ_0 and D_0 , respectively) due to impurity scattering. $\chi(\mathbf{q}, \omega)$ can be calculated within a perturbation theory using a diagrammatic approach, which is described next.

4. Density response theory

We will now review the formulation of a microscopic theory for the density response function $\chi(\mathbf{q}, \omega)$ [eq. (3.18)] based on standard field-theoretic methods. This will yield an explicit expression for the *inverse* of the generalized diffusion coefficient $D(\mathbf{q}, \omega)$ in terms of the irreducible vertex function of the two-particle Green's function. Clearly, a diagrammatic evaluation of such an expression cannot in general be performed exactly, but has to employ approximations. At this point, it is important to bear in mind that in the Anderson localization problem one is particularly interested in the behavior of σ or D near the localization transition, where both quantities vanish. If the conductivity σ was calculated directly from, say, the standard Kubo formula (see, e.g. Rickayzen 1980), this would require a perturbational calculation to (infinitely) high orders in the disorder parameter which ultimately would have to yield $\sigma = 0$ at the transition. This is clearly an impossible task! In this situation it is much more useful to calculate $1/\sigma$ (or $1/D$) as described next, since this quantity (i.e. the resistivity) *diverges* as the transition is approached. Approximations for calculating $1/D$ must then search for the *largest* contributions in some (diagrammatic) expansion, which should be a much more tractable problem.

Let us first formulate the one-particle problem defined by the disorder Hamiltonian (eq. (2.7)) at $T = 0$ (see, e.g. Abrikosov et al. 1963). The one-particle Green's function is given by

$$G(\mathbf{r}, \mathbf{r}'; t - t') = -i\langle \phi_0 | T[\psi(\mathbf{r}, t)\psi^+(\mathbf{r}', t')] | \phi_0 \rangle, \quad (4.1)$$

where $|\phi_0\rangle$ is the ground state of the disordered system. The Fourier transform of eq. (4.1) then takes the form

$$G(\mathbf{k}, \mathbf{k}'; \omega) = \sum_n \varphi_n(\mathbf{k}) \varphi_n^*(\mathbf{k}') \left[\frac{1 - f(\varepsilon_n)}{\omega - \varepsilon_n + i\eta} + \frac{f(\varepsilon_n)}{\omega - \varepsilon_n - i\eta} \right], \quad (4.2)$$

where $\varphi_n(\mathbf{k})$ are the eigenstates of H with energy ε_n , $f(\varepsilon_n)$ is the Fermi function and η is a positive infinitesimal, and we have set $\hbar = 1$. Furthermore,

$$G^{R,A}(\mathbf{k}, \mathbf{k}'; \omega) = \sum_n \frac{\varphi_n(\mathbf{k}) \varphi_n^*(\mathbf{k}')}{\omega - \varepsilon_n \pm i\eta} \quad (4.3)$$

are the associated retarded and advanced Green's functions, respectively. In the case of free electrons without disorder, the one-particle Green's function is given by

$$G^0(\mathbf{k}, \mathbf{k}'; \omega) = \frac{\delta(\mathbf{k} - \mathbf{k}')}{\omega - k^2/2m + i\eta \operatorname{sgn}(k - k_F)}. \quad (4.4)$$

Next, the relevant two-particle quantities for the disorder problem defined by eq. (2.7) are introduced by considering the density response function

$$\chi(\mathbf{r}, \mathbf{r}'; \omega) = i \int_0^\infty dt \exp[i(\omega + i\eta)t] \langle \phi_0 | [\rho(\mathbf{r}, t), \rho(\mathbf{r}', 0)]_- | \phi_0 \rangle \quad (4.5a)$$

$$= \sum_{n, n'} \varphi_n^*(\mathbf{r}) \varphi_{n'}(\mathbf{r}) \varphi_n^*(\mathbf{r}') \varphi_n(\mathbf{r}') \frac{f(\varepsilon_{n'}) - f(\varepsilon_n)}{\omega + \varepsilon_n - \varepsilon_{n'} + i\eta}, \quad (4.5b)$$

where the density operator is given by

$$\rho(\mathbf{r}, t) = \psi^+(\mathbf{r}, t) \psi(\mathbf{r}, t) \quad (4.6a)$$

$$= \sum_{n, n'} \varphi_n^*(\mathbf{r}) \varphi_{n'}(\mathbf{r}) a_n^+ a_{n'}^- . \quad (4.6b)$$

Here a_n^+ creates a particle in an eigenstate of H with energy ε_n , and ψ^+, a_n^+ etc. are Heisenberg operators. The randomness of the distribution of impurities allows one to average over their spatial position in the usual way (Abrikosov et al. 1963); averages are indicated by a pair of angle brackets $\langle \rangle$. The average of the density response function (eq. (4.5b)), $\langle \chi(\mathbf{r}, \mathbf{r}'; \omega) \rangle \equiv \chi(\mathbf{r} - \mathbf{r}', \omega)$, may now be Fourier transformed to yield

$$\chi(\mathbf{q}, \omega) = \sum_{\mathbf{k}, \mathbf{k}'} \sum_{n, n'} \langle \varphi_{n'}(\mathbf{k}_+) \varphi_n^*(\mathbf{k}'_+) \varphi_n(\mathbf{k}'_-) \varphi_n^*(\mathbf{k}_-) \rangle \frac{f(\varepsilon_{n'}) - f(\varepsilon_n)}{\omega + \varepsilon_n - \varepsilon_{n'} + i\eta} \quad (4.7a)$$

$$= \frac{1}{2\pi i} \int_{-\infty}^{\infty} dE \{ [f(E + \omega) - f(E)] \Phi^{RA}(E, \omega; \mathbf{q}) + f(E) \Phi^{RR}(E, \omega; \mathbf{q}) \\ - f(E + \omega) \Phi^{AA}(E, \omega; \mathbf{q}) \}, \quad (4.7b)$$

where $\mathbf{k}_\pm = \mathbf{k} \pm \mathbf{q}/2$. Here we have introduced the abbreviation

$$\Phi^{RA}(E, \omega; \mathbf{q}) \equiv \sum_{\mathbf{k}, \mathbf{k}'} \langle G^R(\mathbf{k}_+, \mathbf{k}'_+; E + \omega) G^A(\mathbf{k}'_-, \mathbf{k}_-; E) \rangle, \quad (4.8)$$

with Φ^{RR} , Φ^{AA} given by analogous expressions.* In particular, at $T = 0$ and in the limit of small ω and $|\mathbf{q}|$, eq. (4.7b) reduces to (Maleev and Toperberg 1975)

$$\chi(\mathbf{q}, \omega) = -\frac{1}{2\pi i} \omega \Phi^{RA}(E_F, \omega; \mathbf{q}) + \chi_0 + O(\omega, q^2), \quad (4.9)$$

where $\chi_0 = N_F$ is the isothermal compressibility. Furthermore, we introduce the two-particle quantity $\Phi_{kk'}(\mathbf{q}, \omega)$:

$$\Phi_{kk'}(\mathbf{q}, \omega) \equiv \langle G^R(\mathbf{k}_+, \mathbf{k}'_+; E_F + \omega) G^A(\mathbf{k}'_-, \mathbf{k}_-; E_F) \rangle, \quad (4.10)$$

so that

$$\sum_{\mathbf{k}\mathbf{k}'} \Phi_{kk'}(\mathbf{q}, \omega) = \Phi^{RA}(E_F, \omega; \mathbf{q}) \quad (4.11a)$$

$$\equiv \Phi(\mathbf{q}, \omega). \quad (4.11b)$$

* Note that, in the original papers by Vollhardt and Wölfle (1980a, b) and Wölfle and Vollhardt (1982), the average Φ^{RA} was introduced as $\Phi^{RA} = -2\pi i \phi^{RA}$.

Comparing eq. (4.9) with the general structure of $\chi(\mathbf{q}, \omega)$ [eq. (3.18)] for $q \rightarrow 0$, we find

$$\Phi(\mathbf{q}, \omega) = \frac{2\pi N_F}{-\text{i}\omega + D(\mathbf{q}, \omega)q^2}, \quad (4.11c)$$

i.e. $\Phi(\mathbf{q}, \omega)$ itself has a diffusion pole.

We now have to introduce the effect of the disorder, i.e. of the random impurities, on the electrons. This is done within standard renormalized perturbation theory for $\Phi_{kk'}$ (eq. (4.10)) making use of skeleton diagrams (Abrikosov et al. 1963); hence, in the diagrams for two-point and four-point functions self-energy insertions do not appear. The exact averaged single-particle Green's functions $G_k^{R,A}$ are then given by

$$G_k^R(E) = \frac{1}{E - k^2/2m - \Sigma_k^R(E)} \quad (4.12)$$

and $G^A = (G^R)^*$, where $\Sigma_k^R(E)$ is the self-energy. Typical diagrams contributing to $\Sigma_k^R(E_F + \omega)$ are shown in fig. 8, where a solid line represents G^R (directed to the right); the representation of Σ_k^A is analogous, with G^A going from right to left. Here the dashed lines with a cross indicate electron-impurity scatterings, each being associated with a factor

$$U_0(\mathbf{k} - \mathbf{k}') = n_{\text{imp}} |V_{\mathbf{k}-\mathbf{k}'}|^2, \quad (4.13)$$

where n_{imp} is the density of impurities and $V_{\mathbf{k}}$ is given by eq. (2.8).

The impurity average over $G^R G^A$ may now be expressed as

$$\Phi_{kk'}(\mathbf{q}, \omega) = G_{k+}^R G_{k-}^A \delta(\mathbf{k} - \mathbf{k}') + G_{k+}^R G_{k-}^A \Gamma_{kk'}(\mathbf{q}, \omega) G_{k+}^R G_{k-}^A, \quad (4.14)$$

where $\Gamma_{kk'}(\mathbf{q}, \omega)$ is the vertex function. A diagrammatic representation of eq. (4.14) is shown in fig. 9. Since $\Gamma_{kk'}(\mathbf{q}, \omega)$ contains both reducible and irreducible diagrams, it is convenient to introduce a completely *irreducible* vertex function $U_{kk'}(\mathbf{q}, \omega)$, in terms of which $\Gamma_{kk'}$ is expressible as

$$\Gamma_{kk'} = U_{kk'} + \sum_{k''} U_{kk''} G_{k+}^R G_{k''-}^A \Gamma_{k''k'} \cdot \quad (4.15)$$

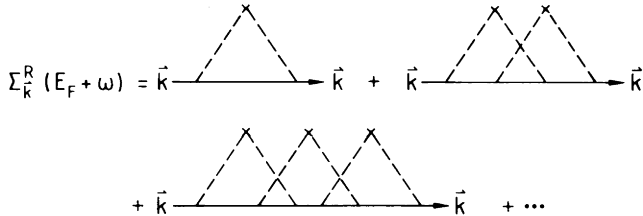


Fig. 8. Typical diagrams contributing to the self-energy $\Sigma_k^R(E_F + \omega)$ entering the averaged single-particle Green's function $G_k^R(E + \omega)$.

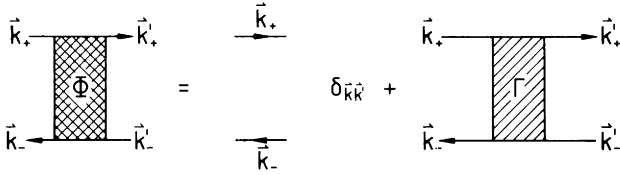


Fig. 9. Diagrammatic representation of the two-particle quantity $\Phi_{kk'}(\mathbf{q}, \omega)$ [eq. (4.10)] in terms of the vertex function $\Gamma_{kk'}(\mathbf{q}, \omega)$.

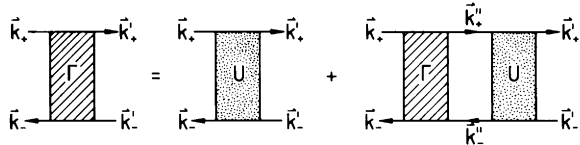


Fig. 10. Diagrammatic representation of $\Gamma_{kk'}(\mathbf{q}, \omega)$ in terms of the irreducible vertex function $U_{kk'}(\mathbf{q}, \omega)$.

This is diagrammatically represented in fig. 10. Typical diagrammatic contributions to $U_{kk'}$ are shown in fig. 11.

As discussed earlier, in the absence of a magnetic field or magnetic impurities one has time-reversal invariance, i.e. single-particle states \mathbf{k} and $-\mathbf{k}$ are equivalent. This important symmetry must also be present in the full vertex function $\Gamma_{kk'}$ and, indeed, is expressed by the relation

$$\Gamma_{kk'}(\mathbf{q}, \omega) = \Gamma_{(k - k' + \mathbf{q})/2, (k' - k + \mathbf{q})/2}(\mathbf{k} + \mathbf{k}', \omega). \quad (4.16a)$$

The validity of eq. (4.16a) is easily verified diagrammatically, as shown in fig. 12a-d. The vertex function in 12a is contorted by turning over its lower part (see 12b). Since Γ is the *full* vertex function, i.e. contains *all* diagrams, such a contortion of its diagrams leaves Γ unchanged (see 12c). Making use of time-reversal invariance by reversing the directions of, say, the arrows at the bottom of the diagram, one is led to 12d. Comparison of 12a and 12d verifies eq. (4.16a). Note that eq. (4.16a) also holds for $\Phi_{kk'}$. Time-reversal invariance obviously relates a set of diagrams, denoted by P , with the set \bar{P} composed of the contorted

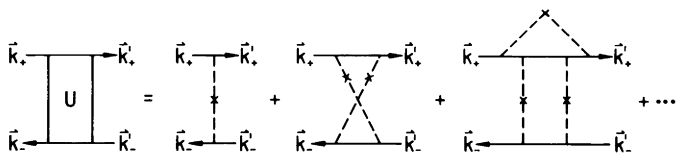


Fig. 11. Typical diagrams contributing to the irreducible vertex function $U_{kk'}(\mathbf{q}, \omega)$.

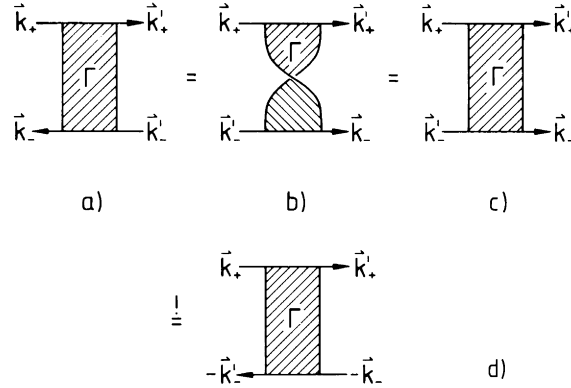


Fig. 12. Diagrammatic representation of the symmetry of the vertex function $\Gamma_{kk'}(\mathbf{q}, \omega)$ in the case of time-reversal invariance.

images of these diagrams, i.e. those obtained by twisting the hole-line as indicated in fig. 12b. This leads to the useful relation

$$\bar{P}_{kk'}(\mathbf{q}, \omega) = P_{(\mathbf{k} - \mathbf{k}' + \mathbf{q})/2, (\mathbf{k}' - \mathbf{k} + \mathbf{q})/2}(\mathbf{k} + \mathbf{k}', \omega). \quad (4.16b)$$

In general, $\bar{P}_{kk'}(\mathbf{q}, \omega) \neq P_{kk'}(\mathbf{q}, \omega)$, since P is only a subclass of the full vertex function Γ . Only in the case of Γ itself does one have $\Gamma_{kk'}(\mathbf{q}, \omega) = \bar{\Gamma}_{kk'}(\mathbf{q}, \omega)$, which therefore leads to the general relation (4.16a).

The irreducible vertex $U_{kk'}$ may be used to set up a Bethe-Salpeter equation for the response function $\Phi_{kk'}$:

$$\Phi_{kk'}(\mathbf{q}, \omega) = G_{\mathbf{k}_+}^R G_{\mathbf{k}_-}^A \delta(\mathbf{k} - \mathbf{k}') + G_{\mathbf{k}_+}^R G_{\mathbf{k}_-}^A \sum_{\mathbf{k}''} U_{kk''}(\mathbf{q}, \omega) \Phi_{k''k'}(\mathbf{q}, \omega), \quad (4.17)$$

which is shown diagrammatically in fig. 13. We now rewrite eq. (4.17) as a kinetic equation. Employing the definition of G^R , G^A (eq. (4.12)), we rewrite $G^R G^A$ as

$$G_{\mathbf{k}_+}^R G_{\mathbf{k}_-}^A = -\frac{\Delta G_{\mathbf{k}}}{\omega - (\mathbf{k} \cdot \mathbf{q})/m - \Delta \Sigma_{\mathbf{k}}}, \quad (4.18)$$

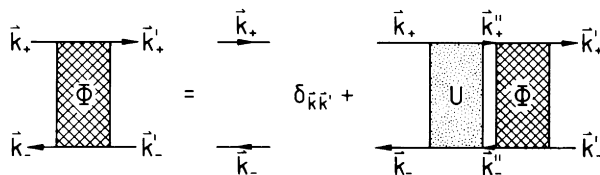


Fig. 13. Bethe-Salpeter equation for $\Phi_{kk'}(\mathbf{q}, \omega)$ in terms of $U_{kk}(\mathbf{q}, \omega)$.

where

$$\Delta G_k \equiv G_{k+}^R - G_{k-}^A, \quad (4.19a)$$

$$\Delta \Sigma_k = \Sigma_{k+}^R(E_F + \omega) - \Sigma_{k-}^A(E_F). \quad (4.19b)$$

Multiplication of eq. (4.17) by the denominator of eq. (4.18) yields the fundamental relation

$$\left(\omega - \frac{\mathbf{k} \cdot \mathbf{q}}{m} - \Delta \Sigma_k \right) \Phi_{kk'} = - \Delta G_k \left[\delta(\mathbf{k} - \mathbf{k}') + \sum_{k''} U_{kk''} \Phi_{k''k'} \right]. \quad (4.20)$$

Summing eq. (4.20) over k, k' , we obtain

$$\omega \Phi(\mathbf{q}, \omega) - q \Phi_j(\mathbf{q}, \omega) = 2\pi i N(E_F), \quad (4.21)$$

where we have introduced

$$\Phi_j(\mathbf{q}, \omega) \equiv \sum_{k,k'} \left(\frac{\mathbf{k} \cdot \hat{\mathbf{q}}}{m} \right) \Phi_{kk'}(\mathbf{q}, \omega), \quad (4.22a)$$

which is essentially the first moment of $\Phi_{kk'}$. Using eq. (4.11c), it follows that

$$\Phi_j(\mathbf{q}, \omega) = 2\pi N_F \frac{q D(\mathbf{q}, \omega)}{-i\omega + D(\mathbf{q}, \omega)q^2}. \quad (4.22b)$$

In deriving eq. (4.21) we made use of the Ward identity

$$\Delta \Sigma_k = \sum_{k'} U_{kk'} \Delta G_{k'}, \quad (4.23)$$

which has been proved earlier (Vollhardt and Wölfle 1980b). This identity expresses the fact that the irreducible vertex $U_{kk'}$ may be systematically generated from the skeleton self-energy Σ_k^R by differentiating Σ_k^R with respect to G_k^R (“cutting Green’s function lines”).

Relation (4.21) is equivalent to the continuity equation. For $q \rightarrow 0$ it reduces to eq. (4.9) since $\chi(0, \omega) = 0$, showing that $\Phi(0, \omega)$ diverges as $1/\omega$ for $\omega \rightarrow 0$. The quantities $\Phi(\mathbf{q}, \omega)$ and $\Phi_j(\mathbf{q}, \omega)$ describe, respectively, the relaxation of the mass density and the mass current of electrons due to scattering from the impurities, and are therefore referred to as density relaxation function (Φ) and current relaxation function (Φ_j), respectively.

The kinetic equation (4.20) for the disordered system, and hence also eq. (4.21), is exact for $T = 0$, and small q and ω . No approximations have so far been introduced (except perhaps for the underlying assumption that the Anderson localization problem may at all be approached by a perturbation theory in the disorder). However, in order to proceed further, e.g. to be able to derive an equation for Φ_j to close the system of equations, we will have to make certain assumptions. First of all we make use of the peculiar fact that in Anderson localization *single-particle* quantities (e.g. the density of states) are *smoothly*

varying functions of disorder (Wegner 1979). Hence, as one goes beyond small impurity concentrations (and even across the localization transition itself, if there is one) such quantities may be expected to remain essentially unchanged. Therefore, it is reasonable to approximate the self-energy Σ in the single-particle Green's function by the lowest-order result in the impurity scattering, $U_0(\mathbf{k} - \mathbf{k}')$, i.e. by the Born approximation. A more quantitative approximation, the so-called single-site approximation or CPA, will be discussed in section 10. Within the simplest approximation, given by the first diagram in fig. 8, one finds

$$\gamma \equiv \text{Im } \Sigma_{k_F}^A(E_F) \quad (4.24a)$$

$$\approx \pi N(E_F) \int \frac{d\Omega_{k'}}{4\pi} U_0(k_F(\hat{\mathbf{k}} - \hat{\mathbf{k}}')) \quad (4.24b)$$

in dimensions $d = 3$. Since we assume the scatterers to be point-like ($V_{\mathbf{k}} = V$), we have

$$\gamma = \pi N_F n_{\text{imp}} V^2 \quad (4.25a)$$

$$= \pi N_F U_0. \quad (4.25b)$$

In particular, using the familiar result from weak-coupling transport theory for the elastic scattering rate:

$$\frac{1}{\tau} = 2\gamma - 2\pi n_{\text{imp}} \sum_{\mathbf{k}'} \delta\left(E_F - \frac{\mathbf{k}'^2}{2m}\right) |V_{\mathbf{k}-\mathbf{k}'}|^2 (\hat{\mathbf{k}} \cdot \hat{\mathbf{k}}'), \quad (4.26)$$

and observing that the last term in eq. (4.26) vanishes for isotropic scattering, we see that in this case $\gamma = 1/2\tau$. For the small impurity concentrations (n_{imp}) assumed here, one has $\gamma/E_F \ll 1$. In fact, $\gamma/E_F = \pi\lambda$, where λ is the small disorder parameter introduced in eq. (3.1). As a consequence of the discussion preceding eq. (4.24), the single-particle Green's functions will be used in the form

$$G_{\mathbf{k}}^R(E) = \frac{1}{E - k^2/2m + i/2\tau}, \quad (4.27)$$

and $G^A = (G^R)^*$. This will suffice for calculating the critical (i.e. singular) behavior of two-particle properties (as e.g. the density correlation function) with respect to ω .

The form of G^R in eq. (4.27) is now employed for expanding $\Phi_{kk'}$ in angular variables. This will lead to an equation for Φ_j . Noting that $\text{Im } G_{\mathbf{k}} \propto \Delta G_{\mathbf{k}}$ [eq. (4.19a)] is strongly peaked at $k = k_F$, with width γ and height γ^{-1} , the dependence of $\Phi_{kk'}$ (and hence of $\sum_{k'} \Phi_{kk'}$) on the magnitude of the wave vectors will be dominated by this structure of $\Delta G_{\mathbf{k}}$. The remaining angular dependence is extracted using a Legendre expansion, which is terminated after the $l = 1$ term. Hence we write

$$\sum_{\mathbf{k}'} \Phi_{kk'} \approx \frac{\Delta G_k}{-2\pi i N_F} \sum_{\mathbf{k}''\mathbf{k}'} \left[1 + \frac{d}{k_F^2} (\mathbf{k} \cdot \hat{\mathbf{q}})(\mathbf{k}'' \cdot \hat{\mathbf{q}}) \right] \Phi_{k''k'}. \quad (4.28)$$

Clearly, eq. (4.11b) for Φ and eq. (4.21) for Φ_j follow immediately from this. Multiplying eq. (4.22) with $(\mathbf{k} \cdot \hat{\mathbf{q}})\tau/im$ and summing over \mathbf{k}, \mathbf{k}' then yields a second equation; this time for the current relaxation function Φ_j :

$$K(\mathbf{q}, \omega)\Phi_j(\mathbf{q}, \omega) + iqD_0\Phi(\mathbf{q}, \omega) = 0, \quad (4.29)$$

where D_0 is the d -dimensional diffusion constant, and where we have neglected a term of $O(\omega\tau) \ll 1$. In eq. (4.29) we have introduced the dimensionless *current relaxation kernel*

$$\begin{aligned} K(\mathbf{q}, \omega) = 1 &+ \frac{\tau}{\pi mn} \sum_{\mathbf{k}\mathbf{k}'} (\mathbf{k} \cdot \hat{\mathbf{q}}) \Delta G_{\mathbf{k}} [U_{\mathbf{k}\mathbf{k}'}(\mathbf{q}, \omega) \\ &- U_0(\mathbf{k} - \mathbf{k}')] \Delta G_{\mathbf{k}'}(\mathbf{k}' \cdot \hat{\mathbf{q}}), \end{aligned} \quad (4.30)$$

which is explicitly given by the irreducible vertex $U_{\mathbf{k}\mathbf{k}'}$. (Note that in eq. (4.30) we subtracted $U_0(\mathbf{k} - \mathbf{k}')$, the lowest-order contribution to $U_{\mathbf{k}\mathbf{k}'}$ (the first diagram in fig. 11), from $U_{\mathbf{k}\mathbf{k}'}$, since the former term has already been included and gives the first term in eq. (4.30), i.e. unity. Hence, in lowest-order perturbation theory $K(\mathbf{q}, \omega) = 1$.)

Equations (4.21) and (4.29) form a closed set for Φ and Φ_j . With eq. (4.11b) the density response function $\chi(\mathbf{q}, \omega)$ is easily found from eq. (4.1). Comparison with the general form, eq. (3.18), yields the generalized diffusion coefficient $D(\mathbf{q}, \omega)$:

$$D(\mathbf{q}, \omega) = \frac{D_0}{K(\mathbf{q}, \omega)}. \quad (4.31)$$

Hence, the current relaxation function $K(\mathbf{q}, \omega)$ is simply the *inverse* of the generalized diffusion coefficient, normalized by the weak-coupling diffusion constant D_0 , i.e. is something like a generalized resistivity $\rho(\mathbf{q}, \omega)/\rho_0$, where $\rho_0 = 1/\sigma_0$. Therefore, as the localization transition is approached ($D \rightarrow 0$), K will *diverge*. The divergent behavior is obtained by considering the dynamical conductivity $\sigma(\omega)$ and the electrical polarizability $\alpha(\omega)$, which are found from $\chi(\mathbf{q}, \omega)$ as

$$\sigma(\omega) = -i\omega\alpha(\omega) \quad (4.32a)$$

$$= e^2 \lim_{\mathbf{q} \rightarrow 0} \frac{-i\omega}{\mathbf{q}^2} \chi(\mathbf{q}, \omega). \quad (4.32b)$$

In what follows, we are mainly interested in the $\mathbf{q} = 0$ limit of $K(\mathbf{q}, \omega)$, i.e. of $D(\mathbf{q}, \omega)$ and $\sigma(\mathbf{q}, \omega)$. In this case we set

$$K(\omega) \equiv K(0, \omega), \quad D(\omega) \equiv D(0, \omega), \quad \sigma(\omega) \equiv \sigma(0, \omega), \quad (4.33a)$$

$$K(\omega) = \frac{\sigma_0}{\sigma(\omega)} = \frac{D_0}{D(\omega)}. \quad (4.33b)$$

In the conducting regime at weak coupling ($\gamma/E_F \ll 1$), $\sigma(0)$ is given by the

Boltzmann conductivity σ_0 [eq. (2.11)] and the polarizability diverges as $\alpha(\omega) \rightarrow \sigma_0/(-i\omega)$. By contrast, on the insulating side where $\sigma(0) = 0$, the polarizability $\alpha(0)$ is finite, i.e. there is a finite restoring force against unlimited polarization of the medium. In this case $\alpha(0) = \sigma_0/\omega_0^2\tau$, where ω_0 is some “oscillator frequency”. Therefore, for an insulator $K(\omega)$ diverges in the limit $\omega \rightarrow 0$:

$$\begin{aligned} \lim_{\omega \rightarrow 0} K(\omega) &= 1, && \text{for a conductor,} \\ &= 1 + \frac{i\omega_0^2\tau}{\omega}, && \text{for an insulator.} \end{aligned} \quad (4.34a)$$

The same result may be obtained by a simple hydrodynamic model of a fluid in which the random scatterers introduce effective macroscopic forces (Vollhardt and Wölfle 1980a, b). For $\omega \rightarrow 0$ eq. (4.34a) implies

$$\operatorname{Re} \sigma(\omega) = \sigma_0 \frac{(\omega\tau)^2}{(\omega_0\tau)^4 + (\omega\tau)^2}, \quad (4.34b)$$

$$\operatorname{Im} \sigma(\omega) = -\sigma_0 \frac{\omega\tau(\omega_0\tau)^2}{(\omega_0\tau)^4 + (\omega\tau)^2}. \quad (4.34c)$$

For a conductor ($\omega_0 = 0$) one finds $\operatorname{Re} \sigma(0) = \sigma_0$, $\operatorname{Im} \sigma(0) = 0$, and for an insulator ($\omega_0 > 0$) $\operatorname{Re} \sigma(\omega) \propto \omega^2$, $\operatorname{Im} \sigma(\omega) \propto -\omega$.

Clearly, the characteristic feature of localization is the behavior $D(\omega) \propto \sigma(\omega) \propto -i\omega$, i.e. is indicated by the *divergence* of $D_0/D = K \propto 1/\omega$ at small ω (infrared divergence) – a result which is independent of the spatial dimension of the system. This divergent contribution must originate from the second term in eq. (4.30), which is due to the irreducible vertex $U_{kk'}$. Since we are interested in divergent contributions to K , the factors ΔG_k in eq. (4.30) may be written in a convenient form as $\Delta G_k \approx -(i/\tau)G_{k+}^R G_{k-}^A$, i.e the term $\omega - \mathbf{k} \cdot \hat{\mathbf{q}}/m$ can be neglected in comparison with $1/\tau$. Equation (4.30) then takes the form

$$\frac{D_0}{D(\mathbf{q}, \omega)} = 1 - \lambda \frac{2E_F}{mn} \sum_{\mathbf{k}, \mathbf{k}'} (\mathbf{k} \cdot \hat{\mathbf{q}}) G_{k+}^R G_{k-}^A [U_{kk'}(\mathbf{q}, \omega) - U_0] G_{k+}^R G_{k-}^A (\mathbf{k}' \cdot \hat{\mathbf{q}}). \quad (4.35)$$

Note that the form of eq. (4.35) is very similar to that of the usual Kubo formula for the conductivity σ (or D) itself (see, e.g. Rickayzen 1980) except for the term $U_{kk'}$ in place of the full vertex $\Gamma_{kk'}$. We now discuss the origin of divergent contributions to $U_{kk'}$.

4.1. Infrared divergences of the irreducible vertex

In the Anderson localization problem, where noninteracting electrons are scattered by random impurity potentials, divergent contributions to the full vertex function $\Gamma_{kk'}(\mathbf{q}, \omega)$ are easily obtained even in perturbation theory. This is due to the fact that in this model the particle number is the only conserved

quantity, so that the quantity describing the relaxation of the density, $\Phi(\mathbf{q}, \omega)$, has a diffusion pole [see eq. (4.11c)] which is divergent in the limit $\omega, q \rightarrow 0$.

The diffusion pole in eqs. (3.18) or (4.11c) contains the full diffusion coefficient $D(\mathbf{q}, \omega)$. In the metallic regime at weak coupling, where $\gamma/E_F \ll 1$, the diffusion coefficient $D(\mathbf{q}, \omega)$ reduces to the simple diffusion constant D_0 . This is also precisely the result of lowest-order perturbation theory for $\Phi(\mathbf{q}, \omega)$ and may be obtained immediately from eqs. (4.21) and (4.29) for Φ and Φ_j containing the relaxation kernel K ; in this theory the irreducible vertex $U_{kk'}$ is given by $U_0(\mathbf{k} - \mathbf{k}')$, i.e. the first diagram in fig. 11, so that $K(\mathbf{q}, \omega) = 1$. From eq. (4.31) we then see that in this limit $D(\mathbf{q}, \omega) = D_0$.

The full vertex function $\Gamma_{kk'}$ is obtained by iterating $U_{kk'}$ (eq. (4.15)). Hence, approximating $U_{kk'}$ by the lowest-order contribution $U_0(\mathbf{k} - \mathbf{k}')$ corresponds to approximating $\Gamma_{kk'}$ by a particle-hole ladder $\Gamma_{kk'}^0$ shown in fig. 14. This contribution is immediately obtained as

$$\Gamma_{kk'}^0(\mathbf{q}, \omega) = \frac{U_0}{1 - U_0 \sum_{\mathbf{k}''} G_{\mathbf{k}_+}^R G_{\mathbf{k}_-}^A}. \quad (4.36)$$

For small q, ω we have

$$\sum_{\mathbf{k}} G_{\mathbf{k}_+}^R G_{\mathbf{k}_-}^A = \frac{\pi N_F}{\gamma} - \frac{\pi N_F}{2\gamma^2} (-i\omega + D_0 q^2), \quad (4.37)$$

so that, with eq. (4.25b),

$$\Gamma_{kk'}^0(\mathbf{q}, \omega) = \lambda \frac{2\pi E_F U_0}{-i\omega + D_0 q^2}. \quad (4.38)$$

The particle-hole ladder is seen to give rise to a diffusion pole, which in principle may lead to a divergence for $\omega, q \rightarrow 0$. Therefore, $\Gamma_{kk'}^0$ (which, in fact, is *independent* of \mathbf{k} and \mathbf{k}') is referred to as *bare diffusion propagator* or *diffuson*.

Since Γ^0 is explicitly particle-hole-reducible, it does not contribute to $U_{kk'}$ and thus also not to $K(\mathbf{q}, \omega)$. One might think that a single particle-hole ladder could, nevertheless, contribute to $K(\mathbf{q}, \omega)$ if it was made irreducible by including vertex corrections across the ladder. However, one can prove that even in the presence of arbitrary vertex corrections the bare diffusion propagator Γ^0 does not give rise to a divergent contribution to $K(\mathbf{q}, \omega)$, since the diffusion pole exactly cancels once all vertex corrections are included (Vollhardt and Wölfle 1980b).

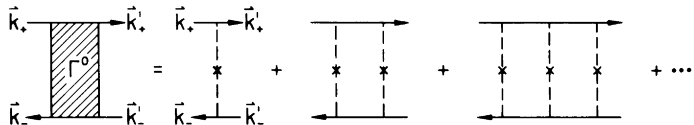


Fig. 14. Particle-hole ladder $\Gamma_{kk'}^0(\mathbf{q}, \omega)$ (“diffuson”).

Besides the particle-hole diffusion propagator, which is merely a consequence of particle conservation and thus also occurs for scattering of classical particles, there exists another divergent diagrammatic contribution (the particle-particle ladder shown at the top of fig. 15) in perturbation theory, which is of exclusively quantum-mechanical nature, and which is only present in the case of time-reversal invariance. The contribution of this type of scattering to the localization problem was first discussed by Abrahams et al. (1979) in their fundamental paper on the absence of diffusion in two-dimensional systems, as well as by Gorkov et al. (1979). The sum of the particle-particle ladder, $\Lambda_{kk'}^0(\mathbf{q}, \omega)$, is easily obtained, as shown in fig. 15. In the case of time-reversal invariance this sum is seen to be given by the twisted bare diffusion propagator Γ^0 in the particle-hole channel (see eq. (4.16)):

$$\Lambda_{kk'}^0(\mathbf{q}, \omega) = \bar{\Gamma}_{kk'}^0(\mathbf{q}, \omega) \quad (4.39a)$$

$$= \Gamma_{(k - k' + q)/2, (k' - k + q)/2}^0(\mathbf{k} + \mathbf{k}', \omega) \quad (4.39b)$$

$$= \lambda \frac{2\pi E_F U_0}{-i\omega + D_0(\mathbf{k} + \mathbf{k}')^2}. \quad (4.40)$$

The bare particle-particle propagator Λ^0 is seen to be singular for $\omega = 0$ and $\mathbf{k} + \mathbf{k}' = 0$, i.e. if the total momentum of the two particles vanishes. This singularity is called a *Cooper-pole* or *Cooperon*, since it resembles the pair correlation of two electrons in a Cooper pair. The condition $\mathbf{k}' = -\mathbf{k}$ implies *backscattering* of particles, whereby the momentum changes by $2k_F$; hence the pole in eq. (4.39) is also referred to as a “ $2k_F$ -pole”. Diagrammatically, this kind of scattering is seen to be represented by the sum of *maximally crossed* diagrams in the particle-hole channel (fig. 15), discussed earlier in a different context by Langer and Neal (1966); see also the intuitive discussion by Bergmann (1983, 1984). Each of these diagrams describes the backscattering of a particle in the course of independent scattering events, leading to the subtle interference of the electron waves on time-reversed paths. This scattering process is exactly the

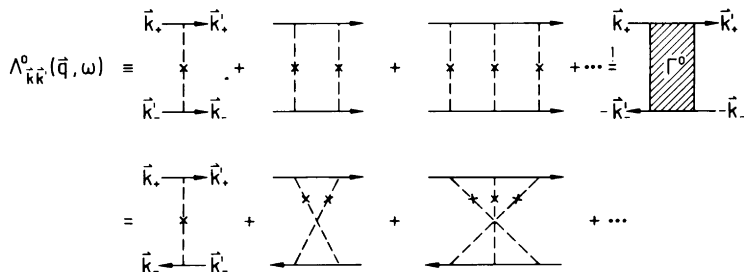


Fig. 15. Particle-particle ladder $\Lambda_{kk'}^0(\mathbf{q}, \omega)$ (“Cooperon”) and its transformation into *maximally crossed diagrams* in the case of time-reversal invariance.

same as that explained in detail in section 4 by means of Feynman paths in a random medium, i.e. by an argument in position space.

The maximally crossed diagrams are particle-hole-irreducible and are therefore part of the irreducible vertex $U_{kk'}$. Their contribution to the current relaxation kernel, $K(\omega) = D_0/D(\omega)$, is found by inserting eq. (4.40), with $Q = \mathbf{k} + \mathbf{k}'$, into eq. (4.35) with $\mathbf{q} = 0$:

$$\frac{D_0}{D(\omega)} = 1 + \frac{1}{\pi N_F} \sum_Q \frac{1}{-i\omega + D_0 Q^2} \quad (4.41)$$

$$= 1 + \lambda d k_F^{2-d} \int_0^{1/l} dQ \frac{Q^{d-1}}{-i\omega/D_0 + Q^2}. \quad (4.42)$$

The integration in eq. (4.42) is restricted to momenta smaller than the inverse mean free path $1/l$ (hydrodynamic regime), where the diffusion pole has its familiar form. The correction to $D_0/D(\omega)$ obtained from the $2k_F$ -backscattering mechanism is indeed seen to be linear in the small disorder parameter λ (eq. (3.1)), i.e. it yields the lowest-order correction to D_0 . Nevertheless, for $\omega \rightarrow 0$ this correction is seen to *diverge* in dimensions $d \leq 2$:

$$\frac{D_0}{D(\omega)} - 1 \propto \lambda \times \begin{cases} \frac{1}{\sqrt{\omega\tau}}, & d = 1, \\ \ln \frac{1}{\omega\tau}, & d = 2. \end{cases} \quad (4.43)$$

Hence, for perturbation theory to remain valid for $d \leq 2$ the frequency must not be too small ($\omega\tau \gtrsim 1$); in that case the limit $\omega \rightarrow 0$ for $D(\omega)$ cannot be obtained from eqs. (4.42) and (4.43).

Since the second term on the right-hand side of eq. (4.42) is small, and since $D(\omega)/D_0 = \sigma(\omega)/\sigma_0$, the correction $\delta\sigma(\omega) = \sigma(\omega) - \sigma_0$ is obtained from eq. (4.42):

$$\frac{\delta\sigma(\omega)}{\sigma_0} = -\lambda d k_F^{2-d} \int_0^{1/l} dQ \frac{Q^{d-1}}{-i\omega/D_0 + Q^2}. \quad (4.44)$$

This result is valid at $T = 0$ in an infinitely large system. In particular, for $d = 2$ one finds the frequency-dependent correction

$$\frac{\delta\sigma(\omega)}{\sigma_0} = -\lambda \ln \frac{1}{\omega\tau}, \quad (4.45a)$$

which implies the *universal* correction (Abrahams et al. 1979, Gorkov et al. 1979)

$$\delta\sigma(\omega) = -\frac{1}{2\pi^2} \left(\frac{e^2}{\hbar} \right) \ln \frac{1}{\omega\tau}. \quad (4.45b)$$

In a d -dimensional finite system with volume L^d the momentum integral in eq. (4.44) is cut off from below at $1/L$; as a result the correction in eqs. (4.43) or

(4.44) is seen to diverge for $d \leq 2$ as the system size is increased ($\omega\tau \rightarrow (L/l)^{-2}$ in eq. (4.43)). For $d = 2$ the length-dependent correction to σ_0 is given by (Abrahams et al. 1979)

$$\delta\sigma(L) = -\frac{1}{\pi^2} \left(\frac{e^2}{\hbar} \right) \ln \frac{L}{l}. \quad (4.46)$$

At finite temperatures and in an infinite system, for $\omega = 0$ the integral in eq. (4.44) is restricted to momenta larger than $1/L_{\text{in}}$, since the inelastic diffusion length $L_{\text{in}} = \sqrt{D_0 \tau_{\text{in}}}$ is the maximal length over which coherent self-interference is possible (see the discussion following eq. (3.10)). In this case one obtains the temperature-dependent correction ($L_{\text{in}} = \alpha T^{-p/2}$)

$$\frac{\delta\sigma(T)}{\sigma_0} = -\lambda \times \begin{cases} \alpha k_F T^{-p/2}, & d = 1, \\ p \ln \frac{1}{T}, & d = 2. \end{cases} \quad (4.47)$$

This result is identical to that obtained in eq. (3.12) using the Feynman-path arguments. For $d = 2$ we have

$$\delta\sigma(T) = -\frac{p}{2\pi^2} \left(\frac{e^2}{\hbar} \right) \ln \frac{T_0}{T}, \quad (4.48)$$

where T_0 is some reference temperature.

The divergence of the correction to the conductivity due to the pole in the particle-particle ladder is seen to be determined by the respective parameter which effectively cuts off the diffusion pole.

5. Beyond perturbation theory: the self-consistent equation for $D(\omega)$

We found that for $d \leq 2$, even the lowest-order correction in λ to the inverse diffusion coefficient $K(\omega) = D_0/D(\omega)$ yields a contribution which, in principle, diverges in the limit $\omega \rightarrow 0$. This infrared divergence explicitly depends on the dimension d and, above all, leads to a breakdown of perturbation theory. Therefore, one is still far from the localization transition itself, where $K(\omega)$ diverges as $1/\omega$. Nevertheless, the perturbation results (eqs. (4.41)–(4.48)) may be taken as a precursor of the Anderson transition (which in dimensions $d \leq 2$ is expected to occur for arbitrarily small disorder), since the divergences are present for all $\lambda > 0$.

Since the transition cannot be obtained in any finite order of perturbation theory, one has to resort to a different approach. In particular, the formulation of a one-parameter scaling theory of the dimensionless conductance g pioneered by Abrahams et al. (1979) and the elucidation of the connection between the Anderson localization problem and the theory of critical phenomena by Wegner

(1979) have opened the way for significant progress. Here we follow a different concept, namely that of *self-consistency*. This concept was first introduced into the localization problem by Götze (1978) within a mode-coupling approach (see also section 9). In this approach, one seeks to express $D(\omega)$ by an equation of the form

$$D(\omega) = \mathcal{F}[D(\omega)], \quad (5.1)$$

where the functional \mathcal{F} contains $D(\omega)$ itself. The self-consistent solution of eq. (5.1) should then provide $D(\omega)$ for all values of ω and disorder parameter λ . Clearly, for this to be successful, eq. (5.1) has to be compatible with exactly known limiting cases, e.g. it has to agree with perturbation theory for $\lambda \ll 1$ [eq. (4.40)]. Self-consistency is then used to extend the theory beyond perturbation theory.

5.1. Method I

As discussed earlier, the perturbational result (4.41) is valid only for not too small ω . Indeed, the diffusion coefficient $D(\omega)$ can only be represented by the diffusion constant D_0 as long as $D(\omega)$ does not change too much. For $\omega \rightarrow 0$ this condition is no longer fulfilled and one should therefore replace D_0 in the particle-particle diffusion pole on the right-hand side of eq. (4.41) by the full $D(\omega)$. (That this is permitted at all is a consequence of time-reversal invariance and the connection between the particle-hole and the particle-particle channel expressed by eq. (4.39).) In this way one obtains the self-consistent equation (Vollhardt and Wölfle 1980a, b)

$$\frac{D_0}{D(\omega)} = 1 + \frac{1}{\pi N(E_F)} \sum_Q \frac{1}{-i\omega + D(\omega)Q^2}. \quad (5.2)$$

The momentum integration is still restricted to $Q < 1/l$ (hydrodynamic regime). Later it will become clear that contributions from higher momenta are indeed unimportant for the critical properties of the system.

5.2. Method II

Equation (5.2) may actually be *derived* diagrammatically by calculating $D(\omega)$ [eq. (4.35)] from the largest, i.e. the most singular, diagrammatic contributions to $U_{kk'}$ (Wölfle and Vollhardt 1982). To this end we write the full vertex function $\Gamma_{kk'}$ as

$$\begin{aligned} \Gamma_{kk'}(\mathbf{q}, \omega) &= \gamma_{kk'}(\mathbf{q}, \omega) + \Gamma^0(\mathbf{q}, \omega) + \Gamma^0(\mathbf{q}, \omega) \sum_{k_1} R_{k_1} \gamma_{k_1 k'}(\mathbf{q}, \omega) \\ &\quad + \Gamma^0(\mathbf{q}, \omega) \sum_{k_1} \gamma_{kk_1}(\mathbf{q}, \omega) R_{k_1} \\ &\quad + (\Gamma^0(\mathbf{q}, \omega))^2 \sum_{k_1 k_2} R_{k_1} \gamma_{k_1 k_2}(\mathbf{q}, \omega) R_{k_2}. \end{aligned} \quad (5.3)$$

Equation (5.3) is shown diagrammatically in fig. 16a. Here $R_k \equiv G_{k+}^R G_{k-}^A$ and the auxiliary vertex function $\gamma_{kk'}(\mathbf{q}, \omega)$ is defined as the sum of all those diagrams that have no particle-hole ladders, or parts thereof, on the very left or right of the diagram (i.e. no scattering lines running vertically from particle- to hole-line). Using eqs. (4.11b) and (4.14), the density relaxation function $\Phi(\mathbf{q}, \omega)$ is obtained from eq. (5.3) as:

$$\Phi = R + Z + \Gamma^0 R^2 + 2\Gamma^0 R Z + (\Gamma^0)^2 R^2 Z \quad (5.4a)$$

$$= R(1 + \Gamma^0 R) + Z(1 + \Gamma^0 R)^2, \quad (5.4b)$$

where $R(\mathbf{q}, \omega) = \sum_k R_k$ and

$$Z(\mathbf{q}, \omega) \equiv \sum_{kk'} R_k \gamma_{kk'}(\mathbf{q}, \omega) R_{k'}. \quad (5.5)$$

From eq. (4.36) it follows that $1 + \Gamma^0 R = \Gamma^0 U_0^{-1}$; hence we have the identity

$$[\Gamma^0(\mathbf{q}, \omega)]^2 Z(\mathbf{q}, \omega) = U_0^2 \Phi(\mathbf{q}, \omega) - \Gamma^0(\mathbf{q}, \omega) + U_0. \quad (5.6)$$

The fact that $\Gamma_{kk'}(\mathbf{q}, \omega)$ is the full vertex function implies that $\Gamma = \bar{\Gamma}$, so that Γ may equally be expressed by the twisted diagrams of fig. 16a. This is shown in

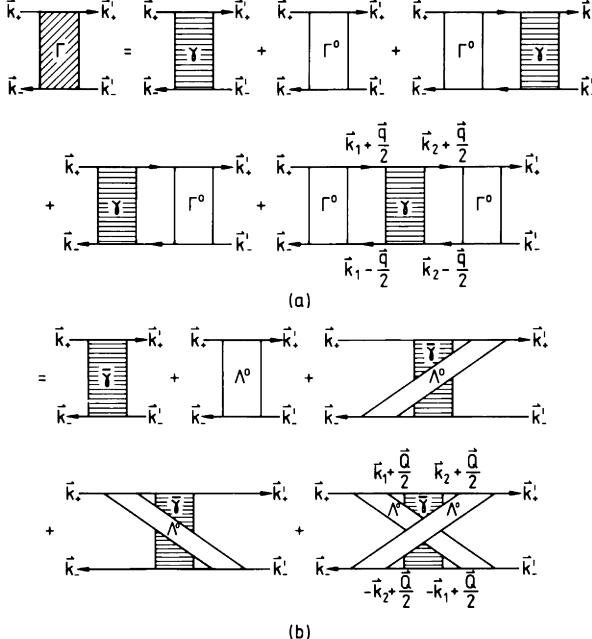


Fig. 16. (a) Exact diagrammatic representation of the full vertex function $\Gamma_{kk}(\mathbf{q}, \omega)$ in terms of the auxiliary vertex function $\gamma_{kk}(\mathbf{q}, \omega)$ and particle-hole ladders Γ^0 . (b) Transformation of the above diagrams in the case of time-reversal symmetry.

fig. 16b, where we have used $\bar{\Gamma}^0 = \Lambda^0$ [eq. (4.39a)]. We see that the last four diagrams are explicitly particle-hole-irreducible and are thus part of the irreducible vertex $U_{kk'}$. In particular, the last diagram in fig. 16b has a unique and peculiar property: it has two *identical* Cooperons $\Lambda^0(\mathbf{Q}, \omega)$, $\mathbf{Q} = \mathbf{k} + \mathbf{k}'$, running diagonally across the diagram, thus leading to the *square* of a diffusion pole. Using eq. (4.16b), the contribution of this diagram is immediately found to be given by eq. (5.6) with \mathbf{q} replaced by $\mathbf{Q} = \mathbf{k} + \mathbf{k}'$.

The contribution from a diagram in $U_{kk'}$ having a factor $[\Gamma^0(\mathbf{k} + \mathbf{k}', \omega)]^2$ will clearly dominate the contributions from diagrams containing only a single power of this diffusion pole (third and fourth diagram in fig. 16b). This conclusion neither depends on the particular (and, in general, unknown*) form of $\bar{\gamma}$, i.e. is not based on perturbation theory nor on the dimension d . Hence, it follows that of the last four diagrams in fig. 16b the diagrammatic contribution to $U_{kk'}$ from the very last will be the most divergent in all dimensions. Furthermore, the contribution from the irreducible part of $\bar{\gamma}_{kk'}$ (the first diagram in fig. 16b) can be neglected, since (i) it contains no diffusion poles $\Gamma^0(\mathbf{k} + \mathbf{k}', \omega)$ connecting the external vertices at all and, (ii) the angular integrals over the factor $(\mathbf{k} \cdot \mathbf{q}), (\mathbf{k}' \cdot \mathbf{q})$ lead to additional factors of $(\mathbf{k} + \mathbf{k}')^2$ which make this contribution even smaller.

The dominant contribution to $U_{kk'}$ is therefore given by

$$U_{kk'}^{\text{domin}} = \Gamma^0(\mathbf{k} + \mathbf{k}', \omega) + [\Gamma^0(\mathbf{k} + \mathbf{k}', \omega)]^2 Z(\mathbf{k} + \mathbf{k}', \omega). \quad (5.7)$$

Here we have explicitly included $\Gamma^0(\mathbf{k} + \mathbf{k}', \omega)$, which we had earlier identified as the lowest-order correction in the disorder to the Boltzmann conductivity; in this way $U_{kk'}$ is guaranteed to yield the correct result in lowest-order perturbation theory. From eq. (5.6) we then find

$$U_{kk'}^{\text{domin}}(\mathbf{q}, \omega) - U_0 = U_0^2 \Phi(\mathbf{k} + \mathbf{k}', \omega). \quad (5.8)$$

Hence the dominant contribution to $U_{kk'}$ is given by the *full* density relaxation function Φ at momentum $\mathbf{k} + \mathbf{k}'$.

Inserting eq. (5.6) into eq. (4.35) for D_0/D and performing the integration, one obtains, for small $Q = |\mathbf{k} + \mathbf{k}'|$,

$$\frac{D_0}{D(\mathbf{q}, \omega)} = 1 + \frac{1}{2(\pi N_F)^2} \sum_Q \Phi(\mathbf{Q}, \omega) \quad (5.9a)$$

$$= 1 + \frac{k_F^{2-d}}{\pi m} \int_0^{1/l} dQ \frac{Q^{d-1}}{-i\omega + D(\mathbf{Q}, \omega) Q^2}. \quad (5.9b)$$

This result is independent of the (small) external momentum \mathbf{q} (in fact, in deriving eq. (5.9) we already neglected terms of the order of $(ql)^2 \ll 1$); we

* Note that the auxiliary vertex $\gamma_{kk'}$ can itself, in principle, be further analyzed, e.g. by expressing it as an infinite sequence of new vertices $\pi_{kk'}$ and particle-hole diffusion poles Γ^0 . This series is easily summed up.

therefore put $\mathbf{q} = 0$ in $D(\mathbf{q}, \omega)$. Furthermore, since we are anyway considering small momenta only (only for small momenta does the density propagator have its simple diffusion-pole structure), we can neglect the \mathbf{Q} -dependence of $D(\mathbf{Q}, \omega)$ in the diffusion pole of eq. (5.9b), i.e. $D(\mathbf{Q}, \omega)Q^2 \approx D(\omega)Q^2$. Thereby we obtain

$$\frac{D_0}{D(\omega)} = 1 + \frac{k_F^{2-d}}{\pi m} \int_0^{1/l} dQ \frac{Q^{d-1}}{-i\omega + D(\omega)Q^2}. \quad (5.9c)$$

This amounts to deriving the self-consistent equation (5.2) for the dynamical conductivity $\sigma(\omega)$ or the diffusion coefficient $D(\omega)$. It should be stressed again that this derivation is not based on perturbation theory and, in particular, is not limited to a certain range of dimensions d . This implies that the self-consistent equation [(5.2), (5.9c)] can be expected to be valid not only in dimensions $d \leq 2$, as suggested by the derivation using method I, but also in dimensions $d > 2$.

For later purposes it is useful to rewrite eq. (5.9c) by multiplying both sides with $D(\omega)/D_0$, yielding

$$\frac{D(\omega)}{D_0} = 1 - \lambda dk_F^{2-d} \int_0^{1/l} dQ \frac{Q^{d-1}}{-i\omega/D(\omega) + Q^2} \quad (5.10)$$

$$= 1 - \frac{d}{\pi} (\pi\lambda)^{d-1} [\tilde{\xi}(\omega)]^{2-d} \int_0^{\tilde{\xi}(\omega)} dy \frac{y^{d-1}}{1+y^2}, \quad (5.11)$$

where

$$\tilde{\xi}^2(\omega) \equiv \frac{D(\omega)}{-i\omega} \frac{1}{l^2} \quad (5.12a)$$

$$= \frac{D(\omega)}{D_0} \frac{1}{(-i\omega\tau)} \frac{1}{d}. \quad (5.12b)$$

5.3. Anisotropic systems and general angle-dependent scattering

Many of the doped semiconductors for which the present theory has been developed, are highly anisotropic systems. Not only is the single-particle energy $\epsilon_{\mathbf{k}}$ anisotropic, but also the impurity scattering probabilities are anisotropic functions of momentum. The assumption of isotropic scattering made in all the preceding sections is unrealistic under these circumstances. Of course, one expects that the scaling behavior does not depend on these details. It is nonetheless interesting to actually derive the scaling property for this case. This may be done in full generality for an arbitrary, anisotropic single-particle energy $\epsilon_{\mathbf{k}}$ and a scattering probability $W_{\mathbf{kk'}}$ for processes in which the electron is scattered from Bloch state $|\mathbf{k}\rangle$ to state $|\mathbf{k}'\rangle$ (only one single Bloch band is considered). Using an eigenfunction expansion one may show that the effect of anisotropy can be completely absorbed into an anisotropic diffusion coefficient (Wölfle and Bhatt 1984).

The lowest-order scale-dependent term of the conductivity is calculated, following eqs. (4.36)–(4.45), by considering the sum of the ladder diagrams $\Gamma_{kk'}^0(\mathbf{q}, \omega)$ shown in fig. 14. In the general case considered here, $\Gamma_{kk'}^0$ satisfies the integral equation

$$\Gamma_{kk'}^0(\mathbf{q}, \omega) = W_{kk'} + \sum_p W_{kp} G_p^R(E + \omega) G_{p-k/2}^A(E) \Gamma_{pk'}^0(\mathbf{q}, \omega), \quad (5.13)$$

where

$$G_k^{R,A}(E) = (E - \varepsilon_k \pm i/2\tau_k)^{-1} \quad (5.14)$$

is the single-particle Green's function and τ_k is the single-particle lifetime given by

$$\begin{aligned} \frac{1}{2\tau_k} &= \sum_{k'} W_{kk'} \operatorname{Im} G_{k'}^A \\ &= \pi \langle W_{kk'} \rangle_{\hat{k}}. \end{aligned} \quad (5.15)$$

Here and in what follows, the angular brackets denote an angular average in k -space weighted with the density of states $N(E; \hat{k})$ along the directions \hat{k} :

$$\begin{aligned} \langle A_k \rangle_k &\equiv \sum_k A_k \delta(\varepsilon_k - E) \\ &= \int \frac{d\Omega_k}{S_d} N(E; \hat{k}) A_k, \end{aligned} \quad (5.16)$$

and S_d is the surface of the unit sphere in d dimensions.

Introducing the eigenfunctions ϕ_k^n of the integral operator in eq. (5.13) in the limit $\mathbf{q}, \omega \rightarrow 0$ as

$$\sum_p W_{kp} |G_p^A|^2 \phi_p^n = \lambda_n \phi_k^n, \quad n = 0, 1, 2, \dots, \quad (5.17)$$

the integral equation (5.13) may be solved in the limit of small ω, q . The functions ϕ_p^n form a complete basis and satisfy the orthonormality relation

$$\sum_k \phi_k^n |G_k^A|^2 \phi_k^{n'} = \langle \phi_k^n \tau_k \phi_k^{n'} \rangle_k = \delta_{nn'}. \quad (5.18)$$

Accordingly, the integral kernel W_{kp} may be expressed as

$$W_{kp} = \sum_n \lambda_n \phi_k^n \phi_p^n. \quad (5.19)$$

With the aid of this representation, the general solution of eq. (5.13) is found to be

$$\Gamma_{kk'}(\mathbf{q}, \omega) = \sum_{n, \lambda_n \neq 1} \frac{\lambda_n}{1 - \lambda_n} \phi_k^n \phi_{k'}^n + \Gamma_{kk'}^{\text{sing}}(\mathbf{q}, \omega). \quad (5.20)$$

Here the term Γ^{sing} contains any singular contribution (in the limit $q, \omega \rightarrow 0$)

arising from eigenvalues $\lambda_n = 1$. Physically, the appearance of such an eigenvalue signals the existence of a conservation law. In the present case there is only one relevant conservation law: the law of particle conservation. The corresponding eigenfunction is given by

$$\phi_{\mathbf{k}}^0 = \frac{1}{z} \frac{1}{\tau_{\mathbf{k}}}, \quad (5.21)$$

with $z = (\langle 1/\tau_{\mathbf{k}} \rangle_{\mathbf{k}})^{1/2}$.

The singular contribution $\Gamma_{kk'}^{\text{sing}}$ is obtained by calculating the small q, ω correction to the eigenvalue $\lambda_0 = 1$. One finds

$$\Gamma_{kk'}^{\text{sing}}(\mathbf{q}, \omega) = \frac{1}{2\pi N(E)} \frac{\zeta_{\mathbf{k}}(\mathbf{q}) \zeta_{\mathbf{k}'}(\mathbf{q})}{-\text{i}\omega + \sum_{\mu\nu} D_{\mu\nu}^0 q_{\nu} q_{\mu}}, \quad (5.22)$$

where

$$\zeta_{\mathbf{k}}(\mathbf{q}) = \frac{1}{\tau_{\mathbf{k}}} - 2\pi\text{i} \sum_{n \neq 0} \langle \mathbf{q} \cdot \mathbf{v}_{\mathbf{k}'} \tau_{\mathbf{k}'} \phi_{\mathbf{k}'}^n \rangle_{\mathbf{k}'} \frac{\lambda_n}{1 - \lambda_n} \phi_{\mathbf{k}}^n \quad (5.23)$$

and the eigenvalues of the diffusion tensor are given by

$$D_{\mu\mu}^0 = \frac{1}{N(E)} \langle v_{k\mu} j_{k\mu} \tau_{\mathbf{k}} \rangle_{\mathbf{k}}. \quad (5.24)$$

Here $j_{k\mu}$ is the renormalized current vertex obtained by dressing the bare vertex with the sum of the ladder diagrams:

$$j_{k\mu} = v_{k\mu} + \sum_{n \neq 0} \frac{\lambda_n}{1 - \lambda_n} \langle v_{k'\mu} \tau_{\mathbf{k}'} \phi_{\mathbf{k}'}^n \rangle_{\mathbf{k}'} \phi_{\mathbf{k}}^n. \quad (5.25)$$

The DC conductivity, given by the current-current correlation function, is obtained in the ladder approximation as

$$\begin{aligned} \sigma_{\mu\mu}^0 &= e^2 \sum_{\mathbf{k}} v_{k\mu} |G_{\mathbf{k}}|^2 j_{k\mu} \\ &= e^2 N(E) D_{\mu\mu}^0. \end{aligned} \quad (5.26)$$

The leading scale-dependent correction to the conductivity arises from the maximally crossed diagrams depicted in fig. 15 and two additional diagrams of the same type, with an impurity line connecting the two ends of the upper (or lower) Green's function line across the Cooperon:

$$\begin{aligned} \delta\sigma_{\mu\mu} &= -\frac{1}{\pi} e^2 \left\{ \sum_{\mathbf{k}} j_{k\mu}^2 |G_{\mathbf{k}}^A|^4 \sum_{\mathbf{q}} \Gamma_{\mathbf{k}-\mathbf{k}}^0(\mathbf{q}, \omega) \right. \\ &\quad \left. - \sum_{\mathbf{k}, \mathbf{k}'} (G_{\mathbf{k}}^R)^2 G_{\mathbf{k}}^A j_{k\mu} j_{-k'\mu} W_{kk'} (G_{\mathbf{k}'}^R)^2 G_{\mathbf{k}'}^A \sum_{\mathbf{q}} \Gamma_{\mathbf{k}-\mathbf{k}}^0(\mathbf{q}, \omega) \right\}. \end{aligned} \quad (5.27)$$

Using the relation

$$j_{k\mu} - \sum_{k'} W_{kk'} G_k^R G_{k'}^A j_{k'\mu} = v_{k\mu}, \quad (5.28)$$

eq. (5.27) may be simplified to give

$$\delta\sigma_{\mu\mu} = -\frac{2e^2}{\pi} D_{\mu\mu}^0 \sum_q \frac{1}{-i\omega + \sum_v D_{vv}^0 q_v^2}. \quad (5.29)$$

It follows that up to first order in the Cooperon contribution, the eigenvalues of the conductivity tensor in two dimensions take the form

$$\frac{\sigma_{\mu\mu}}{\sigma_{\mu\mu}^0} = 1 - \frac{e}{2\pi^2} \frac{1}{\bar{\sigma}^0} \ln(1/\omega\tau), \quad (5.30)$$

where $\bar{\sigma}^0 = (\sigma_{xx}^0 \sigma_{yy}^0)^{1/2}$, and $\sigma_{\mu\mu}^0$ is given by eq. (5.26). Thus, the anisotropy of $\sigma_{\mu\mu}$ scales with that of $\sigma_{\mu\mu}^0$ and the coupling constant λ is given by the average of the eigenvalues of the Boltzmann conductivity tensor, $\bar{\sigma}_0$, in agreement with the one-parameter scaling picture (Altshuler et al. 1981).

This general behavior can be shown to be true in all orders (Wölfle and Bhatt 1984), indicating that the anisotropy in $\sigma_{\mu\nu}$ may be removed by scaling distances along the principal axis μ by $(\sigma_{\mu\mu}^0/\bar{\sigma}^0)^{1/2}$, or equivalently, by scaling momenta by $q_\mu \rightarrow q_\mu(\bar{\sigma}^0/\sigma_{\mu\mu}^0)^{1/2}$. This property can be shown to hold also for the scale-dependent correction terms introduced by Coulomb interaction (Altshuler and Aronov 1979a, b, Bhatt et al. 1984, 1985).

The corresponding generalization of the self-consistent equation (5.2) is given by

$$\frac{D_{\mu\mu}^0}{D_{\mu\mu}(\omega)} = 1 + \frac{1}{\pi N(E_F)} \sum_Q \frac{1}{-i\omega + \sum_v D_{vv}(\omega) Q_v^2}. \quad (5.31)$$

Here the \mathbf{Q} summation extends up to the anisotropic cutoff wave vector $Q_\mu < l_\mu^{-1}$, with l_μ as the mean free path along the principal axis μ .

6. Solution of the self-consistent equation: scaling behavior of the dynamical conductivity

In the insulating state, where $D(\omega) \propto -i\omega$, the density relaxation function $\Phi(\mathbf{q}, \omega)$ takes the form (Götze 1978, 1979)

$$\lim_{\omega \rightarrow 0} \Phi(\mathbf{q}, \omega) = \frac{1}{-i\omega} \frac{2\pi N_F}{1 + (q\xi)^2} \quad (6.1)$$

describing exponential localization, with the localization length ξ given by

$$\frac{1}{\xi} = \lim_{\omega \rightarrow 0} \left(\frac{-i\omega}{D(\omega)} \right)^{1/2}. \quad (6.2)$$

In this case $\tilde{\xi}(0)$ [eq. (5.12a)] is given by $\tilde{\xi} \equiv \tilde{\xi}(0) = \xi/l$. Clearly, Φ diverges as $1/(-i\omega)$ in this limit. Hence, in the localized limit eq. (5.8) takes the form of a transcendental equation for $\tilde{\xi}$:

$$1 = \frac{d}{\pi} (\pi\lambda)^{d-1} \tilde{\xi}^{2-d} \int_0^{\tilde{\xi}} dy \frac{y^{d-1}}{1+y^2}. \quad (6.3)$$

6.1. Solution in dimensions $d \leq 2$

We will first discuss the situation for low dimensions ($d \leq 2$) (Vollhardt and Wölfle 1980a, b). In dimensions $0 < d < 2$ the integral in eq. (6.3) converges for arbitrary ξ . In particular, for $d = 1$ ξ is given by the solution of $\pi/z = \tan^{-1} z$, which is independent of λ . One finds

$$\xi = 2.61 v_F \tau. \quad (6.4)$$

This compares well with the exact result for $d = 1$ (Berezinskii 1973, Abrikosov and Ryshkin 1978), given by $\xi = 4v_F \tau$. Hence, in one dimension ξ is of the order of the mean free path.

For weak disorder ($\lambda \ll 1$) and $1 < d < 2$, the localization length is found to be

$$\xi = \frac{p_{1,d}}{k_F} \frac{1}{\lambda^{1/(2-d)}}, \quad (6.5)$$

where $p_{1,d} = (\sin x/x)^{1/(2-d)}$, $x = \pi d/2$.

For $d = 2$ one finds

$$\xi/l = \left[\exp \frac{1}{\lambda} - 1 \right]^{1/2} \quad (6.6)$$

$$\begin{aligned} &= \exp \frac{1}{2\lambda}, \quad \lambda \ll 1, \\ &= \frac{1}{\sqrt{\lambda}}, \quad \lambda \gg 1. \end{aligned} \quad (6.7)$$

For weak disorder the localization length is seen to grow, i.e. localization is exponentially weak. For $\lambda \lesssim 0.02$, ξ would be larger than typical experimental probes and, therefore, localization phenomena are detectable only via the effects of weak localization discussed in section 2. Altogether, one finds that in dimensions $d \leq 2$ particles are *always* localized, irrespective of how small the disorder concentration is.

The localization length determines also the static electric polarizability $\alpha(0)$ via eq. (4.32a):

$$\alpha(0) = \frac{e^2 n d}{2 E_F} \xi^2. \quad (6.8)$$

Thus, in two dimensions $\alpha(0)$ increases exponentially with decreasing disorder.

The low-frequency dependence of the dynamic conductivity $\sigma(\omega) = (\sigma_0/D_0)D(\omega)$ in dimensions $d \leq 2$ is easily obtained from eq. (5.8):

$$\operatorname{Re} \sigma(\omega) = b_d \sigma_0(\omega\tau)^2, \quad (6.9)$$

where $b_1 = 512$ and $b_2 = (4\lambda)^{-1} \exp(2/\lambda)$. For $d = 2$ the prefactor of the ω^2 -dependence increases exponentially with decreasing disorder. It should be noted that the level repulsion effect (Mott 1970, Berezinskii 1973, Abrikosov and Ryshkin 1978), which actually leads to an additional factor $(\ln \omega)^{d+1}$ in the ω^2 -dependence of $\operatorname{Re} \sigma(\omega)$, is not obtained in the present theory. This is not surprising, since our theory is only expected to yield the dependence $\sigma(\omega) \propto -i\omega$ correctly; the level repulsion effect is clearly of higher order.

6.2. Solution in dimensions $d > 2$

We now discuss the solution of the self-consistent equation (5.9) for dimensions $d > 2$ (Vollhardt and Wölfle 1982). In this case there also exists a solution $D(0) \neq 0$; for this the disorder λ has to be smaller than a critical value λ_c . Using $y^{d-1}/(1+y^2) = y^{d-3}[1-1/(1+y^2)]$, eq. (5.9c) is rewritten as

$$\frac{\sigma(\omega)}{\sigma_0} = 1 - \frac{d}{d-2} \frac{1}{\pi} (\pi\lambda)^{d-1} + \frac{d}{\pi} \frac{(\pi\lambda)^{d-1}}{\tilde{\xi}^{d-2}(\omega)} \int_0^{\tilde{\xi}(\omega)} dy \frac{y^{d-3}}{1+y^2}. \quad (6.10)$$

For $\lambda < \lambda_c$ and in the limit $\omega \rightarrow 0$, where $\tilde{\xi} \rightarrow \infty$, the third term on the right-hand side of eq. (6.10) vanishes for all dimensions $d > 2$; namely, as $\tilde{\xi}^{2-d}$ for $2 < d < 4$, as $\tilde{\xi}^{-2} \ln \tilde{\xi}$ for $d = 4$ and as $\tilde{\xi}^{-2}$ for $d > 4$. In this limit eq. (6.10) yields

$$\frac{\sigma(0)}{\sigma_0} = 1 - \left(\frac{\lambda}{\lambda_c} \right)^{d-1}, \quad \lambda \leq \lambda_c \quad (6.11a)$$

$$= c \left(\frac{\lambda}{\lambda_c} \right) \left(1 - \frac{\lambda}{\lambda_c} \right), \quad \lambda \leq \lambda_c, \quad (6.11b)$$

where $c(x) = \sum_{n=0}^{d-2} x^n$ and the critical disorder λ_c is given by

$$\lambda_c = \left(\frac{d-2}{d\pi^{d-2}} \right)^{1/(d-1)}, \quad d \geq 2. \quad (6.12)$$

The DC conductivity $\sigma(0)$ is seen to vanish at $\lambda = \lambda_c$, where the Anderson transition to the localized state occurs. The transition is approached as

$$\sigma(0) \propto \lambda_c - \lambda \quad (6.13a)$$

for any $d > 2$, indicating that the critical exponent s of the conductivity, $\sigma(0) \propto |\lambda_c - \lambda|^s$, is

$$s = 1, \quad d > 2 \quad (6.13b)$$

This result was first obtained by Abrahams et al. (1979) within a one-parameter scaling theory for the dimensionless conductance.

In the insulating regime ($\lambda > \lambda_c$), the general low-frequency solution for $\sigma(\omega)$ is given by $\sigma(\omega) = -i\omega\alpha(0) + O(\omega^2)$ for any d . The localization length $\xi = \tilde{\xi}l$ is obtained from eq. (6.10) as follows:

$$1 = \left(\frac{\lambda}{\lambda_c}\right)^{d-1} \left[1 - (d-2)\tilde{\xi}^{2-d} \int_0^\infty dy \frac{y^{d-3}}{1+y^2} + O(\tilde{\xi}^{-2}) \right], \quad 2 < d < 4, \quad (6.14)$$

so that

$$\xi = p_{2,d}l \left| 1 - \frac{\lambda}{\lambda_c} \right|^{-1/(d-2)}, \quad (6.15a)$$

where $p_{2,d} = [2(d-1)\sin(\pi d/2)/(2-d)\pi]^{-1/(d-2)}$. Hence, the critical exponent v of the localization length, $\xi \propto |\lambda_c - \lambda|^{-v}$, is

$$v = \frac{1}{d-2}, \quad 2 < d < 4. \quad (6.15b)$$

This also agrees with the result of the scaling theory by Abrahams et al. (1979). For $d > 4$, we find from eq. (6.10)

$$1 = \left(\frac{\lambda}{\lambda_c}\right)^{d-1} \left[1 - \frac{d-2}{d-4} \tilde{\xi}^{-2} + O(\tilde{\xi}^{-4}) \right], \quad (6.16)$$

so that $\xi \propto (\lambda - \lambda_c)^{-1/2}$ ($\lambda > \lambda_c$), and

$$v = \frac{1}{2}, \quad d > 4. \quad (6.17)$$

Thus, $d = 4$ is the upper critical dimension, above which v assumes the classical mean-field behavior. For $d = 4$ one has $\tilde{\xi}^2 \ln(1/\tilde{\xi}^2) \propto (\lambda - \lambda_c)$, which leads to logarithmic corrections to the mean-field behavior.

For $2 < d < 4$, the critical exponents s and v obey the relation

$$s = v(d-2), \quad 2 < d < 4, \quad (6.18)$$

which was first derived by Wegner (1976) based on an approach similar to that used in the theory of critical phenomena.

For $2 < d < 4$ the frequency dependence of $\sigma(\omega)$ in the immediate vicinity of the Anderson transition, i.e. for $\omega\tau \ll |1 - \lambda/\lambda_c|$, is obtained from eq. (6.10) by setting $\tilde{\xi} = \infty$ in the integral and using eq. (5.12b):

$$\frac{\sigma(\omega)}{\sigma_0} = (d-1) \left(1 - \frac{\lambda}{\lambda_c} \right) + r_d \left(\frac{-i\omega\tau}{\sigma(\omega)/\sigma_0} \right)^{(d-2)/2}, \quad (6.19)$$

where $r_d = d^{(d-2)/2}(x/\sin x)$, $x = (d-2)\pi/2$. From eq. (6.19) we see that $\sigma(\omega)$ has a scaling form (Shapiro 1982b)

$$\frac{\sigma(\omega)}{\sigma_0} = (-i\omega\tau)^{(d-2)/d} F \left(\frac{-i\omega}{\omega_c} \right), \quad (6.20)$$

with $\omega_c \tau = |1 - \lambda/\lambda_c|^{d/(d-2)} \propto \xi^{-d}$. Clearly, this scaling form for $\sigma(\omega)$ is also valid for the frequency-dependent diffusion coefficient $D(\omega)$, which may be written as

$$D(\omega) = \xi^{2-d} D^* f(-i\omega/\omega_c), \quad (6.21a)$$

with

$$f(z) = x_d z^{(d-2)/d} F(z), \quad (6.21b)$$

$D^* = [(d-2)N_F/2]^{-1}$ and $x_d = \Gamma(2-d/2)/[(d-1)2^{d-1}\pi^{(d+2)/2}]$. The above two scaling forms are in accordance with the results of explicit scaling theories for $\sigma(\omega)$ and $D(\omega)$ (Wegner 1976, Hikami 1981, Shapiro and Abrahams 1981, Imry et al. 1981).

From eq. (6.19) we see that the scaling function $F(z)$ is determined by the equation

$$F(z) = (d-1)z^{(2-d)/d} + r_d [F(z)]^{(2-d)/2}. \quad (6.22)$$

Thus, the self-consistent theory presented here allows for an explicit calculation of $F(z)$. Its limiting behavior is easily obtained (Shapiro 1982b): for $z \ll 1$ one has

$$\begin{aligned} F(z) &\propto z^{2/d}, & \lambda > \lambda_c, \\ &\propto z^{(2-d)/d}, & \lambda < \lambda_c, \end{aligned} \quad (6.23a)$$

and for $z \gg 1$ one finds

$$F(z) = \text{constant}. \quad (6.23b)$$

The limit $z \gg 1$ is valid in the scaling regime, where

$$\sigma(\omega) \propto \omega^{(d-2)/d}. \quad (6.24)$$

Similar scaling forms have been obtained by Wegner (1976), Götze (1978, 1979, 1981a, b), Hikami (1981, 1982) and Shapiro and Abrahams (1981).

For $d = 3$ in particular, eq. (6.19) yields a cubic equation which may be solved in closed form. In the scaling regime one has $\sigma(\omega) \propto \omega^{1/3}$.

7. Length dependence of the conductance in finite samples

Up to now we have derived the results of the self-consistent theory for the conductivity σ or the diffusion coefficient D as a function of frequency ω in an infinitely extended system. In particular, we obtained a scaling behavior of $\sigma(\omega)$ as expressed by eq. (6.20). We will now discuss the opposite limit, namely the length dependence of σ or D in the case of a finite sample of length L and volume L^d at $\omega = 0$ (Vollhardt and Wölfle 1982, Wölfle and Vollhardt 1982). Indeed, in view of the spatial localization of particles in the problem under investigation, the length dependence should be expected to exhibit the most natural scaling

behavior. Furthermore, the dependence on sample size allows one to make contact with the scaling theory of Abrahams et al. (1979) and with field-theoretic treatments (Wegner 1976, 1979, Oppermann and Wegner 1979, Hikami 1981, 1982).

The scattering mechanism responsible for the localization of an independent quantum-mechanical particle moving in a disordered medium does not depend on the size of the system. Hence, it is present even in finite systems of length L . However, in this case there is a finite probability for the particle to reach the end of the sample before being scattered back into the sample. This effect is taken care of, if the allowed wave vectors of the diffusion mode are restricted to $k > 1/L$. To calculate the length dependence of the diffusion coefficient D , or of the conductivity σ , from the self-consistent equation (5.10) (which is effectively a momentum integral over a correlation function describing the spatial decay of density fluctuations; see eq. (5.9a)), we therefore introduce a lower cutoff at $k = 1/L$. At the same time we take the limit $\omega \rightarrow 0$ in eq. (5.10). To this end we replace $-i\omega/D(\omega)$ in the denominator of the integral by ξ^{-2} (see eq. (6.2)), where ξ is the localization length of the *infinite* system. This expresses the fact that for a given disorder the states of the finite sample are localized, whenever the states of the infinite system are localized (see the above discussion). In other words, ξ depends only on microscopic quantities and *not* on the length of the sample. This is also consistent with renormalization group treatments, where $-i\omega/D(\omega)$ is found to be independent of L (Efetov et al. 1980, Hikami 1982). Therefore, eq. (5.10) yields

$$\frac{D(L)}{D_0} = 1 - d\lambda k_F^{2-d} \int_{1/L}^{1/\tilde{L}} dQ \frac{Q^{d-1}}{\xi^{-2} + Q^2}. \quad (7.1)$$

Subtracting from eq. (7.1) the equation for ξ [eq. (6.3)] leads to

$$\frac{D(L)}{D_0} = d\lambda (k_F \xi)^{2-d} \int_0^{1/\tilde{L}} dy \frac{y^{d-1}}{1 + y^2}, \quad (7.2)$$

where $\tilde{L} \equiv L/\xi$. We note that eq. (7.2) is no longer a self-consistent equation for D ; rather, $D(L)$ is given explicitly by the right-hand side of eq. (7.2).

In fact, the physically appropriate quantity to study in the case of a finite system is not the diffusion coefficient $D(L)$, or the conductivity $\sigma(L)$ itself, but the *conductance* (Thouless 1974, 1977)

$$G = 1/R, \quad (7.3)$$

i.e. the inverse resistance of the d -dimensional system. The resistance may be expressed as $R = \rho L/A$, where $\rho = 1/\sigma$ is the resistivity, and L and A are the side length and the cross section of the system, respectively. For a hypercube the conductance is thus given by

$$G = \sigma L^{d-2}. \quad (7.4)$$

In particular, Thouless (1974, 1977) realized that one may introduce a dimensionless conductance g in units of e^2/h , i.e. $g = (e^2/h)^{-1} G$, so that

$$g(L) = \left(\frac{e^2}{h} \right)^{-1} \sigma L^{d-2}. \quad (7.5)$$

In the ohmic regime, σ is independent of L and hence, $g \propto L^{d-2}$. According to the scaling theory of Abrahams et al. (1979), the conductance $g(L)$ is the quantity obeying a scaling relation. We will now calculate $g(L)$ explicitly within the self-consistent theory. To this end one has to compute the current density J flowing in a sample of finite length L under the influence of an applied electric field E . Such a calculation is made nontrivial by the fact that the density response of localized electrons is *nonlocal*.* We determine J by requiring it to be equal and opposite to the diffusion current under open-circuit conditions. At the end of the sample ($x = L$) the current density is then given by

$$J = eD(L) \frac{d(\delta\rho)}{dx} \Big|_{x=L}, \quad (7.6)$$

where $\delta\rho(x)$ is the density change induced by the electric potential $U(x) = eE(L - x)$:

$$\delta\rho(x) = - \int_0^L dx' \chi(x - x') U(x'). \quad (7.7)$$

Here $\chi(x)$ is the Fourier transform of $\chi(\mathbf{q}, 0)$ [eq. (3.18)], i.e. of the static density response function

$$\chi(\mathbf{q}, 0) = \frac{q^2}{\xi^{-2} + q^2} N_F, \quad (7.8)$$

and has the form

$$\chi(x) = N_F \left[\delta(x) - \frac{1}{2\xi} \exp(-|x|/\xi) \right]. \quad (7.9)$$

Thereby one obtains

$$J(L) = e^2 D(L) N_F \left(1 + \frac{L}{\xi} \right) \exp(-L/\xi) E. \quad (7.10)$$

* Note that for the critical properties of the system, this nonlocality is unimportant since the localization length, $\xi \rightarrow \infty$, is the only relevant length in this case. Hence, for a given length L of the system, ξ can always be chosen such that $L/\xi \ll 1$. However, away from the transition itself, in the strongly localized regime, nonlocality is an important factor.

Inserting eq. (7.2) we find

$$J(L) = c_d e^2 E \xi^{2-d} \left(1 + \frac{L}{\xi}\right) \exp(-L/\xi) \int_0^{\xi/L} dy \frac{y^{d-1}}{1+y^2}, \quad (7.11)$$

where we have used $N_F = [S_d/(2\pi)^d] m k_F^{d-2}$, with S_d as the surface area of the unit sphere in d dimensions, and

$$c_d \equiv \frac{2}{\pi} \frac{S_d}{(2\pi)^d}. \quad (7.12)$$

Since $J(L)/E$ is the conductivity $\sigma(L)$, the conductance $g(L)$ in the insulating regime is obtained from eq. (7.5) as

$$g(L) = c_d (1+x) \exp(-x) h_d(x) \quad (x = L/\xi), \quad (7.13)$$

where we have defined

$$h_d(x) = \int_0^1 dy \frac{y^{d-1}}{x^2 + y^2}. \quad (7.14)$$

Thus, $g(L)$ is seen to depend on the coupling constant λ only via the scaled length of the sample $L/\xi(\lambda)$, i.e. $g(L)$ is a *scaling function*. This agrees completely with the assumption underlying the scaling theory of Abrahams et al. (1979), as well as with the renormalization group treatments of field-theoretic models (Wegner 1976, 1979, Oppermann and Wegner 1979, Efetov et al. 1980, Hikami 1981, 1982, McKane and Stone 1981, Abrahams and Lee 1986). The integral in eq. (7.14) may easily be solved using the recurrence relation

$$h_d(x) = 1/(d-2) - x^2 h_{d-2}(x) \quad \text{for } d > 2,$$

and

$$h_1(x) = (1/x) \tan^{-1}(1/x), \quad h_2(x) = \frac{1}{2} \ln(1 + 1/x^2).$$

Hence, in the insulating regime

$$\begin{aligned} g(L) &= \frac{2}{\pi^2} (1+x) \exp(-x) \frac{1}{x} \tan^{-1}(1/x), \quad d=1, \\ &= \frac{1}{2\pi^2} (1+x) \exp(-x) \ln\left(1 + \frac{1}{x^2}\right), \quad d=2. \end{aligned} \quad (7.15)$$

On the other hand, in the conducting regime ($d > 2$, $\lambda < \lambda_c$), eq. (7.1) yields ($\xi \rightarrow \infty$)

$$g(L) = \frac{c_d}{d-2} \left[1 + \Gamma\left(\frac{d}{2}\right) \Gamma\left(2 - \frac{d}{2}\right) \left(\frac{L}{\xi'}\right)^{d-2} \right], \quad (7.16)$$

where the correlation length ξ' is given by the expression for the localization length ξ [eq. (6.15a)] for $\lambda < \lambda_c$. For $L/\xi' \rightarrow 0$, $g(L)$ approaches the constant $g_c = c_d/(d-2)$, which is independent of the coupling.

Since $g(L)$ depends only on a single variable, there exists a corresponding scaling equation. In particular, we may explicitly calculate the scaling function (β -function)

$$\beta[g(L)] \equiv \frac{d \ln g}{d \ln L} \quad (7.17)$$

from eq. (7.13), which is a crucial quantity in a field-theoretic approach. One obtains

$$\beta[g(L)] = d - 2 - \frac{c_d(1+x)\exp(-x)}{g} - \frac{x^2}{1+x}, \quad (7.18)$$

where $x = L(g)/\xi$ with $L(g)$ as the inverse function of $g(L)$ [eq. (7.13)]. Clearly, β is a function of g only.

Due to the exponential decrease of $g(L)$ for $L/\xi \gg 1$ (this effect is a consequence of the nonlocal character of the density response discussed earlier), one has

$$\beta(g) = \ln g + O\left[\ln\left(\ln\frac{1}{g}\right)\right], \quad g \ll 1 \quad (7.19)$$

for all dimensions. On the other hand, for large g (and, in dimensions $d \leq 2$, for correspondingly small L/ξ) eq. (7.13) yields

$$\beta(g) = d - 2 - \frac{c_d}{g} - x^2\left(1 - \frac{3}{2}\frac{c_d}{g}\right) + O(x^3). \quad (7.20)$$

By contrast, in dimensions $d > 2$, g can only become large if L/ξ' is large [see eq. (7.16)]. The β -function is shown explicitly in fig. 17 for $d = 1, 2, 3, 4$, where it is plotted as a function of $\ln g$.

We see that for $d \leq 2$, one has $\beta(g) < 0$ for any finite g . This implies that, irrespective of the initial condition $g_0 \equiv g(L_0)$ at some given length L_0 , g always decreases when the length of the system is increased. Accordingly, states are always localized in $d \leq 2$, *irrespective of the strength of the disorder* $\lambda > 0$. Therefore in dimensions $d \leq 2$ the system is always insulating in the limit $L \rightarrow \infty$, the localization length ξ increasing exponentially with decreasing λ in the case of $d = 2$ [see eq. (6.7)]. On the other hand, for $d > 2$, the β -function has a zero point (*fixed point*) at $g_c = c_d/(d-2)$. For $g < g_c$, an increase of L drives the system into the localized regime, where $g(L) \propto \exp(-L/\xi)$ [see eq. (7.13)]. By contrast, for $g > g_c$, g scales as L^{d-2} for large d (Ohm's law), i.e. scales into the conducting regime according to $\beta = d - 2 - c_d/g$ [see eq. (7.20)]. At $\beta(g_c) = 0$, the slope of β is continuous and is given by

$$\left.\frac{d\beta}{d \ln g}\right|_{g_c} = \frac{1}{v}, \quad d > 2 \quad (7.21)$$

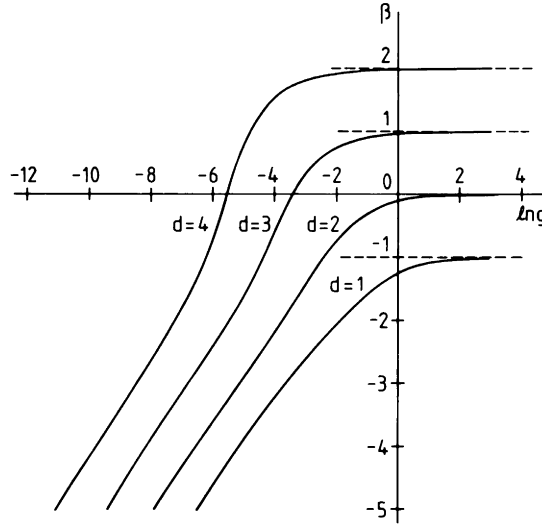


Fig. 17. The β -function for the length-dependent conductance $g(L)$, $\beta[g(L)] = d\ln g/d\ln L$, for dimensions $d = 1, 2, 3, 4$ (Vollhardt and Wölfle 1982).

in agreement with the scaling theory (Abrahams et al. 1979). By linearizing $\beta(g)$ around $\beta = 0$ and integrating the resulting expression, one arrives at the relations $\xi \propto |\lambda - \lambda_c|^{-v}$ for the localization length, with $v = 1/(d - 2)$ for $2 < d < 4$, and $\sigma(0) \propto |\lambda - \lambda_c|^{v(d-2)}$ for the conductivity in the conducting regime, thus reproducing the relation $s = (d - 2)v = 1$ expressed by eqs. (6.13b), (6.15b) and (6.18).*

The most interesting dimension is $d = 2$, where

$$\begin{aligned} \beta(g) &= -\frac{1}{\pi^2 g} - \left(1 - \frac{3}{2\pi^2 g}\right) \exp(-2\pi^2 g) + O(\exp(-3\pi^2 g)), \quad g \gg 1, \\ &= \ln g + O\left(\ln\left(\ln\frac{1}{g}\right)\right), \quad g \ll 1. \end{aligned} \tag{7.22}$$

Most importantly, in this case $\beta(g)$ is found to be *nonanalytic* for $g \rightarrow \infty$ (nonperturbative contribution). Hence, in a formal expansion of $\beta(g)$ in powers

* It should be noted that the overall form of the β -function is not universal, only the behavior at the fixed point will be universal. Hence, experimental attempts to determine whether the conductance is really a scaling variable are only important in that they may verify the existence of a scaling function $\beta[g(L)]$ (Soonpaa and Schwalm 1984, Zavaritskaya and Zvyagin 1985). However, the importance of the actual agreement between the form of $\beta[g(L)]$ obtained thereby with that obtained theoretically should not be overestimated.

of $1/g$ all coefficients of $(1/g)^n$, $n \geq 2$, are zero. In fact, using a mapping of the disorder problem onto a nonlinear σ -model (Wegner 1979), a systematic calculation of the β -function shows that the coefficients of the $1/g^2$ - and $1/g^3$ -terms do indeed vanish (Hikami 1982); see the discussion in section 8. Assuming all higher-order terms to be even zero (which is equivalent to *assuming* a form of $\beta(g)$ as in eq. (7.22)), the integration of the renormalization group equation for the diffusion coefficient yields precisely the form of the self-consistent equation (6.19) (Hikami 1982). However, most recently Wegner (1989) succeeded in calculating the four-loop order contribution to the β -function and thereby found the equivalent of a *finite* $1/g^4$ -term. The additional $1/g^4$ term in the β -function changes the critical exponents s and v (Wegner 1989). While eq. (7.22) cannot therefore be an exact result, the corrections appear only in rather high orders. This suggests that they become important only very close to the transition. (See also the discussion of the validity of the self-consistent theory in section 11.)

In analogy to the length-dependent problem discussed earlier, a scaling function $\beta(F(-i\omega/\omega_c))$ may also be derived for the frequency-dependent “conductance”, $F(-i\omega/\omega_c) \propto \sigma(\omega)(-i\omega/\omega_c)^{(2-d)/d}$ [eq. (6.20)], in the limit $L = \infty$ (Wölfle and Vollhardt 1982). Note that in two dimensions $\sigma(\omega)$ is itself the scaling function; this fact was first noted by Gorkov et al. (1979), who obtained a renormalization group equation for $1/\sigma(\omega)$. Again, β does not change sign for $d \leq 2$, corresponding to an insulating behavior for all strengths of disorder, while for $d > 2$, β has a fixed-point solution, implying the existence of an Anderson transition.

The scaling behavior of the dielectric function near the mobility edge with respect to ω and q has been considered by several authors. In the long wavelength limit ($q \rightarrow 0$), the scaling behavior of $\Phi(q = 0, \omega)$ has been discussed by Wegner (1976), Hikami (1981), Shapiro and Abrahams (1981) and Shapiro (1982b). For finite q , a heuristic discussion has been given by Imry et al. (1982). These authors argue that for $q\xi \gg 1$, the diffusion coefficient scales as $D(\mathbf{q}, \omega) \propto q^{d-2}$.

A full renormalization group treatment for arbitrary q, ω has been carried out by Abrahams and Lee (1986). These authors discuss the scaling behavior of the density relaxation function Φ in analogy with the transverse spin correlation function of the ordinary $O(n)$ spin model below the ferromagnetic transition temperature T_c . The frequency ω and the diffusion coefficient D in the localization problem translate into the external magnetic field and the spin-stiffness constant of the spin model, respectively. It was found that the diffusion coefficient scales as

$$D(\mathbf{q}, \omega) = D^* \xi^{2-d} f(x, y), \quad (7.23)$$

with

$$x = -iN_F \omega \xi^d, \quad y = q \xi \quad (7.24)$$

and

$$D^* = \left[\left(\frac{d-2}{2} \right) N_F \right]^{-1}. \quad (7.25)$$

In the limit $v_F q \ll \omega$, Abrahams and Lee (1986) found

$$\begin{aligned} f(x, y) &= 1 + \bar{x}^{(d-2)/d}, \quad \bar{x} \gg 1, \\ &= 1 + \bar{x}^{(d-2)/2}, \quad \bar{x} \ll 1. \end{aligned} \quad (7.26)$$

where $\bar{x} = -i\omega\xi^d N_F / [(d-2)/2]$. This result is identical to the one obtained for $D(\omega)/D_0$ within the self-consistent theory (see eqs. (6.20), (6.21), (6.22)). On the other hand, in the limit $v_F q \gg \omega$ they obtained

$$f(x, y) = 1 + \left(\frac{\bar{x}}{y^{d-2} + 1} \right)^{(d-2)/2} \quad (7.27)$$

This shows that the correction term near $d = 2$ is of order $[(d-2)/2]^2 \ln y$, which is beyond the range of validity of their expansion in powers of $d-2$.

The investigation of the q -dependence of the diffusion coefficient $D(\mathbf{q}, \omega)$ has been taken up again most recently by Chalker and Nahm (1989) within the n-orbital model (Oppermann and Wegner 1979, Jüngling and Oppermann 1980). They calculated the q -dependence of $D(\mathbf{q}, \omega)$ in two dimensions in the weakly localized regime, taking into consideration all types of scattering – potential, magnetic and spin-orbit. In second-order perturbation theory, they found terms with a length-dependence proportional to $(\ln L)^2$. While such terms are known to be absent in the expression for conductivity $\sigma(\omega)$ (Gorkov et al. 1979), they appear here in the diffusion coefficient at finite q , where q and ω are small but $D_0 q^2 / \omega \gg 1$. The corrections to D were found to be proportional to $[\ln(D_0 q^2 / \omega)]^2$ for all three types of scatterings. A related behavior had been noted by Chalker et al. (1988) in a model for the quantum Hall effect; see also Chalker (1990). The above results may signal a crossover from simple diffusive behavior to a critical regime with a new type of variation of $D(\mathbf{q}, \omega)$.

8. Alternative derivations and extensions of the self-consistent theory

Self-consistent theories of Anderson localization of the type presented in the last three sections and generalizations thereof have been considered by a number of authors. The first self-consistent theory of the Anderson transition had been developed by Götze (1978, 1979, 1981a, b). It is based on a memory-function approximation for the density relaxation function, somewhat analogous to the theory of ion mobility in liquid ${}^3\text{He}$ proposed by Josephson and Lekner (1969) and discussed in detail by Wölfle et al. (1980). The theory described the

qualitative features of the Anderson transition correctly, in particular, the low-frequency behavior of the diffusion coefficient, $D(\omega) \propto -i\omega$, in the localized regime and the associated nonergodicity. However, since the derivation was not based on a systematic perturbation theory, but involved instead certain approximations motivated by the dynamical behavior of classical systems, the first version of this theory failed to take into account the contribution from quantum-interference processes, as described by the maximally crossed diagrams (Cooperons). Consequently, the theory did not contain the so-called weak localization effects discussed in section 3, which appear in lowest-order perturbation theory, and hence predicted a metal-insulator transition in two dimensions. A modification of the theory, which did find localization for arbitrarily weak disorder (Götze et al. 1979), was later shown to be incomplete and erroneous (Vollhardt and Wölfle 1980a, b). The theory was subsequently amended (Belitz et al. 1981) by adding a contribution to the current relaxation kernel to restore the time-reversal symmetry as expressed by eq. (4.16a). The same modification of Götze's theory was suggested by Prelovsek (1981). In the theory of Belitz et al. (1981), this additional contribution governs the critical behavior. The relaxation kernel thus consists of two parts: a Cooperon contribution of quantum-mechanical nature and a diffuson contribution supposed to describe classical localization. It is unclear at present whether the diffuson contribution to the current relaxation is of any importance in the usual case of short-ranged potential fluctuations. The results of a quantitative self-consistent theory using only the Cooperon mechanism (see section 10) suggest that the role of any additional contributions must be small. In the opposite case of long-ranged potential fluctuations, the situation may be different (Gold 1987).

The mode-coupling theory of the Anderson transition discussed above has also been applied to the case of off-diagonal disorder, i.e. randomly varying, hopping transition elements and a fixed energy level (Belitz and Götze 1982). Furthermore, Kotov and Sadvorskii (1983) derived the self-consistent equation (5.2) starting from the disorder model of Anderson (1958) [eq. (2.1)] and applying the diagrammatic theory discussed in section 5.

A somewhat different derivation of the self-consistent equation (5.2) has been given by Kawabata (1981). This author analyzed the diagrams of the conductivity itself and found that a self-consistent calculation of (essentially) the current relaxation function $K(\omega)$ leads to eq. (5.2). The Anderson transition in three dimensions was also discussed.

A very different derivation of the self-consistent equation [(5.2), (5.9c)] has been carried out by Hikami (1981, 1982), who followed the ideas of Wegner (1979) and mapped the disorder problem onto a nonlinear σ -model. This model is renormalizable in the sense of a perturbation theory in $\varepsilon \equiv d - 2$. The coupling constant t , which plays the role of $1/g$ in eq. (7.17), then scales according to $\partial t / \partial \ln L = \beta(t)$, where β is the so-called Gell-Mann low function and L is the system size. (Note that this definition of β differs from that in eq.

(7.17) by a factor of t .) One finds that $\beta = et - 2t^2$ up to and including terms of order t^4 . Assuming all higher-order terms to be zero, one may integrate the renormalization group equation for the two-point vertex function, i.e. the diffusion coefficient, to obtain the self-consistent equation (5.2). It is interesting to note, however, that a recent calculation of the four-loop order contribution to the β -function (Wegner 1989) yields a finite term $\propto t^5$, thus invalidating the assumption underlying Hikami's derivation of the self-consistent equation. As discussed in the concluding section 11, we should not be too surprised to find that the self-consistent theory is not exact. However, the high order in t in which the correction terms appear suggests that they are important only very close to the transition point, although a formal proof of this conjecture does not exist yet.

As discussed in section 7, a full renormalization group treatment of $D(\mathbf{q}, \omega)$ for arbitrary \mathbf{q}, ω has been performed by Abrahams and Lee (1986). In the limit $v_F q < \omega$, they derive a scaling behavior of $D(\mathbf{q}, \omega)$ which is identical to the one for $D(\omega)/D_0$ obtained within the self-consistent theory.

The self-consistent theory of localization has been generalized by Kirkpatrick (1986) to include the effect of a finite, uniform electric field on the disordered solid. In contrast to a magnetic field, which breaks time-reversal symmetry and thus removes the singularity of the Cooperon (see below), an electric field preserves this symmetry. However, it introduces a new length scale l_F corresponding to that length on which the kinetic energy acquired by the electron in the field is equal to the total energy of the electron. Due to this length, the singularities of *both* the Cooperon and the diffuson are cut off, i.e. are removed. Kirkpatrick (1986) found that for $d = 1$ the generalized self-consistent theory essentially reproduces the exact results of Prigodin (1980), who had extended the diagrammatic technique of Berezinskii (1973) to the case of a finite electric field. For weak fields, or strong disorder, there is power-law localization, while for strong fields a mobility edge appears, leading to extended states. In two and higher dimensions, where Berezinskii's method cannot be applied, Kirkpatrick (1986) found that for finite fields electronic states are always extended, i.e. localization does not occur. Clearly, in a real experiment the problem of Joule heating (Anderson et al. 1979) will invalidate the basic assumptions of the model, unless the number of charge carriers is very small and the electric field is not too large.

There have been several attempts to generalize the self-consistent theory of localization to the case of broken time-reversal invariance, as realized in the presence of an external magnetic field or magnetic impurities. Yoshioka et al. (1981) constructed a set of two coupled self-consistent equations for the diffusion coefficients associated with the poles in the particle-hole (diffuson) and particle-particle (Cooperon) channels. These channels are no longer equal in the presence of a field. (The field was assumed to be small enough to only weaken, but not completely suppress, the Cooperon.) In two dimensions all states were

found to be localized. A similar analysis was performed by Ting (1982), who obtained localization in two dimensions only for sufficiently weak magnetic fields, i.e. only if the extension of the lowest Landau orbit is much bigger than the localization length.

In the limit of a strong field, a self-consistent theory for electrons in the N th Landau level ($N \geq 0$) was worked out by Ono (1982a, b, 1983a, b, 1984). He found that all states are localized, except for state(s) in the sub-band center. The localization length was found to increase exponentially with energy as the band center of the N th sub-band was approached. It was pointed out by Benedict and Chalker (1986) that the limit of high Landau level indices ($N \rightarrow \infty$) represents a weak-localization regime specific to the integer quantum Hall effect, which can be treated exactly. Controlled calculations are possible via a $1/N$ expansion (Chalker et al. 1988). According to Carra (1987) the set of diagrams involved in a self-consistent theory for the integer quantum Hall effect can thereby be obtained in a controlled way, too. Unfortunately, subsequent work revealed that the most significant feature of the results, namely, extended states at the center of the Landau level, depends crucially on the impurity distribution and therefore is probably fortuitous (Carra et al. 1989).

The derivations of a self-consistent theory of localization for the case of broken time-reversal invariance have been faced with the problem of how to connect this theory with the correct perturbation theory for weak disorder. Once the Cooperons are suppressed by the magnetic field or magnetic impurities, localization can only be due to divergences coming from particle-hole diffusion poles. As first shown by Hikami (1981, 1982) and Oppermann (1981) in a field-theoretic approach, the conductivity acquires a logarithmic correction for $d = 2$ even in this situation. However, the prefactor is now proportional to the square of the small disorder parameter λ , i.e. perturbation theory starts one order higher than in the case of time-reversal invariance. So the correction is one order of λ smaller in this case. Nevertheless, within a renormalization group approach the lower critical dimension is still $d = 2$, i.e. states are localized in dimensions $d \leq 2$ (with a localization length even larger than for normal scattering). This implies that for $d \leq 2$, infrared divergent terms, which can only be due to diffusion poles, do exist. Hikami (1982) obtained a self-consistent equation for the diffusion coefficient $D(\omega)$ in two dimensions, even for the case of broken time-reversal invariance, by employing the same field-theoretic methods as used for systems where this invariance is intact (see the preceding discussion). He calculated the Gell-Mann low function in the coupling constant t , obtaining $\beta(t) = \epsilon t - 2t^3 + O(t^5)$, which shows that the one- and three-loop contributions vanish. Assuming that indeed all t^α -terms vanish for $\alpha > 3$, the integration of β again yields a self-consistent equation. However, its structure is quite different from that for zero magnetic field [eq. (5.2)], namely, the left-hand side factor D_0/D in eq. (5.2) is replaced by $(D_0/D)^2$ and there is an additional factor of D_0/D in the second term on the right-hand side. It is not clear how such an equation

can be derived from a purely diagrammatic theory. The recent calculation of the four-loop order correction by Wegner (1989), which yields a finite coefficient of the t^5 -term also in this case, shows that this self-consistent result cannot be exact. It should be noted, however, that the observation of the integer quantum Hall effect has been argued to indicate a breakdown of one-parameter scaling. Pruisken (1983a, b, 1988) and Levine et al. (1983) have shown this to happen within an effective field theory, where the Hall conductance appears besides the (dissipative) conductance, thus leading to two-parameter scaling. A very different aspect of the failure of one-parameter scaling, namely, a novel scaling behavior of eigenfunction correlations, has been discussed by Chalker (1988) and Chalker and Daniell (1988).

The difficulties for constructing a self-consistent theory are even greater in the case of systems with spin-orbit scattering (scattering from impurities with heavy nuclei), which leaves time-reversal invariance intact. Perturbation theory reveals a logarithmic correction to σ , the form of which is identical to the one for normal scattering (see eqs. (4.45), (4.46)), but the sign of which is *positive* (Hikami et al. 1980, Oppermann and Jüngling 1980). The conductivity therefore *increases* with decreasing frequency or temperature (*anti-localization*). A simple quantum-mechanical explanation of this effect in terms of multiple scattering (as discussed in section 3) and experimental results fully supporting this finding have been presented by Bergmann (1984). In spite of this result from lowest-order perturbation theory in the disorder, it has generally been expected that for increasing disorder the conductivity should eventually decrease, rather than become infinite, and that states should be localized in the strongly disordered regime. However, there existed no indication from perturbation theory for such a tendency for a long time. Indeed, both the two- and three-loop order corrections to the Gell-Mann low function β in the coupling constant t vanish in this case (Hikami 1982). The four-loop order result by Wegner (1989) now seems to have resolved this problem too. Exploiting the symmetry relation $\beta_{sp}(t) = -2\beta_o(-t/2)$ between the β -function for normal scattering (*orthogonal* symmetry, β_o) and spin-orbit scattering (*symplectic* symmetry, β_{sp}), he found that the finite t^5 -contribution in β_{sp} makes this β -function bend over. This suggests that there indeed exists a nontrivial fixed point in two dimensions, i.e. there is a metal-insulator transition for $d = 2$ in the case of spin-orbit scattering. Such a nonmonotonic form of β implies a very nontrivial scaling behavior. The construction of a self-consistent theory of this transition starting from perturbation theory would require the inclusion of this four-loop order contribution. This is clearly a very hard task.

There have been efforts to incorporate electron-electron interaction effects into the self-consistent theory of localization (Sadovskii 1986), in order to extend the results of Altshuler and Aronov (1979a, b, 1985) from the metallic to the insulating side. Assuming explicitly that the (one-particle) concept of localization applies to a system with interactions, Sadovskii (1986) considered the

influence of the first-order correction in the interaction within the framework of the self-consistent theory. In the case of the first-order correction, the irreducible vertex $U_{kk}(\mathbf{q}, \omega)$ does not have to be modified, i.e. the interaction does not actually enter in a self-consistent way. On the other hand, higher-order corrections in the interaction will clearly become important as one moves towards the mobility edge or to the Fermi level.

9. Application of the self-consistent theory of localization to electronic systems and classical waves

9.1. Electrons in disordered systems with a specific geometry

A two-dimensional, weakly disordered electronic system, where the disorder does not reside in the system itself, but is instead provided by a rough surface with random profile, off which the electrons scatter, has been investigated by McGurn and Maradudin (1984). Calculating $\sigma(\omega)$ and the localization length ξ by applying the self-consistent theory of localization, they found that states are always localized and $\xi \propto \exp(d^3/r^3)$. Here d is the film thickness and r is a characteristic length depending on the Fermi energy and the surface roughness. In particular, their results suggest that in this system ξ can be shorter than a typical sample size even in the case of rather weak disorder, so that one is in a strongly localized regime even in two dimensions. Similar effects can be obtained in the case of scattering of light from a rough grating (see section 9.2).

As already discussed in detail, disordered electronic systems show a very different physical behavior in dimensions $d = 1, 2$ (localization for arbitrarily small disorder) from that in $d = 3$ (existence of an Anderson localization transition). Although there exist physical structures in nature which are essentially one-dimensional (i.e. chains) or two-dimensional (i.e. layers), there always exist small perturbations and couplings which ultimately make the system three-dimensional. In view of the drastic difference between $d = 1, 2$ and $d = 3$ for disordered systems, one may then ask as to what extent interchain or interlayer coupling will change the localization properties in reduced dimensions. The existence of an Anderson transition in a weakly disordered quasi-one-dimensional system was first investigated by Prigodin and Firsov (1983) and Firsov and Prigodin (1984) making use of the self-consistent theory of localization. They found an abrupt transition from a one-dimensional dielectric to three-dimensional metallic behavior when the interchain exchange integral ω was increased above a critical value $\omega_c \sim 1/(\tau\tau_2)^{1/2}$, where $\tau^{-1} = \tau_1^{-1} + \tau_2^{-1}$, and τ_1 and τ_2 are the characteristic times for forward and backward scattering, respectively, (see also Apel and Rice 1983). A qualitatively identical, but quantitatively slightly different result was obtained by Dorokhov (1986) with a numerical calculation. By the same technique the behavior of an electron moving in a system of N parallel, coupled chains was investigated (Prigodin

et al. 1986). Such a system may be viewed as an anisotropic thin wire. For $N \rightarrow \infty$, the quasi-one-dimensional system discussed earlier is recovered.

The case of quasi-two-dimensional systems in the presence of weak disorder was investigated in a similar way (Prigodin and Firsov 1984). Since $d = 2$ is the lower critical dimension, localization is found to be destroyed already by exponentially small interlayer tunnelling, i.e. for $\omega > \omega_c \sim \exp(-E_F\tau/\hbar)$. An observation of two-dimensional behavior therefore requires highly anisotropic layered materials.

The low-temperature dependence of the hopping conductivity $\sigma(T)$ in a two-dimensional weakly disordered system was investigated by Gogolin and Zimanyi (1983). Taking the low-frequency behavior of $\sigma(\omega)$ from the self-consistent theory and making the substitution $\omega \rightarrow i/\tau_{in}(T)$, these authors found a power-law behavior $\sigma(T) \propto T^n$, bridging the logarithmic T -dependence of weak localization and the exponential behavior due to variable range hopping (Mott 1968).

9.2. Localization of classical waves and other wave-like entities moving in a random medium

As discussed in section 3, the effects of weak localization are a consequence of the coherent wave interference on time-reversed paths, described diagrammatically by the Cooperons. Therefore, these effects are expected to be relevant to any kind of wave propagation in a static random medium, irrespective of whether the waves have a quantum-mechanical origin (as in the case of electrons), or whether they are classical (e.g. electromagnetic or acoustic waves). In particular, making use of field-theoretic methods developed earlier for the investigation of electron localization, John et al. (1983) studied the critical behavior of phonons in a disordered elastic medium. They found that all finite-frequency states are localized in dimensions $d \leq 2$ and that there exists a *phonon mobility edge* at $d > 2$. (The modes with $\omega = 0$ must always be extended, because this corresponds to a uniform translation of the whole system.) Similarly, John (1984, 1987) studied the critical behavior of electromagnetic absorption in a disordered medium, i.e. the *photon mobility edge*. Anderson (1985) discussed several more examples of localization phenomena involving classical waves. Since then there have been numerous theoretical (but only very few experimental) investigations of the localization of such wave-like entities.

Localization of electromagnetic waves due to randomness has been studied by several groups using the self-consistent theory of localization. McGurn et al. (1985) used this theory to calculate the resonant scattering of light from surface polaritons on a randomly rough dielectric grating (see also Celli et al. 1985). These surface polaritons are localized due to the surface roughness, i.e. they are no longer propagating surface excitations. These effects should be observable in the angular dependence of the light scattered nonspecularly from the grating.

Similarly, the localization of a surface plasmon polariton parallel to a metal surface, caused by scattering on the rough surface, has also been studied (Arya et al. 1985). Localization effects should be observable in surface-enhanced experiments; they are expected to be appreciable only if radiative losses are small, i.e. they will occur only in a certain frequency-range. Localization of the exciton-polariton (a mixed mode of a photon and an exciton) in semiconductors containing randomly distributed metallic spheres, has been discussed by Cheng et al. (1988). They conclude that the condition for strong localization may be satisfied in such a system and that the effects may be observable in optical absorption experiments. The observability of optical localization was analyzed by Condat and Kirkpatrick (1987). They obtained a phase diagram which suggests that the sudden onset of localization should not be very far from the values of scatterer densities used in weak-localization experiments (van Albada and Lagendijk 1985, Wolf and Maret 1985). Related investigations have been performed by Schmeltzer and Kaveh (1987); for a review see Kaveh (1987).

As mentioned in the beginning of this section, localization of sound waves (phonons) in a disordered medium in dimensions $d = 2$ and 3 has been a subject of considerable interest. Apart from a theoretical treatment of weak-localization effects (Akkermans and Maynard 1985a, b, Akkermans et al. 1986), there have been numerous investigations of the critical properties near the phonon mobility edge, which were initiated by John et al. (1983).

Making use of the self-consistent theory of localization Kirkpatrick (1985) studied the localization of sound waves moving in a random array of hard scatterers in two and three dimensions. While for $d = 2$ acoustic waves were found to be localized for all frequencies, for $d = 3$ they were found to be localized only between an intermediate and a high-frequency mobility edge. It has been proposed that one might employ third sound (i.e. surface waves in a superfluid, such as He-II) on a randomly disordered substrate to study localization in two dimensions (Cohen and Machta 1985) or in one dimension (Condat and Kirkpatrick 1985a, b, 1986). By imposing a uniform flow onto this system, time-reversal invariance is broken. Thereby, the mechanism of localization is changed as in the electronic counterpart (see section 8). The crossover in the critical behavior induced by the flow field has been described by Cohen et al. (1987) within a field-theoretic approach. The influence of the flow for one-dimensional systems has been investigated by Condat et al. (1987) using the formalism of Berezinskii (1973); they found that localization was not essentially modified by the flow in this case. The observability of acoustical localization by random arrays of scatterers was analyzed by Condat and Kirkpatrick (1987). Employing the self-consistent theory of localization they concluded that in three dimensions acoustic localization would not be observable unless the scatterers are more efficient than hard spheres. The same approach has been used to study scalar-wave localization in a two-component composite (Sheng and Zhang 1986). Localization was shown to occur only above a critical impedance

contrast of the medium (i.e. ratio of the indices of refraction of the two components). Besides that, it was found that localization is closely related to resonant scattering, leading to a series of mobility edges and, hence, localization regions.

A very different system was investigated by Igarashi (1987), who addressed the problem of Anderson localization of spin waves in Heisenberg antiferromagnets with random uniaxial anisotropy energy and random exchange interaction. Since the longitudinal spin correlation function is governed by diffusive motion at small q, ω , its evaluation may be related to the localization problem. An estimate of the quantum fluctuations reveals that they are unimportant for diffusive motion. Accordingly, it was found that the most important diagrams of the theory are the same as those in the self-consistent theory of electron localization. Thereby he found that in the presence of a random anisotropy energy spin waves are localized in the long wavelength limit, and that there is a mobility edge in the vicinity of the bottom of the spin wave band. Igarashi (1987) stressed in particular that the localization will also strongly affect the transverse spin-correlation function.

10. Self-consistent theory of the tight-binding model with site-diagonal disorder

In solid state theory, the most suitable formulation of a model of noninteracting electrons in a strongly disordered solid is expected to be the one using Wannier functions $|i\rangle$ located at lattice sites \mathbf{R}_i , with transition matrix elements t_{ij} for hopping of electrons from \mathbf{R}_i to \mathbf{R}_j and with random diagonal elements V_i (see eq. (2.1))

$$H = \sum_{i,j} t_{ij} |i\rangle \langle j| + \sum_i V_i |i\rangle \langle i|. \quad (10.1)$$

To simplify things further, one may restrict the possible hopping processes to nearest-neighbor sites, i.e. to $t_{ij} = t\delta_{ii+\delta}$, where δ labels the nearest-neighbor sites on a hypercubic lattice. The site energies V_i are assumed to be distributed according to a probability distribution $P(V_i)$. Typical distributions are given by the box distribution (2.2) or the Gaussian distribution (2.3). In both cases, W is the width of the distribution and is the single parameter characterizing the disorder in these models. The model (10.1) with the random distribution (2.2) was considered by Anderson in his seminal paper (Anderson 1958).

The above models lend themselves more readily to numerical diagonalization for finite-size lattices than do the continuum models discussed before. In fact, there are a number of results available on quasi-one-dimensional systems of sizes up to $(3 \times 10^5) \times 13 \times 13$ lattice sites (MacKinnon and Kramer 1981, 1982, 1983, MacKinnon 1982, Sak and Kramer 1981, Pichard and Sarma

1981a, b, Soukoulis et al. 1982, Zdetsis et al. 1985, Bulka et al. 1987, Soukoulis et al. 1987). These authors determined the localization length and (with an additional assumption for $d = 3$) the conductivity by a real-space scaling procedure with respect to the dimensions perpendicular to the axis of the quasi-one-dimensional sample rods. The results constitute important “experimental data” against which one may test theoretical results. A quantitative comparison of the self-consistent theory described in the preceding sections with these data is hampered by the fact that the noncritical quantities (e.g. the density of states and the coupling constant in the self-consistent equation) have not been calculated quantitatively within that theory, although this is easily done for the density of states by employing the coherent-potential approximation, i.e. CPA (Soven 1967). There remain two questions: (i) What is the precise structure of the self-consistent theory in the strong coupling regime? (ii) How does one calculate the equivalent of the bare diffusion constant D_0 and of the coupling constant λ ?

These questions have been addressed in a qualitative way by connecting the self-consistent theory to the problem of a quantum-mechanical bound state in a potential well (Economou and Soukoulis 1983, Economou et al. 1984, Soukoulis et al. 1986). This connection is established by observing that the self-consistent equation for $D(\omega)$ [eqs. (5.2), (5.9c)] in the localized regime, i.e. for $\lim_{\omega \rightarrow 0} D(\omega) = -i\omega\xi^2$, where ξ is the localization length, takes the form

$$\pi D_0 N_F = \sum_{Q, Q < Q_c} \frac{1}{Q^2 + \xi^{-2}}; \quad (10.2)$$

for a scaled version of this equation see eq. (6.3). Equation (10.2) is reminiscent of the Schrödinger equation for a particle of mass m^* in a potential well of depth $V_0 (> 0)$,

$$\frac{1}{|V_0|} = \frac{2m^*}{\hbar^2} \sum_k \frac{1}{k^2 + k_b^2}, \quad (10.3)$$

where k_b^{-1} is the extension of a bound state located at the well. The following picture is suggested: localization is a property associated with the state of a single particle in an average potential well of depth $|V_0| = \hbar/(2\pi m^* N_F D_0)$. Thus, the depth of the potential well is determined by noncritical quantities, such as D_0 , N_F and m^* , which may be evaluated in effective medium approximation (CPA). Note that a quantum-mechanical particle is always bound to a potential well in dimensions $d = 1, 2$, which explains the absence of extended states for $d \leq 2$ in this picture. In three dimensions the potential well needs to be sufficiently attractive for a particle to be bound, which explains that a localization transition takes place at a critical value of $N(E)$ and $D_0(E)$. By calculating $N(E)$ and $D_0(E)$ within CPA and adjusting the cutoff parameters in the original self-consistent theory suitably, the above-mentioned authors find a phase boundary separating metallic and insulating regions for the model (10.1) – a

result which is in reasonable agreement with numerical data. The values for the localization length and the conductivity obtained in this model are also in qualitative agreement with the computer data.

A complete (within the limits of the self-consistent theory) derivation of a self-consistent equation for the diffusion coefficient, where all the noncritical quantities are expressed in terms of the single-site approximation (CPA) has been given recently (Kroha et al. 1990, Kroha 1990). This version of the self-consistent theory was partly developed earlier by Kopp (1984a, b). These authors chose to use the locator formalism (originally introduced by Anderson (1958)) rather than the propagator formalism discussed in the previous sections, because it appears to be better adapted to the strong localization limit. The locator formalism may also be expected to give a more accurate description near the localization transition. However, an equivalent representation within the propagator formalism also exists (Kroha 1990). In what follows, we present the discussion given by Kroha et al. (1990).

10.1. Locator expansion

A single locator \hat{g}_n is defined as the atomic Green's function at site n :

$$\hat{g}_n^{R/A}(E) = \frac{1}{E - V_n \pm i0}, \quad (10.4)$$

where R/A refers to the retarded/advanced Green's function. The full single-particle Green's function $\hat{G}_{nm}(E)$ may be expanded in powers of the hopping matrix element as

$$\begin{aligned} \hat{G}_{nm}^R(E) &= \left\langle n \left| \frac{1}{E - H + i0} \right| m \right\rangle \\ &= \hat{g}_n^R \left\{ \delta_{nm} + \left[t_{nm} + \sum_l t_{nl} \hat{g}_l^R t_{lm} + \dots \right] \hat{g}_m^R \right\}. \end{aligned} \quad (10.5)$$

Each term in this series can be represented by a diagram consisting of propagator lines for t and locator lines attached to their endpoints, labelled by a given site (see fig. 18).

As before, we are interested in the one- and two-particle Green's functions averaged over the energy level distribution $P(V_n)$, e.g.

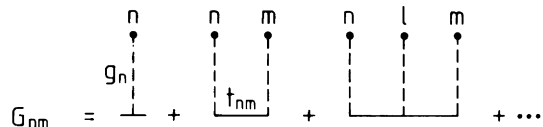


Fig. 18. Locator expansion of the unaveraged Green's function.

$$\begin{aligned} G(E) &\equiv \langle \hat{G}(E) \rangle \\ &= \int \prod_n [dV_n P(V_n)] \hat{G}(E). \end{aligned} \quad (10.6)$$

Using the expansion (10.5), $G(E)$ may be calculated in terms of averaged locator products (Matsubara and Toyozawa 1961, Aiyer et al. 1969)

$$\langle (\hat{g}_n^R)^k \rangle = \int dV_n P(V_n) (\hat{g}_n^R)^k. \quad (10.7)$$

Diagrammatically, $\langle (\hat{g}_n^R)^k \rangle$ is represented by connecting k locator lines to the common endpoint labelled n . The first few terms of the perturbation series for $\langle G_{nm} \rangle$ are shown in fig. 19.

It is useful to introduce a quantity S_{nm} as the sum of all one-particle irreducible diagrams with respect to cutting a t -line (fig. 20). Then, G satisfies the Dyson equation

$$G = S + StG, \quad (10.8)$$

where G, S, t are matrices in the site variables. Furthermore, one introduces a renormalized hopping matrix by

$$T = t + tGt, \quad (10.9)$$

where T satisfies the Dyson equation

$$T = t + tST. \quad (10.10)$$

T will be represented diagrammatically by a double line (fig. 21). The averaged Green's function may be represented in terms of S and T as

$$G = S + STS. \quad (10.11)$$

$$\begin{aligned} \langle g \rangle &= \text{---} + \text{---} + \text{---} + \dots \\ \langle G_{nm} \rangle &= \text{---} + \text{---} + \text{---} + \dots \end{aligned}$$

Fig. 19. Locator expansion of the averaged Green's function.

$$\begin{aligned} S_{nm} &= \text{---} + \text{---} + \text{---} + \dots \end{aligned}$$

Fig. 20. Diagrammatic definition of S_{nm} .

$$T_{nm} = \dots - \overbrace{\hspace{1cm}}^{\text{---}} + \overbrace{\hspace{1cm}}^{\overset{n}{\leftarrow} \overset{m}{\leftarrow}} + \overbrace{\hspace{1cm}}^{\overset{l}{\leftarrow} \overset{n}{\leftarrow} \overset{m}{\leftarrow}} + \dots$$

Fig. 21. Renormalized hopping element T_{nm} .

All the averaged quantities defined above are translation-invariant matrices in the site labels, i.e. $G = G_{mn} = G_{n-m}$, and may be diagonalized by a Fourier transform. One obtains for the retarded Green's function

$$G_k^R(E) = \frac{1}{E - \varepsilon_k - \Sigma_k^R(E)}, \quad (10.12)$$

where ε_k are the Bloch energies and Σ_k is the self-energy given by

$$\Sigma_k^R(E) = E - \frac{1}{S_k^R(E)}. \quad (10.13)$$

It is well known (Aiyyer et al. 1969) that the summation of higher-order contributions, or even of infinite orders in perturbation theory, within the locator expansion poses a technical difficulty which is peculiar to all lattice models: in any given diagram locators belonging to the same site are connected at the same point, but all these locator endpoints correspond to different sites. One may still sum internally over all lattice sites, provided the overcounted contributions are subtracted. The formal procedure by which these so-called *multiple occupancy corrections* or MOCs are determined is sketched in fig. 22. MOC diagrams for any given diagram are generated by successively breaking apart locator lines ending at a common site.

With the help of these definitions and rules, the self-resolvent S may be calculated in the single-site (or CPA) approximation, by summing all diagrams contributing to S involving only one site and subtracting all the MOCs. The result is the self-consistent CPA equation (Leath 1970)

$$\left\langle \frac{\hat{g}_0^R - S_0^R}{1 - (\hat{g}_0^R - S_0^R) T_0^R} \right\rangle = 0. \quad (10.14)$$

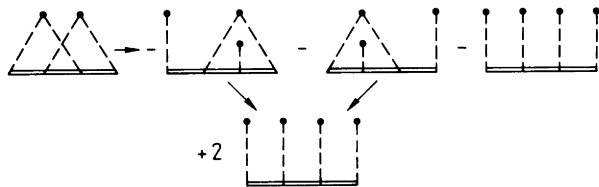


Fig. 22. Construction of multiple occupancy corrections (MOCs).

This equation can be solved numerically for $S_0^R(E)$. The density of states may then be calculated from

$$N(E) = -\frac{1}{\pi} \sum_{\mathbf{k}} \text{Im } G_{\mathbf{k}}^R(E), \quad (10.15)$$

where the \mathbf{k} -summation extends over momenta in the first Brillouin zone. With the bare energy values $\varepsilon_{\mathbf{k}} = 2t \sum_{i=1}^d \cos k_i a$, where a is the lattice constant and k_i are the components of the momentum vector, one finds for the box distribution the density of states shown in fig. 23. Also shown in this figure are the results of the numerical diagonalization of Bulka et al. (1987). As expected, the agreement is good.

As discussed in section 4, the averaged single-particle Green's function does not contain the relevant information about the localization transition. In order to calculate the conductivity or the diffusion coefficient one needs to consider two-particle properties, in particular the averaged product $\langle G^R G^A \rangle$.

It is useful to first discuss a simple approximation for this quantity, the generalization of the ladder approximation (4.36). The ladder consists of a series of bare vertex functions I_0 joined by particle-hole propagators in coherent potential approximation (fig. 24). The bare vertex is defined as the complete

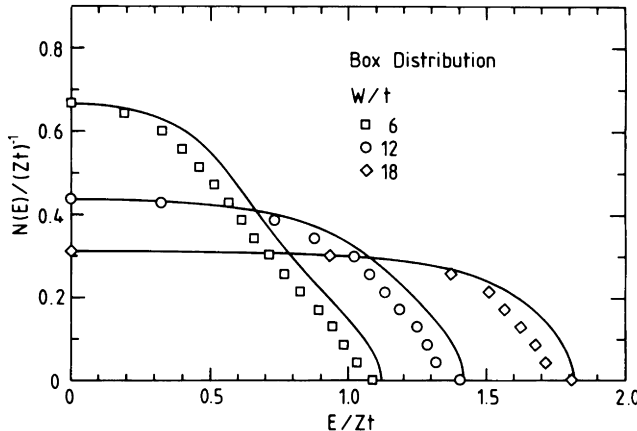


Fig. 23. Density of states in CPA for the box-shaped level distribution. [After Kroha (1990); data points taken from Bulka et al. (1987).]

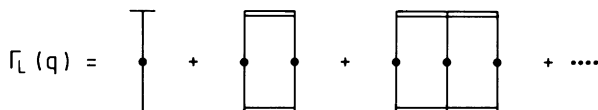


Fig. 24. Sum of ladder diagrams Γ_L .

0	1	2
\vdots		

Fig. 25. Diagrammatic definition of the bare vertex I_0 including MOCs.

single-site vertex, i.e. the sum of all locator ‘‘stars’’, with the appropriate MOCs (see fig. 25). The resulting expression is given by (Kopp 1984a)

$$I_0(\omega) = \frac{S_0^A - S_0^R - \omega S_0^R S_0^A}{\omega(1 + T_0^R S_0^R + T_0^A S_0^A) + T_0^A - T_0^R}. \quad (10.16)$$

Later we will need a slightly different quantity, the vertex \tilde{I}_0 , which is identical to I_0 except that MOCs at the external point on the right-hand side are not included. One finds (Kopp 1984a)

$$\tilde{I}_0(\omega) = \frac{G_0^A - G_0^R}{\omega(1 + T_0^R S_0^R + T_0^A S_0^A) + T_0^A - T_0^R}. \quad (10.17)$$

The sum of the ladder diagrams (fig. 24) is easily obtained as

$$\Gamma_L(\mathbf{q}, \omega) = \frac{I_0}{1 - I_0 \sum_k T_{k+}^R T_{k-}^A}. \quad (10.18)$$

In the limit $\omega, q \rightarrow 0$, the denominator of eq. (10.18) may be cast into the form of a diffusion pole (Kopp 1984a)

$$\Gamma_L(\mathbf{q}, \omega) = \frac{(I_0)^2 (T_0^A - T_0^R)/\tilde{I}_0}{\omega + iD_0 q^2}, \quad (10.19)$$

with the bare diffusion constant

$$D_0 = \frac{1}{\pi N(E_F)} \frac{1}{N} \sum_k (\mathbf{v}_k \cdot \hat{\mathbf{q}})^2 (\text{Im } G_k^A(E))^2, \quad (10.20)$$

where

$$\mathbf{v}_k = \nabla_k \epsilon_k \quad (10.21)$$

is the bare velocity of the tight-binding band. Expression (10.19) contains all MOCs, in particular those from the left and right endpoints of the diagrams. This is appropriate if Γ_L is used as a building block in another diagram, such that all four end-points are summed over without further constraints. If, on the other hand, we were to calculate the density correlation function Φ directly from Γ_L , the pairs of endpoints on the left and on the right are connected to the same site and MOCs involving separate endpoints do not occur. In this case, the renormalized locator pairs at the ends of the diagrams should be replaced by \tilde{I}_0 , i.e. eq. (10.19) has to be multiplied by the factor $(\tilde{I}_0/I_0)^2$. Note that the numerator of eq. (10.19) modified in this way reduces to the density of states $N(E)$ for $\omega \rightarrow 0$, as it should.

The quantity $\Gamma_L(\mathbf{q}, \omega)$ is obviously the counterpart of the diffuson defined in eq. (4.38) in the locator expansion. Similarly, the sum of all maximally crossed diagrams is given from the relation (4.39) by

$$\bar{\Lambda}_{kk'}^0(\mathbf{q}, \omega) = \Gamma_L(\mathbf{k} + \mathbf{k}', \omega). \quad (10.22)$$

At this point it is very helpful to note the existence of a kind of gauge symmetry in the locator expansion. Consider a shift in the zero of energy such that $\epsilon_k \rightarrow \epsilon_k + E_0$ and simultaneously $E \rightarrow E + E_0$. Obviously, all observable quantities, such as $G_k(E)$ (or rather the density of states $N(E)$) and the diffusion coefficient $D(\omega)$, must be invariant under this transformation. Indeed, $N(E)$ and D_0 as given by eqs. (10.17) and (10.22) possess this property. On the other hand, quantities like S_0 or I_0, \tilde{I}_0 need not be invariant and, in fact, inspection of eqs. (10.16) and (10.18), (10.19) shows that they are not! The transformation law for S_0 is $S_0^{-1} \rightarrow S_0^{-1} + E_0$. In any gauge-invariant formulation of the theory, the choice of E_0 must be irrelevant in the end. One may use the freedom of choice of E_0 to one's advantage, if it happens that in a certain limit things become simpler. As is shown later, this is indeed the case in the limit $E_0 \rightarrow \infty$, where certain "vertex corrections" simplify considerably.

10.2. Derivation of the self-consistent equation for the diffusion coefficient

In analogy with the derivation of eq. (4.20) for the correlation function $\Phi_{kk'}(\mathbf{q}, \omega)$ defined by eq. (4.10), one may show that within the locator formalism $\Phi_k = \sum_{k'} \Phi_{kk'}$ satisfies the equation (Kopp 1984a)

$$\begin{aligned} & ((G_{k+}^R)^{-1} - (G_{k-}^A)^{-1}) S_{k+}^R S_{k-}^A \Phi_k(\mathbf{q}, \omega) \\ &= (G_{k-}^A - G_{k+}^R) \left\{ \tilde{I}_k + \sum_p I_{kp} \epsilon_{p+} \epsilon_{p-} \Phi_p(\mathbf{q}, \omega) \right\}, \end{aligned} \quad (10.23)$$

where I_{kp} is the irreducible vertex function. By definition I_{kp} does not contain

diagrams which can be separated in two by cutting a particle-hole propagator pair $T_{\mathbf{p}_+}^{\text{R}} T_{\mathbf{p}_-}^{\text{A}}$. The quantity $\tilde{I}_{\mathbf{k}}$ is defined as $\tilde{I}_{\mathbf{k}} = \sum_{\mathbf{k}'} [I_{\mathbf{k}\mathbf{k}'} - (\text{MOC at end point})]$. The irreducible vertex part satisfies the following Ward identity (Kopp 1984a)

$$S_{\mathbf{k}_+}^{\text{R}}(E + \omega) - S_{\mathbf{k}_-}^{\text{A}}(E) = \sum_{\mathbf{p}} \{ I_{\mathbf{k}\mathbf{p}}(\mathbf{q}) [T_{\mathbf{p}_+}^{\text{R}}(E + \omega) - T_{\mathbf{p}_-}^{\text{A}}(E)] - \omega \tilde{I}_{\mathbf{k}\mathbf{p}} \}, \quad (10.24)$$

which is the analog of the Ward identity (4.23) in the propagator formalism.

One can solve the integral equation (10.23) approximately in the limit of small ω, q by employing the same strategy as in section 4. In the hydrodynamic limit, the dominant components of $\Phi_{\mathbf{k}}$ are given by the density and current density response functions $\Phi(\mathbf{q}, \omega)$ and $\Phi_j(\mathbf{q}, \omega)$ as defined in eqs. (4.11b) and (4.22a). One may therefore expand $\Phi_{\mathbf{k}}$ in terms of these quantities as

$$\Phi_{\mathbf{k}}(\mathbf{q}, \omega) = A_{\mathbf{k}} \Phi(\mathbf{q}, \omega) + B_{\mathbf{k}}(\mathbf{q}) \Phi_j(\mathbf{q}, \omega). \quad (10.25)$$

The expansion coefficients $A_{\mathbf{k}}$ and $B_{\mathbf{k}}$ are determined by comparison with the explicitly given result for the ladder approximation discussed earlier. Using eq. (10.18) we find

$$\Phi_{\mathbf{k}}^{(\text{L})}(\mathbf{q}, \omega) = \frac{T_{\mathbf{k}_+}^{\text{R}} T_{\mathbf{k}_-}^{\text{A}}}{\varepsilon_{\mathbf{k}_+} \varepsilon_{\mathbf{k}_-}} \Gamma_{\text{L}}(\mathbf{q}) \frac{\tilde{I}_0}{I_0}, \quad (10.26)$$

$$\Phi^{(\text{L})}(\mathbf{q}) = \Gamma_{\text{L}}(\mathbf{q}) \left(\frac{\tilde{I}_0}{I_0} \right)^2, \quad (10.27)$$

$$\Phi_j^{(\text{L})}(\mathbf{q}) = \Gamma_{\text{L}}(\mathbf{q}) \frac{\tilde{I}_0}{I_0} \sum_{\mathbf{p}} (\mathbf{v}_{\mathbf{p}} \cdot \hat{\mathbf{q}}) \frac{T_{\mathbf{p}_+}^{\text{R}} T_{\mathbf{p}_-}^{\text{A}}}{\varepsilon_{\mathbf{p}_+} \varepsilon_{\mathbf{p}_-}}, \quad (10.28)$$

and from here, after expanding in \mathbf{q} and ω (Kopp 1984b),

$$A_{\mathbf{k}} = \frac{\text{Im } G_{\mathbf{k}}^{\text{A}}}{\sum_{\mathbf{p}} \text{Im } G_{\mathbf{p}}^{\text{A}}}, \quad (10.29)$$

$$B_{\mathbf{k}}(\mathbf{q}) = \frac{(\mathbf{v}_{\mathbf{k}} \cdot \hat{\mathbf{q}}) (\text{Im } G_{\mathbf{k}}^{\text{A}})^2}{\sum_{\mathbf{p}} (\mathbf{v}_{\mathbf{p}} \cdot \hat{\mathbf{q}})^2 (\text{Im } G_{\mathbf{p}}^{\text{A}})^2}. \quad (10.30)$$

Summing eq. (10.23) over \mathbf{k} and using the Ward identity (10.24), one derives the continuity equation (4.21)

$$\omega \Phi(\mathbf{q}, \omega) - q \Phi_j(\mathbf{q}, \omega) = 2\pi i N(E_{\text{F}}). \quad (10.31)$$

Multiplying eq. (10.23) by $\mathbf{v}_{\mathbf{k}} \cdot \hat{\mathbf{q}}$ and summing over \mathbf{k} , one obtains using eq. (10.24)

$$qL\Phi + M\Phi_j = qR, \quad (10.32)$$

with

$$L = \sum_{\mathbf{p}} (\mathbf{v}_{\mathbf{k}} \cdot \hat{\mathbf{q}}) \frac{1}{q} \Delta G^{-1} \left[S_{\mathbf{k}_+}^{\text{R}} S_{\mathbf{k}_-}^{\text{A}} A_{\mathbf{k}} - G_{\mathbf{k}_+}^{\text{R}} G_{\mathbf{k}_-}^{\text{A}} \sum_{\mathbf{p}} I_{\mathbf{k}\mathbf{p}} \varepsilon_{\mathbf{p}_+} \varepsilon_{\mathbf{p}_-} A_{\mathbf{p}} \right], \quad (10.33a)$$

$$M = \sum_k (\mathbf{v}_k \cdot \hat{\mathbf{q}}) \Delta G^{-1} \left[S_{k_+}^R S_{k_-}^A B_k - G_{k_+}^R G_{k_-}^A \sum_p I_{kp} \epsilon_{p_+} \epsilon_{p_-} B_p \right], \quad (10.33b)$$

$$R = \frac{1}{q} \sum_k (\mathbf{v}_k \cdot \hat{\mathbf{q}}) \Delta G \tilde{I}_k, \quad (10.33c)$$

where $\Delta G^{-1} = (G_{k_+}^R)^{-1} - (G_{k_-}^A)^{-1}$ and $\Delta G = G_{k_-}^A - G_{k_+}^R$.

From eqs. (10.31) and (10.32) the density relaxation function Φ and the density response function χ are calculated as

$$\Phi(\mathbf{q}, \omega) = \frac{2\pi i N(E_F) M + q^2 R}{\omega M + q^2 L} \quad (10.34)$$

and

$$\chi(\mathbf{q}, \omega) = \frac{q^2 L N(E_F)}{\omega M + q^2 L}. \quad (10.35)$$

Using eq. (4.32), the dynamical conductivity follows:

$$\sigma(\omega) = -i e^2 N(E_F) \frac{L(\omega)}{M(\omega)}, \quad (10.36)$$

and the diffusion coefficient is given by

$$D(\omega) = -i \frac{L(\omega)}{M(\omega)}. \quad (10.37)$$

Using the Ward identity (10.24) one may show that

$$L(\omega) = -i \frac{S_0^A - S_0^R}{\text{Im } G_0^A} \sum_p (\mathbf{v}_p \cdot \hat{\mathbf{q}})^2 \epsilon_p^2 (\text{Im } G_p^A)^2 + O(\omega), \quad (10.38)$$

i.e. $L(\omega)$ is expressible in terms of single-particle quantities.

It remains to calculate $M(\omega)$, which requires an approximation for the irreducible vertex I_{kp} . Following the arguments presented in section 5 one may again classify all diagrams of I_{kp} according to the number of Cooperons \tilde{A}_{kp}^0 (see eq. (10.21)) running diagonally across a diagram. Again, the dominant contribution is given by the block of diagrams enclosed by two diagonally crossing Cooperons (see fig. 16). In section 5 we were able to conclude that these diagrams add up to the complete density relaxation function $\Phi(\mathbf{q}, \omega)$. The same conclusion is essentially correct here, except for the fact that the diagrams for $\Phi(\mathbf{q}, \omega)$ have different MOCs at the endpoints associated with them, compared to $I_{kk'}$. In the case of the ladder approximation (10.18) we were able to explicitly account for the difference in the MOCs. In the general case this is not possible, because these corrections will have an exceedingly complex momentum dependence for diagrams in which locators reach from the endpoint deep into the interior of the diagram. Fortunately, in this situation we can make use of the

gauge transformation discussed in the text following eq. (10.22). It may be shown that in the limit $E_0 \rightarrow \infty$ (renormalized) locator pairs I_0 at the endpoints give the leading contribution, all other diagrams being smaller by factors of $1/E_0$. The relation of $I_{kk'}$ and Φ is thus given by

$$I_{kk'} = \lim_{E_0 \rightarrow \infty} \left(\frac{I_0}{\tilde{I}_0} \right)^2 \Phi(\mathbf{q}, \omega), \quad (10.39)$$

with I_0 and \tilde{I}_0 given by eqs. (10.16) and (10.17).

Substituting into the definition (10.33b) of M , one obtains the self-consistent equation for the diffusion coefficient $D(\omega)$ from eq. (10.38) in the form

$$D(\omega) = D_0 + \lambda_{sc} \sum_{k, k'} (\mathbf{v}_k \cdot \mathbf{q}) \frac{\text{Im } G_k^A (\text{Im } G_k^A)^2}{(\mathbf{k} + \mathbf{k}')^2 - i\omega/D(\omega)} (\mathbf{v}_{k'} \cdot \mathbf{q}), \quad (10.40)$$

where

$$\lambda_{sc} = 2 \text{Im } \Sigma^A / [\pi^2 N^2(E) D_0]. \quad (10.41)$$

In eq. (10.40) the momentum sums are taken to extend over the first Brillouin zone. This is appropriate in the limit of strong localization, when the mean free path is of the order of the Fermi wavelength, which in turn is comparable to the lattice constant (except very close to the band edge). For weak localization, the diffusion-pole structure of $\Phi(\mathbf{q}, \omega)$ is strictly applicable only in the momentum regime $q \gtrsim 1/l$, where l is the mean free path. We shall neglect the small corrections introduced by the cutoff in the following.

Equation (10.40) should be compared with the self-consistent equation [(5.2), (5.9c)] derived in section 5. The structure of both these equations is very similar, except for an additional factor of $\text{Im } G_k^A$ in eq. (10.40). The coupling constant λ_{sc} defined by eq. (10.41) is expressed in terms of single-particle quantities, which are calculated in the single-site approximation (CPA). The Green's function G_k^A , the self-energy Σ^A , the density of states $N(E)$ and the bare diffusion constant D_0 are given by eqs. (10.12–10.15). In the limit of weak disorder and for energies near the band center, eq. (10.40) reduces to the result (5.2), with the following identifications (for definiteness we assume a box-shaped distribution of energy levels as defined by eq. (2.3)):

$$\Sigma^A(E) = \frac{1}{12} E G_0^A(E) (W/E)^2, \quad (10.42a)$$

$$D_0(E) = (1/d) \tau \bar{v}_F^2, \quad (10.42b)$$

where

$$\frac{1}{\tau} = 2 \text{Im } \Sigma^A \quad (10.42c)$$

and

$$\bar{v}_F^2 = \Sigma_k \mathbf{v}_k^2 \delta(\varepsilon_k - E_F). \quad (10.42d)$$

10.3. Results of a numerical evaluation of the self-consistent equation

The self-consistent equation (10.40) for $D(\omega)$, with $\text{Im } \Sigma^A$ and $\text{Im } G^A$ determined from eqs. (10.12–10.14) and D_0 given by eq. (10.20), has been solved numerically by Kroha et al. (1990) and Kroha (1990). In this evaluation the two d -dimensional momentum integrals in eq. (10.40) were approximated using the isotropic energy-momentum relation $N_0(\varepsilon_k) = 4\pi k^2 |\text{dk}/\text{d}\varepsilon_k|/(2\pi)^d$, with $N_0(E)$ given by eq. (10.43). In three dimensions they found a metal-insulator phase transition along a line in the (W, E) -plane. This is shown in fig. 26 for the box-shaped distribution and in fig. 27 for the Gaussian distribution. The agreement with the exact numerical diagonalization results of Bulka et al. (1987) (shown as data points in figs. 26, 27) is very good, considering that the theory is *free* of adjustable parameters. In particular, the reentrant behavior near the band edge is nicely reproduced. For weak disorder the phase boundary is seen to follow the CPA band edge. (Note that Bulka et al. (1987) defined the band edge as the energy where $N(E) = 2.5 \times 10^{-3} N(0)$). This is a consequence of the fact that for the energy E near the band edge the density of states and hence, the effective hopping probability increases with increasing disorder. The qualitative shape of the phase boundary had been discussed previously by several authors (Prelovsek 1981, Kotov and Sadovskii 1983, Economou and Soukoulis 1983, Zdetsis et al. 1985, Dersch and Thomas 1985). The good agreement of the above self-consistent theory with the numerical data suggests that the quantum-interference effect, believed to cause localization in the band center as discussed

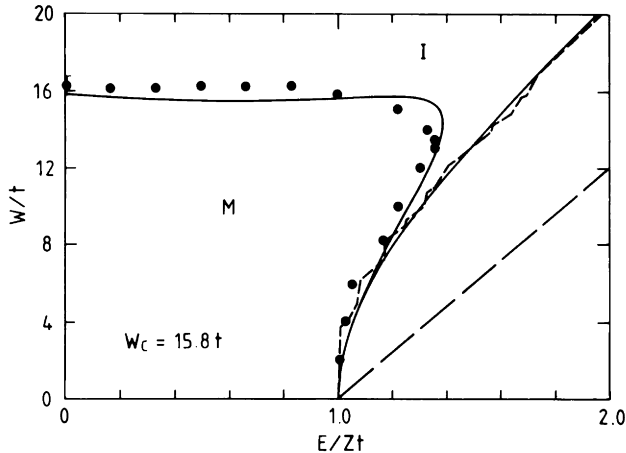


Fig. 26. Phase diagram in the (W, E) -plane for the box-shaped level distribution showing metal (M) and insulator (I) regions: phase boundary curve after Kroha et al. (1990), data points from Bulka et al. (1987). Also shown is the band edge: exact (— — —), numerical data (---), CPA (—).

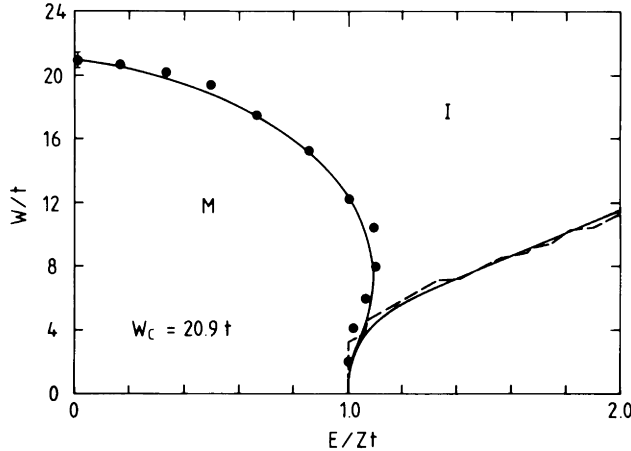


Fig. 27. Phase diagram in the (W, E) -plane for the Gaussian level distribution showing metal (M) and insulator (I) regions: phase boundary curve after Kroha (1990), data points from Bulka et al. (1987). Also shown is the band edge: numerical data (---), CPA (—).

at length in section 6, is responsible for localization near the band edges as well. This is in contrast to a conjecture put forward by Bulka et al. (1987) that near the band edges a different type of localization mechanism, the so-called potential localization, is operative. The latter mechanism is based on the occurrence of large and deep potential-well configurations, which should be more important for electrons at low energy.

The localization length has also been calculated from eq. (10.40). For the box-shaped distribution and for energy $E = 0$, the result is shown in fig. 28 together with the numerical results of Bulka et al. (1987). Again, the agreement is good, in particular in dimensions one and two. In three dimensions, the comparison is more difficult as the choice of the critical value W_c of the disorder is crucial. The value used in fig. 28 is $W_c = 16.2$ for the numerical data and $W_c = 15.8$ for the theoretical curve. Naturally, the scaling procedure employed in the numerical work is less reliable in higher dimensions. According to fig. 28, a crossover from weak-coupling to strong-coupling behavior takes place at $W/t \sim 10$ for $d = 1, 2$ and $(W - W_c)/t \sim 10$ for $d = 3$. The dependence of the localization length ξ on W in the various regimes is indicated in the figure. In particular, in three dimensions the localization length diverges as $(W - W_c)^{-1}$ for $W \rightarrow W_c$.

In fig. 29 the DC conductivity in three dimensions as calculated from eq. (10.40) is shown as a function of the disorder variable W for various values of energy E . Of particular interest is the reentrant behavior for energies near the band edge. As discussed in section 6, the conductivity vanishes linearly with the distance from the critical value of disorder, i.e. $\sigma \propto W_c - W$.

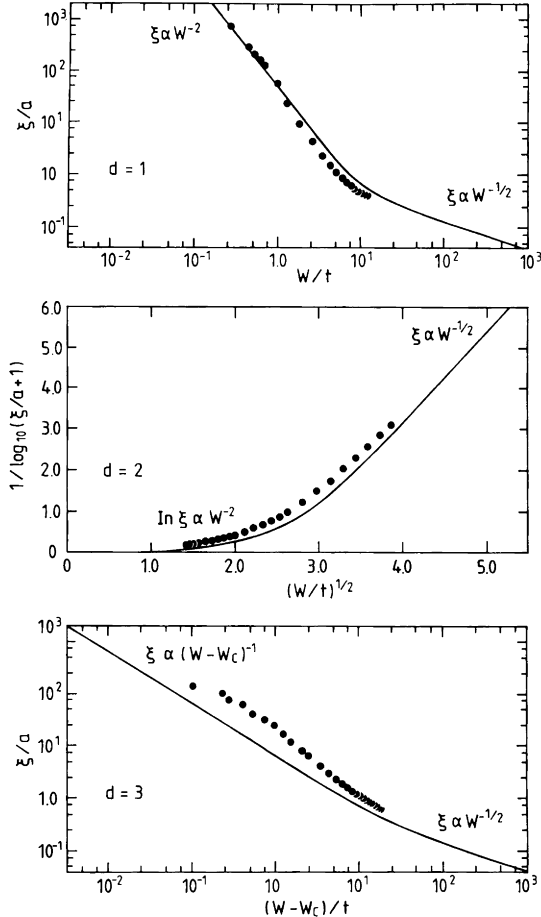


Fig. 28. Localization length as a function of disorder W for $E = 0$ in $d = 1, 2$ and 3 dimensions. (a) ξ/a versus W/t for $d = 1$. (b) $1/\log_{10}(\xi/a + 1)$ versus $(W/t)^{1/2}$ for $d = 2$. (c) ξ/a versus $(W/W_c)/t$ for $d = 3$. Theoretical curves after Kroha et al. (1990), data points after Bulka et al. (1987). Also indicated is the asymptotic behavior.

Finally, the dynamical conductivity in three dimensions for $E = 0$ and various values of disorder is shown in fig. 30. For $W < W_c$, $\text{Re } \sigma(\omega)$ shows a cusp at $\omega = 0$, which cuts deeper and deeper into the Drude peak as W approaches W_c . At $W = W_c$, $\text{Re } \sigma(\omega)$ varies as $\omega^{1/3}$ for small ω (see eq. (6.22)). The spectral weight under $\sigma(\omega)$, removed by the cusp at small ω , is shifted to higher frequencies such that the sum rule on $\text{Re } \sigma$,

$$\int_0^\infty d\omega \text{Re } \sigma(\omega) = \frac{\pi}{2} e^2 \frac{n}{m}, \quad (10.43)$$

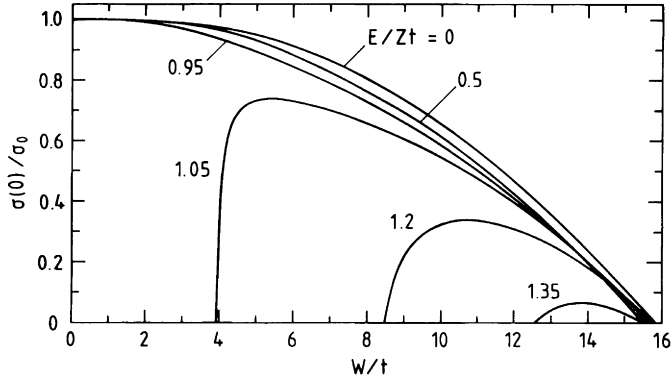


Fig. 29. DC conductivity in $d = 3$ dimensions as a function of disorder W for various values of energy E (after Kroha 1990).

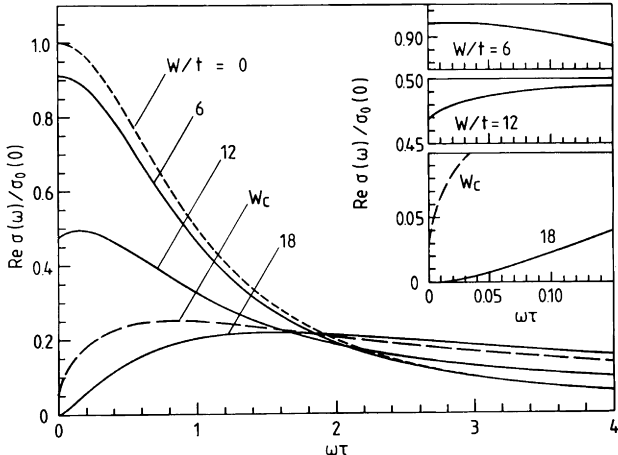


Fig. 30. Dynamical conductivity $\text{Re } \sigma(\omega)$ normalized to the CPA conductivity $\sigma_0(0)$ versus normalized frequency $\omega\tau$ for various values of disorder W (after Kroha 1990). The insert shows the low-frequency behavior.

is satisfied. Beyond W_c , the conductivity is found to increase as $\sigma(\omega) \propto \omega^2$. This is in conflict with the picture of resonance tunnelling processes introduced by Mott (1970), which lead to a dependence $\sigma(\omega) \propto \omega^2 [\ln \omega]^{d+1}$ (for description of an attempt to incorporate resonance tunnelling into the self-consistent theory, see Kopp 1984b). The additional factors of $\ln \omega$ will tend to increase the prefactor of ω^2 , leading to a faster rise of $\sigma(\omega)$ for small ω than that given by the self-consistent theory. This is borne out by a detailed comparison of results in

one dimension (Saso et al. 1985). These authors show that the exact weak-coupling result for $\sigma(\omega)$ (Berezinskii 1973, Abrikosov and Ryshkin 1978), which agrees well with numerical diagonalization data (Saso 1984), rises somewhat faster than $\sigma(\omega)$ obtained from the self-consistent theory.

11. Conclusion

In this chapter we have reviewed some of the recent developments in the theory of quantum particles in disordered systems. Particular emphasis has been placed on the discussion of the self-consistent theory of Anderson localization developed by us in 1980–1982. We have shown that this theory may be derived diagrammatically by summing the most strongly divergent terms. Technically speaking, the theory corresponds to a self-consistent one-loop approximation, i.e. the interaction of fluctuations is taken into account at the lowest level in a self-consistent way. Such theories are known to provide good results in the so-called weak-interaction regime, i.e. not too close to the transition point. Although we have not attempted here to estimate the correction terms, and therefore the regime of validity, one may expect that this regime is broad and well-defined. The reason is that the next two orders in the renormalization group β -function, following the one-loop contribution, are actually zero; meaning that the corrections to the one-loop result appear only in a regime of large-amplitude fluctuations, or close to the transition point. This then implies that the critical behavior obtained in the self-consistent theory, in particular the critical exponents, will not be the correct critical exponents valid in the critical regime proper. Rather, one may expect these exponents to apply in an intermediate regime, as the transition is approached. The excellent agreement of the quantitative version of the self-consistent theory with exact diagonalization results, discussed in section 10, demonstrates that such an intermediate regime does indeed exist.

In the light of the above discussion it is understandable that a generalization of the self-consistent theory to the cases of time-reversal symmetry breaking fields, such as an external magnetic field or magnetic impurities, and to the case of spin-orbit scattering is difficult (see section 8). In these cases, an expansion in higher than one-loop order in the fluctuations is necessary. In the presence of a strong magnetic field it can be shown that the corresponding field theory is characterized by a topological term in the Lagrangian with a coefficient proportional to the Hall conductivity or, equivalently, by two scaling parameters. Nonperturbative contributions of this kind cannot be expected to be easily included in a self-consistent theory of the type described in this chapter.

The self-consistent theory of Anderson localization for the time-reversal invariant case has been widely used for a variety of different physical systems. The theory as reviewed in this article is based on a simple physical argumentation corroborated by an explicit diagrammatic derivation which is easily

adapted to new situations, such as localization of phonons, photons or other classical waves, as discussed in section 9.

The results of the self-consistent theory agree surprisingly well with the exact results available in one dimension. Furthermore, the more quantitative version of the theory presented in section 10 provides results for the crossover from the weak-coupling into the strong-coupling regime in dimensions $d = 1, 2$ and 3 , which are in excellent agreement with the results of numerical diagonalization of finite-size systems. Thus, the self-consistent theory of Anderson localization described here appears to give a reliable picture of the global behavior of disordered systems, even if it should turn out that the critical behavior at the Anderson transition is not described exactly.

Acknowledgements

We are grateful to J. Kroha and T. Kopp for useful discussions. We also thank Ms. Rose Schrempp for her expert typing of the manuscript. This work was partially supported by Sonderforschungsbereich 341 der Deutschen Forschungsgemeinschaft (DV) and by NSF grant DMR-8607941 (PW).

References

(i) Conference Proceedings

Anderson Localization, 1982, eds Y. Nagaoka and H. Fukuyama, Springer Series in Solid State Sciences, Vol. 39 (Springer, Berlin).

Anderson Localization, 1985, ed. Y. Nagaoka, Progress of Theoretical Physics Supplement Nr. 84.

Anderson Localization, 1988, eds T. Ando and H. Fukuyama, Springer Proceedings in Physics, Vol. 28 (Springer, Berlin).

Localization, Interaction, and Transport Phenomena, 1985, eds B. Kramer, G. Bergmann and Y. Bruynseraede, Springer Series in Solid State Sciences, Vol. 61 (Springer, Berlin).

Localization in Disordered Systems, 1984, eds W. Weller and P. Ziesche, Teubner Texte zur Physik, Band 3 (Teubner, Leipzig).

Localization in Disordered Systems, 1988, eds W. Weller and P. Ziesche, Teubner Texte zur Physik, Band 16 (Teubner, Leipzig).

(ii) Articles and Books

Abrahams, E., and P.A. Lee, 1986, Phys. Rev. B **33**, 683.

Abrahams, E., P.W. Anderson, D.C. Licciardello and T.V. Ramakrishnan, 1979, Phys. Rev. Lett. **42**, 673.

Abrikosov, A.A., and I.A. Ryshkin, 1978, Adv. Phys. **27**, 147.

Abrikosov, A.A., L.P. Gor'kov and I.E. Dzyaloshinskii, 1963, Methods of Quantum Field Theory in Statistical Physics (Prentice-Hall, Englewood Cliffs, NJ).

Aiyer, R.N., R.J. Elliott, J.A. Krumhansl and P.L. Leath, 1969, Phys. Rev. **181**, 1006.

Akkermans, E., and R. Maynard, 1985a, Phys. Rev. B **32**, 7850.

Akkermans, E., and R. Maynard, 1985b, J. Phys. (Paris) Lett. **46**, 1045.

Akkermans, E., P.E. Wolf and R. Maynard, 1986, Phys. Rev. Lett. **56**, 1471.

- Altshuler, B.L., and A.G. Aronov, 1979a, Solid State Commun. **39**, 115.
- Altshuler, B.L., and A.G. Aronov, 1979b, Zh. Eksp. & Teor. Fiz. **77**, 2028 [Sov. Phys.-JETP **50**, 968].
- Altshuler, B.L., and A.G. Aronov, 1985, in: Electron-Electron Interactions in Disordered Systems, eds A.L. Efros and M. Pollak (North-Holland, Amsterdam) p. 1.
- Altshuler, B.L., A.G. Aronov and B.Z. Spivak, 1981, Pis'ma Zh. Eksp. & Teor. Fiz. **33**, 101 [JETP Lett. **33**, 94].
- Altshuler, B.L., A.G. Aronov, D.E. Khmelnitskii and A.I. Larkin, 1983, in: Quantum Theory of Solids, ed. I.M. Lifshitz (MIR, Moscow).
- Altshuler, B.L., V.E. Kravtsov and I.V. Lerner, 1986a, Pis'ma Zh. Eksp. & Teor. Fiz. **43**, 342 [JETP Lett. **43**, 441].
- Altshuler, B.L., V.E. Kravtsov and I.V. Lerner, 1986b, Zh. Eksp. & Teor. Fiz. **91**, 2276 [Sov. Phys.-JETP **64**, 1352].
- Anderson, P.W., 1958, Phys. Rev. **109**, 1492.
- Anderson, P.W., 1985, Philos. Mag. B **52**, 505.
- Anderson, P.W., E. Abrahams and T.V. Ramakrishnan, 1979, Phys. Rev. Lett. **44**, 1288.
- Apel, W., and T.M. Rice, 1983, J. Phys. C **17**, L1151.
- Arya, K., Z.B. Su and J.L. Birman, 1985, Phys. Rev. Lett. **54**, 1559.
- Belitz, D., and W. Götze, 1982, J. Phys. C **15**, 981.
- Belitz, D., A. Gold and W. Götze, 1981, Z. Phys. B **44**, 273.
- Benedict, K.A., and J.T. Chalker, 1986, J. Phys. C **19**, 3587.
- Berezinskii, V.L., 1973, Zh. Eksp. & Teor. Fiz. **65**, 1251 [1974, Sov. Phys.-JETP **38**, 620].
- Bergmann, G., 1983, Phys. Rev. B **28**, 2914.
- Bergmann, G., 1984, Phys. Rep. **101**, 1.
- Bhatt, R.N., P. Wölfle and T.V. Ramakrishnan, 1984, Proc. 17th Int. Conf. Low Temp. Phys. LT-17, Part II (North-Holland, Amsterdam) p. 887.
- Bhatt, R.N., P. Wölfle and T.V. Ramakrishnan, 1985, Phys. Rev. B **32**, 569.
- Borland, R.E., 1963, Proc. R. Soc. London Ser. A **274**, 529.
- Bulka, B., M. Schreiber and B. Kramer, 1987, Z. Phys. B **66**, 21.
- Carra, P., 1987, J. Phys. C **20**, L823.
- Carra, P., J.T. Chalker and K.A. Benedict, 1989, Ann. Phys. **194**, 1.
- Castellani, C., and C. DiCastro, 1986, Phys. Rev. B **34**, 5935.
- Castellani, C., C. DiCastro, P.A. Lee and M. Ma, 1984a, Phys. Rev. B **30**, 527.
- Castellani, C., C. DiCastro, P.A. Lee, M. Ma, S. Sorella and E. Tabet, 1984b, Phys. Rev. B **30**, 1596.
- Castellani, C., C. DiCastro, P.A. Lee, M. Ma, S. Sorella and E. Tabet, 1986, Phys. Rev. B **33**, 6169.
- Castellani, C., G. Kotliar and P.A. Lee, 1987, Phys. Rev. Lett. **59**, 323.
- Celli, V., A.A. Maradudin, A.M. Marvin and A.R. McGurn, 1985, J. Opt. Soc. Am. **2**, 2225.
- Chakravarty, S., and A. Schmid, 1986, Phys. Rep. **140**, 193.
- Chalker, J.T., 1988, J. Phys. C **21**, L119.
- Chalker, J.T., 1990, Physica A **167**, 253.
- Chalker, J.T., and G.J. Daniell, 1988, Phys. Rev. Lett. **61**, 593.
- Chalker, J.T., and I.H. Nahm, 1989, J. Phys. Condens. Mat. **1**, 3615.
- Chalker, J.T., and S. Siak, 1990, J. Phys.: Condens. Matter **2**, 2671.
- Chalker, J.T., P. Carra and K.A. Benedict, 1988, Europhys. Lett. **5**, 163.
- Cheng, Z., S.W. Gu and J.X. Fang, 1988, J. Phys. C **21**, L925.
- Cohen, A., Y. Roth and B. Shapiro, 1988, Phys. Rev. B **38**, 12125.
- Cohen, S.M., and J. Machta, 1985, Phys. Rev. Lett. **54**, 2242.
- Cohen, S.M., J. Machta, T.R. Kirkpatrick and C.A. Condat, 1987, Phys. Rev. Lett. **58**, 785.
- Condat, C.A., and T.R. Kirkpatrick, 1985a, Phys. Rev. B **32**, 495.
- Condat, C.A., and T.R. Kirkpatrick, 1985b, Phys. Rev. B **32**, 4392.
- Condat, C.A., and T.R. Kirkpatrick, 1986, Phys. Rev. B **33**, 3102.
- Condat, C.A., and T.R. Kirkpatrick, 1987, Phys. Rev. Lett. **58**, 226.

- Condat, C.A., T.R. Kirkpatrick and S.M. Cohen, 1987, Phys. Rev. B **35**, 4653.
- Dersch, U., and P. Thomas, 1985, J. Phys. C **18**, 5815.
- Dorokhov, O.N., 1986, Pis'ma Zh. Eksp. & Teor. Fiz. **43**, 94 [JETP Lett. **43**, 123].
- Economou, E.N., and C.M. Soukoulis, 1983, Phys. Rev. B **28**, 1093.
- Economou, E.N., C.M. Soukoulis and A.D. Zdetsis, 1984, Phys. Rev. B **30**, 1686.
- Edwards, S.F., 1958, Philos. Mag. **3**, 1020.
- Efetov, K.B., 1983, Adv. Phys. **32**, 53.
- Efetov, K.B., 1984a, Pis'ma Zh. Eksp. & Teor. Fiz. **40**, 17 [JETP Lett. **40**, 738].
- Efetov, K.B., 1984b, Zh. Eksp. & Teor. Fiz. **88**, 1032 [Sov. Phys.-JETP **51**, 606].
- Efetov, K.B., 1987a, Zh. Eksp. & Teor. Fiz. **92**, 638 [Sov. Phys.-JETP **65**, 360].
- Efetov, K.B., 1987b, Zh. Eksp. & Teor. Fiz. **93**, 1125 [Sov. Phys.-JETP **66**, 634].
- Efetov, K.B., 1988, Zh. Eksp. & Teor. Fiz. **94**, 357 [Sov. Phys.-JETP **67**, 199].
- Efetov, K.B., A.I. Larkin and D.E. Khmel'nitskii, 1980, Zh. Eksp. & Teor. Fiz. **79**, 1120 [Sov. Phys.-JETP **52**, 568].
- Erdős, P., and R.C. Herndon, 1982, Adv. Phys. **31**, 65.
- Finkelstein, A.M., 1983, Zh. Eksp. & Teor. Fiz. **84**, 168 [Sov. Phys.-JETP **57**, 97].
- Finkelstein, A.M., 1984a, Z. Phys. B **56**, 189.
- Finkelstein, A.M., 1984b, Zh. Eksp. & Teor. Fiz. **86**, 367 [Sov. Phys.-JETP **59**, 212].
- Finkelstein, A.M., 1984c, Pis'ma Zh. Eksp. & Teor. Fiz. **40**, 63 [JETP Lett. **40**, 796].
- Firsov, Yu.A., and V.N. Prigodin, 1984, in: Localization in Disordered Systems, eds W. Weller and P. Ziesche, Teubner Texte zur Physik, Band 3 (Teubner, Leipzig) p. 194.
- Foster, D., 1975, Hydrodynamic Fluctuations, Broken Symmetry and Correlation Functions (Benjamin, Reading).
- Gogolin, A.A., and G.T. Zimanyi, 1983, Solid State Commun. **46**, 469.
- Gold, A., 1987, Solid State Commun. **64**, 823.
- Gorkov, L.P., A.I. Larkin and D.E. Khmel'nitskii, 1979, Pis'ma Zh. Eksp. & Teor. Fiz. **30**, 248, [JETP Lett. **30**, 248].
- Götze, W., 1978, Solid State Commun. **27**, 1393.
- Götze, W., 1979, J. Phys. C **12**, 1279.
- Götze, W., 1981a, Philos. Mag. B **43**, 219.
- Götze, W., 1981b, in: Recent Developments in Condensed Matter Physics, Vol. I, ed. J.T. Devreese (Plenum Press, New York) p. 133.
- Götze, W., 1983, in: Modern Problems in Solid State Physics, Vol. I: Two-dimensional Electron Systems, eds Yu.E. Lozovik and A.A. Maradudin (North-Holland, Amsterdam).
- Götze, W., P. Prelovsek and P. Wölfle, 1979, Solid State Commun. **30**, 369.
- Henrichs, J., 1988, Phys. Rev. B **37**, 1051.
- Hershfield, S., and V. Ambegaokar, 1986, Phys. Rev. B **34**, 2147.
- Hikami, S., 1981, Phys. Rev. B **24**, 2671.
- Hikami, S., 1982, in: Anderson Localization, eds Y. Nagaoka and H. Fukuyama, Springer Series in Solid State Sciences, Vol. 39 (Springer, Berlin) p. 15.
- Hikami, S., A.I. Larkin and Y. Nagaoka, 1980, Prog. Theor. Phys. **63**, 707.
- Igarashi, J., 1987, Phys. Rev. B **35**, 5151.
- Imry, Y., 1986, in: Directions in Condensed Matter Physics, eds G. Grinstein and G. Mazenko (World Scientific, Singapore).
- Imry, Y., Y. Gefen and D. Bergman, 1981, Phys. Rev. B **24**, 4889.
- Imry, Y., Y. Gefen and D. Bergman, 1982, Phys. Rev. B **26**, 3436.
- Ioffe, A.F., and A.R. Regel, 1960, Prog. Semicond. **4**, 237.
- John, S., 1984, Phys. Rev. Lett. **53**, 2169.
- John, S., 1987, Phys. Rev. Lett. **58**, 2486.
- John, S., H. Sompolinsky and M.J. Stephen, 1983, Phys. Rev. B **27**, 5592.
- Josephson, B., and J. Lekner, 1969, Phys. Rev. Lett. **23**, 111.
- Jüngling, K., and R. Oppermann, 1980, Z. Phys. B **38**, 93.

- Kaveh, M., 1987, *Philos. Mag. B* **56**, 693.
- Kawabata, A., 1981, *Solid State Commun.* **38**, 823.
- Khmelnitskii, D.E., 1984, *Physica B & C* **126**, 235.
- Kirkpatrick, T.R., 1985, *Phys. Rev. B* **31**, 5746.
- Kirkpatrick, T.R., 1986, *Phys. Rev. B* **33**, 780.
- Kirkpatrick, T.R., and D. Belitz, 1990, *Phys. Rev. B* **41**, 11082.
- Kopp, T., 1984a, *J. Phys. C* **17**, 1897.
- Kopp, T., 1984b, *J. Phys. C* **17**, 1919.
- Kotov, E.A., and M.V. Sadovskii, 1983, *Z. Phys. B* **51**, 17.
- Kroha, H., 1990, *Physica A* **167**, 231.
- Kroha, H., T. Kopp and P. Wölfle, 1990, *Phys. Rev. B* **41**, 888.
- Kunz, H., and B. Souillard, 1983, *J. Phys. (Paris) Lett.* **44**, 503.
- Landauer, R., 1957, *IBM J. Res. Rev.* **1**, 223.
- Landauer, R., 1970, *Philos. Mag.* **21**, 683.
- Langer, J.S., and T. Neal, 1966, *Phys. Rev. Lett.* **16**, 984.
- Leath, P.L., 1970, *Phys. Rev. B* **2**, 3078.
- Lee, P.A., and T.V. Ramakrishnan, 1985, *Rev. Mod. Phys.* **57**, 287.
- Levine, H., S.B. Libby and A.M.M. Pruisken, 1983, *Phys. Rev. Lett.* **51**, 1915.
- MacKinnon, A., 1982, in: *Anderson Localization*, eds Y. Nagaoka and H. Fukuyama, Springer Series in Solid State Sciences, Vol. 39 (Springer, Berlin).
- MacKinnon, A., and B. Kramer, 1981, *Phys. Rev. Lett.* **47**, 1546.
- MacKinnon, A., and B. Kramer, 1982, *Phys. Rev. Lett.* **49**, 695.
- MacKinnon, A., and B. Kramer, 1983, *Z. Phys. B* **53**, 1.
- Maleev, S.V., and B.P. Toperverg, 1975, *Zh. Eksp. & Teor. Fiz.* **69**, 1440, [Sov. Phys.-JETP **42**, 734].
- Matsubara, T., and Y. Toyozawa, 1961, *Prog. Theor. Phys.* **26**, 739.
- McGurn, A.R., and A.A. Maradudin, 1984, *Phys. Rev. B* **30**, 3136.
- McGurn, A.R., A.A. Maradudin and V. Celli, 1985, *Phys. Rev. B* **31**, 4866.
- McKane, A.J., and M. Stone, 1981, *Ann. Phys. (NY)* **131**, 36.
- Metzner, W., and D. Vollhardt, 1989, *Phys. Rev. Lett.* **62**, 324.
- Milovanovic, M., S. Sachdev and R.N. Bhatt, 1989, *Phys. Rev. Lett.* **63**, 82.
- Mott, N.F., 1966, *Philos. Mag.* **13**, 989.
- Mott, N.F., 1967, *Adv. Phys.* **16**, 49.
- Mott, N.F., 1968, *J. Non-Cryst. Solids* **1**, 1.
- Mott, N.F., 1970, *Philos. Mag.* **22**, 7.
- Mott, N.F., 1974, *Metal-Insulator Transitions* (Taylor & Francis, London).
- Mott, N.F., and E.A. Davis, 1979, *Electronic Processes in Non-Crystalline Materials*, 2nd Ed. (Clarendon Press, Oxford).
- Mott, N.F., and W.D. Twose, 1961, *Adv. Phys.* **10**, 107.
- Muttalib, K.A., J.L. Pichard and A. Stone, 1987, *Phys. Rev. Lett.* **59**, 2475.
- Ono, Y., 1982a, *J. Phys. Soc. Jpn.* **51**, 2055.
- Ono, Y., 1982b, *J. Phys. Soc. Jpn.* **51**, 3544.
- Ono, Y., 1983a, *J. Phys. Soc. Jpn.* **52**, 2492.
- Ono, Y., 1983b, *J. Phys. Soc. Jpn.* **52**, 247.
- Ono, Y., 1984, *J. Phys. Soc. Jpn.* **53**, 2342.
- Oppermann, R., 1981, *J. Phys. C* **14**, 3757.
- Oppermann, R., and K. Jüngling, 1980, *Phys. Lett. A* **76**, 449.
- Oppermann, R., and F. Wegner, 1979, *Z. Phys. B* **34**, 327.
- Parks, R.D., and W.A. Little, 1964, *Phys. Rev. A* **133**, 97.
- Pichard, J.L., and G. Sarma, 1981a, *J. Phys. C* **14**, L127.
- Pichard, J.L., and G. Sarma, 1981b, *J. Phys. C* **14**, L617.
- Prelovsek, P., 1981, in: *Recent Developments in Condensed Matter Physics*, ed. J.T. Devreese (Plenum Press, New York) Vol. 2, p. 191.

- Prigodin, V.N., 1980, *Zh. Eksp. & Teor. Fiz.* **79**, 2338 [Sov. Phys.-JETP **52**, 1185].
- Prigodin, V.N., and Yu.A. Firsov, 1983, *Pis'ma Zh. Eksp. & Teor. Fiz.* **38**, 241 [JETP Lett. **38**, 284].
- Prigodin, V.N., and Yu.A. Firsov, 1984, *J. Phys. C* **17**, L979.
- Prigodin, V.N., Yu.A. Firsov and W. Weller, 1986, *Solid State Commun.* **59**, 729.
- Pruisken, A.M.M., 1983a, *Nucl. Phys. B* **285** [FS19] 719.
- Pruisken, A.M.M., 1983b, *Nucl. Phys. B* **290** [FS20] 61.
- Pruisken, A.M.M., 1988, *Phys. Rev. Lett.* **61**, 1297.
- Rammer, J., and H. Smith, 1986, *Rev. Mod. Phys.* **58**, 323.
- Rickayzen, G., 1980, *Green's Functions and Condensed Matter* (Academic Press, London).
- Sadovskii, M.V., 1986, in: *Soviet Science Review A, Physics Review*, Vol. 7 (Harwood, Chur) p. 1.
- Sak, J., and B. Kramer, 1981, *Phys. Rev. B* **24**, 1761.
- Saso, T., 1984, *J. Phys. C* **17**, 2905.
- Saso, T., Y. Suzumura and H. Fukuyama, 1985, *Prog. Theor. Phys. Suppl.* **84**, 269.
- Schäfer, L., and F. Wegner, 1980, *Z. Phys. B* **38**, 113.
- Schmeltzer, D., and M. Kaveh, 1987, *J. Phys. C* **20**, L175.
- Shapiro, B., 1982a, *Phys. Rev. B* **25**, 4266.
- Shapiro, B., 1982b, *Phys. Rev. Lett.* **48**, 823.
- Shapiro, B., 1986, *Phys. Rev. B* **34**, 4394.
- Shapiro, B., 1990, *Phys. Rev. Lett.* **65**, 1510.
- Shapiro, B., and E. Abrahams, 1981, *Phys. Rev. B* **24**, 4889.
- Sharvin, D.Yu., and Yu.V. Sharvin, 1981, *Pis'ma Zh. Eksp. & Teor. Fiz.* **34**, 285 [JETP Lett. **34**, 272].
- Sheng, P., and Z.Q. Zhang, 1986, *Phys. Rev. Lett.* **57**, 1879.
- Soonpaa, H.H., and W.A. Schwalm, 1984, *Phys. Lett. A* **100**, 156.
- Soukoulis, C.M., I. Webman, G.S. Grest and E.N. Economou, 1982, *Phys. Rev. B* **26**, 1838.
- Soukoulis C.M., S. Zdetsis and E.N. Economou, 1986, *Phys. Rev. B* **34**, 2253.
- Soukoulis, C.M., E.N. Economou and G.S. Grest, 1987, *Phys. Rev. B* **36**, 8649.
- Soven, P., 1967, *Phys. Rev.* **156**, 809.
- Suslov, I.M., 1986, *Pis'ma Zh. Eksp. & Teor. Fiz.* **43**, 544 [JETP Lett. **43**, 704].
- Thouless, D.J., 1974, *Phys. Rep.* **13**, 93.
- Thouless, D.J., 1977, *Phys. Rev. Lett.* **39**, 1167.
- Ting, C.S., 1982, *Phys. Rev. B* **26**, 678.
- van Albada, M.P., and A. Lagendijk, 1985, *Phys. Rev. Lett.* **55**, 2692.
- van Dongen, P., and D. Vollhardt, 1990, *Phys. Rev. Lett.* **65**, 1663.
- Vollhardt, D., 1987, in: *Festkörperprobleme* (Vieweg, Braunschweig) **27**, 63.
- Vollhardt, D., and P. Wölfle, 1980a, *Phys. Rev. Lett.* **45**, 482.
- Vollhardt, D., and P. Wölfle, 1980b, *Phys. Rev. B* **22**, 4666.
- Vollhardt, D., and P. Wölfle, 1982, *Phys. Rev. Lett.* **48**, 699.
- Washburn, S., and R.B. Webb, 1986, *Adv. Phys.* **35**, 375.
- Wegner, F., 1976, *Z. Phys. B* **25**, 327.
- Wegner, F., 1979, *Z. Phys. B* **35**, 207.
- Wegner, F., 1982, in: *Anderson Localization*, eds Y. Nagaoka and H. Fukuyama, Springer Series in Solid State Phys., Vol. 39 (Springer, Berlin) p. 8.
- Wegner, F., 1989, *Nucl. Phys. B* **316**, 663.
- Wolf, P.E., and G. Maret, 1985, *Phys. Rev. Lett.* **55**, 2696.
- Wölfle, P., and R.N. Bhatt, 1984, *Phys. Rev. B* **30**, 3542.
- Wölfle, P., and D. Vollhardt, 1982, in: *Anderson Localization*, eds Y. Nagaoka and H. Fukuyama, Springer Series in Solid State Phys., Vol. 39 (Springer, Berlin) p. 26.
- Wölfle, P., P. Götze, J. Kurkijärvi and H. Smith, 1980, *J. Phys. C* **13**, 2461.
- Yoshioka, D., Y. Ono and H. Fukuyama, 1981, *J. Phys. Soc. Jpn.* **50**, 3419.
- Zavaritskaya, E.I., and I.P. Zvyagin, 1985, *Pis'ma Zh. Eksp. & Teor. Fiz.* **41**, 393, [JETP Lett. **41**, 482].

- Zdetsis, A.D., C.M. Soukoulis, E.N. Economou and G.S. Grest, 1985, Phys. Rev. B **32**, 7811.
Zirnbauer, M., 1986a, Nucl. Phys. B **265**, 375.
Zirnbauer, M., 1986b, Phys. Rev. B **34**, 6394.
Zirnbauer, M., 1988, Phys. Rev. Lett. **60**, 1450.

CHAPTER 2

Spin Glasses

D. SHERRINGTON

*Department of Theoretical Physics
University of Oxford, UK*

Electronic Phase Transitions
Edited by
© Elsevier Science Publishers, B.V., 1992

W. Hanke and Yu.V. Kopaev

Contents

1. Introduction	81
2. The key ingredients	86
3. Analytic theory	88
3.1. Replica theory	90
3.2. Replica mean-field theory	91
3.2.1. Replica-symmetric Ansatz	93
3.2.2. Parisi Ansatz	98
3.3. The Sherrington–Kirkpatrick model	106
3.4. Further subtleties	107
4. Short-ranged spin glasses	109
5. Vector spin glasses	118
6. Beyond conventional spin glasses	122
6.1. Bipartitioning of random graphs	123
6.2. Neural networks	127
7. Conclusion	130
References	131

1. Introduction

The expression “spin glass” was originally coined* to describe a situation in some magnetic alloys in which there was observed non-periodic or amorphous “freezing” of the orientations of the magnetic moments (or spins). On closer examination, this ordering has turned out to be highly unusual, with many subtle and interesting characteristics, and the attempt to unravel its mysteries has led to a wealth of new concepts and techniques with ramifications far beyond magnetism. In particular, apart from having implications in other areas of solid-state physics, the study of spin glasses has influenced the treatment of hard optimization problems and the quantitative and qualitative analysis of neural networks, and is also being applied to other complex biological problems, such as evolution and immunology. In this chapter I shall introduce and partially overview the key concepts and theoretical techniques, with only limited discussion of experiments and history† and no attempt at completeness.

Despite the caveat of the last sentence, a brief historical introduction to set the scene does seem appropriate.

The earliest experiments drawing attention to spin glasses as potentially interesting systems were performed on substitutional alloys of magnetic and non-magnetic metals. One set of experiments was suggestive of the random freezing mentioned earlier. For example, the observations of the onset of Mossbauer line-splitting beneath a characteristic temperature (Borg et al. 1963) was indicative of local freezing of the electronic magnetic moments over the corresponding lifetimes, while the absence of macroscopic magnetizations or of new magnetic Bragg peaks in neutron diffraction demonstrated that the freezing was not periodic. Further evidence of the aferromagnetic freezing was provided by the observation of a corresponding maximum in the susceptibility as a function of temperature (Owen et al. 1957, Lutes and Schmit 1964), but its rounded nature and, even more, that of a maximum in the specific heat at a slightly higher

* It is generally attributed to Bryan Coles (see, e.g. Anderson 1973).

† For brief discussions of early history see Coles (1984, 1985). For extensive reviews with greater cover of experiment see Binder and Young (1986) and Fischer (1983, 1985). As a more extensive theoretical text concentrating on spin glass mean-field theory the reader is referred to Mézard et al. (1987).

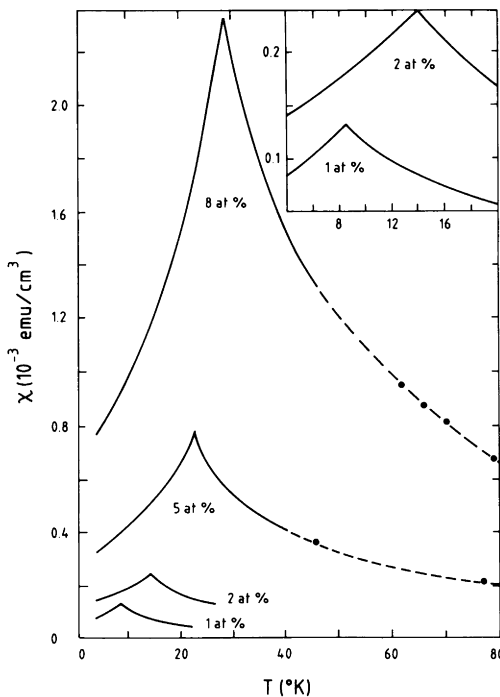


Fig. 1. A.c. susceptibility of the canonical spin glass AuFe at various atomic percentages of Fe; from: Cannella and Mydosh 1972.

temperature, suggested that the “freezing” was the onset of sluggish response rather than a sharp phase transition. It was only when later a.c. susceptibility measurements (Cannella and Mydosh 1972) in which static magnetic fields were kept very low showed quite sharp cusps (see fig. 1) that the possibility of a true new phase transition was recognized. The attempt by Edwards and Anderson (1975) to produce a theory of this transition was the spark for a theoretical revolution, opening a magical box of novel techniques and concepts.

Random freezing is certainly a novelty and, as noted above, it was the attempt to explain the occurrence of this feature which stimulated discoveries of great subtlety. However, a second set of early experiments exposed the presence of another, even more remarkable feature. These experiments demonstrated that the spin glass alloys acquired severe preparation-dependence effects and considerable slowing-down of response to external perturbations beneath the same characteristic temperature as that found in the susceptibility experiments. Although its significance was not appreciated until later, one of these striking preparation-dependent features was observed in a d.c. susceptibility experiment;

the susceptibility obtained by cooling the system in the measurement field (FC: field cooling) yielded a higher value than that obtained by first cooling in zero field and then applying the measurement field (ZFC: zero field cooling) (Tholence and Tournier 1974). Figure 2 shows a more recent demonstration. Similarly, dramatic preparation-dependence was observed in measurements of the remanent magnetization, which, if measured by cooling in the field and then removing it (TRM: thermoremanent magnetization), is greater than the isothermal remanent magnetization (IRM) obtained by first cooling, then applying and finally removing the field (see fig. 3). These observations demonstrate that in the new "phase" there are many metastable states whose relative free energies vary in different ways with external perturbations and which have significant energy barriers impeding motion from one state to another. We now have a mental picture of free-energy surfaces in phase space as having many, non-equivalent, quasi-fractal minima, as illustrated schematically in fig. 4, in contrast to a simple structure with only global-symmetry-related equivalent minima as in a conventional periodic magnet; this is illustrated for a ferromagnet in fig. 5. An explanation of the onset of preparation-dependence/difference between field-cooled and zero-field-cooled measurements comes from different modifications with field of the relative energies of different minima, so that the "trough" containing the lowest minimum at zero field (which has zero magnetization) is no longer the lowest in even a small finite field, with inter-trough barriers which are difficult to

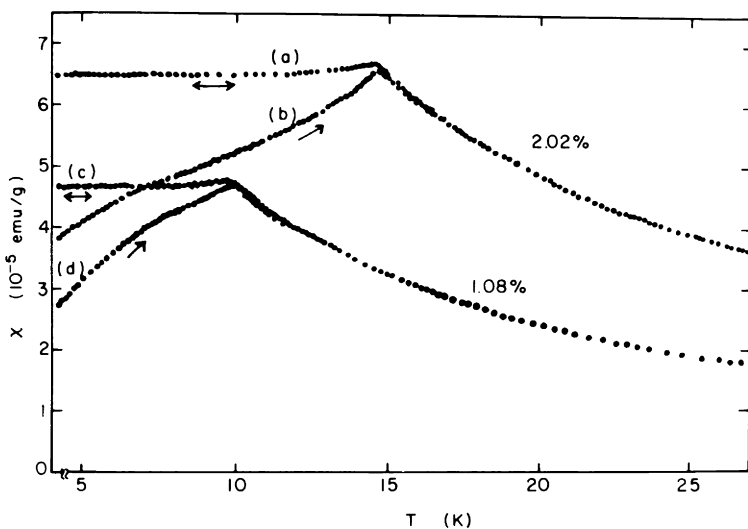


Fig. 2. D.c. susceptibility measurements for two CuMn alloys with 1.08 and 2.02 at.% Mn. Curves (a) and (c) were obtained by cooling in the measurement field (FC), (b) and (d) are the results of zero-field-cooled (ZFC) experiments; from: Nagata et al. 1979.

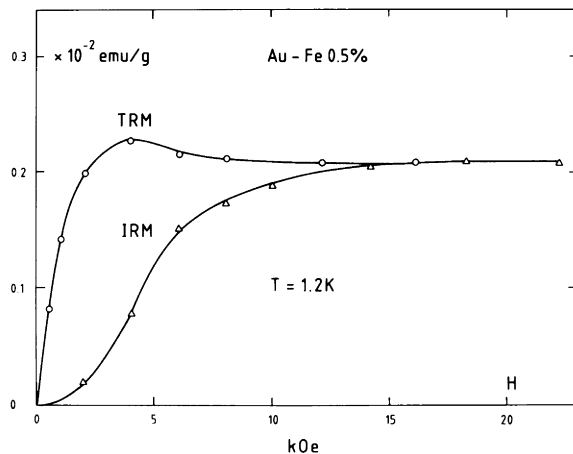


Fig. 3. Remanent magnetization as measured in Au-0.5% Fe at 1.2 K. IRM denotes isothermal remanent magnetization, TRM denotes thermoremanent magnetization; from: Tholence and Tournier 1974.

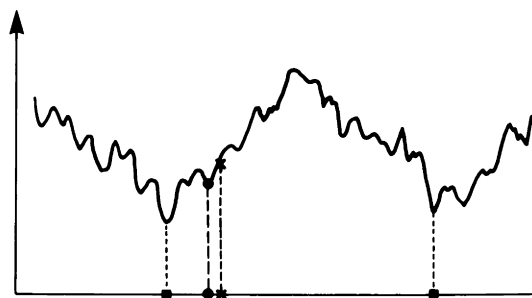


Fig. 4. Schematic plot of free energy as a function of position in macroscopic phase space for a frustrated or *NP*-complete system; also energy or cost as a function of position in microscopic phase space.

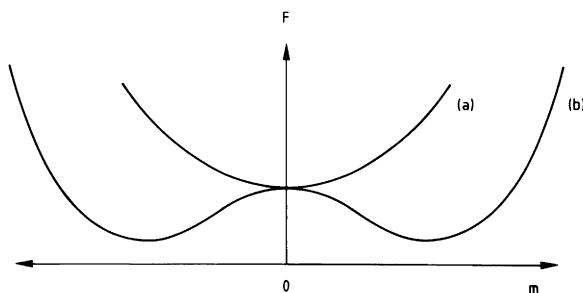


Fig. 5. Schematic plot of free energy as a function of magnetization for a ferromagnet (a) above, (b) below the ordering temperature T_c .

surmount at low temperature, but of less consequence if the field is applied at a high temperature which is then reduced.

The relevance of this image of a complex energy surface to other hard optimization problems is readily envisaged by interpreting fig. 4 as the cost function to be minimized in a hard optimization problem, with the abscissa representing position in the high-dimensional variable space. Consider particularly systems in which it would be prohibitive to calculate the cost function for all values of the N variables: e.g. in graph bipartitioning problems there are 2^N combinations, in the travelling salesman problem $N!$, both of which rapidly become enormous. One requires a shorter algorithm. With a simple form such as illustrated in fig. 6, it clearly suffices to choose a starting value of the parameters (e.g. \times in fig. 6), evaluate the local gradient of the cost function at that value, and iterate downwards to the global minimum (\bullet in fig. 6); this is known as iterative improvement or gradient descent. On the other hand, however, for a cost function such as in fig 4, this procedure will almost always lead to a higher secondary local minimum and not to the global minimum or even a state of similar quality. Spin glasses are in this class of hard optimization problems and the conceptual comparison between the problems of finding the ground state of a spin glass and that of finding the minimum cost of other NP-hard optimization problems has led to valuable transfer to the hard optimization arena of techniques, analytical and computer-simulational, developed to understand spin glass thermodynamics (Kirkpatrick et al. 1983, Fu and Anderson 1986, Banavar et al. 1987).

Figure 4 also provides a hint at the potential for analogy between spin glasses and neural networks for memory. Aside from any further details of the latter, other than the fact that they involve the global behaviour of many simple elements which operate cooperatively, it is clear that many memories require many steady states, closely analogous to the many local minima of the free energy of an NP-hard system. We shall explore this analogy more deeply in the sequel.

The features discussed above, as exhibited by the canonical metallic spin glasses, are now realized to be much more common, as the comments in the

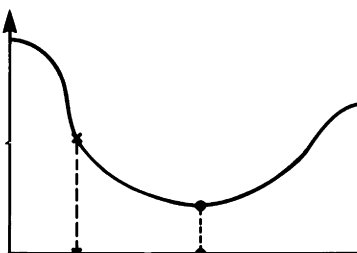


Fig. 6. Schematic plot of free energy as a function of position in macroscopic phase space for an unfrustrated system; also energy or cost as a function of position in microscopic phase space.

last two paragraphs may have led the reader to anticipate (if he was not already aware). Thus, random freezing and preparation dependence are now well-established also in several insulating alloys and model spin systems, as also in related systems with other variables. In the next section we discuss the necessary ingredients and hence extension of the spin glass concept. In the rest of this chapter we discuss analysis, simulations, implications and applications.

2. The key ingredients

Spin glass behaviour seems to require two essential ingredients. These are *quenched disorder* and *frustration*.

“Quenched disorder” refers to constrained disorder in the interactions between the spins and/or their locations. The spin orientations themselves are variables, (i.e. not constrained), governed by the interactions, external fields and thermal fluctuations, free to order or not as thermodynamics tells them. The spin glass phase is an example of spontaneous cooperative freezing (or order) of the spin orientations in the presence of the constrained disorder of the interactions or spin locations. It is thus “order in the presence of disorder”. At a deeper level, in real solids the time scale for the ordering of the spin orientations is short but that of ordering of the atoms or interactions is very long.

“Frustration” refers to conflicts between interactions, or other spin-ordering forces, such that not all can be obeyed simultaneously.

These features are readily visualized in a simple model Hamiltonian appropriate to an idealization of magnetic interactions between atoms with well-defined local moments:

$$H = - \sum_{(ij)} J_{ij} \mathbf{S}_i \cdot \mathbf{S}_j, \quad (2.1)$$

where the i, j label the magnetic moments/spins, the \mathbf{S}_i are the corresponding spin orientation vectors, and J_{ij} measures the “exchange” interaction between the pair of spins (ij) . The variables are the $\{\mathbf{S}_i\}$, while the $\{J_{ij}\}$ are quenched/constrained. In conventional experimental spin glass systems, the spin locations \mathbf{R}_i are randomly located (on a lattice in the case of the substitutional alloys mentioned earlier) and J_{ij} is a function of $(\mathbf{R}_i - \mathbf{R}_j)$ which oscillates in sign with separation. Frustration arises in that pairs of spins get different ordering instructions through the various paths which link i and j , either directly or via intermediate spins.

The hint that spin glass behaviour has its origin in competing interactions and randomness came from studies of the scaling with the concentration of the magnetic ingredient of the characteristic temperatures for the onset of strong preparation dependence, or peaks in the susceptibility or specific heat of the canonical metallic spin glass alloys (Souletie and Tournier 1969). This scaling

pointed the finger at the R^{-3} decay with distance of the Ruderman–Kittel–Kasuya–Yosida (RKKY) interaction, coupled with its oscillations as a function of distance (with period π/k_F , where k_F is the Fermi wavevector);

$$J(R) \sim \frac{1}{R^3} \cos 2k_F R. \quad (2.2)$$

This interaction is ferromagnetic or antiferromagnetic as a function of distance, giving frustration, while the random site occupation makes that frustration non-equivalent at different sites, so that, for example, different nearest-neighbour pairs might react differently because their environments are different. The recognition of the combination of disorder and frustration in the ordering forces led Edwards and Anderson to propose a more convenient model in which there are spins S_i on all the sites of a lattice but the J_{ij} are chosen randomly from a Gaussian distribution centred at zero. The symmetric distribution was chosen to eliminate the possibility of a conventional periodic phase, and the Gaussian form for mathematical convenience. Both restrictions have since been lifted. Computer simulations demonstrated that indeed this model exhibits the characteristic features discussed earlier.

A natural corollary of the recognition of the key ingredients is also that experimentally the behaviour should not be restricted to metallic systems, provided one has disorder and frustration, and indeed the effects have now been seen in several insulating alloys. The canonical insulating example is $\text{Eu}_x\text{Sr}_{1-x}\text{S}$, in which only Eu is magnetic and for which the nearest-neighbour interactions are ferromagnetic, next-nearest interactions are antiferromagnetic.

The relevance of frustration is readily envisaged by considering a simple example of a set of four Ising spins ($\sigma_i = \pm 1$) located on the corners of a square and interacting with their nearest neighbours only via pairwise energies,

$$E_{ij} = -J_{ij}\sigma_i\sigma_j, \quad (2.3)$$

with the J_{ij} either $+J$ (ferromagnetic) or $-J$ (antiferromagnetic). If the number of antiferromagnetic bonds around the square is even, the $\{\sigma_i\}$ can be chosen so as to minimize simultaneously all the exchange bonds, giving a total energy $-4J$. However, if there is an odd number of negative bonds around the square, then not all the bonds can be satisfied simultaneously. At least one must be dissatisfied, the system is frustrated, and the minimum energy is $-2J$. Furthermore, whereas the only ground-state degeneracy in the former (unfrustrated) case is associated with global spin inversion ($\sigma_i \rightarrow -\sigma_i$; all i), in the latter (frustrated) case it is four times greater, since there is further degeneracy associated with which of the four bonds to disobey. Generally, *frustration increases the energy and the degeneracy of the lowest energy states*.

In an extensive system, frustration can have major consequences. For example, consider a square lattice of Ising spins with nearest-neighbour interactions $\pm J$. If all the fundamental cells, or plaquettes, are unfrustrated then the

ground state is cooperatively ordered with only two-fold global inversion degeneracy and there is an order-disorder phase transition at finite temperature. On the other hand, if all the plaquettes are frustrated, the phase transition is suppressed and the ground state has extensive entropy (Villain 1977). Frustration is a necessary ingredient for spin glasses, but too much can suppress cooperative order completely.

The concept of frustration is not restricted to systems all of whose bonds are of the same strength, nor to Ising spins, nor to interactions of fixed character (e.g. ferromagnetic and antiferromagnetic). Antiferromagnetic interactions alone can provide frustration. A classic demonstration is given by the nearest-neighbour Ising model on a triangular lattice; if all the interactions are ferromagnetic, it exhibits the usual paramagnet–ferromagnet transition at finite temperature, but if the interactions are all antiferromagnetic and equal then the resultant frustration around each plaquette suppresses cooperative order. $\text{Cd}_{1-x}\text{Mn}_x\text{Te}$ is an example of a random substitutional alloy spin glass with purely antiferromagnetic interactions, both nearest- and next-nearest neighbour being antiferromagnetic, but in conflict with one another. Amorphous antiferromagnets are another interesting case, although the precise degree of topological disorder necessary to yield a spin glass rather than suppress cooperative order remains unclear (McLenaghan and Sherrington 1984, 1987, Sherrington 1987). Another interesting case requiring only ferromagnetic bonds concerns spins located on the vertices of a randomly connected network, interacting via ferromagnetic nearest-neighbour bonds but subject to a constraint of zero overall magnetization; minimizing the energy of this system is mathematically isomorphic with that of finding a partitioning of a random graph so as to separate it into two partitions each containing half the vertices but such as to minimize the number of edges (lines) connecting the two partitions (Kirkpatrick et al. 1983); this isomorphism has led to the application of spin glass techniques to the partitioning problems (Fu and Anderson 1986, Banavar et al. 1987, Goldschmidt and Lai 1988).

3. Analytic theory

Let us now turn to an analysis of spin glasses, taking as prototype the random-bond Ising model with Hamiltonian

$$H = - \sum_{(ij)} J_{ij} \sigma_i \sigma_j; \quad \sigma_i = \pm 1, \quad (3.1)$$

where the i label the spins and the J_{ij} are drawn randomly from distributions $P(J_{ij})$ which are the same for all equivalent pairs of spin locations. Initially, we shall consider the spins to be on a lattice of sites (i, j) .

Several of the novel features can already be hinted at even within a relatively straightforward extension of conventional mean-field theory (but employing

only a subset of the assumptions usually made in mean-field theory). Allowing for the lack of spatial symmetry, but ignoring self/cavity field and thermodynamic fluctuation effects, a simple extension of a conventional approximation yields the set of self-consistent mean-field equations

$$\langle \sigma_i \rangle = \tanh \left(\sum_j J_{ij} \langle \sigma_j \rangle / kT \right), \quad (3.2)$$

where the $\langle \rangle$ brackets indicate a (possibly symmetry-broken) thermodynamic average

$$\langle O \rangle = \frac{\text{Tr } O \exp(-\beta H)}{\text{Tr } \exp(-\beta H)}, \quad (3.3)$$

where

$$\text{Tr} \equiv \sum_{\{\sigma_i\} = \pm 1}, \quad (3.4)$$

and

$$\beta = (kT)^{-1}. \quad (3.5)$$

Conventionally, within mean-field approximation, the critical temperature T_c for the onset of frozen order is given by the existence of a non-trivial solution ($\langle \sigma \rangle \neq 0$) to the linearized mean-field equation. In the present case this corresponds to

$$\langle \sigma_i \rangle = \sum_j J_{ij} \langle \sigma_j \rangle / kT_c. \quad (3.6)$$

Averaging over sites and bonds and (without justification) ignoring correlations between those averages yields

$$[\langle \sigma_i \rangle] = \sum_j [J_{ij}] [\langle \sigma_j \rangle] / kT_c, \quad (3.7)$$

where the $[]$ brackets denote an average over the bond or site disorder. For a symmetric exchange distribution $[J_{ij}]$ is zero and there is no non-trivial solution to eq. (3.7) at finite T_c . There is no ferromagnetic solution. An analogous consideration similarly eliminates any other periodic order in this case. If, however, eq. (3.6) is first squared on each side and then averaged, again ignoring correlations and using $[J_{ij}] = 0$, there results

$$[\langle \sigma_i \rangle^2] = \sum_j [J_{ij}^2] [\langle \sigma_j \rangle^2] / (kT_c)^2, \quad (3.8)$$

which has a non-trivial solution at a critical temperature given by

$$kT_c = \left(\sum_j J_{ij}^2 \right)^{1/2}, \quad (3.9)$$

with “order parameter” [$\langle \sigma_i \rangle^2$]. Thus, beneath this temperature one has a “frozen-spin” state but without periodic order. Of course, even within mean-field theory this analysis is questionable in detail, but, as we shall see below, sophisticated mean-field theory also yields a frozen-spin state without periodic order.

Equation (3.2) is also the equation for the extrema of the free-energy functional within mean-field theory. The number of solutions to eq. (3.2) thus relates to the number of extrema of the free energy. Analysis shows the number of such solutions grows exponentially with the number of spins (Bray and Moore 1980, Tanaka and Edwards 1980), giving weight to the image of a free-energy surface with much structure.

3.1. Replica theory

Much of the further progress in understanding and quantifying the spin glass problem has employed an artifice known as replica theory. This was introduced by Edwards and Anderson (1975) to aid in the analysis of physical averages over quenched disorder.

We are generally interested in statistically representative quantities, rather than specific instances. It is therefore of interest to look at averages over specific disorder. Indeed, it is a traditional tenet that physical macroscopic measurements on nominally equivalent random systems are overwhelmingly dominated by their mean values; for example, the susceptibility per unit mass of one piece of CuMn alloy is expected to be the same as another of the same concentration provided they are similarly prepared and subject to the same external fields, even though the precise locations of the individual atoms differ. Recently, we have come to realize that subtleties of macroscopic fluctuations are possible and we shall reconsider this assumption later. For the present, however, we shall study the disorder-averaged system. It is, however, important that one averages physical observables if one is to obtain physically relevant results. Thus it is sensible to average the free energy $F = -kT\ln Z$, where Z is the partition function

$$Z = \text{Tr} \exp(-\beta H), \quad (3.10)$$

but not to average Z itself (Brout 1959). Unfortunately, whereas Z is relatively easy to average, being a sum of exponentials, $\ln Z$ is much harder to average. The replica trick is an artifice to transform the hard average over $\ln Z$ into an easier one over an effective Z .

In particular, the replica trick starts with the mathematical identity

$$\ln Z = \lim_{n \rightarrow 0} \frac{1}{n} (Z^n - 1). \quad (3.11)$$

Z^n may be interpreted as the partition function of n identical replicas of the

original system. Introducing a replica label $\alpha = 1, \dots, n$, Z^n may be written as

$$Z^n = \text{Tr}_n \exp \left(- \sum_{\alpha=1}^n H^\alpha / kT \right), \quad (3.12)$$

where H^α is the Hamiltonian with dummy variables labelled by an extra index α and Tr_n is the trace over all the variables. Because Z^n is a sum over exponentials it is relatively straightforward to average in terms of cumulants. For the random-bond Ising model one obtains

$$[Z^n] = \text{Tr}_n \exp \left\{ \sum_{(ij)} \sum_r [J'_{ij}]_c / (kT)^r \sum_{\alpha, \beta, \dots, \delta_r} (\sigma_i^\alpha \sigma_i^\beta \cdots \sigma_i^{\delta_r})(\sigma_j^\alpha \sigma_j^\beta \cdots \sigma_j^{\delta_r}) \right\}, \quad (3.13)$$

where $[J'_{ij}]_c$ indicates the r th cumulant average of J_{ij} and $\alpha, \beta, \dots, \delta_r$ indicate r replica labels, each taking values from 1 to n .

The advantage of a Gaussian distribution of J_{ij} , as used by Edwards and Anderson (1975), is that all the cumulant averages above $r = 2$ vanish, so that eq. (3.13) truncates. Further restricting that range of J_{ij} to nearest neighbours yields

$$[F] = -kT \lim_{n \rightarrow 0} \frac{1}{n} \left\{ \text{Tr}_n \exp \left[\sum_{(ij)} (\beta \tilde{J}_0 \sum_\alpha \sigma_i^\alpha \sigma_j^\alpha + \beta^2 \tilde{J}^2 \sum_{\alpha, \beta} \sigma_i^\alpha \sigma_i^\beta \sigma_j^\alpha \sigma_j^\beta) \right] - 1 \right\}, \quad (3.14)$$

where \tilde{J}_0 is the mean and \tilde{J} the standard deviation of the nearest-neighbour $P(J_{ij})$ and the sum (ij) now refers to nearest neighbours. Thus we have effectively replaced the original disordered system of eq. (3.1) by one with a periodic effective temperature-dependent Hamiltonian

$$H_{\text{eff}} = - \sum_{(ij)} \left(\tilde{J}_0 \sum_{\alpha=1}^n \sigma_i^\alpha \sigma_j^\alpha + \beta \tilde{J}^2 \sum_{\alpha, \beta=1}^n \sigma_i^\alpha \sigma_i^\beta \sigma_j^\alpha \sigma_j^\beta \right) \quad (3.15)$$

involving higher-dimensional spins with more complicated interactions and requiring analysis in the limit $n \rightarrow 0$. If the distribution $P(J_{ij})$ is not Gaussian, one still has a mapping to an effective periodic Hamiltonian but involving further multi-spin interactions.

3.2. Replica mean-field theory

In general the expression in eq. (3.14) cannot be evaluated exactly. By analogy with conventional magnetism, it is natural to consider first a mean-field approximation in which an interacting problem is replaced by an effective non-interacting system with self-consistently determined ‘‘fields’’. Thus one replaces

$$\sum_{(ij)} \sigma_i^\alpha \sigma_j^\alpha \rightarrow \sum_{ij} (\sigma_i^\alpha m_j^\alpha - (m_i^\alpha m_j^\alpha)/2), \quad m_i^\alpha = \langle \sigma_i^\alpha \rangle_n, \quad (3.16)$$

$$\sum_{(ij)} \sigma_i^\alpha \sigma_i^\beta \sigma_j^\alpha \sigma_j^\beta \rightarrow \sum_{ij} (\sigma_i^\alpha \sigma_i^\beta q_j^{(\alpha\beta)} - q_i^{(\alpha\beta)} q_j^{(\alpha\beta)}/2), \quad q_i^{(\alpha\beta)} = \langle \sigma_i^\alpha \sigma_i^\beta \rangle_n, \quad \alpha \neq \beta, \quad (3.17)$$

where $\langle \rangle_n$ refers to a thermodynamic average against the effective Hamiltonian and the order parameters m_i^α , $q_i^{(\alpha\beta)}$ are to be determined self-consistently. Since eq. (3.15) is translationally invariant, we can assume, in the usual fashion, a similar property for m_i^α , $q_i^{(\alpha\beta)}$, provided J_0 is non-negative; if J_0 were negative we would need to allow for antiferromagnetic order instead.

The evaluation of $[F]$ now becomes a single-site problem:

$$[F] = -NkT \lim_{n \rightarrow 0} \frac{1}{n} \left\{ \text{Tr}_n \exp \left[\beta \tilde{J}_0 z \sum_\alpha (\sigma^\alpha m^\alpha - (m^\alpha)^2/2) + (\beta \tilde{J})^2 z \left(n + 2 \sum_{(\alpha\beta)} (\sigma^\alpha \sigma^\beta q^{(\alpha\beta)} - q^{(\alpha\beta)2}/2) \right) \right] - 1 \right\}, \quad (3.18)$$

where z is the coordination number, the trace is now single-site, m^α and $q^{(\alpha\beta)}$ are given by

$$m^\alpha = \frac{\text{Tr}_n \sigma^\alpha \exp(-\beta \tilde{H}_n)}{\text{Tr}_n \exp(-\beta \tilde{H}_n)}, \quad (3.19)$$

$$q^{(\alpha\beta)} = \frac{\text{Tr}_n \sigma^\alpha \sigma^\beta \exp(-\beta \tilde{H}_n)}{\text{Tr}_n \exp(-\beta \tilde{H}_n)}, \quad (3.20)$$

where $-\beta \tilde{H}_n$ is the argument of the exponential in eq. (3.18), or, equivalently, by the extremal equations

$$\frac{\delta \tilde{F}_n}{\delta m^\alpha} = \frac{\delta \tilde{F}_n}{\delta q^{(\alpha\beta)}} = 0, \quad (3.21)$$

where

$$\tilde{F}_n = -kT \ln \text{Tr}_n \exp(-\beta \tilde{H}_n). \quad (3.22)$$

These mean-field equations can only be considered an approximation for short-ranged spin glasses and there is (a) controversy as to the extent to which their predictions can be considered representative of such real systems, (b) great technical difficulty in using them as the basis around which to perform renormalization group analysis to get true short-range critical behaviour. However, (c) they have been instrumental in providing qualitative and quantitative results which have stimulated much further theoretical analysis and experimentation, and (d) they are believed to be exact for the infinite-ranged model introduced by Sherrington and Kirkpatrick (1975) as an artificial soluble model for a spin glass but now recognized as highly relevant to extensions to some hard graph partitioning problems (Kirkpatrick et al. 1983) and to neural networks (Amit et al. 1985a).

Let us defer until later a demonstration that these equations are exact for the SK model mentioned earlier and just concentrate now on their predictions.

3.2.1. Replica-symmetric Ansatz

Equations (3.18)–(3.22) represent a set of self-consistent equations. Were n a fixed finite integer, they would be straightforward to solve (Sherrington 1980), but with the limiting procedure $n \rightarrow 0$ the problem is more difficult, requiring an appropriate analytic continuation. For this reason a further simplifying Ansatz was proposed (Edwards and Anderson 1975), the so-called replica-symmetric Ansatz in which one assumes

$$\begin{aligned} m^\alpha &= m, \quad \text{all } \alpha, \\ q^{(\alpha\beta)} &= q, \quad \text{all } \alpha \neq \beta. \end{aligned} \tag{3.23}$$

This Ansatz is natural, since the replicas are mathematical artifices and are apparently indistinguishable. In fact, however, the situation is more subtle, but we defer further discussion of the subtlety until later.

The computational advantage of the replica-symmetric Ansatz is two-fold; firstly it permits eq. (3.18) to be expressed in terms of readily evaluable effective independent spin terms, and secondly it provides for straightforward analytic continuation. To see the first of these properties, note that the “interacting” term in the exponent

$$2 \sum_{(\alpha\beta)} \sigma^\alpha \sigma^\beta q^{(\alpha\beta)} \rightarrow q \left\{ \left(\sum_\alpha \sigma^\alpha \right)^2 - 1 \right\} \tag{3.24}$$

can be reduced to single- σ form via the identity

$$\exp(\mu x^2) = (2\pi)^{-1/2} \int dy \exp(-y^2/2 + (2\mu)^{1/2} xy). \tag{3.25}$$

Here we take $\mu = (\beta\tilde{J})^2 zq$ and $x = \sum \sigma^\alpha$. The simple analytic continuation occurs because now all σ^α enter linearly with the same coefficient. Evaluation of the trace and taking of the limit $n \rightarrow 0$ yields

$$[F] = N \left\{ \frac{Jm^2}{2} - \frac{\beta J^2}{4}(1-q)^2 - kT \int dh P(h) \ln(2 \cosh \beta h) \right\}, \tag{3.26}$$

where $J_0 = \tilde{J}_0 z$, $J = \tilde{J} z^{1/2}$ and m and q are determined self-consistently from

$$m = \int dh P(h) \tanh \beta h, \tag{3.27}$$

$$q = \int dh P(h) (\tanh \beta h)^2, \tag{3.28}$$

with

$$P(h) = (2\pi J q^2)^{-1/2} \exp(- (h - J_0 m)^2 / 2Jq^2). \quad (3.29)$$

Within this approximation m and q can also be identified as

$$m = [\langle \sigma_i \rangle], \quad (3.30)$$

$$q = [\langle \sigma_i \rangle^2], \quad (3.31)$$

i.e. as the average magnetization and mean-square disorder averaged local moment (Sherrington and Kirkpatrick 1975, Kirkpatrick and Sherrington 1978).* Hence non-zero q implies a cooperatively frozen magnetic state, while non-zero m implies that that frozen state has a non-zero magnetization, a ferromagnetic component. Thus, solutions to eqs. (3.27)–(3.30) fall into three possible categories:

- (a) paramagnetic if both m and q are zero.
- (b) ferromagnetic if both m and q are non-zero.
- (c) spin glass if q is non-zero but m is zero.

The resultant phase diagram is shown in fig. 7a, while fig. 7b shows for comparison a typical experimental phase diagram. When account is taken of the different scalings with concentration of effective interactions J_0, J there is a qualitative accord between the figures (Sherrington and Southern 1975).

Let us concentrate now on the spin glass phase. As the temperature is lowered beneath the critical temperature $T_g = J/k$, q grows continuously from zero as

$$q = \tau + \frac{1}{3}\tau^2 + O(\tau^3); \quad \tau = (T_g - T)/T_g. \quad (3.32)$$

This yields a cusp in the zero-field susceptibility $\chi(T)$, as is observed experimentally. This is most readily seen from the fluctuation correlation form for the differential susceptibility[†]:

$$\chi(T) = (kT)^{-1} N^{-1} \sum_{ij} (\langle \sigma_i \sigma_j \rangle - \langle \sigma_i \rangle \langle \sigma_j \rangle). \quad (3.33)$$

*This identification (and extensions of it) follows from writing $\langle \sigma_i \rangle^r$ as the trace of $\sigma_i^1 \cdots \sigma_i^r$ over r replicas of the disordered system,

$$\langle \sigma_i \rangle^r = \frac{\text{Tr}_r \sigma_i^1 \cdots \sigma_i^r \exp(-\beta(H^1 + \cdots + H^r))}{\text{Tr}_r \exp(-\beta(H^1 + \cdots + H^r))},$$

multiplying numerator and denominator by Z^{n-r} , taking the limit $n \rightarrow 0$ and averaging over the disorder to yield

$$[\langle \sigma_i \rangle^r] = \lim_{n \rightarrow 0} \langle \sigma_i^{\alpha_1} \cdots \sigma_i^{\alpha_r} \rangle_n; \quad \alpha_1 \neq \alpha_2 \neq \cdots \neq \alpha_r.$$

[†]This result follows from formal differentiation of the expression for the magnetization in an external field b ;

$$M = \frac{\sum_{\{\sigma\}} \sigma_i \exp(-(H - b \sum_j \sigma_j)/kT)}{\sum_{\{\sigma\}} \exp(-(H - b \sum_j \sigma_j)/kT)}.$$

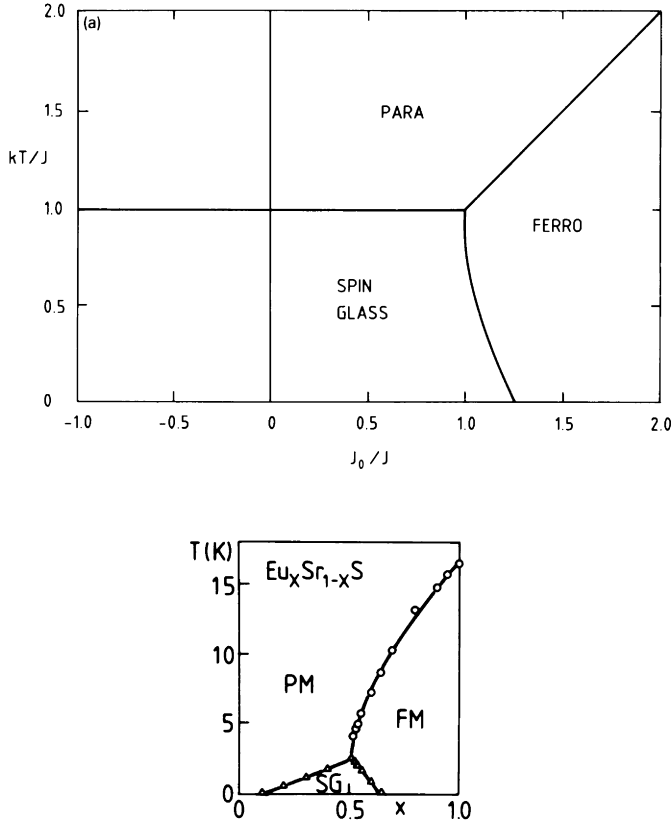


Fig. 7. (a) Phase diagram obtained in replica-symmetric mean-field theory for a random-bond Ising model; from: Sherrington and Kirkpatrick 1975. (b) Phase diagram of $\text{Eu}_x\text{Sr}_{1-x}\text{S}$; from: Maletta and Convert 1979.

For the case $J_0 = 0$, the terms in the summand are zero on average unless $i = j$ and

$$\chi(T) = \chi_0(T) = (NkT)^{-1} \sum_i (1 - \langle \sigma_i \rangle^2), \quad (3.34)$$

or, passing to the average

$$\chi_0(T) = (kT)^{-1} (1 - [\langle \sigma_i \rangle^2]) \quad (3.35)$$

$$= (kT)^{-1} (1 - q). \quad (3.36)$$

Hence, in the vicinity of $T = T_g$ one has

$$\chi_0(T) = (kT_g)^{-1} (1 - |\tau| + O(\tau^2)), \quad T > T_g, \quad (3.37a)$$

$$= (kT_g)^{-1} (1 - \frac{1}{3}\tau^2 + O(\tau^3)), \quad T < T_g. \quad (3.37b)$$

For $J_0 \neq 0$, χ has a similar cusp but with an overall enhancement factor (Sherrington and Kirkpatrick 1975), giving

$$\chi(T) = \chi_0(T)/(1 - J_0\chi_0(T)). \quad (3.38)$$

In the presence of a finite external field b , $P(h)$ of eq. (3.29) is modified by replacing $h \rightarrow h - b$ and $\chi(T)$ is rounded, as shown in fig. 8a. A similar rounding of the cusp in χ is found experimentally (fig. 8b); indeed it is the great sensitivity to such rounding which delayed the experimental discovery of a sharp transition.

For phase transitions of higher than first order one is used to looking for a diverging response function. Clearly, the uniform susceptibility is not such a response function for a spin glass transition. Rather, the divergent susceptibilities are the q -response to a random field and the related non-linear uniform susceptibility. The first of these, sometimes called the spin glass susceptibility, is defined as

$$\chi_{SG} = \partial^2 Q / \partial \tilde{b}^2, \quad (3.39)$$

where

$$Q = \sum \langle \sigma_i \rangle_{\tilde{b}}^2; \quad (3.40)$$

here $\langle \cdot \rangle_{\tilde{b}}$ refers to a thermodynamic average against a system with a random applied field $\{h_i\} = \{\tilde{b}\xi_i\}$, and the $\xi_i = \pm 1$ are random and quenched. Formally performing the differentiation of eq. (3.38) yields the fluctuation form* (Chen and Lubensky 1977, Fisch and Harris 1977)

$$\chi_{SG} = \beta^2 N^{-1} \sum_{ij} (\langle \sigma_i \sigma_j \rangle - \langle \sigma_i \rangle \langle \sigma_j \rangle)^2. \quad (3.41)$$

For $J_0 = 0$ and for $T > T_g$ one obtains within mean-field theory

$$\chi_{SG} = (T^2 - T_g^2)^{-1}, \quad (3.42)$$

which diverges as $T \rightarrow T_g$. For a finite uniform b , higher-order susceptibilities can be defined by

$$M = N^{-1} \sum_i \langle \sigma_i \rangle = \chi b + \chi_3 b^3 + \chi_5 b^5 + \dots \quad (3.43)$$

Within the present mean-field theory, the non-linear susceptibilities χ_3, χ_5 etc. also diverge at T_g ; in fact, χ_3 and χ_{SG} are linearly related. A similar divergence of these higher-order susceptibilities has been observed experimentally (Monod and Bouchiat 1982, Barbara et al. 1981), albeit with a critical exponent different from that given by mean-field theory.

In fact, however, the replica-symmetric Ansatz is not everywhere stable, even within mean-field theory. The problem is clearly exposed by looking at the

* In the limit of infinite N we expect physical observables to be self-averaging: $N^{-1} \sum_i O_i = [O_i]$.

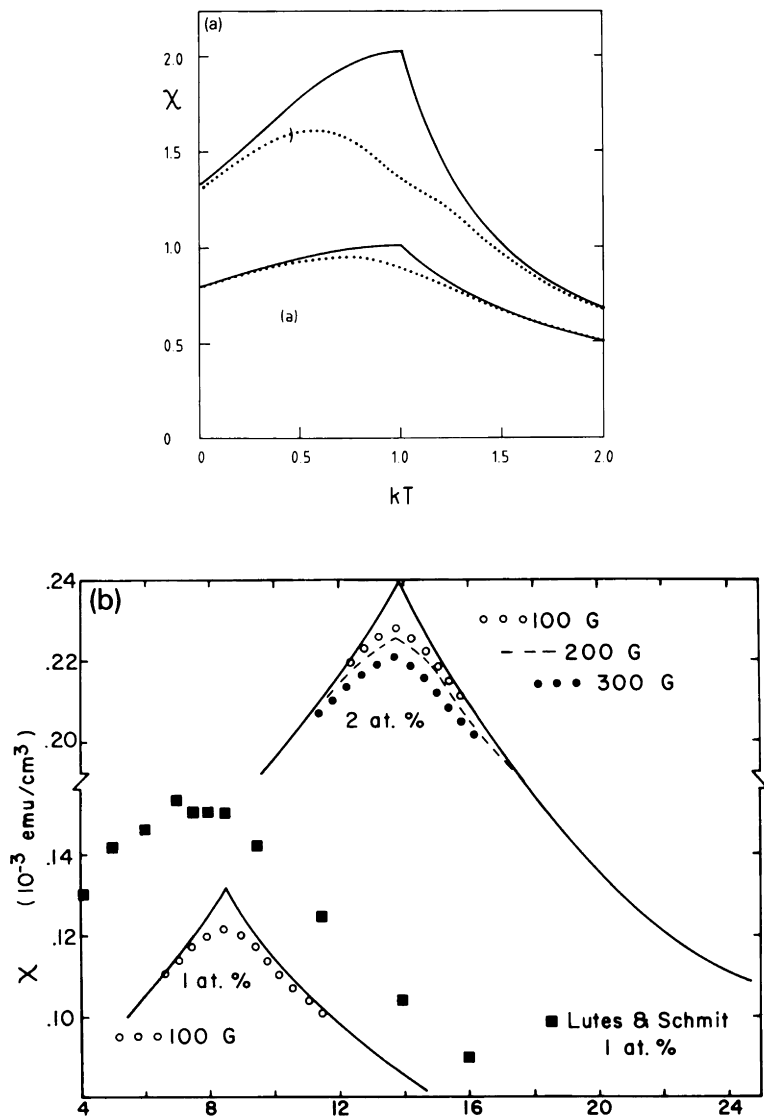


Fig. 8. (a) Differential susceptibility of a random-bond spin glass as given by replica-symmetric mean-field theory. Solid curves are for zero field, dotted curves for $b = 0.1J$. Curves (a) are for $J_0/J = 0$, curves (b) are for $J_0/J = 0.5$; Sherrington and Kirkpatrick 1975. (b) External field dependence of a.c. susceptibility of AuFe. From: Cannella and Mydosh 1972.

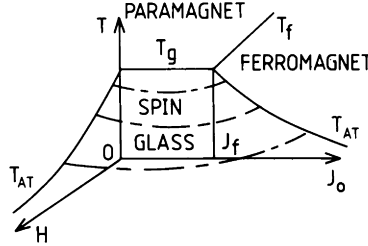


Fig. 9. De Almeida–Thouless surface (indicated by chain-hatching) for the limit of stability of the replica-symmetric Ansatz for mean-field theory for a random-bond Ising model. The Ansatz is unstable on the side of the surface closer to the origin. The phase line beneath the AT surface is calculated within the Parisi Ansatz.

normal modes of fluctuation of $q^{(\alpha\beta)}$ and m^α in replica space about their replica-symmetric values (de Almeida and Thouless 1978). Thus one introduces fluctuation terms η , ε by

$$q^{(\alpha\beta)} = q + \eta^{(\alpha\beta)}, \quad (3.44)$$

$$m^\alpha = m + \varepsilon^\alpha, \quad (3.45)$$

where q , m are the replica-symmetric values, one expands the free energy expression [F] to second order in the fluctuations and studies its normal-mode spectrum in the limit $n \rightarrow 0$. Beneath a surface in $(T/J, J_0/J, b/J)$ space, shown in fig. 9 and including all of the spin glass phase, the replica-symmetric Ansatz is found to be unstable against the replica-symmetry breaking η -modes (de Almeida and Thouless 1978). This instability surface is known, after its discoverers, as the de Almeida–Thouless (AT) surface, its projections as AT lines.

The inadequacy of the replica-symmetric Ansatz has shown up in other ways. The first of these was the prediction, as a consequence of its application, of an unphysical (negative) form for the zero-temperature entropy of the random-bond Ising model (Sherrington and Kirkpatrick 1975). Another is in the result of an evaluation of the spin glass susceptibility χ_{SG} beneath T_g , taking account of fluctuations to harmonic order, which yields a negative value (Pytte and Rudnick 1979, Bray and Moore 1979), despite the manifestly positive-definite form of eq. (3.41).

Beneath the AT surface a more subtle Ansatz is required for a stable solution to the mean-field equations (3.18)–(3.20). Various schemes were proposed, whose analysis suggested that many levels of symmetry breaking were necessary to achieve stability. One due to Parisi (Parisi 1979) has proven to satisfy all stability tests to date.

3.2.2. Parisi Ansatz

The Parisi scheme involves an infinite hierarchy of replica subdivisions. It may be formulated as follows. Consider $q^{\alpha\beta}$ as a symmetric $n \times n$ matrix with zeros

on its diagonals, taking the value $q^{\alpha\beta} = q^{(\alpha\beta)}$ on the off-diagonals*. The replica-symmetric Ansatz corresponds to taking all the off-diagonal elements to be identical, equal to q . Parisi's method may be viewed as a series of subdivisions. First the $(n \times n)$ matrix is subdivided into $(m_1 \times m_1)$ blocks and all the elements of the off-diagonal blocks given the value q . The $(m_1 \times m_1)$ blocks on the diagonal of the $(n \times n)$ matrix are subdivided further into $(m_2 \times m_2)$ subblocks and all the elements of the off-diagonal subblocks given the value q_2 . The $(m_2 \times m_2)$ subblocks on the diagonal are subdivided further, into $(m_3 \times m_3)$ sub-sub-blocks. The elements of the off-diagonal $(m_3 \times m_3)$ sub-sub-blocks are given the value q_3 , while the diagonal sub-sub-blocks are further divided, and so on, giving an infinite regression of subdivisions of the diagonal blocks, with

$$n \geq m_1 \geq m_2 \geq \dots \geq 1. \quad (3.46)$$

So far in this discussion of subdivision, we have been envisaging n, m_i as integers, but the next step in the analysis is to consider analytic continuation to $n \rightarrow 0$, and with it the inversion of the order of eq. (3.46),

$$0 \leq m_1 \leq m_2 \leq \dots \leq 1, \quad (3.47)$$

together with relabellings with

$$m_k/m_{k+1} \rightarrow 1 - dx/x, \quad (3.48)$$

$$q_k \rightarrow q(x), \quad 0 \leq x \leq 1. \quad (3.49)$$

Finally, $q(x)$ is treated as a variational-parameter function and the extremum of $[F]$ with respect to $q(x)$ is taken in analogy with eqs. (3.21); a more precise discussion of extremization is given below.

Within the region of parameters for which replica symmetry is stable, $q(x)$ is a constant for all x ($0 \leq x \leq 1$), but in the region for which the RS-Ansatz is unstable $q(x)$ is not flat. For small reduced temperature $\tau = (T_g - T)/T_g$ the leading behaviour of $q(x)$ is shown in fig. 10.

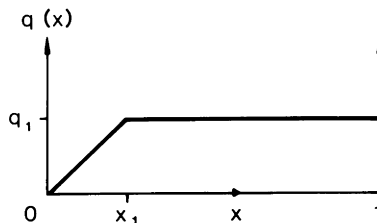


Fig. 10. Parisi order function $q(x)$ for the random-bond Ising model in zero external field at small reduced temperature τ . To leading order in τ , $q_1 = x_1 = \tau$.

* Recall that the notation $(\alpha\beta)$ refers to pairs of *different* labels α, β .

Before turning to a discussion of the implications of the Parisi Ansatz for observables such as the susceptibility, let us consider its interpretation (Parisi 1980). To this end, it is useful first to introduce another concept, that of overlap, and of its distribution.

The overlap between two microscopic Ising states s, s' is defined by

$$q^{ss'} = N^{-1} \sum_i \sigma_i^s \sigma_i^{s'}, \quad (3.50)$$

where $\{\sigma_i^s\}$ is the spin configuration in microstate s . The distribution of microscopic-state overlaps is given by

$$\tilde{P}(q) = \sum_{s, s'} p_s p_{s'} \delta(q - q^{ss'}), \quad (3.51)$$

where p_s is the probability of the microstate s . In a conventional thermodynamic ensemble

$$p_s = \frac{\exp(-H_s/kT)}{\text{Tr} \exp(-H_s/kT)}, \quad (3.52)$$

where H_s is the value of the Hamiltonian in state s .

The application of the replica procedure to the evaluation of $[\tilde{P}(q)]$, together with mean-field theory using the Parisi Ansatz, yields

$$[\tilde{P}(q)] = \int_0^1 \delta(q - q(x)) dx \equiv dx/dq. \quad (3.53)$$

Equation (3.53) thus provides an interpretation of $q(x)$ as the inverse of the average microstate distribution.

The relation (3.53) becomes more conceptually valuable when a further connection is also made. This concerns the distribution of overlaps between thermodynamic macrostates. The overlap distribution between two thermodynamic macrostates S, S' is defined by

$$q^{SS'} = N^{-1} \sum_i m_i^S m_i^{S'}, \quad (3.54)$$

where $\{m_i^S\}$ is the thermodynamic average of $\{\sigma_i\}$ in macrostate S . The macrostate overlap distribution is given by

$$P(q) = \sum_{SS'} P_S P_{S'} \delta(q - q^{SS'}), \quad (3.55)$$

where P_S is the probability of macrostate S ,

$$P_S = \frac{\exp(-F_S/kT)}{\sum_{S'} \exp(-F_{S'}/kT)} \quad (3.56)$$

with F_S being the free energy of state S .

The further important conceptual link arises from the fact that $P(q)$ can be shown to be identical to $\tilde{P}(q)$ for a system in Boltzmann–Gibbs thermodynamic equilibrium. Hence,

$$[P(q)] = dx/dq \quad (3.57)$$

and (dx/dq) is interpreted as giving the average overlap distribution of thermodynamic macrostates in a Boltzmann–Gibbs ensemble.

A conventional Ising ferromagnet has only two thermodynamic states, spin up and spin down and

$$P(q) = \frac{1}{2}(\delta(q - m^2) + \delta(q + m^2)), \quad (3.58)$$

where m is the magnetization per spin. An infinitesimal field suffices to eliminate the peak at $q = -m^2$. Correspondingly, $q(x)$ is a constant at $q = m^2$ for all x .

Similarly, in a region of replica symmetry, in which $q(x)$ is constant as a function of x , say with $q(x) = q_0$, $[P(q)]$ has a single delta function peak at $q = q_0$, which we interpret as implying a single thermodynamic state. By contrast, in the region of replica-symmetry breaking, in which $q(x)$ has structure, $[P(q)]$ has weight over a range of q , indicating the existence of many thermodynamic states. For example, for T just smaller than T_g and in the absence of a magnetic field, where $q(x)$ has the form shown in fig. 10, $[P(q)]$ has a delta function at $q = q(1)$, arising from the plateau in $q(x)$, together with a continuum between $q = 0$ and $q = q(1)$, arising from the ramp in $q(x)$; this is a general structure for any $T < T_g$, $b = 0$, although the detailed shape of the continuum varies with temperature. The delta function is interpreted as the overlap of a thermodynamic state with itself ($S = S'$ in eq. (3.54)), while the continuum corresponds to a range of overlaps between different non-equivalent states.

This identification of $P(q)$ as an overlap distribution of thermodynamic states leads to the expression of thermodynamic observables as integrals over $q(x)$. For example, we recall eq. (3.35) for the zero-field susceptibility of a system with symmetric $P(J_{ij})$:

$$\chi(t) = (kT)^{-1}(1 - [\langle\sigma_i\rangle^2]). \quad (3.55)$$

Averages such as $[\langle\sigma_i\rangle^2]$ follow directly from $[P(q)]$, from relations such as

$$[\langle\sigma_1\sigma_2\cdots\sigma_k\rangle^2] = \int dq q^k [P(q)] = \int_0^1 dx q(x)^k. \quad (3.59)$$

Hence, in particular,

$$[\langle\sigma_1\rangle^2] = \int dq q [P(q)] \quad (3.60)$$

$$= \int_0^1 dx q(x), \quad (3.61)$$

so that

$$\chi(T) = (kT)^{-1} \left(1 - \int_0^1 q(x) dx \right). \quad (3.62)$$

For $T > T_g$, $q(x)$ is zero and eq. (3.39) reproduces the Curie law. For $T < T_g$, Parisi theory gives

$$1 - \int_0^1 q(x) dx = T/T_g \quad (3.63)$$

and

$$\chi = (kT_g)^{-1}, \quad \text{all } T < T_g. \quad (3.64)$$

This result of Curie-like behaviour above T_g and flat $\chi(T)$ beneath T_g will be seen to match the experimental field-cooled results, as shown in fig. 2. On the other hand, if $q(x)$ is replaced by $q(1)$ in eq. (3.40), the resultant $\chi(T)$ is similar to the replica-symmetric result, with $\chi(T)$ decreasing monotonically beneath T_g . This is reminiscent of the zero-field cooled or a.c. susceptibility measurements. Thus one has apparent correspondences between field cooling and the exploration of all thermodynamic states, and between zero-field cooling and trapping in a single thermodynamic state.

It is interesting to note that the onset of replica-symmetry breaking represents an unusual type of phase transition which can lead to discontinuities in observables even in the presence of a finite conjugate field. Thus, for example, in an external field, $q(x)$ is non-zero for all x , but as long as the temperature is above that of the de Almeida-Thouless instability $q(x)$ is a constant. As the temperature is reduced through the AT value corresponding to the field, $q(x)$ acquires structure and the Gibbs average and single-state (or field-cooled and zero-field-cooled) susceptibilities start to diverge, despite the fact that the discontinuity in the former in the zero-field limit is removed in a finite field. The evolution of $q(x)$ with temperature in a finite field H is illustrated in fig. 11, while the resultant susceptibility is shown in fig. 12. In fig. 11, curve (a) corresponds to

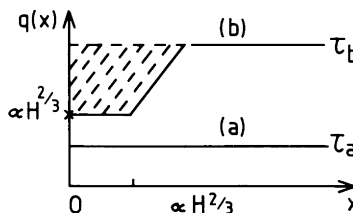


Fig. 11. $q(x)$ for a random-bond Ising model in Parisi mean-field theory for (a) $T > T_{AT}$, (b) $T < T_{AT}$. The hatched area determines the anomaly $\Delta = \chi_{FC} - \chi_{ZFC}$.

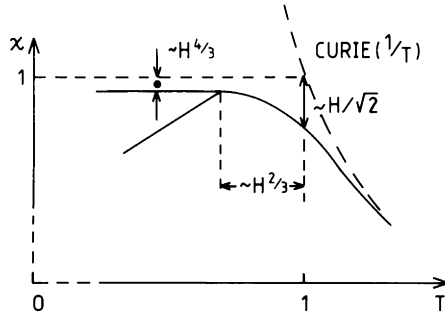


Fig. 12. Susceptibility of an Ising spin glass in an applied field H , as predicted by Parisi's mean-field theory. The upper curve shows the full Gibbs average, obtained from the full $q(x)$ and interpreted as the field-cooled (FC) susceptibility. The lower curve shows the result of restricting to one thermodynamic state, as obtained from $q(1)$ and interpreted as the zero-field-cooled susceptibility.

a value of the reduced temperature $\tau = (T_g - T)/T_g$ (where $T_g = J/k$) which is less than a critical value $\alpha H^{2/3}$ (where $\alpha = [3/(4J^2)]^{1/3}$) and yields

$$q(x) = \tau_a = \frac{1}{2}(\tau + (\tau^2 + 2H)^{1/2} + \dots). \quad (3.65)$$

As the temperature is lowered τ_a increases until it reaches $\alpha H^{2/3}$. Beyond this temperature $q(0)$ is pinned at $\alpha H^{2/3}$ but $q(1)$ continues to rise, as shown in curve (b). The difference between the two susceptibilities, Gibbs (or FC) and single-state (or ZFC), is given by

$$\Delta = (kT)^{-1} \left(q(1) - \int_0^1 q(x) dx \right) \quad (3.66)$$

and is indicated (without the $(kT)^{-1}$ factor) by the hatched region of the curve. The susceptibility curves of fig. 12 follow directly from*

$$\chi_{\text{FC}} = (kT)^{-1} \left(1 - \int_0^1 q(x) dx \right), \quad (3.67)$$

and

$$\chi_{\text{ZFC}} = (kT)^{-1}(1 - q(1)). \quad (3.68)$$

The Parisi solution exhibits several other interesting features. In particular we shall mention ultrametricity (Rammal et al. 1986, Mézard et al. 1984) and non-self-averaging (Rammal et al. 1986, Bray et al. 1984).

Ultrametricity. A space is described as “ultrametric” if distances in that space obey the following property: given three points a, b, c separated by “distances” in

* For convenience we use the labels FC, ZFC, although strictly the quantities given are the Gibbs ensemble and single-state susceptibilities, whose relation to FC, ZFC is strictly a conjecture.

some space d_{ab} , d_{bc} , d_{ca} and labelled such that

$$d_{ab} \geq d_{bc} \geq d_{ca}, \quad (3.69)$$

then

$$d_{ab} = d_{bc}; \quad (3.70)$$

i.e. the two largest distances between three points are equal. To relate this to the present study, we note that distance and overlap are complementary; distance is a measure of separation, overlap of similarity. Thus, a space of overlaps is ultrametric if for three states S , S' , S'' labelled so that

$$q^{SS'} \leq q^{S'S''} \leq q^{S''S}, \quad (3.71)$$

one has

$$q^{SS'} = q^{S'S''}; \quad (3.72)$$

i.e. the two smallest overlaps are equal.

With the definition of overlap given in eq. (3.54), Parisi theory predicts such ultrametricity of a non-trivial nature (trivial ultrametricity corresponding to when all the q are equal). A particular interest in this result lies in its implication of hierarchical order. This implication is obvious if one considers a hierarchical tree as shown in fig. 13, takes its endpoints as the states and their pairwise overlap as determined by how far back in the evolutionary tree one needs to go to find a common ancestor, the overlap being smaller the farther back one needs to go. One readily sees that for any three states the two smallest overlaps are

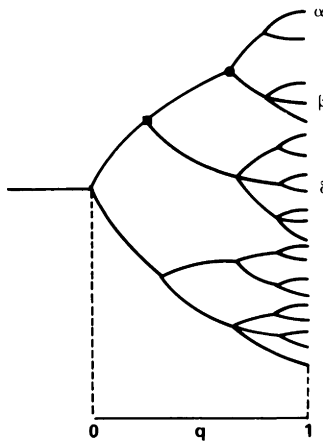


Fig. 13. An evolutionary tree, illustrating the occurrence of ultrametricity. If the overlap between two final states is measured by the degree of evolution of their nearest common ancestor, as shown, then for any group of three final states, the two smallest overlaps are equal.

equal. This observation of ultrametricity of magnetization overlaps within the Parisi analysis of spin glasses (Mézard et al. 1984), and similar ones of ultrametricity of energy overlaps (Athanasius et al. 1987), further justify* the conception of spin glasses as having free-energy surfaces with hierarchical hills-and-valleys structure (see fig. 4.), since if one considers valleys in a mountain landscape as “states” and the height of the lowest col separating two valleys as their “separation” (or inverse measure of their “overlap”) then those separations are ultrametrically ordered.

Non-self-averaging. As discussed earlier, intuition from ergodic-type ideas in conventional statistical mechanics leads one to expect that physical observables will possess the self-averaging feature; i.e. for an observable A of positive expectation value,

$$\lim_{N \rightarrow \infty} \left\{ \frac{\{[A^2] - [A]^2\}^{1/2}}{[A]} \right\} = 0. \quad (3.73)$$

The Parisi Ansatz indeed maintains self-averaging for the normal observables such as energy, free energy and their derivatives. On the other hand, however, the distribution of overlaps is not self-averaging and therefore neither are its moments. For example, consider

$$A = q = N^{-1} \sum_i \langle \sigma_i \rangle^2. \quad (3.74)$$

Now

$$(\Delta q)^2 = [q^2] - [q]^2 \quad (3.75)$$

$$= \int_0^1 q^2(x) dx - \left(\int_0^1 q(x) dx \right)^2, \quad (3.76)$$

which is zero if $q(x)$ is flat (replica-symmetric) but not if $q(x)$ has structure; i.e. replica-symmetry breaking leads to non-self-averaging of the overlaps, again a manifestation of the many non-equivalent states. In fact, within the Parisi Ansatz the overlap probability measure which is self-averaging is the distribution function of the distribution function $P(P(q))$ (Mézard et al. 1984).

The full Parisi analysis, or an equivalent temporal analysis of Sompolinsky (1981), Sompolinsky and Zippelius (1981, 1982) and De Dominicis et al. (1981) leads to a further deduction [Sompolinsky (unpublished)] that the free-energy landscape evolves chaotically as the parameters are changed; i.e. a small change in the actual set of $\{J_{ij}\}$ or of the temperature or applied field causes a non-trivial change in the hill-valley structure. Indeed one might have anticipated this

*They were originally conceived as a result of more philosophical considerations and via computer simulations, e.g. Kirkpatrick and Sherrington 1978.

result from the quality of the folklore mappings between Gibbs/single-state and FC/ZFC susceptibilities.

3.3. The Sherrington–Kirkpatrick model

Although mean-field theory can only be considered approximate for systems with short-range interactions, the above analysis is believed to be exact for a special model in which every spin interacts with every other spin, but via quenched random interactions with an appropriate scaling with N . This is the Sherrington–Kirkpatrick (SK) model (Sherrington and Kirkpatrick 1975), characterized in its Ising version by a Hamiltonian

$$H = - \sum_{(ij)} J_{ij} \sigma_i \sigma_j, \quad (3.77)$$

where the sum is over all pairs (ij) and the J_{ij} are quenched parameters chosen randomly and independently from a distribution with moments

$$[J_{ij}] = \tilde{J}_0 = J_0/N, \quad (3.78)$$

$$[J_{ij}^2] = \tilde{J}^2 = J^2/N. \quad (3.79)$$

Equation (3.18) is readily derived by the following procedure: (1) Replica theory is used to express $[F]$ as in eq. (3.14) but with (ij) now running over all pairs of sites. (2) The σ -summations in the exponent are expressed as complete squares,

$$\sum_{(ij)} \sigma_i^\alpha \sigma_j^\alpha = \frac{1}{2} \left(\left(\sum_i \sigma_i^\alpha \right)^2 - 1 \right), \quad (3.80)$$

$$\sum_{(ij)} \sigma_i^\alpha \sigma_i^\beta \sigma_j^\alpha \sigma_j^\beta = \frac{1}{2} \left(\left(\sum_i \sigma_i^\alpha \sigma_i^\beta \right)^2 - 1 \right), \quad (3.81)$$

and eq. (3.25) used to express $[F]$ in terms of integrals of effective single-site paramagnets over auxiliarily fields as

$$[F] = -kT \lim_{N \rightarrow \infty} \lim_{n \rightarrow 0} \frac{1}{n} \left[\int \prod_\alpha d\tilde{m}^\alpha \prod_{(\alpha\beta)} d\tilde{q}^{(\alpha\beta)} \exp(-N\beta g(\{\tilde{m}^\alpha\}, \{\tilde{q}^{(\alpha\beta)}\})) - 1 \right], \quad (3.82)$$

where

$$\begin{aligned} g(\{\tilde{m}^\alpha\}, \{\tilde{q}^{(\alpha\beta)}\}) &= kT \ln \text{Tr} \exp \left[\beta J_0 \sum_\alpha \sigma^\alpha \tilde{m}^\alpha \right. \\ &\quad \left. + (\beta J)^2 \left(n + 2 \sum_{(\alpha\beta)} \sigma^\alpha \sigma^\beta \tilde{q}^{(\alpha\beta)} \right) \right]. \end{aligned} \quad (3.83)$$

Because g is independent of N , the integral of eq. (3.82) is overwhelmingly dominated by the values of $\{\tilde{m}^\alpha\}$, $\{\tilde{q}^{(\alpha\beta)}\}$ for which g is minimized. This ex-

tremum has

$$\tilde{m}^\alpha = m^\alpha, \quad (3.84)$$

$$\tilde{q}^{(\alpha\beta)} = q^{(\alpha\beta)}, \quad (3.85)$$

where $m^\alpha, q^{(\alpha\beta)}$ are as given in eqs. (3.19)–(3.22). The free energy $[F]$ is as given in eq. (3.18).

3.4. Further subtleties

Before leaving this mean-field analysis, two further subtleties are worthy of note since they illustrate the need for caution in passing conventional procedures to unconventional phase transition problems.

If the replica-symmetric Ansatz is employed and the extremum of $[F]$ with respect to q considered, then the extremum giving the phases correctly is that maximizing $[F]$ with respect to q , in stark contrast to conventional minimization. At a simple level this can be interpreted as a consequence of the fact that the number of $(\alpha\beta)$ -combinations is $n(n - 1)/2$ so that the number of $q^{(\alpha\beta)}$ becomes negative as n tends to zero.

A second unconventional-looking feature is that if one analytically continues the high temperature free energy $[F]$, with $m = q = 0$, to $T < T_g$, the result is lower than the free energy of the spin glass solutions. In fact, however, the analytic continuation of a state beyond the limit of its validity is strictly meaningless.

The relevant criterion, which gives both the above points correctly, is that the system must be stable against all fluctuations. In the present problem this means that g must be stable against all $m^\alpha, q^{(\alpha\beta)}$ -fluctuations.

Computer simulations of the SK model (Kirkpatrick and Sherrington 1978, Young 1983, Bhatt and Young 1985, 1987, 1988) confirm the above pictures. For example, in figs. 14a, b are shown the results of simulations (Young 1983, 1985) of $[P(q)]$, (a) above the AT line for $H \neq 0$ and (b) below the AT line for $H = 0$, for a series of sample sizes N . As N is increased, the curves approach the Parisi predictions of eq. (3.57).

Other studies (Bhatt and Young 1985, 1987, 1988, 1989, Parga et al. 1984) demonstrate the occurrence of ultrametricity and non-self-averaging (Bray et al. 1984).

Finally, in this section, we note that the free energy in the Parisi Ansatz for $J_0 = 0$ is given by

$$\begin{aligned} [F] = & -\frac{1}{4}\beta J^2 N \left\{ 1 - 2q(1) + \int_0^1 q^2(x) dx \right\} \\ & - \frac{1}{(2\pi)^{1/2}} N k T \int_{-\infty}^{\infty} e^{-z^2/2} G(0, H + q(0)^{1/2}z) dz, \end{aligned} \quad (3.86)$$

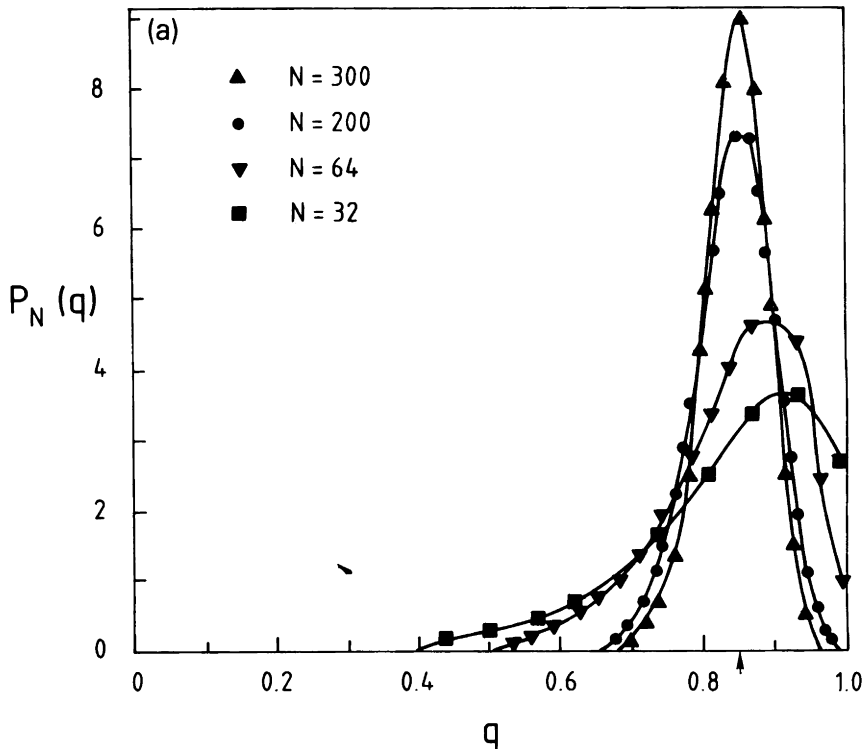


Fig. 14. (a)

where $G(x, y)$ is the solution of the partial differential equation

$$\frac{\partial G}{\partial x} = -\frac{1}{2}J^2 \frac{\partial q}{\partial x} \left[\frac{\partial^2 G}{\partial y^2} + x \left(\frac{\partial G}{\partial y} \right)^2 \right] \quad (3.87)$$

with the boundary condition

$$G(1, y) = \log[2 \cosh(\beta y)]. \quad (3.88)$$

The reader will probably have noticed that in fig. 12 the full Gibbs-averaged zero-field susceptibility is constant in the spin glass phase at

$$\chi(T < T_g) = (kT_g)^{-1}. \quad (3.89)$$

This result can be obtained either from a perturbative solution to the Parisi equations, or directly by gauge transformation of the variables mentioned earlier (Sommers 1983). This constant behaviour of $\chi(T < T_g)$ reflects itself in the vertical character of the phase line separating spin glass and ferromagnet in fig. 9

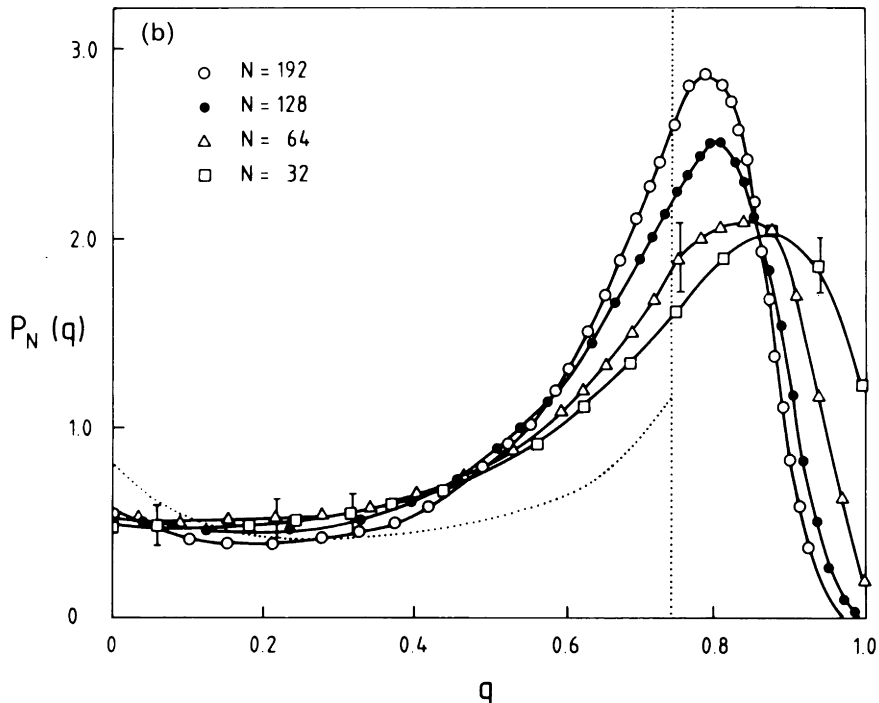


Fig. 14. (a) Monte Carlo simulations of $[P_N(q)]$ for the SK model for several sizes at $T = 0.4J$, $H = 1.2J$, which is above the AT line. The results are consistent with a Gaussian distribution centred on the value of q given by replica mean-field theory (indicated by the arrow) and of width scaling as $N^{-1/2}$; from: Young 1985. (b) Monte Carlo simulations of $[P_N(q)]$ for the SK model for several sizes at $T = 0.4$, $H = 0$, which is below the AT line. The dotted line is an approximate solution of Parisi's equations and consists of a delta function of width $\frac{4}{3}$ at $q = 0.744$ and a continuum with finite weight down to $q = 0$; from: Young 1983.

(Toulouse 1980); indeed the predicted values of $\chi(T < T_g)$ and the phase line $J_0(T)$ separating spin glass and ferromagnet are related by the condition (Toulouse 1980)

$$J_0(T) \chi(T) = J, \quad (3.90)$$

hence further relating the different characters also of the replica-symmetric results for these curves.

4. Short-ranged spin glasses

The SK model is effectively range-free; often referred to as infinite-ranged. As we have noted, mean-field theory, in its sophisticated form, is believed to be exact

for this model, so that the results of the last section hold. Real experimental spin glass materials have exchange interactions which die off with distance. Because of thermodynamic fluctuations, mean-field theory cannot be relied on. For conventional systems, mean-field theory gives the correct exponents only above an upper critical dimension (u.c.d.), while a phase transition itself only persists above a lower critical dimension (l.c.d.). The questions therefore arise as to what is the lower critical dimension for short-ranged spin glasses, whether there is a finite upper critical dimension and whether the novel concepts obtained from mean-field theory, such as ultrametricity and non-self-averaging, persist in real spin glasses. Several of these questions remain controversial and will not be pursued here. We shall only concentrate on some evaluations of the l.c.d. and comment that perturbation analysis around mean-field theory shows significant subtleties compared with conventional magnets*. There is now universal agreement that the l.c.d. of the short-range Ising spin glass lies between two and three. It is interesting to consider some of the evidence, which falls into two categories, computer-simulative and analytical, the latter from high-temperature series expansions, e.g. for the spin glass susceptibility χ_{SG} . Here we shall concentrate on the first of these categories, numerical studies.

The earliest computer evidence for the absence of spin glass ordering in two dimensions came from computer-simulative studies of the averaged squared spin correlation function [$\langle \sigma(\mathbf{R} - \mathbf{R}')\sigma(\mathbf{R}') \rangle^2$], using transfer matrix techniques to show decay with \mathbf{R} (Morgenstern and Binder 1979).

A more recent demonstration relies on the scaling with distance of the effective exchange interaction between blocks of spins (Bray and Moore 1984). The effective block-spin interaction strength may be determined as follows. Consider the same randomly generated sample of linear dimension L with first periodic and second antiperiodic boundary conditions in one direction. The difference in the ground-state energies associated with these two types of boundary conditions gives a measure of the interaction at scale L . For a spin glass system with a symmetric exchange distribution at the microscopic level, this energy difference can be either positive or negative depending on the particular choice of microscopic exchanges; i.e. the random sign character is preserved as the scale is varied, continuing the spin-glass-like character of the effective Hamiltonian. From the distribution over microscopic choices of $\{J_{ij}\}$ one generates a distribution $P_L(J)$ at scale L . Just as it is convenient to characterize a symmetric microscopic $P(J_{ij})$ in terms of its standard deviation J , so too a useful measure of the effective width of the spin distribution at scale L is the standard deviation of the energy difference between periodic and anti-periodic boundary conditions. Another is the average modulus. In each case, the relevant measure is to normalize the energy difference by L to give the effective

* See e.g. De Dominicis and Kondor (1985).

exchange strength at length L , $J(L)$. By studying the asymptotic behaviour as $L \rightarrow \infty$ one may deduce whether there is cooperative order in the ground state of the infinite system. Thus one has

$$\begin{aligned} \lim_{L \rightarrow \infty} J(L) &= 0, \quad \text{no order,} \\ &= \infty, \quad \text{order.} \end{aligned} \tag{4.1}$$

Bray and Moore (1984) used such a zero-temperature scaling procedure to assess the existence or otherwise of an ordered spin glass phase in an Ising system in two and three dimensions. In numerical studies of a system with an initially symmetric $P(J_{ij})$ they found that this symmetry was preserved at scale L and that $J(L)$ scaled as

$$J(L) \sim JL^y \tag{4.2}$$

with $y < 0$ for $d = 2$, $y > 0$ for $d = 3$. Thus they deduced that Ising spin glass order is possible in three dimensions but not in two.

Another piece of numerical evidence that the lower critical dimension of an Ising spin glass with short-ranged interactions lies between two and three comes from the Monte Carlo simulation studies of Bhatt and Young (1985, 1987, 1988) and of Ogielski and Morgenstern (1985a, b) (see also Ogielski 1987).

In Monte Carlo simulations of statistical mechanics, one devises a computer algorithm which dynamically and probabilistically generates a temporal distribution which matches the Boltzmann–Gibbs ensemble distribution over long times*. There are several ways to effectuate this, although to be viable one needs to employ importance sampling† (Metropolis et al. 1953). For the results to be representative of thermal equilibrium, it is essential that the simulations be carried out long enough to allow the system to come to equilibrium and be independent of the starting state before commencing any sampling which is to be used in determining thermodynamic averages, and also to extend for a further period which is longer than this equilibrium time, during which measurements providing the average can be taken. In spin glasses and other frustrated systems, this equilibrium time is very long and increases with decreasing temperature and with increasing size of sample, placing severe restrictions on simulations, even with powerful (Bhatt and Young 1985, 1987, 1988) or special-purpose computers (Ogielski and Morgenstern 1985a, b, Ogielski 1987).

It is clearly relevant to be able to assess when equilibration has been achieved. Bhatt and Young (1985, 1987, 1988) devised a particularly elegant test involving the use of two different simulational approaches to the spin glass susceptibility, approaching the thermodynamic value from above and from below, with the

* If one wishes to simulate real dynamics, more conditions are required.

† For a discussion of Monte Carlo principles and procedures see e.g. Binder 1979.

coalescence and subsequent quiescence determining a measure of the equilibration time; thus

$$q^{(2)} = N^{-1} \sum_{ij} [\langle \sigma_i \sigma_j \rangle^2] \quad (4.3)$$

is the long-time limit of both

$$q_U^{(2)}(t) = \left[N^{-2} \sum_{ij} \sigma_i(t + t_0) \sigma_j(t + t_0) \sigma_i(t_0) \sigma_j(t_0) \right] \quad (4.4a)$$

$$= \left[\left(N^{-1} \sum_i \sigma_i(t + t_0) \sigma_i(t_0) \right)^2 \right], \quad (4.4b)$$

and

$$q_L^{(2)}(t) = \left[\frac{1}{t} \int_{t_0}^{t_0+t} dt' N^{-2} \sum_{ij} \sigma_i^{(1)}(t') \sigma_j^{(1)}(t') \sigma_i^{(2)}(t') \sigma_j^{(2)}(t') \right] \quad (4.5a)$$

$$= \frac{1}{t} \int_{t_0}^{t_0+t} dt' \left[\left(N^{-1} \sum_i \sigma_i^{(1)}(t') \sigma_i^{(2)}(t') \right)^2 \right]. \quad (4.5b)$$

$q_U^{(2)}(t)$ can be obtained in the simulation of single systems with correlations in time. At $t = 0$, $q_U^{(2)}(t = 0) = 1$ and $q_U^{(2)}(t)$ approaches the limit $q_U^{(2)}(t = \infty) = q^{(2)}$ from above. $q_L^{(2)}(t)$ can be obtained from the comparison of a pair of systems with identical $\{J_{ij}\}$ evolving independently. At $t = 0$ these systems will be uncorrelated so that $q_L^{(2)}(t = 0) = 0$ and $q_L^{(2)}(t)$ approaches $q_L^{(2)}(t = \infty) = q^{(2)}$ from below. In both cases t_0 is a time greater than the equilibration time (determined a posteriori).

For a finite-sized system phase transitions are smoothed but finite-size scaling can be used to sharpen their identification. In particular, if one assumes a single correlation length ξ , which diverges as $T \rightarrow T_g$, then the order parameter distribution over systems of size L near T_g is given by the scaling form.

$$P(q) = L^{\beta/\nu} \tilde{P}(qL^{\beta/\nu}, L^{1/\nu} \tau) + \text{less singular corrections}, \quad (4.6)$$

where $L = N^{1/d}$, $P(x, y)$ is a universal function (for any particular universality class), $\tau = (T_g - T)/T_g$, and β and ν are critical exponents. A convenient measure to estimate the transition temperature is thus (Bhatt and Young 1985, 1987, 1988)

$$g_L(T) = \frac{1}{2} \left\{ 3 - \left[\frac{\langle q^4 \rangle}{\langle q^2 \rangle^2} \right] \right\}, \quad (4.7)$$

where the spin glass order parameter q ,

$$q = N^{-1} \sum_i \langle \sigma_i \rangle^2, \quad (4.8)$$

is here obtained either by temporal correlations of a single system

$$q(t) = N^{-1} \sum_i \sigma_i(t + t_0) \sigma_i(t_0) \quad (4.9)$$

or by cross-correlation between two replicas

$$q(t) = N^{-1} \sum_i \sigma_i^{(1)}(t) \sigma_i^{(2)}(t). \quad (4.10)$$

Clearly, in the limit $N \rightarrow \infty$, for $T > T_g$, $P(q)$ will be Gaussian-distributed around zero,

$$[\langle q^4 \rangle] = 3[\langle q^2 \rangle^2], \quad (4.11)$$

and $g_L(T > T_g)$ will be zero, whereas for $T < T_g$, assuming a single thermodynamic state, $P(q)$ will have an essentially delta function peak and $g_L(T < T_g)$ will be equal to 1. Hence $g(T)$ will have a step function form at T_g ,

$$\begin{aligned} g_\infty(T) &= \theta(T_g - T) = 1, & T_g > T, \\ &= 0, & T_g < T. \end{aligned} \quad (4.12)$$

For finite L this step-function form will be smoothed out more so the smaller is L , but one would expect the curves to cross at $T = T_g$, thereby pin-pointing the transition temperature. More precisely, the scaling law (4.6) implies as leading behaviour

$$g_L(T) = \tilde{g}(L^{1/v} \tau), \quad (4.13)$$

where $g(x)$ is universal, again implying that the curves cross at $\tau = 0$ ($T = T_g$), with the slope at crossing yielding the exponent v . A further check is provided by fitting g and P to scaling plots.

In fig. 15 are shown curves (Bhatt and Young 1985, 1987, 1988) for $g_L(T)$ for a four-dimensional random-bond Ising model. They clearly demonstrate the transition. For the two-dimensional case the curves for $g_L(T)$ for decreasing T appear only to be coming together at $T = 0$ implying that there is no finite-temperature phase transition in this case. For $d = 3$, the situation is more unusual; the curves for $g_L(T)$ coalesce at a critical $T = T_g$ (see fig. 16a), obeying scaling plots for $T \geq T_g$ (see figs. 16b, 17), but for $T < T_g$ they remain together. This suggests that there is a spin glass phase transition for the three-dimensional short-range Ising model, but leaves open the possibility that this transition may be more complicated than the single-phase/single-correlation length which was assumed in the scaling analysis.

It is now universally accepted that indeed there is a phase transition for the three-dimensional short-range spin glass, but it remains controversial as to whether the spin glass phase is single-phase (Bray and Moore 1987a, Fischer and Huse 1988), as in a conventional magnet, or multi-phase (Sourlas 1988, Caracciolo et al. 1990), as in the SK model.

Irrespective of the question of the number of phases at low temperature, there does seem to be evidence that the energy landscape of finite-dimensional short-

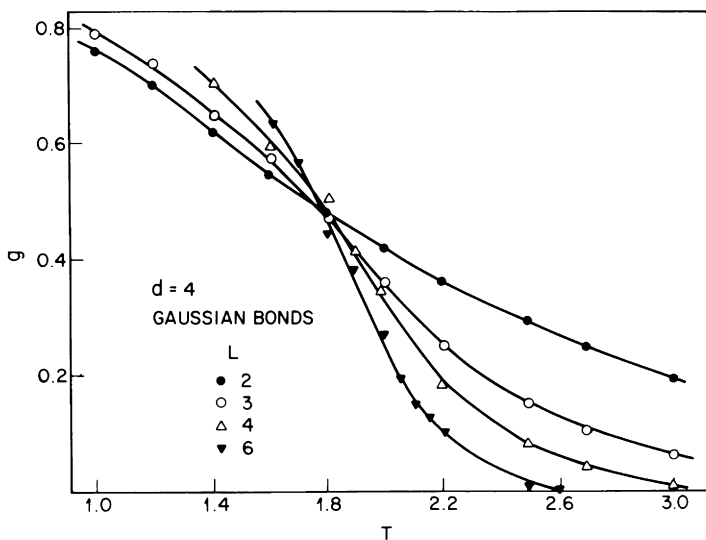


Fig. 15. $g_L(T)$ curves for a nearest-neighbour Ising spin glass in four dimensions; from: Bhatt and Young 1987.

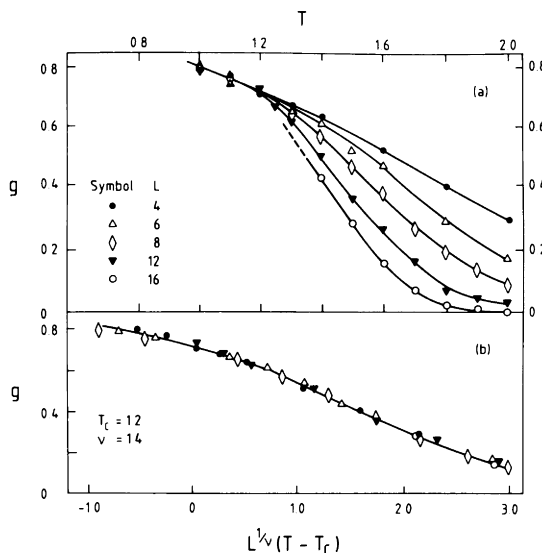


Fig. 16. (a) $g_L(T)$ for the $\pm J$ spin glass on a three-dimensional simple cubic lattice for a range of L . Curves for different sizes merge together at the spin glass transition. (b) Scaling plot of $g_L(T)$ showing how data for all sizes fall on a universal curve above T_g , when plotted against $L^{1/\nu}(T - T_g)$; from: Bhatt and Young 1985.

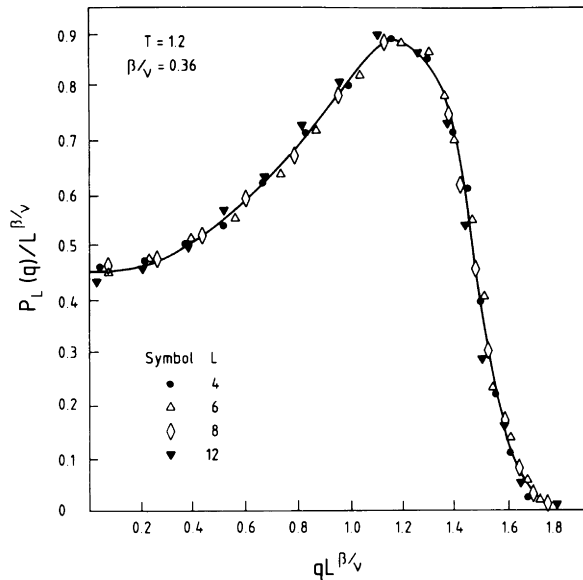


Fig. 17. Scaling plot of the order-parameter distribution function $P_L(q)$; from: Bhatt and Young 1985.

range spin glasses evolves chaotically with changes in parameters, much as has already been deduced for the infinite-ranged SK model. Bray and Moore (1987b) repeated their scaling study of $J(L)$, now comparing the case of two slightly different sets of $\{J_{ij}\}$, viz.

$$\{J_{ij}^{(1)}\} = \{J_{ij}\}, \quad (4.14a)$$

and

$$(J_{ij}^{(2)}) = \{J_{ij}\} + \{\Delta_{ij}\}, \quad (4.14b)$$

where $\{J_{ij}\}$ and $\{\Delta_{ij}\}$ are drawn randomly from Gaussian distributions of width J and $\varepsilon \ll J$ respectively. The resultant block-spin exchanges in each case (again based on the difference between periodic and antiperiodic boundary conditions) were used to generate corresponding effective block-spin distributions of widths $J(L)$ and $\varepsilon(L)$ respectively, and the scaling of $\varepsilon(L)$ and $J(L)$ was studied. Apart from the $J(L)$ scaling discussed above, it was found that

$$\varepsilon(L)/J(L) \sim L^\xi, \quad (4.15)$$

with $\xi > 0$ even for $d = 2$. It was argued that this inequality is true for all d . Small deviations in the initial J_{ij} distribution lead to diverging ground-state

differences. A similar chaotic evolution is expected to result from other perturbations, such as the temperature and applied field.

Another set of computer simulation experiments offers further evidence for a non-trivial free-energy structure/dynamic behaviour even above the critical temperature for a true thermodynamic phase transition (Derrida and Weisbuch 1988, Ogielsky 1985). In these experiments, a single disordered system is allowed to evolve from two different starting configurations via Monte Carlo dynamics with identical random numbers at each stage for each of the two sequences and the instantaneous configurations are compared. A useful monitor is the Hamming “distance” between the two configurations, A and B, defined by

$$D^{AB}(t) = (4N)^{-1} \sum_i (\sigma_i^A(t) - \sigma_i^B(t))^2 \quad (4.16)$$

and simply related to the overlap

$$q^{AB}(t) = N^{-1} \sum_i \sigma_i^A(t) \sigma_i^B(t) \quad (4.17)$$

by

$$D^{AB}(t) = (1 - q^{AB}(t)). \quad (4.18)$$

The long-time behaviour of $[D^{AB}(t)]$ was studied by Derrida and Weisbuch (1988) up to $t \sim 500$. It was found that for a three-dimensional system there are three temperature regions:

- (1) $T > T_2$: $D(t \rightarrow \infty)$ goes to zero independently of $D(0)$.
- (2) $T_2 > T > T_1$: $[D(t \rightarrow \infty)]$ goes to a temperature-dependent value (increasing monotonically as T decreases) independently of $D(0)$.
- (3) $T_1 > T$: $D(t)$ tends to a different non-zero value for different $D(0)$.

In the last two cases there was found little dependence of $D(t \rightarrow \infty)$ on size. T_1 was found to be comparable with the phase-transition temperature determined by other methods. T_2 was found to be some three times larger. The temperature region beneath T_1 is identified as that of the true spin glass phase. The temperature range between T_1 and T_2 is identified as having a free-energy structure with many valleys separated by high barriers so that the systems are effectively trapped in single valleys for long periods, but insufficient for a true phase transition. A similar separation of the region above the phase transition was found by Ogielski (1985) in his extensive simulations of the $3d \pm J$ spin glass, in terms of the decay of $q(t)$, the spin autocorrelation function; he found a high-temperature region with $q(t)$ decreasing exponentially in time and an intermediate region with slow (stretched exponential) decay.

In two dimensions $T_1 \rightarrow 0$ while T_2 remains finite. A further analysis of $D(t)$ from random starting configuration pairs ($\{S_i(0)\}$, $\{-S_i(0)\}$) gives extra confirmatory weight to the interpretation of T_2 as a dynamic phase transition by studying the finite-size scaling of the relaxation times away from the

initial state:

$$\tau_n = \sum_{t=0}^{t_e} t^n D(t) / \sum_t D(t), \quad (4.19)$$

where t_e is the time for the two configurations to become equal with

$$[\tau_1] \sim L^z f(L^{1/v}(T - T_2)/T_2), \quad (4.20)$$

and

$$[\tau_2/\tau_1^2] \sim g(L^{1/v}(T - T_2)/T_2), \quad (4.21)$$

so that a crossing-analysis analogous to that used for the static transition by Bhatt and Young determines T_2 and v , while $[\tau_1]$ yields z . Neumann and Derrida (1988) found for $d = 2$

$$T_2/J = 1.6 \pm 0.1, \quad (4.22)$$

$$z = 1.7. \quad (4.23)$$

This identification of an intermediate region of free-energy hills and valleys, together with chaotic evolution upon changing parameters presumably underlies the observation of Kinzel (1979), in Monte Carlo simulations of remanent magnetization in a two-dimensional random-bond Ising model, of a difference between TRM and IRM beneath a temperature-dependent critical field (see fig.

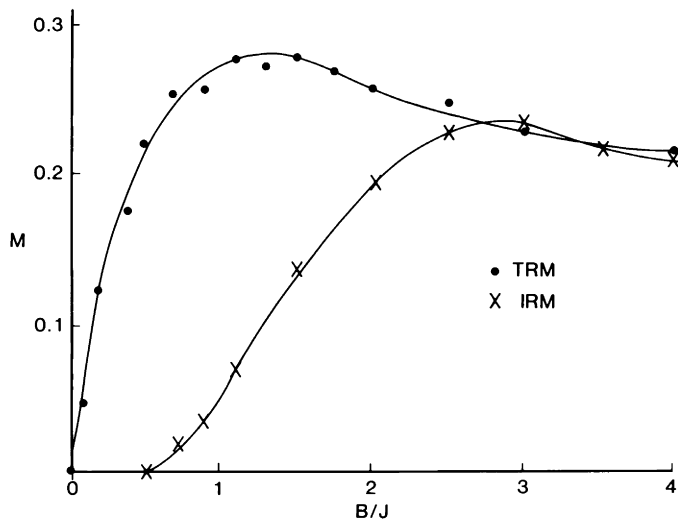


Fig. 18. Results of Monte Carlo simulations of isothermal remanent magnetization (IRM) and thermoremanent magnetization (TRM) for a Gaussian random-bond Ising model on a square net at $T = J/4k$; from: Kinzel (1979).

18) with results which are remarkably reminiscent of the experimental curves, e.g. AuFe (see fig. 3), despite the fact that it is now believed there is no true equilibrium phase transition in this case.

5. Vector spin glasses

So far we have discussed only Ising spin systems in which the spins are allowed only two orientations. Most (but not all) experimental systems have spins with greater orientational freedom and it is therefore of interest to consider the case of more general m -vector spin glasses, in which fixed-length spins* are free to orient in m -dimensional space, determined by a Hamiltonian

$$H = - \sum_{(ij)} J_{ij} \mathbf{S}_i \cdot \mathbf{S}_j, \quad (5.1)$$

where the \mathbf{S}_i are fixed-length vectors in m -space and either the sum is over magnetic site-pairs with J_{ij} a function of the site separation, or the $\{J_{ij}\}$ are distributed randomly according to a distribution $P(J_{ij})$. Provided that $P(J_{ij})$ is symmetric and there is no external field, replica mean-field theory is readily extended and believed to be exact for an infinite-range interaction. It yields an isotropic spin glass order on average[†]. The order parameter is

$$q_{\mu\nu}^{\alpha\beta} = N^{-1} \sum_i \langle S_{i\mu}^\alpha S_{i\nu}^\beta \rangle = q^{\alpha\beta} \delta_{\mu\nu}, \quad (5.2)$$

where μ, ν label Cartesian directions. On the other hand, if there is a magnetic field or a spontaneous ferromagnetic moment, then the orientational symmetry is broken and the direction of the magnetization is singled out with average orientational symmetry only among the components orthogonal to this direction. Even though an external field always induces a magnetization along its direction, a spin glass phase transition still occurs in the orthogonal directions (Gabay and Toulouse 1981); for small external fields H and symmetric $P(J_{ij})$, this transverse spin-glass ordering temperature is given by (Gabay and Toulouse 1981).

$$T_\perp = T_g - [(m^2 + 4m + 2)H^2/4(m + 2)^2 T_g^3] + O(H^4) \quad (5.3)$$

where $T = J/\sqrt{m}$ is the spin glass transition temperature for $H = 0$. Similarly, for $H = 0$ but J_0 large enough for spontaneous ferromagnetism, two ferromagnetic phases are predicted by mean-field theory, a higher-temperature phase in which the ferromagnetic ordering is collinear, and a lower-temperature phase in which there is (apparently) random canting around the ferromagnetic axis; or

* It is also interesting to consider itinerant and other soft-spin situations but this we shall not do here; see however, Sherrington and Mihill (1974), Hertz (1979) and Sherrington (1981).

[†] There is an exception to the isotropic ordering for the four-state clock model; Nobre et al. 1989.

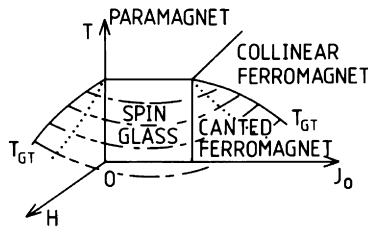


Fig. 19. Schematic mean-field phase diagram for $m > 1$ vector model. Phase transition lines are indicated by solid curves. Chain hatching indicates the Gabay–Toulouse surface. Dotted lines designate cross-overs; from: Sherrington 1983.

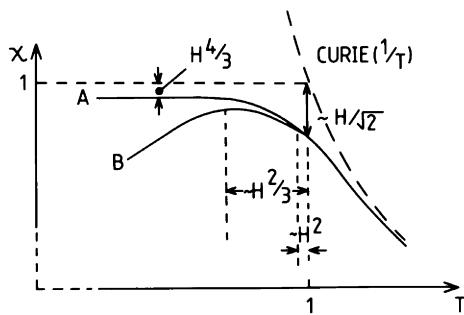


Fig. 20. Schematic plot of the longitudinal susceptibility of an $m > 1$ vector spin glass. Curve A indicates the full Gibbs average/field-cooled. Curve B indicates the single-state average/zero-field-cooled case; from: Sherrington 1983.

equivalently there is transverse spin glass order as well as longitudinal ferromagnetism*. The mean-field phase diagram is illustrated schematically in fig. 19.

Replica-symmetry breaking occurs in the mean-field theory of the vector spin glass too. For the isotropic case it occurs everywhere inside the spin glass phase; in the case of anisotropy induced by an applied field or spontaneous ferromagnetism, replica-symmetry breaking occurs within the region with transverse spin glass ordering (Cragg et al. 1982). In each case, however, the effect is weak as the temperature is lowered through the transition until a lower “cross-over” temperature is reached, reminiscent in its (H, J_0) -dependence of the de Almeida–Thouless surface (Cragg et al. 1982, Elderfield and Sherrington 1983). The consequences for the longitudinal susceptibility are shown in fig. 20, showing the onset of irreversibility $\Delta(T)$, or difference between Gibbs and single-state susceptibility, and its cross-over from a weak to a strong effect. Similar effects are observed experimentally (Hamzic and Campbell 1981, Lauer and Keune 1982,

* Of course even in the collinear ferromagnetic state not all the spin averages on different sites are the same, just as is the case in the frustrated ferromagnets obtained in the higher J_0/J part of the phase diagram of the Ising examples discussed earlier.

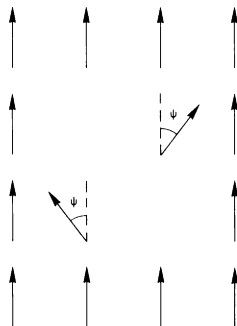


Fig. 21. Illustration of the canting which occurs in the ground state of a two-dimensional square lattice with R in the range $\frac{1}{2} > R > \frac{2}{3}$ when diagonal sites are removed in a single unit cell, with the spins outside the cell pinned to be ferromagnetic; from: Dunlop and Sherrington 1985.

Kett et al. 1981). For more complete reviews of replica theory of the vector spin glass the reader is referred to Elderfield and Sherrington (1984) and Sherrington (1983).

Since replica theory is rather formal and an infinite-range system rather difficult to envisage, it is perhaps helpful to note how transverse spin glass ordering can occur in a short-range frustrated ferromagnet. This can be done for either random-site or random-bond disorder but let us consider here the former, with interactions which are nearest-neighbour (J_1) ferromagnetic, next-nearest-neighbour (J_2) antiferromagnetic. For the undiluted system to be collinearly ferromagnetic, the ratio $R = J_1/|J_2|$ must exceed a critical value;* this we assume to be the case. Now consider diluting the pure ferromagnet. As one removes spins, the balance of forces acting on the remaining spins changes. Thus, removing a single spin means that its neighbours have one less neighbour favouring ferromagnetic order, while the number of neighbours favouring anti-ferromagnetism is unchanged. As dilution increases this can cause local canting to occur as more near neighbours are removed compared with next neighbours, as is illustrated in fig. 21 for the ground-state order of a two-dimensional square lattice with an intermediate value of R (Dunlop and Sherrington 1985). Furthermore, for isolated dilution regions there is degeneracy in the canting. For an m -vector system the degeneracy corresponds to orientational symmetry in $(m - 1)$ spin dimensions and the situation can be viewed as having an $(m - 1)$ -dimensional free ‘‘pseudospin’’ embedded in a ferromagnetic matrix. In the case illustrated in fig. 21, the ‘‘pseudospin’’ is actually associated with a pair of sites and for $m = 2$ can have two opposed internal conformations. As account is taken of several such ‘‘pseudospins’’ and of the distortion they cause in the ferromagnetic matrix, one recognizes that they influence one another through

* Otherwise, one gets a more complicated modulated phase.

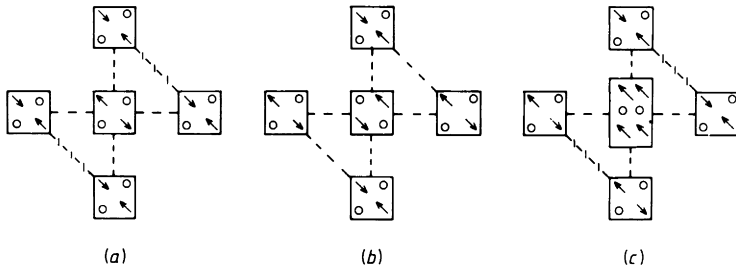


Fig. 22. Artificial/special groupings of impurities (shown for $m = 2$) to illustrate both the mixture of ferromagnetic and antiferromagnetic interactions between pseudospins (the spin-pairs inside the square plaquettes) and also frustration. $--$ denotes satisfied bonds, $-/-/-$ denotes unsatisfied bonds. (a) and (c) are conformations with frustration, (b) is unfrustrated. In this illustration isolated (real) spin impurities are assumed not to exist. If present they can reverse the character of an interaction between pseudospins; from: Dunlop and Sherrington 1985.

an effective “indirect exchange” via the ferromagnetic medium. Furthermore, this interaction can be either “ferromagnetic” or “antiferromagnetic”, favouring either “parallel” or “antiparallel” alignment of the pseudospins, depending on relative positioning in the matrix. This is illustrated in fig. 22 for the case of the ground-state ordering of a two-dimensional $m = 2$ model system. One therefore has the ingredients for spin glass ordering of the pseudospins. Since the effective interactions between the pseudospins are smaller than those giving rise to the underlying ferromagnetism, possible transverse pseudospin glass ordering, and hence canting of the ferromagnetism, occurs at a lower temperature than that for collinear ferromagnetism. Of course, the usual issues of critical dimensionalities apply for these short-ranged models.

Turning now to the issue of lower critical dimension for vector spin glasses, there is now significant evidence, based on Monte Carlo extensions (Olive et al. 1986, Chakrabarti and Dasgupta 1986) of the Ising study of Bhatt and Young (1985, 1987, 1988) discussed earlier, that a short-range isotropic classical Heisenberg model does not have a finite-temperature spin glass phase. Rather, there appears to be a $T = 0$ transition. This absence of a transition in three dimensions is indicated both for a short-range random-bond model (Olive et al. 1986) and for a random-site system with RKKY oscillatory exchange (Chakrabarti and Dasgupta 1986), as expected to model real metallic systems. On the other hand, the addition of random anisotropy, e.g. due to Dzyaloshinski–Moriya interactions (Chakrabarti and Dasgupta 1987) or crystal-field effects, does appear to be sufficient to reduce the critical dimensionality and yield spin glass order in three dimensions. It is thought that such anisotropy, which is inevitably present in a random alloy, underlies the apparent experimental observation of spin glass order in real three-dimensional Heisenberg alloys. This presumably also underlies the observation that the

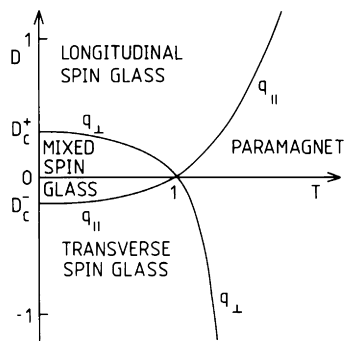


Fig. 23. Phase diagram predicted by replica-symmetric mean-field theory for a system characterized by a Hamiltonian with random-bond isotropic Heisenberg exchange together with uniaxial anisotropy contribution $-D\sum(S_i^z)^2$; the exchange is Gaussian distributed and temperature is normalized to the $D = 0$ spin glass ordering temperature, the labelled q_{\perp} and q_{\parallel} indicate the onset of transverse and longitudinal spin glass order; from: Roberts and Bray 1982.

critical exponents of experimental spin glasses are comparable more with those found in simulations of short-range Ising spin glasses rather than in isotropic Heisenberg ones (Olive et al. 1986).

Uniaxial anisotropy leads to a further range of spin glass behaviours, with qualitative accord between theoretical predictions (Roberts and Bray 1982, Cragg and Sherrington 1982, Elderfield and Sherrington 1984) and experimental observations (Albrecht et al. 1982, Fert et al. 1982, Murayama et al. 1986). Figure 23 shows replica mean-field predictions for a system with isotropic Heisenberg exchange plus local uniaxial anisotropy contributing $-D\sum(S_i^z)^2$ to the Hamiltonian; in the longitudinal spin glass phase there is spin glass freezing only in the z direction, in the transverse spin glass phase only in the plane orthogonal to z , while in the mixed phase there is spin glass freezing in all directions (albeit anisotropically for $D \neq 0$). For a discussion of replica-symmetry breaking see Elderfield and Sherrington (1984), where also will be found a discussion of the effect of the further addition of a magnetic field.

6. Beyond conventional spin glasses

The spin glass concept arose, as we have indicated earlier, to describe the properties of certain magnetic metallic alloys and has been shown to be appropriate also to other magnetic alloys. It is also relevant to other analogous situations in solids where combined randomness and frustration occur, e.g. in charge density wave systems with random pinning. In this section, however, we note that it has had further applications in several problems which are physically very distinct but which are related in their mathematical formulation. We

shall discuss explicitly only two of these, the optimal equipartitioning of random graphs and a class of neural network models. At the outset, however, we comment that both of these examples, as well as other related analogous problems, are naturally range-free so that mean-field theory is relevant. Thus we have the situation that although there remains controversy over the relevance to real magnetic alloys of the detailed predictions of the replica mean-field theory developed to model them, there is general agreement that theory is relevant to a wealth of other interesting “real” problems.

6.1. Bipartitioning of random graphs

In many problems of planning and design one is faced with the task of drawing the best compromise between conflicting desires. Here we shall be concerned only with such problems which can be quantified and formulated in terms of minimizing some cost function with respect to variable parameters, subject to any constraint. A classic problem of this kind is that of bipartitioning a graph so that half of its vertices are in one partition and half in the other, in such a way that the number of edges (lines) connecting the partitions is minimized. If the graph is effectively random, this is a hard combinatorial optimization problem (Cristofides 1979, Papadimitriou and Steglitz 1982), of the kind known as NP-complete (Garey and Johnson 1979). It can be considered as an idealization of many practical problems, such as that of distributing the elements of an electronic circuit between two microchips so as to have an equal number on each but minimize the wires passing between them, or to distribute a computing task between two processors so that the load is equally distributed but the number of signals passing between the processors is minimized. Our interest here is that this graph partitioning problem is closely analogous to that of finding the ground state of an infinite-ranged Ising spin glass (Kirkpatrick et al. 1983, Fu and Anderson 1986, Banavar et al. 1987).

Let us now show the correspondence mathematically. Let us label the vertices of the graph by (i, j, \dots) and their location in the partitioning by $(\sigma_i, \sigma_j, \dots)$ where

$$\begin{aligned}\sigma_j &= +1 && \text{if } i \text{ is in the first partition,} \\ &= -1 && \text{if } i \text{ is in the second partition.}\end{aligned}\tag{6.1}$$

The edges of the graph are given by the connectivity matrix \mathbf{a} where

$$\begin{aligned}a_{ij} &= 1 && \text{if edge } (ij) \text{ is present,} \\ &= 0 && \text{if edge } (ij) \text{ is absent.}\end{aligned}\tag{6.2}$$

Then the number of edges passing between the two partitions is

$$N_{ce} = \sum_{(ij)} a_{ij} \frac{1}{2}(1 - \sigma_i \sigma_j),\tag{6.3}$$

while the condition of equipartitioning is

$$\sum_i \sigma_i = 0. \quad (6.4)$$

Except for a constant, eq. (6.3) is the Hamiltonian of a (randomly connected) ferromagnet,

$$H = -\frac{1}{2} \sum_{(ij)} a_{ij} \sigma_i \sigma_j, \quad (6.5)$$

which it is desired to minimize subject to a constraint of zero total magnetization (eq. (6.4)). Since the preferred ground state of a ferromagnet has

$$\left| \sum_i \sigma_i \right| = N, \quad (6.6)$$

it is clear that these requirements are in conflict, i.e. are frustrated. If the connectivity matrix is randomly constructed, then one has both frustration and quenched disorder, the key ingredients for a spin glass, and consequently a quasi-fractal energy landscape similar to that found for a spin glass. The spin glass analogy can be made closer by replacing the “hard” constraint of eq. (6.4) by a “soft” constraint in terms of a penalty added to the Hamiltonian

$$\Delta H = \lambda \left(\sum_i \sigma_i \right)^2, \quad (6.7)$$

with λ independent of N , but $\{\sigma_i\}$ now unrestricted. Now

$$H = -\frac{1}{2} \sum_{(ij)} (a_{ij} - 4\lambda) \sigma_i \sigma_j, \quad (6.8)$$

i.e. one has a random-bond Ising model with effective exchange interactions which are sometimes ferromagnetic, sometimes antiferromagnetic.

Several subdivision classes exist even for this simple random-graph bipartitioning. We mention here only the union of two interesting subsets (see also Sherrington 1987). The first subset concerns the scaling of the average valence c (number of connections per vertex) with the total number of vertices N . We consider first cases with c proportional to N , which we refer to as having extensive valence, and second cases with c independent of N , which we refer to as intensive valence. The second subclassification concerns whether each vertex is connected to exactly c other vertices, a situation we shall refer to as “fixed valence”, or whether each edge has an equal chance of being present with only the average valence equal to c , a situation we shall refer to as “average valence”.

For the optimization problem, only the minimization of H is required (with or without constraint on $\{\sigma_i\}$, depending on the formulation). Statistical mechanics can, however, be applied by introducing a complementary “temperature” T ,

with states $\{\sigma_i\}$ determined according to the resulting Boltzmann distribution, evaluating the free energy $F(T)$ and obtaining the “ground-state energy” E by the limiting procedure

$$E = \lim_{T \rightarrow 0} F(T). \quad (6.9)$$

The determination of E (and the corresponding ground-state configuration $\{\sigma_i\}_{\langle H \rangle=0}$) by Monte Carlo simulation with decreasing T is known as “Optimization by Simulated Annealing” (Kirkpatrick et al. 1983) and relies on analogy with the real annealing procedure used by a metallurgist to overcome the energy barriers to ideal crystallization consequential to a rapid quench; in terms of the schematic fig. 4, interpreted as the energy or cost, the circular dots show the result of a rapid quench from a state indicated by the cross, whereas the squares show true ground states – heating provides the thermal energy to overcome energy barriers, or rounds out free-energy landscapes.

Here, however, we shall concentrate on an analytical investigation of the minimum cost, averaged over statistically equivalent networks. Since the physical quantities are energies, this implies an average over $\ln Z$, where Z is the effective partition function. It is therefore natural to use replica theory. Since for random graphs there is no lattice and the interactions have no “range”, or are effectively infinite-ranged, replica mean-field theory (or steepest descent analysis) is exact (without thermal fluctuations), although all its internal subtleties, as partially discussed earlier, apply.

For the cases of average valence, the free energy averaged over all graphs of average valence c is given by (Fu and Anderson 1986)

$$[F] = -kT \lim_{n \rightarrow 0} \frac{1}{n} \left\{ \text{Tr}' \exp \left[\sum_{m=1}^{\infty} \beta^m C_m \sum_{\{\alpha_m\}} \left(\sum_i \sigma_i^{\alpha_1} \sigma_i^{\alpha_2} \cdots \sigma_i^{\alpha_m} \right)^2 \right] - 1 \right\}, \quad (6.10)$$

where the C_m are functions of the probability $p = c/N$ that an edge is present. The prime on Tr indicates that the trace is to be performed subject to constraint (6.4). Because of the constraint, the term $m=1$ can be eliminated from the sum on m . In the usual fashion (see eq. (3.25)), $\exp(\cdots (\sum_i \sigma_i^{\alpha_1} \cdots \sigma_i^{\alpha_m})^2)$ can be replaced by a Gaussian average over an effective system with linear interaction with an auxiliary field $q^{\alpha_1 \cdots \alpha_m}$, viz.

$$\begin{aligned} \exp \left(\cdots \left(\sum_i \sigma_i^{\alpha_1} \cdots \sigma_i^{\alpha_m} \right)^2 \right) &\rightarrow \int dq^{\alpha_1 \cdots \alpha_m} \exp(- (q^{\alpha_1 \cdots \alpha_m})^2 / 2) \\ &\times \exp \left(\cdots q^{\alpha_1 \cdots \alpha_m} \sum_i \sigma_i^{\alpha_1} \cdots \sigma_i^{\alpha_m} \right). \end{aligned} \quad (6.11)$$

Steepest descents analysis then leads to self-consistent equations for the q and hence to $[F]$.

In the case of extensive average valence, p is independent of N . If, further, β is chosen to scale as

$$\beta = \tilde{\beta} N^{-1/2}, \quad (6.12)$$

then in terms of intensive β the m summation in eq. (6.11) terminates after $m = 2$ and the problem is exactly equivalent to that of the SK spin glass (Fu and Anderson 1986). In terms of the total number of edges

$$N_{\text{ed}} = pN/2, \quad (6.13)$$

there results

$$\frac{N_{\text{ce}}}{N_{\text{ed}}} = \frac{1}{2} \left\{ 1 - c((1-p)/pN)^{1/2} \right\} + O(N^{-1}), \quad (6.14)$$

where $c = 1.5266 \pm 0.0002$.

For intensive average valence, $p = z/N$, the C_m scale as N^{-1} and all $m \geq 2$ are relevant, yielding an infinite set of order parameters $q^{\alpha_1 \dots \alpha_m}$; $m = 2, \dots, \infty$ (Kanter and Sompolinsky 1987, Mézard and Parisi 1987). This is closely analogous to another range-free spin glass model, due to Viana and Bray (1985), in which one has spins distributed on a random network of average intensive valence c , with the bonds which are present having quenched randomness drawn from a distribution $P(J_{ij})$ whose moments are independent of N . Locally the structure of a network of intensive valence is tree-like, and self-consistent Bethe lattice analogies have also been employed to understand spin glasses on such networks (Bowman and Levin 1985, Thouless 1986, Sherrington and Wong 1987). In replica-symmetric theory a useful Ansatz is

$$q_m = \int dh P(h) (\tanh \beta h)^m, \quad (6.15)$$

where q_m denotes the m th order replica-symmetric order function

$$q_m = q^{\alpha_1 \dots \alpha_m}, \quad \alpha_1 \neq \alpha_2 \neq \dots \neq \alpha_m, \quad (6.16)$$

and $P(h)$ satisfies self-consistency equations; for the $\pm J$ exchange spin glass model

$$\begin{aligned} P(h) &= \sum_{k=0}^{\infty} \alpha^k \frac{e^{-\alpha}}{k!} \int dh_1 \dots dh_k P(h_1) \dots P(h_k) \\ &\times \delta \left(h - \beta^{-1} \sum_{i=1}^k \tanh^{-1}(\tanh \beta J \tanh \beta h_i) \right), \end{aligned} \quad (6.17)$$

with

$$\int dh P(h) \tanh \beta h = 0. \quad (6.18)$$

The correct self-consistent solution $P(h)$ does however involve subtlety, insofar as it involves a continuum even as $T \rightarrow 0$, not just delta functions (Katsura 1987a, b, Mottishaw and De Dominicis 1987, Wong et al. 1988).

For fixed valence, the extensive case is essentially equivalent to the corresponding average valence case (Wiethege and Sherrington 1987), but the intensive case has some minor further subtleties (Wong and Sherrington 1987).

As might be expected, replica-symmetry breaking occurs in all these problems, but its analysis remains only partial (de Almeida and De Dominicis 1989, De Dominicis and Goldschmidt 1989) for the case of intensive valence, due to the larger number of order parameters needed.

Spin glass concepts and techniques have been applied to other hard optimization problems, including the famous travelling salesman problem (Lawler et al. 1985, Kirkpatrick and Toulouse 1985, Mézard and Parisi 1986) in which one tries to minimize the route of a salesman visiting a set of effectively randomly located cities.

6.2. Neural networks

Another interesting problem with close affinity to the spin glass problem concerns a simple idealized model of associative neural memory due to Hopfield (Hopfield 1982). The human cortex contains of many neurons (of order 10^{10}) which are highly and apparently randomly interconnected (of order 10^4 – 10^5 connections per neuron) over all ranges. In a severe (but useful) idealization due to McCulloch and Pitts (McCulloch and Pitts 1943), the neurons can be viewed as having just two states, firing and non-firing. The interest for associative memory is envisaged as not in the state of a single neuron, but in the global activity patterns or sequences. Recall is the retrieval of these patterns from some noisy initial conditions. The actual dynamic states are determined by the character of the connections between the neurons, with modifications of these connections during the learning process. Because the relevant activity and storage are global, one is considering content-addressable memory.

To store many memories it is essential that there be many stable dynamic states. This requires frustration.

The operation can be idealized as follows. If a neuron fires, it sends potentials through axons and synapses to other neurons. These potentials can be excitatory (positive) or inhibitory (negative). Any one neuron receives such potentials from all its afferent neurons which are firing and contributing either positive or negative potentials. Its subsequent action is determined by the collective accumulation of all these input potentials. A steady state is reached when the activity of each neuron matches the input instructions it receives.

In the case of symmetric synapses this simple picture can be related mathematically to the extremization of a frustrated cost function. Let us denote the neurons by $\{i\}$ and their states by $\{\sigma_i\}$; $\sigma_i = 1$ corresponding to firing, $\sigma_i = -1$

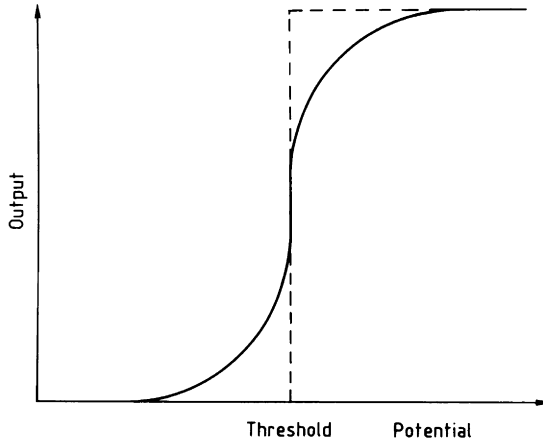


Fig. 24. Output probability function for a neuron to fire given an input potential. For a potential much greater than threshold the firing probability is unity, for a potential much less than threshold it is zero. The dashed step function is an idealization, corresponding to $T = 0$ in the Hamiltonian analogue.

to not firing. If neuron j fires, it sends a potential J_{ij} to neuron i . The total synaptic potential received by neuron i is thus

$$V_i = \sum_j J_{ij} \frac{1}{2}(\sigma_j + 1), \quad (6.19)$$

taking J_{ij} to be zero if there is no connection between j and i . The probability of i now firing is determined by a sigmoidal function, as illustrated in fig. 24.

Let us initially consider a further idealization of the firing probability p_i to the step function form

$$p_i = \theta(V_i - W_i), \quad (6.20)$$

where W_i is a threshold. The condition for steady-state activity is then

$$\sigma_i = \text{sgn}(V_i - W_i) = \text{sgn}\left(\frac{1}{2} \sum_j J_{ij} \sigma_j + \frac{1}{2} \sum_j J_{ij} - W_i\right), \quad \text{all } i. \quad (6.21)$$

The connection to a problem characterized by a cost function follows by noting that if a field term $-\sum b_i \sigma_i$ is added to the Hamiltonian H of eq. (3.1), then the condition for a state $\{\sigma\}$ to be stable against any single spin flip $\sigma_i \rightarrow -\sigma_i$ is

$$\sigma_i = \text{sgn}\left\{\sum_j J_{ij} \sigma_j - b_i\right\}, \quad \text{all } i. \quad (6.22)$$

With an appropriate identification of b_i , eqs. (6.21) and (6.22) are clearly identical. The Hamiltonian formulation does however require that

$$J_{ij} = J_{ji}. \quad (6.23)$$

This observation of a mathematical isomorphy between the condition for steady-state dynamics of a model “brain” with symmetric synapses and that for states of a corresponding Hamiltonian model to be stable against single spin flips opened the door to both conceptional and technical application of spin glass theory to the analysis of neural networks.

We have already considered temperature in the thermodynamic context. In the neural context it corresponds to allowing for the sigmoidal rounding of p_i illustrated in fig. 24, replacing p_i by

$$p_i = [1 + \exp(-\beta(V_i - W_i))]^{-1}. \quad (6.24)$$

In this case the mapping is between average activity states, the average dynamic states of the network corresponding to minima of the corresponding free-energy surface. Note however, that the interest is not now just in the overall minimum, but also in the secondary minima. The extent of these minima characterize the domains of attraction of the dynamic steady states.

Clearly, to make useful memories the networks must be trained so that the dynamic steady states correspond to learned patterns. That is, if a stored pattern is $\{\sigma_i\} = \{\xi_i\}$, then one wishes that if the system starts with $\{\sigma\}$ having a sufficient overlap with $\{\xi_i\}$, then the iteration will be towards a strong overlap with $\{\xi_i\}$, sufficient to “recognize” it.

One can imagine many algorithmic codings of memories in the $\{J_{ij}\}$. One which has received significant and influential study is that attributed to Hebb,

$$J_{ij} = N^{-1} \sum_{\mu=1}^p \xi_i^\mu \xi_j^\mu, \quad (6.25)$$

where $\mu = 1, \dots, p$ label the patterns $\{\xi_i^\mu\}$ to be stored. We concentrate on random patterns $\{\xi_i^\mu\}$ and on extensive storage; i.e. p is proportional to N . Interest will be in statistically significant results, as obtained by appropriate averages over particular choices of $\{\xi^\mu\}$. Replica theory may be used to perform this analysis (Amit et al. 1985a). Because of the infinite-range of the interactions, again one may use auxiliary fields and/or order parameters with extremal dominance of integrals. In fact, however, as pointed out earlier, interest is not just in absolute extrema, but also in secondary ones. The resulting analysis (Amit et al. 1985a, b) yields the phase diagram shown in fig. 25. Cooperatively frozen states of the Hamiltonian system include both retrieval states having finite overlap with a single memory,

$$m^\mu = N^{-1} \sum_i \langle \sigma_i \rangle \xi_i^\mu \neq 0; \quad \text{only one } \mu, \quad (6.26)$$

and others which are mixture states, having overlap with more than one memory, and spin glass states having all m^μ scaling to zero as $N \rightarrow \infty$ but with

$$q = N^{-1} \sum_i \langle \sigma_i \rangle^2 \neq 0. \quad (6.27)$$

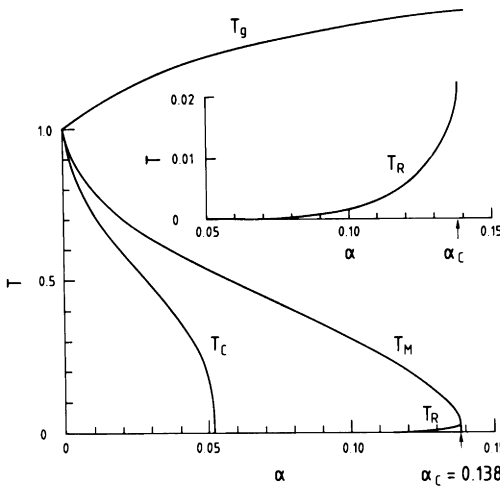


Fig. 25. Phase diagram of the Hopfield model with Hebb synapses storing $p = \alpha N$ uncorrelated patterns; from: Amit et al. 1985a, b. T_M indicates a boundary beneath which there are retrieval states. T_g is the boundary for extremal states which have non-zero $q = |\langle \sigma_i \rangle^2|$ but which are uncorrelated with the memories (spin glass states). Beneath T_c the retrieval states are global minima. T_R bounds a region of replica-symmetry breaking.

It is seen from fig. 25 that there is a limit on capacity at $p = \alpha_c N$, with $\alpha_c \sim 0.138$ for Hebb synapses.

Replica theory can also be used to determine optimal storage (Gardner 1987, 1988), in which the $\{J_{ij}\}$ are chosen to ensure that the largest number of patterns $\{\xi^\mu\}$ can be stored, all obeying equations such as eq. (6.21). It can also be extended to networks with other Boolean-dynamics rules and with different degrees of noise or signal rounding, particularly for dilute networks (Wong and Sherrington 1989, 1990).

7. Conclusion

In this article I have tried to show how the observations of unusual behaviour of some magnetic alloys, known as spin glasses, have led to a number of new and interesting concepts and techniques. The mean-field theory developed as a first step to understand them has itself proven very subtle and instructive, although its detailed relevance remains controversial with regard to the short-range systems for whose description it was originally devised. For these short-range systems yet other techniques have been introduced and studied, themselves leading to new concepts. Furthermore, mathematical mappings have led to the

realization of a widespread relevance far beyond physics, with continuing exciting developments.

Spin glass theory is truly an example of a situation in which the attempt to understand apparently fairly obscure but unusual physical properties of systems without obvious practical applications has revolutionized concepts and techniques on a wide scale and with far-reaching consequences.

References

- Albrecht, H., E.F. Wassermann, F.T. Hedgecock and P. Monod, 1982, Phys. Rev. Lett. **48**, 819.
 Amit, D.J., H. Gutfreund and H. Sompolinsky, 1985a, Phys. Rev. Lett. **55**, 1530.
 Amit, D.J., H. Gutfreund and H. Sompolinsky, 1985b, Ann. Phys. **173**, 30.
 Anderson, P.W., 1973, in: Amorphous Magnetism, eds H.O. Hooper and A.M. de Graaf (Plenum Press, New York) p. 1.
 Athanasiou, G.G., C.P. Bachas and W.F. Wolff, 1987, Phys. Rev. B **35**, 1965.
 Banavar, J.R., D. Sherrington and N. Sourlas, 1987, J. Phys. A **20**, L1.
 Barbara, B., A.P. Malozemoff and Y. Imry, 1981, Phys. Rev. Lett. **47**, 1852.
 Bhatt, R.N., and A.P. Young, 1985, Phys. Rev. Lett. **54**, 924.
 Bhatt, R.N., and A.P. Young, 1987, Numerical studies of spin glasses, in: Heidelberg Colloquium on Glassy Dynamics, eds J.L. van Hemmen and I. Morgenstern (Springer, Berlin) p. 215.
 Bhatt, R.N., and A.P. Young, 1988, Phys. Rev. B **37**, 5606.
 Bhatt, R.N., and A.P. Young, 1989, J. Phys. Condens. Mat. **1**, 2997.
 Binder, K., ed., 1979, Monte Carlo Methods in Statistical Physics (Springer, Berlin).
 Binder, K., and A.P. Young, 1986, Rev. Mod. Phys. **58**, 801.
 Borg, R.J., R. Booth and C.E. Violet, 1963, Phys. Rev. Lett. **11**, 464.
 Bowman, D.R., and K. Levin, 1985, Phys. Rev. B **25**, 3438.
 Bray, A.J., and M.A. Moore, 1979, J. Phys. C **12**, 79.
 Bray, A.J., and M.A. Moore, 1980, J. Phys. C **13**, L469.
 Bray, A.J., and M.A. Moore, 1984, J. Phys. C **17**, L463.
 Bray, A.J., and M.A. Moore, 1987, Phys. Rev. Lett. **58**, 57.
 Bray, A.J., and M.A. Moore, 1987a, Phys. Rev. Lett. **58**, 57.
 Bray, A.J., and M.A. Moore, 1987b, Scaling theory of the ordered phase of spin glasses, in: Heidelberg Colloquium on Glassy Dynamics, eds J.L. van Hemmen and I. Morgenstern (Springer, Berlin).
 Bray, A.J., M.A. Moore and A.P. Young, 1984, J. Phys. C **17**, L155.
 Brout, R., 1959, Phys. Rev. **115**, 824.
 Canella, V., and J.A. Mydosh, 1972, Phys. Rev. B **6**, 4220.
 Caracciolo, S., G. Parisi, S. Patarnello and N. Sourlas, 1990, J. Phys. (Paris) **51**, 1877.
 Chakrabarti, A., and C. Dasgupta, 1986, Phys. Rev. Lett. **56**, 1404.
 Chakrabarti, A., and C. Dasgupta, 1987, Phys. Rev. B **36**, 793.
 Chen, J.H., and T.C. Lubensky, 1977, Phys. Rev. B **16**, 2106.
 Coles, B.R., 1984, in: Multicritical Phenomena, eds R. Pynn and A. Skjeltorp (Plenum Press, New York) p. 363.
 Coles, B.R., 1985, Ann. Phys. (Paris) **10**, 63.
 Coles, B.R., 1985, Ann. Phys. (Paris) **10**, 63.
 Coles, B.R., 1985, Ann. Phys. (Paris) **10**, 63.
 Cragg, D.M., and D. Sherrington, 1982, Phys. Rev. Lett. **46**, 1190.
 Cragg, D.M., D. Sherrington and M. Gabay, 1982, Phys. Rev. Lett. **49**, 158.
 Cristofides, N., 1979, Combinatorial Optimization (Wiley, New York).

- de Almeida, J.R., and C. De Dominicis, 1989, in: New Trends in Magnetism, eds J.R. de Almeida, Coutinho and Rezende (World Scientific, Singapore).
- de Almeida, J.R., and D.J. Thouless, 1978, *J. Phys. A* **11**, 983.
- De Dominicis, C., and Y.Y. Goldschmidt, 1989, *J. Phys. A* **22**, L775.
- De Dominicis, C., and I. Kondor, 1985, in: Application of Field Theory to Statistical Mechanics, ed. L. Garrido (Springer, Berlin).
- De Dominicis, C., M. Gaba and H. Orland, 1981, *J. Phys. (Paris) Lett.* **42**, L523.
- Derrida, B., and G. Weisbuch, 1988, *Europhys. Lett.* **7**, 113.
- Dunlop, M.W., and D. Sherrington, 1985, *J. Phys. C* **18**, 1465.
- Edwards, S.F., and P.W. Anderson, 1975, *J. Phys. F* **5**, 965.
- Elderfield, D., and D. Sherrington, 1983, *J. Phys. A* **15**, L513.
- Elderfield, D., and D. Sherrington, 1984, *J. Phys. C* **17**, 5595.
- Fert, A., P. Pureur, F. Hippert, K. Baberschke and F. Bruss, 1982, *Phys. Rev. B* **26**, 5300.
- Fisch, R., and A.B. Harris, 1977, *Phys. Rev. Lett.* **37**, 756.
- Fischer, D.S., and D.A. Huse, 1988, *Phys. Rev. B* **38**, 386.
- Fischer, K.H., 1983, *Phys. Status Solidi B* **116**, 357.
- Fischer, K.H., 1985, *Phys. Status Solidi B* **130**, 3.
- Fu, Y., and P.W. Anderson, 1986, *J. Phys. A* **19**, 1605.
- Gabay, M., and G. Toulouse, 1981, *Phys. Rev. Lett.* **47**, 201.
- Gardner, E., 1987, *Europhys. Lett.* **4**, 481.
- Gardner, E., 1988, *J. Phys. A* **21**, 257.
- Garey, M.R., and D.S. Johnson, 1979, Computers and Intractability (Freeman, San Francisco, CA).
- Goldschmidt, Y.Y., and P.-Y. Lai, 1988, *J. Phys. A* **21**, L1043.
- Hamzic, A., and I.A. Campbell, 1981, *J. Phys. (Paris) Lett.* **42**, L309.
- Hertz, J., 1979, *Phys. Rev. B* **19**, 4796.
- Hopfield, J.J., 1982, *Proc. Natl. Acad. Sci.* **79**, 2554.
- Kanter, I., and H. Sompolinsky, 1987, *Phys. Rev. Lett.* **58**, 164.
- Katsura, S., 1987a, *Prog. Theor. Phys. Jpn., Suppl.* **87**, 139.
- Katsura, S., 1987b, *Physica A* **141**, 556.
- Kett, H., W. Gebhart and U. Krey, 1981, *J. Magn. & Magn. Mater.* **25**, 215.
- Kinzel, W., 1979, *Phys. Rev. B* **19**, 4595.
- Kirkpatrick, S., and D. Sherrington, 1978, *Phys. Rev. B* **17**, 4384.
- Kirkpatrick, S., and G. Toulouse, 1985, *J. Phys. (Paris)* **46**, 1277.
- Kirkpatrick, S., C.D. Gelatt and M.P. Vecchi, 1983, *Science* **220**, 671.
- Lauer, J., and W. Keune, 1982, *Phys. Rev. Lett.* **48**, 1850.
- Lawler, E.L., J.K. Lenstra, A.H.G. Rinnoy Kan and D.M. Schmoys, 1985, The Traveling Salesman Problem (Wiley, New York).
- Lutes, O.S., and J.L. Schmit, 1964, *Phys. Rev. A* **134**, 676.
- Maletta, H., and P. Convert, 1979, *Phys. Rev. Lett.* **42**, 108.
- McCulloch, W.S., and W. Pitts, 1943, *Bull. Math. Biophys.* **5**, 115.
- McLenaghan, I.R., and D. Sherrington, 1984, *J. Phys. C* **17**, 1531.
- McLenaghan, I.R., and D. Sherrington, 1987, *J. Phys. C* **20**, 1701.
- Metropolis, N., A.W. Rosenbluth, M.N. Rosenbluth, A.H. Teller and E. Teller, 1953, *J. Chem. Phys.* **21**, 1087.
- Mézard, M., and G. Parisi, 1986, *J. Phys. (Paris)* **47**, 1285.
- Mézard, M., and G. Parisi, 1987, *Europhys. Lett.* **3**, 1067.
- Mézard, M., G. Parisi, N. Sourlas, G. Toulouse and M.A. Virasoro, 1984, *J. Phys. (Paris)* **45**, 843.
- Mézard, M., G. Parisi and M.A. Virasoro, 1987, Spin Glass Theory and Beyond (World Scientific, Singapore).
- Monod, P., and H. Bouchiat, 1982, *J. Phys. (Paris) Lett.* **43**, 145.
- Morgenstern, I., and K. Binder, 1979, *Phys. Rev. Lett.* **43**, 1615.
- Mottishaw, P., and C. De Dominicis, 1987, *J. Phys. A* **20**, L375.

- Murayama, S., K. Yokosawa, Y. Miyako and E.F. Wassermann, 1986, Phys. Rev. Lett. **57**, 1785.
- Nagata, S., P.H. Keesom and H.R. Harrison, 1979, Phys. Rev. B **19**, 1633.
- Neumann, A.U., and B. Derrida, 1988, J. Phys. (Paris) **49**, 1647.
- Nobre, F.D., D. Sherrington and A.P. Young, 1989, J. Phys. A **22**, 2835.
- Ogielski, A.T., 1987, Phase transitions and equilibrium dynamics in strongly random Ising spin systems, in: Heidelberg Colloquium on Glassy Dynamics, eds J.L. van Hemmen and I. Morgenstern (Springer, Berlin).
- Ogielski, A.T., and I. Morgenstern, 1985, Phys. Rev. Lett. **54**, 928.
- Ogielski, A.T., and I. Morgenstern, 1985, J. Appl. Phys. **57**, 3382.
- Ogielsky, A.T., 1985, Phys. Rev. B **32**, 7384.
- Olive, J.A., A.P. Young and D. Sherrington, 1986, Phys. Rev. B **34**, 6341.
- Owen, J., M.E. Browne, V. Arp and A.F. Kip, 1957, J. Phys. Chem. Solids **2**, 85.
- Papadimitriou, C.H., and K. Steglitz, 1982, Combinatorial Optimization (Prentice-Hall, Englewood Cliffs, NJ).
- Parga, N., G. Parisi and M.A. Virasoro, 1984, J. Phys. (Paris) Lett. **46**, L1063.
- Parisi, G., 1979, Phys. Rev. Lett. **43**, 1754.
- Parisi, G., 1980, J. Phys. A **13**, 1887.
- Pytte, E., and J. Rudnick, 1979, Phys. Rev. B **19**, 3603.
- Rammal, R., G. Toulouse and M.A. Virasoro, 1986, Rev. Mod. Phys. **58**, 765.
- Roberts, S.A., and A.J. Bray, 1982, J. Phys. C **15**, L527.
- Sherrington, D., 1980, J. Phys. A **13**, 637.
- Sherrington, D., 1981, J. Phys. C **14**, L371.
- Sherrington, D., 1983, The infinite-ranged m-vector spin glass, in: Heidelberg Colloquium on Spin Glasses (Springer, Berlin).
- Sherrington, D., 1983, J. Phys. Soc. Jpn. **52**, Suppl. 229.
- Sherrington, D., 1987, in: Time-Dependent Effects in Disordered Systems, eds R. Pynn and A. Skjeltorp (Plenum Press, New York).
- Sherrington, D., and S. Kirkpatrick, 1975, Phys. Rev. Lett. **35**, 1972.
- Sherrington, D., and K. Mihill, 1974, J. Phys. Colloq. (Paris) **5-C4-199**.
- Sherrington, D., and B.W. Southern, 1975, J. Phys. F **5**, 965.
- Sherrington, D., and K.Y.M. Wong, 1987, J. Phys. A **20**, L785.
- Sommers, H.-J., 1983, J. Phys. A **16**, 447.
- Sompolinsky, H., (unpublished).
- Sompolinsky, H., 1981, Phys. Rev. Lett. **47**, 935.
- Sompolinsky, H., and A. Zippelius, 1981, Phys. Rev. Lett. **47**, 359.
- Sompolinsky, H., and A. Zippelius, 1982, Phys. Rev. B **25**, 6860.
- Souletie, J., and R. Tournier, 1969, J. Low Temp. Phys. **1**, 95.
- Sourlas, N., 1988, Europhys. Lett. **6**, 561.
- Tanaka, F., and S.F. Edwards, 1980, J. Phys. F **10**, 2471.
- Tholence, J.L., and R. Tournier, 1974, J. Phys. (Paris) **35**, C4-229.
- Thouless, D.J., 1986, Phys. Rev. Lett. **56**, 1082.
- Toulouse, G., 1980, J. Phys. (Paris) Lett. **41**, L447.
- Viana, L., and A.J. Bray, 1985, J. Phys. C **18**, 3037.
- Villain, J., 1977, J. Phys. C **10**, 1717.
- Wiethege, W., and D. Sherrington, 1987, J. Phys. A **20**, L9.
- Wong, K.Y.M., and D. Sherrington, 1987, J. Phys. A **20**, L793.
- Wong, K.Y.M., and D. Sherrington, 1989, Europhys. Lett. **10**, 419.
- Wong, K.Y.M., and D. Sherrington, 1990, J. Phys. A **23**, 4659.
- Wong, K.Y.M., D. Sherrington, P. Mottishaw, R. Dewar and C. de Dominicis, 1988, J. Phys. A **21**, L99.
- Young, A.P., 1983, Phys. Rev. Lett. **51**, 1206.
- Young, A.P., 1985, J. Appl. Phys. **57**, 3361.

This page intentionally left blank

CHAPTER 3

Ab Initio Statistical Mechanics of Structural Phase Transitions

K.M. RABE

*Applied Physics
Becton Center, Yale University
New Haven, CT 06520, USA*

and

J.D. JOANNOPOULOS

*Department of Physics
Massachusetts Institute of Technology
Cambridge, MA 02139, USA*

Contents

1. Introduction	137
2. Ab initio calculations of the structural properties of solids	137
3. Structural phase transitions	142
3.1. Phenomenology	142
3.2. Landau and renormalization group theories	144
4. Ab initio statistical mechanics: general considerations for structural transitions	145
5. Ab initio statistical mechanics: GeTe	146
5.1. Rocksalt–rhombohedral transition of GeTe	147
5.2. GeTe at zero temperature: ab initio calculations	148
5.3. Model Hamiltonian	153
5.4. Calculation of model Hamiltonian parameters	157
5.5. Statistical mechanics	163
5.5.1. Partition function	163
5.5.2. Analysis and results	164
5.6. Discussion	169
6. Future prospects	171
References	173

1. Introduction

Modern theories of critical phenomena have been developed to a very high degree of sophistication. However, the application of these methods to the study of phase transitions in real materials, rather than model systems, is generally conducted by starting with a highly simplified model Hamiltonian or free-energy functional for which the parameters are determined phenomenologically, without explicit connection to the microscopic physics of the system. Even when a reasonably microscopic model Hamiltonian could be found, the accuracy to which the configuration energies would need to be known was, before recent developments, beyond the scope of the available calculational techniques and computing capabilities.

In the last few years, progress in the tractability and accuracy of ab initio total-energy techniques has reached the point at which their application to the calculation of finite-temperature phenomena, such as structural phase transitions, can be realized. In section 2, density functional theory and the ab initio pseudopotential total-energy method are discussed. The basic concepts of structural phase transitions and the current state of the application of modern statistical-mechanics techniques to these systems are summarized in section 3. In section 4, we put forward the principles of “ab initio statistical mechanics”, a synthesis between a microscopic chemical understanding of the solid obtained from ab initio methods and the analysis of the transition through modern techniques of critical phenomena. In section 5, this approach is implemented for the rocksalt-rhombohedral structural phase transition in GeTe. Lastly, in section 6 we discuss the prospects for further ab initio statistical-mechanics studies, identifying some systems of interest and important questions which can be addressed by these techniques, and also discuss some theoretical issues which could lead to an increase of the scope of such studies.

2. Ab initio calculations of the structural properties of solids

For present purposes, a crystal is an infinite collection of electrons, of charge $-e$, and atomic nuclei, which can be regarded as point charges $+Ze$, interacting via Coulomb forces. Although a complete solution of this quantum-

mechanical many-body problem is impossible, a great deal can be learned even without such a solution. First, through the Born–Oppenheimer approximation, the nuclear coordinates are transformed from dynamical variables into the parameters of an external potential for the electrons. Then, through the use of density functional theory (DFT)*, the ground-state energy and charge density of the resulting “inhomogeneous electron gas” can be obtained by solving an equivalent one-body problem, in principle exactly though in practice only approximately, as will be further explained in what follows. This procedure is ab initio in that no experimental input about the system is required beyond the atomic numbers of the constituent atoms, and the calculated quantities are directly useful in extracting information about the measurable properties of solids.

The central result of density functional theory is the Hohenberg–Kohn theorem (Hohenberg and Kohn 1964): *the total ground-state energy of an interacting electron system in an external potential $v(\mathbf{r})$ can be expressed as a universal functional of the charge density $\rho(\mathbf{r})$.* It is usual to decompose the functional as follows:

$$E[\rho(\mathbf{r})] = \int d\mathbf{r} v(\mathbf{r})\rho(\mathbf{r}) + \frac{1}{2} \int d\mathbf{r} \frac{\rho(\mathbf{r})\rho(\mathbf{r}')}{|\mathbf{r} - \mathbf{r}'|} + G[\rho(\mathbf{r})],$$

where the third term contains the quantum-mechanical kinetic energy and the exchange and correlation energies of the interacting electrons.

The proof of this theorem is based on the quantum-mechanical variational principle, and thus has the useful feature that $E[\rho(\mathbf{r})]$ is a functional which attains its minimum for the “correct” $\rho(\mathbf{r})$ corresponding to the given $v(\mathbf{r})$. Thus an equation relating $v(\mathbf{r})$ and $\rho(\mathbf{r})$ can be obtained by setting $\delta E/\delta\rho$ to zero, subject to the constraint that $N = \int d\mathbf{r} \rho(\mathbf{r})$. By far the most convenient representation of $\rho(\mathbf{r})$, which has the added benefit of treating the kinetic energy quantum mechanically, is

$$\rho(\mathbf{r}) = \sum \psi_n^*(\mathbf{r})\psi_n(\mathbf{r}),$$

where the $\psi_n(\mathbf{r})$ are the single-particle wave functions of the non-interacting electron gas system which has the charge density $\rho(\mathbf{r})$ in its ground state. Then the variation $\delta E/\delta\psi_n$ gives rise to the following system of Schrödinger-like equations, called the Kohn–Sham equations (Kohn and Sham 1965):

$$[-\frac{1}{2}\nabla^2 + v_{\text{eff}}(\mathbf{r})]\psi_n(\mathbf{r}) = \epsilon_n\psi_n(\mathbf{r}),$$

which is precisely that of a system of non-interacting electrons in an effective

* A good review of DFT is Kohn and Vashishta (1980) and of its applications is Williams and von Barth (1980).

one-body potential given by

$$v_{\text{eff}}(\mathbf{r}) = v(\mathbf{r}) + \int d\mathbf{r}' \frac{\rho(\mathbf{r}')}{|\mathbf{r} - \mathbf{r}'|} + \frac{\delta E_{\text{xc}}[\rho]}{\delta \rho(\mathbf{r})},$$

where we have written $G = T_{\text{nonint}} + E_{\text{xc}}$.

In principle, the density functional method could yield the total energy and charge density exactly. In practice, however, the explicit functional dependence of E_{xc} on $\rho(\mathbf{r})$ is unknown and thus an approximate form must be used. The most widely used form is the local-density approximation (LDA) (Kohn and Sham 1965) in which E_{xc} is written as $\int d\mathbf{r} \epsilon_{\text{xc}}(\rho(\mathbf{r})) \rho(\mathbf{r})$ and the function ϵ_{xc} is obtained from knowledge of the properties of the homogeneous electron gas (Ceperley 1978, Ceperley and Alder 1980, Perdew and Zunger 1981). This form is very simple to handle and turns out to be a surprisingly accurate representation of the true functional, as will be further discussed subsequently.

Thus, through DFT, the problem has been reduced to a system of one-body Schrödinger equations which, because of the dependence of v_{eff} on $\rho(\mathbf{r})$, must be solved self-consistently. One could now proceed directly using the appropriate nuclear charges for the material of interest to perform an all-electron total-energy calculation. For the kinds of results we will be interested in, which involve small energy differences between similar crystal configurations, such an approach has some serious drawbacks. These arise from the fact that while the low lying “core electrons” are basically unaffected by the solid-state environment and thus do not contribute to energy differences, i.e. can be regarded as a “frozen core”, they dominate the total energy and, through the requirements of orthogonality, force a very highly structured wave function for the valence electrons in the core region. Consequently, the total energies have to be calculated to high precision and the basis sets needed to achieve the proper description of the valence wave functions in the core region are large or complicated.

These problems are solved by the elimination of the explicit appearance of the core electrons through the pseudopotential approximation (Starkloff and Joannopoulos 1977, Bachelet et al. 1982), in which the all-electron problem is mapped to that of the valence electrons moving in an effective external field in which the lowest-lying levels reproduce the valence-electron eigenvalues and the charge density in the interstitial region outside the ion cores. The construction of this effective field can be accomplished in a number of ways, and is indeed somewhat arbitrary. The scheme which is currently most widely used (Starkloff and Joannopoulos 1977, Bachelet et al. 1982, Hamann et al. 1979) preserves the ab initio character of the all-electron calculations by superimposing ionic pseudopotentials which are constructed from ab initio calculations for the constituent atoms. More precisely, the ionic pseudopotential reproduces the valence eigenvalues and wave functions outside some chosen core radius

obtained from an all-electron calculation for a given atomic reference configuration. To do this exactly in general requires a nonlocal (angular-momentum dependent) ionic pseudopotential. The norm-conserving character of these ionic pseudopotentials is crucial for the self-consistent density functional calculations and in determining their transferability into different crystal environments (Shaw and Harrison 1967, Topp and Hopfield 1974).

The primary practical problems which limit the complexity of the systems that can be studied and the accuracy of the calculations are the size of the basis set in which the one-electron wave functions are expanded and the density of k -point sampling in the computation of quantities, such as $\rho(\mathbf{r})$, which involve averaging over the Brillouin zone. While a variety of basis sets can be used, one advantage of using the pseudopotential approximation is that it is usually possible to use a plane-wave basis. Despite the fact that it is generally larger than sets of basis functions tailored for a specific problem, there is a payoff in flexibility (different atomic arrangements are treated in an unbiased way) and simplicity (ease in computing matrix elements and charge densities). The effects of the limitations on basis set and k -point set size can be systematically investigated by raising the cutoffs and checking the convergence of the total-energy differences of interest.

With this scheme and currently available computers, it is possible to compute ground-state total energies for a wide variety of materials and for quite complicated structures. From the location and curvatures of energy minima, predictions can be obtained for structural properties such as the lattice constants, cohesive energy, bulk modulus, elastic constants (and even phonon frequencies), surface reconstructions, and atomic relaxation at defects, at zero temperature and in temperature regimes where energy considerations are expected to dominate. Indeed, there is already a large body of work in which these predictions compare favorably with experimental observations (Cohen 1982, Joannopoulos 1985). In addition, examination of the valence charge density, the bandstructure and the individual terms contributing to the total energy provides microscopic insight into the nature of bonding in the materials and the factors favoring structural changes.

The quantitative success obtained in these studies suggests that the approximations involved must be very good. In the case of the local-density approximation, this is particularly surprising. Although the density functional scheme is exact in principle, here a functional derived from results for a homogeneous electron gas is being applied to systems which are highly inhomogeneous, including ionic and covalently bonded solids. The situation was at first made even more mysterious by the failure of attempts to improve the functional by including higher-order terms in a gradient expansion (Langreth and Perdew 1979). However, some understanding of the success of the LDA has been achieved. In the case of systems with nearly constant density, the validity of linear response gives an independent expression, which over a range of q is

better approximated by the LDA than by gradient corrections (Geldart et al. 1972). Also, the LDA satisfies exactly the sum rules required by charge neutrality (Gunnarsson and Lundqvist 1976). Lastly, $v_{xc}(\mathbf{r})$ and $n(\mathbf{r})$ for certain systems, obtained through constructions which include some many-body effects, are negligibly different from those in the LDA (Godby et al. 1986, 1987).

In contrast, the pseudopotential scheme is inherently approximate. The validity of the frozen-core approximation, which is in fact an independent approximation buried in the pseudopotential, has been examined in detail (von Barth and Gelatt 1980). The transferability of the pseudopotential is good by construction: the norm conservation ensures that the logarithmic derivative of the wave function with respect to energy is exactly reproduced outside the core radius, and thus that the scattering properties of the ion are well reproduced in different crystal environments (Shaw and Harrison 1967, Topp and Hopfield 1974). Remaining problems can be dealt with by changing the choice of atomic reference configuration, and in cases where the core and valence charge distributions overlap in space, the errors due to the linearization of the exchange-correlation potential can be eliminated by storing the charge distribution of the frozen core (Louie et al. 1982).

When performing these density functional calculations, it is very important not to lose sight of their intrinsic limitations. For example, although the ground-state charge density is correctly given, the wave function is not a Slater determinant of the ψ_n used in the construction of the Kohn–Sham equations. Also, in general the one-electron eigenvalues ε_n are not directly related to single-particle energies despite their resemblance to the bands observed in experiments such as photoemission, and in particular, there is no theoretical basis for the idea that the difference of ε_n will yield the correct fundamental gap for a semiconductor like Si, and indeed it does not (Godby et al. 1986, 1987).

Since the construction of a DFT actually only depends on the existence of a variational principle, one can in fact imagine a DFT for excited states, but with a functional which is quantum-number dependent and at present unknown. The situation for a density functional theory for systems at finite temperature is somewhat brighter (Mermin 1965), since one can use the existing results for a homogeneous electron gas at low but finite temperature to construct an appropriate local density functional. However, since this scheme has seen very little practical use (Ghazali and Leroux Hugon 1978), it is difficult to judge the reliability of the finite-temperature LDA, particularly in strongly inhomogeneous semiconducting materials where the gap at $T = 0$ is incorrectly given by DFT.

In the absence of a practical scheme for obtaining electronic contributions to the entropy, ab initio calculations for finite-temperature properties are confined to situations where the lattice contribution to the entropy dominates, since this can be obtained within the Born–Oppenheimer approximation keeping the electrons at zero temperature. Thus, natural candidates for an ab initio study

can be found among systems which undergo structural phase transitions as a function of temperature, which will be discussed in the next section.

3. Structural phase transitions

3.1. Phenomenology

Phase transitions in solids can occur as a result of varying external parameters such as temperature, pressure, and magnetic field. They are characterized by a quantity called the order parameter, which distinguishes the disordered phase, in which it is single-valued, from the ordered phase, in which it becomes multiple-valued, reflecting the presence of a broken symmetry (Lifshitz and Pitaevskii 1980). The order parameter is a thermal expectation value of some combination of the microscopic degrees of freedom of the system. The transition can be classified according to the nature of the operators as an electronic transition, e.g. magnetic or superconducting, or as a structural transition, in which the ordering occurs in the ionic parameters. The latter can be considered to include ferroelectric transitions, in which the order parameter is the electrical polarization and thus involves both electronic and ionic operators.

In a structural transition, the crystal distortion is usually strongly coupled to other degrees of freedom in the system such as strain. This leads to the concept of a secondary order parameter, which is a quantity which is not in itself critical, but in which ordering is induced by the nonzero primary order parameter (Cochran 1971). These considerations are important when looking at the structural changes between the high- and low-temperature phases, and also when examining the critical behavior of the system, especially the phase diagram and other nonuniversal quantities.

As discussed above, within a ground-state density functional approach it is only the structural transitions which are accessible, and moreover, only in those systems where the transition is driven by lattice entropy rather than electronic entropy. This is clearly the case in a system where there is a gap for electronic excitations which is larger than the transition temperature. Other possibilities exist, e.g. charge density wave systems with a short coherence length (McMillan 1977). In contrast, the martensitic transitions in the A-15 compounds Nb_3Sn and V_3Si are cases in which the electronic contributions to the entropy appear to dominate (Bhatt and McMillan 1976).

There is a further classification of the lattice-driven structural phase transitions which reflects properties of the microscopic potential and has a corresponding phenomenological signature due to differences in the dynamics of the soft mode (Lines and Glass 1977). At one end of the spectrum are the order-disorder transitions, for which the high-temperature phase is microscopically distorted, although the thermal-averaged distortion is zero. This corresponds to a strongly anharmonic, deep double-well potential for local distortions, and a diffusive character for the soft mode which arises from the

hopping between wells. In such a case, it is natural to use a discrete-spin picture to model the system. At the other end of the spectrum are the displacive transitions, in which the distribution of atomic positions is a phonon-like single peak about the average position, which corresponds to a weakly anharmonic lattice potential and phonon-like excitations with a temperature-dependent dispersion relation. In this picture, the transition occurs when the frequency of the phonon mode whose polarization vector corresponds to the atomic displacements of the transition decreases to zero.

Experimental studies of structural phase transitions focus on the detection of the occurrence of a transition and the measurements of various quantities as the external parameters are varied around the transition point. Static structural determinations are used to study the order parameter in the ordered and disordered phases. These methods include X-ray diffraction and elastic neutron scattering (Frazer 1971), which probe the order on long-length scales, and LEED spectroscopy (Van Hove and Tong 1979), which is useful for detecting symmetry changes on surfaces. EXAFS yields information about the local order and in particular, can distinguish between displacive and order-disorder transitions (Islam and Bunker 1987). Dynamic structural determinations, such as inelastic neutron scattering (Frazer 1971), Raman scattering and infrared spectroscopy (Lines and Glass 1977) probe the characteristics of the collective modes, in particular, their frequencies and linewidths. Lastly, measurements of thermodynamical and mechanical quantities such as the specific heat, response functions and elastic constants can be used to characterize the transition further.

Structural phase transitions have been found to occur in numerous and widely diverse systems. Surfaces provide many examples of transitions in two dimensions. Phase transitions between different surface reconstructions occur for many clean metal and semiconductor surfaces, including Si(100), Si(111), W(001) and Mo(001) (Tosatti 1980). In addition, phase transitions can occur in the ordering of physisorbed and chemisorbed surface layers, either driven by adsorbate-adsorbate interactions or by modifications caused by the adsorbate of the interactions which drive the reconstructions of the substrate layer. Interesting examples of adsorbed-layer systems include rare gas atoms on graphite, O and Se on Ni(111), and H on W(100) and Mo(100) (Sinha 1980).

There is also a rich variety of systems in three dimensions. These include transitions between different forms of polymorphic crystals, among which are silica (Behnke et al. 1986), ice (Behnke et al. 1986) and tin (Ihm and Cohen 1981). Ionic molecular crystals such as LiKSO₄ show interesting effects due to the coupling between the translational and rotational degrees of freedom of the components (Choudry et al. 1986, Kurzynski and Halawa 1986), and some, such as Rb₂ZnCl₄, possess incommensurate phases (Katkanant et al. 1986). Another example of long-period ordering (which, however, may be a kinetic rather than an equilibrium phenomenon) is a polytypic material such as ZnS, which occurs in about 200 different forms all composed of structurally identical layers appearing in a variety of stacking orders (Mardix 1986). Ferroelectrics are a group of

materials which share certain characteristic properties because the ordering in local atomic rearrangements gives rise to local electrical polarization. Related systems are antiferroelectrics and ferroelastics, in which the electrical polarization is induced by a transition in the strain degrees of freedom (Lines and Glass 1977). Another class of transitions which primarily involves local rearrangements of atoms are ordering transitions in metal and semiconductor alloys. In the latter, the fabrication of strained alloys in heterostructures permits the observation of additional types of ordered phases (Martins and Zunger 1986, Littlewood 1986). Martensitic transformations, on the other hand, do not involve atomic rearrangements within the unit cell but rather the development of long-wavelength strains which change its shape. Examples include the A-15 compounds Nb_3Sn and V_3Si , mentioned earlier, and $\beta\text{-NaN}_3$ (Sahu 1986).

3.2. Landau and renormalization group theories

The vast amount of data relating to phase transitions in this great variety of materials can be systematized and comprehended through the theoretical concept of "universality". Close to a second-order transition, in the so-called critical region, quantities such as the order parameter, correlation functions, specific heat and susceptibility are observed to scale according to simple power laws specified by the critical exponents. The values of the exponents, which determine the universality class of the transition, are in general independent of the details of the system, being related only to the nature of the order parameter, the spatial dimensionality and the symmetry.

A simple description of a given phase transition, called the Landau theory (Lifshitz and Pitaevskii 1980), can be constructed with these three pieces of information and one additional assumption, as follows. The free energy is expanded as an *analytic* function of a symmetry-breaking quantity, such as the charge density, whose observed value is obtained by minimizing this expression. From this can be deduced that in a second-order transition, the order parameter transforms according to an irreducible representation of the symmetry group of the high-symmetry phase, and thus the permitted ordered phases can be obtained. However, because of the assumption of analyticity, it turns out that the critical exponents are fixed at the so-called "classical" values, and thus this theory cannot account for the variety of observed universality classes.

A similar expansion in invariants, where now the order parameter is a function of position, yields a Landau–Ginzburg–Wilson Hamiltonian, in terms of which the free energy can be expressed as a functional integral (Amit 1978). Evaluating the functional integral via the stationary-phase approximation, one recovers the Landau theory. A renormalization group (RG) evaluation, which is designed to incorporate the effects of fluctuations, yields a natural explanation of the universality and possible nonclassicality of the critical exponents (a good introduction is Pfeuty and Toulouse (1977) and an additional source is Ma (1976)). Given the nature of the order parameter, the spatial dimensionality and

the symmetry, a Hamiltonian is constructed. Then, by integration over a subset of the degrees of freedom of the system, a new partition function is obtained and cast in the same form as the old, but in which the Hamiltonian has a new set of parameters which are expressed in terms of the old by recursion relations. The recursion relations are used to generate flow diagrams in Hamiltonian parameter space.

The fixed points of these flows play a central role in determining the properties of the transitions that a system will undergo. To describe a second-order transition, the fixed points are located, their stability studied, and critical exponents extracted. First-order transitions can be identified from the topology of the flows or the absence of stable fixed points. From this information a phase diagram can be constructed.

Nonuniversal aspects of critical behavior are also of interest. These depend on the actual values of coupling for a particular system, and can be also obtained within an RG analysis (Rudnick and Nelson 1976). The simplest is the location of a particular system in the phase diagram, and from that the value of the critical temperature. Crossover phenomena, where the system is governed by a certain fixed point in one part of the critical region, and then by another (or becomes first order) closer to criticality, can be studied. Lastly, the thermodynamic quantities can be obtained by evaluating the scaling functions via RG.

The RG approach, with its emphasis on universality, leaves open questions which relate to the specific features of the behavior of individual materials. First, attention focuses on the global topology of flows and on the properties of fixed points, rather than on the accurate prediction of the properties of a system with a given microscopic Hamiltonian, not necessarily in a Landau–Ginzburg–Wilson form. While universality leads to a natural emphasis on relevant variables, irrelevant variables can significantly modify nonuniversal properties before they renormalize to zero (Natterman 1976), and in general, the calculations of nonuniversal properties are more involved and less technically developed than issues of universal behavior. In addition, the phenomenological determination of coupling parameters can lead to ambiguities in identifying the critical behavior of a particular system, and such an approach cannot give insight into the chemical origin of the couplings, such as is necessary in the selection of materials to embody a certain type of critical behavior.

4. Ab initio statistical mechanics: general considerations for structural transitions

In striving to understand the behavior of a specific material, we can address the questions which are left open by the statistical-mechanical approach by introducing quantitative realism at the level of an appropriate microscopic Hamiltonian, constructed with the use of total-energy calculations.

Because this is in some sense the most natural approach to the statistical mechanics of structural transitions in real systems, several attempts have been previously made to carry out such a program. Phase transitions on the Si and Ge(100) surfaces have been examined using a semi-empirical tight-binding total-energy method (Ihm et al. 1983). Transitions in the fluorine-based perovskite RbCaF_3 , using a Gordon–Kim total-energy method, have been studied within the anharmonic crystal model (Boyer and Hardy 1981). These schemes suffered from the lack of accuracy of the total-energy methods. Recent work on Zr (Ye et al. 1987) used an accurate ab initio total-energy method, but the self-consistent phonon treatment of the model chosen did not permit the examination of critical behavior.

It is clearly crucial to formulate a procedure in which both tractability and accuracy are ensured. More specifically, these requirements are expressed as follows. The model Hamiltonian must be realistic in the sense that the temperature-dependent structural quantities of interest obtained from it are accurate. However, the model must also be simple. It must contain only a small number of parameters, which must be straightforwardly obtainable from a reasonable number of ab initio total-energy calculations, and it must also be of such a form that it is possible to perform a statistical-mechanical analysis of the model, accurate and valid in the critical region.

The reconciliation between the conflicting demands of realism and simplicity is possible. The key is to drop the requirement for complete generality and to design the model Hamiltonian for a specific transition, expressing the model only in terms of those degrees of freedom which are important for describing this particular transition. In addition, simplicity is gained by including only those interactions which are significant, as based on an understanding of the chemistry of the system and information about the properties of the lattice potential obtained either phenomenologically or from ab initio investigations. The realism of the model, on the other hand, is preserved by fitting the model to the structural energies calculated using ab initio methods, which are obtained independently of any assumptions in the model and which represent the best available solutions to the full crystal Hamiltonian.

Using this simple microscopic Hamiltonian, one can then derive a Landau–Ginzburg–Wilson free-energy functional, either by a coarse-graining procedure or a Hubbard–Stratonovich transformation. With this step, the problem is cast into a form suitable for the application of powerful statistical mechanical techniques such as RG, and the extensive work done in this area can be exploited to obtain information about the specific material of interest.

5. Ab initio statistical mechanics: GeTe

To illustrate the concepts outlined above and demonstrate their usefulness, we describe in this section the implementation of this approach for a particular

structural transition: the rocksalt–rhombohedral transition of GeTe (Rabe and Joannopoulos 1987a, b). First, we summarize the relevant experimental observations of the GeTe structural transition. Then, we lay the foundations for the finite-temperature calculation by applying the ab initio pseudopotential total-energy method to the $T = 0$ structural properties of GeTe. Next, we give a detailed account of the derivation of the form of the model Hamiltonian and of the computation of the parameters that appear in it through total-energy calculations for a variety of structural configurations. Lastly, we examine the finite-temperature properties of the model using first mean-field theory, then a renormalization group analysis, discuss the accuracy of the results and compare them to experimental observations.

5.1. Rocksalt–rhombohedral transition of GeTe

At high temperatures, the IV–VI narrow-gap semiconductor GeTe has the rocksalt structure. At low temperatures the system exists in a rhombohedral structure. This structure, shown in fig. 1, can be described as a rocksalt structure slightly distorted by freezing in a $k = 0$ optical phonon along the [111] direction, corresponding to the order parameter of the transition, with a subsequent shear relaxation along [111], corresponding to the secondary order parameter. The other group IV tellurides, SnTe and PbTe, also have the rocksalt structure at high temperatures and show the same tendency to lattice instability as the temperature is lowered. However, the transition in SnTe occurs at a much lower temperature, and in PbTe not at all, the lattice instability manifesting itself only through the softness of the $k = 0$ optical phonon. Experimental studies of the GeTe transition and their interpretation are somewhat difficult because of the high transition temperature and intrinsic limitations on the quality of the sample. The latter arises because the compound GeTe is not in the range of homogeneity of the alloy, which for a nominal stoichiometric composition results in the coexistence of free Ge with a 50.3% Te-phase (Shelimova et al. 1965, Bigava et al. 1976, Abrikosov et al. 1977a). This phase exhibits the rhombohedral–rocksalt transition and contains free holes arising mainly from Ge vacancies. The temperature dependence of the order parameter near the transition has not been observed, as it has been in SnTe using elastic neutron

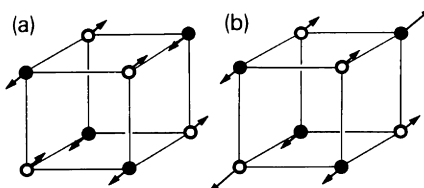


Fig. 1. Rhombohedral structure of GeTe is obtained from the rocksalt structure by a two-step distortion: (a) relative displacement of the two fcc sublattices by $a_0\tau(111)$ and (b) rhombohedral shear along (111).

scattering (Iizumi et al. 1975). However, transition temperatures in the range 625–700 K have been extracted from measurements of the temperature dependence of the volume and rhombohedral angle α using X-ray diffraction (Bigava et al. 1976, Schubert and Fricke 1951a, b, 1953a, b, Bierly et al. 1963, Zhukova and Zaslavskii 1967), calorimetric determinations of the heat evolution associated with the transition (Abrikosov et al. 1983) and studies of anomalies in the thermal expansion (Shelimova et al. 1965, Abrikosov et al. 1977a, Novikova et al. 1971, 1972, 1977) and electrical resistivity (Novikova et al. 1975, Abrikosov et al. 1977b). In some measurements (Zhukova and Zaslavskii 1967), small discontinuities in volume and α have been detected at the transition, suggesting that it may be weakly first-order, in contrast to the second-order transition observed in SnTe. It is the calculation of the transition temperature and the explanation of the weakly first-order character of the transition that will be the focus of the theoretical analysis.

5.2. GeTe at zero temperature: ab initio calculations

The validity of the model Hamiltonian and thus of the finite-temperature properties derived from it depends crucially on the accurate calculation of structural total energies for the material and structures of interest. This should be possible for GeTe because of the structural simplicity of the two phases and the smoothness and high transferability of the Ge and Te pseudopotentials. We show this in the sequel by computing structural properties which are directly related to energy differences. In the process, calculational cutoffs are established by studying convergence. Results are compared with experimental values to verify the ability of these calculations to describe GeTe. Also, charge densities and bandstructures are examined to obtain an understanding of the character of bonding in the material and to aid in the development of simple qualitative physical ideas about structural energies.

The calculations of quantum-mechanical total energies of various structural configurations of GeTe are performed using the self-consistent pseudopotential total-energy method, described in section 2, with details as follows (Rabe and Joannopoulos 1987c). The Ge and Te pseudopotentials used are the relativistic nonlocal potentials of Bachelet et al. (1982). The need for a relativistic potential arises from the enhancement of the s–p splitting, which must be included for a correct description of the effect of s–p hybridization on distortion energies. The spin–orbit splitting should play a comparatively minor role, because of the gap, as we have verified in calculations of the sublattice-displacement energy in SnTe. Hence, except for generating bandstructures, we use spin–orbit averaged potentials. Exchange and correlation are included through the local-density approximation using the Ceperley–Alder–Perdew–Zunger parametrization (Ceperley 1978, Ceperley and Alder 1980, Perdew and Zunger 1981). Eigenfunctions are expanded in a plane-wave basis with energy cutoff $E_1 = 10.5$ Ry, and

Löwdin perturbation theory (Löwdin 1951) is used to include the effect of plane waves up to $E_2 = 16.5$ Ry. Brillouin-zone averages are performed using Monkhorst–Pack special k -point sets (Monkhorst and Pack 1976), which depend on the Bravais lattice and the chosen sampling density. Cutoffs are chosen to give convergence on 1% level for the rocksalt-structure lattice constant, 10% for the bulk modulus and 10% for the curvature of $E(\tau)$ (energy of sublattice displacement at fixed volume). We find that convergence is limited in the $E(V)$ case by the energy cutoff; in the $E(\tau)$ case it is limited by k -points.

The results of the calculation are as follows. By calculating $E(V)$ at various atomic volumes V (fig. 2) and fitting to a polynomial quadratic in V , we can extract the lattice constant $a_0 = 5.85 \text{ \AA}$ and bulk modulus $B = 0.51 \text{ Mbar}$ of a hypothetical rocksalt form at $T = 0$. Comparing this to the experimental “zero-temperature” lattice constant 5.92 \AA (estimated using $a_0 = 6.01 \text{ \AA}$ at 670 K and a linear thermal-expansion coefficient of 20×10^{-6} for $T > T_c$ (Novikova et al. 1970)) we see that the calculated values are $\sim 1\%$ too small. Although there are no measurements of the bulk modulus for GeTe, the calculated value of

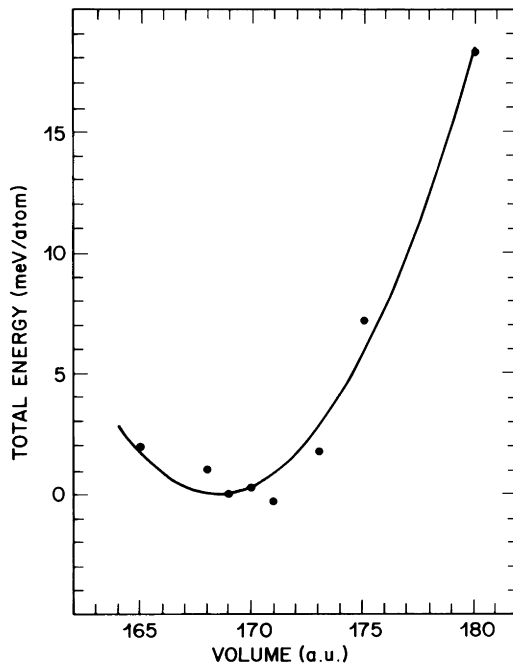


Fig. 2. Total energy of the rocksalt structure, in meV/atom, as a function of varying atomic volume. The minimum of the parabolic fit shown as a solid line is selected as the zero of energy. The lattice constant a_0 at the minimum is 5.85 \AA and the curvature at the minimum yields a bulk modulus of 0.51 Mbar .

0.51 Mbar is, as expected, roughly the same as measurements in SnTe and PbTe, which fall in the range 0.4–0.5 Mbar (Beattie 1969, Houston et al. 1968).

The bandstructure, total pseudocharge density and band-by-band pseudocharge densities (figs. 3, 4 and 5, respectively) support a simple tight-binding picture of the competition of ionic and covalent bonding, as we have previously found in SnTe and PbTe (Rabe and Joannopoulos 1985). In the rocksalt structure, the low lying s-level on both the cation and anion are filled. The bands near the Fermi level are half filled, with mostly p-character. This resonant bonding results in a large electron–phonon coupling which drives the lattice instability, while the ionic character, on the other hand, stabilizes the rocksalt structure. Examination of the total and band-by-band charge densities (figs. 4 and 5) illustrates this competition. The ionic component is apparent from the charge transfer from the cation Ge to the anion Te, while the deviation of the charge densities of the ions from spherical symmetry indicates the covalent nature of the p-bonding. Comparison with calculated pseudocharge densities of PbTe (Rabe and Joannopoulos 1985) shows that in PbTe there is more charge transfer and less deviation from spherical symmetry of the ions, and thus the balance shifts between ionic and covalent bonding, stabilizing the rocksalt

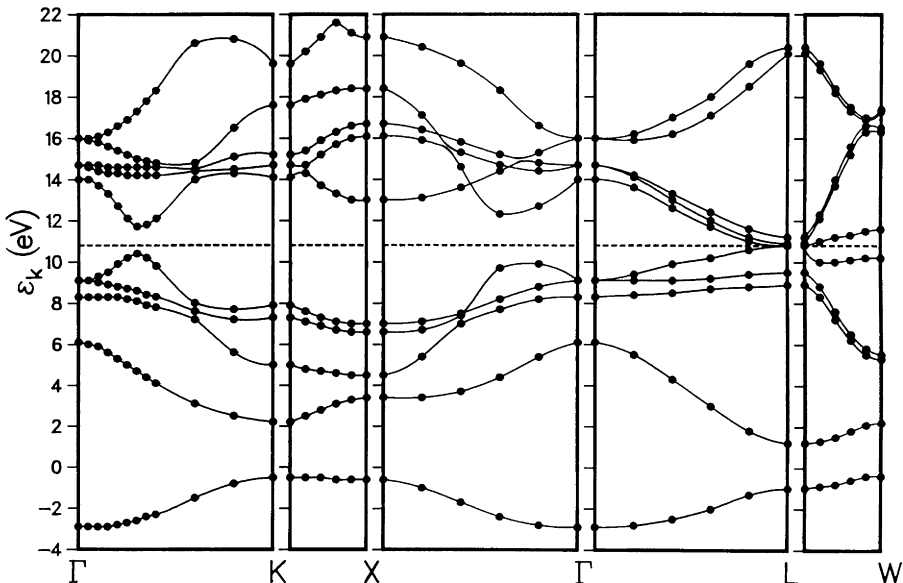


Fig. 3. Pseudopotential bandstructure of GeTe in the rocksalt structure with lattice constant $a_0 = 5.85 \text{ \AA}$, including spin-orbit coupling. In units of $2\pi/a_0$, $\Gamma = (0, 0, 0)$, $L = (1/2, 1/2, 1/2)$, $W = (1, 1/2, 0)$, $K = (1, 1/4, -1/4)$ and $X = (1, 0, 0)$. The gap of 0.04 eV at L is too small to be visible on this plot. The energy of the top of the valence band is indicated by a dashed line.

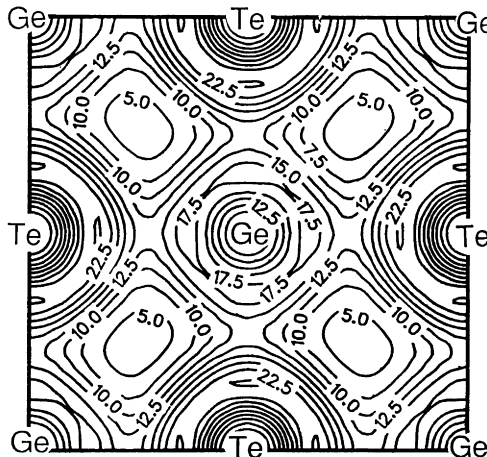


Fig. 4. Total pseudocharge density of rocksalt GeTe with lattice constant $a_0 = 5.85 \text{ \AA}$ in the (100) plane. Densities are given in units of electrons per two-atom unit cell.

structure. In fact, in SnTe this competition is so finely drawn, as reflected in the low T_c , that the total-energy calculations incorrectly predict the minimum-energy structure to be the rocksalt structure, albeit with a very low-energy cost for sublattice displacement. This failure is produced by the equilibrium-volume underestimate, characteristic of LDA calculations, which leads to an overstabilization of the rocksalt structure relative to the lower-symmetry rhombohedral structure. This volume dependence is also the reason for the observed $dT_c/dP < 0$. With correction of this problem by fixing the lattice constant to the SnTe experimental value, calculations show that sublattice displacement does in fact significantly lower the total energy.

We study a range of values of τ and α to determine the zero-temperature equilibrium lattice parameters for GeTe. The results are fitted with a polynomial in τ and α to within 10^{-4} Ry and the fit is shown in fig. 6 as a contour plot. The resulting lattice parameters are $\alpha = 58.8^\circ$ and $\tau = 0.025$ to be compared with the experimental values ($57.9^\circ, 0.026$) (Goldak et al. 1966) and ($58.0^\circ, 0.034$) (Zhukova and Zaslavskii 1967). Through an argument analogous to that for SnTe, the underestimate of the rhombohedral distortion can be seen to arise from the LDA underestimate of the minimum-energy volume, although the size of this effect relative to the size of the instability is much smaller in GeTe.

Finally, we vary α , with $\tau = 0$ and $a_0 = 5.85 \text{ \AA}$ (fig. 7), to obtain a value for the shear elastic constant of the rocksalt structure, $C_{44} = 1.8 \times 10^{11} \text{ dyne/cm}^2$. Since there is no experimental measurement of C_{44} for GeTe, we compare the calculation to the SnTe value $C_{44} = 1.4 \times 10^{11} \text{ dyne/cm}^2$ (Seddon et al. 1976), finding reasonable agreement.

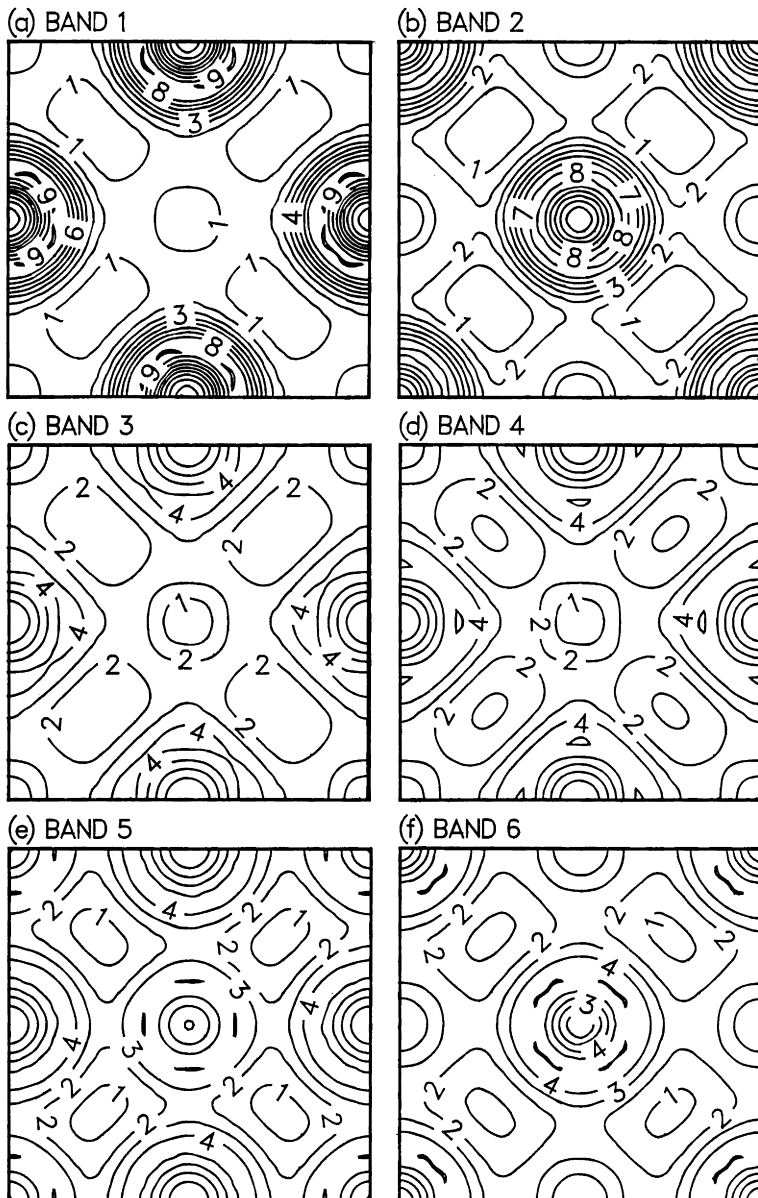


Fig. 5. Band-by-band pseudocharge densities of rocksalt GeTe in the (100) plane for (a)–(e) bands 1–6, respectively, in units of electrons per unit cell. Positions of Ge and Te atoms are the same as in fig. 4.

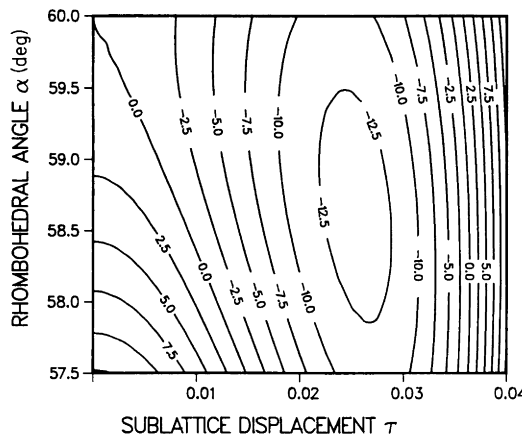


Fig. 6. Contour plot of the fit to $\Delta E_{\text{tot}}(\alpha, \tau) = E_{\text{tot}}(\alpha, \tau) - E_{\text{tot}}(\alpha = 60^\circ, \tau = 0)$. Energies shown are in meV/atom.

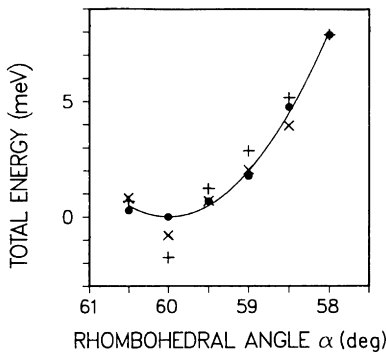


Fig. 7. Total energy in meV/atom of GeTe as a function of α with $\tau = 0$. Vertical crosses are results of calculations done with 125 k -points, filled circles with 343 k -points and crosses with 729 k -points in the full Brillouin zone. The minimum of the parabolic fit, shown as a solid line, is selected as the zero of energy. The curvature yields a value for C_{44} of 1.8×10^{11} dyne/cm 2 .

The general level of agreement of calculated quantities with experimental measurements, which is typical of applications of this total-energy method to other materials, leads us to conclude that the ab initio scalar relativistic pseudopotential total-energy method can be used to provide an accurate description of the structural properties of GeTe.

5.3. Model Hamiltonian

To incorporate information about structural energies into an understanding of the structural transition, it is of central importance to have an appropriate

model Hamiltonian form. In this section, the guidelines set out in section 4 are followed to manipulate the full crystal Hamiltonian for GeTe into a form which is both simple and realistic.

For a displacive transition such as the rocksalt–rhombohedral transition in GeTe, it is appropriate to use an anharmonic lattice Hamiltonian (Cochran 1960, Anderson 1960) in which only the ionic degrees of freedom appear explicitly, and the electronic effects are included through the Born–Oppenheimer approximation. This Hamiltonian, simplified by expanding to fourth order about the prototype configuration (in this case, the rocksalt structure) is the basis for the soft-mode theory of structural phase transitions. However, for present purposes it is far too complicated. First, it contains too many free parameters – not only the full phonon dispersion relation of the crystal, but also all the wave-vector-dependent higher-order couplings. Second, it is too difficult to analyze the finite-temperature behavior beyond the lowest-order self-consistent phonon approximation, which breaks down in the critical region.

To find a model Hamiltonian with a simpler form and a greatly reduced number of parameters, we identify the important degrees of freedom for describing the transition though the local-mode approximation (Lines 1969). For each unit cell, the local-mode variable is defined as the projection of local ionic displacements onto the polarization vectors of the $k = 0$ optical modes, referred to the mean positions in the high-temperature structure. To a large extent, the requirement that the local mode have the lattice symmetry restricts the possible implementations of this definition. Moreover, the approximations which will be essential for obtaining a Hamiltonian with a small number of parameters necessitate that the precise choice of local mode incorporate a physical understanding of the lattice instability. The charge flow and energy gain resulting from the symmetry breaking by the distortion of the six equivalent nearest-neighbor bonds of the rocksalt structure involves primarily Te p-like states (Rabe and Joannopoulos 1985, Littlewood 1980a, b), while the main anharmonic contribution to the energy originates in the nonlinear Te polarizability (Bussmann–Holder et al. 1983). Thus, for GeTe, the best choice of local mode emphasizes the distortion of the Te ion environment:

$$\xi_i = a_0^{-1} \left(\Delta \mathbf{r}_{\text{Te}}^i - \frac{1}{6} \sum_j \Delta \mathbf{r}_{\text{Ge}}^j \right),$$

where a_0 is the length of the side of the fcc conventional unit cell and the displacements $\Delta \mathbf{r}$ are measured relative to the rocksalt structure (fig. 8).

The next step is to write a model Hamiltonian expressed purely in terms of the local-mode variables by expanding in symmetry-allowed powers of the local-mode variables, with on-site terms kept up to some arbitrary order and intersite interactions to quadratic order only. This “local-anharmonicity” approximation is crucial in keeping the form of the model Hamiltonian simple.

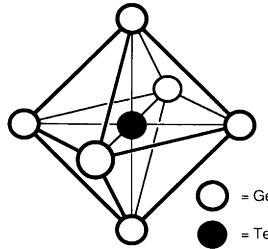


Fig. 8. The local-mode variable is defined as $\xi_i = a_0^{-1}(\mathbf{r}_{\text{Te}}^i - \frac{1}{6} \sum_j \mathbf{r}_{\text{Ge}}^j)$. The sum runs over the six nearest neighbor Ge atoms, which in the rocksalt structure form an octahedron with the Te atom at the center.

Before giving the explicit approximate expression for the model Hamiltonian H_{mod} which will be used in the calculation, we study its properties using the exact form, obtained from the relation:

$$\exp(-\beta H_{\text{mod}}(\{\xi_i\}) = \int \left[\prod_i (\mathrm{d}\sigma_i) \right] \exp(-\beta H_{\text{lat}}(\{\xi_i\}, \{\sigma_i\})),$$

where $\sigma_i = a_0^{-1}(\Delta \mathbf{r}_{\text{Te}}^i + \frac{1}{6} \sum_j \Delta \mathbf{r}_{\text{Ge}}^j)$ and $H_{\text{lat}}(\{\xi_i\}, \{\sigma_i\})$ is the full anharmonic lattice Hamiltonian, for which the values at certain $\{\xi_i\}$, $\{\sigma_i\}$ can be obtained through ab initio total-energy calculations. We note that at fixed $\{\xi_i\}$, H_{mod} in principle depends on the energies of a $\frac{3}{2}N$ dimensional space of ionic configurations and the temperature.

However, to a good approximation the situation is much simpler. We decompose H_{lat} as follows:

$$H_{\text{lat}}(\{\xi_i\}, \{\sigma_i\}) = H_1(\{\xi_i\}) + H_2(\{\sigma_i\}) + H_3(\{\xi_i\}, \{\sigma_i\}).$$

Because the physically important anharmonicity is associated with the $\{\xi_i\}$, it should be sufficient to include the $\{\sigma_i\}$ in the expansion of H_{lat} up to quadratic order only. The Gaussian integration over the $\{\sigma_i\}$ replaces $\{\sigma_i\}$ by the values which minimize H_{lat} at fixed $\{\xi_i\}$, and therefore the coefficients of H_{mod} are independent of temperature in this approximation.

For general $\{\xi_i\}$, the minimization of H_{lat} over the $\{\sigma_i\}$ is an extremely difficult problem. For $\{\xi_i\}$ with high space-group symmetry, it can be greatly simplified by approximating H_3 by its lowest order term $\sum_{\alpha\beta ij} V_{\alpha\beta}(\mathbf{R}_j - \mathbf{R}_i) \xi_\alpha(\mathbf{R}_i) \sigma_\beta(\mathbf{R}_j)$. With

$$\xi_\alpha(\mathbf{R}_i) = \frac{1}{N} \sum_{\mathbf{k}} \xi_\alpha(\mathbf{k}) \exp(i\mathbf{k} \cdot \mathbf{R}_i), \quad \sigma_\alpha(\mathbf{R}_i) = \frac{1}{N} \sum_{\mathbf{k}} \sigma_\alpha(\mathbf{k}) \exp(i\mathbf{k} \cdot \mathbf{R}_i),$$

and

$$V_{\alpha\beta}(\mathbf{R}_i) = \sum_{\mathbf{k}} V_{\alpha\beta}(\mathbf{k}) \exp(i\mathbf{k} \cdot \mathbf{R}_i),$$

this can be written as $\sum_{\alpha\beta k} V_{\alpha\beta}(k) \xi_\alpha(k) \sigma_\beta(-k)$. Thus, if we choose a local-mode configuration with a single nonzero $\xi(k) = \xi^*(-k)$, the only nontrivial minimization is with respect to the component of $\sigma(-k) = \sigma^*(k)$ which does not break any further symmetry beyond that of $\xi(k)$. For $k \rightarrow 0$, however, $V_{\alpha\beta}(k)$ goes like k^2 , since $\sigma_\alpha(k=0)$ is a uniform translation of the crystal which cannot change the energy and the linear term in k is not permitted by inversion symmetry. For such local-mode configurations, we instead approximate H_3 by the terms which describe the lowest-order coupling of the long-wavelength strain (the gradient of σ) to the local-mode variable ξ :

$$\begin{aligned} & \sum_{\alpha\beta\gamma ij} V_{\alpha\beta\gamma}(\mathbf{R}_j - \mathbf{R}_i) \sigma_\alpha(\mathbf{R}_j) \xi_\beta(\mathbf{R}_i) \xi_\gamma(\mathbf{R}_i) \\ &= \frac{1}{N} \sum_{\alpha\beta\gamma kk'} V_{\alpha\beta\gamma}(k) \sigma_\alpha(k) \xi_\beta(-k') \xi_\gamma(k' - k), \end{aligned}$$

where for $k \rightarrow 0$, $V_{\alpha\beta\gamma}(k) \rightarrow V_{\alpha\beta\gamma\delta} k_\delta$. Rather than integrate this term out immediately, we will for the time being keep the long-wavelength strains explicitly in order to study the physics arising from this coupling.

The construction of H_{mod} for the GeTe transition proceeds as follows. The local-mode variables “sit” on the sites of an fcc lattice and only cubic-symmetry invariants appear in the expansion of the Hamiltonian. We truncate the on-site potential at fourth order in the local-mode variable but keep isotropic terms to eighth order. Intersite interactions up to second order are included, since the constraints imposed by the sharing of Ge atoms by first- and second-neighbor local-mode octahedra suggest the coupling is important. The lowest-order terms involving long-wavelength strain fields are included explicitly, as discussed earlier.

Carrying out this construction, we obtain the following explicit form for H_{mod} . The expression for the on-site potential is

$$\sum_i \left\{ A |\xi(\mathbf{R}_i)|^2 + u_0 |\xi(\mathbf{R}_i)|^4 + v_0 \sum_\alpha \xi_\alpha(\mathbf{R}_i)^4 + D |\xi(\mathbf{R}_i)|^6 + E |\xi(\mathbf{R}_i)|^8 \right\},$$

with the first-neighbor intersite interactions

$$\begin{aligned} & -\frac{1}{2} \sum_i \left\{ \xi_x(\mathbf{R}_i) [a_1 \sum \xi_x(\mathbf{R}_i + a_0 \mathbf{d}/2) + a_2 \sum \xi_x(\mathbf{R}_i + a_0 \mathbf{d}/2) \right. \\ & \quad \left. + a_3 \sum (\mathbf{d} \cdot \hat{\mathbf{x}})(\mathbf{d} \cdot \hat{\mathbf{y}}) \xi_y(\mathbf{R}_i + a_0 \mathbf{d}/2) \right. \\ & \quad \left. + a_3 \sum (\mathbf{d} \cdot \hat{\mathbf{x}})(\mathbf{d} \cdot \hat{\mathbf{z}}) \xi_z(\mathbf{R}_i + a_0 \mathbf{d}/2)] + \text{cyc. perm.} \right\}, \end{aligned}$$

and second-neighbor intersite interactions

$$-\frac{1}{2} \sum_i \left\{ \xi_x(\mathbf{R}_i) [b_1 \sum \xi_x(\mathbf{R}_i + a_0 \mathbf{d}) + b_2 \sum \xi_x(\mathbf{R}_i + a_0 \mathbf{d})] + \text{cyc. perm.} \right\},$$

where $\xi(\mathbf{R}_i)$ is the local-mode variable at the fcc lattice site \mathbf{R}_i .

With the strain tensor $e_{\alpha\beta} = (du_\beta/dx_\alpha + du_\alpha/dx_\beta)/2$, the lowest-order terms which describe long-wavelength strain deformations and their coupling to the order parameter are

$$(\Omega_0)^{-1} \int d^3r \left[C_{11} \sum_\alpha e_{\alpha\alpha}(\mathbf{r})^2/2 + C_{12} \sum_{\alpha \neq \beta} e_{\alpha\alpha}(\mathbf{r}) e_{\beta\beta}(\mathbf{r})/2 + C_{44} \sum_{\alpha \neq \beta} e_{\alpha\beta}(\mathbf{r})^2 \right. \\ \left. - g_0 \sum_\alpha e_{\alpha\alpha}(\mathbf{r}) |\xi_i|^2/3 - g_1 \sum_{\alpha < \beta} e_{\alpha\beta}(\mathbf{r}) \xi_{i,\alpha} \xi_{i,\beta} \right. \\ \left. - g_2 \sum_\alpha e_{\alpha\alpha}(\mathbf{r}) (\xi_{i,\alpha}^2 - |\xi_i|^2/3) \right].$$

These expressions define the model Hamiltonian coefficients $A, u_0, v_0, D, E, a_1, a_2, a_3, b_1, b_2, C_{11}, C_{12}, C_{44}, g_0, g_1$ and g_2 which will be calculated in the next section.

5.4. Calculation of model Hamiltonian parameters

The values of the coefficients for GeTe are obtained by fitting the model Hamiltonian to the energies of a variety of local-mode configurations, which, to facilitate the calculations, are chosen to be as highly symmetric as possible while still separately determining the coefficients. For the zero-strain coefficients $A, u_0, v_0, D, E, a_1, a_2, a_3$ and $b_1 + 2b_2$ we must consider configurations with the full fcc translational symmetry (fig. 9a) as well as configurations with two translationally inequivalent types of local-mode variables on fcc lattice sites. For the fcc lattice, there are only two ways to divide the sites into two inequivalent classes, giving rise to an arrangement with a tetragonal unit cell (fig. 9b) and to one with a rhombohedral unit cell (fig. 9c). In each type of unit cell, we study two families

Table 1

Specifications of the families of local mode configurations for which total energies were calculated, the combinations of quadratic parameters determined and the Monkhorst–Pack (1976) k -point sets used.

Open and filled circles are used to label translationally inequivalent lattice sites (see fig. 9)

Configuration	Unit cell type	Local mode variables	Quadratic parameters determined	k -point sets (no. of points in full BZ)
		Open circles	Filled circles	[smaller, larger]
(a)	fcc	$\tau(111)$	—	$A + 4a_1 + 2a_2 + b_1 + 2b_2$ [125, 343]
(b)	fcc	$\tau(010)$	—	$A + 4a_1 + 2a_2 + b_1 + 2b_2$ [125, 343]
(c)	tetragonal	$\tau(010)$	$-\tau(010)$	$A - 4a_1 + 2a_2 + b_1 + 2b_2$ [48, 100]
(d)	tetragonal	$\tau(101)$	$-\tau(101)$	$A - 2a_2 + b_1 + 2b_2$ [48, 100]
(e)	rhombohedral	$\tau(111)$	$-\tau(111)$	$A - 4a_3 - b_1 - 2b_2$ [27, 125]
(f)	rhombohedral	$\tau(112)$	$-\tau(112)$	$A + 2a_3 - b_1 - 2b_2$ [27, 125]

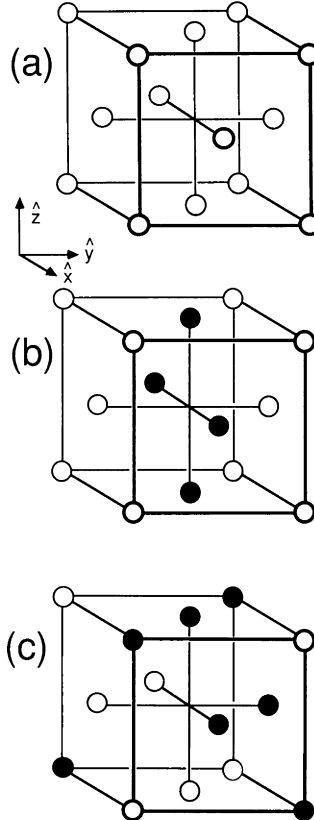


Fig. 9. The translational symmetries of the various local-mode configurations studied are illustrated. An fcc lattice with all sites equivalent is shown in (a). The division of lattice sites into two inequivalent types, as indicated by filled and open circles, yields (b) a tetragonal unit cell with equivalent sites lying in (010) planes, and (c) a rhombohedral unit cell with equivalent sites lying in (111) planes.

of local-mode configurations, specified by a fixed polarization vector at each inequivalent site and a varying amplitude τ . Details of the six families (a)–(f) are given in table 1. For each family, the energy as a function of τ determines one combination of coefficients at each order. Unfortunately, the second-neighbor couplings b_1 and b_2 cannot be separately determined without using still larger unit cells.

To obtain the strain coefficients C_{11} , C_{12} , C_{44} , g_0 , g_1 and g_2 , it is sufficient to consider configurations in which the local mode is uniform and only the lattice changes. We study three types of variation corresponding to pure volume change ($e_{xx} = e_{yy} = e_{zz}$), pure rhombohedral angle change at fixed volume

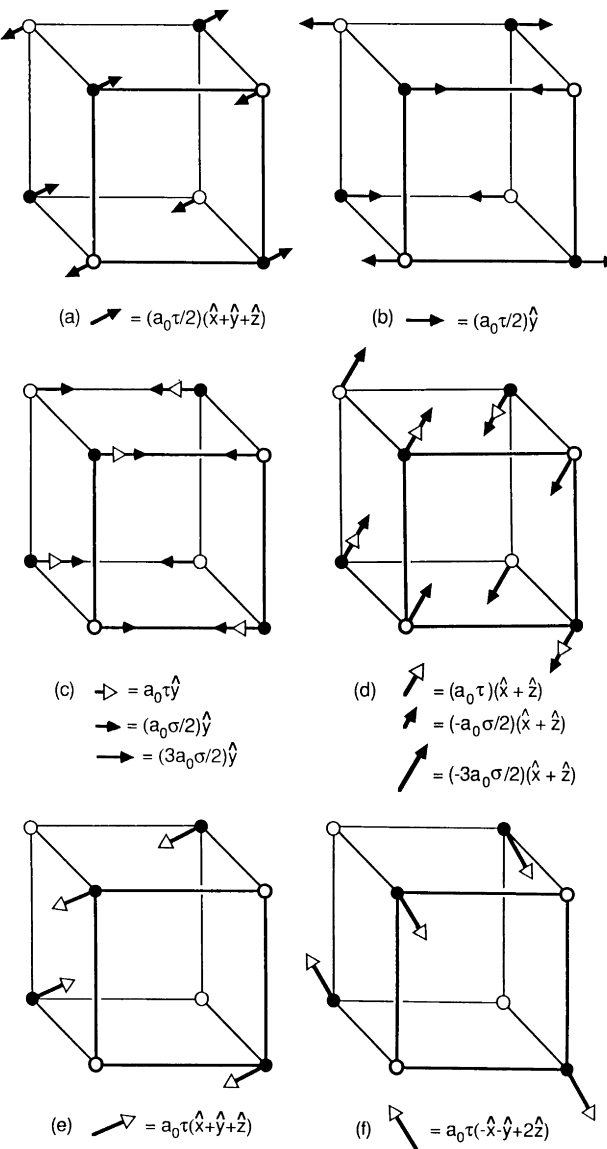


Fig. 10. For each family of zero-strain local mode configurations, labelled (a)–(f) as in table 1, the type of ionic configurations for which total energies are calculated is shown. These ionic configurations are constructed according to the symmetry of the corresponding local-mode configuration, as described in the text. Open and filled circles here represent Ge and Te ions, respectively. For (a), (b), (e) and (f) a fixed τ corresponds to a single ionic configuration. For (c) and (d), the requirements imposed by symmetry are less stringent and a one-dimensional space of ionic configurations, parametrized by σ , corresponds to fixed τ .

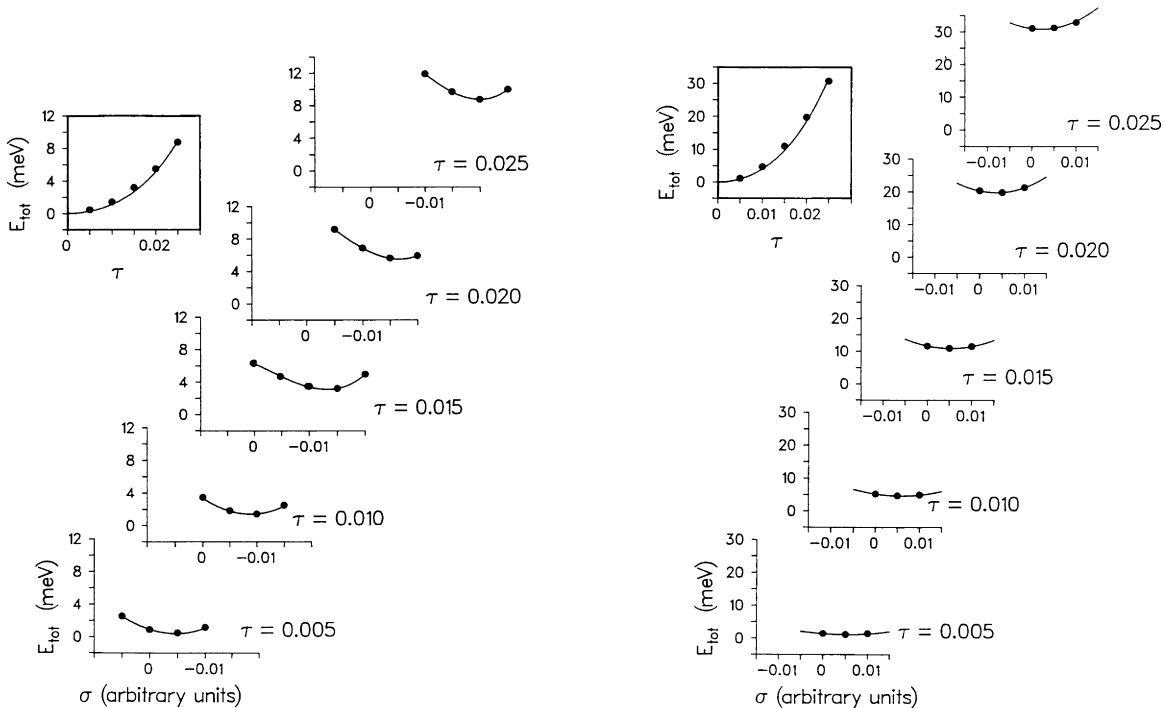


Fig. 11. For each member of a family of local-mode configurations, parametrized by τ , the space of corresponding ionic configurations of same translational and point symmetry, parametrized by σ , is searched for the minimum energy, which is assigned to the local-mode configuration (inset). For (a) the longitudinal tetragonal family and (b) the transverse tetragonal family shown here, the corresponding space is one-dimensional. Energies are given relative to the rocksalt-structure minimum in meV per atom.

($e_{xx} = e_{yy} = e_{zz}$, $e_{xy} = e_{yz} = e_{xz}$), and uniaxial strain (e_{zz}). The coefficients C_{11} , C_{12} and C_{44} are obtained from configurations with $\tau = 0$, while for g_0 , g_1 and g_2 a configuration with nonzero τ must be included at each \mathbf{e} .

As discussed in section 5.3, the exact relationship between the local-mode configuration energies and the ionic configuration energies, involving a highly complicated integration over the non-local-mode degrees of freedom, can be replaced to a good approximation by a simple rule, which permits the extraction of a given local-mode configuration energy from one or a small number of ionic-configuration calculations. This rule is that the local-mode configuration energy can be taken as the minimum over the energies of ionic configurations with the same translational and point symmetries. For families (a), (b), (e) and (f) and the strained configurations, the choice of τ and the symmetry requirement completely specify the ionic configuration. For families (c) and (d), the symmetry

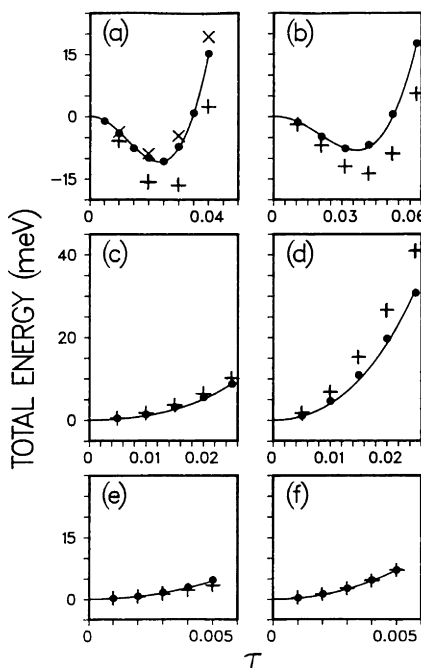


Fig. 12. Calculated local mode configuration energies, given relative to the rocksalt-structure minimum in meV per atom. Solid lines show fit using model Hamiltonian parameters given in table 2. The energies for six families of local-mode configurations with zero strain are shown – longitudinal and transverse: (a), (b) fcc; (c), (d) tetragonal and (e), (f) rhombohedral. The vertical crosses show the results of calculations with the smaller k -point sets given in table 1, filled circles with the larger k -point sets, and the crosses in (a) with 729 k -points in the full Brillouin zone.

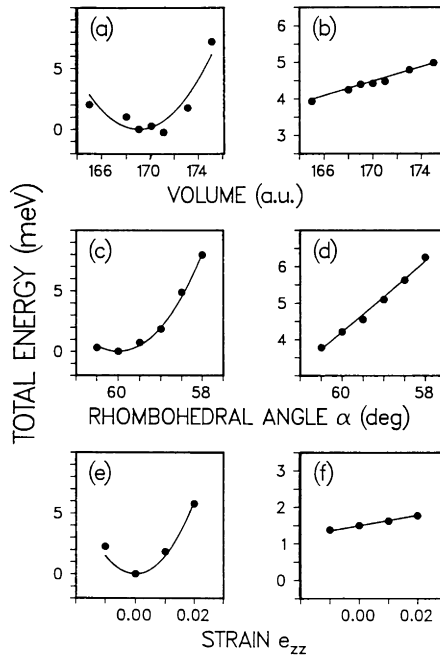


Fig. 13. Same conventions as fig. 12. The energies of configurations which include strain are shown: (a), (c) and (e) are pure strain distortions with $\tau = 0$. Parabolic fits, shown as solid lines, yield values for the elastic constants C_{11} , C_{12} and C_{44} . In (b), (d) and (f), which show $E(\mathbf{e}, \tau = 0.01) - E(\mathbf{e}, \tau = 0.00)$, the slopes of the straight-line fits determine the order-parameter strain coupling constants g_0 , g_1 and g_2 . Note the differences in energy scale among (a), (c), (e); (b), (d), (f), and fig. 12.

requirement is less restrictive, resulting in a one-dimensional space of ionic configurations, here parametrized by σ , which must be searched for the energy minimum. The resulting ionic configurations for all six families are shown in fig. 10. Calculations of the ionic-configuration energies are performed as described in sections 5.2. Details of the minimization procedure are illustrated in fig. 11.

The results for the energies of all the zero-strain local-mode configurations are shown in fig. 12. Energies of configurations including strain are shown in fig. 13. We include the results for smaller k -point sets in fig. 12 to demonstrate the level of convergence, which we find is dominated by k -point sampling. With the cutoffs used, energy curvatures are determined to about 10% accuracy.

The model Hamiltonian parameters were obtained through a two-step fitting process. First, the zero-strain coefficients were fitted to the zero-strain local-mode configuration energies, measured relative to the energies at $\tau = 0$. Then, the strain parameters were fitted to the energies of strained configurations,

Table 2
Model Hamiltonian parameters for GeTe (eV)

On-site		Intersite		Elastic		Coupling	
A	59.3	a_1		6.08	C_{11}	29.7	g_0
u_0	8.73×10^3	a_2		10.5	C_{12}	0.12	g_1
v_0	4.12×10^3	a_3		4.38	C_{44}	5.75	g_2
D	-7.32×10^5	$b_1 + 2b_2$		42.0			
E	2.36×10^7						

holding the zero-strain coefficients fixed and letting a_0 in the definition of ξ vary with \mathbf{e} . The quality of the fit can be seen from the solid lines in figs. 12 and 13. The resulting parameters are given in table 2.

5.5. Statistical mechanics

5.5.1. Partition function

Given this microscopic Hamiltonian, the transition temperature and critical properties follow from the evaluation of the partition function

$$Z = \int \left[\prod_i d\xi_i \right] \mathcal{D}\mathbf{e}(\mathbf{r}) \exp[-\beta H_{\text{mod}}(\{\xi_i\}, \mathbf{e}(\mathbf{r}))].$$

A systematic approach begins with manipulating it into a standard form. First, we perform a Hubbard–Stratonovich transformation, the purpose of which is to make the temperature dependence of the contribution of the intersite interactions to the instability of the high-symmetry configuration appear explicitly in the functional (Amit 1978). Through an exact Gaussian integral identity, we introduce a new field ϕ_i which couples linearly to the order parameter:

$$\begin{aligned} Z \propto & \int \left[\prod_i d\phi_i \right] \left[\prod_i d\xi_i \right] \mathcal{D}\mathbf{e}(\mathbf{r}) \exp \left[-\frac{1}{2} \sum_{i\alpha j\beta} (J^{-1})_{i\alpha j\beta} \phi_{i\alpha} \phi_{j\beta} \right] \\ & \times \exp \left[\sum_i \phi_i \cdot \xi_i + V_{\text{str}}(\xi_i, \mathbf{e}(\mathbf{r})) \right] \exp \left[\sum_i V_{\text{loc}}(\{\xi_i\}) \right], \end{aligned}$$

where for convenience we have written

$$\beta H_{\text{mod}}(\{\xi_i\}, \mathbf{e}(\mathbf{r})) = \sum_i V_{\text{loc}}(\{\xi_i\}) - \frac{1}{2} \sum_{i\alpha j\beta} J_{i\alpha j\beta} \xi_{i\alpha} \xi_{j\beta} + V_{\text{str}}(\xi_i, \mathbf{e}(\mathbf{r})).$$

The integral over the $\{\xi_i\}$ now factors into single-site traces. Expanding the

$\exp[\sum_i \phi_i \cdot \xi_i + V_{\text{str}}(\xi_i, \mathbf{e}(\mathbf{r}))]$, numerically evaluating the integrals

$$\langle p(\xi) \rangle = \frac{\int d^3\xi \exp(-\beta[A|\xi|^2 + u_0|\xi|^4 + v_0 \sum_\alpha \xi_\alpha^4 + D|\xi|^6 + E|\xi|^8]) p(\xi)}{\int d^3\xi \exp(-\beta[A|\xi|^2 + u_0|\xi|^4 + v_0 \sum_\alpha \xi_\alpha^4 + D|\xi|^6 + E|\xi|^8])}$$

and re-exponentiating gives a functional of the same form as the original Hamiltonian:

$$\begin{aligned} \beta H_{\text{HS}} = & \int d^3r \left\{ (r_0(T - T_0)|\phi(\mathbf{r})|^2 + |\nabla \phi(\mathbf{r})|^2)/2 \right. \\ & + \frac{1}{2} \left(\sum_\alpha f(\partial_\alpha \phi_\alpha)^2 - \sum_{\alpha \neq \beta} h(\partial_\beta \phi_\alpha)(\partial_\alpha \phi_\beta) \right) \\ & + \bar{u}|\phi(\mathbf{r})|^4 + \bar{v} \sum_\alpha \phi_\alpha(\mathbf{r})^4 + O(\phi^6) \\ & + (6\pi^2)^{-1} \left[\bar{Z}_3 \sum_\alpha e_{\alpha\alpha}(\mathbf{r})/3 + \bar{C}_{11} \sum_\alpha e_{\alpha\alpha}(\mathbf{r})^2/2 + \bar{C}_{12} \sum_{\alpha \neq \beta} e_{\alpha\alpha}(\mathbf{r}) e_{\beta\beta}(\mathbf{r})/2 \right. \\ & + \bar{C}_{44} \sum_{\alpha \neq \beta} e_{\alpha\beta}(\mathbf{r})^2 \\ & - \bar{g}_0 \sum_\alpha e_{\alpha\alpha}(\mathbf{r}) |\phi(\mathbf{r})|^2/3 - \bar{g}_1 \sum_{\alpha < \beta} e_{\alpha\beta}(\mathbf{r}) \phi_\alpha(\mathbf{r}) \phi_\beta(\mathbf{r}) \\ & \left. \left. - \bar{g}_2 \sum_\alpha e_{\alpha\alpha}(\mathbf{r}) (\phi_\alpha(\mathbf{r})^2 - |\phi(\mathbf{r})|^2/3) \right] \right\}. \end{aligned}$$

In anticipation of the RG analysis to follow, we have taken the continuum limit, defined the length scale so that the Brillouin zone is approximated by a sphere of radius 1 and normalized the $\phi(\mathbf{r})$ so that the $|\phi(\mathbf{r})|^2$ term has coefficient $\frac{1}{2}$. This expression is precisely of the standard Landau–Ginzburg–Wilson form for a three-component model on a three-dimensional compressible lattice with cubic symmetry, which has been studied previously (Natterman 1977, Murata 1977, Bender 1976). However, rather than being regarded as free parameters, in the present case the coefficients have values which are completely specified as functions of the microscopic Hamiltonian parameters calculated for GeTe in section 5.4.

5.5.2. Analysis and results

With the partition function in this functional-integral form, the finite-temperature behavior of the system can be investigated using standard methods. The simplest of these is the stationary-phase approximation, which after minimizing with respect to the strain, leads to an expression for the free energy

$$F(\phi) = \frac{1}{2} r_0(T - T_{c,\text{mf}}) |\phi|^2 + u_{\text{eff}} |\phi|^4 + v_{\text{eff}} \sum_\alpha \phi_\alpha^4,$$

where

$$\begin{aligned} u_{\text{eff}} &= \bar{u} - (6\pi^2)^{-1} \left\{ \bar{g}_0^2 / (6(\bar{C}_{11} + 2\bar{C}_{12})) + \bar{g}_0\bar{g}_2 / (9(\bar{C}_{11} + 2\bar{C}_{12})) \right. \\ &\quad \left. + \bar{g}_2^2 \bar{C}_{11} \bar{C}_{12}^2 / (9(\bar{C}_{11} + 2\bar{C}_{12})^2 (\bar{C}_{11} - \bar{C}_{12})^2) + \bar{g}_1^2 / (16\bar{C}_{44}) \right\} \\ v_{\text{eff}} &= v - (6\pi^2)^{-1} \left\{ \bar{g}_0\bar{g}_2 / (3(\bar{C}_{11} + 2\bar{C}_{12})) + \bar{g}_2^2 \bar{C}_{11} \bar{C}_{12}^2 / (3(\bar{C}_{11} + 2\bar{C}_{12})^2) \right. \\ &\quad \left. \times (\bar{C}_{11} - \bar{C}_{12})^2 + \bar{g}_1^2 / (16\bar{C}_{44}) \right\}, \end{aligned}$$

and the mean-field theory transition temperature $T_{c,\text{mf}} = T_0 - 2\bar{g}_0\bar{Z}_3 / (18\pi^2 r_0(\bar{C}_{11} + 2\bar{C}_{12}))$. For GeTe, we find $T_0 = 669$ K while the contribution from strain coupling contributes +4 K, giving $T_{c,\text{mf}} = 673$ K. The order of the transition within this treatment is determined by the sign of the quartic coefficient $u_{\text{eff}} + \frac{1}{3}v_{\text{eff}}$, with the phase diagram on the u - v plane shown in fig. 14. The u_{eff} and v_{eff} obtained by setting $\bar{g}_i = 0$ place the system well within the second-order region, while the inclusion of strain-coupling changes the character of the quartic anisotropy considerably, as shown in fig. 15a, b. The system is shifted well toward the phase boundary, although a second-order character is still predicted.

The effect of fluctuations on the transition temperature and on the order of the transition can be understood through the use of the momentum-space renormalization group approach in the ε -expansion (Wilson and Kogut 1974). Briefly, this involves identifying the Hamiltonian with a point in a multidimensional parameter space and describing the integration over progressively longer wavelength fluctuations through changes in the effective Hamiltonian parameters, which are expressed in the form of recursion relations. To obtain explicit forms for the recursion relations and confine them to a finite-dimensional parameter space, the integrals are expanded, regarding the Hamiltonian parameters and the parameter $\varepsilon = 4 - d$ (d is the spatial dimensionality) as small. The flow diagrams generated by the recursion relations and, in particular, the fixed points can be analyzed to obtain the critical behavior.

In performing this analysis for the present case, the following simplifications are made. First, since the critical temperature dependence is contained in the vanishing of $T - T_{c,\text{mf}}$, all other coefficients in βH_{HS} are evaluated at $T_{c,\text{mf}}$ and

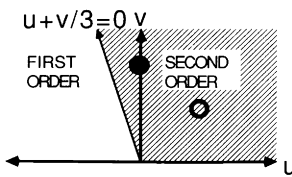


Fig. 14. Phase diagram in u - v plane ($v > 0$) within mean-field theory. The open circle shows the position of the system with strain coupling neglected; the filled circle gives the values for (u, v) which incorporate the effects of strain coupling within mean-field theory.

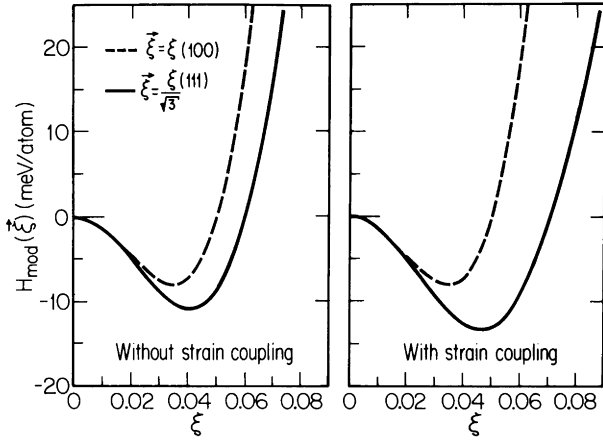


Fig. 15. The effect of strain coupling on the quartic anisotropy is demonstrated. On the left is shown $H_{\text{mod}}(\{\xi_i = \xi\}, \mathbf{e} = 0)$ for ξ along (100) and (111) (dashed and solid lines, respectively). $H_{\text{mod}}(\{\xi_i = \xi\}, \mathbf{e}_0)$, where \mathbf{e}_0 is the strain which minimizes H_{mod} at fixed ξ , is shown on the right. While for ξ along (100) the curves are indistinguishable, for ξ along (111) there is a large coupling to the strain and thus the quartic anisotropy is considerably increased.

their temperature dependence is neglected, resulting in the values of the coefficients given in table 3. Next, we perform the Gaussian integrals over the strain degrees of freedom, retaining only the infinite-range intersite quartic couplings generated by the homogeneous strain terms. This leads to:

$$\begin{aligned} \beta H_{\text{LGW}} = & \int d^3r \left\{ (r_0(T - T_{c,\text{mf}}) |\phi(r)|^2 + |\nabla \phi(r)|^2)/2 + u |\phi(r)|^4 \right. \\ & + v \sum_{\alpha} \phi_{\alpha}(r)^4 + O(\phi^6) \\ & \left. + \frac{1}{2} \left(f \sum_{\alpha} (\partial_{\alpha} \phi_{\alpha})^2 - h \sum_{\alpha \neq \beta} (\partial_{\alpha} \phi_{\alpha})(\partial_{\beta} \phi_{\beta}) \right) \right\} \\ & + \int d^3r \int d^3r' \left\{ w_0 \sum_{\alpha} \phi_{\alpha}(r)^2 \phi_{\alpha}(r') + w_1 \sum_{\alpha < \beta} \phi_{\alpha}(r)^2 \phi_{\beta}(r')^2 \right. \\ & \left. + w_2 \sum_{\alpha < \beta} \phi_{\alpha}(r) \phi_{\beta}(r) \phi_{\alpha}(r') \phi_{\beta}(r') \right\}. \end{aligned}$$

Lastly, in analyzing this model, we neglect the higher-order anharmonicities and the anisotropic components of the gradient terms since these are marginal or irrelevant fields, which do not affect the fixed-point structure and which will modify the flows significantly only in extreme cases. Thus, we consider the differential recursion relations to first order in $\varepsilon = 4 - d = 1$ in the six-dimen-

Table 3
Coefficients in the functional $\beta H_{\text{HS}}(\{\xi_i\}, \{\mathbf{e}(\mathbf{r})\})$

On-site	Intersite		Elastic		Coupling	
r_0	3.68 (eV) ⁻¹	f	0.00	\bar{C}_{11}	1.03×10^3	\bar{g}_0
$k_B T_0$	669 K	h	0.10	\bar{C}_{12}	3.72	\bar{g}_1
\bar{u}	0.0175			\bar{C}_{44}	194	\bar{g}_2
\bar{v}	0.0133			Z_3	-5.75	

sional parameter space $r = r_0(T - T_{c,\text{mf}})$, u , v , w_0 , w_1 and w_2 :

$$\begin{aligned} dr/dl &= 2r + (8\pi^2)^{-1}(20u + 12v + 4w_0 + 4w_1)/(1+r), \\ du/dl &= u - (8\pi^2)^{-1}u(44u + 24v)/(1+r)^2, \\ dv/dl &= v - (8\pi^2)^{-1}v(36u + 48v)/(1+r)^2, \\ dw_0/dl &= w_0 - (8\pi^2)^{-1}(24w_0u + 8w_1u + 24w_0v + 4w_0^2)/(1+r)^2, \\ dw_1/dl &= w_1 - (8\pi^2)^{-1}(32w_1u + 8w_0u + 24w_1v + 2w_1^2 + 4w_0w_1)/(1+r)^2, \\ dw_2/dl &= w_2 - (8\pi^2)^{-1}(8w_2u + 2w_2^2)/(1+r)^2. \end{aligned}$$

To illustrate the issues which arise in the analysis of these flows, we first discuss the simpler cases of the isotropic model, parametrized by r and u , and the cubic anisotropy model, parametrized by r , u and v (Aharony 1973, 1976). The computation of the transition temperature for the isotropic model is shown in fig. 16. As the physical temperature, and thus r , is varied, the system moves along the line of constant u . The critical surface, containing the nontrivial fixed point, separates the r -regime which flows to the low-temperature fixed point from that which flows to high temperature, yielding the critical value of r and thus the transition temperature.

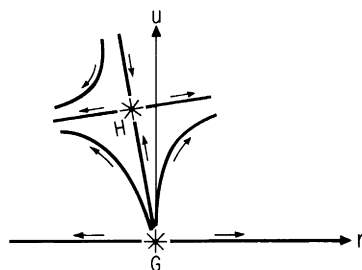


Fig. 16. Flow diagram for the isotropic vector model. G is the unstable Gaussian fixed point; H is the Heisenberg fixed point, which governs the critical behavior.

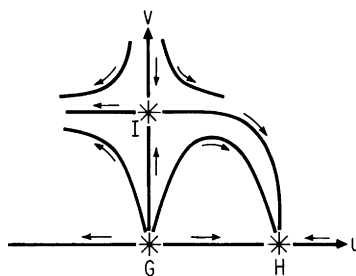


Fig. 17. Flows on the critical surface of the cubic anisotropy model, projected on the u - v plane. G is the unstable Gaussian fixed point; H is the Heisenberg fixed point, which governs the critical behavior for $u > 0$; I is the Ising fixed point, which is unstable with respect to u . For $u < 0$, none of the fixed points is accessible and the transition is first-order.

The projection of the critical flows on the u - v plane is shown in fig. 17 to illustrate the analysis of the RG phase diagram. For $u > 0$, the critical flows terminate on the Heisenberg fixed point at $u \neq 0, v = 0$, yielding second-order behavior. However, for $u < 0$, the critical flows lead away from all known fixed points. This type of runaway has been shown to be associated with the occurrence of a first-order transition (Rudnick and Nelson 1976). Thus the phase boundary within RG lies at $u = 0$, in contrast to the MFT $u + \frac{1}{3}v = 0$. Systems which lie between these two lines are said to have “fluctuation-driven first-order transitions”, i.e. first-order in RG but second-order in MFT.

To obtain the temperature and order of the transition in GeTe, we apply these principles to the full six-dimensional strain-coupled model. First, by iterating the recursion relations numerically, we examine the changes in the flows as the system moves along the line in parameter space as the physical temperature T changes. In this way, we find that the shift in T_c due to fluctuations is only -16 K , yielding $T_c = 657\text{ K}$. Thus, we see that the transition temperature obtained in MFT is not changed significantly with this more correct treatment.

This RG analysis also yields an understanding of the observed first-order character of the transition. At the fixed points of the pure cubic-anisotropy model ($w_i = 0$), the w_i are relevant (Natterman 1977). There are new fixed points with $w_i^* > 0$, but these are not accessible to flows starting in the $w_i < 0$ region of parameter space, as in the present case where $w_0 = -2.71 \times 10^{-3}$, $w_1 = -3.83 \times 10^{-4}$ and $w_2 = -3.60 \times 10^{-2}$. To see that this runaway behavior of the strain-generated couplings, particularly of w_2 , provides a plausible mechanism for the observed character of the transition, recall that within mean-field theory, the effect of the strain coupling is to shift the effective values of (u, v) towards the mean-field phase boundary $u_{\text{eff}} + \frac{1}{3}v_{\text{eff}} = 0$, from $(0.018, 0.013)$ to $(-6.1 \times 10^{-4}, 0.028)$. This substantial shift suggests that although the transition within mean-field theory is still second-order, the

strain effects could be large enough to produce an observable discontinuity within RG, and thus the transition is fluctuation-driven first-order.

5.6. Discussion

Here we review the calculation to see where important approximations and calculational inaccuracies enter, in the process distinguishing the features which are special to the GeTe transition from aspects applicable to other systems. At the end of this section, we discuss the comparison with experimental observations.

We started by assuming that the transition could be described by a pure lattice Hamiltonian expanded about the prototype structure. Although models have been proposed in which the near-band-gap electronic states are the direct source of the temperature dependence of the structure (Korzhuev et al. 1981, Volkov and Kopaev 1973), it seems unlikely that this effect could be significant compared to the lattice anharmonicity in the case of GeTe, as these states involve only a small part of the Brillouin zone. Defining a local-mode variable, we formally obtained a model Hamiltonian that exactly reproduced the thermal behavior of the original. Then we approximated the model by a truncated expansion – local anharmonicity, no intersite interactions beyond second neighbor, lowest-order local-mode-strain coupling – with no temperature dependence in the coefficients. These truncations, which are crucial in keeping the form of the model Hamiltonian simple, determine the quantitative accuracy of the interpolation between the calculated configuration energies. All of them, most notably the choice of local-mode variable so as to cast the most important anharmonicity into a local form, are motivated by the physical understanding of the GeTe transition. Thus, the details of this part of the procedure would need to be rethought when applied to other systems. In particular, although the local-mode approximation can be used to obtain model Hamiltonians for both displacive and order-disorder structural transitions (Lines and Glass 1977), the large local anharmonicity in the latter case probably implies that nonlocal anharmonic terms must also be included for a good quantitative description. Therefore this approach is generally feasible only for transitions, like those in GeTe, which have displacive character.

In contrast, once we have obtained the numerical form of the model, the statistical mechanical analysis depends mainly on the universality class of the transition. We have examined the effects of dropping terms from H_{LGW} and the use of the ε -expansion for the nearest-neighbor Ising model on an fcc lattice. A treatment completely analogous to that of the GeTe model Hamiltonian gives a shift in T_c of -14% , comparable to that of -18% obtained from numerical studies (Domb and Miedema 1964) for $d = 3$. The smaller shift in the GeTe case results from smaller ratios of the fourth-order couplings to r_0 , as determined by the several independent microscopic coupling constants. Also, many of the

approximations in the statistical mechanical analysis can be systematically improved. For example, the fluctuations could be described using the full Green's function instead of its gradient expansion, the analysis could be carried to higher order in ϵ , and the higher-order anharmonicities, anisotropic fluctuations and the terms generated by the inhomogeneous strains could be included explicitly in the recursion relation analysis. In fact, to first order in ϵ , the sixth-order anharmonicities can be included in the analysis simply by introducing effective values of u and v (Blankschtein and Aharony 1983). For the zero-strain coupling case, we find $(u_{\text{eff}}, v_{\text{eff}})$ shifts only slightly, from $(0.018, 0.013)$ to $(0.013, 0.011)$, so that this correction cannot account for the observed first-order behavior.

The most important calculational errors enter via the total-energy calculations. As discussed in section 4, k -point convergence makes the largest contribution to errors at the level of ionic-configuration energies, resulting in uncertainty in the quadratic coefficients in H_{mod} of about 10%. From the mean-field expression for T_c , to which the fluctuation contribution constitutes only a small correction, it can be shown that the error in T_c is roughly linear in the uncertainty in the quadratic coefficients. Also, some uncertainty is produced by the fact that we did not calculate b_1 and b_2 individually, but only the combination $b_1 + 2b_2$. Since we expect both of these to be positive, we introduce $v \in [0, 1]$ with $b_1 = v(b_1 + 2b_2)$, $b_2 = \frac{1}{2}(1 - v)(b_1 + 2b_2)$. For the RG analysis, we chose $v = 0.37$ which is a reasonable value in view of the lack of strong anisotropy of the first-neighbor interactions and has the additional advantage that $f = 0$. If we had included f explicitly in the RG analysis, it would be possible to obtain quantitative bounds on $T_c(v)$. However, since $T_{c,\text{mf}}$ depends only on $b_1 + 2b_2$ and the fluctuation correction is small, T_c should be fairly insensitive to v . In fact, it can also be shown that including third-neighbor interactions in H_{mod} would not affect $T_{c,\text{mf}}$. Unfortunately, the same argument does not work for fourth neighbors.

With emphasis on the total-energy uncertainties, we make an estimate of the error in T_c to obtain a final answer of 657 ± 100 K. This prediction compares quite favorably with the range of experimental values 625–700 K. In addition, a fluctuation-driven first-order transition is predicted, consistent with experimental indications of a weakly discontinuous transition. Our analysis results in the additional microscopic insight that this character is produced by the presence of the order parameter strain coupling. Although a more refined treatment of the strain degrees of freedom would be required than that given here, experimentally observable quantities such as dT_c/dP , elastic constants and their discontinuity at the transition, and the discontinuity of the thermal-expansion coefficient at the transition could also be calculated using our approach. This provides an encouraging prospect for future applications of the pseudopotential total-energy method to the calculation of finite-temperature properties of solids.

6. Future prospects

Investigating a structural phase transition through an ab initio statistical mechanical approach involves combining results from two independent disciplines of condensed-matter physics. On the one hand, there has been a lot of interest in understanding the energetics of materials which undergo structural phase transitions. These studies focus on the microscopic origin of the character of the bonding that results in different structures being close in energy and also on the development of models that describe the energies of low-lying configurations in a unified way. On the other hand, in a purely statistical mechanical context an ever-increasing number of systems with different types of order parameters and a large variety of interactions are being classified and studied. Multidimensional phase diagrams can be generated within mean-field theory as well as with renormalization group approaches. The latter have also been used to study properties of fixed points and reveal the nature of the various phase boundaries. Thus, it is clear that a great deal of the groundwork for ab initio statistical-mechanics studies already exists, and the establishment of the final links through ab initio total-energy calculations should potentially yield useful insights into structural phase transitions in a number of systems.

In three-dimensional systems, the emphasis will be on understanding the microscopic physics of the transition, and predicting the sequence of phases and transition temperatures. Natural candidates for further studies are transitions in perovskite compounds, such as SrTiO_3 , or, because of the complications involved in working with O potentials, fluorine-based perovskites such as RbCaF_3 (Boyer and Hardy 1981). With applied stress, the critical behavior becomes more interesting, e.g. various multicritical points and three-state Potts model behavior in SrTiO_3 (Fontanari and Theumann 1986).

The primary difficulty in the calculations for the perovskites is the accuracy of the ab initio method. This would be much less of a problem in studying ordering in semiconductor alloys, since there the pseudopotentials are so well behaved that accurate calculations can be performed for complex unit cells containing of the order of 100 atoms (Kaxiras et al. 1986). For this system, the main effort would be in the development of an appropriate microscopic Hamiltonian, and in the selection of an interesting transition to study.

In general, systems in two dimensions exhibit a much richer variety of critical behavior. The (100) surfaces of Si and Ge apparently have a very stable dimerization reconstruction. As a function of temperature, the dimers can then tilt and order in a variety of ways providing a natural mapping onto a two-dimensional Ising Hamiltonian (Ihm et al. 1983). The energy resolution needed for the differentiation of the various ordered structures is beyond that of the semi-empirical tight-binding method, and so ab initio calculations are required for further progress (Needels et al. 1987).

W(001) and Mo(001) are observed to have transitions from (1×1) to $c(2 \times 2)$ and an incommensurate structure, respectively, in what appears to be a charge density wave transition with short coherence length. The adsorption of H can modify the transitions considerably. For these transitions, the development of model Hamiltonians from microscopic Hamiltonians has been discussed in detail, but their quantitative derivation has not been carried out (Ying 1985). It has been suggested that this should be done with the construction of a force-constant model as an intermediate step, but based on the experience with GeTe, it seems likely that a direct fit of the model to configurational energies would give more accurate results.

The microscopic interactions in chemisorbed surface layers cannot be easily extracted from phenomenology as in the case of physisorbed layers of rare gas atoms. It has been suggested that the phase diagram of Se on Ni (100) contains a phase boundary with Ashkin-Teller character, which has nonuniversal continuously varying critical exponents (Bak et al. 1985). An analysis of the structure of the underlying microscopic Hamiltonian shows the presence of terms which could destroy this behavior (Berker et al. 1987). Through the combination of an ab initio determination of the microscopic interactions with the real-space renormalization group phase diagrams (Berker and Caflisch 1984), the controversial aspects of the complex phase diagram of this system could be clarified considerably.

Progress in the application of statistical-mechanics methods to real systems should also stimulate interest in the generation of accurate phase diagrams for specific models using numerical methods such as Monte Carlo. Also, development of ab initio total-energy methods will presumably be accelerated with respect to solving the problems in materials of interest, both in improving numerical algorithms and in increasing the accuracy of the physical approximations.

As discussed in section 2, some progress has been made in developing methods which could permit studies of phase transitions in real materials other than the lattice-driven ones considered here. The capability of calculating electronic entropy contributions to the free energy could make possible the study of transitions where this is an important factor. In addition, there are a number of systems where there is an interesting interplay between structural and electronic phase transitions. For example, KMnF_3 undergoes a series of magnetic and structural phase transitions as a function of temperature (Hidaka 1975, Hidaka et al. 1975). In the perovskite-related compounds $\text{La}_{2-x}\text{Sr}_x\text{CuO}_{4-\delta}$ and $\text{YBa}_2\text{Cu}_3\text{O}_{7-\delta}$ there appears to be a significant relationship between the superconducting and structural phase transitions that may provide some insight into the mechanism for the high- T_c superconductivity (Paul et al. 1987, Horn et al. 1987, Millis and Rabe 1988).

Unfortunately, even if the theoretical problems were solved, the last-mentioned investigations would involve such demanding computations as to be

impossible in a practical sense at this point. However, as discussed above, there are many examples of systems where the necessary calculations do fall within the range of feasibility, and it seems likely that the ab initio approach to statistical mechanics will evolve and yield many interesting results.

Acknowledgement

This work was supported in part by the Office of Naval Research contract No. N00014-86-K-0158.

References

- Abrikosov, N.Kh., O.G. Karpinskii, L.E. Shelimova and M.A. Korzhuev, 1977a, Neorg. Mater. **13**, 2160 [Inorg. Mater. **13**, 1723].
- Abrikosov, N.Kh., M.A. Korzhuev and L.E. Shelimova, 1977b, Neorg. Mater. **13**, 1757 [Inorg. Mater. **13**, 1418].
- Abrikosov, N.Kh., M.A. Korzhuev, L.A. Petrov, O.A. Teplov and G.K. Demenskii, 1983, Neorg. Mater. **19**, 370 [Inorg. Mater. **19**, 334].
- Aharony, A., 1973, Phys. Rev. B **8**, 4270.
- Aharony, A., 1976, in: Phase Transitions and Critical Phenomena, Vol. 6, eds C. Domb and M.S. Green (Academic Press, New York) p. 357.
- Amit, D.J., 1978, Field Theory, the Renormalization Group and Critical Phenomena (McGraw-Hill, New York).
- Anderson, P.W., 1960, in: Fizika Dielektrikov, ed. G. Skanavi (Akad. Nauk, Moscow).
- Bachelet, G.B., D.R. Hamann and M. Schluter, 1982, Phys. Rev. B **26**, 4199.
- Bak, P., P. Kleban, W.N. Unertl, J. Ochab, G. Akinci, N.C. Bartelt and T.L. Einstein, 1985, Phys. Rev. Lett. **54**, 1539.
- Beattie, A.G., 1969, J. Appl. Phys. **40**, 4818.
- Behnke, G., H. Bilz and H. Buttner, 1986, Phys. Rev. Lett. **56**, 1276.
- Bender, G., 1976, Z. Phys. B **23**, 285.
- Berker, A.N., and R.G. Cafisch, 1984, Phys. Rev. B **29**, 1279.
- Berker, A.N., R.G. Cafisch and A. Aharony, 1987, unpublished.
- Bhatt, R.N., and W.L. McMillan, 1976, Phys. Rev. B **14**, 1007.
- Bierly, J.N., L. Muldawer and O. Beckman, 1963, Acta Metall. **11**, 447.
- Bigava, A.D., A.A. Gabedava, E.D. Kunchuliya, S.S. Moiseenko and R.R. Shvngiradze, 1976, Neorg. Mater. **12**, 835 [Inorg. Mater. **12**, 708].
- Blankschtein, D., and A. Aharony, 1983, Phys. Rev. B **28**, 386.
- Boyer, L.L., and J.R. Hardy, 1981, Phys. Rev. B **24**, 2577.
- Bussmann-Holder, A., H. Bilz and P. Vogl, 1983, in: Dynamical Properties of IV-VI Compounds, Springer Tracts in Modern Physics, Vol. 99 (Springer, Berlin).
- Ceperley, D.M., 1978, Phys. Rev. B **18**, 3126.
- Ceperley, D.M., and B.J. Alder, 1980, Phys. Rev. Lett. **45**, 566.
- Choudhury, N., S.L. Chaplot and K.R. Rao, 1986, Phys. Rev. B **33**, 8607.
- Cochran, W., 1960, Adv. Phys. **9**, 387.
- Cochran, W., 1971, in: Structural Phase Transitions and Soft Modes, eds E.J. Samuelsen, E. Andersen and J. Feder (Universitetsforlaget, Oslo) p. 1.

- Cohen, M.L., 1982, Phys. Scr. **T1**, 5.
- Domb, C., and A.R. Miedema, 1964, in: Progress in Low Temperature Physics, Vol. IV, ed. C.J. Gorter (North-Holland, Amsterdam).
- Fontanari, J.F., and W.K. Theumann, 1986, Phys. Rev. B **33**, 3530.
- Frazer, B.C., 1971, in: Structural Phase Transitions and Soft Modes, eds E.J. Samuels, E. Andersen and J. Feder (Universitetsforlaget, Oslo) p. 43.
- Geldart, D.J.W., M. Rasolt and R. Taylor, 1972, Solid State Commun. **10**, 279.
- Ghazali, A., and P. Leroux Hugon, 1978, Phys. Rev. Lett. **41**, 1569.
- Godby, R.W., M. Schluter and L.J. Sham, 1986, Phys. Rev. Lett. **56**, 2415.
- Godby, R.W., M. Schluter and L.J. Sham, 1987, Phys. Rev. B **35**, 4170.
- Goldak, J., C.S. Barrett, D. Innes and W. Youdelis, 1966, J. Chem. Phys. **44**, 3323.
- Gunnarsson, O., and B.I. Lundqvist, 1976, Phys. Rev. B **13**, 4274.
- Hamann, D.R., M. Schluter and C. Chiang, 1979, Phys. Rev. Lett. **43**, 1494.
- Hidaka, M., 1975, J. Phys. Soc. Jpn. **39**, 180.
- Hidaka, M., N. Ohama, A. Okazaki, H. Sakashita and S. Yamakawa, 1975, Solid State Commun. **16**, 1121.
- Hohenberg, P., and W. Kohn, 1964, Phys. Rev. B **136**, 864.
- Horn, P.M., D.T. Keane, G.A. Held, J.L. Jordan-Sweet, D.L. Kaiser, F. Holtzberg and T.M. Rice, 1987, Phys. Rev. Lett. **59**, 2772.
- Houston, B., R.E. Strakna and H.S. Belson, 1968, J. Appl. Phys. **39**, 3913.
- Ihm, J., and M.L. Cohen, 1981, Phys. Rev. B **23**, 1576.
- Ihm, J., D.H. Lee, J.D. Joannopoulos and J.J. Xiong, 1983, Phys. Rev. Lett. **51**, 1872.
- Iizumi, M., Y. Hamaguchi, K.F. Komatsubara and Y. Kato, 1975, J. Phys. Soc. Jpn. **38**, 443.
- Islam, Q.T., and B.A. Bunker, 1987, Phys. Rev. Lett. **59**, 2701.
- Joannopoulos, J.D., 1985, in: Physics of Disordered Materials, eds D. Adler, H. Fritzsche and S.R. Ovshinsky (Plenum Press, New York) p. 19, and references therein.
- Katkanant, V., P.J. Edwardson, J.R. Hardy and L.L. Boyer, 1986, Phys. Rev. Lett. **57**, 2033.
- Kaxiras, E., Y. Bar-Yam, J.D. Joannopoulos and K.C. Pandey, 1986, Phys. Rev. B **33**, 4406.
- Kohn, W., and L.J. Sham, 1965, Phys. Rev. A **140**, 1133.
- Kohn, W., and P. Vashishta, 1980, in: Theory of the Inhomogeneous Electron Gas, eds S. Lundqvist and N.H. March (Plenum Press, New York) p. 79.
- Korzhuev, M.A., L.I. Petrova, G.K. Demenskii and O.A. Teplov, 1981, Fiz. Tverd. Tela **23**, 3387 [Sov. Phys.-Solid State **23**, 1966] and references therein.
- Kurzynski, M., and M. Halawa, 1986, Phys. Rev. B **34**, 4846.
- Landau, L.D., and E.M. Lifshitz, 1980, Statistical Physics, part 1, 3rd Ed., revised and enlarged by E.M. Lifshitz and L.P. Pitaevskii (Pergamon Press, Oxford).
- Langreth, D.C., and J.P. Perdew, 1979, Solid State Commun. **31**, 567.
- Lines, M.E., 1969, Phys. Rev. **177**, 797.
- Lines, M.E., and A.M. Glass, 1977, Principles and Applications of Ferroelectrics and Related Materials (Clarendon Press, Oxford).
- Littlewood, P.B., 1980a, J. Phys. C **13**, 4855.
- Littlewood, P.B., 1980b, J. Phys. C **13**, 4875.
- Littlewood, P.B., 1986, Phys. Rev. B **34**, 1363.
- Louie, S.G., S. Froyen and M.L. Cohen, 1982, Phys. Rev. B **26**, 1738.
- Löwdin, P.O., 1951, J. Chem. Phys. **19**, 1396.
- Ma, S.-K., 1976, Modern Theory of Critical Phenomena (Benjamin/Cummings, Reading, MA).
- Mardix, S., 1986, Phys. Rev. B **33**, 8677.
- Martins, J.L., and A. Zunger, 1986, Phys. Rev. Lett. **56**, 1400.
- McMillan, W.L., 1977, Phys. Rev. B **16**, 643.
- Mermin, N.D., 1965, Phys. Rev. A **137**, 1441.
- Millis, A.J., and K.M. Rabe, 1988, Phys. Rev. B **38**, 8908.
- Monkhorst, H.J., and J.D. Pack, 1976, Phys. Rev. B **13**, 5188.

- Murata, K.K., 1977, Phys. Rev. B **15**, 4328.
- Natterman, T., 1976, J. Phys. C **9**, 3337.
- Natterman, T., 1977, J. Phys. A **10**, 1757.
- Needels, M., M.C. Payne and J.D. Joannopoulos, 1987, Phys. Rev. Lett. **58**, 1765.
- Novikova, S.I., L.E. Shelimova, N.Kh. Abrikosov, V.I. Galyutin and B.A. Evseev, 1970, Fiz. Tverd. Tela **12**, 3623 [Sov. Phys.-Solid State **12**, 2945 (1971)].
- Novikova, S.I., L.E. Shelimova, N.Kh. Abrikosov, V.I. Galyutin and B.A. Evseev, 1971, Fiz. Tverd. Tela **12**, 3623 [Sov. Phys.-Solid State **12**, 2945].
- Novikova, S.I., L.E. Shelimova, N.Kh. Abrikosov and B.A. Evseev, 1972, Fiz. Tverd. Tela **13**, 2764 [Sov. Phys.-Solid State **13**, 2310].
- Novikova, S.I., L.E. Shelimova, E.S. Avilov and M.A. Korzhuev, 1975, Fiz. Tverd. Tela **17**, 2379 [Sov. Phys.-Solid State **17**, 1570].
- Novikova, S.I., L.E. Shelimova, N.Kh. Abrikosov and O.G. Karpinskii, 1977, Fiz. Tverd. Tela **19**, 1171 [Sov. Phys.-Solid State **19**, 683].
- Paul, D.McK., G. Balakrishnan, N.R. Bernhoeft, W.I.F. David and W.T.A. Harrison, 1987, Phys. Rev. Lett. **58**, 1976.
- Perdew, J.P., and A. Zunger, 1981, Phys. Rev. B **23**, 5048.
- Pfeuty, P., and G. Toulouse, 1977, Introduction to the Renormalization Group and to Critical Phenomena (Wiley, Chichester).
- Rabe, K.M., and J.D. Joannopoulos, 1985, Phys. Rev. B **32**, 2302.
- Rabe, K.M., and J.D. Joannopoulos, 1987a, Phys. Rev. Lett. **59**, 570.
- Rabe, K.M., and J.D. Joannopoulos, 1987b, Phys. Rev. B **36**, 6631.
- Rabe, K.M., and J.D. Joannopoulos, 1987c, Phys. Rev. B **36**, 3319.
- Rudnick, J., and D.R. Nelson, 1976, Phys. Rev. B **13**, 2208.
- Sahu, D., 1986, Phys. Rev. B **34**, 4735.
- Schubert, K., and H. Fricke, 1951a, Z. Naturforsch. A **6**, 781.
- Schubert, K., and H. Fricke, 1951b, Struct. Rep. **15**, 72.
- Schubert, K., and H. Fricke, 1953a, Z. Metallkd. **44**, 457.
- Schubert, K., and H. Fricke, 1953b, Struct. Rep. **17**, 44.
- Seddon, T., S.C. Gupta and G.A. Saunders, 1976, Solid State Commun. **20**, 69.
- Shaw, R.W., and W.A. Harrison, 1967, Phys. Rev. **163**, 604.
- Shelimova, L.E., N.Kh. Abrikosov and V.V. Zhdanova, 1965, Russ. J. Inorg. Chem. **10**, 650.
- Sinha, S.K., ed., 1980, Ordering in Two Dimensions (North-Holland, Amsterdam).
- Starkloff, T., and J.D. Joannopoulos, 1977, Phys. Rev. B **16**, 5212.
- Topp, W.C., and J.J. Hopfield, 1974, Phys. Rev. B **7**, 1295.
- Tosatti, E., 1980, in: Modern Trends in the Theory of Condensed Matter, eds A. Pekalski and J. Przystawa (Springer, Berlin) p. 501.
- Van Hove, M.A., and S.Y. Tong, 1979, Surface Crystallography by LEED (Springer, Berlin).
- Volkov, B.A., and Yu.V. Kopaev, 1973, Zh. Eksp. & Teor. Fiz. **64**, 2184 [Sov. Phys.-JETP **37**, 1103].
- von Barth, U., and C.D. Gelatt, 1980, Phys. Rev. B **21**, 2222.
- Williams, A.R., and U. von Barth, 1980, in: Theory of the Inhomogeneous Electron Gas, eds S. Lundqvist and N.H. March (Plenum Press, New York) p. 189.
- Wilson, K.G., and J. Kogut, 1974, Phys. Rep. **12**, 75.
- Ye, Y.-Y., Y. Chen, K.M. Ho, B.N. Harmon and P.A. Lindgard, 1987, Phys. Rev. Lett. **58**, 1769.
- Ying, S.C., 1985, in: Dynamical Phenomena at Surfaces, Interfaces and Superlattices, eds F. Nizzoli, K.H. Rieder and R.F. Willis (Springer, Berlin).
- Zhukova, T.B., and A.I. Zaslavskii, 1967, Kristallografiya **12**, 37 [Sov. Phys.-Crystallogr. **12**, 28].
- Zhukova, T.B., and A.I. Zaslavskii, 1967, Kristallografiya **12**, 37 [Sov. Phys.-Crystallogr. **12**, 28].

This page intentionally left blank

CHAPTER 4

Stable Numerical Simulations of Models of Interacting Electrons in Condensed-Matter Physics

E.Y. LOH Jr and J.E. GUBERNATIS

*Theoretical Division and Center for Nonlinear Studies
Los Alamos National Laboratory
Los Alamos, NM 87545, USA*

© Elsevier Science Publishers B.V., 1992

*Electronic Phase Transitions
Edited by
W. Hanke and Yu.V. Kopaev*

Contents

1. Introduction	180
2. Theoretical framework	182
2.1. Path integrals in imaginary time	182
2.2. The Trotter approximation	183
2.3. The Hubbard–Stratonovich transformation	183
2.4. Boson world lines	185
2.5. The single-electron propagator	189
2.6. The many-electron propagator	189
2.7. The sign problem	190
2.8. “Nodal” surfaces	192
2.9. Importance sampling: single classical particle	192
2.10. The Green’s function	194
3. Mathematical formulation	195
3.1. Matrix representation of single-particle propagators	195
3.2. Checkerboard breakup	197
3.3. Bosonic-configuration weights	198
3.4. Matrix representation of the Green’s function	199
3.5. Metropolis algorithm	200
3.6. Green’s function updating	202
3.7. “Wrapping” Green’s functions	204
3.8. Measurement estimators	205
3.9. Minus signs	209
4. Stabilization	209
4.1. Stable matrix multiplication	211
4.2. Zero-temperature studies	213
4.3. Finite-temperature $\mathbf{G}(\tau, \tau)$: I	214
4.4. Finite-temperature $\mathbf{G}(\tau, \tau)$: II	215
4.5. Unequal-time Green’s function	216
5. Results for Hubbard models	218
5.1. Repulsive Hubbard model	219
5.2. Attractive Hubbard model	220
5.3. Copper-oxide clusters	223
6. Conclusion	224

Appendix I. Extended electronic interactions	226
Appendix II. Bosonic world lines	227
Appendix III. Many-electron propagator	229
Appendix IV. Finite-temperature field weights	231
Appendix V. Determinants of different-size matrices	233
References	233

1. Introduction

With the explosive development of large-scale computers over the past decade, there has been a parallel increase of interest in simulating models of interacting electrons. The desire is not only to “benchmark” analytic approaches to problems – which, except for a few special cases, are perturbation methods based on extreme parameter values and whose accuracy and radii of convergence are unknown – but also to develop a new predictive approach, valid on its own, that is capable of treating intermediate regions of parameter space where existing analytic approaches fail. Indeed, many interesting and novel materials, such as the heavy-fermion and high-temperature superconducting materials, seem to fall in these regimes.

Simulation techniques are still being developed. In many cases, where results are reported, they are as much a demonstration of an algorithm as they are an exploration of new physics. Difficulties in performing the simulations include excessive computation time, probabilities that become negative, fermion wavefunctions that turn bosonic, and numerical instabilities at low temperatures. Progress, however, is being made, and part of our objective is to describe some recent progress in stabilizing simulations at low and zero temperatures (Loh Jr et al. 1989).

In order to eliminate all but the essential electronic degrees of freedom, we work in a limited basis of single-electron orbitals, giving the Hamiltonian

$$H = - \sum_{ij} \sum_{\sigma} T_{ij} (c_{i\sigma}^{\dagger} c_{j\sigma} + c_{j\sigma}^{\dagger} c_{i\sigma}) + \sum_{ij} V_{ij} n_i n_j, \quad (1.1)$$

where the T_{ij} are the hopping integrals and $c_{i\sigma}$ is the annihilation operator for an electron of spin $\sigma = \uparrow$ or \downarrow in orbital i . This Hamiltonian models the kinetic energy of the particles through the inter-orbital hoppings as $-T_{ij} c_{i\sigma}^{\dagger} c_{j\sigma}$. The Coulomb interaction is modelled as a functional $\sum_{ij} V_{ij} n_i n_j$ of the charge density $n_i = c_{i\uparrow}^{\dagger} c_{i\uparrow} + c_{i\downarrow}^{\dagger} c_{i\downarrow}$, where the V_{ij} include the effects of screening. This Hamiltonian is a generic form that includes such condensed-matter physics standards as the Hubbard and extended-Hubbard Hamiltonians and the Anderson Hamiltonian. There is great interest in studying approximate models at zero and finite temperatures to see if they contain features that

explain antiferromagnetism, superconductivity, or other low-temperature phase transitions observed in nature.

In a path-integral representation of the problem, we review how one introduces auxiliary, Hubbard–Stratonovich fields (Hubbard 1959) to eliminate the self-interactions of the electrons. These auxiliary fields mediate the screened interaction V_{ij} , somewhat like photons mediating the standard electromagnetic interaction. Once the direct interactions among the electrons have been eliminated, the resulting “free-fermion” problem is readily solved, albeit only formally, in terms of determinants of single-electron wavefunctions. Finally, we perform “importance sampling” – with Monte Carlo, Langevin, or molecular-dynamics techniques – over the auxiliary bosonic fields.

One difficulty in thermodynamic studies of many-electron systems is that the lowest-energy states are assigned exponentially large weights in the low-temperature limit. Due to the Pauli exclusion of electrons, however, these states are not macroscopically occupied. Instead, low-energy states are filled up to some “Fermi energy”, which controls the physics of the system. Numerically, information about states around this “Fermi energy”, which is exponentially suppressed relative to the bottom of the “band”, must be extracted as small differences of large numbers – a hopelessly noisy procedure for finite-precision computers. Fortunately, recent algorithmic developments allow the explicit separation of exponentially divergent numerical scales associated with different energies, stabilizing numerical simulation at a small computational cost (Loh Jr et al. 1989).

In this chapter, we will discuss finite-temperature and zero-temperature formalisms for simulating systems of fermions that are coupled only with bosonic degrees of freedom – either physical electron–phonon interactions or couplings to a fictitious field that eliminates direct electronic correlations. In section 2, we establish the theoretical framework for performing fermionic simulations by presenting the transformations which replace electronic correlations with intermediate bosonic fields, by characterizing path integrals of coupled electron–boson wavefunctions, and by discussing the importance sampling of bosonic fields. In this section, we also depart from common practice in that we devote considerable attention to developing a specific insight into what goes on in these simulations, where intuition is often a poor guide. This discussion is presented to motivate the generally tedious mathematics that underlies the algorithms and to help the reader in further algorithmic development. In section 3, we formulate algorithms in mathematical terms, giving the details necessary to carry out a calculation.

Unfortunately, the diverse numerical scales present in the simulations make calculations unstable at low temperatures on any computer of finite precision. In section 4, we discuss techniques for decoupling these scales and stabilizing simulations. In section 5, we present results for sampling models with strong

electronic correlations. Finally, in section 6, we discuss and give suggestions for future areas of development.

2. Theoretical framework

In this section, we present the theoretical framework for simulating systems of coupled electrons and bosons. The Trotter approximation (Trotter 1959, Suzuki 1976) is used to discretize quantum path integrals. Intermediate bosonic fields replace direct electronic interactions according to the Hubbard–Stratonovich transformation (Hubbard 1959). We try to give the reader a feeling for the characteristics of the bosonic and fermionic degrees of freedom. Within the approach we describe, only the fermionic degrees of freedom are summed “out” in a formally exact manner. Thus, we discuss importance-sampling strategies for the bosonic fields.

2.1. Path integrals in imaginary time

Feynman formulated quantum mechanics as an integral over all paths of a physical system through phase space (Feynman and Hibbs 1965). For real-time dynamics, any particular path contributes to the integral with a phase that depends exponentially on the integrated action along the path. Hence, two very similar paths can interfere destructively and provide no net contribution to the path integral. On the other hand, near a path of stationary phase, paths have similar phases and can add up constructively. In the classical limit $\hbar \rightarrow 0$, only the stationary-phase path is important, and so in this limit Feynman’s path-integral formulation of quantum mechanics reduces to the principle of least action.

Statistical mechanics, however, entails the study of path integrals in imaginary time (Feynman and Hibbs 1965), in which contributions vary exponentially in magnitude, but not in phase. Therefore, path integrals are dominated by paths of large magnitude, which can be identified by importance-sampling techniques (Creutz and Freedman 1981). For quantum simulations, then, one generally studies the operator $\exp(-\beta H)$ by writing each matrix element as a path integral

$$\langle \psi_L | e^{-\beta H} | \psi_R \rangle = \sum_{|\psi_1\rangle, |\psi_2\rangle, \dots, |\psi_{N_t-1}\rangle} \langle \psi_L | e^{-\Delta\tau H} | \psi_1 \rangle \langle \psi_1 | e^{-\Delta\tau H} | \psi_2 \rangle \dots \times \langle \psi_{N_t-1} | e^{-\Delta\tau H} | \psi_R \rangle \quad (2.1)$$

in imaginary time $\beta = it/\hbar$, where the path integral has been discretized in small “time” steps $\Delta\tau = \beta/N_t$. In contrast, the real-time dynamics of quantum systems is characterized by many interfering paths which resist similar importance-sampling treatments.

For finite-temperature statistical mechanics, the partition function is

$$Z = \text{Tr } e^{-\beta H} = \sum_{|\psi\rangle} \langle \psi | e^{-\beta H} | \psi \rangle, \quad (2.2)$$

where $\beta = 1/k_B T$ is the reciprocal temperature; i.e. the integral is over all paths that are periodic in imaginary time, with $|\psi\rangle = |\psi_L\rangle = |\psi_R\rangle$.

In the zero-temperature limit, $\beta = 1/k_B T$ diverges and the boundary condition in imaginary time becomes unimportant. Thus, we may fix the endpoints of the paths and study

$$Z = \langle \psi_L | e^{-\beta H} | \psi_R \rangle, \quad (2.3)$$

which projects the ground state out of $|\psi_L\rangle$ and $|\psi_R\rangle$ for very large β .

We will develop finite- and zero-temperature formalisms for simulations based on eqs. (2.2) and (2.3), respectively.

2.2. The Trotter approximation

Aside from the physical intuition and elegant formalism that accompany path integrals (Feynman and Hibbs 1965), eq. (2.1) has the important computational advantage that it is possible to approximate the matrix elements of $\exp(-\Delta\tau H)$ for $\Delta\tau \rightarrow 0$ even though the matrix elements of $\exp(-\beta H)$ are, in practice, impossible to evaluate. Typically, one breaks the Hamiltonian H into any number of pieces $H = H_1 + H_2 + \dots + H_n$, which possibly do not commute, and writes the Trotter approximation (Trotter 1959, Suzuki 1976)

$$e^{-\Delta\tau H} = e^{-\Delta\tau H_1} e^{-\Delta\tau H_2} \dots e^{-\Delta\tau H_n} + \mathcal{O}(\Delta\tau)^2, \quad (2.4)$$

for each factor in eq. (2.1). In the limit $\Delta\tau \rightarrow 0$, the approximation for the path integral becomes exact. Since numerical calculations are performed for nonzero $\Delta\tau$, results must be extrapolated to $\Delta\tau = 0$.

2.3. The Hubbard–Stratonovich transformation

The Trotter approximation may be used to separate out direct electronic interactions. These interactions may then be replaced by couplings to bosonic fields using the Hubbard–Stratonovich transformation (Hubbard 1959). As an example, we consider the Hamiltonian

$$H = H_0 + U(n_\uparrow - \frac{1}{2})(n_\downarrow - \frac{1}{2}), \quad (2.5)$$

where n_σ is the number of electrons of spin $\sigma = \uparrow$ or \downarrow in some impurity orbital. Hubbard (1959) originally used time-ordering conventions to handle the path integral. With eq. (2.4), the action in the path integral can be simplified. Through the Trotter approximation, $\exp(-\Delta\tau H) \approx \exp(-\Delta\tau H_0)\exp(-\Delta\tau U(n_\uparrow - \frac{1}{2})(n_\downarrow - \frac{1}{2}))$, the impurity-orbital repulsion is separated from the factor $\exp(-\Delta\tau H_0)$ at each time interval in eq. (2.1). This

can be written as the Gaussian integral

$$\begin{aligned}
 & \exp(-\Delta\tau U(n_\uparrow - \frac{1}{2})(n_\downarrow - \frac{1}{2})) \\
 &= \exp(-\Delta\tau U((n_\uparrow - \frac{1}{2})^2 + (n_\downarrow - \frac{1}{2})^2)/2) \exp(\Delta\tau U(n_\uparrow - n_\downarrow)^2/2) \\
 &= \exp(-\Delta\tau U/4) \exp(\Delta\tau U(n_\uparrow - n_\downarrow)^2/2) \\
 &= \exp(-\Delta\tau U/4) \frac{1}{\sqrt{2\pi}} \int_{-\infty}^{\infty} dx \exp(-x^2/2 + \sqrt{\Delta\tau U} x(n_\uparrow - n_\downarrow)). \quad (2.6)
 \end{aligned}$$

By casting the exponent in the form of a perfect square and introducing the auxiliary field x , one can rewrite $U(n_\uparrow - \frac{1}{2})(n_\downarrow - \frac{1}{2}) = U(c_\uparrow^\dagger c_\uparrow - \frac{1}{2})(c_\downarrow^\dagger c_\downarrow - \frac{1}{2})$, which is quartic in fermion creation and annihilation operators, in a form which is only quadratic in these operators. The repulsive Coulomb interaction has been replaced by an intermediate bosonic field x , which couples to the net spin $n_\uparrow - n_\downarrow$ in the impurity orbital. Physically, the effect of a positive value of U is to create a spin moment in this orbital.

We have engineered the transformation so that the auxiliary field is always real. Had we not done so, insurmountable computational difficulties would have arisen since, as we will see, we would like to have real exponentials. Had U been negative, we would have written

$$\begin{aligned}
 \exp(-\Delta\tau U(n_\uparrow - \frac{1}{2})(n_\downarrow - \frac{1}{2})) &= \exp(-\Delta\tau U/4) \frac{1}{\sqrt{2\pi}} \int_{-\infty}^{+\infty} dx \exp((-x^2/2) \\
 &\quad + \sqrt{\Delta\tau |U|} x(n_\uparrow + n_\downarrow - 1)), \quad (2.7)
 \end{aligned}$$

coupling the field to a charge degree of freedom. Physically, the effect of a negative value of U is to create charge fluctuations in the impurity orbital.

Since it must be effected at each value of the imaginary time, the Hubbard–Stratonovich transformation produces a functional integral over some field $x(\tau)$. By restricting fluctuations in this field, one may derive the Hartree–Fock and random-phase approximations RPA (Evenson et al. 1970, Hamann 1970, Hassing and Esterling 1973). By treating the fields numerically, one may sum over all fluctuations of the fields and so systematically improve these approximations to any desired accuracy.

All interactions in condensed-matter physics can, in principle, be derived by eliminating the bosonic fields that appear in the electromagnetic field equations. We are not interested in solving all of condensed-matter physics ab initio, however, but only a very approximate model that is nonrelativistic, tight-binding, screened, etc. The auxiliary, Hubbard–Stratonovich variables are the bosonic fields that, when eliminated, produce the reduced interaction. These fields have several characteristics. First, like the electromagnetic photon, the field introduced in eq. (2.6) is massless and so provides an instantaneous interaction. Second, the field is entirely localized at the site and so results only in an

on-site repulsion. Extended Coulomb interactions can be modelled either by bosonic fields that are localized on bonds between the orbitals or by coupling fields on different sites. (See Appendix I.) Third, the field could be discrete. This observation, due to Hirsch (1985), is motivated by the fact that the fermion occupation is also discrete: the occupation numbers n_\uparrow and n_\downarrow of up and down electrons can only be 0 or 1. Again, working only with real auxiliary fields, we use one of two different transformations,

$$\begin{aligned} e^{-\Delta\tau U(n_\uparrow - 1/2)(n_\downarrow - 1/2)} &= \frac{1}{2} e^{(-\Delta\tau|U|/4)} \sum_x e^{\alpha x(n_\uparrow - n_\downarrow)}, \quad U > 0, \\ &= \frac{1}{2} e^{(-\Delta\tau|U|/4)} \sum_x e^{\alpha x(n_\uparrow + n_\downarrow - 1)}, \quad U < 0, \end{aligned} \tag{2.8}$$

depending on the sign of U . In both cases, $\cosh \alpha = \exp(\Delta\tau|U|/2)$ and the bosonic field is discrete: $x = \pm 1$. We remark again that for an on-site repulsion, the auxiliary field couples to the spin degree of freedom, while for an on-site attraction it couples to the charge. Simulations using discrete transformations produce results with error bars about half of those for the continuous transformation (Hirsch 1985, Buendia 1986) presumably due to the decreased phase space. In Appendix II, we will see that the discrete and continuous transformations are equivalent in the limit $\Delta\tau \rightarrow 0$.

Once the auxiliary fields have been introduced, the sums (2.2) and (2.3) become nested sums

$$Z = \sum_{\{x\}} \sum_{\text{fermionic}} \exp(-S) = \sum_{\{x\}} p[x] \tag{2.9}$$

over bosonic $\{x\}$ and fermionic degrees of freedom, where S is some fermion–boson action that we will write out explicitly for some cases later. For a fixed configuration of bosonic field variables x , we will sum over the fermions exactly to calculate the weight $p[x]$ of that configuration. Then, we will sum over the $x(\tau)$ stochastically using importance sampling.

2.4. Boson world lines

To develop a physical intuition for the configurations generated in the simulations, we now discuss world line pictures, the imaginary-time evolutions of bosons and fermions. For a bosonic field, the world line is the value of the field as a function $x(\tau)$ of time. These fields may be auxiliary, massless Hubbard–Stratonovich variables or they could be massive, physical phonons. For fermions, the world lines are the positions of the fermions in real space, again, as functions of time.

While the world line of a quantum particle may be continuous in imaginary time, it is never differentiable. There are always components of very high frequency, which cannot be represented by a finite number of degrees of freedom on a computer. On the other hand, these high-frequency components contribute

negligibly to most physical observables, such as the potential energy or the average displacement of the particle; hence, cutting off the very high frequency components causes no practical limitations in calculations (Loh Jr 1988). Specifically, the error caused by discretizing the path integral in finite imaginary-time units $\Delta\tau$ is due principally to the Trotter approximation (2.4) and not to the elimination of the high frequencies.

Let us now examine the effects of the mass of a quantum particle on the world lines of the particle. Consider massive Einstein phonons in the Holstein Hamiltonian

$$H = H_{el} + \sum_i \left(\frac{p_i^2}{2m} + \frac{kx_i^2}{2} \right) + \lambda \sum_i x_i n_i, \quad (2.10)$$

where H_{el} is the purely electronic part of the Hamiltonian and x_i and p_i are the positions and momenta of the site phonons which couple to the electronic charge density n_i . The energy expended in lattice distortion is modelled with the harmonic term $k\sum x_i^2/2$. In this model, an electron distorts the ionic lattice through its coupling λ to the phonons. In certain parameter regimes, it is energetically favorable for a second electron to remain close to this first electron rather than to distort another portion of the crystal structure. Thus, the phonons induce an effective attraction between electrons, much as the massless Hubbard–Stratonovich fields mediate an attraction in eq. (2.7). Due to their finite mass, the physical phonons do not react instantaneously to electronic motions and so provide a retarded attraction.

For the massive phonons, the mass m governs the time variation of the phonon world lines through the velocity term

$$\dot{x}_i(\tau) = \frac{x_i(\tau) - x_i(\tau - \Delta\tau)}{\Delta\tau}$$

in the discretized action

$$S = \sum_{\tau=\Delta\tau}^{\beta} \Delta\tau \left(H_{el} + \sum_i (\frac{1}{2}m\dot{x}_i(\tau)^2 + \frac{1}{2}kx_i(\tau)^2) + \lambda \sum_i x_i(\tau) n_i(\tau) \right). \quad (2.11)$$

In the limit $\Delta\tau \rightarrow 0$, then, the world line $x(\tau)$ must be continuous.

In contrast, eq. (2.7) has only distortion ($-x^2/2$) and fermion–boson ($\sqrt{\Delta\tau U} x(n-1)$) terms. Since there is no kinetic-energy term, field variables on adjacent time slices, τ and $\tau - \Delta\tau$, are not directly coupled: in contrast to physical, massive bosons, the world lines of the Hubbard–Stratonovich fields are not even continuous, let alone differentiable! Indeed, if we had employed Hirsch's discretized transformation (2.8), then $x(\tau) = \pm 1$ and the lines could not be continuous.

World lines, generated by purely bosonic actions, are shown in fig. 1. The world lines are piecewise constant for the duration $\Delta\tau = 0.04$ of a time slice, but

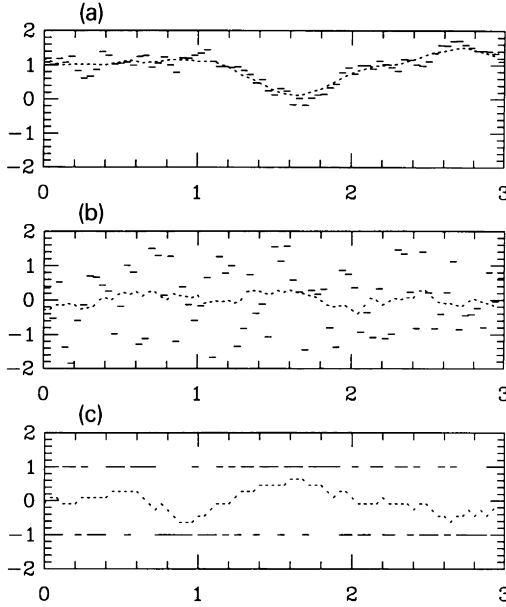


Fig. 1. Sample bosonic world lines: (a) massive field, (b) massless, continuous field, and (c) massless, discrete $x = \pm 1$ field. The massless fields have large fluctuations, which average out to produce a low-frequency average order $\sqrt{\Delta\tau}$. Since the coupling to massless fields is larger, however, the net effect of bosonic fields is always of the same order.

then jump to new constant values. Thus, each line is described by a sequence of values $X_l = x(l\Delta\tau)$ for $l = 1, 2, \dots, N_t$. The world lines are generated by the weights

$$p[x] \sim \exp\left(-\Delta\tau \sum_l \left(\frac{m}{2} \left(\frac{X_l - X_{l-1}}{\Delta\tau}\right)^2 + \frac{k}{2} X_l^2\right)\right),$$

with $m = k = 1$ for the massive boson in fig. 1a;

$$p[x] \sim \exp\left(-\sum_l \frac{X_l^2}{2}\right)$$

for the massless, continuous field in fig. 1b; and

$$p[x] \sim \exp\left(-\sum_l (\delta(X_l - 1) + \delta(X_l + 1))\right)$$

for the massless, discrete field in fig. 1c.

Figure 1a shows the world line for a massive boson. Given that it is required to be piecewise constant, the line is reasonably “continuous”: $x(\tau)$ is highly

correlated between successive time slices. Nevertheless, it is not “differentiable” (in the limit $\Delta\tau \rightarrow 0$). The field variable is typically of order 1. Hence, electron–boson and purely electronic contributions enter the action to the same order in $\Delta\tau$.

This balance between electron–boson and purely electronic contributions is somewhat more subtle for massless bosons. Consider a massless field $x(\tau)$ that mediates the single-orbital interactions as in eq. (2.5). Possible world lines for $x(\tau)$ are sketched in figs. 1b, c for continuous fields [eqs. (2.6) or (2.7)] and discrete fields $x = \pm 1$ [eq. (2.8)], respectively. Now, successive values $x(\tau - \Delta\tau)$ and $x(\tau)$ of the field variable are completely uncorrelated. Over some finite time τ , the electron feels $N_x = \tau/\Delta\tau$ random fields with a mean field of order $1/\sqrt{N_x} \sim \sqrt{\Delta\tau}$. Thus, for massless bosons the effective field on the electron is reduced by a factor $\sqrt{\Delta\tau}$ due to random fluctuations. The dotted lines in figs. 1b, c show the reduced, effective field after the high-frequency oscillations have been eliminated by averaging over a short imaginary time. On the other hand, the effective coupling of the electrons to this reduced field is much stronger. While the electron–boson contribution to the action goes as $\sum \Delta\tau x$ for the massive boson, it goes as $\sum \sqrt{\Delta\tau|U|}x$ in eqs. (2.6) and (2.7) and as $\sum \alpha x \sim \sum \sqrt{\Delta\tau|U|}x$, as $\Delta\tau \rightarrow 0$, in eq. (2.8). Hence, the effective coupling increases by a factor $\sqrt{\Delta\tau}$ to compensate for the reduction in the effective, time-averaged field. In short, the electron–boson contribution enters the action to the same order as the purely electronic contribution. For massive bosons, however, $x(\tau)$ guides the electrons smoothly, while for massless bosons the field achieves the same effect by jerking the electrons wildly.

(As we shall see, round-off errors in the numerical calculations pose severe difficulties for simulations. One effect of the wild fluctuations in massless fields is to accentuate these numerical instabilities since the fields require larger-scale computations to effect smaller-scale ($\sqrt{\Delta\tau}$) averages.)

The electronic degrees of freedom, then, are determined to equal order in $\Delta\tau$ both by purely electronic contributions and by the coupling to bosonic fields. We have shown this for massless and massive fields that were generated by purely bosonic actions. In Appendix II, we will see that the result remains the same even when the bosonic fields are generated by the full electron–boson action. While it appears that we have relied on a different electron–boson coupling for the massless- and massive-field cases, the redefinition of the coupling is, in fact, quite natural. If we had simply followed the conventions of the massive fields and let the mass go to zero, the electron–boson coupling and the time-averaged field would have been of order 1. Fluctuations in the field, however, would have grown to order $1/\sqrt{\Delta\tau}$. We choose, instead, to keep the field values of unit order. Thus, for massless bosons, we must rescale the field and the coupling and the time-averaged field drops to order $\sqrt{\Delta\tau}$.

2.5. The single-electron propagator

For any particular configuration of field variables, the single-electron, imaginary-time propagator $\mathbf{B}(\tau_2, \tau_1)$ for $\tau_2 \geq \tau_1$ is given by the matrix elements

$$B_{ij}(\tau_2, \tau_1) = \langle 0 | c_i \left(\mathcal{T} \exp \left(- \int_{\tau_1}^{\tau_2} S(\tau) d\tau \right) \right) c_j^\dagger | 0 \rangle, \quad (2.12)$$

where \mathcal{T} is the time-ordering operator, S the imaginary-time electron–boson action containing the dependence on the $x(\tau)$, and $|0\rangle$ is the vacuum state. This propagator obeys the identities

$$\mathbf{B}(\tau_3, \tau_2)\mathbf{B}(\tau_2, \tau_1) = \mathbf{B}(\tau_3, \tau_1), \quad \mathbf{B}(\tau, \tau) = \mathbf{1}. \quad (2.13)$$

Since the up and down electrons can couple differently to the bosonic fields, we will compute the single-particle propagator (2.12) separately for each electronic spin \uparrow and \downarrow . In a homogeneous bosonic field, $\mathbf{B}^\sigma(\tau_2, \tau_1)$ causes the wavefunction of an electron with spin σ , injected at a specific site at imaginary time τ_1 , to diffuse evenly throughout the spatial lattice and grow or decrease in magnitude. From eqs. (2.12) and (2.13), the solution of the equations of motion is

$$\begin{aligned} c_i(\tau_2) &= \sum_j B_{ij}(\tau_2, \tau_1) c_j(\tau_1), \\ c_i^\dagger(\tau_2) &= \sum_j c_j^\dagger(\tau_1) B_{ji}^{-1}(\tau_2, \tau_1). \end{aligned} \quad (2.14)$$

Notice that $c_i(\tau)$ and $c_i^\dagger(\tau)$ are not Hermitian conjugates since we are working in imaginary time.

2.6. The many-electron propagator

Up to this point, we have neglected the statistics of the identical fermions. While the spin σ of a fermion distinguishes it from a fermion of opposite spin $-\sigma$, all fermions of the same spin are indistinguishable. Indistinguishable fermions obey Fermi–Dirac statistics, i.e. the wavefunction changes sign under the exchange of any two identical fermions. An important consequence of this is the Pauli exclusion principle for identical fermions in the same state. When the Fermi–Dirac nature of the particles becomes important – at low temperatures and high densities – it is the delicate, nearly perfect cancellation of opposite-sign contributions to the partition function that gives rise to the distinctly fermionic phenomena that we hope to measure. Thus, while we can use importance sampling for the bosonic fields, summing stochastically over fermion configurations would be an ineffective means of capturing fermionic character. Our strategy will be to use importance sampling to sum over configurations of the bosons, but to sum, even if only formally, over all fermionic paths exactly. This,

we will see, does not eliminate the cancellation or “sign” problem completely, but it does make many calculations possible.

Of course, there is nothing “fermionic” about the single-particle propagator (2.12), since statistics is meaningless for a single particle. So we now consider the imaginary-time propagator for N_σ identical fermions, each of which has spin σ and couples identically to the external, time-varying field, but all of which are independent of each other except for their statistics. The advantage of having independent fermions is that many-fermion propagators are easily expressed in terms of single-particle propagators as (see Appendix III)

$$\begin{aligned} & \langle 0 | c_{i_1} c_{i_2} \cdots c_{i_{N_\sigma}} \left(\mathcal{T} \exp \left(- \int_{\tau_1}^{\tau_2} S(\tau) d\tau \right) \right) c_{j_{N_\sigma}}^\dagger \cdots c_{j_2}^\dagger c_{j_1}^\dagger | 0 \rangle \\ &= \det \begin{pmatrix} B_{i_1 j_1}(\tau_2, \tau_1) & B_{i_1 j_2}(\tau_2, \tau_1) & \cdots & B_{i_1 j_{N_\sigma}}(\tau_2, \tau_1) \\ B_{i_2 j_1}(\tau_2, \tau_1) & B_{i_2 j_2}(\tau_2, \tau_1) & \cdots & B_{i_2 j_{N_\sigma}}(\tau_2, \tau_1) \\ \vdots & \vdots & \ddots & \vdots \\ B_{i_{N_\sigma} j_1}(\tau_2, \tau_1) & B_{i_{N_\sigma} j_2}(\tau_2, \tau_1) & \cdots & B_{i_{N_\sigma} j_{N_\sigma}}(\tau_2, \tau_1) \end{pmatrix}. \end{aligned} \quad (2.15)$$

The determinant automatically incorporates the odd parity of particle exchange into the calculation. We remark that while the number $N! / N_\sigma!(N - N_\sigma)!$ of many-body states grows exponentially with the number N of possible single-particle states, the factorization of the problem into single-particle propagators reduces the calculation to a manipulation of $N \times N$ matrices and makes the calculation scale as N^3 at worst*. Thus, the effort of introducing auxiliary fields to eliminate direct electron-electron interactions has already brought us some advantages.

To summarize, since the evolving particles are “independent”, the many-particle propagator should simply be a product of single-particle propagators. Having injected N_σ identical particles at time τ_1 into orbitals $j_1, j_2, \dots, j_{N_\sigma}$, we do not, however, know which of these particles arrive at the various orbitals $i_1, i_2, \dots, i_{N_\sigma}$ at time τ_2 . The determinant (2.15) is a sum over all such arrivals with the appropriate minus signs inserted to account for an even or odd number of permutations of the identical fermions.

2.7. The sign problem

We now imagine that we inject two particles at τ_1 at sites j_1 and j_2 , as in fig. 2. In the figure, the space axis is vertical and one assumes periodic boundary conditions. The imaginary-time axis runs from right to left. We assume the sign of the electron–boson coupling to be such that shaded regions of space are unfavorable for electron propagation. In the figure, the bosonic field variables happen to

* “Conjugate-gradient” methods, which we will not discuss here, scale nominally as N since they iterate with sparse representations of $N \times N$ matrices. Unfortunately, such methods require a divergent number of iterations at low temperatures, making them impractical.

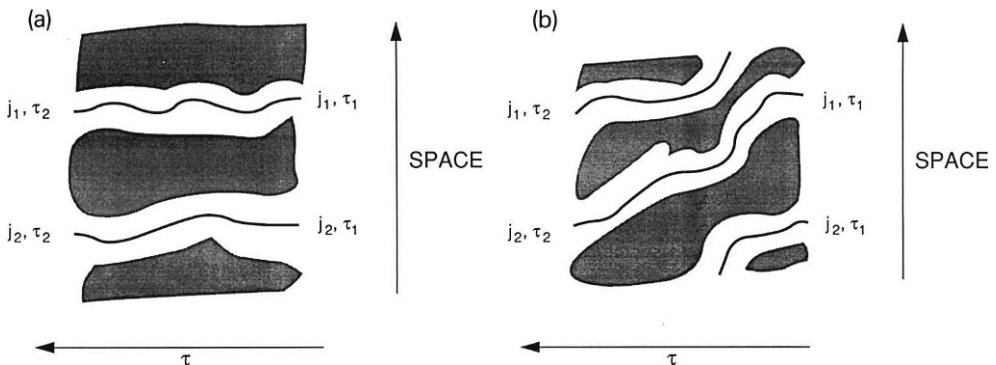


Fig. 2. Bosonic field configurations of different “sign”. The electron–boson coupling is chosen such that shaded regions of space–time are unfavorable for electron propagation. In (a), well-defined channels lead electrons at j_1 and j_2 back to themselves. In (b), the channels force an exchange of the electrons. The fields in (b), therefore, would appear in a simulation with opposite signs relative to (a).

provide well-defined channels for the electrons. In fig. 2a, these channels guide the electrons from j_1 and j_2 back to themselves. Hence, the configuration of field variables represented in fig. 2a contributes to the partition function with a positive weight. In contrast, the auxiliary variables represented in fig. 2b force an exchange of the electrons and their contribution appears in the partition function with a negative weight. These pictures correspond to high temperatures (short imaginary times and few chances for exchanges), low particle densities, and massive bosons (slowly varying fields in time). In practice, particularly for massless bosonic fields, which mediate instantaneous interactions, the fields are very noisy and hence do not provide well-defined channels. Thus, in the limit of low temperature, high fermion densities, and massless fields, there are many exchanges and it is difficult to characterize the sign of the determinant. The picture becomes one of fermions tunnelling through an amorphous medium. Nevertheless, it is clear that the space–time structure of the x -fields can lead to determinants (2.15) of opposite signs.

This is unfortunate because we rely on importance sampling to make measurements in the hopelessly large phase space of field variables x , and importance sampling is incapable of keeping track of delicate cancellations of contributions with opposite signs. To a large extent, the fermionic nature of the particles has already been accounted for by the exact evaluation of determinants. Thus, “determinantal” simulations have had a number of successes while “world-line” methods*, which sum stochastically over assignments between

* “World-line” methods (Hirsch et al. 1981, 1982) work for fermions in one dimension, which are isomorphic via the Jordan–Wigner transformation to quantum spin chains. Above one dimension, these methods are useful for fermions only at high temperatures and low densities, when the short imaginary time $\beta = 1/k_B T$ and large interparticle spacing make fermion exchange improbable – in short, when the fermionic nature of the particles is unimportant.

identical particles, work only for systems with no essential fermionic characteristics. Nevertheless, as we will see, even “determinantal” methods will fail due to sign difficulties.

2.8. “Nodal” surfaces

The net weight with which a particular set of bosonic fields enters the partition function (2.9) takes the form of a determinant. This determinant, as we have seen, may be either a positive or a negative functional of the field variables $\{x\}$, particularly at low temperatures, for which a sufficiently long imaginary time is available for particles to exchange many times. Clearly, in the phase space of the $\{x\}$, the determinant has nodal surfaces that separate these positive and negative regions and on which a configuration of field variables would have vanishing weights. We may think of this vanishing weight as being due to an infinite “potential energy” for the configuration.

Further, for a simulation to produce unbiased averages, it must be ergodic, i.e. it must be able to sample all of configuration space and not just one subspace bounded by potential barriers. Such a sampling is difficult to achieve with a gradual evolution of the field variables in the presence of “nodal” surfaces. On the other hand, a large change in even a single field variable may cause a nodal crossing if the discretization parameter $\Delta\tau$ is sufficiently large.

2.9. Importance sampling: single classical particle

Importance sampling is the technique of generating states of a physical system stochastically with the same probability distribution as in thermal equilibrium. While many samples are generated to reduce the statistical fluctuations in this stochastic process, the number of samples needed to make reasonably good measurements on the physical system is many orders of magnitude smaller than the size of phase space, which is prohibitively large. Typically, importance sampling takes the form of a Markov chain, a trajectory through phase space in which each new sample is closely related to the previous one.

We begin by discussing importance sampling in the context of a very simple example: a single classical particle in a potential well at finite temperature. In thermodynamic equilibrium, the probability of the particle being at position x is $\exp(-\beta V(x))$, where $V(x)$ is the external potential and $\beta = 1/k_B T$ is, once again, the reciprocal temperature. Of course, for this classical model, the action is diagonal in any basis and we no longer have an imaginary-time dimension. While the partition-function integral is best evaluated with numerical quadratures, such methods are impractical in evaluating the high-dimensional integrals that occur in many-body problems. Hence, we will discuss strategies for importance sampling that are appropriate for many-body problems.

The Monte Carlo method is perhaps the most popular approach for sampling phase space.* In this method one proposes a change in the system configuration and then accepts or rejects the change in accordance with “detailed balance”. For example, in the Metropolis algorithm (Metropolis et al. 1953), given a particle at position x , one proposes a new position $x' = x + \delta x$, with δx chosen at random from some symmetric distribution, and accepts the point with probability

$$\begin{aligned} P(x \rightarrow x') &= 1 && \text{if } e^{-\beta V(x')} > e^{-\beta V(x)}, \\ &= e^{-\beta(V(x') - V(x))} && \text{if } e^{-\beta V(x')} < e^{-\beta V(x)}. \end{aligned} \quad (2.16)$$

Another popular choice for the transition probability is (Binder 1987)

$$P(x \rightarrow x') = \frac{e^{-\beta V(x')}}{e^{-\beta V(x)} + e^{-\beta V(x')}}, \quad (2.17)$$

which would arise if we had frozen the system so that the particle could only move between position x and the randomly chosen position x' and then put the system in contact with a heat bath. These two algorithms maintain detailed balance

$$P(x \rightarrow x')e^{-\beta V(x)} = P(x' \rightarrow x)e^{-\beta V(x')}, \quad (2.18)$$

ensuring that the equilibrium distribution $\exp(-\beta V(x))$ of x remains fixed. In simulation time, the classical particle would appear to jump around in phase space under these rules.

An alternative approach would be to let the particle evolve by simulating its dynamics. We have not specified the dynamics of the particle, since originally we were interested only in its equilibrium properties. Nevertheless, we may introduce a fictitious dynamics that does not affect the particle’s equilibrium properties. For example, the addition of a kinetic energy $p^2/2m$ leaves the partition function

$$Z = \int dx \int dp e^{-\beta(p^2/2m + V(x))} \sim \int dx e^{-\beta V(x)} \quad (2.19)$$

unchanged to within some arbitrary multiplicative factor. If we choose some momentum p from the Gaussian distribution $\exp(-\beta p^2/2m)$, we may then let the particle evolve according to the equations of motion:

$$\dot{x} = \frac{p}{m}, \quad \dot{p} = -\frac{\partial V(x)}{\partial x}. \quad (2.20)$$

In molecular dynamics, these equations are commonly integrated using the leap-frog algorithm, which is fast, stable, and easy to implement (Verlet 1968). In

* For more details on classical Monte Carlo methods, including both the Metropolis and heat bath algorithms, see, e.g. Binder (1987).

molecular dynamics, the classical particle would trace long, smooth trajectories through phase space. A many-body system would appear to undergo a complicated, “breathing” motion. To sample the thermodynamic ensemble, we must thermalize p periodically, i.e. we must pick p afresh. If we choose p from the Gaussian distribution at each time-evolution step, we are using the Langevin method, which leads to a Brownian motion in the degrees of freedom.

One drawback of using a continuous evolution of the $\{x\}$, such as in a molecular-dynamics or Langevin method, is that it is difficult to tunnel through the potential barriers of the nodal surfaces of the determinantal functional. In contrast, Monte Carlo updating may “step” across such a potential barrier with the update of even only one field variable if $\Delta\tau$ is not too small.

Finally, a combination of Monte Carlo, molecular-dynamics, or Langevin methods may be used to perform the importance sampling. Indeed, a popular “hybrid” combination is to let the system evolve according to some fictitious dynamics using molecular dynamics (updating the momenta in the system occasionally and so including occasional Langevin steps), but then to correct for step-size errors in the numerical integration by accepting or rejecting the evolved system according to the Metropolis rule (Scalettar et al. 1987).

2.10. The Green’s function

The matrix elements of the Green’s function \mathbf{G}^σ are

$$G_{ij}^\sigma(\tau', \tau) = \langle c_{i\sigma}(\tau') c_{j\sigma}^\dagger(\tau) \rangle_x. \quad (2.21)$$

Here, the angular brackets denote averages over all electron paths for a *particular* configuration of the bosonic fields x . This average, of course, is taken with respect to whichever imaginary-time boundary condition [eq. (2.3) or eq. (2.2)] is appropriate and must be calculated separately for $\sigma = \uparrow$ and $\sigma = \downarrow$. While the Green’s function is customarily defined with a time-ordering operator inside the brackets to serve field-theoretic purposes, this convention is not needed and will not be used in our numerical development.

The Green’s function is the central object in numerical simulations, playing at least two essential roles. The first is in the importance sampling of the bosonic fields. For example, one may propose and then (using Metropolis or heat bath algorithms) accept or reject a change in a single field variable $x_i(\tau)$ at site i and imaginary time τ . In the spirit of perturbation theory, we could estimate the changes in the electron–boson contribution to the action, under the assumption that the electronic degrees of freedom remain fixed under this change in a single field variable. Then, since $x_i(\tau)$ couples only to $n_{i\uparrow}(\tau)$ and $n_{i\downarrow}(\tau)$, the only information we need about the electrons are the $G_{ii}^\sigma(\tau, \tau) = 1 - \langle n_{i\sigma}(\tau) \rangle_x$ for both spin-up and for spin-down electrons. Indeed, Blankenbecler, Scalapino, and Sugar (Scalapino and Sugar 1981, Blankenbecler et al. 1981a, b) have shown that the $G_{ii}^\sigma(\tau, \tau)$ are all that one needs to evaluate changes in the electron–boson

contribution to the action exactly. Similarly, the $G_{ii}^\sigma(\tau, \tau)$ provide all the information needed to perform Langevin or molecular-dynamics sampling, since the forces on the bosonic field variables depend only on local electronic densities.

The second important role that the Green's function plays in simulations is in measurements of the electronic degrees of freedom. If A is a measurement operator that contains electron creation and annihilation operators, then

$$\langle A \rangle = \frac{1}{N_m} \sum'_{\{x\}} \langle A \rangle_x, \quad (2.22)$$

where the primed sum is over N_m bosonic field variables sampled in proportion to their probabilities in thermal equilibrium, and $\langle A \rangle_x$ is the expectation value of A for a fixed set of fields x . Since $\langle A \rangle_x$ is an average for fermions which interact only with fixed bosons and not with each other, we may apply Wick's theorem (Fetter and Walecka 1971) to express it as a sum over products of contractions of fermion operators. Each such contraction, of course, is a specific element of the \mathbf{G}^σ .

One final note on these Green's functions is that their matrix elements need not fall in the numerical ranges we would normally expect. For example, $G_{ii}^\sigma(\tau, \tau) = 1 - \langle n_{i\sigma}(\tau) \rangle_x$ and so should fall in the range $0 \leq G_{ii}^\sigma(\tau, \tau) \leq 1$. For fermions evolving in imaginary time through time-varying fields, however, this is no longer the case. Indeed, near the nodal surfaces discussed earlier, the elements of \mathbf{G}^σ diverge.

3. Mathematical formulation

In this section, we develop the simulation algorithms in detail, focussing on a particular example to make the discussion more transparent. We work with the two-dimensional Hubbard model, eliminating the interactions between the fermions using the discrete Hubbard–Stratonovich transformation (Hirsch 1985). Importance sampling is then performed using single-site-update Monte Carlo. After each change is accepted, the Green's function is updated by the procedure suggested by Blankenbecler, Scalapino, and Sugar (BSS) (Scalapino and Sugar 1981, Blankenbecler et al. 1981a, b). The two-dimensional Hubbard Hamiltonian is a convenient example. Other Hamiltonians may be treated by steps similar to those outlined here.

3.1. Matrix representation of single-particle propagators

The Hamiltonian we consider is

$$\begin{aligned} H &= H_t + H_U + H_\mu \\ &= - \sum_{ij,\sigma} T_{ij}(c_{i\sigma}^\dagger c_{j\sigma} + c_{j\sigma}^\dagger c_{i\sigma}) + U \sum_i (n_{i\uparrow} - \tfrac{1}{2})(n_{i\downarrow} - \tfrac{1}{2}) - \mu \sum_i n_i, \end{aligned} \quad (3.1)$$

where the T_{ij} are the hopping integrals, $U > 0$ is the strength of the on-site Hubbard repulsion, and μ is the chemical potential, chosen to be zero at half filling. Sums over i are taken over sites on a periodic, square lattice, and we will consider nonzero hopping T_{ij} only between nearest-neighbor sites i and j . We will use N for the number of sites on the lattice and work in the real-space basis of sites i .

Using the Trotter approximation, we break each of the N_t factors $\exp(-\Delta\tau H)$ in eq. (2.1) into two additional factors

$$e^{-\Delta\tau H} \approx e^{-\Delta\tau(H_U + H_\mu)} e^{-\Delta\tau H_t}, \quad (3.2)$$

which are diagonal and off-diagonal, respectively, in a site-occupation representation. Since the terms which make up H_U and H_μ are diagonal, they commute among themselves and their exponentials can be factored into

$$e^{-\Delta\tau(H_U + H_\mu)} = \prod_i e^{-\Delta\tau U(n_{i\uparrow} - 1/2)(n_{i\downarrow} - 1/2)} \prod_i e^{\Delta\tau\mu n_i}$$

without approximation. We reduce the exponential of the quartic terms $-\Delta\tau U(n_{i\uparrow} - \frac{1}{2})(n_{i\downarrow} - \frac{1}{2})$ by invoking Hirsch's discrete Hubbard–Stratonovich transformation (2.8).

The up and down fermions couple to the external fields differently. Hence, we compute two single-particle propagators \mathbf{B}^\dagger and \mathbf{B}^\downarrow . For a given configuration of field variables,

$$\mathbf{B}^\sigma(\tau_2, \tau_1) = \mathbf{B}^\sigma(\tau_2, \tau_2 - \Delta\tau) \mathbf{B}^\sigma(\tau_2 - \Delta\tau, \tau_2 - 2\Delta\tau) \cdots \mathbf{B}^\sigma(\tau_1 + \Delta\tau, \tau_1),$$

where

$$\mathbf{B}^\sigma(\tau, \tau - \Delta\tau) \approx \mathbf{A}^\sigma(\tau) \exp(\Delta\tau\mu) \exp(\Delta\tau\mathbf{T}) \quad (3.3)$$

gives eq. (3.2) in our single-particle, real-space basis. The particles diffuse in real space for a small imaginary time $\Delta\tau$ according to $\exp(\Delta\tau\mathbf{T})$, their propagators are amplified or attenuated through the scalar factor $\exp(\Delta\tau\mu)$, and finally are scattered by the external potentials described by

$$\mathbf{A}^\sigma(\tau) = \begin{pmatrix} e^{\sigma\alpha x_1(\tau)} & & 0 \\ & e^{\sigma\alpha x_2(\tau)} & \\ & & \ddots \\ 0 & & e^{\sigma\alpha x_N(\tau)} \end{pmatrix},$$

where the exponents $\sigma\alpha x = \pm\alpha x$ flip signs depending on whether $\sigma = \uparrow$ or \downarrow , and where $\cosh(x) = \exp(\Delta\tau U/2)$ as in eq. (2.8). Since we couple the external fields only to local fermionic degrees of freedom, \mathbf{A}^σ is diagonal. The σ -dependence of the \mathbf{A}^σ reflects the fact that the two types of fermions, $\sigma = \uparrow$ or \downarrow , couple to the auxiliary fields differently. Indeed, it is only because of the \mathbf{A}^σ that the propagators \mathbf{B}^\dagger and \mathbf{B}^\downarrow are different.

3.2. Checkerboard breakup

Generally, we will choose to break the kinetic-energy matrix $\exp(\Delta\tau \mathbf{T})$ in eq. (3.3) further. While the computational cost of diagonalizing and then exponentiating \mathbf{T} is relatively small, the resulting matrix is dense, making the number of operations needed to perform a matrix multiplication scale as N^3 . Alternatively, for uniform hopping integrals, one may utilize fast-fourier transforms (FFT) and apply the kinetic-energy factors $\exp(\Delta\tau \mathbf{T})$ in momentum space, in which \mathbf{T} is diagonal. This approach, unfortunately, does not allow for nonuniform hoppings, and efficient use of the FFT restricts the linear size of the system one studies to powers of 2.

A sparse and extremely convenient approximate form for $\exp(\Delta\tau \mathbf{T})$ results from a further application of the Trotter approximation to the kinetic energy. In the single-particle, real-space basis, the exponential of the hopping part of the Hamiltonian may be written as

$$\exp(\Delta\tau \mathbf{T}) = \exp\left(\Delta\tau \sum_{\langle ij \rangle} \mathbf{T}^{(ij)}\right) \approx \prod_{\langle ij \rangle} \exp(\Delta\tau \mathbf{T}^{(ij)}). \quad (3.4)$$

The sparse matrices $\mathbf{T}^{(ij)}$, with only $T_{ij}^{(ij)} = T_{ji}^{(ij)} = T_{ij}$ nonzero, are easily exponentiated, giving

$$\begin{aligned} \exp(\Delta\tau \mathbf{T}^{(ij)}) &= \exp \Delta\tau \begin{pmatrix} 0 & \cdots & 0 & \cdots & 0 & \cdots & 0 \\ \vdots & & \vdots & & \vdots & & \vdots \\ 0 & \cdots & 0 & \cdots & T_{ij} & \cdots & 0 \\ \vdots & & \vdots & & \vdots & & \vdots \\ 0 & \cdots & T_{ij} & \cdots & 0 & \cdots & 0 \\ \vdots & & \vdots & & \vdots & & \vdots \\ 0 & \cdots & 0 & \cdots & 0 & \cdots & 0 \end{pmatrix} \\ &= \begin{pmatrix} 1 & \cdots & 0 & \cdots & 0 & \cdots & 0 \\ \vdots & & \vdots & & \vdots & & \vdots \\ 0 & \cdots & \cosh(\Delta\tau T_{ij}) & \cdots & \sinh(\Delta\tau T_{ij}) & \cdots & 0 \\ \vdots & & \vdots & & \vdots & & \vdots \\ 0 & \cdots & \sinh(\Delta\tau T_{ij}) & \cdots & \cosh(\Delta\tau T_{ij}) & \cdots & 0 \\ \vdots & & \vdots & & \vdots & & \vdots \\ 0 & \cdots & 0 & \cdots & 0 & \cdots & 1 \end{pmatrix}. \end{aligned}$$

Each $\exp(\Delta\tau \mathbf{T}^{(ij)})$ is also sparse, with only the ii , ij , ji , and jj elements differing from those of the unit matrix. If we replace the multiplication of the dense matrix by the series (3.4) of sparse-matrix multiplications, the number of operations for

multiplication onto an $N \times N$ matrix is reduced from N^3 to $N \times N_b$, where the number of bonds N_b grows linearly with the number of sites for local hoppings. For the square lattice, for example, $N_b = 2N$. For historical reasons, eq. (3.4) is referred to as the checkerboard breakup.*

Not only is the checkerboard breakup of the kinetic energy reasonably fast, it is extremely versatile and convenient. No diagonalization or FFT is required and changes in the hopping integrals – as when one incorporates a fixed lattice distortion – may be effected immediately. Further, evaluation of the inverse $\exp(-\Delta\tau \mathbf{T})$ requires no extra work: one has only to reverse the sign of the off-diagonal elements. In subsequent discussions, we may write $\exp(\Delta\tau \mathbf{T})$ even when we use the checkerboard, approximate form.

3.3. Bosonic-configuration weights

Within the zero-temperature framework suggested by eq. (2.3), let us write $|\psi_L\rangle$ and $|\psi_R\rangle$ as products of single-particle states. Then, using eq. (2.15), the field weights in eq. (2.9) become

$$p[x] = \prod_{\sigma=\uparrow,\downarrow} \det(\mathbf{P}_L^\sigma \mathbf{B}^\sigma(\beta, 0) \mathbf{P}_R^\sigma), \quad (3.5)$$

where the introduction of the auxiliary fields x has decoupled the system into separate $\sigma = \uparrow, \downarrow$ problems. The field-variable dependence of the right-hand side of eq. (3.5) enters through the single-particle propagator \mathbf{B} .

In eq. (3.5), we have written $|\psi_L\rangle$ and $|\psi_R\rangle$ as products of up- and down-electron single-particle states in order to use eq. (2.15). The rows (columns) of the rectangular $N_\sigma \times N$ ($N \times N_\sigma$) matrices \mathbf{P}_L^σ (\mathbf{P}_R^σ) give the single-particle states of $|\psi_L\rangle$ ($|\psi_R\rangle$) of spin $\sigma = \uparrow, \downarrow$ in our N -state basis. For example, let $|\psi_R\rangle = |\psi_R^\uparrow\rangle |\psi_R^\downarrow\rangle$ and let

$$\begin{aligned} |\psi_R^\sigma\rangle &= (P_{11}c_{1\sigma}^\dagger + P_{21}c_{2\sigma}^\dagger + \cdots + P_{N1}c_{N\sigma}^\dagger) \\ &\quad (P_{12}c_{1\sigma}^\dagger + P_{22}c_{2\sigma}^\dagger + \cdots + P_{N2}c_{N\sigma}^\dagger) \\ &\quad \cdots \\ &\quad (P_{1N_\sigma}c_{1\sigma}^\dagger + P_{2N_\sigma}c_{2\sigma}^\dagger + \cdots + P_{NN_\sigma}c_{N\sigma}^\dagger)|0\rangle, \end{aligned}$$

where $|0\rangle$ is the vacuum state. Then

$$\mathbf{P}_R^\sigma = \begin{pmatrix} P_{11} & P_{12} & \cdots & P_{1N_\sigma} \\ P_{21} & P_{22} & \cdots & P_{2N_\sigma} \\ \vdots & \vdots & \ddots & \vdots \\ P_{N1} & P_{N2} & \cdots & P_{NN_\sigma} \end{pmatrix}.$$

* The Trotter formula first became popular in numerical simulations for one-dimensional chains. There, the alternation of even and odd bonds laid out a checkerboard in space-time. See, e.g. Barma and Shastry (1978).

Typically, we will choose $|\psi_L\rangle = |\psi_R\rangle$, so that the \mathbf{P}_L^σ are the Hermitian conjugates of the \mathbf{P}_R^σ . The numbers N_\uparrow and N_\downarrow of up- and down-spin electrons need not be equal. These numbers are fixed over the course of any one simulation however, so that the zero-temperature algorithm is carried out in the canonical ensemble.

For the finite-temperature partition function (2.2), we are no longer interested in matrix elements of $\exp(-\beta H)$ between specified initial and final many-body wavefunctions, but we would like to sum over all $|\psi_L\rangle = |\psi_R\rangle$ of all occupations N_\uparrow and N_\downarrow . Now,

$$p[x] = \prod_{\sigma=\uparrow,\downarrow} \det(\mathbf{1} + \mathbf{B}^\sigma(\beta, 0)). \quad (3.6)$$

We derive this result in Appendix IV. Here, we only note that if we simply had $\det(\mathbf{B})$, we would have had eq. (2.15) with a packed lattice: a fermion on each site. On the other hand, $\det(\mathbf{1})$ is the many-particle propagator for zero particles. In eq. (3.6), $\det(\mathbf{1} + \mathbf{B})$ samples both of these terms and so generates the grand-canonical partition function for a particular set of field variables, summing over all states with all occupation numbers of electrons.

3.4. Matrix representation of the Green's function

To derive \mathbf{G} in terms of the single-particle propagator, let us begin by examining matrix elements of the equal-time Green's function

$$G_{ij}^\sigma(\tau, \tau) = \langle c_{i\sigma}(\tau) c_{j\sigma}^\dagger(\tau) \rangle = \Delta_{ij} - \langle c_{j\sigma}^\dagger(\tau) c_{i\sigma}(\tau) \rangle,$$

where Δ_{ij} is the Kronecker delta function. The expectation $\langle c_{j\sigma}^\dagger(\tau) c_{i\sigma}(\tau) \rangle$ may be evaluated by coupling the action to $c_{j\sigma}^\dagger c_{i\sigma}$ for an instant at imaginary time τ :

$$\begin{aligned} \mathcal{T} \exp\left(-\int_0^\beta S(t) dt\right) &= \mathcal{T} \exp\left(-\int_\tau^\beta S(t) dt\right) \exp\left(-\int_0^\tau S(t) dt\right) \\ &\rightarrow \mathcal{T} \exp\left(-\int_\tau^\beta S(t) dt\right) \exp(h c_{j\sigma}^\dagger c_{i\sigma}) \exp\left(-\int_0^\tau S(t) dt\right). \end{aligned}$$

Under this transformation of the action, the weight $p[x]$ becomes a function $p_h[x]$ of the coupling constant h . For example, in the zero-temperature formalism,

$$p_h[x] = \det(\mathbf{P}_L^\sigma \mathbf{B}^\sigma(\beta, \tau) e^{h\mathbf{O}} \mathbf{B}^\sigma(\tau, 0) \mathbf{P}_R^\sigma) \det(\mathbf{P}_L^{-\sigma} \mathbf{B}^{-\sigma}(\beta, 0) \mathbf{P}_R^{-\sigma}),$$

where the only nonzero matrix element of \mathbf{O} is $O_{ji} = 1$. With the definitions

$$\mathbf{L}^\sigma(\tau) = \mathbf{P}_L^\sigma \mathbf{B}^\sigma(\beta, \tau) \quad (3.7)$$

and

$$\mathbf{R}^\sigma(\tau) = \mathbf{B}^\sigma(\tau, 0) \mathbf{P}_R^\sigma, \quad (3.8)$$

the expectation becomes

$$\begin{aligned}\langle c_{j\sigma}^\dagger(\tau)c_{i\sigma}(\tau) \rangle &= \frac{\partial}{\partial h} \ln p_h[x]|_{h=0} = \text{Tr} \frac{\partial}{\partial h} \ln (\mathbf{L}^\sigma e^{h\mathbf{O}} \mathbf{R}^\sigma)|_{h=0} \\ &= \text{Tr}(\mathbf{L}^\sigma \mathbf{R}^\sigma)^{-1} \mathbf{L}^\sigma \mathbf{O} \mathbf{R}^\sigma = (\mathbf{R}^\sigma (\mathbf{L}^\sigma \mathbf{R}^\sigma)^{-1} \mathbf{L}^\sigma)_{ij}.\end{aligned}$$

The equal-time Green's function in the zero-temperature formalism becomes

$$\mathbf{G}^\sigma(\tau, \tau) = \mathbf{1} - \mathbf{R}^\sigma(\tau)(\mathbf{L}^\sigma(\tau)\mathbf{R}^\sigma(\tau))^{-1}\mathbf{L}^\sigma(\tau). \quad (3.9)$$

In the finite-temperature formalism, we can play the same tricks, coupling to $c_j^\dagger c_i$, writing the resulting field weight as a function of h , and taking a logarithmic derivative. Now,

$$\mathbf{G}^\sigma(\tau, \tau) = (\mathbf{1} + \mathbf{B}^\sigma(\tau, 0)\mathbf{B}^\sigma(\beta, \tau))^{-1}. \quad (3.10)$$

For unequal arguments, we transform the Green's function using the integrated equations of motion (2.14) for the fermion operators to get

$$\mathbf{G}(\tau', \tau) = \mathbf{B}(\tau', \tau)\mathbf{G}(\tau, \tau) = \mathbf{G}(\tau', \tau')\mathbf{B}(\tau', \tau). \quad (3.11)$$

3.5. Metropolis algorithm

As we have seen, the weight of a configuration of the bosonic field variables is a product [eq. (3.5) or (3.6)] of two determinants. Such determinants are too expensive to evaluate for each set $\{x\}$ of field variables that we encounter in the course of a simulation. Fortunately, importance sampling via either the Metropolis or heat bath algorithm requires only the ratio $\mathcal{R} = p[x']/p[x]$ of weights. As we will now see, these ratios are straightforward to evaluate when $\{x'\}$ differs from $\{x\}$ in the value of only one field variable.

The change of only one field variable, at site i and at imaginary time τ , from $x_i(\tau)$ to $x'_i(\tau)$ affects the time evolution of the fermions through the matrix \mathbf{A} :

$$\begin{aligned}\mathbf{A}^\sigma(\tau) &\rightarrow \begin{pmatrix} e^{\sigma\alpha x_1(\tau)} & & & 0 \\ & \ddots & & \\ & & e^{\sigma\alpha x'_i(\tau)} & \\ 0 & & & \ddots & e^{\sigma\alpha x_N(\tau)} \end{pmatrix}, \\ &= (\mathbf{1} + \Delta^\sigma(i, \tau))\mathbf{A}^\sigma(\tau),\end{aligned}$$

where the only nonzero matrix element of $\Delta^\sigma(i, \tau)$ is $\Delta_{ii}^\sigma(i, \tau) = \exp(\sigma\alpha(x'_i(\tau) - x_i(\tau))) - 1$. The accompanying change in the single-particle propagator \mathbf{B}^σ is

$$\begin{aligned}\mathbf{B}^\sigma(\beta, 0) &= \mathbf{B}^\sigma(\beta, \tau)\mathbf{B}^\sigma(\tau, 0) \\ &\rightarrow \mathbf{B}^\sigma(\beta, \tau)(\mathbf{1} + \Delta^\sigma(i, \tau))\mathbf{B}^\sigma(\tau, 0).\end{aligned}$$

For the zero-temperature algorithm, we now have $\mathcal{R} = \mathcal{R}^\dagger \mathcal{R}^\downarrow$, with

$$\mathcal{R}^\sigma = \frac{\det(\mathbf{L}^\sigma(\tau)(\mathbf{1} + \Delta^\sigma(i, \tau))\mathbf{R}^\sigma(\tau))}{\det(\mathbf{L}^\sigma(\tau)\mathbf{R}^\sigma(\tau))},$$

using the definitions (3.7) and (3.8). Dropping a number of indices to simplify the equations, the probability-ratio factors become

$$\begin{aligned}\mathcal{R}^\sigma &= \frac{\det(\mathbf{L}(\mathbf{1} + \Delta)\mathbf{R})}{\det(\mathbf{L}\mathbf{R})} \\ &= \frac{\det(\mathbf{L}\mathbf{R} + \mathbf{L}\Delta\mathbf{R})}{\det(\mathbf{L}\mathbf{R})} \\ &= \det(\mathbf{1} + (\mathbf{L}\mathbf{R})^{-1}\mathbf{L}\Delta\mathbf{R}).\end{aligned}\quad (3.12)$$

The last expression is the determinant of $N_\sigma \times N_\sigma$ matrices. What is remarkable is that this determinant is equal to that of a larger, $N \times N$, matrix:

$$\mathcal{R}^\sigma = \det(\mathbf{1} + \Delta\mathbf{R}(\mathbf{L}\mathbf{R})^{-1}\mathbf{L}) = \det(\mathbf{1} + \Delta(\mathbf{1} - \mathbf{G}^\sigma)). \quad (3.13)$$

(See Appendix V.) We finally write the ratio of probabilities as

$$\mathcal{R} = \mathcal{R}^\dagger \mathcal{R}^\downarrow = \prod_{\sigma=\uparrow, \downarrow} \det(\mathbf{1} + \Delta^\sigma(i, \tau)(\mathbf{1} - \mathbf{G}^\sigma(\tau, \tau))). \quad (3.14)$$

For the finite-temperature algorithm, we proceed in a similar fashion:

$$\begin{aligned}\mathcal{R}^\sigma &= \frac{\det(\mathbf{1} + \mathbf{B}^\sigma(\beta, \tau)(\mathbf{1} + \Delta^\sigma(i, \tau))\mathbf{B}^\sigma(\tau, 0))}{\det(\mathbf{1} + \mathbf{B}^\sigma(\beta, \tau)\mathbf{B}^\sigma(\tau, 0))} \\ &= \frac{\det(\mathbf{1} + \mathbf{B}^\sigma(\beta, 0) + \mathbf{B}^\sigma(\beta, \tau)\Delta^\sigma(i, \tau)\mathbf{B}^\sigma(\tau, 0))}{\det(\mathbf{1} + \mathbf{B}^\sigma(\beta, 0))} \\ &= \det(\mathbf{1} + (\mathbf{1} + \mathbf{B}^\sigma(\beta, 0))^{-1}\mathbf{B}^\sigma(\beta, \tau)\Delta^\sigma(i, \tau)\mathbf{B}^\sigma(\tau, 0)) \\ &= \det(\mathbf{1} + \Delta^\sigma(i, \tau)\mathbf{B}^\sigma(\tau, 0)(\mathbf{1} + \mathbf{B}^\sigma(\beta, 0))^{-1}\mathbf{B}^\sigma(\beta, \tau)) \\ &= \det(\mathbf{1} + \Delta^\sigma(i, \tau)(\mathbf{1} - \mathbf{G}^\sigma(\tau, \tau))).\end{aligned}$$

This time, the cyclic rearrangement of factors in the determinant is straightforward since the factors are square matrices with well-defined inverses. The ratio of probabilities has exactly the same form [eq. (3.14)] in terms of the Green's function as in the zero-temperature case.

At this point, one might seem hard pressed to justify all this formalism. In fact, however, eq. (3.14) provides us with a very fast means of evaluating the ratio $p[x']/p[x]$. Since field variables couple only to local fermionic degrees of freedom, a change in only field variable leads to correction matrices Δ^σ which have only one nonzero matrix element. The determinants in eq. (3.14) become

very easy to evaluate and the Metropolis ratio reduces to

$$\mathcal{R} = \mathcal{R}^\dagger \mathcal{R}^\downarrow = \prod_{\sigma=\uparrow,\downarrow} (1 + \Delta_{ii}^\sigma(i, \tau)(1 - G_{ii}^\sigma(\tau, \tau))). \quad (3.15)$$

This final expression is not a product of matrix determinants, but of simple scalars which are readily computed provided that the diagonal matrix elements of the equal-time Green's functions $\mathbf{G}^\sigma(\tau, \tau)$ are known. If each bosonic field were coupled to fermionic degrees of freedom on several near-neighbor sites or if several field variables were changed, then Δ^σ would be less sparse and eq. (3.15) would be, correspondingly, more involved.

3.6. Green's function updating

At first glance, it appears that we have accomplished nothing. While the updating probability $\mathcal{R} = p[x']/p[x]$ can be simply expressed in terms of elements of the Green's functions (3.9) or (3.10), the evaluation of the \mathbf{G}^σ , requiring inverses of matrices, is at least as difficult as calculating the determinants (3.5) or (3.6) outright.

In simulations, however, we compute the inverses fairly infrequently. Whenever we change either an external field $x_i(\tau)$ or the time τ , we use the BSS algorithm (Scalapino and Sugar 1981, Blankenbecler et al. 1981a,b) to update the Green's functions in the finite-temperature approach. We will describe similar procedures for maintaining the relevant inverse for the zero-temperature algorithm. It must be conceded that all elements of the inverse must be updated – even if the field is changed on only one site in space–imaginary-time. Thus, the computation is still relatively expensive – of order N_σ^2 operations per update for the zero-temperature algorithm and of order N^2 operations at finite temperatures – and is the dominant portion of the computation. On the other hand, we will generally avoid the more expensive procedure of calculating the inverses from scratch, which would be of order N_σ^3 and N^3 operations at zero and finite temperature, respectively. The question is then, “If a change is made in the field variables, how may we update the inverses in eqs. (3.9) and (3.10) efficiently?” In answering the question we will again assume the changes in the single-particle propagators to be described in terms of the correction matrices Δ^σ as $\mathbf{B}^\sigma(\tau, 0) \rightarrow (\mathbf{1} + \Delta^\sigma(i, \tau))\mathbf{B}^\sigma(\tau, 0)$.

For the zero-temperature case,

$$\begin{aligned} (\mathbf{L}^\sigma \mathbf{R}^\sigma)^{-1} &\rightarrow (\mathbf{L}^\sigma (\mathbf{1} + \Delta^\sigma) \mathbf{R}^\sigma)^{-1} \\ &= (\mathbf{L}^\sigma \mathbf{R}^\sigma + \mathbf{L}^\sigma \Delta^\sigma \mathbf{R}^\sigma)^{-1} \\ &= (\mathbf{1} + (\mathbf{L}^\sigma \mathbf{R}^\sigma)^{-1} \mathbf{L}^\sigma \Delta^\sigma \mathbf{R}^\sigma)^{-1} (\mathbf{L}^\sigma \mathbf{R}^\sigma)^{-1}. \end{aligned}$$

Of course, we already have $(\mathbf{L}^\sigma \mathbf{R}^\sigma)^{-1}$, it is inverse before updating. We compute the other inverse, $(\mathbf{1} + (\mathbf{L}^\sigma \mathbf{R}^\sigma)^{-1} \mathbf{L}^\sigma \Delta^\sigma \mathbf{R}^\sigma)^{-1}$, by making use of the fact that the Δ^σ are sparse. General solutions are given by the Sherman–Woodbury and

Morrison formulas (Press et al. 1988, Rice 1983). For our simple case, where the only nonzero matrix element of Δ^σ is Δ_{ii}^σ , we assume

$$(\mathbf{1} + (\mathbf{L}^\sigma \mathbf{R}^\sigma)^{-1} \mathbf{L}^\sigma \Delta^\sigma \mathbf{R}^\sigma)^{-1} = (\mathbf{1} + x(\mathbf{L}^\sigma \mathbf{R}^\sigma)^{-1} \mathbf{L}^\sigma \Delta^\sigma \mathbf{R}^\sigma),$$

where x is some scalar which we must determine. Since

$$\Delta^\sigma \mathbf{R}^\sigma (\mathbf{L}^\sigma \mathbf{R}^\sigma)^{-1} \mathbf{L}^\sigma \Delta^\sigma = \Delta^\sigma (\mathbf{1} - \mathbf{G}^\sigma) \Delta^\sigma = \Delta_{ii}^\sigma (1 - G_{ii}^\sigma) \Delta^\sigma$$

is simply a scalar multiple of Δ^σ , our Ansatz gives

$$\begin{aligned} \mathbf{1} &= (\mathbf{1} + (\mathbf{L}^\sigma \mathbf{R}^\sigma)^{-1} \mathbf{L}^\sigma \Delta^\sigma \mathbf{R}^\sigma)(\mathbf{1} + x(\mathbf{L}^\sigma \mathbf{R}^\sigma)^{-1} \mathbf{L}^\sigma \Delta^\sigma \mathbf{R}^\sigma) \\ &= \mathbf{1} + (1 + x + x \Delta_{ii}^\sigma (1 - G_{ii}^\sigma)) (\mathbf{L}^\sigma \mathbf{R}^\sigma)^{-1} \mathbf{L}^\sigma \Delta^\sigma \mathbf{R}^\sigma, \end{aligned}$$

or

$$x = -\frac{1}{1 + \Delta_{ii}^\sigma (1 - G_{ii}^\sigma)}.$$

This, of course, is simply $-1/\mathcal{R}^\sigma$. The updating equation is now

$$(\mathbf{L}^\sigma \mathbf{R}^\sigma)^{-1} \rightarrow (\mathbf{L}^\sigma \mathbf{R}^\sigma)^{-1} \frac{1}{\mathcal{R}^\sigma} (\mathbf{L}^\sigma \mathbf{R}^\sigma)^{-1} \mathbf{L}^\sigma \Delta^\sigma \mathbf{R}^\sigma (\mathbf{L}^\sigma \mathbf{R}^\sigma)^{-1} \quad (3.16)$$

for single-variable updating. The updating is fast because the Δ^σ are sparse. Since the Green's functions are $N \times N$ matrices while the $(\mathbf{L}^\sigma \mathbf{R}^\sigma)^{-1}$ are only $N_\sigma \times N_\sigma$, we will maintain only the $(\mathbf{L}^\sigma \mathbf{R}^\sigma)^{-1}$ in zero-temperature calculations, computing elements of the \mathbf{G}^σ as they are needed. Nevertheless, one could still write updating equations for the real-space Green's functions. From eqs. (3.9) and (3.16),

$$\mathbf{G}^\sigma \rightarrow \mathbf{G}^\sigma - \frac{1}{\mathcal{R}^\sigma} \mathbf{G}^\sigma \Delta^\sigma (\mathbf{1} - \mathbf{G}^\sigma). \quad (3.17)$$

The corresponding derivation for the finite-temperature algorithm is more straightforward:

$$\begin{aligned} \mathbf{G}^\sigma(\tau, \tau) &= (\mathbf{1} + \mathbf{B}^\sigma)^{-1} \\ &\rightarrow (\mathbf{1} + (\mathbf{1} + \Delta^\sigma(\tau, \tau)) \mathbf{B}^\sigma)^{-1} \\ &= (\mathbf{1} + \mathbf{B}^\sigma)^{-1} (\mathbf{1} + \Delta^\sigma(\tau, \tau) \mathbf{B}^\sigma (\mathbf{1} + \mathbf{B}^\sigma)^{-1})^{-1} \\ &= \mathbf{G}^\sigma (\mathbf{1} + \Delta(\mathbf{1} - \mathbf{G}))^{-1}, \end{aligned}$$

writing $\mathbf{B}^\sigma(\tau, 0) \mathbf{B}^\sigma(\beta, \tau)$ simply as \mathbf{B}^σ . Using an Ansatz $(\mathbf{1} + x \Delta^\sigma (\mathbf{1} - \mathbf{G}^\sigma))$ again for the inverse $(\mathbf{1} + \Delta^\sigma (\mathbf{1} - \mathbf{G}^\sigma))^{-1}$, we find $x = -1/\mathcal{R}^\sigma$ and

$$\mathbf{G}^\sigma \rightarrow \mathbf{G}^\sigma - \frac{1}{\mathcal{R}^\sigma} \mathbf{G}^\sigma \Delta^\sigma (\mathbf{1} - \mathbf{G}^\sigma)$$

as before.

3.7. “Wrapping” Green’s functions

Up to this point, we have described algorithms for determining the Metropolis acceptance/rejection ratio \mathcal{R} and for updating the Green’s functions \mathbf{G}^σ in the event of one accepting a proposed field-variable change. These algorithms are formally equivalent for the zero- and finite-temperature approaches. Our discussion, however, has always involved the equal-time Green’s functions $\mathbf{G}^\sigma(\tau, \tau)$ at a particular imaginary time τ . What happens when we wish to consider Monte Carlo hits at other imaginary times?

For the zero-temperature formalism, we construct the Green’s functions out of the products $\mathbf{L}(\tau)$ and $\mathbf{R}(\tau)$ from eqs. (3.7) and (3.8). The inverse

$$\begin{aligned} (\mathbf{L}(\tau)\mathbf{R}(\tau))^{-1} &= (\mathbf{P}_L \mathbf{B}(\beta, \tau) \mathbf{B}(\tau, 0) \mathbf{P}_R)^{-1} \\ &= (\mathbf{P}_L \mathbf{B}(\beta, 0) \mathbf{P}_R)^{-1}, \end{aligned}$$

that we must compute is independent of the imaginary time τ at which we perform our Metropolis updates. The way we use this inverse to evaluate elements of the Green’s functions $\mathbf{G}(\tau, \tau) = \mathbf{1} - \mathbf{R}(\tau)(\mathbf{L}(\tau)\mathbf{R}(\tau))^{-1}\mathbf{L}(\tau)$, however, does depend on τ . Thus, when we move from one time to another, we must modify $\mathbf{L}(\tau)$ and $\mathbf{R}(\tau)$. For example, for $\tau' > \tau$,

$$\mathbf{L}(\tau') = \mathbf{L}(\tau)\mathbf{B}(\tau', \tau)^{-1}$$

and

$$\mathbf{R}(\tau') = \mathbf{B}(\tau', \tau)\mathbf{R}(\tau).$$

Modification of the left and right matrices $\mathbf{L}(\tau)$ and $\mathbf{R}(\tau)$ as we move from one value of τ to another, then, involves moving factors of \mathbf{B} from the left side of \mathbf{R} to the right side of \mathbf{L} or vice versa. This can be achieved by one of two means. In the first option, suitable for small changes in τ , we tack on factors of \mathbf{B} on the side by straightforward multiplication and delete these factors from the other side by multiplication of the corresponding inverses. From eq. (3.3) and the checkerboard breakup, we see that such multiplications are made up of factors \mathbf{A} and $\exp(\Delta\tau \mathbf{T})$ that are sparse and trivial to invert.

The second option, suitable for large changes in τ , eliminates a number of these multiplications. In such a case, as one builds up \mathbf{L} and \mathbf{R} from \mathbf{P}_L and \mathbf{P}_R , one stores partial products along the way. To string additional factors of \mathbf{B} onto one side requires the multiplications we just discussed. Deletion of such factors from the other side, however, is performed more trivially by recalling a previously stored partial product. For example, in fig. 3a, the partial products \mathbf{P}_L , $\mathbf{L}(\beta - \tau_0), \dots, \mathbf{L}(\tau + \tau_0)$, and $\mathbf{L}(\tau)$, generated in the computation of $\mathbf{L}(\tau)$ are stored, as are the by-products \mathbf{P}_R , $\mathbf{R}(\tau_0)$, $\mathbf{R}(2\tau_0), \dots, \mathbf{R}(\tau)$ of the $\mathbf{R}(\tau)$ computation. To move from τ to a fairly distant imaginary time $\tau + \tau_0$, we need the factors $\mathbf{L}(\tau + \tau_0)$ and $\mathbf{R}(\tau + \tau_0)$. The right factor $\mathbf{R}(\tau + \tau_0) = \mathbf{B}(\tau + \tau_0, \tau)\mathbf{R}(\tau)$ is easily computed by successively multiplying by $\mathbf{B}(\tau + \tau_0, \tau)$, a series of sparse

$$\begin{array}{ccccccccc}
 \mathbf{L}(\beta) = \mathbf{P}_L & \mathbf{L}(\beta - \tau_0) & \dots & \mathbf{L}(\tau + \tau_0) & \mathbf{L}(\tau) & \mathbf{R}(\tau) & \dots & \mathbf{R}(2\tau_0) & \mathbf{R}(\tau_0) & \mathbf{R}(0) = \mathbf{P}_R \\
 \Downarrow & \Downarrow & \dots & \Downarrow & \Downarrow & \Downarrow & \dots & \Downarrow & \Downarrow & \Downarrow \\
 \mathbf{L}(\beta) = \mathbf{P}_L & \mathbf{L}(\beta - \tau_0) & \dots & \mathbf{L}(\tau + \tau_0) & \mathbf{R}(\tau + \tau_0) & \mathbf{R}(\tau) & \dots & \mathbf{R}(2\tau_0) & \mathbf{R}(\tau_0) & \mathbf{R}(0) = \mathbf{P}_R
 \end{array}$$

Fig. 3. Computer storage scheme. As one builds up $\mathbf{L}(\tau)$ and $\mathbf{R}(\tau)$, needed for updating at time τ , one stores the intermediate partial products $\mathbf{P}_L, \dots, \mathbf{L}(\tau)$ and $\mathbf{P}_R, \dots, \mathbf{R}(\tau)$, as in (a). When one moves to imaginary time $\tau + \tau_0$, $\mathbf{L}(\tau + \tau_0)$ is already available as a previously stored partial product. Further, $\mathbf{R}(\tau + \tau_0)$ is easily computed from $\mathbf{R}(\tau)$ and may be stored in lieu of $\mathbf{L}(\tau)$, which is no longer needed, as in (b).

matrices, with the partial product $\mathbf{R}(\tau)$, which of course is already available. The left factor $\mathbf{L}(\tau + \tau_0)$ has already been stored in a previous calculation. At $\tau + \tau_0$, matrices are stored as in fig. 3b.

Storing partial products in this manner has the added advantage that roundoff errors will not accumulate from the repeated adding-on of factors and the subsequent deletion by inverse multiplication. As we will discuss, difficulties from roundoff errors can be devastating. In practice, we sweep over all times τ , through a combination of coarse and fine movements in imaginary time, using both of the previous approaches.

For the finite-temperature approach, we advance to a later imaginary time $\tau' > \tau$ by writing the Green's function as

$$\begin{aligned}
 \mathbf{G}(\tau', \tau') &= (\mathbf{1} + \mathbf{B}(\tau', 0)\mathbf{B}(\beta, \tau'))^{-1} \\
 &= (\mathbf{1} + \mathbf{B}(\tau', \tau)\mathbf{B}(\tau, 0)\mathbf{B}(\beta, \tau)\mathbf{B}(\tau', \tau)^{-1})^{-1} \\
 &= \mathbf{B}(\tau', \tau)\mathbf{G}(\tau, \tau)\mathbf{B}(\tau', \tau)^{-1}.
 \end{aligned} \tag{3.18}$$

Of course, $\mathbf{B}(\tau', \tau) = \mathbf{B}(\tau', \tau - \Delta\tau) \cdots \mathbf{B}(\tau + \Delta\tau, \tau)$. In eq. (3.18), we are simply taking factors of $\mathbf{B}(\tau + \Delta\tau, \tau)$ off the right side of \mathbf{G} (by inverse multiplication) and “wrapping” them onto the left side. It is this picture that we describe as “wrapping” matrices around the Green's functions. Naturally, to go from larger imaginary times to smaller ones, we simply wrap matrices in the opposite direction. As before, multiplication by \mathbf{B} matrices and inverse multiplication by \mathbf{B}^{-1} matrices is straightforward and relatively fast, since the components of the \mathbf{B} 's are either diagonal or they are easy to approximate with the checkerboard breakup. Of course, we may also choose to compute and store partial products of $\mathbf{B}(\beta, \tau)$ and $\mathbf{B}(\tau, 0)$ in a way similar to that in the zero-temperature case.

3.8. Measurement estimators

Physical measurements of electronic properties appear in analytical calculations and in numerical simulations as expectation values of products of fermion creation and annihilation operators. In this section, we discuss several practical points as to how to measure such expectation values in simulations.

In simulations, as in analytical calculations, Wick's Theorem is used to convert expectation values of products of operators into sums of products of expectation values of all possible pair-wise contractions of creation and annihilation operators. The expectation values of these contractions are elements of the Green's functions, which must be calculated and maintained for updating field variables. (In the zero-temperature formalism, we maintain the inverse $(\mathbf{L}^* \mathbf{R}^*)^{-1}$, from which elements of the Green's functions are readily calculated.) Thus, Wick's Theorem expresses results of measurements in terms of the central objects of a simulation.

As an example, consider the z -component of the antiferromagnetic structure factor

$$S(\pi, \pi) = \frac{1}{N} \sum_{ij} (-)^{i-j} \langle (n_{i\uparrow} - n_{i\downarrow})(n_{j\uparrow} - n_{j\downarrow}) \rangle, \quad (3.19)$$

where N is the number of sites on the lattice, $n_{i\sigma}$ is the number of electrons with spin σ on site i , and $(-)^{i-j}$ is $+1$ if i and j are on the same sublattice, but -1 if they are not. We estimate S in eq. (3.19) by averaging measurements over N_m different samples of the bosonic field variables, where N_m is sufficiently large so that we can gather good statistics. Thus,

$$\begin{aligned} S(\pi, \pi) &= \frac{1}{N_m} \sum_{\{x\}} \frac{1}{N} \sum_{ij} (-)^{i-j} (\langle n_{i\uparrow} n_{j\uparrow} \rangle_x + \langle n_{i\downarrow} n_{j\downarrow} \rangle_x \\ &\quad - \langle n_{i\uparrow} n_{j\downarrow} \rangle_x - \langle n_{i\downarrow} n_{j\uparrow} \rangle_x), \end{aligned} \quad (3.20)$$

where the expectation values $\langle \rangle_x$ are now for specific configurations of field variables $\{x\}$. For any such configuration, the electrons are completely decoupled from each other, which allows us to apply Wick's Theorem. Since the Hubbard–Stratonovich transformation block diagonalizes the problem in electron spin, contractions $\langle c_{i\sigma}^\dagger c_{j-\sigma} \rangle_x$ between operators of different spins are necessarily zero. Hence, the cross products

$$\langle n_{i\sigma} n_{j-\sigma} \rangle_x = \langle n_{i\sigma} \rangle_x \langle n_{j-\sigma} \rangle_x = (1 - G_{ii}^\sigma)(1 - G_{jj}^{-\sigma})$$

in eq. (3.20) decouple nicely. In contrast, products in eq. (3.20) of like-spin factors produce more nonzero contractions:

$$\begin{aligned} \langle c_{i\sigma}^\dagger c_{i\sigma} c_{j\sigma}^\dagger c_{j\sigma} \rangle_x &= \langle c_{i\sigma}^\dagger c_{i\sigma} \rangle_x \langle c_{j\sigma}^\dagger c_{j\sigma} \rangle_x + \langle c_{i\sigma}^\dagger c_{j\sigma} \rangle_x \langle c_{i\sigma} c_{j\sigma}^\dagger \rangle_x \\ &= (1 - G_{ii}^\sigma)(1 - G_{jj}^\sigma) + (\Delta_{ij} - G_{ji}^\sigma)G_{ij}^\sigma, \end{aligned} \quad (3.21)$$

where Δ_{ij} is the Kronecker delta function, which we use in reordering operators in the form required by our definition of the Green's function. Notice that in the case $i = j$, eq. (3.21) reduces to $(1 - G_{ii}^\sigma)$, which we would expect for $\langle n_{i\sigma} n_{i\sigma} \rangle_x = \langle n_{i\sigma} \rangle_x$.

Using Wick's Theorem, any electronic observable is easily reduced to averages of combinations of Green's function elements. Accordingly, the measurement process is straightforward in principle. There are several observations and points, however, that are useful to discuss.

In stochastic simulations, long computer runs are needed to collect many measurements and so reduce the statistical error. When the time that is needed to generate independent statistical samples is relatively large, it is necessary to gather as much data as possible from each sample. Thus, symmetries of the Hamiltonian are often exploited to construct many estimators of the same quantity. For example, to estimate the bond charge (kinetic energy)

$$\langle c_i^\dagger c_{i+\hat{a}} \rangle,$$

we may average measurements of

$$\langle c_{i\sigma}^\dagger(\tau) c_{i+\hat{a}\sigma}(\tau) \rangle$$

over many values of lattice position i , electronic spin σ , spatial neighbors \hat{a} , and, in the case of the finite-temperature formalism which is periodic in τ , imaginary time τ . Due to fluctuations in the bosonic field variables $\{x\}$, individual configurations will not obey the symmetries of the Hamiltonian. Averages of measurements over many configurations will.

On the other hand, there may well be features in a simulation that break symmetry artificially. For example, in the Hubbard model, the staggered magnetization

$$M_{(\pi,\pi)}^z = \sum_i (-)^i (c_{i\uparrow}^\dagger - c_{i\downarrow}^\dagger) \sigma^z \begin{pmatrix} c_{i\uparrow} \\ c_{i\downarrow} \end{pmatrix},$$

is rotationally invariant, σ^z being the Pauli spin matrices. Due to the symmetry breaking of the Hubbard–Stratonovich transformation, however, the longitudinal estimator

$$\frac{1}{N} \langle (M_{(\pi,\pi)}^z)^2 \rangle$$

produces much noisier estimates of the antiferromagnetic structure factor in finite-temperature simulations (Hirsch 1987) than the rotationally equivalent transverse estimator

$$\frac{1}{2N} \langle (M_{(\pi,\pi)}^x)^2 + (M_{(\pi,\pi)}^y)^2 \rangle.$$

In ground-state calculations, symmetries may be broken still further by the trial wavefunction $|\psi\rangle$ (Sorella et al. 1988). Thus, the symmetrized measurement

$$\frac{1}{3N} \langle (M_{(\pi,\pi)}^x)^2 + (M_{(\pi,\pi)}^y)^2 + (M_{(\pi,\pi)}^z)^2 \rangle$$

may provide very good estimates of the structure factor (3.19), while a surprisingly long imaginary time β may be required to project a symmetric ground state out of $|\psi\rangle$. In summary, while the true quantum-mechanical wavefunction may be the symmetric superposition of many symmetry-breaking contributions, any one sample in a numerical simulation will not be symmetric. Hence, symmetrized estimators often provide great improvements in performance.

While it may be advantageous to collect formally redundant measurements, there is an added computational cost associated with computing the extra averages. In addition, these extra measurements are correlated to some degree so that they may give little additional information and hence may not be worth the extra cost. In practice, then, one averages over only a limited set of estimators. Further, while the elements of the Green's functions are always available during the course of a simulation, one typically chooses to employ several updating sweeps through the space-time lattice between measurements, since successive configurations may well be correlated.

Simulations generate extremely long streams of measurements. By "binning" these streams – dividing the streams into bins of equal lengths and reporting bin averages instead of individual measurements – one can both reduce the volume of output and estimate the statistical uncertainties in the measurements. The length of the bins must be long compared to the correlation time of the simulation. Thus, while consecutive samples of the simulations are generally highly correlated, averages from successive bins may be treated as being statistically independent. If A_i are the bin averages for a certain observable A , then

$$\bar{A} = \frac{1}{N_{\text{bin}}} \sum_i A_i \quad (3.22)$$

is, of course, the estimate of the observable, while

$$\sigma(A) \approx \frac{1}{\sqrt{N_{\text{bin}} - 1}} \sigma(A_i) = \frac{1}{\sqrt{N_{\text{bin}} - 1}} \sqrt{\frac{\sum_i A_i^2}{N_{\text{bin}}} - \bar{A}^2} \quad (3.23)$$

is the statistical uncertainty in the estimate (3.22). Here, N_{bin} is the number of bins.

A typical Monte Carlo run may entail 10 to 20 bins of 250 to 500 measurements each, with two to five sweeps of the space-time lattice between measurements. The configuration of the system is generally initialized randomly, so that 500–1000 sweeps should be performed to equilibrate the system before measurements are made. Experimentation and individual standards are the final arbiters in deciding how to set these parameters. Since different physical observables generally have different statistical properties, run parameters will also depend on the quantities to be measured.

The errors associated with measurements reported will be due to both the nonzero discretization parameter $\Delta\tau$ and to statistical fluctuations. Our use of

path integrals requires us to study the limit $\Delta\tau \rightarrow 0$. In practice, measurements obey small- $\Delta\tau$ scaling laws (Suzuki 1985, Fye 1986, Fye and Scalettar 19xx) – in most cases, either as $\Delta\tau$ or as $\Delta\tau^2$ – for surprisingly large values of $\Delta\tau$. This is fortunate since the reduced number of degrees of freedom for large- $\Delta\tau$, coarsely discretized path integrals allows faster sweeps through the space–time lattice and more movement through phase space for each sweep. The size of statistical errors depends greatly on the quantity being measured. For several thousand sweeps, we would expect path-integral simulations to estimate the energy – generally the best-behaved observable – to fractions of one percent. In contrast, long-range observables, such as the antiferromagnetic structure factor, may well have up to 10% fluctuations for the same number of sweeps.

3.9. Minus signs

Importance sampling requires that the weights $p[x]$ all be positive definite so that they may be interpreted as probabilities. In case they are not, the weights governing the importance sampling should be the absolute values $|p[x]|$. The expectation value (2.22) becomes

$$\frac{\sum_{\{x\}} \langle A \rangle_x p[x]}{\sum_{\{x\}} p[x]} = \frac{\sum_{\{x\}} \langle A \rangle_x s[x] |p[x]|}{\sum_{\{x\}} s[x] |p[x]|} = \frac{\sum'_{\{x\}} \langle A \rangle_x s[x]}{\sum'_{\{x\}} s[x]}, \quad (3.24)$$

where $s[x]$ is the sign of $p[x]$ and the primed sums are over configurations $\{x\}$ generated according to the weights $|p[x]|$.

Of course, the “minus-sign” problem in simulations of fermions is that the numerator and denominator in eq. (3.24) can be much smaller than the statistical fluctuations in the measurement process. In such a case, the simulation is defeated. Further, “nodal surfaces” can possibly exist in $\{x\}$ -phase space, even if there is no sign problem. In eqs. (3.5) and (3.6), we see that each weight $p[x] = \prod_{\sigma} p^{\sigma}[x]$ is a product of $\sigma = \uparrow$ and \downarrow contributions. As long as the individual p^{σ} can change sign, phase space will be partitioned by “potential barriers” or “nodal surfaces”. If these surfaces coincide throughout phase space, however, the product $p[x]$ will have the same sign in every partition. This is in fact the case for the half-filled Hubbard model and the symmetric Anderson lattice.

4. Stabilization

As we have seen, the Green’s function, and not the partition function, is the central object of the simulations. It is needed to perform importance sampling and to make measurements. As one sweeps from one imaginary time τ to another, \mathbf{G} can be produced on the new time slice by “wrapping” matrices, as described in the previous section. Unfortunately, round-off errors accumulate in

this procedure, making it necessary occasionally to recompute the Green's function from scratch. The more serious difficulty is that at low temperatures, as β becomes large, the Green's function cannot be computed at all. The reason is that as many \mathbf{B} matrices are multiplied together, the product becomes more and more ill-conditioned, with exponentially divergent numerical scales. In calculating the Slater determinants in eqs. (3.5) and (3.6), one computes small differences of large matrix elements. These differences are very inaccurate, dominated by the noise in the least significant bits of the matrix elements when the calculations are performed on finite-precision computers.

More physically, the single-particle propagator \mathbf{B} amplifies “low-energy” states for any particular configuration of the bosonic fields while attenuating the “high-energy” states. In addition, the states near some intermediate “Fermi energy”, buried exponentially by the states at the bottom of the “band”, describe the important physical phenomena in fermionic systems. Although this correspondence to a single-particle band picture is loose – our strongly correlated systems are actually sums over *many* single-particle, time-varying problems – the fact remains that the fermionic behavior of a model gets “drowned” by other large numerical scales. Conventional simulations ultimately fail simply because these important small-scale features cannot be extracted from $\mathbf{B}(\beta, \tau)$ and $\mathbf{B}(\tau, 0)$ using computers with finite precision.

The sparse matrices (3.3), which make up \mathbf{B} , can be represented with high precision on a finite-precision computer. Likewise the matrix elements of the Green's function can also be represented, since these elements are generally well-behaved numbers. It is only the intermediate products in the calculation of \mathbf{G} , the single-particle propagator for large imaginary times, that are difficult to represent on finite-precision machines without loss of important information. It is our task, then, to organize the calculation of \mathbf{G} such that no essential information is lost.

Several recent efforts (White et al. 1988, Hirsch 1988) at low-temperature stabilization use matrices of higher dimensions, at a substantial cost of computer time and memory. In this section, we describe even more recent developments (Loh Jr et al. 1989) in efficiently stabilizing the computation of the matrix products and the matrix inversions needed to get the Green's function. There are two keys to this approach. First, in forming matrix products, small scales are maintained explicitly, rather than implicitly as small differences of large numbers. Second, the varied numerical scales are combined only at the last step in the calculation of the Green's function, using some scales to cut off smaller, inconsequential scales. Resorting, once again, to a band picture, the numerical scale associated with a single-particle state of energy E relative to the chemical potential μ is $\exp(-\beta(E - \mu))$, which diverges or vanishes exponentially with β . On the other hand, the occupation of that state, a Green's function element, is $1/(\exp(\beta(E - \mu)) + 1)$, which ranges between 0 and 1. More generally, if we are able to keep the numerical scales $\exp(\beta(E - \mu))$ separated, we will be able to cut

off the ill-behaved scales in the final step in calculating \mathbf{G} by adding terms of unit scale.

We will begin this section by discussing the stable multiplication of matrices. Then we will discuss various ways of cutting off the large and small scales to compute the Green's function for a variety of simulation applications.

4.1. Stable matrix multiplication

The *condition number* of a matrix is roughly the ratio of the largest singular value of the matrix to the smallest one and represents an upper bound to be amplification of errors in matrix multiplications. Our aim is to decompose ill-conditioned matrices by representing them in the form \mathbf{UDV} , where the diagonal matrix \mathbf{D} contains the diverging singular values explicitly and has the large condition number, but where \mathbf{U} and \mathbf{V} are “sufficiently well-conditioned”, a property which will be made more precise later. If we choose both \mathbf{U} and \mathbf{V} to be orthogonal, the resulting decomposition is the singular-value decomposition (SVD), which is known to be very stable in performance. Unfortunately, the inner loops of SVD subroutines have vanishingly small lengths and so perform slowly on vector computers. In practice, the modified Gram–Schmidt (MGS) factorization \mathbf{UDV} , where \mathbf{U} is orthogonal and \mathbf{D} is diagonal, but \mathbf{V} is unit triangular, is preferable. The computation time for an MGS decomposition is, in some cases, up to 20 times less than that for SVD. Fortunately, unit-triangular matrices are sufficiently well-conditioned, so that large numbers of them can be multiplied in simulations without destroying stability.

To understand what we gain in decomposing an ill-conditioned matrix into such a \mathbf{UDV} factorized form, consider the schematic multiplication

$$\begin{aligned} \mathbf{UDV} &= \begin{pmatrix} x & x & x & x \\ x & x & x & x \\ x & x & x & x \\ x & x & x & x \end{pmatrix} \begin{pmatrix} X & & & \\ & X & & \\ & & X & \\ & & & X \end{pmatrix} \begin{pmatrix} x & x & x & x \\ x & x & x & x \\ x & x & x & x \\ x & x & x & x \end{pmatrix} \\ &= \begin{pmatrix} X & X & X & X \\ X & X & X & X \\ X & X & X & X \\ X & X & X & X \end{pmatrix}. \end{aligned}$$

Here, \mathbf{U} and \mathbf{V} are sketched as having only matrix elements of unit scale, while \mathbf{D} has elements of many scales, which we have pivoted into descending order. Notice that once the multiplication has been performed, all of the elements of the product matrix are of the largest scale. The product is, essentially, an outer product of the first column of \mathbf{U} and the first row of \mathbf{V} . The smallest numerical

scales exist only implicitly, as small differences of large matrix elements, and they can never be recovered on a computer of finite precision.

In contrast, a matrix which displays its small scales explicitly can be factorized stably. Consider, for example, the factorization of a column-stratified matrix \mathbf{M} :

$$\begin{aligned}\mathbf{U}^{-1}\mathbf{M}\mathbf{V}^{-1} &= \begin{pmatrix} x & x & x & x \\ x & x & x & x \\ x & x & x & x \\ x & x & x & x \end{pmatrix} \begin{pmatrix} X & X & X & X \\ X & X & X & X \\ X & X & X & X \\ X & X & X & X \end{pmatrix} \begin{pmatrix} x & x & x & x \\ x & x & x & x \\ x & x & x & x \\ x & x & x & x \end{pmatrix} \\ &= \begin{pmatrix} X & & & \\ & X & & \\ & & X & \\ & & & X \end{pmatrix} = \mathbf{D}.\end{aligned}$$

Multiplication on the left of \mathbf{M} by a transformation matrix only combines elements within a given column – elements of the same scale – and so causes no loss of information. Multiplication on the right by \mathbf{V}^{-1} combines columns of different scales. This multiplication, however, does not overwrite any small-scale information so long as large-scale columns are scaled down appropriately before they are added into columns of smaller scale. Such factorization is in fact possible for both the SVD and MGS decompositions.

To compute the product of many matrices stably, we decouple the various scales present throughout the calculation. To illustrate this, we first imagine we have decomposed some partial product $\mathbf{B}(\tau, 0) = \mathbf{UDV}$. To extend the single-particle propagator to imaginary time $\tau + \tau_0$, we write

$$\begin{aligned}\mathbf{B}(\tau + \tau_0, 0) &= \mathbf{B}(\tau + \tau_0, \tau)\mathbf{UDV} = (\mathbf{B}(\tau + \tau_0, \tau)\mathbf{UD})\mathbf{V} \\ &= \left(\mathbf{B}(\tau + \tau_0, \tau)\mathbf{U} \begin{pmatrix} X & & & \\ & X & & \\ & & X & \\ & & & X \end{pmatrix} \right) \mathbf{V} \\ &= \begin{pmatrix} X & X & X & x \\ X & X & X & x \\ X & X & X & x \\ X & X & X & x \end{pmatrix} \mathbf{V} \\ &= (\mathbf{U}'\mathbf{D}'\mathbf{V}')\mathbf{V} = \mathbf{U}'\mathbf{D}'(\mathbf{V}'\mathbf{V}),\end{aligned}\tag{4.1}$$

giving the decomposition of the new partial product $\mathbf{B}(\tau + \tau_0, 0)$. Here, τ_0 is the length of imaginary time for which the single-particle propagator can be

extended without swamping the machine precision. We have decomposed the stratified matrix $\mathbf{B}(\tau + \tau_0, \tau)\mathbf{UD}$ into $\mathbf{U}'\mathbf{D}'\mathbf{V}'$. The \mathbf{V} matrices must be sufficiently well-conditioned in order that we can multiply many of them together stably; we can do this for both orthogonal (for SVD) and unit-triangular (for MGS) \mathbf{V} matrices. The product $\mathbf{B}(\tau + \tau_0, \tau)\mathbf{U}$ is formed as a series of sparse-matrix multiplications (3.3) on \mathbf{U} .

Gram–Schmidt orthogonalization has long been used to stabilize matrix products (Wilkinson 1965). In the calculation of characteristic Lyapunov exponents from time series, transformations are linearized and represented as matrices at each time step. The stable computation of a long product of many such matrices is often carried out by decomposing partial products (Benettin and Galgani 1979, Shimada and Nagashima 1979). MacKinnon and Kramer (1983) have used orthogonalization in the scaling theory of electrons in disordered solids. Sugiyama and Koonin (1986) first proposed limited applications of these techniques to Monte Carlo simulations of fermions. Only recently (Loh Jr et al. 1989), have decomposition techniques been applied widely, and in a greater variety of contexts, to fermionic simulations. We will now describe how to use decomposed forms of the single-particle propagator to simulations of fermions.

4.2. Zero-temperature studies

Sugiyama and Koonin (1986) first used matrix-decomposition techniques in fermion Monte Carlo for equal-time measurements in a zero-temperature context. Recently, Sorella et al. (1989) used this stabilized approach with a Langevin updating of the auxiliary fields.

In the zero-temperature approach, the Green's function (3.9) is

$$\mathbf{G}^\sigma(\tau, \tau) = \mathbf{1} - \mathbf{R}^\sigma(\tau)(\mathbf{L}^\sigma(\tau)\mathbf{R}^\sigma(\tau))^{-1}\mathbf{L}^\sigma(\tau).$$

The factorized forms for the \mathbf{L} and \mathbf{R} matrices are

$$\mathbf{L}^\sigma = \mathbf{V}_L^\sigma \mathbf{D}_L^\sigma \mathbf{U}_L^\sigma, \quad \mathbf{R}^\sigma = \mathbf{U}_R^\sigma \mathbf{D}_R^\sigma \mathbf{V}_R^\sigma,$$

where the order of the \mathbf{U} , \mathbf{D} , and \mathbf{V} matrices has been reversed for $\mathbf{L}^\sigma = \mathbf{P}_L^\sigma \mathbf{B}^\sigma(\beta, \tau)$ since the product is built up on the right side, instead of on the left side as in eq. (4.1). In the zero-temperature, canonical (fixed-number) approach, \mathbf{L}^σ (\mathbf{R}^σ) are $N_\sigma \times N$ ($N \times N_\sigma$) rectangular matrices, where the \mathbf{U}_L^σ (\mathbf{U}_R^σ) are also $N_\sigma \times N$ ($N \times N_\sigma$) rectangular matrices, while the \mathbf{D}_L^σ (\mathbf{D}_R^σ) and \mathbf{V}_L^σ (\mathbf{V}_R^σ) are “small” $N_\sigma \times N_\sigma$ square matrices. Using the factorized forms in the expression for the Green's function, we find that

$$\begin{aligned} \mathbf{G}^\sigma &= \mathbf{1} - (\mathbf{U}_R^\sigma \mathbf{D}_R^\sigma \mathbf{V}_R^\sigma)((\mathbf{V}_L^\sigma \mathbf{D}_L^\sigma \mathbf{U}_L^\sigma)(\mathbf{U}_R^\sigma \mathbf{D}_R^\sigma \mathbf{V}_R^\sigma))^{-1}(\mathbf{V}_L^\sigma \mathbf{D}_L^\sigma \mathbf{U}_L^\sigma) \\ &= \mathbf{1} - \mathbf{U}_R^\sigma (\mathbf{U}_L^\sigma \mathbf{U}_R^\sigma)^{-1} \mathbf{U}_L^\sigma, \end{aligned}$$

i.e. the Green's function depends only on the rectangular \mathbf{U}_L^σ and \mathbf{U}_R^σ matrices but not at all on the square \mathbf{V}_L^σ , \mathbf{D}_L^σ , \mathbf{V}_R^σ , or \mathbf{D}_R^σ transformation matrices.

In zero-temperature simulations, then, we can stabilize the calculation by orthonormalizing the rows of \mathbf{L}^σ and the columns of \mathbf{R}^σ without ever keeping or manipulating the linear transformations which effect the orthonormalization.

4.3. Finite-temperature $\mathbf{G}(\tau, \tau)$: I

For finite-temperature simulations, however, we are not interested in the effect of the single-electron propagator \mathbf{B} on the preselected set of single-particle states represented in \mathbf{P}_L and \mathbf{P}_R . Rather, we trace over all possible states. Thus, the transformation matrices must be kept. Since only $\mathbf{G}(\tau, \tau)$ is needed to update the Hubbard–Stratonovich field variables, we will begin by examining the equal-time Green's function. Fortunately, there is a simple prescription for calculating the $\mathbf{G}^\sigma(\tau, \tau)$ that can be added as a module to stabilize standard BSS codes.

The equal-time Green's function (3.10) is

$$\mathbf{G}^\sigma(\tau, \tau) = (\mathbf{1} + \mathbf{B}(\tau, 0)\mathbf{B}(\beta, \tau))^{-1}. \quad (4.2)$$

We build up the decomposition for the product of sparse factors of which $\mathbf{B}(\tau, 0)\mathbf{B}(\beta, \tau)$ is composed in the manner suggested by eq. (4.1). Now the Green's function becomes

$$\begin{aligned} \mathbf{G} &= (\mathbf{1} + \mathbf{UDV})^{-1} = \mathbf{V}^{-1}(\mathbf{U}^{-1}\mathbf{V}^{-1} + \mathbf{D})^{-1}\mathbf{U}^{-1} \\ &= \mathbf{V}^{-1}(\mathbf{U}'\mathbf{D}'\mathbf{V}')^{-1}\mathbf{U}^{-1} = (\mathbf{V}'\mathbf{V})^{-1}(\mathbf{D}')^{-1}(\mathbf{U}\mathbf{U}')^{-1}. \end{aligned} \quad (4.3)$$

Once we have formed the sum $\mathbf{U}^{-1}\mathbf{V}^{-1} + \mathbf{D}$, we decompose it into $\mathbf{U}'\mathbf{D}'\mathbf{V}'$ and the remaining factors are easily inverted and combined in any order.

What we have done is to isolate the divergent scales in \mathbf{D} until they are combined with the unit elements of $\mathbf{U}^{-1}\mathbf{V}^{-1}$, which cut off these divergent scales much like the unit term cuts off $\exp(\beta(E - \mu))$ in the standard band picture.

In all, we define numerical stability in an operational fashion. While the implication all along has been that we do not lose information when the numerical scales of the problem are maintained explicitly, in fact, much information is lost. For example, if we multiply the inverse $(\mathbf{U}^{-1}\mathbf{V}^{-1} + \mathbf{D})^{-1}$ in eq. (4.3) by the original matrix $(\mathbf{U}^{-1}\mathbf{V}^{-1} + \mathbf{D})$, we would never recover the identity matrix – even if the original matrix and its computed inverse were both kept in decomposed form. Similarly, if we perform many operations, such as “wrapping”, on the “stably” computed Green's function, small errors that are present in our representation of the Green's function on any finite-precision machine – even if \mathbf{G} is kept in decomposed form – would accumulate until the errors became larger than the calculated matrix elements. Our operational definition of stability, then, is simply that we should be able to calculate matrix elements of the Green's function, the only object needed for the simulation importance sampling and measurement process, to several significant figures. The overwriting of small scales by unit numbers and of unit scales by big numbers in the

addition $\mathbf{U}^{-1}\mathbf{V}^{-1} + \mathbf{D}$ does not introduce any significant errors into the computation of the Green's function. Rather, this addition simply cuts off certain numerical scales. In a simple band picture, it is not important whether a state deep in the band is amplified by 10^{100} or by 10^{1000} – all that is important is that states deep in the band are filled. Similarly, it is not important whether high-energy states are attenuated by 10^{-100} or by 10^{-1000} – it only matters that such states are cut off. In our calculation of the Green's function, we generate the single-particle propagator in decomposed form, identifying the “transformation” matrices \mathbf{U} and \mathbf{V} , which describe the “single-particle” states for a given set of Hubbard–Stratonovich fields, and the scales \mathbf{D} associated with the different states. At this point, addition of $\mathbf{U}^{-1}\mathbf{V}^{-1}$ cuts off the divergent scales to identify which states have been amplified and which have been attenuated. It is for this reason that the overwriting of scales, which we have so tediously been avoiding, can be performed in this last step on $\mathbf{U}^{-1}\mathbf{V}^{-1} + \mathbf{D}$ without introducing any errors into the computation of Green's function. Indeed, in practice the exponentially divergent elements of \mathbf{D} cannot be stored on a computer of finite dynamic range and so we cut them off at, say, 10^{+100} and 10^{-100} . It is enough for us to know simply which scales are “big” and which are “small”.

Again, even while we are able to compute the matrix elements of the Green's function to reasonably high accuracy, we may “wrap” \mathbf{G} only for a short imaginary time – of the scale τ_0 , which was introduced in the discussion of eq. (4.1). Thus, \mathbf{G} must be recomputed from scratch from time to time. The number of times \mathbf{G} must be recomputed in one sweep of all time slices goes as β/τ_0 . The number of decompositions one must perform in each such recomputation also goes as β/τ_0 . Thus, the overhead associated with stabilizing the computation scales as $(\beta/\tau_0)^2$. While this scaling may dominate the computation at very low temperatures (large β) or for unstable problems on machines of small world lengths (small τ_0), we have found that for sets of problems – such as sufficiently low temperatures to study the ground state of a single-band Hubbard model on up to 16×16 lattices on a 64-bit machine – the stabilization overhead represents only a fraction of the running time.

4.4. Finite-temperature $\mathbf{G}(\tau, \tau)$: II

An alternative to the great deal of recomputation involved in re-evaluating eq. (4.3) for many different τ is to use computer memory to store partial products. Now, we imagine we have the decompositions of two partial products. Building up a partial product from the right, we define

$$\mathbf{B}(\tau, 0) = \mathbf{U}_R \mathbf{D}_R \mathbf{V}_R, \quad (4.4)$$

and building up the remaining factors from the left, we define

$$\mathbf{B}(\beta, \tau) = \mathbf{V}_L \mathbf{D}_L \mathbf{U}_L, \quad (4.5)$$

where the order of the factorization is reversed. In contrast with the zero-temperature case, all these matrices are square. Now, from eq. (4.2), we obtain

$$\begin{aligned}\mathbf{G}(\tau, \tau) &= (\mathbf{1} + \mathbf{U}_R \mathbf{D}_R \mathbf{V}_R \mathbf{V}_L \mathbf{D}_L \mathbf{U}_L)^{-1} \\ &= \mathbf{U}_L^{-1} (\mathbf{U}_R^{-1} \mathbf{U}_L^{-1} + \mathbf{D}_R \mathbf{V}_R \mathbf{V}_L \mathbf{D}_L)^{-1} \mathbf{U}_R^{-1}. \end{aligned}\quad (4.6)$$

Again, the inverse of the ill-conditioned sum can be stabilized by decomposing the sum and then inverting its individual pieces. Schematically, the piece to be inverted is

$$\begin{aligned}&\left(\begin{array}{cccc} x & x & x & x \\ x & x & x & x \\ x & x & x & x \\ x & x & x & x \end{array} \right) + \left(\begin{array}{cccc} X & & & \\ & X & & \\ & & X & \\ & & & X \end{array} \right) \left(\begin{array}{cccc} x & x & x & x \\ x & x & x & x \\ x & x & x & x \\ x & x & x & x \end{array} \right) \left(\begin{array}{cccc} X & & & \\ & X & & \\ & & X & \\ & & & X \end{array} \right) \\ &= \left(\begin{array}{cccc} x & x & x & x \\ x & x & x & x \\ x & x & x & x \\ x & x & x & x \end{array} \right) + \left(\begin{array}{cccc} XX & XX & XX & XX \\ XX & XX & XX & XX \\ xX & xX & XX & XX \\ xX & xX & xX & XX \end{array} \right). \end{aligned}$$

Because we have kept the diagonal matrices on the outsides of the terms, elements of different scales are added together only in the last step, to “cut off scales”, as before.

In building up the partial product $\mathbf{B}(\tau, 0)$, one may store the decompositions of the partial products $\mathbf{B}(\tau_0, 0)$, $\mathbf{B}(2\tau_0, 0)$, $\mathbf{B}(3\tau_0, 0)$, and so on. Thereafter, to move from some imaginary time τ to $\tau + \tau_0$, one must perform the appropriate series of sparse-matrix multiplications and another decomposition, as in eq. (4.1). To move from τ backward to $\tau - \tau_0$, on the other hand, one need only recall a previously stored partial product. This procedure is both faster and accumulates fewer roundoff errors than when applying and then stripping off factors with multiplication of matrices and then their inverses. Similarly, one may store the partial products $\mathbf{B}(\beta, \beta - \tau_0)$, $\mathbf{B}(\beta, \beta - 2\tau_0)$, $\mathbf{B}(\beta, \beta - 3\tau_0)$, and so on, in building up $\mathbf{B}(\beta, \tau)$. In all, storage of these partial products and utilization of eq. (4.6) brings the stabilization overhead down to scaling as (β/τ_0) . While it becomes necessary to store the decompositions of many partial products, the memory costs are affordable.

4.5. Unequal-time Green's function

Finally, while equal-time measurements can always be expressed in terms of averages of the equal-time Green's function $\mathbf{G}(\tau, \tau)$, application of Wick's

Theorem to time-dependent quantities such as susceptibilities

$$\chi(i\omega_n) = \int_0^\beta \langle \mathbf{A}^\dagger(\tau) \mathbf{A}(0) \rangle e^{i\omega_n \tau} d\tau$$

will generate contractions between fermion operators at different imaginary times. Thus, we will require matrix elements of the unequal-time Green's function

$$\mathbf{G}(\tau', \tau) = \mathbf{B}(\tau', \tau)(\mathbf{1} + \mathbf{B}(\tau, 0)\mathbf{B}(\beta, \tau))^{-1}.$$

For small changes $\tau' \rightarrow \tau''$ in the arguments of \mathbf{G} , multiplication by the single-particle propagator $\mathbf{B}(\tau'', \tau')$ produces the appropriate Green's function:

$$\mathbf{G}(\tau'', \tau) = \mathbf{B}(\tau'', \tau')\mathbf{G}(\tau', \tau).$$

As with “wrapping”, however, this procedure cannot propagate Green's functions for more than some imaginary time – again, roughly τ_0 . In this section, we describe two methods of stably forming

$$\mathbf{G}(\tau, 0) = \mathbf{B}(\tau, 0)(\mathbf{1} + \mathbf{B}(\beta, 0))^{-1} = (\mathbf{B}(\tau, 0)^{-1} + \mathbf{B}(\beta, \tau))^{-1}. \quad (4.7)$$

First, we can pattern our approach as closely as possible to eq. (4.3). Using the decompositions (4.4) and (4.5), we get

$$\mathbf{G}(\tau, 0) = (\mathbf{V}_R^{-1} \mathbf{D}_R^{-1} \mathbf{U}_R^{-1} + \mathbf{V}_L \mathbf{D}_L \mathbf{U}_L)^{-1}.$$

We then isolate the most ill-conditioned diagonal matrix. For example, if $\tau > \beta - \tau$, we write

$$\mathbf{G}(\tau, 0) = \mathbf{U}_R(\mathbf{D}_R^{-1} + \mathbf{V}_R \mathbf{V}_L \mathbf{D}_L \mathbf{U}_L \mathbf{U}_R)^{-1} \mathbf{V}_R = \mathbf{U}_R(\mathbf{U}' \mathbf{D}' \mathbf{V}')^{-1} \mathbf{V}_R, \quad (4.8)$$

proceeding somewhat as before. If, on the other hand, $\tau < \beta - \tau$, one would isolate \mathbf{D}_L . In preliminary tests, this decomposition has proven to behave surprisingly well, even in the case of $\tau \approx \beta - \tau$, where it is not clear which diagonal matrix to isolate.

Alternatively, we can arrange the factors in eq. (4.7) so that the two terms in the final, “cutoff” addition are stratified matrices with explicitly maintained small scales. We write

$$\mathbf{G}(\tau, 0) = \mathbf{U}_L^{-1}(\mathbf{P} \mathbf{D}_R^{-1} \mathbf{U}_R^{-1} \mathbf{U}_L^{-1} + \mathbf{P} \mathbf{V}_R \mathbf{V}_L \mathbf{D}_L)^{-1} \mathbf{P} \mathbf{V}_R. \quad (4.9)$$

Since we have been pivoting the largest singular values to the upper left-hand corner of the diagonal matrices, (4.9) includes a pivoting matrix

$$\mathbf{P} = \begin{pmatrix} & & & 1 \\ & \ddots & & \\ 1 & & & \end{pmatrix}$$

to order the elements of \mathbf{D}_R^{-1} in the same way. Schematically, the sum to be inverted in eq. (4.9) is

$$\begin{pmatrix} X & X & X & X \\ X & X & X & X \\ X & X & X & X \\ x & x & x & x \end{pmatrix}^+ \begin{pmatrix} X & X & X & x \\ X & X & X & x \\ X & X & X & x \\ X & X & X & x \end{pmatrix}.$$

Clearly, the small scales in the problem are kept explicitly until this addition, when we would expect that the cutting off of scales would not introduce any significant errors. Indeed, eq. (4.9) generally outperforms eq. (4.8) in tests of Green's function computation on finite-precision machines, calculating matrix elements of \mathbf{G} with errors one order of magnitude below those from eq. (4.8). Unfortunately, the algorithm also seems to fail occasionally. This is not currently understood.

5. Results for Hubbard models

The stabilization algorithms of the previous section have been tested in a variety of circumstances. As we noted in section 2, the massless Hubbard–Stratonovich fields are characterized predominantly by their fluctuations. Thus, a simple test of stability is to calculate the matrix elements of the Green's function in both single and double precision for random configurations of the auxiliary variables. The agreement between the elements from these two different calculations is typically at least to ten significant figures when the tests are performed on 64-bit computers. Further, Monte Carlo results on very small lattices (4 sites) can be compared to results from exact diagonalizations. Results for energies and ground-state correlation functions have been checked down to temperatures of $T = 0.01$ ($\beta = 100$), almost two orders of magnitude beyond the temperatures at which unstable calculations fail or the temperatures that are needed to project out the ground-state properties of this small system.

At the time this chapter was finished (March, 1989), work utilizing the recently developed stabilization techniques were just reaching the published literature. Here, we report some results for Hubbard models in two dimensions (White et al. 1989a, Scalettar et al. 1989, Scalettar et al. 1991). Simulations have been run on lattices up to 18×18 sites at reciprocal temperatures as high as $\beta = 32$. The Green's functions were never propagated very far ($\tau_0 \sim 0.5\text{--}1$) in imaginary time before the computation was restabilized. These results come from simulations using the discrete Hubbard–Stratonovich transformation and Monte Carlo updating with both the finite- and zero-temperature formulations. The longest runs needed the order of 10 hours on a CRAY X-MP computer.

5.1. Repulsive Hubbard model

The single-band, repulsive Hubbard model is the model most studied by quantum Monte Carlo methods. The bulk of these studies has occurred in the past two years in connection with various proposals regarding mechanisms for high-temperature superconductivity. These recent studies have confirmed the basic results of the original study by Hirsch (1987): at half filling, the model is antiferromagnetic and this antiferromagnetism rapidly diminishes as one dopes with electrons or holes to move away from half filling. The newer studies have also, quite naturally, focussed on calculations of various superconducting pairing correlation functions and susceptibilities over a range of dopings and on-site Coulomb interaction strengths. All calculations to date have shown that these measures of superconductivity are suppressed relative to their values when the Coulomb interaction is zero. Recently, other procedures for calculating attractive pairings have been suggested, but even with their use the superconducting state is yet to be seen (White et al. 1989b).

A traditional difficulty with simulations of fermions has been achieving sufficiently low temperatures to study the ground-state properties of a system. With the stabilized methods discussed in section 4, not only is it now numerically possible to go to extremely low temperatures, but the overhead associated with the stabilization is negligible. By computing with both the zero-temperature and finite-temperature algorithms, White et al. (1989a) have shown that by $\beta = 20$ the finite-temperature simulation measures ground-state properties. Because of the efficiency of these methods, computation time can be devoted to studies on increased lattice sizes rather than on stabilizing small-lattice calculations. For example, in fig. 4 the antiferromagnetic structure factor (3.19) is plotted against the reciprocal temperature β for various sizes of square lattices at

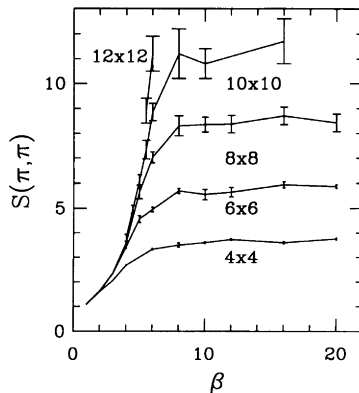


Fig. 4. The antiferromagnetic structure factor (3.19) as a function of reciprocal temperature β at $U = 4t$ for the repulsive Hubbard model in two dimensions (White et al. 1989a).

a coupling $U = 4t$, i.e. half of the bandwidth (White et al. 1989a). It is clear from this figure that there is no essential difficulty in going well below the temperature that is needed to isolate the ground state. At high temperatures (low β) there is little size dependence. At low temperatures, however, the structure factor is seen to diverge with lattice size. Fits of the data to finite-size corrections predicted from spin wave theory suggest long-range antiferromagnetism in the ground state (White et al. 1989a).

The original work of Hirsch (1987) was also the first to discuss and illustrate the existence of a severe sign problem in simulations of this model. White et al. (1989a) also measured the average sign, the denominator in eq. (3.24), as a function of doping at low temperatures. At half filling, a particle-hole symmetry ensures that $\langle s \rangle = 1$. At extreme fillings – either very few particles or very few holes – there are so few opportunities for exchange that the fermionic nature of the model becomes unimportant and the average sign is close to 1. What is surprising is that the determinants incorporate so much fermionic nature into the calculations of configuration weights (3.5) and (3.6) that the ‘‘low-density’’ value of $\langle s \rangle \approx 1$ holds even up to quarter filling. What is disconcerting is that the drop off of the sign as one moves away from half filling is extremely fast. It is unfortunate that so near half filling, where the possibility of superconductivity in a repulsive model exists, the simulations are the most difficult to perform.

5.2. Attractive Hubbard model

While no convincing explanation has yet been given for the pairing mechanism binding charge carriers in the novel high-temperature superconductors, the short coherence lengths in these materials have prompted many researchers to explore local, real-space pairing models. Neglecting the question as to what gives rise to the effective interaction, one can, nonetheless, assume a local, on-site attraction between fermions and study the resulting $U < 0$ Hubbard model.

In addition to its possible relevance to high T_c , the negative- U model in two dimensions is interesting in its own right, displaying curious phenomenology near half filling. Due to the high degree of symmetry ($O(3)$) at half filling, the model is expected to have no finite transition temperature. (At half filling, the model is isomorphic to the half-filled, repulsive Hubbard model, which belongs to the same universality class as the Heisenberg antiferromagnet and has long-range order only in the ground state.) Doping off of half filling in the negative- U model, however, reduces the symmetry of the ground state and gives rise to a finite, Kosterlitz–Thouless transition temperature (Scalettar et al. 1989).

In fig. 5, the number of singlet pairs in the pair condensate at zero temperature, normalized to the number of sites in the system, is plotted against the reciprocal of the linear size of the system for $U = -2$, -4 , and -8 at quarter filling on lattices of up to 18×18 sites (Scalettar et al. 1989). Again, finite-size corrections from spin wave theory predict a straight-line extrapolation of the

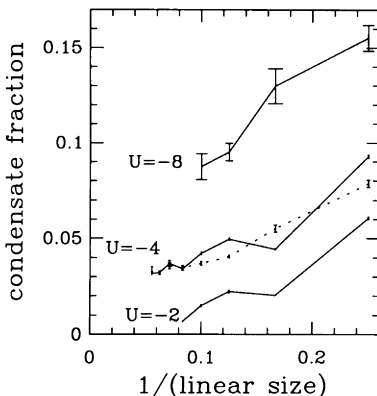


Fig. 5. Spin wave extrapolation of the ground-state fraction of singlet pairs in the pair condensate for the quarter-filled, two-dimensional, attractive Hubbard model (Scalettar et al. 1989). At weak coupling $U = -2$, finite-size modulations make extrapolations difficult. At a stronger coupling $U = -8$, error bars increase dramatically. The numerical simulation performs best at an intermediate coupling $U = -4$, for which analytical approaches are most limited. Data are shown for periodic boundary conditions (solid lines) and open boundaries (dotted line).

data to the infinite-system limit. Several features are apparent from the plot. First, at weak couplings $U = -2$ and -4 , the data have a fairly irregular dependence on lattice size. The reason for this is easy to deduce from the $U = 0$ limit. In this limit, the fermions no longer interact and the Hamiltonian is easily diagonalized in momentum space. The single-particle density of states in this limit is very sparse for finite-size lattices. In order to achieve a particular filling for a given lattice size, the Fermi energy must sometimes lie on a single-particle energy and sometimes between levels. Thus, the effective density of states at the Fermi surface varies widely. This irregular dependence on lattice size, of course, diminishes with N , as the interlevel spacing gets smaller, and with $|U|$, as the single-particle levels get mixed.

Due to these irregularities, it is impossible to extrapolate the $U = -2$ data to the thermodynamic limit. By the time $U = -4$, however, it is clear that a macroscopic fraction of the fermions are in the pair condensate. Increasing the magnitude of the electron-electron coupling to $U = -8$, the pairs become more defined and the macroscopic fraction grows. The irregularities with lattice size have, presumably, been damped out by the electronic correlations. Now, however, this is difficult to tell since the error bars have increased dramatically. From the discrete Hubbard-Stratonovich transformation (2.8), we see that the coupling α of the electrons to the fluctuating field grows with $|U|$. Thus, for weak couplings $U = -2$ and $U = -4$, the statistical errors associated with sampling only a finite number of field configurations are small. As we see from fig. 5, however, these fluctuations increase dramatically as one goes to the strong-coupling limit.

In short, simulations are difficult to perform in weak coupling, due to the severe lattice-size dependence, and also in strong coupling, due to the increasing statistical fluctuations. The parameter regime in which numerical simulations perform best is one that is difficult to study with analytical techniques.

In fig. 6, the charge-density-wave structure factor

$$\text{CDW}(q) = \frac{1}{N} \sum_{r_1 r_2} e^{iq \cdot (r_1 - r_2)} n_{r_1} n_{r_2} \quad (5.1)$$

is plotted as a function of wavenumber q for two-dimensional lattices of up to 18×18 sites for $U = -4$ (Scalettar et al. 1989). Other than for the smallest (4×4) lattice, results generally lie on top of one another for the different numbers of sites. While there is structure in the plot, the peaks do not diverge with lattice size. Thus, we characterize the system as a liquid, rather than as a solid. The peak in $\text{CDW}(q)$ at half filling is, of course, at $q = (\pi, \pi)$ due to the perfect nesting of the Fermi surface. At quarter filling, the peak occurs on the lines $q = (q_x, \pi)$ and $q = (\pi, q_y)$, as predicted in the RPA.

Consider a charge excitation

$$|\psi_q\rangle = \rho_q |\psi_0\rangle / \langle \psi_0 | \rho_{-q} \rho_q | \psi_0 \rangle^{1/2}$$

of wavenumber q , where

$$\rho_q = \frac{1}{N} \sum_r e^{iq \cdot r} n_r$$

and $|\psi_0\rangle$ is the ground state. Then the energy of the excitation is

$$\omega(q) = \langle \psi_q | H | \psi_q \rangle - \langle \psi_0 | H | \psi_0 \rangle = \frac{2}{3} \frac{E_0}{N} \left(1 - \frac{1}{4} \varepsilon_q \right) / \text{CDW}(q),$$

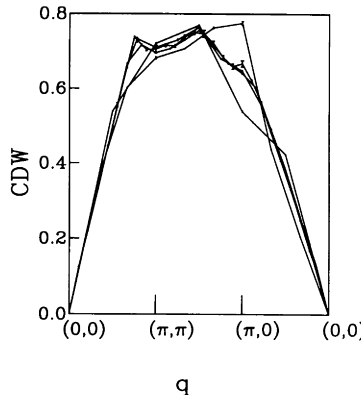


Fig. 6. The charge-density-wave structure factor (5.1) as a function of wave number q for quarter filled, two-dimensional, Hubbard lattices of up to 18×18 sites for $U = -4$ (Scalettar et al. 1989).

where (E_0/N) is the ground-state energy per site and $\varepsilon(q) = -2t(\cos q_x + \cos q_y)$. Thus, peaks in $\text{CDW}(q)$ can become dips in $\omega(q)$. The weak structure in fig. 6, however, is not strong enough to lead to a roton minimum in the excitation spectrum $\omega(q)$.

5.3. Copper-oxide clusters

Of course, more directly relevant to the high-temperature superconductors are multiband Hubbard models that have the structure of the CuO_2 planes. In the planes, each Cu site is surrounded by four nearest-neighbor O sites, while each O site has two nearest-neighbor Cu sites. While the debate over which orbitals of the Cu and O atoms are relevant – or even if the physics of the superconductivity is contained in the planes – continues, a great deal of attention remains focussed on the “Emery” model (Emery 1987) which considers only the $d_{x^2-y^2}$ Cu and p- σ bonding/antibonding O orbitals. The largest orbital overlap is between neighboring d- and p-orbitals and the largest Coulomb repulsion is the on-site Hubbard repulsion U_d . Thus, Scalettar et al. (1991) have studied

$$H = -t \sum_{\langle ij \rangle \sigma} (c_{i\sigma}^\dagger c_{j\sigma} + c_{j\sigma}^\dagger c_{i\sigma}) + \varepsilon \sum_j n_j + U_d \sum_i n_{i\uparrow} n_{i\downarrow}, \quad (5.2)$$

where the hopping sum is over nearest-neighbor Cu–O pairs, the site-energy sum is over O sites j , and the correlation sum is over Cu sites i . The creation and annihilation operators are actually for holes, with the reference “undoped” system having one hole per cell. We will choose $t = 1$, $\varepsilon = 1$, and $U_d = 4$, all energies nominally in eV.

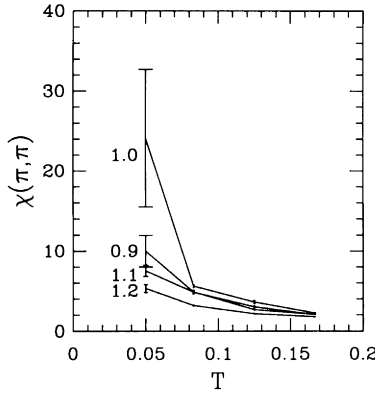


Fig. 7. The antiferromagnetic susceptibility $\chi(\pi, \pi)$ on the copper sublattice as a function of temperature for different lattice fillings on a two-dimensional CuO_2 cluster (Scalettar et al. 1991). Slight doping suppresses the antiferromagnetism.

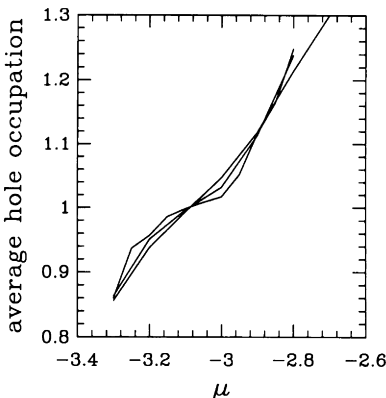


Fig. 8. The average number of holes per cell on the CuO_2 cluster as a function of the chemical potential μ for reciprocal temperatures $\beta = 12, 16, 20$ (Scalettar et al. 1991). As the temperature is lowered, a broad, flat plateau develops about the reference filling of 1 hole/cell.

In fig. 7, the antiferromagnetic susceptibility $\chi(\pi, \pi)$ on the copper sublattice is plotted as a function of temperature for different lattice fillings (Scalettar et al. 1991). The lattice is made up of 16 CuO_2 cells arranged in a 4×4 cluster. Thus, there are 48 sites in the system. This should be large enough to observe a bound-pair of holes since the coherence lengths in these systems are only several cell lengths. The effect of the site-energy difference is to place the holes predominantly on the Cu sites. Antiferromagnetic superexchange between Cu sites leads to the divergence in χ at low temperatures. Upon doping, however, itinerant holes wash out the staggered order. Figure 7 shows the low-temperature behavior of the antiferromagnetism as the doping is varied from 0.9, 1.0, 1.1, to 1.2 holes per unit cell.

In eq. (5.2), the filling of the lattice is controlled with a chemical potential term. In fig. 8, the average number of holes per cell is plotted as a function of the chemical potential μ for reciprocal temperatures $\beta = 12, 16, 20$ (Scalettar et al. 1991). As the temperature is lowered, a broad, flat plateau develops about the reference filling of 1 hole/cell. This is a clear signature of the stability of that filling.

6. Conclusion

In this chapter, we have briefly reviewed “determinantal” methods of simulating many-electron systems. In such methods, direct electronic interactions are replaced by couplings to auxiliary bosonic fields. Sums over the fermionic degrees of freedom are performed exactly for fixed configurations of the bosonic

fields. In contrast, sums over these fields are performed stochastically, using the determinantal weights to guide the importance sampling.

We have concentrated on providing a more heuristic exposition of the simulation formalism. Further, we have described recently developed methods for stabilizing the calculations at low temperatures.

Alternative stable algorithms do exist for specialized problems. The first approach is the world-line method for one-dimensional systems of interacting electrons (and quantum spin systems). This method has been reviewed by De Raedt and Lagendijk (1985). The second approach is the “impurity” algorithm of Hirsch and Fye (1986). In this approach, electrons interact on a small number N_i of impurity orbitals. The non-interacting part of the Hamiltonian is integrated out and the impurities may be regarded as being embedded in an infinite medium. Procedures exist for performing the updating (Hirsch and Fye 1986) and for restoring correlations between the impurities and the non-interacting degrees of freedom (Gubernatis 1987). Unfortunately, the updating process needs the elements of the Green’s function between all imaginary times instead of just the equal-time elements. Hence, the computing time scales as $(N_i \beta)^3$. For the one and two-impurity Anderson Hamiltonians, the method is stable and efficient. For a lattice of impurity sites, however, this approach is very expensive. Other algorithms (White et al. 1988, Hirsch 1988) have reduced the prefactor for many-impurity problems, but methods that stabilize simulations by expanding Green’s function matrices remain very costly.

In contrast, the overhead associated with explicitly maintaining essential small scales is modest. It is possible to stabilize a variety of simulation algorithms in this manner. Thus, one must choose a particular implementation. It appears that the Monte Carlo updating of discrete Hubbard–Stratonovich fields has the most desirable properties. Since the phase space of discrete fields is smaller than for continuous fields, the importance sampling is much more effective. The correlations (Buendia 1986, Lin and Hirsch 1986) and integration errors of Langevin and molecular-dynamics approaches make those methods less efficient and more difficult to implement well. Finally, Monte Carlo updating appears to be the most successful algorithm in crossing the “nodal barriers” which divide the bosonic-field phase space.

These efficient stabilization techniques have allowed relatively inexpensive explorations of the low-temperature phases of a variety of models of strongly correlated electrons. In most cases, it is no longer necessary to extrapolate to low temperatures. Rather, it is now possible simply to run at temperatures that are low enough to extract ground-state properties. Further, the overhead associated with the stabilization is only a small portion of the computational cost. Thus, low-temperature simulations (White et al. 1989a) of the two-dimensional Hubbard model can easily be realized at costs one order of magnitude below those previously possible (Tang and Hirsch 1988).

Nevertheless, important algorithmic difficulties remain in the numerical studies of fermions. Undoubtedly, the most important of these is the “minus-sign” problem. To date, this obstacle can really only be overcome by avoiding it. (Sorella et al. (1989) speculate that the sign problem can be ignored in the limit of zero temperature.) Hence, studies of the single-band Hubbard model are performed either for the $U < 0$ model or for the half-filled $U > 0$ model. Studies of the Anderson lattice are best limited to the symmetric case. These limitations can be extremely unfortunate. For example, the simplest explanation for high-temperature superconductivity would be the single-band Hubbard model. However, the validity of such a theory cannot be checked with numerical methods because it is just close to half filling, the only doping at which the repulsive Hubbard model could superconduct, that the sign problem is worst.

Large-scale simulations always benefit by faster algorithms. The most serious factor in limiting the speed of fermionic simulations is the dependence on lattice size. Determinantal methods scale as the cube of the number of lattice sites. The linear dependence of conjugate-gradient methods on N is highly attractive. Unfortunately, despite many attempts, such as “preconditioning”, at controlling of the number of conjugate-gradient iterations needed at low temperatures, these techniques tend to lose their desirable scaling properties.

Acknowledgements

We would like to thank D.J. Scalapino, R.T. Scalettar, R.L. Sugar, and S.R. White for many useful discussions and productive collaborations and D.K. Campbell and R. Gupta for reading the manuscript. This work was supported by the U.S. Department of Energy.

Appendix I. Extended electronic interactions

In section 2, we considered only on-site interactions between electrons. Here, we briefly consider the case of interactions

$$\sum_{ij} V_{ij} n_i n_j \tag{I.1}$$

extended to other sites as well.

The standard approach is to rewrite each term $-\Delta\tau V_{ij} n_i n_j$ as a perfect square, which may be eliminated with an auxiliary field, and an on-site repulsion. Then, the on-site repulsions may be collected and eliminated with eq. (2.8). Unfortunately, the introduction of a new field for each term further expands the phase space that must be explored, making efficient simulations more difficult.

As the range of the interaction is increased, this approach simply becomes intractable.

The alternative is to couple auxiliary fields not only to the local electronic degrees of freedom but also to bosonic fields on other orbitals. For example, generalizing the Hubbard–Stratonovich transformation, we can write (Negele and Orlando 1988)

$$\begin{aligned} \exp\left(\frac{1}{2}\mathbf{n}^T \mathbf{M} \mathbf{n}\right) &\sim \int d\mathbf{x} \exp\left(-\frac{1}{2}\mathbf{x}^T \mathbf{M}^{-1} \mathbf{x} + \mathbf{x}^T \mathbf{n}\right) \\ &\sim \int d\mathbf{y} \exp\left(-\frac{1}{2}\mathbf{y}^T \mathbf{M} \mathbf{y} + \mathbf{y}^T \mathbf{M} \mathbf{n}\right), \end{aligned} \quad (\text{I.2})$$

where $\mathbf{n}^T = (n_1, n_2, \dots)$ is a vector of electron occupation numbers in orbitals 1, 2, ..., N . All of the eigenvalues of \mathbf{M} must be positive in order that the integrals converge. In the first integral, the electronic charge \mathbf{n} couples only to the local bosonic field \mathbf{x} , while the field \mathbf{x} on each site couples to the field on each of the other sites through \mathbf{M}^{-1} . In the second integral, if \mathbf{M} has a limited-range interaction, then the boson–electron coupling $\mathbf{y}^T \mathbf{M} \mathbf{n}$ and boson–boson coupling $\mathbf{y}^T \mathbf{M} \mathbf{y}$ are also of limited-range.

For a general repulsive interaction, however, the left-hand side of (I.2) is $\exp(-\Delta\tau \mathbf{n}^T \mathbf{V} \mathbf{n})$ with $V_{ij} > 0$. To make the eigenvalues of $\frac{1}{2}\mathbf{M} = -\Delta\tau \mathbf{V}$ all positive in such cases, we must add an offset to the action. The contribution to the path integral from this generalized repulsion becomes

$$\begin{aligned} \exp\left(-\Delta\tau \sum_{ij} V_{ij} n_i n_j\right) &= \exp\left(\Delta\tau V_0 \sum_i n_i^2 - \Delta\tau \sum_{ij} V_{ij} n_i n_j\right) \\ &\times \exp\left(-\Delta\tau V_0 \sum_i n_i^2\right). \end{aligned} \quad (\text{I.3})$$

With the use of (I.2), the first factor in (I.3) may now be expressed in terms of a bosonic field whose components couple both to the local electronic charge density and to each other. The second factor may not be so treated as its “matrix” has only negative eigenvalues. This factor has the form of an on-site repulsion; as we have seen, it may be interpreted as resulting from a second intermediate field, whose components couple to the local electronic spin density but not to each other.

Again, we have engineered these transformations so that the auxiliary fields and the couplings are always real.

Appendix II. Bosonic world lines

In this appendix, we will continue the characterization of imaginary-time evolutions of bosonic field variables from section 2.

We first examine the relationship between the discrete [eq. (2.8)] and continuous [eq. (2.6)] transformations in the limit $\Delta\tau \rightarrow 0$, considering, as an example, the case $U > 0$. We average the external potential felt by the electrons over an imaginary time that is infinitesimally small and yet much larger than $\Delta\tau$. The coupling of the electrons to this locally time-averaged field is simply $\alpha x(n_\uparrow - n_\downarrow) \rightarrow \sqrt{\Delta\tau|U|}x(n_\uparrow - n_\downarrow)$, as $\Delta\tau \rightarrow 0$, where x is the averaged field. Phase space for the discrete field variables is uniform. Each such variable has zero mean and unit variance. A local time average x of many such fields, therefore, must have a Gaussian distribution $\exp(-x^2/2)/\sqrt{2\pi}$, from the central-limit theorem. Incorporating this weighting factor, we see that the elimination of high-frequency oscillations in the discrete field of (2.8) produces the continuous transformation (2.6). In the limit $\Delta\tau \rightarrow 0$, then, the discrete and continuous transformations are equivalent.

In section 2, we argued that the massless Hubbard–Stratonovich fields are essentially decoupled in time and that the time averages of such fields are necessarily of order $\sqrt{\Delta\tau}$, but that the electron–boson terms still enter the action to the same order in $\Delta\tau$ as the purely electronic terms, since the coupling to this weak average field is $1/\sqrt{\Delta\tau}$. We presented our case using fields that were generated by purely bosonic actions. Here, we justify our characterization of the massless fields rigorously.

We will examine discrete Hubbard–Stratonovich fields in the limit $\Delta\tau \rightarrow 0$. Further, we will work within the finite-temperature formalism. Our results remain valid within the zero-temperature formalism as well. The correlation of two distinct field variables is

$$\langle x(\tau)x(\tau') \rangle = \frac{\sum_{\{x\}} x(\tau)x(\tau') \text{Tr } \mathcal{T} \exp(-\int_0^\beta S(\tau) d\tau)}{\sum_{\{x\}} \text{Tr } \mathcal{T} \exp(-\int_0^\beta S(\tau) d\tau)}, \quad (\text{II.1})$$

where the trace is over fermionic degrees of freedom and $S(\tau)$ is the action of the electrons evolving through the time-varying Hubbard–Stratonovich fields $\{x\}$. The field variable $x(\tau)$ enters the numerator of (II.1) as

$$\begin{aligned} \sum_{x(\tau) = \pm 1} x(\tau) e^{-\Delta\tau S(\tau)} &= \sum_{x(\tau) = \pm 1} x(\tau) e^{\alpha x(\tau)s(\tau)} \\ &= \tanh(\alpha s(\tau)) \sum_{x(\tau) = \pm 1} e^{\alpha x(\tau)s(\tau)} \\ &= \tanh(\alpha s(\tau)) \sum_{x(\tau) = \pm 1} e^{-\Delta\tau S(\tau)}, \end{aligned}$$

where $s = n_\uparrow - n_\downarrow$ is the local electronic spin. Hence,

$$\langle x(\tau)x(\tau') \rangle = \langle \tanh(\alpha s(\tau)) \tanh(\alpha s(\tau')) \rangle \rightarrow \Delta\tau|U|\langle s(\tau)s(\tau') \rangle = \mathcal{O}(\Delta\tau)$$

as $\Delta\tau \rightarrow 0$. Further, if $\tau = \tau'$, then $\langle x^2 \rangle = \langle 1 \rangle = 1$. The correlation of two field variables, then, drops to order $\Delta\tau$ for even an infinitesimal separation in imaginary time. As a corollary, while field-variable correlations are related to physical measurements, the fluctuations in these quantities make them impractical estimators in simulations.

We can now calculate the characteristic size of the mean field $N_x^{-1} \sum_{\tau} x(\tau)$, averaged over, again, some infinitesimal imaginary time $N_x \Delta\tau$ that is large compared to $\Delta\tau$. The mean-square field is

$$\begin{aligned} \left\langle \left(\frac{1}{N_x} \sum_{\tau} x(\tau) \right)^2 \right\rangle &= \frac{1}{N_x^2} \sum_{\tau} \langle x(\tau)^2 \rangle + \frac{1}{N_x^2} \sum_{\tau \neq \tau'} \langle x(\tau) x(\tau') \rangle \\ &= \frac{1}{N_x} + \frac{1}{N_x^2} \sum_{\tau \neq \tau'} \Delta\tau |U| \langle s(\tau) s(\tau') \rangle = \mathcal{O}(\Delta\tau). \end{aligned}$$

Hence, the time-averaged field is of order $\sqrt{\Delta\tau}$, as in section 2.

Appendix III. Many-electron propagator

In this appendix, we examine the many-electron propagator (2.15). The many-electron propagator naturally takes the form of a determinant since the antisymmetry of electron exchange is automatically incorporated by the odd parity of the row or column exchange in determinantal evaluation.

The inner product of two N_{σ} -electron states is

$$\langle 0 | c_{i_1} c_{i_2} \cdots c_{i_{N_{\sigma}}} c_{j_{N_{\sigma}}}^{\dagger} \cdots c_{j_2}^{\dagger} c_{j_1}^{\dagger} | 0 \rangle = \det \begin{pmatrix} B_{i_1 j_1} & B_{i_1 j_2} & \dots & B_{i_1 j_{N_{\sigma}}} \\ B_{i_2 j_1} & B_{i_2 j_2} & \dots & B_{i_2 j_{N_{\sigma}}} \\ \vdots & \vdots & \ddots & \vdots \\ B_{i_{N_{\sigma}} j_1} & B_{i_{N_{\sigma}} j_2} & \dots & B_{i_{N_{\sigma}} j_{N_{\sigma}}} \end{pmatrix}, \quad (\text{III.1})$$

where the $B_{ij} = \langle 0 | c_i c_j^{\dagger} | 0 \rangle$ are the single-electron inner products. The proof proceeds easily via induction. Clearly, the result holds true for $N_{\sigma} = 1$. Assume eq. (III.1) holds for $N_{\sigma} - 1$. The anticommutation of electron operators gives

$$c_i c_j^{\dagger} = B_{ij} - c_j^{\dagger} c_i,$$

even if c_i and c_j^{\dagger} are expressed in different bases. In eq. (III.1), we may exchange fermion operators to bring $c_{i_{N_{\sigma}}}$ all the way over to the right side until it multiplies the vacuum state $|0\rangle$ directly, producing a null result. The nonzero

remainders of the electron exchanges give

$$\begin{aligned}
& \langle 0 | c_{i_1} c_{i_2} \cdots c_{i_{N_\sigma}} c_{j_{N_\sigma}}^\dagger \cdots c_{j_2}^\dagger c_{j_1}^\dagger | 0 \rangle \\
&= B_{i_{N_\sigma} j_{N_\sigma}} \langle 0 | c_{i_1} c_{i_2} \cdots c_{i_{N_\sigma-1}} c_{j_{N_\sigma-1}}^\dagger \cdots c_{j_2}^\dagger c_{j_1}^\dagger | 0 \rangle \\
&\quad - B_{i_{N_\sigma} j_{N_\sigma-1}} \langle 0 | c_{i_1} c_{i_2} \cdots c_{i_{N_\sigma-1}} c_{j_{N_\sigma-1}}^\dagger c_{j_{N_\sigma-2}}^\dagger \cdots c_{j_1}^\dagger | 0 \rangle \\
&\quad - B_{i_n j_{N_\sigma-2}} \langle 0 | c_{i_1} c_{i_2} \cdots c_{i_{N_\sigma-1}} c_{j_{N_\sigma}}^\dagger c_{j_{N_\sigma-1}}^\dagger c_{j_{N_\sigma-3}}^\dagger \cdots c_{j_1}^\dagger | 0 \rangle \\
&\quad + \cdots .
\end{aligned} \tag{III.2}$$

Expressing the $(N_\sigma - 1)$ -electron inner products as determinants, we see that eq. (III.2) is simply the cofactor expansion of the $N_\sigma \times N_\sigma$ determinant in eq. (III.1).

Now consider the imaginary-time propagation of a N_σ -electron state. We may expand the imaginary-time propagator as

$$\begin{aligned}
\mathcal{T} \exp \left(- \int_0^\beta S(\tau) d\tau \right) &= \exp(-\Delta\tau S(\beta)) \cdots \exp(-\Delta\tau S(2\Delta\tau)) \\
&\quad \times \exp(-\Delta\tau S(\Delta\tau))
\end{aligned}$$

in terms of piecewise-constant contributions $S(l\Delta\tau)$ in the limit $\Delta\tau \rightarrow 0$. With the quartic terms in the electron operators reduced by the Hubbard–Stratonovich transformations, the contributions $S(l\Delta\tau)$ are at most quadratic in c and c^\dagger . Further, we will require that each piece $S(l\Delta\tau)$ is Hermitian and number-conserving. (While each $\exp(-\Delta\tau S(l\Delta\tau))$ must be Hermitian, the product of many such factors need not.) Then, the imaginary-time propagator becomes

$$\begin{aligned}
\mathcal{T} \exp \left(- \int_0^\beta S(\tau) d\tau \right) &= \text{constant} \times \exp(-c^\dagger \mathbf{M}_{N_t} c) \cdots \exp(-c^\dagger \mathbf{M}_2 c) \\
&\quad \times \exp(-c^\dagger \mathbf{M}_1 c),
\end{aligned}$$

where we have written the creation and annihilation operators

$$c^\dagger = (c_1^\dagger \quad c_2^\dagger \quad \cdots \quad c_N^\dagger)$$

and

$$c = \begin{pmatrix} c_1 \\ c_2 \\ \vdots \\ c_N \end{pmatrix}$$

as vectors and the contributions to the action explicitly as number-conserving operators in matrix form.

Working in the basis in which \mathbf{M} is diagonal, we can easily prove that

$$e^{-c^\dagger \mathbf{M} c} c^\dagger = c^\dagger e^{-\mathbf{M}} e^{-c^\dagger \mathbf{M} c}. \tag{III.3}$$

Using (III.3) to propagate the N_σ -electron wavefunction

$$\begin{aligned} & (e^{-c^\dagger \mathbf{M}_{N_t} c} \cdots e^{-c^\dagger \mathbf{M}_1 c}) c^\dagger v_{j_{N_\sigma}} \cdots c^\dagger v_1 |0\rangle \\ &= (c^\dagger e^{-\mathbf{M}_{N_t}} \cdots e^{-\mathbf{M}_1} v_{j_{N_\sigma}}) \cdots (c^\dagger e^{-\mathbf{M}_{N_t}} \cdots e^{-\mathbf{M}_1} v_1) |0\rangle, \end{aligned}$$

we may invoke eq. (III.1) to prove eq. (2.15).

Appendix IV. Finite-temperature field weights

Here, we show that eq. (3.6) is the weight of a configuration of field variables $\{x\}$ within the finite-temperature formalism. For a fixed configuration of bosonic field variables, the electrons evolve through a time-dependent field described by $\{x\}$. The electrons are decoupled from each other, however, so that the weight can be expressed in terms of the single-electron propagator \mathbf{B} , which depends on $\{x\}$. We would like to show that the trace

$$p[x] = \text{Tr } \mathcal{T} \exp \left(- \int_0^\beta S(\tau) d\tau \right) \quad (\text{IV.1})$$

over electronic degrees of freedom is $\det(\mathbf{1} + \mathbf{B}(\beta, 0))$, where \mathbf{B} is given by eq. (2.12) and the action S depends on the configuration of the bosonic fields $\{x\}$. Here, we will consider electrons of only one particular spin σ since the generalization to electrons of many spins is trivial.

Here, we use the grand-canonical trace over all numbers N_σ of electrons. Since Pauli exclusion allows at most one electron per orbital, the number N_σ of electrons must fall in the range $0 \leq N_\sigma \leq N$, where N is the total number of orbitals. For each choice of N_σ , we must sum over the states

$$c_{i_{N_\sigma}}^\dagger \cdots c_{i_2}^\dagger c_{i_1}^\dagger |0\rangle,$$

where the sum over the $i_1, i_2, \dots, i_{N_\sigma}$ must be over all distinct subsets of the orbitals $1, 2, \dots, N$.

For a particular number N_σ of electrons and a particular subset $i_1, i_2, \dots, i_{N_\sigma}$ of orbitals, the contribution

$$\begin{aligned} & \langle 0 | c_{i_1} c_{i_2} \cdots c_{i_{N_\sigma}} \left(\mathcal{T} \exp \left(- \int_0^\beta S(\tau) d\tau \right) \right) c_{i_{N_\sigma}}^\dagger \cdots c_{i_2}^\dagger c_{i_1}^\dagger | 0 \rangle \\ &= \det \begin{pmatrix} B_{i_1 i_1}(\beta, 0) & B_{i_1 i_2}(\beta, 0) & \dots & B_{i_1 i_{N_\sigma}}(\beta, 0) \\ B_{i_2 i_1}(\beta, 0) & B_{i_2 i_2}(\beta, 0) & \dots & B_{i_2 i_{N_\sigma}}(\beta, 0) \\ \vdots & \vdots & \ddots & \vdots \\ B_{i_{N_\sigma} i_1}(\beta, 0) & B_{i_{N_\sigma} i_2}(\beta, 0) & \dots & B_{i_{N_\sigma} i_{N_\sigma}}(\beta, 0) \end{pmatrix} \end{aligned}$$

to the trace is given by eq. (2.15).

Further, the determinant

$$\det(\mathbf{1} + \mathbf{B}(\beta, 0)) = \det \begin{pmatrix} 1 + B_{11} & B_{12} & \dots & B_{1N} \\ B_{21} & 1 + B_{22} & \dots & B_{2N} \\ \vdots & \vdots & \ddots & \vdots \\ B_{N1} & B_{N2} & \dots & 1 + B_{NN} \end{pmatrix} \quad (\text{IV.2})$$

can be expanded as

$$\begin{aligned} & \det(1) \\ & + \det(B_{11}) + \det(B_{22}) + \dots + \det(B_{NN}) \\ & + \det \begin{pmatrix} B_{11} & B_{12} \\ B_{21} & B_{22} \end{pmatrix} + \det \begin{pmatrix} B_{11} & B_{13} \\ B_{31} & B_{33} \end{pmatrix} + \dots \\ & \quad + \det \begin{pmatrix} B_{N-1\ N-1} & B_{N-1\ N} \\ B_{N\ N-1} & B_{N\ N} \end{pmatrix} \\ & + \dots \\ & + \det \begin{pmatrix} B_{11} & B_{12} & \dots & B_{1N} \\ B_{21} & B_{22} & \dots & B_{2N} \\ \vdots & \vdots & \ddots & \vdots \\ B_{N1} & B_{N2} & \dots & B_{NN} \end{pmatrix} \end{aligned}$$

in terms of the number of factors of B . We can easily see that this sum is precisely the grand-canonical trace that we are trying to evaluate. The first term is the contribution from the vacuum state. The next line is made up of contributions from all single-electron states. The following line is made up of contributions from all two-electron states. The last term, finally, is the contribution from the N -electron state, which packs each orbital with an electron.

In the special case that the fields are time independent, the trace (IV.1) can be evaluated in terms of stationary states. Once again, writing the electron creation and annihilation operators as vectors, the time-independent Hamiltonian

$$H = -c^\dagger \mathbf{M} c = -c^\dagger (\mathbf{O}^\dagger \mathbf{D} \mathbf{O}) c = -d^\dagger \mathbf{D} d = -\sum_i D_{ii} d_i^\dagger d_i$$

may be diagonalized with the unitary transformation \mathbf{O} in terms of the stationary states $\mathbf{d} = \mathbf{O}c$ of the system. The grand-canonical trace

$$\begin{aligned} \text{Tr } e^{-\beta H} &= \text{Tr } \exp \left(\beta \sum_i D_{ii} d_i^\dagger d_i \right) = \prod_i \sum_{d_i^\dagger d_i = 0, 1} e^{\beta D_{ii} d_i^\dagger d_i} \\ &= \prod_i (1 + e^{\beta D_{ii}}) \end{aligned} \quad (\text{IV.3})$$

is easily found using the diagonalized form. The final expression is just the partition function for free electrons. Rewriting it in basis-invariant form, we find

$$\text{Tr } e^{-\beta H} = \det(\mathbf{1} + e^{\beta \mathbf{D}}) = \det(\mathbf{1} + e^{\beta \mathbf{M}}),$$

the time-independent form of (IV.2).

Appendix V. Determinants of different-size matrices

To produce eq. (3.13) from eq. (3.12), we used an identity

$$\det(\mathbf{1}_N + \mathbf{A}\mathbf{B}) = \det(\mathbf{1}_M + \mathbf{B}\mathbf{A}), \quad (\text{V.1})$$

where \mathbf{A} is an $N \times M$ rectangular matrix while \mathbf{B} is an $M \times N$ rectangular matrix. To highlight the fact that (V.1) relates determinants of matrices of different sizes, we have written the $N \times N$ unit matrix as $\mathbf{1}_N$ and the $M \times M$ unit matrix as $\mathbf{1}_M$.

To prove (V.1), let us simply prove that $f_N(\lambda) = f_M(\lambda)$, where

$$f_N(\lambda) = \det(\mathbf{1}_N + \lambda\mathbf{A}\mathbf{B})$$

and

$$f_M(\lambda) = \det(\mathbf{1}_M + \lambda\mathbf{B}\mathbf{A}).$$

It is clear that f_N and f_M are polynomials in λ of order at most N and M , respectively, and that $f_N(0) = f_M(0) = 1$. Expanding the logarithm of $f_N(\lambda)$ as a power series about $\lambda = 0$ and using the relation $\det(\mathbf{M}) = \exp(\text{Tr} \ln \mathbf{M})$, we find

$$\ln(f_N(\lambda)) = \text{Tr} \ln(\mathbf{1}_N + \lambda\mathbf{A}\mathbf{B}) = -\text{Tr} \sum_{n=1}^{\infty} \frac{(-\lambda\mathbf{A}\mathbf{B})^n}{n}.$$

Due to the cyclic nature of the trace, the order of \mathbf{A} and \mathbf{B} can be reversed. This gives the power-series expansion of $\ln(f_M(\lambda))$, proving the relationship between f_N and f_M .

References

- Barma, M., and B.S. Shastry, 1978, Phys. Rev. B **18**, 3351.
- Benettin, G., and L. Galgani, 1979, Lyapunov characteristic exponents and stochasticity, in: International Workshop on Intrinsic Stochasticity in Plasmas, June 17–23, Institut d'Etudes Scientifique de Cargese, Corse, France, eds G. Laval and D. Grésillon (Editions de Physique, Orsay).
- Binder, K., 1987, Monte Carlo Methods in Statistical Physics (Springer, Berlin).
- Blankenbecler, R., D.J. Scalapino and R.L. Sugar, 1981a, Phys. Rev. D **24**, 2278.
- Blankenbecler, R., D.J. Scalapino and R.L. Sugar, 1981b, Phys. Rev. B **24**, 4295.
- Buendia, G.M., 1986, Phys. Rev. B **33**, 3519.

- Creutz, M., and B. Freedman, 1981, Ann. Phys. **132**, 427.
- DeRaedt, H., and A. Lagendijk, 1985, Phys. Rep. **127**, 233.
- Emery, V.J., 1987, Phys. Rev. Lett. **58**, 2794.
- Evenson, W.E., J.R. Schrieffer and S.Q. Wang, 1970, J. Appl. Phys. **41**, 1199.
- Fetter, A.L., and J.D. Walecka, 1971, Quantum Theory of Many-Particle Systems (McGraw-Hill, New York).
- Feynman, R.P., and A.R. Hibbs, 1965, Quantum Mechanics and Path Integrals (McGraw-Hill, New York).
- Fye, R.M., 1986, Phys. Rev. B **33**, 6271.
- Fye, R.M., and R.T. Scalettar, 1987, Phys. Rev. B **37**, 3833.
- Gubernatis, J.E., 1987, in: Quantum Monte Carlo Methods, ed. M. Suzuki (Springer, Berlin) p. 216.
- Hamann, D.R., 1970, Phys. Rev. B **2**, 1373.
- Hassing, R.F., and D.M. Esterling, 1973, Phys. Rev. B **7**, 432.
- Hirsch, J., R.L. Sugar, D.J. Scalapino and R. Blankenbecler, 1982, Phys. Rev. B **26**, 5033.
- Hirsch, J.E., 1985, Phys. Rev. B **31**, 4403.
- Hirsch, J.E., 1987, Phys. Rev. B **35**, 1851.
- Hirsch, J.E., 1988, Phys. Rev. B **38**, 12023.
- Hirsch, J.E., and R.M. Fye, 1986, Phys. Rev. Lett. **56**, 2521.
- Hirsch, J.E., D.J. Scalapino, R.L. Sugar and R. Blankenbecler, 1981, Phys. Rev. Lett. **47**, 1628.
- Hubbard, J., 1959, Phys. Rev. Lett. **3**, 77.
- Lin, H.Q., and J.E. Hirsch, 1986, Phys. Rev. B **34**, 1964.
- Loh Jr, E.Y., 1988, Multigrid Monte Carlo methods, in: Computer Simulation Studies in Condensed Matter Physics; Recent Developments, eds D.P. Landau and H.B. Schüttler, Springer Proc. Phys. Vol. 3 (Springer, Berlin).
- Loh Jr, E.Y., J.E. Gubernatis, R.T. Scalettar, R.L. Sugar and S.R. White, 1989, Stable matrix-multiplication algorithms for the low-temperature numerical simulations of fermions, in: Interacting Electrons in Reduced Dimensions, eds D. Baeriswyl and D.K. Campbell (Plenum Press, New York).
- MacKinnon, A., and B. Kramer, 1983, Z. Phys. B **53**, 1.
- Metropolis, N., A.W. Rosenbluth, M.N. Rosenbluth, A.H. Teller and E. Teller, 1953, J. Chem. Phys. **21**, 1087.
- Negele, J.W., and H. Orlando, 1988, Quantum Many-Particle Systems (Addison-Wesley, Redwood City, CA).
- Press, W.H., B.P. Flannery, S.A. Teukolsky and W.T. Vetterling, 1988, Numerical Recipes: The Art of Scientific Computing (Cambridge University Press, Cambridge).
- Rice, J.R., 1983, Numerical Methods, Software and Analysis (McGraw-Hill, New York).
- Scalapino, D.J., and R.L. Sugar, 1981, Phys. Rev. Lett. **46**, 519.
- Scalettar, R.T., 1989, Physica C **162-164**, 313.
- Scalettar, R.T., D.J. Scalapino, R.L. Sugar and D. Toussaint, 1987, Phys. Rev. B **36**, 8632.
- Scalettar, R.T., E.Y. Loh Jr, J.E. Gubernatis, A. Moreo, S.R. White, D.J. Scalapino, R.L. Sugar and E. Dagotto, 1989, Phys. Rev. Lett. **62**, 1407.
- Scalettar, R.T., S.R. White, D.J. Scalapino and R.L. Sugar, 1991, Phys. Rev. B, to be published.
- Shimada, I., and T. Nagashima, 1979, Prog. Theor. Phys. **61**, 1605.
- Sorella, S., E. Tosatti, S. Baroni, R. Car and M. Parrinello, 1988, Int. J. Mod. Phys. B **1**, 993.
- Sorella, S., S. Baroni, R. Car and M. Parrinello, 1989, Europhys. Lett. **8**, 663.
- Sugiyama, G., and S.E. Koonin, 1986, Ann. Phys. **168**(1), 1-26.
- Suzuki, M., 1976, Commun. Math. Phys. **51**, 183.
- Suzuki, M., 1985, Phys. Lett. A **113**, 199.
- Tang, S., and E. Hirsch, 1988, Phys. Rev. B **37**, 9546.
- Trotter, H.F., 1959, Proc. Am. Math. Soc. **10**, 545.
- Verlet, L., 1968, Phys. Rev. **165**, 21.

- White, S.R., R.L. Sugar and R.T. Scalettar, 1988, Phys. Rev. B **38**, 11665.
- White, S.R., D.J. Scalapino, R.L. Sugar, E.Y. Loh Jr, J.E. Gubernatis and R.T. Scalettar, 1989a, Phys. Rev. B **40**, 506.
- White, S.R., D.J. Scalapino, R.L. Sugar, N.E. Bickers and R.T. Scalettar, 1989b, Phys. Rev. B **39**, 839.
- Wilkinson, J.H., 1965, *The Algorithmic Eigenvalue Problem* (Clarendon Press, Oxford) p. 607.

This page intentionally left blank

CHAPTER 5

Modulated and Localized Structures of Spin Density Waves in Itinerant Antiferromagnets

V.V. TUGUSHEV

*I.V. Kurchatov Institute of Atomic Energy
123182 Moscow, USSR*

*Translated from the Russian
by Artavaz BEKNAZAROV*

© Elsevier Science Publishers, B.V., 1992

*Electronic Phase Transitions
Edited by
W. Hanke and Yu.V. Kopaev*

Contents

1. Introduction	239
2. Spin density wave (SDW) model: a brief discussion	241
3. Modulated spin structures in itinerant antiferromagnets	246
3.1. Peculiarities of the phase diagram and incommensurate SDW states in “nesting”-type models of antiferromagnetic phase transition	246
3.2. SDW soliton lattice state in the model with an infinite-capacity electron reservoir	255
3.3. Influence of impurity scattering and a finite-capacity electron reservoir on the formation of the SDW soliton lattice	263
4. Localized impurity states and short-range order in SDW antiferromagnets	270
4.1. Formation of resonance impurity levels in SDW systems below the Néel point	270
4.2. Defect-induced short-range antiferromagnetic ordering above and below the Néel point: formation of “localized” spin-density waves	279
5. Experimental results for some dilute chromium alloys	287
6. Conclusions	296
Appendix I	297
Appendix II	298
Appendix III	300
Appendix IV	300
References	300

1. Introduction

It is known that in the theory of itinerant magnetism there is a qualitative criterion – the generalized Stoner–Hubbard criterion (Herring 1966) – for instability of the ground paramagnetic state with respect to the type of spin ordering. For the simplest model with an effective point potential of electron–electron exchange interaction $I(\mathbf{r} - \mathbf{r}') = I\delta(\mathbf{r} - \mathbf{r}')$, this criterion has the form

$$1 \lesssim I\dot{\chi}(\mathbf{q}), \quad (1.1)$$

where $\dot{\chi}(\mathbf{q})$ is the spin susceptibility of noninteracting quasi-particles and \mathbf{q} is the wave vector. At $\mathbf{q} = 0$, eq. (1.1) changes to the ferromagnetism criterion $1 \lesssim IN(0)$, where $N(0) = \dot{\chi}(0)$ is the density of states on the Fermi surface. If the quantity $\dot{\chi}(\mathbf{q})$ has a singularity at $\mathbf{q} = \mathbf{Q}$, then the criterion (1.1) can be satisfied even with $IN(0) < 1$, provided that there is no ferromagnetic instability. In this case, an antiferromagnetic state of an itinerant magnetic material is likely to appear. Although the criterion (1.1) itself is of an approximate character and requires a number of additional solutions (e.g. the calculation of the quantities I and $\dot{\chi}(\mathbf{q})$ from first principles is an independent problem), its applicability for a wide class of itinerant magnetic materials is generally accepted at present and provides a good qualitative agreement with experiments.

The instability of the paramagnetic ground state from the viewpoint of the criterion (1.1) was first pointed out by Overhauser (1962) in a one-dimensional model of a metal, whose energy spectrum satisfies the condition $\varepsilon(\mathbf{p}) = -\varepsilon(\mathbf{p} + 2\mathbf{p}_F)$, where \mathbf{p}_F is the Fermi momentum. Because of the logarithmic divergence of the quantity $\dot{\chi}(\mathbf{q} \rightarrow 2\mathbf{p}_F)$, the criterion (1.1) is satisfied at as small a value of the potential I as desired, and hence, under the Hartree–Fock approximation an absolute instability [a spin density wave (SDW)] appears toward the formation of an antiferromagnetic structure.

We are not going to discuss here the validity of the Overhauser model and the correlational effects, which are of fundamental importance in one-dimensional systems. What is of interest to us is the fact that for a number of three-dimensional metals (transition or rare-earth metals) and alloys the Fermi surface in the paramagnetic phase has almost congruent (i.e. coinciding upon translation by the vector \mathbf{Q} specified by the geometry of the Brillouin zone) electron- and hole-segments near which the spectrum condition $\varepsilon_1(\mathbf{p}) \approx -\varepsilon_2(\mathbf{p} + \mathbf{Q})$

("nesting") is satisfied for a rather large region of vectors \mathbf{p} . Because of the logarithmic divergence of $\chi(\mathbf{q} \rightarrow \mathbf{Q})$ in these systems, an instability appears toward the formation of a SDW state, which may, however, be destroyed with increasing temperature or with a change in the degree of incongruence of the Fermi surface by way of a phase transition at the Néel point. Lomer (1962) and Fedders and Martin (1966) applied the SDW concept in order to describe antiferromagnetism in chromium and its alloys, and thereby laid the foundation for a completely new trend in the band theory of magnetism which had been developing for more than two decades.

At present we know of a class of models describing the effect of the special topology of the electronic spectrum on electronic and magnetic phase transitions in crystals. Of particular interest here are the following systems having the characteristic features of an electronic band structure:

(a) One-band metals obeying the dispersion law $\varepsilon(\mathbf{k}) \approx -\varepsilon(\mathbf{k} + \mathbf{Q})$ in a certain region of the vectors \mathbf{k} : a particular mention may be made of metals having Fermi surface with nearly planar segments. In this case the SDW instability is very similar to Overhauser instability;

(b) Two-band metals or narrow-band semiconductors, for which the following relation is satisfied: $\varepsilon_1(\mathbf{k}) \approx -\varepsilon_2(\mathbf{k} + \mathbf{Q})$, where the numbers 1 and 2 are the band indices. At $\mathbf{Q} = 0$, we have in particular the model of a straight-band semimetal (semiconductor), which is unstable toward electron–hole coupling (Keldysh and Kopaev 1964).

To the class of systems indicated above belong some rare-earth antiferromagnets with so-called *ribbon* portions of the Fermi surface (Coqueblin 1977) and quasi-one-dimensional organic conductors with open Fermi surfaces (Gor'kov 1984). For systems having Fermi surface with nearly planar segments, a substantial role is played by lateral corrugation, which suppresses one-dimensional fluctuations and provides a choice of the optimal wave vector \mathbf{Q} for the antiferromagnetic structure.

In a number of transition metals and their compounds there exist closed Fermi surfaces, which are corrugated polyhedrons. If the corrugation parameter W_{\perp} is small as compared to the bandwidth W_{\parallel} along the direction of the normal to the face, then by virtue of small W_{\perp}/W_{\parallel} the effect of the face "joints" is neglected, and the problems for open and closed Fermi surfaces become almost identical. But if $W_{\perp} \sim W_{\parallel}$, i.e. if the Fermi surface cannot be visualized in the form of a set of intersecting weakly deformed planes, then use is made of the spherical or elliptic approximation. The structure of a spin density wave is, as a rule, only slightly sensitive to the specification of the Fermi surface; what is important is the very existence of the congruent regions of the Fermi surface.

The classical examples of antiferromagnets with spin density waves are chromium and its dilute alloys (see e.g. the reviews by Fawcett 1988, Kulikov and Tugushev 1984) and some quasi-one-dimensional conductors (Gor'kov 1984). Less known examples are the ordered alloys FeRh (Kulikov et al. 1982,

Kulatov et al. 1986), MnNi (Egorushkin et al. 1983), Pt₃Fe (Kulatov et al. 1986, Kulikov 1985), the Manvelli phases V_nO_{2n+1} (Kopaev and Mokerov 1982, Idlis and Kopaev 1983), the compound CrB₂ (Liu et al. 1975) and some complex sulfides of the type V₃S₄ and V₅S₈ (Kitaoka et al. 1979, Kitaoka and Yasuoka 1980). Probably, in an external magnetic field a spin density wave appears also in NbSe₃ (Coleman et al. 1985) and in 2H-TaS₂ (Butz et al. 1986). Finally, there is ground for treating the magnetic properties of mixed metal oxides of the type La–Sr–Cu–O and Y–Ba–Cu–O in the spirit of the band approach through the use of the SDW scheme (Eyert et al. 1988, Shraishi et al. 1988, Schluter 1988, Chui et al. 1988, Kasowski et al. 1987). The last-named group of materials is of special interest at present in connection with the search for mechanisms of high-temperature superconductivity and the relationship between these mechanisms and the effects of antiferromagnetic correlations of itinerant electrons. Unfortunately, the results of the latest investigations (see e.g. Moriya 1985) in the field of the band theory of magnetism leave the problem of antiferromagnetic ordering in crystals almost untouched and are mainly associated with the study of Stoner ferromagnets. Meanwhile, the specificity of itinerant antiferromagnetism requires in a number of cases the elaboration of problems that have no direct analogs in the ferromagnetic situation. Some of these problems are discussed in this chapter.

2. Spin density wave (SDW) model: a brief discussion

The model of itinerant antiferromagnetism discussed here is a special case of the more general model of electronic phase transitions in metals, with a specific topology of the Fermi surfaces of electrons and holes (the so-called *excitonic insulator* model). This model has been proposed by Keldysh and Kopaev (1964) (see also the works of Kozlov and Maksimov 1965, Halperin and Rice 1968, and De Cloiseaux 1965). The model has made it possible to describe a number of properties of crystals with electronic and magnetic phase transitions (the metal–insulator transition (Keldysh and Kopaev 1964), and ferroelectric (Elesin and Kopaev 1976), antiferromagnetic (Kozlov and Maksimov 1965) and ferromagnetic (Volkov et al. 1979a) ordering). Such a diversity is possible due to the presence of a large number of “degrees of freedom” in the model Hamiltonian. The order parameter, which characterizes an electronic transition, has in a general case the form of a four-component spinor:

$$\hat{A} = A^s \hat{I} + A^t \cdot \hat{\sigma}, \quad A^s = A_{Re}^s + i A_{Im}^s, \quad A^t = A_{Re}^t + A_{Im}^t, \quad (2.1)$$

where \hat{I} is a unit matrix and $\hat{\sigma}$ is a vector composed of Pauli matrices. The scalar order parameters $A_{Re, Im}^s$ characterize the singlet electron–hole coupling associated with the generation of a charge density wave (CDW) and an orbital current density wave (OCDW), and the vector order parameters $A_{Re, Im}^t$

characterize the triplet coupling associated with the formation of a spin density wave and a spin current density wave (SCDW).

Let us write the Hamiltonian of the two-band excitonic insulator model in the second-quantization representation:

$$\begin{aligned} \hat{H} = & \sum_{i,k,\alpha} \varepsilon_i(\mathbf{k}) a_{ik\alpha}^+ a_{ik\alpha} + \sum_{k,k',q,\alpha,\beta} [g_1 a_{1k\alpha}^+ a_{2k'\beta}^+ a_{2k'-q\beta} a_{1k+q\alpha} \\ & + g_2 (a_{1k\alpha}^+ a_{1k'\beta}^+ a_{2k'-q\beta} a_{2k+q\alpha} + \text{c.c.}) \\ & + g_2 (a_{1k\alpha}^+ a_{2k'\beta}^+ a_{1k'-q\beta} a_{2k+q\alpha} + \text{c.c.})], \end{aligned} \quad (2.2)$$

where $a_{1,2}^+$ and $a_{1,2}$ are, respectively, the electron creation and annihilation operators in bands 1 and 2, g_1 is the potential of the screened interband Coulomb interaction of the density-density type and g_2 is the interaction potential with an interband transition of a pair of particles. For simplicity, all the matrix elements of the Coulomb interaction are assumed to be independent of the momenta.

The transitions to the above-indicated four states are characterized by the corresponding effective point potentials:

$$\begin{aligned} g_{\text{Re}}^s &= g_1 - 3g_2, \\ g_{\text{Im}}^s &= g_{\text{Im}}^l = g_1 - g_2, \\ g_{\text{Re}}^l &= g_1 + g_2. \end{aligned} \quad (2.3)$$

Note that in the Hubbard model $g_1 \equiv g_2$. With $g_2 > 0$ the SDW state is the most favorable, since it corresponds to a larger value of the interaction potential and, accordingly, a higher phase transition temperature. A detailed analysis of the interaction potentials in the excitonic insulator model has been reported in the literature (Buker 1981, Bychkov and Jordanskii 1980).

The model described by eq. (2.2) allows for an asymptotically exact solution with $gN(0) \ll 1$ ($N(0)$ is the reduced density of states on the Fermi surface); the appropriate mathematical approach is analogous to the Gor'kov method in the theory of superconductivity (Abrikosov et al. 1962). In the mean-field approximation one may pass over from eq. (2.2) to the Hamiltonian \tilde{H} of electrons moving in a self-consistent exchange field $\Delta_{ij}^{\alpha\beta}(\mathbf{r})$:

$$\tilde{H} = H_0 - \int \sum_{i,j,\alpha,\beta} [\Delta_{ij}^{\alpha\beta}(\mathbf{r}) a_{i\alpha}^+(\mathbf{r}) a_{j\beta}(\mathbf{r}) + \Delta_{ij}^{\beta\alpha}(\mathbf{r}) \hat{g}^{-1} \Delta_{ji}^{\beta\alpha}(\mathbf{r})] d\mathbf{r}, \quad (2.4)$$

where \hat{g}^{-1} is the matrix composed of the inverse effective potentials $(g_{\text{Re,Im}}^{s,l})^{-1}$. For the real triplet order parameter under consideration, formula (2.4) retains terms with $\Delta_{ij}^{\alpha\beta} = (\Delta^l(\mathbf{r}) \cdot \hat{\sigma})^{\alpha\beta}$ and $\hat{g}^{-1} = (g_{\text{Re}}^+)^{-1} \equiv g^{-1}$. The self-consistency equation at $T = 0$ can be obtained by varying \tilde{H} with respect to the parameter

$\Delta_{ij}^{\alpha\beta}(\mathbf{r})$. At finite temperatures one should vary the free energy $\mathcal{F}(\Delta_{ij}^{\alpha\beta})$ corresponding to eq. (2.4). In the case of spin density waves the self-consistency equation for the potential $\Delta_{ij}^{\alpha\beta}(\mathbf{r})$ has the following form:

$$\begin{aligned}\Delta_{12}^{\alpha\beta} &= \Delta_{21}^{*\beta\alpha} = (\Delta^t \cdot \hat{\sigma})^{\alpha\beta}, \\ \Delta^t(\mathbf{r}) &= \frac{1}{2}gT \text{Tr} \left[\sum_n \text{Re}(\hat{G}_{12}(\mathbf{r}, \mathbf{r}'; \omega_n) \hat{\sigma}) \right], \\ \omega_n &= \pi T(2n + 1), \quad n = 0, \pm 1, \dots,\end{aligned}\tag{2.5}$$

where $\hat{G}_{ij}(\mathbf{r}, \mathbf{r}'; \omega_n)$ are the temperature Green's functions of the Hamiltonian \tilde{H} . For a linearly polarized structure the components $\Delta_{ij}^{\alpha\beta}(\mathbf{r})$ have the form

$$\Delta_{ij}^{zz}(\pm \mathbf{q}) = -\Delta_{ij}^{zz}(\pm \mathbf{q}) = \Delta^{tz};\tag{2.6}$$

the direction of the vector Δ^t is chosen to be along the axis of quantization. If $\mathbf{q} = \frac{1}{2}\mathbf{G}$, where \mathbf{G} is the reciprocal lattice vector, then eq. (2.6) describes the simplest antiferromagnetic structure with a doubling of the period along the vector \mathbf{G} . However, if $\mathbf{q} \neq \frac{1}{2}\mathbf{G}$, then the linearly polarized structure [eq. (2.6)] with one pair of wave vectors $\mathbf{q} = \pm \mathbf{Q}$ does not satisfy the self-consistency equation (2.5). At the same time, the transverse helicoidal SDW structure

$$\Delta_{12}^{zz}(\mathbf{q}) = \Delta_{21}^{zz}(-\mathbf{q}) = \Delta^{t\perp}\tag{2.7}$$

always satisfies eq. (2.5) (the z axis is directed along the helicon axis). The question whether the linearly polarized or the helicoidal SDW structure is realized must be answered for each individual case, depending on the parameters of the model.

The dispersion relations $\varepsilon_i(\mathbf{k})$ in eq. (2.2) are written down in the form

$$\varepsilon_1(\mathbf{k}) = k^2/2m^* - \varepsilon_F - \mu, \quad \varepsilon_2(\mathbf{k} + \mathbf{Q}) = -(k^2/2m^* - \varepsilon_F) - \mu.\tag{2.8}$$

Here the quantity μ characterizes the degree of incongruence of the Fermi surface of electrons in bands 1 and 2. Assuming that the phase transition to the SDW state is second-order, we obtain from eq. (2.5) the equation for the Néel temperature $T_N(\mu)$, by linearizing the right-hand side with respect to $\Delta^t(\mathbf{q})$. Here, without imposing any additional restrictions on the choice of the vector \mathbf{q} and the type of the SDW structure, we obtain (Kopaev 1975):

$$\begin{aligned}-\ln(T_N/T_N^0) &= \text{Re} \int_{-1}^1 [\psi(\frac{1}{2} + i(\mu + v_F q z)/2\pi T_N) - \psi(\frac{1}{2})] dz, \\ \partial T_N / \partial \tilde{q} |_{\tilde{q}=\mathbf{q}_0} &= 0, \quad \tilde{\mathbf{q}} = \mathbf{q} - \frac{1}{2}\mathbf{G}\end{aligned}\tag{2.9}$$

where $T_N^0 = 0.57\Delta_0$, $\Delta_0 = W \exp(-1/\bar{g})$, W being the cutoff energy of the order of ε_F ; $\psi(x)$ is the digamma function. The last equation provides the choice of the vector $\tilde{\mathbf{q}} = \mathbf{q}_0$ corresponding to the maximum transition temperature, $\bar{g} = g_{\text{Re}}^t N(0)$.

In fig. 1 the $T_N(\mu)$ lines with $\mu \leq \mu^*$ are seen to limit the region of the commensurate SDW structure (C-phase). It has been shown for the model of spherical Fermi surface segments by Rice (1970) and for the model of planar Fermi segments by Shibatani et al. (1969) and Kotani (1975a, b, 1978a, b) that at a sufficiently large value of $\mu \geq \mu^*$ ($\mu^* \approx 0.604\Delta_0$), incommensurate SDW structure (the I-phase), whose wave vector $\mathbf{q} \neq \mathbf{Q}$, is realized. In the $T_N(\mu)$ diagram there appears a tricritical point ($T_N^* \approx 0.31\Delta_0$, $\mu^* \approx 0.604\Delta_0$) at which the transition lines between the paramagnetic (P), C and I phases of the SDW converge.

The transition line between the P and I phases has been found to be significantly different for the Rice and Kotani models. The $T_I(\mu)$ line shown in fig. 1a was found under the assumption that the P-I transition is second-order: it begins at point (T_N^*, μ^*) and ends at point $(T_N = 0, \mu^c = 0.755\Delta_0)$. However, correctness of this assumption depends significantly on a number of additional parameters of the model, and in a general case the second order of the P-I transition is not realized. The C-I transition line was not found by Rice, and probably, in the spherical segments model it cannot be obtained at all, strictly speaking.

The $T_I(\mu)$ line for the planar segments model (fig. 1b) starts at point (T_N^*, μ^*) and asymptotically approaches the abscissa, but formally, T_I vanishes nowhere. The inclusion of lateral corrugation and also of impurity scattering leads, just as in the spherical segments model, to vanishing of T_I at a certain value of μ^c (Young and Cade 1977, Maki and Sakurai 1972). It is important, however, that the P-I transition in the model of planar segments is always second-order, this being different from the situation in the spherical segments model. Further, one can also find the C-I transition line correctly and also the SDW structure in the entire I phase.

A few words should be said about the two additional parameters of the model, which need to be introduced for a more detailed description of the various systems mentioned earlier. One of these parameters is the *capacity of the*

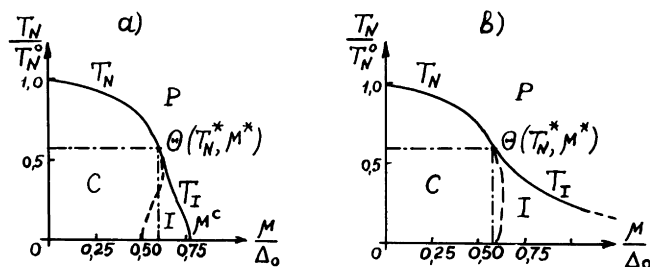


Fig. 1. Phase diagrams. (a) Rice model (Rice 1970). (b) Kotani model (Shibatani et al. 1969, Kotani 1975a, b, 1978a, b).

reservoir (M), which has a strong effect on both the shape of the phase diagram $T_N(\mu)$ and the SDW structure. Let us assume that apart from the congruent segments, there are other segments of the Fermi surface which do not exhibit singularities and which do not participate in the generation of the SDW. The mean density of states on the Fermi surface for these segments (reservoir) is denoted by $N_r(0)$. The shift of the chemical potential μ introduced with respect to the original value μ_0 in the P phase, upon formation of spin density waves, is specified by the condition of conservation of the total number of particles:

$$\delta n(\mu) + N_r(0)(\mu - \mu_0) = 0, \quad (2.10)$$

where $\delta n(\mu)$ is the variation of the total number of particles in bands 1 and 2 ($\delta n(\mu) \sim 2N(0)$). Introducing the parameter $M = N_r(0)/2N(0)$, we can arrive at a combined solution of eqs. (2.5) and (2.10) at different M values. If $M \gg 1$, then by virtue of M^{-1} we assume that $\mu \approx \mu_0$ (the case of fixed chemical potential). But if $M \ll 1$, then μ can change significantly upon antiferromagnetic ordering. For real systems with spin density waves, the results of model calculations are usually in better agreement with experiment when $M \gg 1$, since the fraction of non-singular segments of the Fermi surface in these is very significant, as a rule.

The another additional parameter of the model, which has a strong effect on the form of the phase diagram and the SDW structure, is the so-called *scattering parameter* v . The explicit form of the quantity v for the case of a small concentration of magnetic and nonmagnetic impurities has been given, e.g. by Young and Cade (1977) and Maki and Sakurai (1972). The influence of impurity scattering on the phase diagram $T_N(\mu_0)$ is reflected in the lowering of T_N and T_i and in the contraction of the I-phase region. Detailed analysis of phase diagrams for individual systems is possible only through the use of numerical methods.

It should be noted that a more general statement of the problem includes also the effect of scattering on the choice of the type of solution in the excitonic insulator model (CDW, SDW, OCDW, SCDW); e.g., even with formally lower interaction potentials, the states with imaginary order parameters can be realized at higher temperatures and become more favorable than the CDW or the SDW state [Volkov et al. (1978a, 1979b)].

The scattering of phonons may also, in principle, exert a noticeable influence on the phase diagram. This scattering is usually taken into account by simply introducing a phenomenological temperature dependence $v(T)$ (Sato and Maki 1973). One can also construct a more rigorous scheme taking into account electron–phonon scattering on the basis of equations of the type of the Eliashberg equation (Kulikov and Tugushev 1981).

In this chapter we do not intend to present all the results obtained in the model described by eq. (2.2); we confine ourselves to expounding the general idea of the model. Most of the early results on SDW systems have been dealt with in the literature (see Kulikov and Tugushev 1984 and the extensive

bibliography therein). Here we discuss only some of the latest developments concerning the formation of superstructures and the antiferromagnetic short-range order in SDW systems, which play an important role in understanding the properties of a number of real materials, primarily dilute Cr-based alloys.

3. Modulated spin structures in itinerant antiferromagnets

3.1. Peculiarities of the phase diagram and incommensurate SDW states in “nesting”-type models of antiferromagnetic phase transition

As has been pointed out earlier, with $\mu > \mu^*$ a system with Hamiltonian given by eq. (2.2) is unstable toward the formation of an inhomogeneous structure of the triplet order parameter $A^t(\mathbf{r})$ with a characteristic wave vector $\mathbf{q}_0 \neq 0$. In the Rice model (Rice 1970) the P–I transition line can be found only by a variational technique $M \gtrsim 1$, since the transition in major part of the phase diagram with $\mu > \mu^*$ is first-order (Nakanishi and Maki 1972); although with $\mu \approx \mu^c$ it is again second-order, just as in the case of $\mu < \mu^*$. A calculation has been carried out (Nakanishi and Maki 1972) for two types of SDW structure: the sinusoidal linearly polarized structure and the helicoidal structure. It was found that, in the region of validity of the Ginzburg–Landau expansion for the thermodynamic potential $\Omega(A^t, \mu)$ near the Lifshitz point, the sinusoidal structure is more favorable. Calculation shows that away from the Lifshitz point in the direction of increasing μ , the parameter $v_F q_0 / \max(T, \mu)$ sharply increases and the Ginzburg–Landau expansion becomes invalid. In the case of a first-order transition the role of the higher harmonics of the SDW (the Fourier components $A^t(\mathbf{q})$ with wave vectors that are multiples of \mathbf{q}_0) is increased and the transition line $T_l(\mu)$ cannot be found. The limit $M = 0$ at which the transition is really second-order has been considered by Malaspinas and Rice (1971). Although this limit is hardly of any significance for real itinerant antiferromagnets, even in this case the sinusoidal solution has been found to be more favorable than the helicoidal solution. For an arbitrary power of the reservoir M , it is possible to find a value of $M^* \sim 1$ at which the order of the transition changes from second to first.

It should be noted that it is due to the variational character of all calculations in the Rice model that the sinusoidal solution is found to be more favorable than the helicoidal one; this does not signify that it is absolutely favorable. One can visualize more complicated SDW structures, the exclusion of which from the analysis is not justified at all. For instance, it has been recently demonstrated (Buker 1982) that the bulk SDW structure with three wave vectors $\{\mathbf{q}_0^i\}$, $i = 1, 2, 3$, $|\mathbf{q}_0^i| \equiv q_0$, is more favorable in the Rice model than the linearly polarized sinusoidal one. It should be stressed, however, that the question of the favorableness of one or the other type of SDW structure cannot be regarded to have been solved, in principle, without taking account of the higher harmonics; this cannot be done in the model proposed by Rice (1970).

In the model proposed by Shibatani et al. (1969) and Kotani (1975a, b, 1978a, b) it is possible, at least with $M \gg 1$, to go somewhat further into the understanding of the properties of systems with a modulated antiferromagnetic structure, which is associated with the presence of at least one exact solution for spin density waves which would take account of an infinite series of harmonics (the soliton lattice model). If the corrugation parameter is such that $\varepsilon_F \gg |W_\perp| \gg A^t$, then we may ignore on the one hand, “one-dimensional” fluctuations and make use of the mean-field approximation (otherwise, the “parquet” situation (Gor’kov and Dzyaloshinskii 1974, Dzyaloshinskii and Katz 1972 will occur); and, on the other hand, the explicitly three-dimensional character of the spectrum near the planar segment, of the Fermi surface, with an accuracy of up to corrections $\sim W_\perp/\varepsilon_F$. Note that in such a case, the direction of the SDW vector \mathbf{q}_0 may not coincide with the direction of the velocity vector along the normal to a given segment of the Fermi surface: e.g. in the octahedron model (Shibatani et al. 1969, Kotani 1975a, b, 1978a, b) for the Fermi surface of chromium the direction of \mathbf{q}_0 coincides with the vector $2\pi a(100)$, which combines in pairs the faces of the electron and hole-octahedra oriented at angles of $(\pm\frac{1}{4}\pi, \pm\frac{3}{4}\pi)$ to \mathbf{q}_0 . A variational computation (Buker 1982) shows that the linearly polarized sinusoidal solution for spin density waves appears to be the most favorable among all those considered. By using numerical methods (Harada and Kotani 1982) it is possible to find the second-order transition line between the C and I phases (in calculations use is made of a large number of harmonics) at different values of M . However, no variational method can provide a rigorous proof of the order of the transition between the C and I phases or the true SDW structure inside the I phase. Moreover, as is shown later, the authors of all works devoted to the calculation of incommensurate SDW structures have neglected an important factor – the spatial redistribution of electron density $n(x)$ in the I phase and the attendant loss of electrostatic energy (the long-range part of the electron–electron interaction). This appears to be especially important for systems with $M \lesssim 1$, where the region of existence of the linearly polarized I phase of spin density waves is narrowed, as a result of which the helicoidal structure may become more favorable.

Let us consider (Volkov et al. 1978b, Volkov and Tugushev 1979) the model Hamiltonian \mathcal{H} for systems with congruent segments of the Fermi surface which is unstable toward the formation of a spin density wave (it is assumed that the corresponding coupling constant g^t is at a maximum). Under the mean-field approximation we write the Hamiltonian \mathcal{H} in matrix form:

$$\mathcal{H} = \begin{pmatrix} \left[\varepsilon_1 \left(\frac{\nabla}{i} \right) - e\Phi(\mathbf{r}) \right] \hat{I} & -A^t(\mathbf{r}) \cdot \hat{\sigma} \\ -\hat{A}^t(\mathbf{r}) \cdot \hat{\sigma} & \left[\varepsilon_2 \left(\frac{\nabla}{i} \right) - e\Phi(\mathbf{r}) \right] \hat{I} \end{pmatrix}, \quad (3.1)$$

where \hat{I} is a unit matrix, $\hat{\sigma}$ is a vector composed of Pauli matrices and $\Phi(\mathbf{r})$ is the

self-consistent scalar potential associated with the redistribution of electron density upon incommensurate antiferromagnetic ordering. For the sake of definiteness, we consider the case of a Fermi surface with corrugated planar segments:

$$\varepsilon_1(\mathbf{k}) = v_F k_x + \eta_1(k_\perp), \quad \varepsilon_2(\mathbf{k} + \mathbf{Q}) = -v_F k_x + \eta_2(k_\perp), \quad (3.2)$$

where v_F is the velocity at the Fermi surface in the direction of the normal to the planar segment, $\eta_{1,2}(k_\perp)$ is the transverse corrugation, $|\eta_{1,2}| \ll \varepsilon_F$. However, generally speaking, $|\eta_{1,2}| \gg \Delta^t$, so that “one-dimensional” fluctuations of the order parameter are not important.

In the commensurate case $\Delta^t(\mathbf{r}) \equiv \Delta^t$, it is possible to find eigenfunctions and eigenvalues of the Hamiltonian [eq. (3.1)] and also to solve the self-consistency equation for the amplitude of Δ^t . However, for the incommensurate case in general such a program cannot be realized even ignoring a self-consistent account of the electron density redistribution. Let us write down a system of equations for the Fourier components of the temperature Green's functions

$$\hat{G}_{ij}^{\alpha\beta}(\mathbf{r}, \mathbf{r}'; \tau, \tau') = -i \langle T\psi_{i\alpha}(\mathbf{r}, \tau)\psi_{j\beta}^+(\mathbf{r}', \tau') \rangle, \quad (3.3)$$

where i and j are the band indices, α and β are the spin indices and $\psi_{i\alpha}$ and $\psi_{i\alpha}^+$ are the electron creation and annihilation operators:

$$\begin{aligned} & \left[i\omega_n - \varepsilon_1 \left(\frac{\nabla}{i} \right) + e\Phi(\mathbf{r}) \right] \hat{G}_{11}(\mathbf{r}, \mathbf{r}'; \omega_n) \\ &= \delta(\mathbf{r} - \mathbf{r}') - \Delta^t(\mathbf{r}) \cdot \hat{\sigma} \hat{G}_{21}(\mathbf{r}, \mathbf{r}'; \omega_n), \\ & \left[i\omega_n - \varepsilon_2 \left(\frac{\nabla}{i} \right) + e\Phi(\mathbf{r}) \right] \hat{G}_{21}(\mathbf{r}, \mathbf{r}'; \omega_n) = -\hat{\Delta}^t(\mathbf{r}) \cdot \hat{\sigma} \hat{G}_{11}(\mathbf{r}, \mathbf{r}'; \omega_n). \end{aligned} \quad (3.4)$$

The equations for \hat{G}_{22} and \hat{G}_{12} are obtained in an analogous manner.

For the scalar potential $\Phi(\mathbf{r})$ we write Poisson's equation:

$$\nabla^2 \Phi(\mathbf{r}) = -4\pi e \delta n(\mathbf{r}). \quad (3.5)$$

A local variation of the electron density $\delta n(\mathbf{r})$ is easy to determine if one knows the normal Green's functions $\hat{G}_{ii}(\mathbf{r}, \mathbf{r}'; \omega_n)$. Considering that the local variation of electron density in the reservoir is equal to $N_r(0)[\delta\mu + e\Phi(\mathbf{r})]$, where $\delta\mu = \tilde{\mu} - \mu$ is the change of the chemical potential in the antiferromagnetic phase as compared to the paramagnetic phase, we obtain

$$\delta n(\mathbf{r}) = T \sum_n \text{Tr} \hat{G}_{ii}(\mathbf{r}, \mathbf{r}'; \omega_n) + N_r(0)[\delta\mu + e\Phi(\mathbf{r})] - 2N(0)\mu. \quad (3.6)$$

Since the total number of particles in the system does not change as a result of the phase transition, it is necessary that the following condition be satisfied:

$$\langle \delta n \rangle = \frac{1}{V} \int \delta n(\mathbf{r}) d\mathbf{r} \equiv 0. \quad (3.7)$$

The single-particle Green's functions $G_{ij}(\mathbf{r}, \mathbf{r}'; \omega_n)$ can be written conveniently as follows:

$$G_{ij}(\mathbf{r}, \mathbf{r}'; \omega_n) = \mathcal{G}_{ij}(x, x', \boldsymbol{\rho}_\perp - \boldsymbol{\rho}'_\perp, \omega_n) \\ \times \exp[\pm (\frac{1}{2}iQ_x(x - x') + \frac{1}{2}i\boldsymbol{Q}_\perp \cdot (\boldsymbol{\rho}_\perp - \boldsymbol{\rho}'_\perp))], \quad (3.8)$$

where the plus sign is taken for the components \mathcal{G}_{12} and \mathcal{G}_{11} and the minus sign for \mathcal{G}_{22} and \mathcal{G}_{21} . The order parameter $A^t(\mathbf{r})$ is written in the form

$$A^t(\mathbf{r}) = A^t(x) \exp[iQ_x x + i\boldsymbol{Q}_\perp \cdot \boldsymbol{\rho}_\perp]. \quad (3.9)$$

Let us now perform on the functions \mathcal{G}_{ij} a Fourier transformation along the transverse coordinate $(\boldsymbol{\rho}_\perp - \boldsymbol{\rho}'_\perp)$, and after the substitution

$$\mathcal{G}_{ij}(x, x', \boldsymbol{q}_\perp; \omega_n) = \tilde{\mathcal{G}}_{ij}(x, x'; \tilde{\omega}_n) \exp\left(i\frac{\eta_-}{v_F}(x - x')\right), \quad \tilde{\omega}_n = \omega_n + i\eta_+, \\ \eta_\pm(\boldsymbol{q}_\perp) = \frac{1}{2}[\eta_1(\boldsymbol{q}_\perp + \frac{1}{2}\boldsymbol{Q}_\perp) \pm \eta_2(\boldsymbol{q}_\perp - \frac{1}{2}\boldsymbol{Q}_\perp)], \quad (3.10)$$

we arrive at a one-dimensional equation for the Green's function $\tilde{\mathcal{G}}_{ij}(x, x'; \tilde{\omega}_n)$:

$$[i\hat{I}\tilde{\omega}_n - \tilde{H}] \tilde{\mathcal{G}} = \hat{I}\delta(x - x'), \quad (3.11)$$

$$\tilde{H} = \begin{pmatrix} \left[iv_F \frac{\partial}{\partial x} - e\Phi(x) \right] \hat{I} & -A^t(x) \cdot \hat{\sigma} \\ -A^t(x) \cdot \hat{\sigma} & \left[-iv_F \frac{\partial}{\partial x} - e\Phi(x) \right] \hat{I} \end{pmatrix}. \quad (3.12)$$

The system (3.11) in combination with eqs. (3.5) and (3.6) cannot be solved in a general case. However, we can discuss a few limiting situations that allow for a comparatively rigorous analysis. In this section, we will examine in detail the situation near the Lifshitz point, when the Ginzburg–Landau expansion is valid for the free-energy functional. For simplicity, we will analyze only the case of $\eta_+ \ll \mu$, which can, in principle, be realized with an appropriate choice of \boldsymbol{Q}_\perp . Using the standard Gor'kov method (Abrikosov et al. 1962) for the BCS model and assuming $|A^t(x)|$ to be small ($|A^t| \ll T, \mu$) and a slowly varying quantity ($|A'^t|/|A^t| \ll p_F$), we write the functional $\Omega(A^t, \mu)$ in the following form:

$$\Omega = \Omega_1 + \Omega_2, \quad (3.13)$$

where

$$\Omega_1 = \int \{ c_1 |\mathbf{A}^t|^2 + c_2 |\mathbf{A}^t|^4 + c_3 |\mathbf{A}^t|^6 + v_F^2 c_2 |\mathbf{A}^{t\prime}|^2 + \frac{1}{2} v_F^4 c_3 |\mathbf{A}^{t\prime\prime}|^2 + v_F^2 c_3 [2(\mathbf{A}^t \cdot \mathbf{A}^{t\prime})^2 + 3|\mathbf{A}^t|^2 |\mathbf{A}^{t\prime}|^2] \} dx, \quad (3.14)$$

$$\Omega_2 = \frac{1}{1+M} \int \{ c_4 |\mathbf{A}^t|^4 + c_6 |\mathbf{A}^t|^6 + 3v_F^2 c_5 |\mathbf{A}^t|^2 |\mathbf{A}^{t\prime}|^2 + 4(\mathbf{A}^t \cdot \mathbf{A}^{t\prime})^2 \} dx. \quad (3.15)$$

The expressions for the coefficients $\{c_i\}$ are given in Appendix I. Note that the contribution of the long-range part Ω_2 is specially separated out [formula (3.15)] and is given by the diagrams in fig. 2a. The contribution of Ω_1 is shown in fig. 2b.

Let us explain in more detail the origin of the term (3.15). It is clear that in the derivation of the self-consistency equation and the functional Ω , it is necessary to expand into a series in Ω_1 not only the Green's functions but also the chemical potential μ and the scalar potential $\Phi(x)$. With an accuracy of up to second-order terms in $|\mathbf{A}^t|$, we obtain using eq. (3.6):

$$\delta n(x) = -2N(0) \left\{ \frac{2\varphi_1}{\pi T} |\mathbf{A}^t|^2 + \frac{v_F^2 \varphi_3}{(\pi T)^3} \left(\left| \frac{\partial \mathbf{A}^t}{\partial x} \right|^2 - 2\mathbf{A}^t \cdot \frac{\partial^2 \mathbf{A}^t}{\partial x^2} \right) \right\} + 2N(0)[\delta\mu + e\Phi(x)] + N_r(0)[\delta\mu + e\Phi(x)]. \quad (3.16)$$

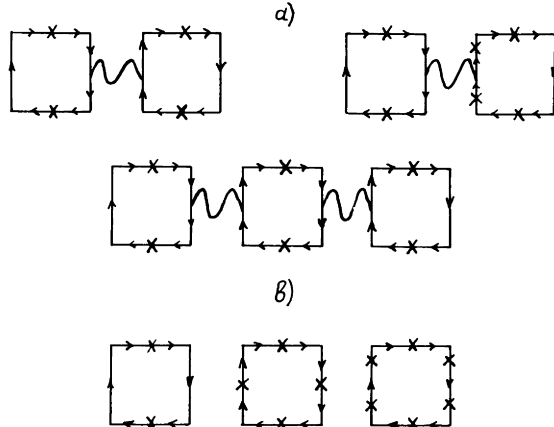


Fig. 2. Contributions to the thermodynamic potential [eq. (3.13)]. (a) Ω_2 . (b) Ω_1 .

The condition of conservation of the number of particles [eq. (3.7)] gives

$$\delta\mu = \frac{1}{1+\beta} \left\{ \frac{2\varphi_1}{\pi T} \langle |\mathbf{A}^t|^2 \rangle + \frac{v_F^2 \varphi_3}{(\pi T)^3} \left[\left\langle \left| \frac{\partial \mathbf{A}^t}{\partial x} \right|^2 \right\rangle - 2 \left\langle \mathbf{A}^t \cdot \frac{\partial^2 \mathbf{A}^t}{\partial x^2} \right\rangle \right] \right\}. \quad (3.17)$$

Here $\langle \dots \rangle$ signifies averaging over the volume and $M = N_r(0)/2N(0)$ is the capacity of the reservoir. The quantity μ_0 is related to the excess number of particles (the difference in the electron and hole concentrations in the unreconstructed phase) by

$$n = [N_r(0) + 2N(0)] \mu. \quad (3.18)$$

In the limit of high particle density, the square of the inverse Debye screening radius $\kappa^2 = 4\pi e^2(N_r(0) + 2N(0)) \ll p_F^2$, and the characteristic SDW wave vector $|\mathbf{q}_0| \lesssim T/v_F$, so that with $T \ll \epsilon_F$ for the long-wavelength components $\Phi(\mathbf{r})$, which are of interest here, we may neglect the left-hand side of eq. (3.5). As a result, we obtain the “local” electroneutrality condition (to a scale $\sim q_0^{-1}$):

$$\delta\mu + e\Phi = \frac{1}{1+\beta} \left\{ \frac{2\varphi_1}{\pi T} |\mathbf{A}^t|^2 + \frac{v_F^2 \varphi_3}{(\pi T)^3} \left[\left| \frac{\partial \mathbf{A}^t}{\partial x} \right|^2 - 2 \mathbf{A}^t \cdot \frac{\partial^2 \mathbf{A}^t}{\partial x^2} \right] \right\}. \quad (3.19)$$

Now it is easy to see why the inclusion of the long-range part of the electron-electron interaction potential is important even for the determination of the form of the functional Ω . Indeed, let us assume that $e = 0$ in formula (3.5). Then it is not difficult to see that, with the requirement expressed by eq. (3.7) in the functional Ω , there appear explicitly nonphysical terms of the type $\langle |\mathbf{A}^t|^2 \rangle$, $\langle |\mathbf{A}^t|^4 \rangle$ corresponding to the effective potential of an infinite radius of action. Such terms have been found in all the studies of incommensurate SDW structures, but the cause of their appearance has not been discussed. But if $e \neq 0$, then since the equations for the Green’s functions contain $\delta\mu$ and $\Phi(x)$ only in the combination $\delta\mu + e\Phi(x)$, the nonphysical terms in the functional do not appear [see formula (3.19)]. It is interesting that this conclusion is valid at any value of the effective charge $e \neq 0$, since in the limit of $q_0 \ll \kappa$ expressions (3.19) and (3.15) do not contain e at all.

Let us now discuss the plausible solutions for the spin density wave corresponding to the commensurate, linearly polarized and helicoidal phases. It is convenient to rewrite the functional (3.13) in a general phenomenological form:

$$\mathbf{A}^t \equiv \mathbf{A}, \quad (3.20)$$

$$\begin{aligned} \Omega = & \int \left[\alpha |\mathbf{A}|^2 + \frac{1}{2} \beta_1 |\mathbf{A}|^4 + \frac{1}{3} \gamma_1 |\mathbf{A}|^6 + a_1 \left| \frac{\partial \mathbf{A}}{\partial x} \right|^2 + a_2 \left| \frac{\partial^2 \mathbf{A}}{\partial x^2} \right|^2 \right. \\ & \left. + b_1 |\mathbf{A}|^2 \left| \frac{\partial \mathbf{A}}{\partial x} \right|^2 + b_2 \left(\mathbf{A} \cdot \frac{\partial \mathbf{A}}{\partial x} \right)^2 \right] dx, \end{aligned} \quad (3.21)$$

where γ_1, a_2, b_1 and $b_2 > 0$, and the coefficients α, β_1 and a_1 may change sign. The notation of eq. (3.21) presupposes the modulation of the spin density waves only along a single specified direction, but one can also deal with the three-dimensional situation, which is realized in the spherical segments model of the Fermi surface.

Since the functionals of the type (3.21) have not been discussed earlier for modulated magnetic structures (according to the terminology used by Izymov (1984), here the appearance of non-Lifshitz invariants is responsible for the modulation of spin density waves), we will give some explanations. The retention of the term $|\partial^2 \Delta / \partial x^2|^2$ is associated with the vanishing of the coefficient a_1 and with the change of its sign; in general the coefficient β_1 may also vanish in our model, which is why it is necessary to retain the terms $\sim b_1$ and b_2 in order to obtain stable solutions in the I phase. The commensurate phase is realized for $\beta_1 > 0, a_1 > 0$ and $\alpha < 0$ (the region to the left of the Lifshitz point in fig. 3). Here the equilibrium value of the order parameter is given by $\Delta_0^2 = -\alpha/\beta_1$. The incommensurate phase becomes favorable when $a_1 < 0$, in which case the characteristic SDW wave vector at the second-order transition line is determined from the maximum of the transition temperature and is given by the relation $q_0^2 = -a_1/2a_2$. The P-I transition line itself is determined from the equation

$$\alpha(q_0) = \alpha + a_1 q_0^2 + a_2 q_0^4 = \alpha_1 - a_1^2/4a_2. \quad (3.22)$$

As one can see by differentiation with respect to μ , this equation, in conjunction with the condition $a_1 = 0$ at the Lifshitz point, implies continuity of the transition temperatures $T_C(\mu)$ and $T_I(\mu)$ and of their derivatives at the point $\mu = \mu^*$. The condition $\alpha(q_0) \leq 0$ determines the region of existence of the I phase on the (T, μ) diagram.

Further, it is necessary to answer two key questions: (1) the possible form of the incommensurate solution and (2) determination of the transition line between the C and I phases. At arbitrary values of the coefficients in eq. (3.21) an appropriate analysis can be performed by numerical techniques alone. In this section we will discuss the limiting case of a small-capacity reservoir for $\beta_1 > 0$ over the entire (T, μ) region of interest near the Lifshitz point. Let us carry out a qualitative investigation within the framework of the variational principle. The essence of its application for searching the line of absolute instability of a certain phase toward transition to another phase consists in the following. Let the equilibrium value of the order parameter Δ in the initial phase be known and be equal to Δ_0 . Then, we have to substitute into the functional (3.21) a trial value of Δ in the form of $\Delta = \Delta_0 + \varepsilon$, where $\varepsilon(x)$ is a small quantity having the symmetry of the new phase; in this case we must evaluate the functional (3.21) to within ε^2 . The boundary of the region of absolute instability of the old phase is determined in this case by the inequality $\delta\Omega/\delta\varepsilon^2 \leq 0$. The same procedure can be applied to

determine the boundary of the region of absolute instability of a phase with symmetry $\varepsilon(x)$ toward transition to a commensurate phase.

Let us find the line of absolute instability of the C phase relative to the I phase. To this end it is sufficient to choose $\varepsilon(x)$ in the form of a linearly polarized plane wave:

$$\varepsilon(x) = e\varepsilon_0 \sin qx. \quad (3.23)$$

For the cases of $e \parallel A_0$ and $e \perp A_0$ we obtain the conditions of absolute instability of the C phase:

$$\begin{aligned} 2|\alpha| - \tilde{a}_1^2/4a_2 &\leq 0, \\ \tilde{a}_1 = a_1 + b_{\parallel, \perp} |\alpha|/\beta_1 &\leq 0, \\ b_{\parallel} = b_1 + b_2, \quad b_{\perp} = b_1. \end{aligned} \quad (3.24)$$

The instability line $T_{C1}^{||}(\mu)$ is shown qualitatively in fig. 3. It is not difficult to see that, as before, at the Lifshitz point $\partial T_{C1}^{||, \perp}/\partial\mu = \partial T_C/\partial\mu = \partial T_I/\partial\mu$.

When choosing $\varepsilon(x)$ in helicoidal form, which is known to be an exact solution of the functional (3.21),

$$\varepsilon(x) = (e_1 \cos qx + e_2 \sin qx)\varepsilon_0, \quad e_1 \parallel A_0, \quad e_2 \perp A_0, \quad (3.25)$$

we obtain the instability condition (3.21) with the replacement $b_{\parallel, \perp} \rightarrow b_1 + \frac{1}{2}b_2$. Thus, formally, upon movement from the commensurate SDW phase (see fig. 3), the first one to set in is the absolute instability toward transition to a state with incommensurate SDW linearly polarized along A_0 . Notice that the $T_{C1}(\mu)$ lines lie inside the region of existence of the C phase ($\alpha < 0$).

Let us now find out the boundaries of the region of absolute instability of the I phase. To do this, it is necessary to specify the equilibrium value of $A(x)$. The

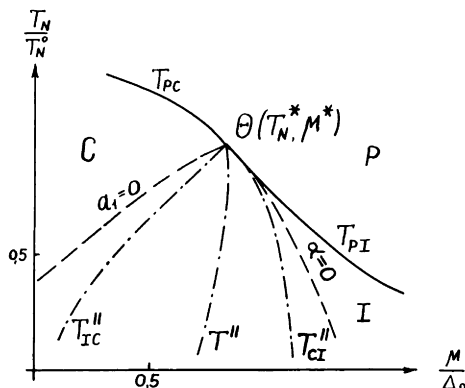


Fig. 3. Region of the phase diagram near the Lifshitz point for a system with a low-capacity reservoir.

simplest way consists in choosing $\Delta(x)$ in the form of a linearly polarized plane wave:

$$\Delta(x) = \Delta_0 \sin q_0 x, \quad (3.26)$$

where Δ_0 and q_0 must be determined in a self-consistent manner from the functional (3.21):

$$q_0^2 = -\frac{1}{2}a_2^{-1}(a_1 + \frac{1}{4}b_{||}\Delta_0^2), \quad \Delta_0^2 = -\frac{\alpha + a_1 q_0^2 + a_2 q_0^4}{\frac{3}{4}\beta_1 + \frac{1}{2}b_{||}q_0^2}. \quad (3.27)$$

The condition of absolute instability of the I phase of the form (3.26) toward transition to the C phase is found in the same way as eq. (3.24). It is easy to see that the condition of nontrivial solvability of eq. (3.27) has the following form in the limit $q_0 \rightarrow 0$:

$$a_1 + \frac{1}{3}b_{||}|\alpha|/\beta_1 \leq 0. \quad (3.28)$$

In the region determined by eq. (3.28) (the $T_{IC}^{II}(\mu)$ line in fig. 3) the solution (3.26) is always stable against a small constant increment ϵ for $\epsilon \parallel \Delta_0$. Analogous conclusions can be made for the increment $\epsilon \perp \Delta_0$ and also for the helicoidal SDW structure. In the latter case, instead of (3.28) we should write:

$$a_1 + b_1|\alpha|/\beta_1 \leq 0. \quad (3.29)$$

On the line defined by eq. (3.28) the energy of the incommensurate linearly polarized phase $\Omega_I = \frac{1}{3}|\alpha|^2/\beta_1$, while the energy of the commensurate phase $\Omega_C = -\frac{1}{2}|\alpha|^2/\beta_1$, implying that the latter phase is energetically more favorable. Thus, the first-order transition line corresponding to the thermodynamic equilibrium of the phases lies between the lines $T_{IC}^{II}(\mu)$ and $T_{CI}^{II}(\mu)$, which may be regarded as the boundaries of the existence of metastable I and C structures, respectively. On the other hand, for the helicoidal SDW structure (3.29) the energies of the I and C phases coincide on the line defined by eq. (3.29), i.e. there is no metastable I phase and the transition between the I and C phases is second-order.

We now discuss the question of the choice of the form of the solution for spin density waves in the I phase. Near the P–I transition line, where in the formulas for q_0^2 we may neglect the contributions $\frac{1}{4}b_{||}\Delta_0^2$ and $\frac{1}{4}b_1\Delta_0^4$ as compared to a_1 , the most favorable phase for $\beta_1 > 0$ is the helicoidal phase:

$$\Omega_{hel} - \Omega_{cos} = -\frac{1}{6}(\alpha - a_1^2/4a_2)^2/\beta_1 < 0. \quad (3.30)$$

However, near the C–I transition line the situation is not so unambiguous. As a matter of fact, if $b_2 > 2b_1$, then the line defined by eq. (3.29) lies to the left of that defined by eq. (3.28) on the (T, μ) diagram. This means that the helicoidal SDW is more favorable near the two boundaries of existence of the I phase than the sinusoidal linearly polarized one. However, when $b_2 < 2b_1$, the former line

lies to the right of the latter, which means that formally the possibility of appearance of the sinusoidal SDW is not excluded, not at least near the I-C transition line. It is clear, however, that sooner or later as the P-I transition boundary is approached the helicoidal SDW must again be realized, i.e. a re-orientational transition must take place. The presence of magnetic anisotropy, which has been neglected in the functional (3.21), can, of course, make the situation more favorable for the sinusoidal structure.

The physical factor responsible for the helicoidal solution being more favorable than the sinusoidal one in the case of a small-capacity reservoir is obvious and consists of an energy loss upon spatial redistribution of the electron density. For the sinusoidal structure such a loss occurs even by virtue of $|\Delta|^4$ (the term $\sim \beta_1$ in eq. (3.21)), and in the gradient terms such a loss occurs by virtue of $|\Delta|^2 |\partial \Delta / \partial x|^2$ (the term $\sim b_1$). The neglect of this circumstance (Kotani 1978b) has led to the incorrect conclusion that the sinusoidal phase is more favorable than the helicoidal one over the entire region of existence of the I phase.

3.2. SDW soliton lattice state in the model with an infinite-capacity electron reservoir

From expression (3.6) it follows that in the limit of large capacity of the reservoir ($M \gg 1$) we may ignore the effect of electron density redistribution on generation of spin density waves and limit ourselves to the inclusion of the short-range part of the electron-electron interaction in the effective potential g . In such a case, in the model of planar segments we can solve exactly the system of equations (3.1) for the Green's functions and also the self-consistency equation for the linearly polarized SDW at any temperature T (Buzdin and Tugushev 1983). Indeed, let us switch over to a diagonal (with respect to the spin index) representation in eq. (3.4):

$$\Delta^t(x) \cdot \hat{\sigma} = \Delta(x) \hat{\sigma}_3. \quad (3.31)$$

The direction of the axis of quantization is chosen along the polarization vector of spin density waves. Then the system of equations for the functions $G_{ij}(x, x'; \tilde{\omega}_n)$ with $\alpha = \pm 1$ will have the form

$$\begin{pmatrix} i\tilde{\omega}_n - iv_F \partial / \partial x & \Delta(x)\alpha \\ \Delta(x)\alpha & i\tilde{\omega}_n + iv_F \partial / \partial x \end{pmatrix} \hat{G}^{\alpha\alpha} = \delta(x - x'). \quad (3.32)$$

Taking the quadrature of the system represented by eq. (3.32) and writing it term by term in an explicit form, we get

$$\begin{aligned} (-\tilde{\omega}_n^2 - H^2) G_{11}^{\alpha\alpha} + iv_F \frac{\partial \Delta \alpha}{\partial x} G_{21}^{\alpha\alpha} &= i\tilde{\omega}_n + \left(iv_F \frac{\partial \Delta \alpha}{\partial x} \right) \delta(x - x'), \\ -iv_F \frac{\partial \Delta \alpha}{\partial x} G_{21}^{\alpha\alpha} + (-\tilde{\omega}_n^2 - H^2) G_{11}^{\alpha\alpha} &= -\Delta(x)\alpha \delta(x - x'), \end{aligned} \quad (3.33)$$

and an analogous pair of equations for $G_{22}^{\alpha\alpha}$ and $G_{12}^{\alpha\alpha}$. Here $H^2 = -v_F^2 \partial^2 / \partial x^2 + \Delta^2(x)$. Setting up then the linear combinations $\mathcal{G}_{\pm} = G_{11}^{\alpha\alpha} \pm iG_{21}^{\alpha\alpha}$ and performing obvious transformations of the “sources” on the right-hand side of eq. (3.33), after a simple rearrangement of the terms, we obtain

$$\begin{aligned}\mathcal{G}_+^{\alpha\alpha} &= -\sum_m \frac{i\tilde{\omega}_n f_{m\alpha}^{(1)}(x) f_{m\alpha}^{*(1)}(x') + \tilde{E}_m f_{m\alpha}^{(1)}(x) f_{m\alpha}^{*(2)}(x')}{\tilde{\omega}_n^2 + \tilde{E}_m^2}, \\ \mathcal{G}_-^{\alpha\alpha} &= -\sum_m \frac{i\tilde{\omega}_n f_{m\alpha}^{(2)}(x) f_{m\alpha}^{*(2)}(x') + \tilde{E}_m f_{m\alpha}^{(2)}(x) f_{m\alpha}^{*(1)}(x')}{\tilde{\omega}_n^2 + \tilde{E}_m^2},\end{aligned}\quad (3.34)$$

where the functions $f_{m\alpha}^{(1,2)}(x)$ are given by the relation

$$f_{m\alpha}^{(1,2)} = \varphi_{m\alpha}^{(1)} \pm i\varphi_{m\alpha}^{(2)}, \quad (3.35)$$

and $\varphi_{m\alpha}^{(1,2)}$ is the solution of the system of Bogoliubov equations:

$$\begin{aligned}iv_F \frac{\partial}{\partial x} \varphi_{m\alpha}^{(1)} - \Delta\alpha \varphi_{m\alpha}^{(2)} &= E_m \varphi_{m\alpha}^{(1)}, \\ -iv_F \frac{\partial}{\partial x} \varphi_{m\alpha}^{(2)} - \Delta\alpha \varphi_{m\alpha}^{(1)} &= E_m \varphi_{m\alpha}^{(2)}, \\ E_m &= \tilde{E}_m + \eta_+(\mathbf{q}_\perp),\end{aligned}\quad (3.36)$$

and E_m are its eigenvalues. With the self-consistency equation

$$\frac{\Delta(x)}{g} = \frac{1}{2} \text{Tr} \alpha T \sum_{n, \mathbf{q}_\perp} G_{12}^{\alpha\alpha}(x, x'; \tilde{\omega}_n), \quad (3.37)$$

we also have a closed system of expressions for the Green's functions and the order parameter. It is not difficult to see that eq. (3.37) can be rewritten in a form analogous to the corresponding equation in the Peierls continuum model with the filling of the band being close to half:

$$\begin{aligned}\frac{\Delta(x)}{g} &= \text{Re} \sum_{\mathbf{q}_\perp, E_m > 0} f_m^{*(1)}(x, \mathbf{q}_\perp) f_m^{(2)}(x, \mathbf{q}_\perp) \\ &\times [n(E_m - \eta_+ - \mu) - n(-E_m - \eta_+ - \mu)],\end{aligned}\quad (3.38)$$

where the subscript α in the functions $f_m^{(1,2)}$ has been taken to be equal to $+1$ and $n(x)$ is the Fermi distribution function. Therefore, we may use the results obtained for this model by Brazovskii et al. (1980) and by Horovitz (1981) at $T = 0$. These authors have found an exact periodic solution for the system described by eqs. (3.37) and (3.36) in the form of a soliton lattice:

$$\Delta(x) = \Delta_2 \text{sn} \left(\frac{\Delta_1 x}{v_F}, \gamma \right), \quad \gamma = \frac{\Delta_2}{\Delta_1}, \quad (3.39)$$

where $\text{sn}(y, \gamma)$ is the Jacobi elliptic function with modulus γ and period $4K(\gamma)$. The functions $f_{m\alpha}^{(1,2)}(x)$ for opposite values of $\alpha = \pm$ are obtained by a shift of the argument by half the period of the soliton lattice defined by eq. (3.39), which is why, in what follows, we will speak only of the functions $f_{m+}^{(1,2)} - f_m^{(1,2)}$, which, according to Brazovskii et al. (1980), are the essence of the solutions of first-order Lame's equations:

$$\left[v_F^2 \frac{\partial^2}{\partial x^2} + E_m^2 - \Delta^2 \pm \frac{\partial \Delta}{\partial x} \right] f_m^{(1,2)}(x) = 0. \quad (3.40)$$

The “potentials” of these equations

$$Q(x), p(x) = \Delta^2 \mp \Delta'(x)$$

may be rewritten, using eq. (3.39), in standard form via the doubly periodic Weierstrass elliptic functions $\wp(y)$ (Whittaker and Watson 1927) with real (ω) and imaginary (ω') periods

$$Q(x) = p(x + \omega) = e_1 + 2\wp(x + \omega'),$$

$$\omega = \frac{K(k)}{(e_1 - e_3)^{1/2}}, \quad \omega' = \frac{iK(k')}{(e_1 - e_3)^{1/2}}, \quad (3.41)$$

$$e_1 - e_3 = \varepsilon_+^2, \quad e_1 - e_2 = \varepsilon_-^2 = k'^2 \varepsilon_+^2, \quad e_1 + e_2 + e_3 = 1:$$

$$\Delta_{1,2} = (1 \pm k')\varepsilon_+, \quad \frac{\Delta_2}{\Delta_1} = \frac{1 - k'}{1 + k'} = \gamma. \quad (3.42)$$

The solutions of eqs. (3.40) may now be written in the form of Bloch functions (see e.g. Whittaker and Watson 1927). Then, imposing the quasi-periodic boundary conditions

$$f_m^{(1,2)}(x + 2\omega) = \exp(2iq_m\omega)f_m^{(1,2)}(x),$$

one can determine the longitudinal (i.e. along the normal to the planar portion) density of states per spin (Mertsching and Fischbeck 1981, Takayama et al. 1980):

$$\begin{aligned} N_{||}(\varepsilon) &= \left| \frac{\partial q_m}{\partial \varepsilon} \right| \frac{1}{v_F} \\ &= \frac{|\varepsilon^2 - \varepsilon_+^2 E(k)/K(k)|}{[(\varepsilon^2 - \varepsilon_+^2)(\varepsilon^2 - \varepsilon_-^2)]^{1/2}} \Theta[(\varepsilon^2 - \varepsilon_+^2)(\varepsilon^2 - \varepsilon_-^2)] \frac{1}{\pi v_F}. \end{aligned} \quad (3.43)$$

The energy spectrum $\varepsilon(q)$ contains two symmetric gaps $\pm \varepsilon_+(1 - k')$, a narrow allowed midband of width $2k'\varepsilon_+$ and two broad bands (see fig. 4).

Analytic treatment based on the exact solution of eq. (3.39) can be carried out to completion in two limiting cases: $T \ll \Delta_2$ or Δ_1 , $\Delta_2 \ll T, \mu$ (the latter condition determines the region near the Lifshitz point where the functional

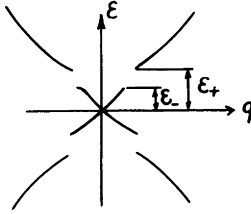


Fig. 4. Electronic spectrum in the SDW soliton lattice model below the Néel point.

approach is operative). In the intermediate region of the values of temperature T and order parameter μ , only a numerical calculation is possible. To simplify the calculations we will assume that $|\eta_+| \ll \mu$, i.e. the choice of the wave vector Q_\perp provides the best geometric coincidence of electron and hole Fermi surfaces.

In the region of low temperatures $T \ll \Delta_2$, we calculate explicitly the thermodynamic potential $\Omega(T, \mu)$:

$$\begin{aligned} \Omega = -2T \cdot 2N(0) & \left\{ \int_{-W_\parallel}^{W_\parallel} \ln(1 + \exp[-(\varepsilon - \mu)/T]) \left| \frac{\partial q}{\partial \varepsilon} \right| d\varepsilon \right\} \\ & + (\bar{g} K(\gamma))^{-1} \int_0^{K(\gamma)} \Delta^2(y) dy \frac{2N(0)}{\pi \Delta_1}, \quad \bar{g} = g N_\perp \frac{1}{\pi v_F} = g N(0), \end{aligned} \quad (3.44)$$

where N_\perp is the transverse density of states.

Using the formula for the longitudinal density of states [eq. (3.43)], we obtain at $T = 0$

$$\begin{aligned} \Omega(0, \mu) = \Omega_0(\mu) + \delta\Omega(0, \mu), \\ \frac{\delta\Omega(0, \mu)}{2N(0)} = -\varepsilon_+^2 \left\{ \ln \frac{\varepsilon_+ k}{\Delta_0} \left[2 \left(\frac{E(k)}{K(k)} - 1 \right) + k^2 \right] + \frac{1+k'^2}{2} - 2 \frac{E(k)}{K(k)} \right\} \\ - \frac{\pi \mu E_+}{K(k)}. \end{aligned} \quad (3.45)$$

For definiteness it is assumed that $\mu > 0$ and lies inside the forbidden band $\varepsilon_+(1 - k')$; $\Omega_0(\mu)$ is the thermodynamic potential of the paramagnetic phase and Δ_0 is the value of the order parameter in the commensurate phase at $T = \mu = 0$.

Minimizing eq. (3.45) with respect to ε_+ and k , we get

$$\begin{aligned} \varepsilon_+ = \frac{\Delta_0}{k}, \quad \frac{E(k)}{k} = \frac{\mu \pi}{2 \Delta_0}, \\ \frac{\Omega(0, \mu) - \Omega_0(\mu)}{2N(0)} = -\Delta_0^2 \frac{1+k'^2}{2k'^2}. \end{aligned} \quad (3.46)$$

The critical value μ^c , which determines the boundary of the region of existence of the I phase, is given at $T = 0$ by the following conditions:

$$\mu^c = (2/\pi)\Delta_0, \quad k = 1. \quad (3.47)$$

The temperature correction to the thermodynamic potential in the region of $T \ll |\varepsilon_+ - \mu|$ is determined by the energy region in the vicinity of the edge of the forbidden band:

$$\varepsilon^2(q) \approx \varepsilon_+^2 + v^*(q - q_0)^2, \quad q_0 = \pm \frac{\pi\varepsilon_+}{2K(k)}, \quad v^* = \frac{K(k)k}{K(k) - E(k)}, \quad (3.48)$$

$$\frac{\delta\Omega(T, \mu) - \Omega(0, \mu)}{2N(0)} = -2(\tfrac{1}{2}\pi)^{1/2} \exp\left(-\frac{\varepsilon_+ - \mu}{T}\right) T^{3/2} \frac{\varepsilon_+^{1/2}}{v^*}. \quad (3.49)$$

Knowing $\Omega(0, \mu)$ and $\Omega(T, \mu)$ from eqs. (3.45) and (3.49), we can determine the low-temperature portion of the $T_l(\mu)$ line, which bounds the region of existence of the I phase when $\mu > (2/\pi)\Delta_0$. Expanding $\Omega(T, \mu)$ near the point $\mu = \mu^c$, $T = 0$, $k' = 0$, we obtain in a first-order approximation which does not vanish with respect to the parameter $L = [\ln(4/k')]^{-1} \ll 1$:

$$\begin{aligned} \frac{\Omega(T, \mu) - \Omega(0, \mu)}{2N(0)} &\approx -(\pi\Delta_0(\mu - \mu^c) - A)L, \\ A &= 2(\tfrac{1}{2}\pi)^{1/2} \exp\left[-\frac{\Delta_0 - \mu^c}{T}\right] T^{3/2} \Delta_0^{1/2}. \end{aligned} \quad (3.50)$$

The condition for the vanishing of the coefficient at L yields

$$\mu^c(T) = \mu^c + \frac{A(T, \mu^c)}{\pi\Delta_0}. \quad (3.51)$$

Thus, the dependence $\mu^c(T)$ is exponential in character in the region of low temperatures and determines the region of absolute instability of the I phase toward the C phase.

It is not difficult to see that, at $\mu = \mu^c$, $T = 0$, for the commensurate phase we obtain $\Delta_2 = \varepsilon_+ = \Delta_0$, $\delta\Omega(0, \mu^c) = 2N(0)(-\Delta_0^2/2)$, i.e. the thermodynamic potentials of the C and I phases coincide and the I-C transition is second-order. An analogous conclusion, at least within the limits of experimental accuracy, is valid for the region of low temperatures at the $\mu^c(T)$ line, which can be confirmed by direct calculation of eq. (3.49). At an arbitrary temperature T , the transition line $\mu^c(T)$ can be found only by numerical methods. In such a case it is convenient to start with the self-consistency equation (3.38), which after simple

but rather tiresome manipulations is reduced to the form

$$\begin{aligned} \ln \frac{\Delta_0}{k\varepsilon_+} &= \int_{\varepsilon_+}^{\infty} [n(\varepsilon + \mu) + n(\varepsilon - \mu)] \frac{\varepsilon d\varepsilon}{[(\varepsilon^2 - \varepsilon_+^2)(\varepsilon^2 - \varepsilon_-^2)]^{1/2}} \\ &+ \int_0^{\varepsilon_-} n(\mu - \varepsilon) - n(\mu + \varepsilon) \frac{\varepsilon d\varepsilon}{[(\varepsilon_+^2 - \varepsilon^2)(\varepsilon_-^2 - \varepsilon^2)]^{1/2}}. \end{aligned} \quad (3.52)$$

The parameter k must be determined from the minimization of the thermodynamic potential [eq. (3.44)]. In analytical form this can be realized near the Lifshitz point, where expansion in the small parameters $\Delta_2 \ll T, \mu$ and $k \ll 1$ is permissible. It is expedient, however, to apply the functional approach, which is completely equivalent to the one used earlier in the region of validity of the Ginzburg–Landau expansion for the potential $\Omega(T, \mu)$ near the Lifshitz point. Let us now specify this approach for the case under consideration.

Consider the functional of the form (3.21) for the linearly polarized SDW. The appropriate Euler–Lagrange equation reads

$$\begin{aligned} a_2 \Delta''' - a_1 \Delta'' + \alpha \Delta + \beta_1 \Delta^3 + \gamma \Delta^5 - b[\Delta(\Delta')^2 + \Delta^2 \Delta''] &= 0, \\ b &= b_1 + b_2. \end{aligned} \quad (3.53)$$

General analysis of the nonlinear equation of the form (3.53) is difficult, but with certain relations between its coefficients some of the solutions can be given. Let us first show that the simple periodic solution of the first modified Korteweg–de Vries (MKDV) equation,

$$\Delta''' - 6A\Delta^2\Delta' + B\Delta' = 0, \quad (3.54)$$

with appropriate choice of the constants A and B and the second integral C of eq. (3.54) is also the solution of eq. (3.53). This solution is known to have the form of the soliton lattice [eq. (3.39)]. The first and second integrals of eq. (3.54) have the familiar form:

$$\Delta'' - 2A\Delta^3 + B\Delta = 0, \quad (3.55)$$

$$(\Delta')^2 - A\Delta^4 + B\Delta^2 = C. \quad (3.56)$$

The equality of the first integral in eq. (3.55) to zero provides the choice of periodic solutions. Now, differentiating eq. (3.54) and combining the resultant expression with eq. (3.55) multiplied by $(\lambda_1 + \lambda_2 \Delta^2)$ and also with (3.56) multiplied by $\lambda_3 \Delta$, where λ_1, λ_2 and λ_3 are numerical multipliers, we obtain an equation of the type (3.53). From the condition of matching of the coefficients in the equations we find

$$\frac{c_1}{c_3} + B \frac{c_2}{c_3} + \frac{1}{2}B^2 + C = 0, \quad (3.57)$$

$$\begin{aligned} A &= 1, \\ \Delta_1^2 + \Delta_2^2 &= B, \\ \Delta_1^2 \Delta_2^2 &= C. \end{aligned} \tag{3.58}$$

One more missing equation should be derived for an unambiguous determination of the coefficients Δ_1 and Δ_2 (or, in other words, B and C) from the condition of minimization of the thermodynamic potential $\Omega(T, \mu)$ upon substitution of the exact solution (3.39) into eq. (3.44):

$$\Omega(T, \mu) - \Omega_0(\mu) = c_1 I_2 \Delta_2^2 + c_2 I_4 \Delta_2^4 + c_3 I_6 \Delta_2^6, \tag{3.59}$$

$$\begin{aligned} I_2 &= J_2, \quad I_4 = 2J_4 + \gamma^{-2} - (\gamma^{-2} + 1)J_2, \\ I_6 &= 8J_6 + (\frac{1}{2}\gamma^{-4} + 6\gamma^{-2} + \frac{1}{2})J_2 - 7(\gamma^{-2} + 1)J_4, \\ J_4 &= \frac{1}{K(\gamma)} \int_0^{K(\gamma)} \operatorname{sn}^n(y, \gamma) dy. \end{aligned} \tag{3.60}$$

Let us also write certain useful relations between the integrals J_n :

$$\begin{aligned} J_2 &= \gamma^{-2} [1 - E(\gamma)/K(\gamma)], \\ J_4 &= \frac{1}{3}\gamma^{-2} [2(\gamma^2 + 1)J_2 - 1], \\ J_6 &= \frac{1}{5}\gamma^{-2} [4(\gamma^2 + 1)J_4 - 3J_2]. \end{aligned} \tag{3.61}$$

It is convenient to vary eq. (3.59) with respect to Δ_2 and to obtain the missing equation:

$$c_1 I_2 + 2c_2 I_4 \Delta_2^2 + 3c_3 I_6 \Delta_2^4 = 0. \tag{3.62}$$

Now we can discuss the question of the I-C transition line near the Lifshitz point. Expanding eq. (3.59) with $\gamma \rightarrow 1$, we obtain up to dominant order in the logarithm $L = (\ln 4/\gamma')^{-1}$

$$\Omega(T, \mu) - \Omega_0(\mu) = (c_1 \Delta_2^2 + c_2 \Delta_2^4 + c_3 \Delta_2^6) - L(c_1 \Delta_2^2 + \frac{2}{3}c_2 \Delta_2^4 + \frac{3}{5}c_3 \Delta_2^6). \tag{3.63}$$

The vanishing of the coefficient at L and also the condition (3.57) give the I-C transition line:

$$c_1 c_3 = \frac{5}{27} c_2^2, \quad c_1 > 0, c_2 < 0, \tag{3.64}$$

the value of $\Delta_2^2 = \Delta_1^2$ at this line being given by

$$\Delta_2^2 = \Delta_1^2 = \frac{5}{9} \frac{|c_2|}{c_3}, \quad c_2 < 0, c_1 > 0. \tag{3.65}$$

Calculating the energies of the I and C phases at the line given by eq. (3.64), we obtain, with logarithmic accuracy,

$$\Omega(T, \mu) - \Omega_0(\mu) = \Omega_c(T, \mu) - \Omega_0(\mu) = -\frac{5^2}{9^3} \frac{|c_2|^3}{c_3^2}. \quad (3.66)$$

Of interest is the comparison of the snoidal solution (eq. (3.39)) with the helicoidal solution. Near the Lifshitz point the existence boundary of the helicoidal phase is given by a relation analogous to (3.29):

$$c_1 c_3 = \frac{2}{3} c_2^2, \quad c_1 > 0, c_2 < 0, \quad (3.67)$$

i.e. it lies much closer to the P–I transition line. From this we can make a qualitative presumption regarding the favorableness of the snoidal solution as compared to the helicoidal one over the entire region of existence of the I phase. The numerical calculation that has been recently performed by Machida and Nakanishi (1984) for a mathematically equivalent model of a quasi-one-dimensional superconductor in a magnetic field in the incommensurate Larkin–Ovchinnikov–Fulde–Ferrell (LOFF) state confirms this inference.

It is interesting to note that the choice of the snoidal solution as a variational one for the functional of the general form (3.21) provides an unambiguous confirmation that it is unfavorable as compared to the helicoidal solution for $\beta_1 > 0$, at least in the immediate vicinity of the Lifshitz point. Indeed, calculations analogous to eq. (3.63) give, up to dominant order in L ,

$$\begin{aligned} \Omega(T, \mu) - \Omega_0(\mu) = & (\alpha \Delta_2^2 + \frac{1}{2} \beta_1 \Delta_2^4 + \frac{1}{3} \gamma_1 \Delta_2^6) - L [\alpha \Delta_2^2 + \frac{2}{3} \Delta_2^4 (\beta_1 - a_1) \\ & + \frac{1}{15} \Delta_2^6 (\frac{23}{3} \gamma_1 - 8a_2 - 2(b_1 + b_2))] . \end{aligned} \quad (3.68)$$

If the coefficient $\beta_1 > 0$ is not anomalously small, then, retaining only the terms $\sim \Delta_2^4$, it is not difficult to show that the stability boundary for the snoidal phase when $a_1 \ll \beta_1$ practically coincides with the $\alpha = 0$ line and that with $a_1 \sim \beta_1$ (far from the Lifshitz point, but still within the range of validity of the Ginzburg–Landau expansion) $a_1 = -\frac{1}{2} \beta_1$. In any case, in fig. 3 this boundary lies much more to the right (closer to the P–I transition line) than the stability limit of the helicoidal phase (3.29) and the sinusoidal phase (3.28).

Thus, in the limit $M \gg 1$, the sinusoidal solution (3.28) is exact and more favorable as compared to the helicoidal one, but the question of its uniqueness and favorableness as compared to the other solutions within the class of linearly polarized spin density waves is still open. Appendix II gives some mathematical arguments regarding the possibility of the existence of more sophisticated solutions for functionals of the type (3.14). In the Peierls model at $T = 0$ such solutions have been discussed by Brazovskii et al. (1981), but no conclusions concerning the region of their realization in SDW systems can be made at present.

The above exactly solvable model of the SDW soliton lattice with an infinite-capacity reservoir can be extended, after altering the notation appropriately, to other systems with electronic and magnetic phase transitions: quasi-one-dimensional superconductors in an exchange field (Buzdin and Tugushev 1983, Buzdin and Polonskii 1987), spin-Peierls antiferromagnets in a magnetic field (Buzdin et al. 1983). At the same time, for CDW and SDW systems restrictions on the application of the model are imposed by the finite capacity of the reservoir and the role of Coulomb long-range interaction. For such systems the solution in the form of a soliton lattice must be regarded only as variational.

3.3. Influence of impurity scattering and a finite-capacity electron reservoir on the formation of the SDW soliton lattice

As pointed out earlier, in the model of an antiferromagnet with spin density waves electron-impurity scattering leads to a decrease in the transition temperature $T_N(\mu)$. Generally speaking, an increase in the impurity concentration x may also lead to a change in the type of magnetic structure (e.g. the disappearance of spin structure modulation) (Kulikov and Tugushev 1984).

Let us examine in more detail the region of the phase diagram (T, μ) in the vicinity of the Lifshitz point. This region is interesting in that the change in the type of magnetic structure may occur even with a very small impurity concentration, i.e. even if the condition $v \ll (T_N, \mu)$, where v is the total frequency of electron-impurity scattering, is satisfied. Let us make it clear immediately that in the sequel v is taken to mean the total frequency of scattering of electrons from the planar segments of the Fermi surface onto impurity atoms, both with and without a transition into the reservoir: $v = 2\pi x [\langle V_{nn}^2 \rangle N_n(0) + \langle V_{nr}^2 \rangle N_r(0)]$, where $N_n(0)$ and $N_r(0)$ are the densities of states of the planar segments and the reservoir, respectively; V_{nn} and V_{nr} are the matrix elements of the electron-impurity scattering potential with and without transition into the reservoir, respectively. Apart from the frequency v , in this case there also appears a frequency $v' = 2\pi x \langle V_{nn}^2 \rangle N_n(0)$, which is less than or of the order of v . As will be seen later, the parameter v'/v ($0 \leq v'/v \leq 1$) exerts a strong influence on the form of the modulated structure of the spin density waves.

Within the framework of the functional approach, which is valid in the vicinity of the Lifshitz point (T_N^*, μ^*) , we examine the thermodynamic potential $\Omega(\Delta(x))$ written in the form of eq. (3.21). The coefficients for the functional Ω are no longer connected by the concrete relations (3.14) and (3.15), and in the general case one cannot say anything about the form of the equilibrium solution $\Delta(x)$. However, in the limit of weak electron-impurity scattering (in the sense indicated above) and a large (but not infinite) capacity of the reservoir we can still go further into the analysis of the functional (3.21).

The influence of impurity scattering on the coefficients of the functional (3.21) can be conveniently accounted for graphically. Figure 5 shows, as an example,

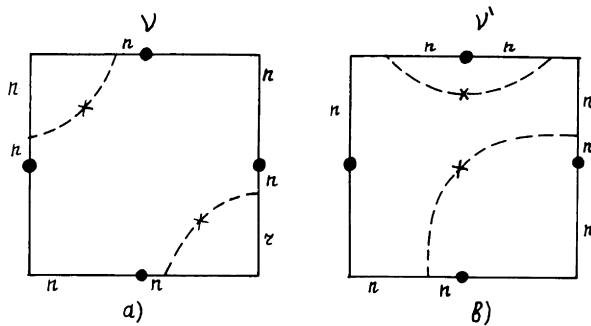


Fig. 5. Contributions of impurity scattering processes to the renormalization of the Landau expansion coefficients for the thermodynamic potential Ω .

some of the terms of fourth order in $\Delta(x)$ in the functional (3.21). The solid line represents the temperature Green's functions in the paramagnetic phase (the subscript n is used for electrons of the planar segments and r for electrons of the reservoir), the circle indicates the order parameter $\Delta(x)$ and the dashed line, the electron-impurity scattering potential.

Within the framework of the standard diagrammatic technique (Abrikosov et al. 1962) the scattering off a nonmagnetic impurity leads to two types of correction. First, there appears a damping in the Green's functions (fig. 1a), which reduces to replacement of the imaginary frequencies $i\omega_k \rightarrow i\tilde{\omega}_k = i\omega_k(1 + v/|\omega_k|)$, $\omega_k = \pi T(2K + 1)$, $k = 0, \pm 1, \dots$. This procedure by itself does not violate relations (3.14) between the coefficients of the functional (3.21) in the limit $M \rightarrow \infty$; instead of c_1, c_2 and c_3 the renormalized values \tilde{c}_1, \tilde{c}_2 and \tilde{c}_3 appear (see Appendix I). Second, it is necessary to accomplish the "dressing", by impurity lines, of the vertices containing single circles and pairs of circles. It is not difficult to see that the contributions of such diagrams are proportional to $v' \sim v(1 + M)^{-1}$ under the assumption that the matrix elements $\langle V_{nn}^2 \rangle$ and $\langle V_{nr}^2 \rangle$ are quantities of the same order of magnitude. In this case, $v'/v \sim (1 + M)^{-1} \rightarrow 0$ when $M \gg 1$. A situation may be envisaged, where due to certain special reasons (e.g. the specificity of the symmetric properties of the wave function) the scattering accompanied by transition into the reservoir (i.e. actually into another band) is suppressed, in which case $v'/v \sim 1$ even when $M \gg 1$. The coefficients of the functional Ω of the form (3.21) are explicitly given in Appendix I.

A concrete calculation has been performed for two limiting cases: $v'/v = 0$ and $v'/v = 1$ for $M \rightarrow \infty$. Note that in the limit $v'/v = 0$ the restriction on the smallness of v as compared to (T, μ) is of no importance in the sense that the soliton solution (3.39) does not change its form even far from the Lifshitz point, where the expansion (3.21) is no longer applicable. If $v'/v \sim 1$, then relations

(3.14) are violated and even if the contribution of (3.15) is neglected, no exact solution in the form (3.39) can be obtained.

Nevertheless, we may hope that this solution will still be valid as a variational solution, at least for $v' \ll (T^*, \mu^*)$, for which we have small corrections to the coefficients $\{c_i\}$ of the exactly solvable model without impurity scattering. The advantage of the choice of the snoidal solution as a variational one as compared to the traditionally used sinusoidal solution for the SDW model is that it is possible to take accurate account of an infinite number of harmonics, which is especially important near the I-C transition line.

Calculations show that for any $v \ll (T, \mu)$ the thermodynamic potential $\Omega_{sn}(T, \mu, v)$ in the class of snoidal solutions $\Delta(x) = \Delta_1 \operatorname{sn}(\Delta_1 x/v_F)\gamma$ is lower than that in the class of sinusoidal solutions $\Delta(x) = \Delta_2 \sin(\Delta_2 x/v_F)$, i.e. $\Omega_{sn}(T, \mu, v) - \Omega_{sin}(T, \mu, v) < 0$. The phase diagrams for the cases $v' = 0$ and $v' = v$ are given in fig. 6. All the transitions (P-I, P-C, and I-C) are of second order. This has been tested by direct computations of the thermodynamic potential $\Omega_{sn}(T, \mu, v)$ obtained by substitution of the variational solution in the form (3.39) and by minimization of Ω_{sn} with respect to the parameters Δ_1 and Δ_2 of the soliton lattice.

Now we are interested in a more correct search for the form of the function $\Delta(x)$ for the case $v'/v \neq 0, M \neq \infty$. An equation of the general form (3.53) has solutions in the class of doubly periodic functions and we are interested in those which satisfy the slowness and smallness criteria used in constructing the functional (3.21).

The corrections to relations (3.14) are assumed to be small with respect to the parameter $(1 + M)^{-1} \ll 1$, which corresponds to the smallness of corrections of

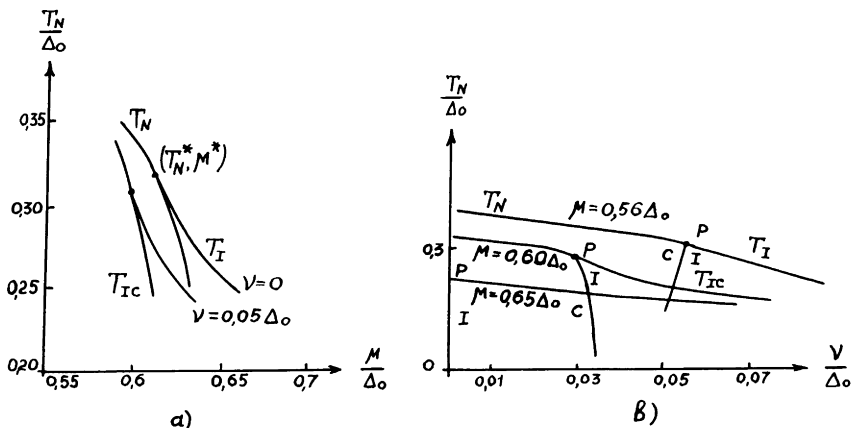


Fig. 6. Effect of impurity scattering on the phase diagram of an itinerant antiferromagnet. (a) $v' = 0$.
(b) $v' = \gamma$.

the type (3.45) and to the relation $v'/v \sim (1 + M)^{-1}$. It is convenient to include immediately all the impurity contributions in the coefficients α , a_1 and a_2 at lower degrees of $\Delta(x)$ (see Appendix I). In eq. (3.53) we thus have

$$\begin{aligned} b &= \frac{10a_2 + b'}{v_F^2}, & \gamma &= \frac{6a_2 + \gamma'}{v_F^4}, & \beta_1 &= \frac{2a_1 + \beta'_1}{v_F^2}, \\ b', \gamma' &\ll a_2, & |\beta'_1| &\ll 2|a_1|. \end{aligned} \quad (3.69)$$

The explicit form of γ' , b' and β'_1 is unimportant here; what is of importance is that all these corrections are $\sim (1 + M)^{-1}$ and are small in the limit of large reservoir capacity M . The most severe restriction on this smallness is imposed by the requirement $|\beta'_1| \ll 2|a_1|$, since a_1 can itself vanish at the Lifshitz point. Therefore, in the immediate vicinity of this point the scheme of calculation of the corrections constructed below is not applicable to the solution of eq. (3.39). As M increases, the region of violation of the relation $|\beta'_1| \ll 2|a_1|$ becomes increasingly narrow and the region of validity of the calculation scheme is widened. Introducing the dimensionless variables

$$\Delta \rightarrow \Delta \left(\frac{|a_1|}{a_2} \right)^{1/2}, \quad x \rightarrow x \left(\frac{a_2}{|a_1|} \right)^{1/2} v_F^{-1}$$

we rewrite eq. (3.69) as follows:

$$\begin{aligned} \Delta'''' - \text{sgn}(a_1)\Delta'' + z\Delta + \left(2\text{sgn}(a_1) + \frac{\beta'_1}{|a_1|} \right)\Delta^3 + \left(6 + \frac{\gamma'}{a_2} \right)\Delta^5 \\ - \left(10 + \frac{b'}{a_2} \right)(\Delta\Delta'^2 + \Delta^2\Delta'') = 0, \quad z = \frac{\tilde{c}_1 \tilde{c}_3}{|\tilde{c}_2|^2}. \end{aligned} \quad (3.70)$$

In the region of existence of the inhomogeneous solution (3.70), $a_1 < 0$.

The correction to the solution (3.39), which is linear in β'_1 , γ' and b' will be sought in the form $\Delta(x) - \Delta_0(x) = \tilde{\varphi}(x)\Delta'_0(x)$. The linearized equation for the function $\tilde{\varphi}(x)$ has the form

$$\begin{aligned} \Delta'_0 \tilde{\varphi}'''' + 4\Delta''_0 \tilde{\varphi}''' + 2(3\Delta''_0 + \Delta'_0(1 - 5\Delta_0^2))\tilde{\varphi}'' \\ + 4(\Delta''''_0 + \Delta''_0(1 - 5\Delta_0^2) - 5\Delta_0^2 \Delta_0)\tilde{\varphi}' = f(x), \end{aligned} \quad (3.71)$$

where $\Delta_0(x)$ is the snoidal function (3.39), and

$$f(x) = -\frac{\beta'_1 \Delta_0^3}{|a_1|} - \frac{\gamma' \Delta_0^5}{a_2} + \frac{b'}{a_2}(\Delta_0 \Delta'^2_0 + \Delta_0^2 \Delta''_0) \quad (3.72)$$

is an odd, periodic [with period $4K(\gamma)$] function. Substitution of $\tilde{\varphi}'(x) = h(x)/\Delta'_0(x)$ makes it possible to lower the order of the differential

equation:

$$h''' + \frac{\Delta_0''}{\Delta_0'} h'' + \left[3 \frac{\Delta_0'''}{\Delta_0'} - 2 \left(\frac{\Delta_0''}{\Delta_0'} \right)^2 + 2 - 10\Delta_0^2 \right] h' + \left[3 \frac{\Delta_0'''}{\Delta_0'} - 4 \frac{\Delta_0'' \Delta_0'''}{\Delta_0'^2} \right. \\ \left. + 2 \left(\frac{\Delta_0''}{\Delta_0'} \right)^3 + (2 - 10\Delta_0^2) \frac{\Delta_0''}{\Delta_0'} - 20\Delta_0' \Delta_0 \right] h = f(x). \quad (3.73)$$

It is not difficult to see that at $f(x) = 0$, the last equation is satisfied by the solutions of the equation

$$h'' + \left[3 \frac{\Delta_0'''}{\Delta_0'} - 2 \left(\frac{\Delta_0''}{\Delta_0'} \right)^2 + 2 - 10\Delta_0^2 \right] h = \frac{C}{\Delta_0'}, \quad (3.74)$$

with an arbitrary constant C . Let us denote the solutions of the homogeneous equation (3.74) ($C = 0$) by $h_1(x)$ and $h_2(x)$ and its Wronski determinant by $W = h_1 h_2' - h_1' h_2$. Then, the special solution of the inhomogeneous equation (3.74) at $C = W$ will have the form

$$h_3(x) = h_2(x) \int^x \frac{h_1(x')}{\Delta_0'(x')} dx' - h_1(x) \int^x \frac{h_2(x')}{\Delta_0'(x')} dx'. \quad (3.75)$$

The set of three functions h_1 , h_2 , h_3 constitute the basis for any solution of eq. (3.73) at $f(x) = 0$. The special solution of the same equation with a non-zero right-hand side has the standard form:

$$h_4(x) = \frac{1}{W} \left[h_2(x) \int^x \frac{h_1(x')}{\Delta_0'(x')} - h_1(x) \int^x \frac{h_2(x')}{\Delta_0'(x')} \right] \int^{x'} \Delta_0'(x'') f(x'') dx'' dx'. \quad (3.76)$$

Let us now write down the general solution of the inhomogeneous equation (3.73):

$$h(x) = \sum_{i=1}^3 A_i h_i(x) + h_4(x) \quad (3.77)$$

and find the functions h_1 and h_2 in an explicit form. First, we rewrite the “potential” in eq. (3.74) as

$$3 \frac{\Delta_0'''}{\Delta_0'} - 2 \left(\frac{\Delta_0''}{\Delta_0'} \right)^2 + 2 - 10\Delta_0^2 = 2 - 3(\Delta_1^2 + \Delta_2^2) + 2 \left(\frac{\Delta_0}{\Delta_0'} \right)^2 (\Delta_1^2 + \Delta_2^2)^2. \quad (3.78)$$

Performing transformations of the elliptic functions (Whittaker and Watson 1927), one can see that

$$\frac{\Delta_0(x)}{\Delta_0'(x)} = - \frac{1}{\Delta_1(1 - \gamma^2)} \frac{\operatorname{cn}(\Delta_1 x + K(\gamma))}{\operatorname{sn}(\Delta_1 x + K(\gamma)) \operatorname{dn}(\Delta_1 x + K(\gamma))}. \quad (3.79)$$

Combining eqs. (3.78) and (3.79) and introducing new variables

$$y = (1 + \gamma)(A_1 x + K(\gamma)), \quad k = (2\gamma^{1/2}/(1 + \gamma)) \quad \text{and} \quad k_1^2 + k^2 = 1,$$

we can rewrite eq. (3.74) at $C = 0$ in the form of a first-power Lamé equation:

$$h''(y) + 2 \left[1 + \frac{1 - \frac{3}{2}B}{4A_1^2} (1 + k_1)^2 - k^2 \operatorname{sn}^2(y + K(k) + iK'(k)) \right] h(y) = 0. \quad (3.80)$$

Its two linearly independent solutions are expressed via the Jacobi eta and theta functions

$$h_{\pm}(y) = \frac{\Theta_1(y + y_0, k)}{H_1(y, k)} \exp[\mp y Z(y_0, k)]. \quad (3.81)$$

Here $Z(y_0, k)$ is the zeta function with argument y_0 , which can be found from the equation

$$k^2 \operatorname{cn}^2(y_0, k) = 1 + \frac{(1 + k_1)^2 (1 - \frac{3}{2}B)}{2A_1^2}. \quad (3.82)$$

Since $\tilde{\varphi} = h/A'_0$, it follows that the boundary conditions $h(x = \pm K(\gamma)/A_1)$ must be imposed on the solutions of eq. (3.73); for these boundary conditions the following linear combinations of the functions (3.81) are satisfied:

$$\begin{aligned} h_1 &= h_+ - h_-, \\ h_2 &= h_+ \exp(2K(k)Z(y_0, k)) - h_- \exp(-2K(k)Z(y_0, k)). \end{aligned} \quad (3.83)$$

Note that here $h_1(x) = h_2(-x)$.

Using the functions $h_{1,2}(x)$ (eq. (3.83)), we write the solution of eq. (3.73) which satisfies the boundary conditions indicated above:

$$\begin{aligned} \tilde{\varphi}'(x) &= \frac{1}{W} \left[\frac{h_2(x)}{A'_0(x)} \int_{-K(\gamma)/A_1}^x \frac{h_1(x')}{A'_0(x')} \left(A_3 + \int_{-K(\gamma)/A_1}^{x'} A'_0(x'') f(x'') dx'' \right) dx' \right. \\ &\quad \left. - \frac{h_1(x)}{A'_0(x)} \int_{K(\gamma)/A_1}^x \frac{h_2(x')}{A'_0(x')} \left(A_3 + \int_{-K(\gamma)/A_1}^{x'} A'_0(x'') f(x'') dx'' \right) dx' \right]. \end{aligned} \quad (3.84)$$

In eq. (3.84) we can, by appropriate choice of the integration limits, perform normalization, with which $A_1 = A_2 = 0$. Let us also require that the sought-for function

$$\tilde{\varphi}(x) = \tilde{\varphi}(0) + \int_0^x \tilde{\varphi}'(x') dx' \quad (3.85)$$

and its derivative $\varphi'(x)$ satisfy the quasi-periodic boundary conditions

$$\tilde{\varphi}\left(\frac{K(\gamma)}{\Delta_1}\right) = \exp\left(\frac{2iqK(\gamma)}{\Delta_1}\right)\tilde{\varphi}\left(-\frac{K(\gamma)}{\Delta_1}\right), \quad (3.86)$$

$$\tilde{\varphi}'\left(\frac{K(\gamma)}{\Delta_1}\right) = \exp\left(\frac{2iqK(\gamma)}{\Delta_1}\right)\tilde{\varphi}'\left(-\frac{K(\gamma)}{\Delta_1}\right), \quad (3.87)$$

where q is the wave number. The last formula may be written, in combination with eq. (3.84), in the form

$$A_3 W[\exp(2iqK(\gamma)/\Delta_1) - 1] = \int_{-K(\gamma)/\Delta_1}^{K(\gamma)/\Delta_1} \Delta'_0(x)f(x)dx. \quad (3.88)$$

Thus, eq. (3.88) defines the constant A_3 . The perturbation theory described here may be applied provided that $|\tilde{\varphi}(x)\Delta'_0(x)| \ll |\Delta_0(x)|$, which is satisfied by choosing $\tilde{\varphi}(0) = 0$. The condition (3.86) in conjunction with the relation $h_1(x) = h_2(-x)$ gives the value of $q = (\pi\Delta_1(2n + 1))/2K(\gamma)$, where n is an integer. Taking into account this result and also the fact that $f(x) = -f(-x)$, we immediately find from eq. (3.88) that $A_3 = 0$. Thus, the final result is

$$\Delta(x) = \Delta_0(x) + \Delta'_0 \int_0^x \frac{h_4(x')}{\Delta'_0(x')} dx', \quad (3.89)$$

where $h_4(x)$ is given by formula (3.76). The qualitative form of the dependence (3.89) is illustrated in fig. 7 for one period of the soliton lattice (the choice of the coordinate origin is made in such a way that $\Delta'(x = 0) > 0$).

Thus, the presence of a finite reservoir capacity M and of impurity scattering leads not only to a change in the amplitude and period of the soliton lattice of a spin density wave (this effect is taken into account in $\Delta_0(x)$ via the variation of the parameters Δ_1 and Δ_2) but also to an unsymmetric distortion of the shape of the SDW on the scale of the new period.

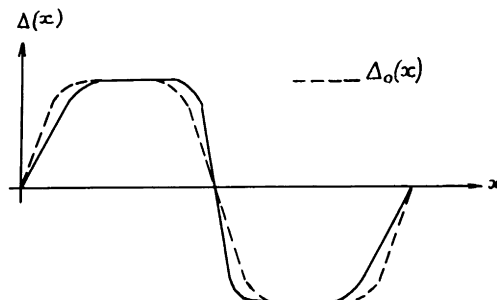


Fig. 7. Distortion of the shape of the SDW soliton lattice under the influence of impurity scattering.

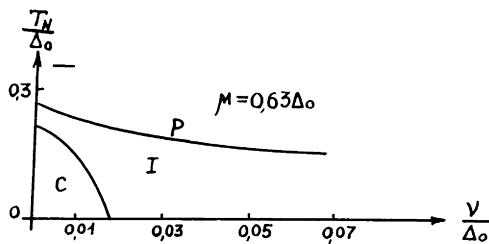


Fig. 8. Phase diagram $T_N(v)$ with an isolated region of the C phase.

The above treatment of the model of the SDW soliton lattice taking into account electron scattering on nonmagnetic impurities allows one to predict the form of the phase diagram of a doped itinerant antiferromagnet in the vicinity of the Lifshitz point. A qualitatively new effect (as compared to the case of the rigid-band approximation (variation of μ)) is firstly, the shift of the Lifshitz point itself upon variation of the impurity concentration and, secondly, the variation of the slopes of the temperatures $T_N(x)$ for transitions from the P phase to the C and I phases and also of the temperature $T_{IC}(x)$ for the transition between the I and the C phase. The temperature $T_{IC}(x)$ varies particularly strongly up to the value at which $\partial T_{IC}(x)/\partial x$ can change sign as compared to the rigid-band case (see e.g. fig. 6b). The phase diagrams of temperature versus impurity concentration can, as a result, assume a rather unusual form, depending on the particular relation between the parameters $\mu(x)$ and $v(x)$ (e.g. of the type given in fig. 8). It is well known (Kulikov and Tugushev 1984) that such a diversity is impossible to account for, even qualitatively, within the framework of a simple model that takes account of only the variation of $\mu(x)$; in the scheme proposed this shortcoming is removed.

The strong restrictions that do not permit one to extend directly the results of the present work to other models with electron soliton lattices are the requirements of high reservoir capacity and small impurity scattering of electrons from the singular segments of the Fermi surface $v' \ll v$.

4. Localized impurity states and short-range order in SDW antiferromagnets

4.1. Formation of resonance impurity levels in SDW systems below the Néel point

The behavior of impurities in itinerant antiferromagnets with spin density waves is traditionally discussed in the context of their effect on the form of phase diagrams $T_N(x)$ (mainly for chromium alloys; see the review by Kulikov and

Tugushev 1984). Practically, all calculations of impurity scattering are performed in the Born approximation through the use of a diagrammatic technique (Abrikosov et al. 1962) by analogy with the theory of superconductivity. As a matter of fact, only the early works (Kopaev and Rusinov 1969, Kopaev and Timerov 1971) have dealt with the problem of formation of local impurity states in the excitonic insulator model for the case of zero reservoir capacity, and self-consistent effect of these states on the rearrangement of the electronic spectrum. The formation of an impurity band in the excitonic insulator model with increasing impurity concentration and the influence of multiple scattering effects in the scheme of the averaged t -matrix have been considered by Evertz and Zittartz (1973). Zawadowski and Tütto (1985) have recently discussed the reorganization of the charge density near a defect for the quasi-one-dimensional SDW model in connection with the calculation of the pinning strength.

In most itinerant antiferromagnets with spin density waves only a relatively small part of the Fermi surface is overlapped by a gap below the Néel point, which is why the influence of the electron reservoir on the properties of the antiferromagnetic phase appears to be very significant. In particular, for systems with defects the presence of a reservoir lends a resonance character to scattering of electrons from the overlapped part of the Fermi surface off localized impurity states which arise in the antiferromagnetic phase inside the dielectric gap (Volkov and Tugushev 1984).

Let us trace out the specific features of the formation of these states taking, as an example, a simple model of a point nonmagnetic impurity in the anti-ferromagnetic matrix of a two-band semimetal unstable toward the generation of spin density waves (the effects of spin fluctuations and exchange polarization of the reservoir are neglected). The Hamiltonian of the model is written in the form

$$H = H_0 + H_{\text{imp}}, \quad (4.1)$$

where

$$\begin{aligned} H_0 &= \sum_{k, i, \alpha} \varepsilon_i(\mathbf{k}) a_{ik\alpha}^+ a_{ik\alpha} - \sum_{k, i \neq j} (\Delta^l \cdot \hat{\sigma})_{\alpha\beta} a_{ik\alpha}^+ a_{jk\beta} \\ &\quad + \sum_{k, \alpha} \varepsilon_r(\mathbf{k}) a_{rk\alpha}^+ a_{rk\alpha}, \quad \varepsilon_1(\mathbf{k}) \approx -\varepsilon_2(\mathbf{k} + \mathbf{Q}), \end{aligned} \quad (4.2)$$

$$\begin{aligned} H_{\text{imp}} &= \sum_{k, k', i, j, \alpha} \{ V_{ij} a_{ik\alpha}^+ a_{jk'\alpha} \} + \sum_{k, k', i, \alpha} \{ V_{ri} a_{ik\alpha}^+ a_{rk'\alpha} + \text{c.c.} \} \\ &\quad + \sum_{k, k', \alpha} V_{rr} a_{rk\alpha}^+ a_{rk'\alpha}. \end{aligned} \quad (4.3)$$

Here the notation is the same as that used earlier; the indices $i, j = 1, 2$ refer to congruent segments of the Fermi surface, r is the reservoir index and V_{ij} , V_{ri} , V_{rr}

are the matrix elements of electron–impurity scattering. For the point potential model we assume that these matrix elements are independent of the momenta \mathbf{k} and \mathbf{k}' . For simplicity we also assume that

$$V_{11} = V_{22} = V_0, \quad V_{12} = V_{21}^* = V_0 \exp(i\mathbf{Q} \cdot \mathbf{R}_0), \quad V_{rr} \equiv V_1, \quad V_{ri} \equiv V_2 \quad (4.4)$$

where \mathbf{R}_0 is the coordinate of the impurity center (for a model with a doubling of $\exp(i\mathbf{Q} \cdot \mathbf{R}_0) = \pm 1$ for various antiferromagnetic sublattices). Let us first consider the case of a commensurate SDW (the C phase) when $\Delta' = \Delta = \text{constant}$. Switching over to the spin-diagonal representation (the axis of quantization is directed along the SDW polarization vector), we write down a system of equations for the Green's functions in the field of a point potential:

$$G_{ij}^{\alpha\alpha}(\mathbf{k}, \mathbf{k}') = \dot{G}_{ij}^{\alpha\alpha}(\mathbf{k})\delta_{kk'} + \sum_{k''} \dot{G}_{i}^{\alpha\alpha}(\mathbf{k}, \mathbf{k}'')\Gamma_{lm}^{\alpha\alpha}\dot{G}_{mj}^{\alpha\alpha}(\mathbf{k}'', \mathbf{k}'), \quad (4.5)$$

where $(l, m) = (i, j, r)$, $\dot{G}_{ij}^{\alpha\alpha}(\mathbf{k})$ are “zero” retarding Green's functions without an impurity potential and $\Gamma_{lm}^{\alpha\alpha}$ is the electron–impurity scattering vertex.

$$\begin{aligned} \dot{G}_{11(22)}^{\alpha\alpha}(\mathbf{k}, \omega) &= (\omega \pm \xi_k)[\omega^2 - \xi_k^2 - (\Delta')^2]^{-1}, \\ \dot{G}_{12}^{\alpha\alpha}(\mathbf{k}, \omega) &= \dot{G}_{21}^{\alpha\alpha}(\mathbf{k}, \omega) = -\alpha\Delta'[\omega^2 - \xi_k^2 - (\Delta')^2]^{-1}, \\ \dot{G}_{rr}^{\alpha\alpha}(\mathbf{k}, \omega) &= [\omega - \varepsilon_r(\mathbf{k})]^{-1}, \\ \xi_k &= \varepsilon_1(\mathbf{k}) = -\varepsilon_2(\mathbf{k} + \mathbf{Q}), \quad \alpha = \pm 1. \end{aligned} \quad (4.6)$$

The solution of the system (4.5) in a general form is extremely laborious, which is why we do not reproduce it here. We are interested only in the pole at the vertex $\Gamma_{lm}^{\alpha\alpha}$, which determines the energy of the bound state on the defect:

$$1 - g_{\text{eff}} I_\alpha(\mathbf{R}_0) = 0, \quad (4.7)$$

$$I_\alpha(\mathbf{R}_0) = \frac{[\alpha|\Delta'| \exp(i\mathbf{Q} \cdot \mathbf{R}_0) - \omega]}{[(\Delta')^2 - \omega^2]^{1/2}}, \quad (4.8)$$

where

$$g_{\text{eff}} = g_0 - ig_2[1 + ig_1]^{-1}, \quad (4.9)$$

$$g_0 = 2\pi V_0 N(0), \quad g_1 = \pi V_1 N_r(0), \quad g_2 = 2\pi^2 V_2^2(0)N(0). \quad (4.10)$$

For the time being we consider a case where there is no scattering with electronic transitions from the congruent segments to the reservoir, i.e. $g_2 = 0$. For the sake of definiteness, we assume that the impurity is in the antiferromagnetic sublattice, where $\exp(i\mathbf{Q} \cdot \mathbf{R}_0) = 1$. Then, depending on the spin state, the product $\alpha|\Delta'|$ may be positive or negative. If $V_0 > 0$, then the solution of eq. (4.7) exists when $\alpha \exp(i\mathbf{Q} \cdot \mathbf{R}_0) > 0$ and a local state with spin “up” (along the SDW

polarization vector) is formed:

$$\omega_{\uparrow} = -|\Delta^{\dagger}| \frac{1 - g_0^2}{1 + g_0^2}. \quad (4.11)$$

With $V_0 < 0$ a local state with spin “down” is formed:

$$\omega_{\downarrow} = |\Delta^{\dagger}| \frac{1 - g_0^2}{1 + g_0^2}. \quad (4.12)$$

For the other sublattice ($\exp(i\mathbf{Q} \cdot \mathbf{R}_0) = -1$) the indices \uparrow and \downarrow should be reversed. Since a spin density wave changes sign upon transition from one lattice point to another, the spin polarization of electrons at the local levels will vary accordingly. It is interesting to note that in the model in question the spin polarization of the local states is complete. This is associated with the choice of the matrix elements of the electron–impurity interaction in the form (4.4). With a different choice, say $V_{11} = V_{22} = V_0$, $V_{12} = V_{21} = 0$, the local levels arise for the two spin projections:

$$\omega_{\uparrow\downarrow} = -\operatorname{sgn} g_0 |\Delta^{\dagger}| \frac{4 - g_0^2}{4 + g_0^2}, \quad (4.13)$$

so that the spin polarization of the impurity state is absent. But if we choose $V_{11} = V_{22} = 0$, $V_{12} = V_{21}^* = V_0 \exp(i\mathbf{Q} \cdot \mathbf{R}_0)$, then

$$\begin{aligned} \omega_{\uparrow} &= \pm |\Delta^{\dagger}| \frac{4 - g_0^2}{4 + g_0^2}, \quad g_0 \exp(i\mathbf{Q} \cdot \mathbf{R}_0) > 0, \\ \omega_{\downarrow} &= \pm |\Delta^{\dagger}| \frac{4 - g_0^2}{4 + g_0^2}, \quad g_0 \exp(i\mathbf{Q} \cdot \mathbf{R}_0) < 0, \end{aligned} \quad (4.14)$$

and for any of the signs of the matrix element V_0 and any of the lattice points \mathbf{R}_0 , there arise two symmetric local levels with fixed spin polarization (Volkov and Nunuparov 1980). In the case of an arbitrary choice of the matrix elements V_{ij} the levels are arranged asymmetrically relative to the midgap and are only partly spin-polarized. The level formation scheme corresponding to eqs. (4.11) and (4.12) is presented in fig. 9.

The radius of the localized state can be evaluated from the formula

$$\rho_0 \approx v_F(1 + g_0^2)/2g_0|\Delta^{\dagger}|. \quad (4.15)$$

The generation of a spin-polarized local state is accompanied by a redistribution of spin density in the vicinity of the defect. Electrons with spin “down” (for $g_0 > 0$) are pushed out of the region $\sim \rho_0$ around the impurity, and inside this region electrons predominate with spin “up”. At distances greater than ρ_0 , there occurs a partial compensation of the local moment. The variation of the spin density as a result of the incorporation of a defect is given by $\delta S = \delta N_{\uparrow} - \delta N_{\downarrow}$,

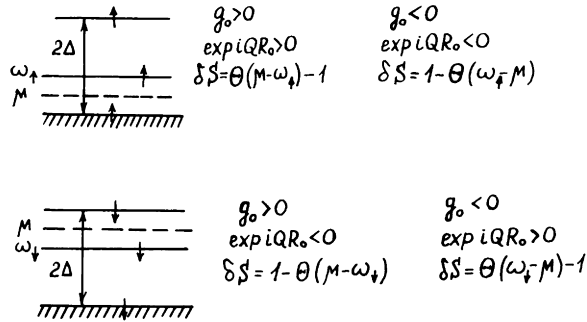


Fig. 9. Structure of spin-polarized energy levels on defects in SDW antiferromagnets.

where $\delta N_{\uparrow,\downarrow}$ is the change in the number of particles with spins “up” and “down”. At $T = 0$, assuming that the Fermi level μ lies inside the gap, after simple but rather cumbersome computations, we get

$$\begin{aligned} \delta S(\omega_{\uparrow} - \mu > 0) &= \begin{cases} -1, & g_0 > 0, \exp(iQ \cdot R_0) > 0, \\ 0, & g_0 < 0, \exp(iQ \cdot R_0) < 0; \end{cases} \\ \delta S(\omega_{\uparrow} - \mu < 0) &= \begin{cases} 0, & g_0 > 0, \exp(iQ \cdot R_0) > 0, \\ 1, & g_0 < 0, \exp(iQ \cdot R_0) < 0; \end{cases} \\ \delta S(\omega_{\downarrow} - \mu > 0) &= \begin{cases} 1, & g_0 > 0, \exp(iQ \cdot R_0) < 0, \\ 0, & g_0 < 0, \exp(iQ \cdot R_0) > 0; \end{cases} \\ \delta S(\omega_{\downarrow} - \mu < 0) &= \begin{cases} 0, & g_0 > 0, \exp(iQ \cdot R_0) < 0, \\ -1, & g_0 < 0, \exp(iQ \cdot R_0) > 0. \end{cases} \end{aligned} \quad (4.16)$$

The physical consequences of result (4.16) are obvious. For instance when $g_0 > 0$ and $\exp(iQ \cdot R_0) > 0$, the level ω_{\uparrow} is split off from the valence band. Further, if $\omega_{\uparrow} > \mu$, then the local state is found to be unoccupied, so that the number of occupied states with spin “up” appears to be one less than that before introduction of the impurity, and if $\omega_{\uparrow} < \mu$ the number of occupied states does not vary. The other cases can be analyzed in an analogous manner.

At temperatures close to T_N we can calculate the average magnetization per lattice site, passing over to the temperature Green's functions through the replacement $\omega \rightarrow i\omega_n$, $\omega_n = \pi T(2n + 1)$, $n = 0, \pm 1, \dots$. To first-order approximation in V_0

$$\delta S = 8V_0N(0) \frac{\mu|\Delta'| \exp(iQ \cdot R_0)}{(\pi T)^2} = \sum_{n \geq 0} \frac{1}{(2n + 1)^3 (1 + \mu^2/\omega_n^2)^2}. \quad (4.17)$$

If μ is close to the middle of the band, i.e. if we have an almost ideal congruence of the Fermi surface segments, it is necessary to retain terms of higher order in

V_0 . At $\mu = 0$, up to an accuracy of V_0^2 we have

$$\delta S = \frac{3}{32} [\pi V_0 N(0)]^2 \frac{|\Delta^t| \exp(i\mathbf{Q} \cdot \mathbf{R}_0)}{T}. \quad (4.18)$$

The general expression for $\delta S(T)$ and arbitrary V_0 is not given here because it is cumbersome.

Let us return to the discussion of eqs. (4.7)–(4.10) in the general case of $g_0 \neq 0$. With $g_{\text{eff}} = g_{\text{Re}} + ig_{\text{Im}}$, where

$$g_{\text{Re}} = \frac{g_0(1 + g_1^2) - g_1 g_2}{1 + g_1^2}, \quad g_{\text{Im}} = -\frac{g_2}{1 + g_1^2}, \quad (4.19)$$

we obtain for $g_0 > 0$, $\exp(i\mathbf{Q} \cdot \mathbf{R}_0) > 0$

$$\omega_\uparrow = -|\Delta^t| \frac{1 - (g_{\text{Re}}^2 + g_{\text{Im}}^2)^2 - 4ig_{\text{Re}}g_{\text{Im}}}{(1 + g_{\text{Re}}^2 - g_{\text{Im}}^2) + 4g_{\text{Re}}^2g_{\text{Im}}^2}. \quad (4.20)$$

Note that in the case of a short-range spherical potential the major contribution to V_0 and V_1 is introduced by single-node matrix elements on the Wannier functions of equivalent orbitals which generate, respectively, congruent segments of the Fermi surface and a reservoir. If we presume that the origin of singular segments of the Fermi surface is different (e.g. in chromium alloys the reservoir is formed to a considerable extent by s and p orbitals and the congruent segments mainly by d orbitals), then the single-node matrix element in the hybridization term V_2 is small and it will be reasonable to assume $g_2 \lesssim g_0, g_1$. It is then not difficult to see that $g_{\text{Re}} \approx g_0$, $g_{\text{Im}} \lesssim g_0$ and

$$\omega_\uparrow \approx -|\Delta^t| \left[\frac{1 - g_0^2}{1 + g_0^2} + \frac{4ig_0g_2}{(1 + g_0^2)^2(1 + g_1^2)} \right]. \quad (4.21)$$

The ionization energy for the level $|\omega_{\uparrow, \downarrow} - |\Delta^t|| = \omega_0 = |\Delta^t| \cdot 2g^2/(1 + g_0^2)$ is found here to be larger than the level width $\gamma = \text{Im}(\omega_\uparrow)$, i.e. the quasi-locality criterion is approximately fulfilled. In principle, when $g_2 \sim g_0, g_1$, the level width may be of the order of the ionization energy.

The generalization of the results obtained here to the case of a magnetic impurity in the matrix of an antiferromagnet has been accomplished by Galkin et al. (1986). In order not to make the treatment cumbersome, let us consider the simplest model of the classical impurity spin s at the lattice point \mathbf{R}_0 . Let us add to the Hamiltonian H_{imp} [eq. (4.3)] the term

$$H'_{\text{imp}} = \sum_{\mathbf{k}, \mathbf{k}', i, j, \alpha, \beta} J_{ij} (\mathbf{s} \cdot \hat{\boldsymbol{\sigma}})_{\alpha\beta} a_{ik\beta}^\dagger a_{jk'\alpha}, \quad (4.22)$$

where J_{ij} are exchange integrals for which we retain relation (4.4). In fact, a more rigorous spin-fluctuational approach within the framework of the statistical approximation also leads to a Hamiltonian of the type given by eq. (4.22).

The total amplitude of electron–impurity scattering $\Gamma_{lm}(\omega)$ averaged over the configurations of a random vector \mathbf{S} in the antiferromagnetic sublattice has now the form of the spinor

$$\Gamma_{lm}(\omega) = \Gamma_{lm}^{(0)}(\omega)\hat{I} + \Gamma_{lm}^{(1)}(\omega)\hat{\sigma}_z, \quad (4.23)$$

where the z axis coincides with the direction of SDW polarization. Considering e.g. the matrix (4.23) in an “even” sublattice $\exp(i\mathbf{Q} \cdot \mathbf{R}_0) = 1$, we obtain the following expression (neglecting scattering into the reservoir):

$$\Gamma^{(0)} = A(\omega)/D(\omega), \quad \Gamma^{(1)} = B(\omega)/D(\omega), \quad (4.24)$$

$$A(\omega) = [V_0 - Q(V_0^2 - J_0^2 \langle |\mathbf{S}|^2 \rangle)][L - 2J_0 \langle \mathbf{S} \cdot \mathbf{n} \rangle P]$$

$$B(\omega) = P[V_0^2 - J_0^2 \langle |\mathbf{S}|^2 \rangle][L - 2J_0 \langle \mathbf{S} \cdot \mathbf{n} \rangle P]$$

$$- J_0 \langle \mathbf{S} \cdot \mathbf{n} \rangle L + 2J_0^2 \langle (\mathbf{S} \cdot \mathbf{n})^2 \rangle P, \quad (4.25)$$

$$D(\omega) = L^2 - 4J_0^2 \langle (\mathbf{S} \cdot \mathbf{n})^2 \rangle P^2,$$

where

$$P = \frac{2\pi N(0)|\mathcal{A}^t|}{[(\mathcal{A}^t)^2 - \omega^2]^{1/2}}, \quad Q = -\frac{2\pi N(0)\omega}{[(\mathcal{A}^t)^2 - \omega^2]^{1/2}},$$

$$L = 1 - 2QV_0 + (Q^2 - P^2)(V_0^2 - J_0^2 \langle |\mathbf{S}|^2 \rangle), \quad (4.26)$$

where \mathbf{n} is a unit vector in the direction of SDW polarization.

The energies of the local impurity levels $\omega_{\uparrow,\downarrow}$ are found from the poles of $\Gamma_{lm}(\omega)$. We will confine ourselves to two limiting cases. When $V_0^2 \gg J_0^2 S^2$, from the condition $D(\omega) = 0$ we obtain

$$\omega_{\uparrow,\downarrow} = -\text{sgn } V_0 |\mathcal{A}^t| \frac{1 - g_0^2}{1 + g_0^2} \pm |\mathcal{A}^t| \frac{\lambda_0 g_0}{(1 + g_0^2)^2} L \langle (\mathbf{S} \cdot \mathbf{n})^2 \rangle^{1/2}, \quad (4.27)$$

and when $V_0^2 \ll J^2 S^2$,

$$\omega_{\uparrow,\downarrow} = \pm |\mathcal{A}^t| \left[1 - \frac{\lambda_0^2 \langle (\mathbf{S} \cdot \mathbf{n})^2 \rangle}{1 + \lambda_0^2 \langle \mathbf{S}^2 \rangle} \right]^{1/2}, \quad (4.28)$$

with

$$\begin{aligned} \lambda_0 &= 2\pi J_0 N(0), & \langle (\mathbf{S} \cdot \mathbf{n})^2 \rangle &= \alpha(x) S^2, & \langle \mathbf{S} \cdot \mathbf{n} \rangle &= S L(x), \\ \langle |\mathbf{S}|^2 \rangle &= S^2, & \alpha(x) &= 1 - \frac{2}{x} \operatorname{ctg} x + \frac{2}{x^2}, & x &= \frac{H_{\text{eff}}}{T}. \end{aligned} \quad (4.29)$$

Here $L(x)$ is the Langevin function and H_{eff} is the effective field at the lattice point \mathbf{R}_0 . To a first-order approximation in the electron–impurity interaction potential, $H_{\text{eff}} = J_0(|\mathcal{A}^t|)/g$.

We will discuss in more detail the structure of impurity levels at $T = 0$. In this limit $\langle (\mathbf{S} \cdot \mathbf{n})^2 \rangle = S^2$ and one of the two poles of the function $\Gamma(\omega)$ cancels out (the numerator in eq. (4.24) vanishes together with the denominator), so that we finally have

$$\begin{aligned}\omega_{\uparrow} &= -\frac{|\Delta^{\dagger}|(1 - \tilde{g}_{0\uparrow}^2)}{1 + \tilde{g}_{0\uparrow}^2}, \quad \tilde{g}_{0\uparrow} > 0, \\ \omega_{\downarrow} &= \frac{|\Delta^{\dagger}|(1 - \tilde{g}_{0\downarrow}^2)}{1 + \tilde{g}_{0\downarrow}^2}, \quad \tilde{g}_{0\downarrow} < 0, \\ \tilde{g}_{0\uparrow\downarrow} &= g_0 \mp \lambda_0 S.\end{aligned}\tag{4.30}$$

This expression closely resembles relations (4.11) and (4.12). For an “odd” sublattice $\exp(i\mathbf{Q} \cdot \mathbf{R}_0) = -1$, the signs of spin projections (\uparrow, \downarrow) should be reversed everywhere.

In the concluding part, we intend to dwell on the question of localized impurity states in the I phase of the SDW. Within the framework of the soliton lattice model it is possible to reduce the problem of finding the energy of the local level to the solution of a comparatively simple equation (Buzdin et al. 1986). We consider the case of a nonmagnetic point impurity with relations of the type (4.4) between the matrix elements V_{ij} . The total vertex of electron–impurity scattering, say for the spin “up” in an “even” sublattice ($\exp(i\mathbf{Q} \cdot \mathbf{R}_0) = 1$) may be written in the form

$$\Gamma^{\uparrow\uparrow}(\omega, \mathbf{R}_0) = V_0 \left[1 - V_0 \sum_{i,j} G_{ij}^{\uparrow\uparrow}(\mathbf{R}_0, \mathbf{R}_0, \omega) \right]^{-1}.\tag{4.31}$$

The Green’s functions $G_{ij}^{\uparrow\uparrow}(\mathbf{r}, \mathbf{r}', \omega)$ for the soliton lattice model of the SDW were given in section 3.2. Introducing the density of states in accordance with eq. (3.43) and performing an appropriate summation over the quasi-momenta and band indices (i, j) , we obtain for the pole ω_{\uparrow} in eq. (4.31) the following relation:

$$1 = -g_0 A(\Omega_{\uparrow}), \quad \Omega_{\uparrow} = \omega_{\uparrow}/\Delta_2,\tag{4.32}$$

$$A(\Omega_{\uparrow}) = \frac{2M(\Omega_{\uparrow})}{\pi\gamma\varepsilon + \Omega_{\uparrow}} [-\Omega_{\uparrow} \operatorname{sn}(\zeta_0, \gamma) + \Omega_{\uparrow}^2 - \frac{1}{4}(1 + \gamma^{-2}) + \frac{1}{2}\operatorname{sn}^2(\zeta_0, \gamma)],\tag{4.33}$$

where

$$\begin{aligned}M(\Omega_{\uparrow}) &= \Pi\left(\frac{\Omega_{\uparrow}^2}{\varepsilon_+^2}, \frac{\varepsilon_-}{\varepsilon_+}\right) + \Pi\left(\frac{\varepsilon_-^2}{\Omega_{\uparrow}^2}, \frac{\varepsilon_-}{\varepsilon_+}\right) - K\left(\frac{\varepsilon_-}{\varepsilon_+}\right), \\ \varepsilon_{\pm} &= \frac{1}{2}(\gamma^{-1} \pm 1), \quad \zeta_0 = x_0 \Delta_1/v_F.\end{aligned}\tag{4.34}$$

Here $\Pi(\Psi, \varepsilon_-/\varepsilon_+)$ is the Schröder elliptic integral. The function $M(\Omega_{\uparrow})$ is such that $M(\Omega_{\uparrow}) \equiv 0$ for $\varepsilon_-^2 > \Omega_{\uparrow}^2 > \varepsilon_+^2$ (recall that ε_{\pm} are the boundaries of the

one-electron spectrum). Thus, the solutions of eq. (4.32) exist when the energies $\varepsilon_-^2 \lesssim \Omega_\uparrow^2 \leq \varepsilon_+^2$, i.e. in the forbidden band.

Let us examine some limiting cases. With $\gamma \rightarrow 1$ (the sparse lattice limit) eq. (4.32) assumes the form

$$1 = -\frac{g_0}{\Omega_\uparrow(1-\Omega_\uparrow^2)^{1/2}} [\Omega_\uparrow \tanh \zeta_0 + \Omega_\uparrow^2 - \frac{1}{2}(1-\tanh^2 \zeta_0)]. \quad (4.35)$$

Let us assume that the impurity is present in the region of a positive half-wave, i.e. $\zeta_0 > 0$. Far away from the soliton wall, a bound state arises when $g_0 > 0$:

$$\Omega_\uparrow = -\frac{1-g_0^2}{1+g_0^2}, \quad \zeta_0 \rightarrow +\infty. \quad (4.36)$$

Analogously, in the region of a negative half-wave, for $g_0 < 0$ we have

$$\Omega_\uparrow = \frac{1-g_0^2}{1+g_0^2}, \quad \zeta_0 \rightarrow -\infty. \quad (4.37)$$

The results (4.36) and (4.37) naturally coincide with those given by eqs. (4.11) and (4.12) for an “even” and an “odd” sublattice, respectively. However, if the defect is near the soliton wall, the situation becomes different. Assume that the position of the lattice point impurity coincides exactly with the middle of the wall ($\zeta_0 = 0$). There then appear two roots:

$$\Omega_\uparrow^{(1,2)} = \pm \frac{1}{\sqrt{2}} \left[1 \mp \frac{\operatorname{sgn} g_0}{(1+g_0^2)^{1/2}} \right]^{1/2}. \quad (4.38)$$

It is easy to see that with any sign of the potential V_0 inside the forbidden band, there are two local levels split off from the conduction band (valence band) and from the central soliton band, respectively. In the limit $\gamma \rightarrow 1$, $\zeta_0 \rightarrow \pm \infty$, one of the levels merges with the soliton band and disappears. Figure 10 shows the dependence $\Omega_\uparrow(g_0)$ for various ζ_0 (the quantity $|\zeta_0|$ is limited by virtue of the

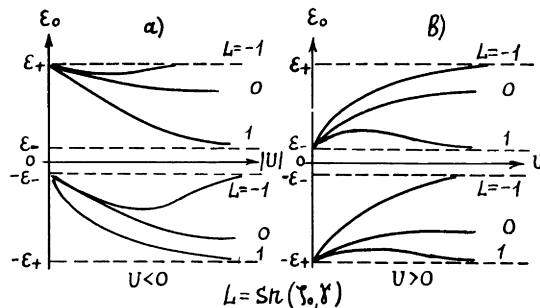


Fig. 10. Dependence of the binding energy (ε_0) of the impurity level on the defect potential (U) in the SDW soliton lattice. (a) $U < 0$. (b) $U > 0$.

periodicity of the function $\text{sn}(\zeta_0, \gamma)$ to the value of $2K(\gamma)$. For the levels $\Omega_\downarrow(g_0)$, all the formulas are analogous to the replacement of the even sublattice by an odd sublattice and ζ_0 by $-\zeta_0$.

The general properties of the impurity states in the soliton lattice allow one to group them into several blocks. With $g_0 < 0$, the level is split off from the conduction band lying in the interval $\Omega^{(+)} < \Omega_{\uparrow,\downarrow} < \varepsilon_+$ and from the central soliton band in the interval $\Omega^{(-)} < \omega_{\uparrow,\downarrow} < -\varepsilon_-$.

With $g_0 > 0$, the level detached from the valence band has an energy $-\varepsilon_+ < \Omega_{\uparrow,\downarrow} < \Omega^{(-)}$ and the one detached from the soliton band has an energy $\varepsilon_+ < \Omega_{\uparrow,\downarrow} < \Omega^{(+)}$. The energies $\Omega^{(+)}$ are obtained as asymptotic values when $g_0 \rightarrow \pm \infty$:

$$\Omega^{(\pm)} = \frac{1}{2}[\text{sn}(\zeta_0, \gamma) \pm (1 + \gamma^{-2} - \text{sn}^2(\zeta_0, \gamma))^{1/2}]. \quad (4.39)$$

If the positions of the defects in the lattice are uncorrelated, the coordinate ζ_0 runs in a random way over all values within the interval $(-2K(\gamma), 2K(\gamma))$. Hence, there is a spread of impurity levels $\Omega_{\uparrow,\downarrow}(\zeta_0)$ which thus fill the entire forbidden band even in the absence of direct overlaps between the wave functions of the impurity states. In the limit of the sparse soliton lattice, the density of impurity states has the form of a sharp peak at energies $\Omega_{\uparrow,\downarrow}(\zeta_0 \rightarrow \pm \infty)$ with a smeared-out region of width $\Delta\Omega \sim 2K(\gamma)^{-1}$, while for the dense lattice the peak width is of the order of $|\varepsilon_+ - \varepsilon_-|$, i.e. it may span the dielectric gap. Thus, in the I phase of spin density waves a gapless structure of the electronic spectrum may be formed (even if the broadening of the impurity level due to scattering to the reservoir is neglected), only because of a topological disorder in the position of the impurity centers in the antiferromagnetic matrix.

The results obtained here are not actually associated with the nature of the defect and their validity is limited only by the requirement of the short-range action of the electron-impurity potential $V(\mathbf{r})$ (the characteristic radius of action q_0 must be small as compared to the congruence length of an electron-hole pair $\zeta = v_F/|\mathcal{A}^\dagger|$). In particular, our model can describe the formation of surface states at the boundary of an itinerant antiferromagnet. For the model of a Fermi surface having planar segments, with the orientation of the surface normal to the vector \mathbf{Q} , the inclusion of lateral corrugation leads, as can easily be shown, to the formation of a surface band with the dispersion law $\omega_{\uparrow,\downarrow} + \eta_+(\mathbf{q}_\perp) = E_{\uparrow,\downarrow}(\mathbf{q}_\perp)$.

Thus, in itinerant antiferromagnets there may appear surface magnetization. If $\eta_+(\mathbf{q}_\perp) < |\mathcal{A}^\dagger|$ (and this may be allowed without violating the conditions of validity of the mean-field theory), then the surface spin-polarized bands lies entirely inside the bulk dielectric gap.

4.2. Defect-induced short-range antiferromagnetic ordering above and below the Néel point: formation of “localized” spin density waves

The incorporation of defects leads to a self-consistent redistribution of the charge and spin density in their vicinity and, as a consequence, to a local

rearrangement of the spin density wave. This rearrangement manifests itself in a most pronounced way in the formation of a region of short-range magnetic order around the defect near the Néel point, on a scale of the order of the correlation length of the order parameter $\zeta \gg a$ (a is the interatomic distance). It is well known that the presence of defects in crystals with electronic, magnetic and structural phase transitions may also lead to the appearance of a short-range order in the vicinity of the defect – the generation of localized states above the point of a homogeneous (bulk) transition. Such a situation occurs e.g., in a case where the transition temperature increases locally near the defect (say, because of fluctuations in the impurity concentration, or the presence of a domain boundary or a twinning plane with a coupling constant larger than that in the bulk). At present many examples of such localized states are known: local structural distortions (Levanyuk et al. 1979), surface magnetism (Allan 1979), localized superconductivity (Khaikin and Khlyustikov 1981). Whereas various cases of transition to the commensurate phase have been studied in sufficient detail here, the short-range-order structures formed upon transitions to the incommensurate state (of the type of SDW I phase) practically have not been explored. It should be noted that this topic is of undoubtedly interest since a large number of systems with phase transitions to an incommensurate structure are known at present: quasi-one-dimensional Peierls (Brazovskii et al. 1981) and spin-Peierls (Buzdin et al. 1983) systems, superconductors in an exchange field (Buzdin and Tugushev 1983), modulated long-period ferromagnets (Izumov 1984), and finally itinerant antiferromagnets with spin density waves, which constitute the subject matter of this chapter. The temperature T_{loc} , at which a short-range order (a local transition) arises on a defect above the temperature of the bulk transition to an incommensurate phase, can be found on the basis of an analysis of the corresponding free-energy functional, in which account must be taken of higher-order terms in order-parameter gradients. The solutions of the linearized equations for order parameters can be found at all times, but in a number of cases of practical interest we can also find solutions to nonlinear equations (e.g. in the model of the SDW soliton lattice). According to Levanyuk et al. (1979), in the case of a short-range potential (i.e. which falls off at a distance smaller than the correlation length) of the defect we can describe its effect by adding to the thermodynamic potential the δ -function source $\Gamma(\mathcal{A}^t)\delta(r)$. Depending on the form of the function $\Gamma(\mathcal{A}^t)$, a distinction is made between two types of sources: the “local field” type ($\Gamma_0 = \mathbf{F}_0 \cdot \mathcal{A}^t$) and “local temperature” type (in the simplest isotropic case $\Gamma_1 = \frac{1}{2}F_1|\mathcal{A}^t|^2$). The explicit form of the coefficients F_0 and F_1 for the microscopic model of the spin density wave is given in Appendix IV.

We will first consider the three-dimensional SDW model (Kostina et al. 1985) in the case one cannot go beyond the solution of linearized equations. In the functional of the general form (3.21) for a linearly polarized SDW, we retain only those terms which are quadratic in $\mathcal{A}^t(r)$. We consider the case of a three-

dimensional source of the “local temperature” type:

$$\Omega = \alpha(\Delta^t)^2 + a_1(\text{grad } \Delta^t)^2 + a_2(\text{div grad } \Delta^t)^2 - \frac{1}{2}F_1(\Delta^t)^2\delta(\mathbf{r}). \quad (4.40)$$

The self-consistency equation has the form

$$\alpha\Delta^t - a_1\nabla^2\Delta^t + a_2\nabla^4\Delta^t = \frac{1}{2}F_1\Delta^t(0)\delta(\mathbf{r}). \quad (4.41)$$

If $a_1 > 0$ and the term $\sim a_2$ may be neglected, the solution (4.41) is known and trivial. In this case the problem reduces to finding the conditions for the existence of a bound state for the Schrödinger equation with a δ -shaped potential. In our case, a_1 may change sign at the Lifshitz point, so that the retention of the term $\sim a_2$ is important. We write down the formal “solution” of eq. (4.41):

$$\Delta^t(\mathbf{r}) = \frac{1}{2}F_1\Delta^t(0)G(\mathbf{r}, 0), \quad (4.42)$$

where $G(\mathbf{r}, 0) = G(\mathbf{r}, \mathbf{r}' = 0)$ and $G(\mathbf{r}, \mathbf{r}')$ is the Green's function for eq. (4.41) with the right-hand side set equal to zero:

$$\begin{aligned} G(\mathbf{r}, \mathbf{r}') = & \{2\pi|\mathbf{r} - \mathbf{r}'|(4\alpha a_2 - a_1^2)^{1/2}\}^{-1} \\ & \times \exp(-\frac{1}{2}|\mathbf{r} - \mathbf{r}'|[(\sqrt{4\alpha a_2} + a_1)/a_2]^{1/2}) \\ & \times \sin(\frac{1}{2}|\mathbf{r} - \mathbf{r}'|[(\sqrt{4\alpha a_2} - a_1)/a_2]^{1/2}). \end{aligned} \quad (4.43)$$

The function $G(\mathbf{r}, 0)$ is finite when $\mathbf{r} \rightarrow 0$; this is due to the highest-order gradient term being $\sim a_2$. Hence, the solution of eq. (4.42) is continuous for $\mathbf{r} \rightarrow 0$ and there is no need to introduce a finite radius of the source or matching conditions at the boundary, as suggested in the literature (Levanyuk et al. 1979). When $\mathbf{r} \rightarrow 0$, we obtain from eq. (4.42) the condition for determination of the temperature T_{loc} at which a short-range order arises:

$$1 = \frac{1}{2}F_1[4\pi(a_2\sqrt{4\alpha a_2} + a_1 a_2)^{1/2}]^{-1}. \quad (4.44)$$

Strictly speaking, it is necessary to make certain that eq. (4.44) really gives the line of absolute instability toward the formation of a local SDW within the interval $T_N < T < T_{\text{loc}}$, for which we should calculate $\Delta^t(0)$; this can be done by retaining those terms in eq. (4.41) which are higher-order in $\Delta^t(\mathbf{r})$, only in accordance with perturbation theory with a small magnitude of the source F_1 . Appropriate calculations have been carried out by Kostina et al. (1985). The qualitative form of the dependence $T_{\text{loc}}(\mu)$ is shown in fig. 11. In region I ($a_1 > \sqrt{4\alpha a_2}$), the local SDW decays exponentially away from the defect. In region II ($a_1 < \sqrt{4\alpha a_2}$), the exponential decay is superimposed by periodic oscillations.

A remarkable situation is the existence of a short-range order with as small a value of the source as desired ($F_1 > 0$) in the region of $a_1 < 0$, where the

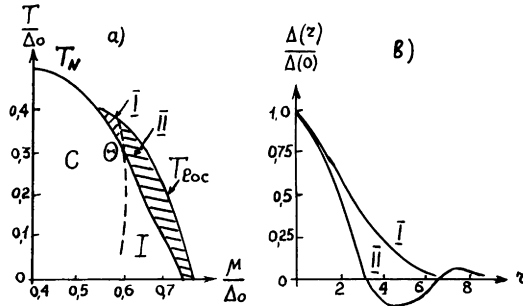


Fig. 11. Model of spherical segments of the Fermi surface. (a) Boundary T_{loc} of the region of short-range antiferromagnetic order at defects T_{loc} . (b) Structure of the order parameter $\Delta(r)$ in the vicinity of the defect.

incommensurate SDW phase is realized. Recall that for the case of the commensurate phase, when there is the earlier-mentioned analogy with the three-dimensional Schrödinger equation in the point potential, a bound state (i.e. a local transition) arises only at a sufficiently large value of the potential F_1 (Landau and Lifshitz 1974). For the incommensurate phase this analogy is absent (eq. (4.41) is of fourth order) and a bound state arises, just as in a one-dimensional system, at as small a value of the potential F_1 as desired. An estimate of the excess of $T_{loc}(\mu)$ over the bulk temperature $T_N(\mu)$ in the region of the I phase gives $T_{loc} - T_N \approx F_1^2$.

Let us briefly consider the case of $T = 0$ for the three-dimensional SDW model. It is known that with $\mu < \mu^c = 0.755\Delta_0$ the paramagnetic phase is absolutely unstable toward transition into the I phase. It can be shown that in the model of a nonmagnetic point defect with $g_0 \ll 1$, in the region of values $\mu^c < \mu < \mu_{loc}$ the self-consistency equation has the following solution:

$$\Delta^I(r) = \frac{\Delta^I(0) \sin q_0 r}{q_0 r} \exp(-0.741q_0 r) \left(\frac{\mu^2}{(\mu^c)^2} - 1 \right)^{1/2},$$

$$q_0 = 2Q_0/v_F, \quad Q_0 \approx 0.91\Delta_0. \quad (4.45)$$

The quantity μ_{loc} is found from the relation

$$\left[1 - \frac{\mu_{loc}^2}{(\mu^c)^2} \right]^{1/2} = \left| \frac{\pi g_0 Q_0^2 I(\mu^c)}{\sqrt{2\varepsilon_F D(\mu^c)}} \right|, \quad (4.46)$$

$$I(\mu^c) = \iint_{-1}^{+1} \frac{dx dy}{y-x} \ln \left| \frac{Q_0 x - \mu^c}{Q_0 y - \mu^c} \right| \approx 7.74 \operatorname{sgn} \mu,$$

$$D(\mu^c) = \frac{1}{4} \left(\frac{Q_0^2}{(\mu^c)^2} - 1 \right)^{-1} \left[4 \frac{Q_0^2}{(\mu^c)^2} - \frac{Q_0^4}{(\mu^c)^4} - 3 \right]^{1/2} \approx 0.466.$$

The appearance of a “local” SDW on the defect signifies the simultaneous formation of a region of short-range (\sim the characteristic size of the SDW decay) magnetic order and nonzero magnetization M . A simple calculation in the approximation linear in F_1 near the Lifshitz point yields:

$$M = 2F_1\mu_B N(0)\Delta^1(0). \quad (4.47)$$

The appearance in the paramagnetic phase of such local moments must lead to an increase in the susceptibility below T_{loc} . At the same time, below T_N these moments must be frozen in the SDW matrix.

Let us now switch over to the examination of short-range order for the quasi-one-dimensional SDW model (the case of corrugated planar segments of the Fermi surface) (Buzdin et al. 1986). In the case of the exactly solvable model of the soliton lattice in view, we will consider the functional (3.14) with a planar source, which can be represented either by the sample surface perpendicular to the SDW wave vector or by the domain boundary. It is convenient to switch over to the dimensionless variables $x \rightarrow v_F(c_3/|c_2|)^{1/2}x$, $\Delta^1 \rightarrow (|c_2|/c_3)^{1/2}\varphi$. Then, after varying the functional (3.14), we obtain an inhomogeneous fourth-order equation:

$$\begin{aligned} \varphi'''' - 10\varphi\varphi^{12} - 10\varphi^2\varphi'' + 6\varphi^5 - 2\operatorname{sgn} c_2(\varphi'' - 2\varphi^3) + 2\tau\varphi &= \delta(x)D(\varphi), \\ \tau = c_1 c_3 / c_2^2, \end{aligned} \quad (4.48)$$

where $D(\varphi) = F_0 c_3 |c_2|^{-2} = \tilde{F}_0$ for a source of “local field” type and $D(\varphi) = F_1 c_3^{1/2} c_2^{3/2} \varphi(0) = \tilde{F}_1 \varphi(0)$ for a source of “local temperature” type (in the dimensionless variables $\delta(x) \rightarrow (|c_2|/c_3)^{1/2} \delta(x) v_F^{-1}$).

We begin with region I on the phase diagram presented in fig. 12, where $(c_1, c_2) > 0$ and the contribution from the terms higher in φ and φ' may be neglected. Equation (4.48) is simplified in this case and takes the form of the first MKDV integral with a point source:

$$\varphi'' - 2\varphi^3 - \tau\varphi = -\frac{1}{2}D(\varphi)\delta(x). \quad (4.49)$$

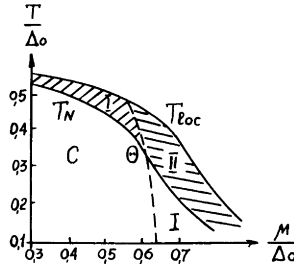


Fig. 12. Boundary T_{loc} of the region of short-range antiferromagnetic order at defects in the model of planar segments of the Fermi surface.

The boundary conditions for $\varphi(x)$ far away from the defect are $\varphi(\pm\infty) = 0$ and $\varphi'(\pm\infty) = 0$, which after integrating eq. (4.49) gives

$$\varphi(x) = \frac{\tau^{1/2}}{\sinh(\tau^{1/2}x + \tilde{\Phi})}, \quad (4.50)$$

where $\tilde{\Phi}$ is an arbitrary constant, which determines the boundary condition on the defect:

$$B = \exp(-2\tilde{\Phi}) = \frac{[\varphi^2(0) + \tau]^{1/2} - \tau^{1/2}}{[\varphi^2(0) + \tau]^{1/2} + \tau^{1/2}}. \quad (4.51)$$

Matching the resultant solutions at the coordinate origin, we find

$$\frac{4\tau(1+B)B^{1/2}}{(1-B)^2} = \frac{1}{2}D(\varphi(0)). \quad (4.52)$$

For a defect of the “local-field” type the problem is completely solved at this point. For a defect of the “local temperature” type eq. (4.52) determines the local transition line. If we take $D(\varphi(0)) = \tilde{F}_1 \varphi(0)$, then in the first-order approximation in $\varphi(0)$ eq. (4.52) yields

$$4(c_1 c_2)^{1/2} = F_1 > 0. \quad (4.53)$$

In the region of $4(c_1 c_2)^{1/2} < F_1$, the amplitude $(\Delta^t(0))^2$ on the defect is equal to

$$(\Delta^t(0))^2 \cong \frac{c_1^{1/2}}{2c_2^{3/2}} [F_1 - 4(c_1 c_2)]^{1/2}. \quad (4.54)$$

In the immediate vicinity of the Lifshitz point, where $c_2 \rightarrow 0$ (but still in region I) we should keep the higher-order terms in φ and φ' in eq. (4.48). In such a case, near the local transition line, using the properties of the exact integrability of the eq. (4.48) with its right hand side set equal to zero, we get

$$(\Delta^t(0))^2 = \frac{(F_1 - 4a\sqrt{c_1 c_3})8a\sqrt{c_1}(4a^2 - b^2)}{c_3^{3/2}[84a^6 - 45a^4b^2 + 10a^2b^4 - b^6]}, \quad (4.55)$$

$$a = \left[\frac{c_1^{1/2}}{(2c_3)^{1/2}} + \frac{c_2}{2c_3} \right]^{1/2}, \quad b = \left[\frac{c_2}{2c_3} - \frac{c_1^{1/2}}{(2c_3)^{1/2}} \right]^{1/2}. \quad (4.56)$$

Let us now focus our attention on region II, where $(c_1/2c_3) > (c_2^2/(4c_3)^2)$, $c_2 < 0$ and the retention of the terms of higher order in φ and φ' in the functional is fundamentally necessary. We are interested in real solutions of eq. (4.48) that are even in x and which tend to zero as $x \rightarrow \pm\infty$. In the absence of the source, eq. (4.48) is satisfied by the solution of the first MKDV equation

$$\varphi''' + A_j \varphi' - 6\varphi^2 \varphi' = 0 \quad (4.57)$$

at $A_j^{1/2} = b' \pm ia'$, $j = 1, 2$, where

$$a' = [(\frac{1}{2}\tau)^{1/2} - \frac{1}{2}]^{1/2}, \quad b' = [(\frac{1}{2}\tau)^{1/2} + \frac{1}{2}]^{1/2}. \quad (4.58)$$

The solutions of eq. (4.58) that fall off as $x \rightarrow \pm\infty$ are two complex-conjugate functions:

$$\begin{aligned}\varphi^{(1)}(x) &= \varphi^{(1)}(0) \left[\cos(A_1^{1/2}x) - i \left(1 - \frac{[\varphi^{(1)}(0)]^2}{A_1} \right)^{1/2} \sin(A_1^{1/2}|x|) \right]^{-1}, \\ \varphi^{(2)}(x) &= (\varphi^{(1)}(x))^*.\end{aligned}\quad (4.59)$$

We introduce the functions $p^{(j)}(x)$ and $q^{(j)}(x)$ related to $\varphi^{(j)}(x)$ by the Miura transformation:

$$p^{(j)}, q^{(j)} = [\varphi^{(j)}]^2 \pm [\varphi^{(j)}]', \quad (4.60)$$

and hence, satisfying the first MKDV equation conjugate to eq. (4.57). The method of constructing an exact real solution to eq. (4.48) from the complex auxiliary solutions of eq. (4.59) is based on the principle of nonlinear superposition (Calogero and Degasperis 1982), which gives in explicit form a new solution of the second CDV equation expressed via the three other solutions of the same equation: an arbitrary solution $(p^{(0)}, q^{(0)})$ and two solutions $(p^{(j)}, q^{(j)}, j = 1, 2)$ connected with $(p^{(0)}, q^{(0)})$ by the Bäcklund transformation (see Appendix IV). The solution $(p^{(0)}, q^{(0)})$ chosen here is the trivial solution $p^{(0)} = q^{(0)} = 0$, in which case the parameters of the Bäcklund transformation should be chosen as follows: $-\frac{1}{2}iA_1^{1/2}$ for $p^{(1)}, q^{(1)}$ and $\frac{1}{2}iA_2^{1/2}$ for $p^{(2)}, q^{(2)}$. Now we write down the solution of interest in the form

$$\varphi(x) = \frac{1}{2}[\mathcal{Q}(|x|) - \mathcal{P}(|x|)], \quad (4.61)$$

where

$$\begin{aligned}\mathcal{Q}, \mathcal{P} &= (A_2^{1/2} - A_1^{1/2})[(A_1^{1/2} + A_2^{1/2})\mathcal{L}(q, p) - i]^{-1}, \\ \mathcal{L}(q, p) &= \left[\int_{|x|}^{\infty} \{(q, p)^{(1)} - (q, p)^{(2)}\} d\xi \right]^{-1}.\end{aligned}\quad (4.62)$$

Let us consider the question of boundary conditions for $x \rightarrow 0$. The solution we are interested in must be continuous and must have continuous derivatives up to second order; this follows from the condition of validity of the Ginzburg–Landau functional (3.14). The third derivative $\varphi'''(0)$ has at $x = 0$ a first-order discontinuity. Thus, the system of equations

$$\begin{aligned}\varphi''(0^+) &= \varphi''(0^-), \\ \varphi'''(0^+) - \varphi'''(0^-) &= D(\varphi(0))\end{aligned}\quad (4.63)$$

determines a pair of arbitrary constants $\varphi_{(0)}^{(1,2)}$. Linearization of expression (4.61) subject to the boundary conditions expressed by eq. (4.63) allows one to find the local transition line in a system with a source of the “local temperature” type:

$$4[c_1(2c_1c_3)^{1/2} + c_1c_2]^{1/2} = F_1. \quad (4.64)$$

Near this line, we have from eq. (4.61)

$$\Delta^t(x) = \Delta^t(0) \exp(-\tilde{a}'|x|) \left\{ \cos \tilde{b}'|x| + \frac{\tilde{a}'}{\tilde{b}'} \sin \tilde{b}'|x| \right\}, \quad (4.65)$$

where $\Delta^t(0)$ is given by relation (4.55) with the replacement $a \rightarrow \tilde{a}'$, $b \rightarrow i\tilde{b}'$, where $(\tilde{b}', \tilde{a}') = (b', a')[|c_2|/c_3]^{1/2}$. The local transition line $T_{loc}(\mu)$ is given in fig. 12. Note that at any value of F_1 , for the one-dimensional SDW model the local transition occurs prior to the bulk transition in the region of $c_2 > 0$, whereas for the three-dimensional model there exists a minimal value of the defect potential $F_{1\min}$, which limits the possibility of the local transition being realized. Such a qualitative difference follows quite distinctly from the known analogy between our problem with $c_2 > 0$ and the criterion of appearance of a local state in the potential well for the Schrödinger equation.

We will now dwell briefly on the short-range structure in the vicinity of the defect at a temperature T lower than the bulk transition temperature. For the sake of simplicity, we will confine ourselves to the simplest case: $c_2 > 0$, $|c_1|c_3 \ll c_2^2$, when we may neglect the terms of higher order in φ and φ' in eq. (4.48). But this time we have $c_1 < 0$ and, hence, $\tau < 0$.

In the absence of a defect the solution of eq. (4.49) below the bulk transition temperature is

$$\varphi_0^2 = +\frac{1}{2}|\tau|. \quad (4.66)$$

The boundary conditions for $\varphi(x)$, away from the defect in the case under consideration, are $\varphi(\pm\infty) = \varphi_0$, $\varphi'(\pm\infty) = 0$, i.e. the solution $\varphi(x)$ has the form of a polaron. Integrating eq. (4.49) and subjecting the integral to these boundary conditions, we obtain two possible solutions:

$$\varphi_+(x) = \varphi_0 \coth[(\frac{1}{2}|\tau|)^{1/2}|x| + \tilde{\Phi}_+], \quad (4.67)$$

$$\varphi_-(x) = \varphi_0 \tanh[(\frac{1}{2}|\tau|)^{1/2}|x| + \tilde{\Phi}_-]. \quad (4.68)$$

In the case of a source of the “local temperature” type $D(\varphi) = \tilde{F}_1 \varphi(0)$, the choice of the solution (4.67) and (4.68) is governed by the sign of the potential \tilde{F}_1 . If $\tilde{F}_1 > 0$ as before, then the boundary conditions on the defect are satisfied only by eq. (4.67), and the phase $\tilde{\Phi}_+$ is found from the condition

$$\coth \tilde{\Phi}_+ = \frac{\tilde{F}_1}{8\varphi_0} + \left[\left(\frac{\tilde{F}_1}{8\varphi_0} \right)^2 + 1 \right]^{1/2}. \quad (4.69)$$

But if $\tilde{F}_1 < 0$, the solution (4.68) is realized, in which case for the phase $\tilde{\Phi}_-$ we have

$$\tanh \tilde{\Phi}_- = - \left| \frac{\tilde{F}_1}{8\varphi_0} \right| + \left[\left(\frac{\tilde{F}_1}{8\varphi_0} \right)^2 + 1 \right]^{1/2}. \quad (4.70)$$

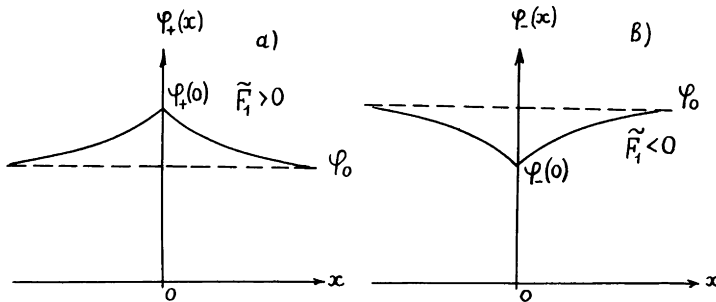


Fig. 13. The structure of the order parameter $\varphi(x)$ in the vicinity of the defect below the Néel point.
 (a) Attractive potential. (b) Repulsive potential.

The physical meaning of the solutions (4.67) and (4.68) is obvious. The solution $\varphi_+(0)$ describes the local crowding of the SDW analogous to that above the bulk transition temperature T_N obtained earlier. The solution $\varphi_-(x)$ describes the local discharge of the SDW and has no analogs above T_N . Both these solutions, which correspond to the potentials $\tilde{F}_1 > 0$ and $\tilde{F}_1 < 0$, are graphically depicted in fig. 13. In the case of a source of the “local field” type, the solutions are chosen in an analogous manner: φ_+ for $\tilde{F}_0 > 0$ and φ_- for $\tilde{F}_0 < 0$. The relevant calculations are omitted here their simplicity.

5. Experimental results for some dilute chromium alloys

As pointed out earlier in section 1, chromium and its dilute alloys are traditional examples of itinerant antiferromagnets with spin density waves. In most of these alloys, in the region of small impurity concentrations (and in CrV and CrNi over the entire region of existence of the antiferromagnetic structure) the SDW I phase of the linearly polarized type is realized (a transverse one when $T > T_{sf}$ and a longitudinal one when $T < T_{sf}$, where T_{sf} is the spin-flip transition temperature). The most favorable candidates for testing the theory of the SDW soliton lattice are pure Cr and its dilute alloys with Mn and V, which are well-described in the rigid-band approximation. A variation in the incongruence parameter μ upon doping is the principal factor that affects the SDW parameters and the dependence $T_N(x)$, where x is the impurity concentration (Kochler et al. 1966). The specific features of the band structure of Cr in the paramagnetic phase (nearly congruent electron and hole octahedra at points Γ and H of the Brillouin zone) (Asano and Yamashita 1967) and the relatively high reservoir capacity ($M \approx 3-4$) allow one to hope that the results of section 3.2 are valid for these systems.

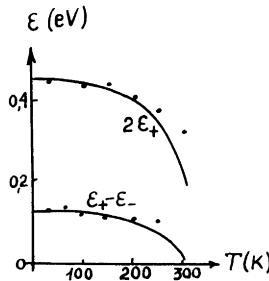


Fig. 14. Temperature dependence of two energy gaps in Cr [— theory (Machida and Fujita 1984), ● experiment (Machida et al. 1984)].

A serious argument in favor of the soliton lattice model is furnished by experiments on the measurement of infrared absorption in pure Cr (Machida et al. 1984). Below the Néel temperature are observed two low-frequency absorption peaks, which have not been adequately interpreted. It is clear that in the case of the electronic spectrum characteristic of the soliton lattice (fig. 14) the frequencies of these peaks are equal to $2\epsilon_+$ and $(\epsilon_+ - \epsilon_-)$ if the Fermi level lies within the region of $-\epsilon_- < \mu < -\epsilon_+$. In pure Cr the peak frequencies are 0.15 (0.13 according to other data) and 0.45 eV, which gives $\gamma \approx \frac{1}{2}$. In $\text{Cr}_{1-x}\text{Mn}_x$ alloys, as x exceeds 0.4 at%, only one absorption peak (~ 0.4 eV) is left; this may be interpreted in terms of the disappearance of the narrow soliton band in the C phase. The experimental plots of ϵ_+ versus T borrowed from the literature (Machida et al. 1984) are given in fig. 14 and the numerical calculations reproduced here have been performed by Machida and Fujita (1984)*.

Information on the structure of the I phase is also provided by data on the peak intensity in the neutron scattering cross section for the higher harmonic components of the SDW: $I_m \sim \Delta_m^2$, where the Fourier components Δ_m are determined from expansion of $\Delta(x)$ into a harmonic series

$$\Delta(x) = \sum_{n=0}^{\infty} \Delta_{2n+1} \sin[(2n+1)qx], \quad (5.1)$$

$$\Delta_{2n+1} = \frac{2\pi\Delta_2}{\gamma K(\gamma)} \frac{\lambda^{(2n+1)/2}}{1 - \lambda^{(2n+1)}}, \quad \lambda = \exp\left[-\pi \frac{K'(\gamma)}{K(\gamma)}\right], \quad q = \pi\Delta_1/2K(\gamma)v_F. \quad (5.2)$$

The third harmonic (Iida et al. 1981a), whose relative intensity $I_3/I_1 = (\Delta_3/\Delta_1)^2 = [\lambda/(\lambda^2 + \lambda + 1)]^2$, is well distinguishable in experiments. This

* Machida and Fujita (1984) have recently reported the contribution to the thermodynamic potential associated with the charge density redistribution [see eq. (3.15)], but with a large reservoir capacity ($M \approx 3-4$); this does not seem to have affected the result of numerical calculations appreciably.

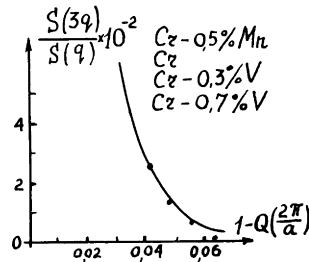


Fig. 15. Neutron scattering intensity ratios of the fundamental and third-harmonic components for several Cr–Mn and Cr–V alloys [— theory (Machida and Fujita 1984), ● experiment (Iida et al. 1981a)].

relation has been independently obtained in experiments by Nakai and Iida (1981). Figure 15 shows the experimental (Iida et al. 1981a) and the calculated data.

Below T_N in the SDW I phase there appears a deformation wave which has been detected by X-ray diffraction (Tsunoda et al. 1974) and neutron diffraction (Iida et al. 1981b). The deformation wave amplitude in CrMn and CrV alloys is proportional to the square of the SDW amplitude and the spectral dependence must contain harmonics even in q (only the second harmonic has been observed experimentally).

According to the SDW soliton lattice model, in the region of the soliton walls there occurs a redistribution of electron density $\delta p(x) \sim \Delta^2(x) - \langle \Delta^2 \rangle$ accompanied (owing to an electron–phonon interaction) by the generation of a deformation wave, which is described by the component of the deformation tensor $\sigma(x)$ along the vector Q :

$$\sigma(x) \sim \delta p(x) \sim \sum_{n=1}^{\infty} \sigma_{2n} \cos(2nqx), \quad \sigma_{2n} = 2n / \sinh[2\pi n K'(k)/K(k)]. \quad (5.3)$$

Unfortunately, the lack of data on the higher harmonics of the deformation wave limits the possibility of comparing the theoretical and experimental data. The only thing that is possible is to construct the dependence σ_2/Δ_1 as a function of the wave vector q (see fig. 16) (the experimental points are from Tsunoda et al. (1974) and Iida et al. (1981b)).

There have been reported in the literature some other interesting experimental results too, which are interpreted qualitatively within the framework of the soliton lattice model. For example, mention can be made of the so-called *hardening* of the SDW wave vector (Ruesink et al. 1980) detected upon measurement of the de Haas–van Alphen effect in Cr under pressure in the region of liquid helium temperatures. The point is that in the I phase of spin density waves the Fermi surface of Cr experiences a substantial rearrangement (Graebner and Marcus 1968) involving the formation of chain sheets for hole ellipsoids at

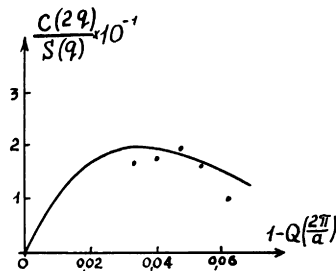


Fig. 16. Wave number dependence of the ratio of the strain wave amplitude to the fundamental component $S(q)$ of the spin density wave [— theory (Machida and Fujita 1984), ● experiment (Iida et al. 1981b)].

points N and electron spheres on the Δ lines of the initial Brillouin zone (it is these regions of the Fermi surface that make up the reservoir). The chain-like model allows one to relate the area of the electron orbit, determined from the de Haas-van Alphen effect, to the magnitude of the vector q , which characterizes the incommensurability of spin density waves; and the measurement of the de Haas-van Alphen effect under pressure makes it possible to determine the pressure derivative $d \ln q / d p \approx -(0.45-0.47) \times 10^{-3} \text{ kbar}^{-1}$ (Vinokurova et al. 1979). This result is in good agreement with neutron diffraction experiments ($-0.5 \times 10^{-3} \text{ kbar}^{-1}$) (Umebayashi et al. 1968). In their experiments carried out at low pressures, Ruesink et al. (1980) have observed an irreversible shift in the de Haas-van Alphen frequency, which means that the vector q did not regain its initial value after the pressure was released. Upon repeated application of the pressure the vector q did not seem to change at first, but once the pressure exceeded the maximum value in the first cycle there occurred a further irreversible change in q at the same rate as at the beginning of the experiment. However, if the samples were annealed at $T \sim 50-200 \text{ K}$ after the pressure was released, the vector q returned to its initial value in the undeformed sample. From the standpoint of the soliton lattice model of spin density waves, such behavior is natural and is associated with the pinning of the soliton walls on the local distortions of the crystalline lattice or on impurities. The microscopic mechanism of this pinning is most likely associated with the formation of a charge density wave and of a deformation wave in the wall region. In experiments carried out by Ruesink et al. (1980), upon removal of the pressure the SDW soliton lattice was found to be frozen in the metastable state. This is so because the charge density wave and the deformation wave coupled rigidly to the lattice have no time to adjust themselves to the equilibrium value of the wave vector q in the region of low temperatures.

The annealing leads to “dissipation” of the nonequilibrium structure of the deformation wave and, as a consequence, to the recovery of the equilibrium

structure of the spin density wave. It is possible that the same pinning mechanism is also responsible, to a certain extent, for the first-order character of the I-C transition in the majority of chromium alloys.

After the congruent segments of the Fermi surface are closed by a gap below the Néel temperature, the major role in metallic conductivity of itinerant antiferromagnets is played by electrons of the reservoir. The appearance of quasi-local states inside the gap is responsible for the fact that the reservoir electrons of energies $\omega \approx \omega_{\uparrow, \downarrow}$ are resonance-scattered off these states. It should be stressed that in our model the resonance levels arise only below T_N and of necessity inside the gap, i.e. in the energy interval $\pm |\Delta^t|$ with respect to the Fermi level at any value of the scattering potential. This constitutes the essential difference from the Wolff and Anderson models, in which the quasi-local impurity level need not lie near the Fermi level and be dependent on the presence or absence of antiferromagnetic ordering. The specificity of the formation of an impurity level in our model manifests itself in a strong dependence of its binding energy and spin polarization on temperature and pressure, and on variation of the degree of congruence of the Fermi surface upon doping, plus other factors that affect spin density waves. In what follows, we discuss some of the experimental consequences of these dependences for dilute Cr-based alloys.

Let us consider the amplitude of resonance scattering of reservoir electrons at the impurity level $\omega_0 = \omega_{\uparrow}, \omega_{\downarrow}$ and assume, for simplicity, $q_1 \ll 1$. After simple calculations we obtain

$$\begin{aligned} \Gamma_r &= \frac{1}{\pi N_r(0)} (-\gamma)(\omega - \omega_0 + i\gamma)^{-1}, \\ \omega_0 &= -\operatorname{sgn} \alpha |\Delta^t| \frac{1 - g_0^2}{1 + g_0^2}, \quad \gamma = \frac{4|\Delta^t||g_0 g_2|}{(1 + g_0^2)^2}. \end{aligned} \quad (5.4)$$

The average scattering time is found in a conventional way from the imaginary part of the scattering amplitude (5.4):

$$\langle \tau_r \rangle = - \int_{-\varepsilon_F}^{\infty} \tau_r(\omega) \frac{\partial f(\omega)}{\partial \omega} d\omega, \quad \tau_r^{-1}(\omega) = \frac{2}{\pi N_r(0)} \frac{\gamma^2}{(\omega - \omega_0)^2 + \gamma^2}, \quad (5.5)$$

where $f(\omega)$ is the Fermi distribution function. As $T \rightarrow 0$, we obtain a resonance contribution to the residual resistivity

$$\rho^0 = \frac{b}{1 + a^2}, \quad a = \frac{\omega_0 - \mu}{\gamma}, \quad b = \frac{2m^* n_{\text{res}}}{n_e e^2 \pi N_r(0)}, \quad (5.6)$$

where n_e is the electron concentration and n_{res} the resonance impurities concentration. The strong dependence $\tau_r(\mu)$ may lead to a sharply nonmonotonic behavior of $\rho^0(x)$, where x is the impurity concentration, and also to the appearance of a resonance peak when $\mu \approx \omega_0$. Indeed, in dilute Cr-based alloys

the position of the Fermi level can be readily changed by the incorporation of an impurity:

$$\mu = \mu_0 + x \frac{m}{N_\Sigma(0)}, \quad N_\Sigma(0) = N_r(0) + 2N(0), \quad (5.7)$$

where μ_0 is the incongruence parameter for pure chromium ($\mu_0 < 0$) and m is the number of electrons per impurity atom transferred to or removed from the band. Combining the various impurities, one can independently change the concentration of scattering centers and the position of the Fermi level; this provides us with reliable information about the character of the residual resistivity of chromium alloys. Recently, precision measurements (Volkov et al. 1979c, Kostina et al. 1986) of $\rho^0(x)$ in ternary Cr-Si-Mn(V) and Cr-Fe-Mn(V) alloys were carried out. A specific feature of these systems is that one can, almost independently, increase or decrease the magnitude of μ without altering the concentration of scattering centers (V and Mn are very weak scatterers in Cr and their effect is well-described in the rigid-band approximation). By successively changing the dopant concentration in these experiments it was found that it is possible to trace out the presence of resonance anomalies of $\rho^0(x)$ in both the C and the I phases of spin density waves, and to determine (using the formulas given in section 3.1 and eq. (5.6)) the energy and width of the resonance levels. The results of the investigations carried out by Volkov et al. (1979c) and by Kostina et al. (1986) are presented in fig. 17. It should also be noted that such anomalies of $\rho^0(x)$ have been observed in the alloys Cr-Co-Mn(V) (Arajs and Dunmyre 1967) and Cr-Fe-Mo (Arajs et al. 1967). There is no doubt that the resonance peaks must also manifest themselves in the pressure dependence $\rho^0(p)$ since the quantity μ depends strongly on pressure.

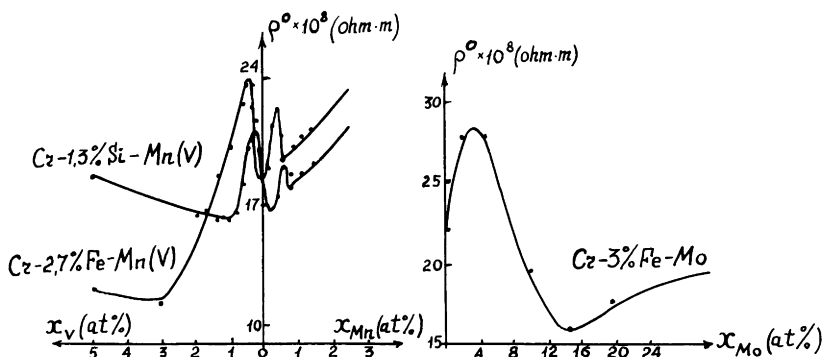


Fig. 17. Concentration dependence of the residual resistivity of ternary chromium alloys (Kostina et al. 1986).

Another remarkable feature of the systems in question is the unusual behavior of resistivity $\rho(T)$ in the region of temperatures $T \lesssim T_N$, because of the strong temperature dependence of the parameters $\omega_0(T)$ and $\gamma(T)$ and of the resonance character of the frequency dependence of the scattering time $\tau_r(\omega)$ in eq. (5.5). If we ignore the first two factors (i.e. if we assume that ω_0 and γ are temperature-independent), then the course of temperature dependence $\rho(T)$ in the region of $T \ll \gamma$ becomes reversed and a direct evaluation of the integral in eq. (5.5) in conjunction with eq. (5.4) yields

$$\rho(T) = \frac{b}{1 + a^2(T)} \left[1 - \frac{\pi^2 T^2}{3\gamma^3(1 + a^2(T))} \right], \quad a(T) = \frac{\omega_0(T) - \mu}{\gamma(T)}. \quad (5.8)$$

Apart from this negative correction to the resistivity of Cr-based alloys at low temperatures, there are also other contributions capable of giving, in sum total, a rather complex dependence $\rho(T)$. For example, when $T > x\Theta_D$ (Θ_D is the Debye temperature) the interference of electron–impurity and electron–phonon scattering may give a positive contribution $\sim (T/\Theta_D)^2$ comparable in magnitude to that given by eq. (5.8). Partial compensation of these contributions may lead to an increase in the region of negative variation, where $\rho(T) \propto -T^{1/2}x^{5/2}$ [the Aronov–Al’tshuler mechanism of quantum corrections (Al’tshuler and Aronov 1979)], and to the appearance of a minimum in $\rho(T)$ at temperatures close to liquid nitrogen temperature. However, one should consider also the dependence $\rho^0(T)$ associated with temperature variation of $\Delta^l(T)$ and, in general, of $\mu(T)$. For example, due to the decrease of $\Delta^l(T)$ even in the region of low temperatures ($T \ll |\Delta^l|$), the local level $\omega_0(T)$ can approach $\mu(T)$ with the result that the resonance condition is fulfilled better than at $T = 0$. The situation may, however, be reversed: $\omega_0(T)$ and $\mu(T)$ may increasingly diverge with increasing T . On the $\rho(T)$ curves, all the singularities indicated manifest themselves in the form of maxima and minima (or their combinations).

The negative low-temperature variation of $\rho(T)$ and the characteristic minimum $\rho(T_{\min})$, $T_{\min} \ll T_N$, have been observed in alloys of Cr with Si, Ge, Ni, Fe and Co (see e.g. Booth 1966, Arajs and Katzenmeyer 1967a, b) and have been traditionally associated with the Kondo effect. It has been well established, however, that Si, Ge and Ni do not at all possess localized moments in alloys with Cr and that the local moment of Co is strongly frozen in the antiferromagnetic matrix when $T < T_N$, which is why the Kondo scattering is found to be suppressed. In order to carry out a detailed analysis of the behavior of $\rho(T)$ with $T \lesssim T_N$, Galkin and Tugusheva (1986) studied ternary Cr–Fe–Mn(V) alloys over a wide range of impurity concentrations and have convincingly demonstrated the impossibility of accounting for the anomalies of $\rho(T)$ with the aid of the Kondo mechanism. Conversely, the resonance scattering model has made it possible to achieve an adequate description of the specific features of the alloys mentioned here; such as (i) the existence of $\rho(T_{\min})$ only in a narrow range of

magnetic impurity concentrations ($x_{\text{Fe}} \lesssim 1.5$ at%), (ii) the presence of a maximum, (iii) the unusual behavior of $T_{\min}(x_{\text{Fe}})$ which does not fit into the Kondo plots, and (iv) the nonmonotonic variation (sometimes even an increase) of T_{\min} with increasing nonmagnetic impurity concentration. It has been possible to trace out the correlation between the appearance of low-temperature minima $\rho(T_{\min})$ and maxima of $\rho^0(x)$ in the residual resistivity, which is, in our opinion, the decisive confirmation of the resonance level model. Finally, in alloys with a high ($\gtrsim 5$ at%) content of vanadium, for which the antiferromagnetic ordering is completely suppressed, "true" Kondo anomalies of $\rho(T)$ have been revealed, which are almost identical for alloys with Fe and Co and which are independent of vanadium concentration.

Some of the characteristic $\rho(T)$ plots obtained by Galkin and Tugusheva (1986) are presented in fig. 18.

Another important argument in favor of the resonance model is presumably the occurrence of a broad maximum in the $\rho(T)$ plot near the Néel temperature. This maximum is usually ascribed to the appearance of a gap at the Fermi surface and to a change in the density of states of the conduction electrons. This effect itself must not depend strongly on the composition of the alloy, but even for alloys in which T_N falls off with increasing impurity concentration or is unlikely to change at all (Cr-Si, Cr-Ni, etc.), the anomaly in $\rho(T)$ increases when $T \approx T_N$. From the viewpoint of our mechanism, this can be accounted for rather easily. When $T \approx T_N$, taking into account the temperature dependence $A^t(T) \sim [T_N - T]^{1/2}$ it is easy to show that

$$\rho(T \rightarrow T_N) = \frac{b\gamma^2}{\mu^2 + 1/3\pi^2 T_N^2} \sim |T_N - T|, \quad (5.9)$$

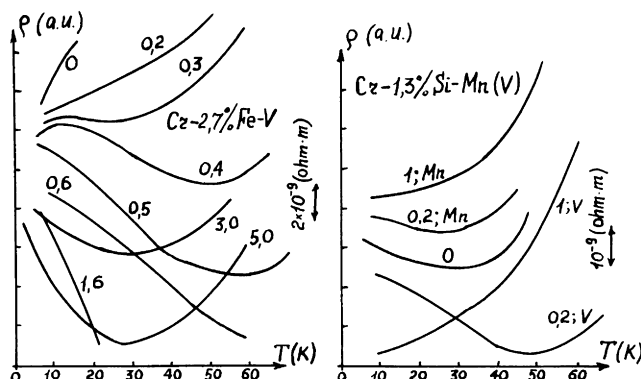


Fig. 18. Temperature dependence of electrical resistivity in ternary chromium alloys (Galkin and Tugushev 1986).

i.e. the electrical resistance increases with decreasing temperature for $T < T_N$. As the dependence $\Delta^i(T)$ becomes weaker, the usual metallic behavior of $\rho(T)$ begins to predominate, this behavior being associated with scattering of phonons, as a result of which there appears a maximum near $T \lesssim T_N$.

Finally, one more feature of the resonance model should be mentioned: the negative contribution to low-temperature magnetoresistance. Neglecting the dependence $\Delta^i(H)$ on magnetic-field H , which is not important in Cr-based alloys with moderate fields, we can show that with $T \ll T_N$

$$\frac{\rho(H, T = 0) - \rho(H = 0, T = 0)}{\rho(H = 0, T = 0)} = -d \left(\frac{\mu_B H}{\gamma} \right)^2, \quad d = \frac{1 - 3a^2}{(1 + a^2)^2}. \quad (5.10)$$

This result differs from the dependence $-H^2/T^2$ in the model proposed by Al'tshuler and Aronov (1979) for $\mu_B H \ll T$.

Unfortunately, the available measurements of magnetoresistance of dilute Cr-based alloys simply reveal the negative variation of $\rho(H)$, without making it possible to account for this effect fully. Qualitatively, in our model the negative magnetoresistance may even increase with increasing temperatures at a certain stage, as a result of a decrease in $\Delta^i(T)$ and hence, in $\gamma(T)$, whereas in the Aronov-Al'tshuler model the negative magnetoresistance falls with increasing T .

The case of local phase transitions in itinerant antiferromagnets does not require much discussion since practically no experiments in the region of $T > T_N$ have been carried out for the purpose of their detection. An exception is the work of Kondorskii et al. (1979), who detected the Curie-Weiss anomaly of the magnetic susceptibility $\chi(T)$ and pointed out its unusual behavior with change in concentration of the nonmagnetic impurity (vanadium). This result has been treated by Kostina et al. (1985) within the framework of the model discussed in section 4.2 and the dependence $T_{loc}(x_V)$ has been constructed qualitatively (see fig. 19). The appearance of local moments below the local transition

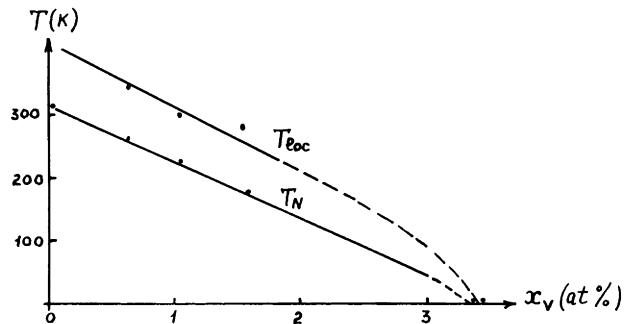


Fig. 19. Concentration dependence of the Néel temperature (T_N) and of the temperature at which short-range order is set up (T_{loc}) in $\text{Cr}_{1-x}\text{V}_x$ alloys (Kostina et al. 1985).

temperature and their freezing below the Néel temperature can be seen rather clearly in the $\chi(T)$ plots, but it would also be interesting to trace out the other characteristics (say, the dependence $\rho(T)$) near the local transition temperature. Unfortunately, such data are not available at present.

An interesting situation may occur in chromium samples with an atomically clean (100) surface, in which surface ferromagnetic ordering may appear below the Curie temperature $T_C \approx 800$ K (Hasegawa 1985), while the antiferromagnetic transition in the bulk takes place at $T_N \approx 312$ K. Presumably, here situation corresponding to a source of the “local field” type discussed in section 4.2 is realized; the role of this source is played by the surface magnetization vector. Neutron diffraction experiments could possibly reveal the presence of the induced antiferromagnetic component in the near-surface layer $\sim \zeta(T)$ above T_N . Moreover, the surface itself may play the role of a nonmagnetic planar defect, leading to the formation of a narrow spin-polarized surface band, which one can try to detect by means of optical methods.

6. Conclusions

The SDW model has made it possible to relate in a qualitative way the fundamental factor responsible for antiferromagnetic ordering to the particular singularities of the Fermi surface in a metal. However, until now this model has been studied only in the limit of a small exchange interaction constant, $\bar{g} \ll 1$, i.e. in the mean-field approximation. Meanwhile, for the majority of antiferromagnets (chromium and its dilute alloys constitute an exception rather than the rule) the interaction constant is not small ($\bar{g} \gtrsim 1$) and an important role is played by spin fluctuations. It is these fluctuations that determine, in particular, rather significant deviations of the real Néel temperature and of the form of the phase diagrams in alloys of transition metals (Kulatov et al. 1986).

There is, however, one more fundamental aspect of the problem, which consists of a qualitatively new effect associated with spin fluctuations – the appearance of a short-range antiferromagnetic order above the Néel temperature even in the absence of structural defects. The attempt (Hasegawa 1978) to include spin fluctuations in the SDW scheme within the framework of the self-consistent field theory of spin fluctuations (Moriya and Kawabata 1973a, b) has boiled down to calculating the corrections (delocalized spin fluctuations with a small amplitude) to the mean-field approximation, which are found to be insignificant in the region of validity of the scheme itself (Moriya and Kawabata 1973a, b). In our opinion, the developments in the modern theory of itinerant magnetism have made it possible to significantly expand the range of validity of the SDW scheme. A number of procedures for calculating the effective thermodynamic short-range magnetic order (of the type of local band theory (Korenman et al. 1977, 1979, Capellmann and Vieira 1982a, b)) available for

itinerant ferromagnets in the Stoner model can also be applied, rather must be applied, to SDW antiferromagnets. This seems to be especially important for a study of the magnetic properties of mixed metal oxides, such as La–Sr–Cu–O and Y–Ba–Cu–O, and also detection of strong short-range antiferromagnetic order effects (Yang et al. 1988, Shirane et al. 1987) in them. In our opinion, there are no serious grounds for rejection of the band scheme in explaining the magnetic properties of the materials indicated above, and it is hoped that a considerable progress will be made in this direction in the near future.

Appendix I

The coefficients of the functional (3.21) calculated in accordance with the standard procedure (Abrikosov et al. 1962) have the following form at $M = \infty$ (with the contribution of eq. (3.15) having been neglected):

$$\alpha = \tilde{c}_1 + 2v' \frac{\psi_2}{\pi T}, \quad (\text{I.1})$$

$$a_1 = \tilde{c}_2 v_F^2 + \frac{5}{4} v' \frac{\psi_4 v_F^2}{(\pi T)^3}, \quad (\text{I.2})$$

$$a_2 = \frac{1}{2} \tilde{c}_3 v_F^4 + \frac{1}{2} v' \frac{\psi_6 v_F^4}{(\pi T)^5}, \quad (\text{I.3})$$

$$\beta_1 = 2\tilde{c}_2 + 4v' \frac{\psi_4}{(\pi T)^3}, \quad (\text{I.4})$$

$$b = 5\tilde{c}_3 v_F^2 + 8v' \frac{\psi_6 v_F^2}{(\pi T)^5}, \quad (\text{I.5})$$

$$\gamma = 3\tilde{c}_3 + 6v' \frac{\psi_6}{(\pi T)^5}, \quad (\text{I.6})$$

$$\tilde{c}_1 = c_1 + v \frac{\psi_2}{\pi T}, \quad (\text{I.7})$$

$$\tilde{c}_2 = c_2 + \frac{3}{4} v \frac{\psi_4}{(\pi T)^3}, \quad (\text{I.8})$$

$$\tilde{c}_3 = c_3 + \frac{5}{8} v \frac{\psi_6}{(\pi T)^5}, \quad (\text{I.9})$$

$$c_1 = \ln \frac{T}{T_N^0} - \psi(\tfrac{1}{2}) + \operatorname{Re} \psi(\tfrac{1}{2} + i\eta), \quad (\text{I.10})$$

where $\psi(z)$ is the digamma function,

$$\eta = \frac{\mu}{2\pi T}, \quad c_2 = \frac{\varphi_2}{2(\pi T)^2}, \quad c_3 = \frac{\varphi_4}{4(\pi T)^4} \quad (\text{I.11})$$

and $T_N^0 = W \exp(-1/g_t N_n(0))$;

$$\varphi_2 = \frac{1}{4} \operatorname{Im} \frac{\partial \psi}{\partial \eta}, \quad (\text{I.12})$$

$$\varphi_4 = \frac{1}{96} \operatorname{Im} \frac{\partial^3 \psi}{\partial \eta^3}, \quad (\text{I.13})$$

$$\varphi_6 = \frac{1}{7680} \operatorname{Im} \frac{\partial^5 \psi}{\partial \eta^5}, \quad (\text{I.14})$$

$$\varphi_2 = \frac{1}{16} \operatorname{Re} \frac{\partial^2 \psi}{\partial \eta^2}, \quad (\text{I.15})$$

$$\varphi_4 = \frac{1}{768} \operatorname{Re} \frac{\partial^4 \psi}{\partial \eta^4}. \quad (\text{I.16})$$

The corrections associated with the contribution of eq. (3.15) have the following form:

$$\Delta \beta_1 = \frac{1}{1+M} 2c_4, \quad (\text{I.17})$$

$$\Delta b = \frac{1}{1+M} 7v_F^2 c_5, \quad (\text{I.18})$$

$$\Delta \gamma = \frac{1}{1+M} 3c_6, \quad (\text{I.19})$$

$$c_4 = \frac{1}{(\pi T)^2} \frac{1}{16} (\operatorname{Re} \psi')^2, \quad (\text{I.20})$$

$$c_5 = \frac{1}{(\pi T)^4} \frac{1}{768} \operatorname{Re} \psi' \cdot \operatorname{Re} \psi''', \quad (\text{I.21})$$

$$c_6 = \frac{1}{(\pi T)^4} \frac{1}{768} \operatorname{Re} \psi' \operatorname{Re} \psi'''' \frac{5+3M}{1+M}. \quad (\text{I.22})$$

Appendix II

For the microscopic model of the Peierls transition with a nearly half-filled band, Brazovskii et al. (1981) have pointed to the existence of a second solution

– a doubly periodic solution – in addition to the simple periodic solution. This result can also be obtained using the functional approach. By making the order parameter in eq. (3.21) and the coordinate x dimensionless, the functional $\Omega(\varphi)$ can be reduced to the form

$$\Omega = \int \{\alpha\varphi^2 + \beta(\varphi^4 + \varphi^{12}) + \varphi''^2 + 10(\varphi\varphi')^2 + 2\varphi^6\} dx. \quad (\text{II.1})$$

The Euler equation here has the form

$$\varphi''' - 10\varphi\varphi^{12} - 10\varphi^2\varphi'' + 6\varphi^5 - \beta(\varphi'' - 2\varphi^3) + \alpha\varphi = 0. \quad (\text{II.2})$$

Using the Miura transformation, we introduce the function $u = \varphi^2 + \varphi'$ and show that it satisfies the second KDV equation, the solution of which is provided exactly by a doubly periodic function. This equation is written in the form

$$\sum_i b_i \frac{\delta I_i}{\delta u} = 0, \quad i = -1, 0, 1, 2, \quad (\text{II.3})$$

where I_i are the integrals of the KDV equation:

$$\begin{aligned} I_{-1} &= \int u dx, & I_0 &= \int u^2 dx, & I_1 &= \int (\frac{1}{2}u'^2 + u^3) dx, \\ I_2 &= \frac{1}{2} \int (u''^2 - 5u^2u'' + 5u^4) dx. \end{aligned} \quad (\text{II.4})$$

We rewrite eq. (II.3) as follows:

$$\begin{aligned} &(b_2 J_2 + b_1 J_1 + b_0 \varphi)' + 2\varphi(b_2 J_2 + b_1 J_1 + b_0 \varphi) \\ &+ b_2 [\varphi''^2 + 10\varphi^2\varphi^{12} - 2\varphi^6 - 2\varphi'\varphi^3] \\ &+ b_1 (\varphi^4 - \varphi'^2) - b_0 \varphi^2 + b_{-1} = 0. \end{aligned} \quad (\text{II.5})$$

Multiplying at the same time eq. (II.2) by φ' , we can write this relation in the form

$$[\alpha\varphi^2 + \beta(\varphi^4 - \varphi^{12}) - (\varphi'' - 2\varphi'\varphi^3 - 2\varphi^6 + 10\varphi^2\varphi^{12})]' = 0. \quad (\text{II.6})$$

Comparing eqs. (II.6) and (II.5) using the relations

$$J_1 = \varphi'' - 2\varphi^3, \quad J_2 = \varphi''' - 10\varphi^2\varphi'' - 10\varphi\varphi^{12} + 6\varphi^5, \quad (\text{II.7})$$

we see that these equations coincide at $b_2 = 1, b_1 = -\beta, b_0 = 0$, i.e. the solution $\varphi(x)$ of (II.2) really leads to the second KDV equation for $u = \varphi^2 + \varphi'$. This means that $\varphi(x)$ is in general a doubly periodic function.

Appendix III

The source function $\Gamma(\Delta^t(r))$, where Δ^t is the order parameter for the case of a magnetic planar defect of the “local field” type in the SDW model, has the form

$$\Gamma_0(\Delta^t) = \mathbf{F}_0 \cdot \Delta^t(r), \quad (\text{III.1})$$

$$\mathbf{F}_0 = -\frac{2U\mathbf{m}}{(1 + \bar{U}^2)\bar{g}}, \quad \bar{U} = 2\pi UN(0), \quad (\text{III.2})$$

where U is the potential of the defect, $U = JM$, M being the local frozen magnetization of the defect, \mathbf{m} is a unit vector in the direction of magnetization and J is the effective exchange integral.

For the case of a nonmagnetic defect of the “local temperature” type we have

$$\Gamma_1(\Delta^t) = \frac{1}{2} F_1(\Delta^t)^2(r), \quad (\text{III.3})$$

$$F_1 = \frac{\bar{U}}{(1 + \bar{U}^2)^2} [2\varphi_1 - \varphi_0 \bar{U} (3 + \bar{U}^2)]. \quad (\text{III.4})$$

Here $\bar{U} = 2\pi UN(0)$, where U is the potential of the nonmagnetic defect.

Appendix IV

The nonlinear transformation formulae used in section 4.2 have been taken from the book of Calogero and Degasperis (1982). The solutions $u^0(\zeta)$ and $u^i(\zeta)$ ($i = 1, 2$) of the KDV equations are interconnected by the Bäcklund transformation if

$$\frac{\partial w^{(0)}}{\partial \zeta} + \frac{\partial w^{(i)}}{\partial \zeta} = \frac{1}{2} [w^{(0)} - w^{(i)}] [4d_i - (w^{(0)} - w^{(i)})], \quad (\text{IV.1})$$

where $w^{(i)} = \int_{\zeta}^{\infty} u_{(y)}^{(i)} dy$ and d_i are parameters.

Performing algebraic manipulations, from eq. (IV.1) we can obtain a new solution of the equation, for which

$$w^{(3)} = w^{(0)} - \frac{(d_1 + d_2)(w^{(1)} - w^{(2)})}{d_1 - d_2 + \frac{1}{2}(w^{(1)} - w^{(2)})}. \quad (\text{IV.2})$$

Formula (IV.2) is called the principle of nonlinear superposition for the solutions of the KDV equation.

References

Abrikosov, A.A., L.P. Gor'kov and I.E. Dzyaloshinskii, 1962, Methods of Quantum Field Theory in Statistical Physics (Fizmatgiz, Moscow), English Ed. Quantum Field Theoretical Methods in Statistical Physics (Prentice Hall, Englewood Cliffs, NJ, Pergamon Press, London).

- Allan, G., 1979, Conditions for the Existence of a Permanent Magnetic Moment Near the Transition-Metal Surface, *Phys. Rev. B* **19**, 4774.
- Altshuler, B.L., and A.G. Aronov, 1979, Concerning the Theory of Disordered Metals and Heavily Doped Semiconductors, *Zh. Eksp. & Teor. Fiz.* **77**, 2028.
- Arajs, S., and G. Dunmyre, 1967, Occurrence of a Minimum in the Electrical Resistivity of Cr Alloys at Low Temperatures, *J. Appl. Phys.* **38**, 1157.
- Arajs, S., and W. Katzenmeyer, 1967a, Electrical Resistivity of Some Cr-Si Alloys, *J. Phys. Soc. Jpn.* **23**, 932.
- Arajs, S., and W. Katzenmeyer, 1967b, Electrical Resistivity of Cr-Ge Alloys, *J. Phys. Chem. Solids* **28**, 1459.
- Arajs, S., G. Dunmyre and S. Dechter, 1967, Electrical Resistivity Studies of Cr-Co Alloys, *Phys. Rev. B* **154**, 448.
- Asano, S., and J. Yamashita, 1967, Band Energy of Antiferromagnetic Chromium, *J. Phys. Soc. Jpn.* **23**, 714.
- Booth, J., 1966, Magnetic Properties of Chromium Alloys Containing Dilute Concentrations of Co, Ni and Fe, *J. Phys. & Chem. Solids* **27**, 1639.
- Brazovskii, S.A., S.A. Gordyunin and N.N. Kirova, 1980, An Exact Solution of the Peierls Model with an Arbitrary Number of Electrons per Unit Cell, *Pis'ma Zh. Eksp. & Teor. Fiz.* **31**, 486.
- Brazovskii, S.A., I.E. Dzyaloshinskii and N.N. Kirova, 1981, Spin States in the Peierls Model and Finite-Band Potentials, *Zh. Eksp. & Teor. Fiz.* **81**, 2279.
- Buker, D., 1981, Selection of the Spin-Density-Wave State, *Phys. Rev. B* **24**, 5713.
- Buker, D., 1982, Spin-Density-Wave State of Chromium, *Phys. Rev. B* **25**, 991.
- Butz, T., K. Ebeling, E. Hagh, S. Saibene, E. Zech and A. Lerf, 1986, Evidence for the Coexistence of CDW and SDW in 2H-TaS₂, *Phys. Rev. Lett.* **56**, 639.
- Buzdin, A.I., and S.A. Polonskii, 1987, The Inhomogeneous State in Quasi-One-Dimensional Superconductors, *Zh. Eksp. & Teor. Fiz.* **93**, 357.
- Buzdin, A.I., and V.V. Tugushev, 1983, Phase Diagram for Electronic and Superconducting Transitions to the Soliton-Lattice State, *Zh. Eksp. & Teor. Fiz.* **85**, 735.
- Buzdin, A.I., M.L. Kulich and V.V. Tugushev, 1983, Spin-Peierls Systems in Magnetic Fields: Phase Transition from the Dimerized to the Soliton Lattice State, *Solid State Commun.* **48**, 483.
- Buzdin, A.I., V.N. Menshov and V.V. Tugushev, 1986, Localized States on Defects upon Electronic Transitions into the Soliton-Lattice Phase, *Zh. Eksp. & Teor. Fiz.* **91**, 2204.
- Bychkov, Yu.A., and S.V. Iordanskii, 1980, Cooperative Excitations in a Semimetal with Electron-Hole Coupling, *Fiz. Tverd. Tela* **22**, 2034.
- Calogero, F., and A. Degasperis, 1982, Spectral Transform and Solitons (North-Holland, Amsterdam).
- Capellmann, H., and V. Vieira, 1982a, Strong Short-Range Magnetic Order in Ferromagnetic Transition Metals Above T_c : A Theoretical Explanation, *Solid State Commun.* **43**, 747.
- Capellmann, H., and V. Vieira, 1982b, Magnetic Properties of Ferromagnetic Transition Metals Above T_c : Qualitative Aspects, *Phys. Rev. B* **25**, 3333.
- Chui, S., R. Kasowski and W. Hsu, 1988, Mean-Field Calculation of the Antiferromagnetic Instability in La_{2-x}Sr_xCuO₄, *Phys. Rev. Lett.* **61**, 207.
- Coleman, R., G. Eiserman, M. Everson, A. Johnson and L. Falicov, 1985, Evidence for Magnetism in the Low-Temperature CDW Phase of NbSe₃, *Phys. Rev. Lett.* **55**, 863.
- Coqueblin, B., 1977, The Electronic Structure of Rare-Earth Metals and Alloys: the Magnetic Heavy Rare Earths (Academic Press, New York).
- De Cloiseaux, J., 1965, Exciton Instability and Crystallographic Anomalies in Semiconductors, *J. Phys. & Chem. Solids* **26**, 259.
- Dzyaloshinskii, I.E., and E. Katz, 1972, Concerning the Theory of Antiferromagnetism of Chromium, *Zh. Eksp. & Teor. Fiz.* **62**, 1104.
- Egorushkin, V.E., S.N. Kulkov and S.E. Kulkova, 1983, Electronic Structure and the Theory of Phase Transformation in NiMn, *Physica B* **123**, 61.

- Elesin, V.F., and Yu.V. Kopaev, 1976, Concerning the Electronic Theory of Ferroelectricity, Pis'ma Zh. Eksp. & Teor. Fiz. **24**, 78.
- Evertz, H., and I. Zittartz, 1973, Impurity in the Excitonic Phase, J. Low Temp. Phys. **11**, 349.
- Eyert, V., J. Sticht and J. Kübler, 1988, Itinerant Magnetism in K_2NiF_4 -Type Compounds, Helv. Phys. Acta **61**, 496.
- Fawcett, E., 1988, Spin-Density Wave Antiferromagnetism in Chromium, Rev. Mod. Phys. **60**, 209.
- Fedders, P., and P. Martin, 1966, Itinerant Antiferromagnetism, Phys. Rev. B **143**, 245.
- Fischbeck, H., 1983, On the Translation Mode of the Kink Lattice of a Quasi-One-Dimensional Peierls-Fröhlich System with a Nearly Half-Filled Band, Phys. Status Solidi B **118**, 595.
- Galkin, V.Yu., and T.E. Tugusheva, 1986, Temperature Anomalies of Electrical Resistivity in Dilute Cr-Fe Alloys, 24th USSR Conference on Low-Temperature Physics, Abstracts, part II, p. 119.
- Galkin, V.Yu., T.E. Tugusheva and V.V. Tugushev, 1986, Resonance Impurity Scattering in Antiferromagnetic Cr-Fe-V(Mn) Alloys, Fiz. Tverd. Tela **28**, 2290.
- Gor'kov, L.P., 1984, Physical Phenomena in New Organic Conductors, Usp. Fiz. Nauk. **144**, 381.
- Gor'kov, L.P., and I.E. Dzyaloshinskii, 1974, Concerning the Possible Phase Transitions in Systems of Interacting Metallic Filaments (Quasi-One-Dimensional Metals) Zh. Eksp. & Teor. Fiz. **67**, 397.
- Graebner, J., and J. Marcus, 1968, De Haas–Van Alphen Effect in Antiferromagnetic Chromium, Phys. Rev. B **175**, 659.
- Halperin, B.I., and T.M. Rice, 1968, The Excitonic State at the Semiconductor–Semimetal Transition, Solid State Phys. **21**, 115.
- Harada, I., and A. Kotani, 1982, Commensurate and Incommensurate States of Spin-Peierls Systems in a Magnetic Field, J. Phys. Soc. Jpn. **51**, 1737.
- Hasegawa, H., 1978, A Study of Spin Fluctuations in Antiferromagnetic Metals Described by a Nesting-Type Model, J. Low Temp. Phys. **31**, 475.
- Hasegawa, H., October 1985, Electrical Structure and Surface Magnetism of Cr(100) at Finite Temperature, Preprint ISSP, Ser. A, No. 1585.
- Herring, C., 1966, Exchange interactions among itinerant electrons, in: Magnetism IV, eds C.T. Rado and H. Suhl (Academic Press, New York).
- Horovitz, B., 1981, Soliton Lattice in Polyacetylene. Spin-Peierls Systems and 2D sine-Gordon Systems, Phys. Rev. Lett. **48**, 742.
- Idlis, B.G., and Yu.V. Kopaev, 1983, On the Theory of Phase Transitions in Vanadium Oxides V_nO_{2n-1} (Magneli Phases), Solid State Commun. **45**, 301.
- Iida, S., Y. Tsunoda, Y. Nakai and N. Kunitomi, 1981a, Third Harmonics of Spin-Density-Waves in Cr and Its Alloys, J. Phys. Soc. Jpn. **50**, 2587.
- Iida, S., M. Kohno, Y. Tsunoda and N. Kunitomi, 1981b, Strain Waves in Cr, CrMn and CrV Alloys, J. Phys. Soc. Jpn. **50**, 2581.
- Izymov, Yu.A., 1984, Modulated or Long-Periodic Magnetic Structures of Crystals, Usp. Fiz. Nauk **144**, 439.
- Kasowski, R., W. Hsu and F. Herman, 1987, Electronic Structure of Oxygen-Deficient High- T_c Superconductors: $YBa_2Cu_xO_x$ ($6 \leq x \leq 8$), Phys. Rev. B **36**, 6904.
- Keldysh, L.V., and Yu.V. Kopaev, 1964, Possible Instability of the Semimetallic State Against Coulomb Interaction, Fiz. Tverd. Tela **6**, 2791.
- Khaikin, M.S., and I.N. Khlyustikov, 1981, The Twinning Plane of a Metallic Crystal – A Two-Dimensional Superconductor, Pis'ma Zh. Eksp. & Teor. Fiz. **33**, 167.
- Kitaoka, Y., and H. Yasuoka, 1980, NMR Investigation of the Spin Fluctuations in Itinerant Antiferromagnets: V_3Se_4 and V_5Se_8 , J. Phys. Soc. Jpn. **48**, 1460.
- Kitaoka, Y., H. Yasuoka, Y. Oka, K. Kosuge and S. Kachi, 1979, Observation of the Antiferromagnetic Order in Metallic Compounds V_3S_4 and V_3Se_4 , J. Phys. Soc. Jpn. **46**, 1381.
- Kochler, W., R. Moon, A. Trego and A. Mackintosh, 1966, Antiferromagnetism in Chromium Alloys, Phys. Rev. B **151**, 405.
- Kondorskii, E.I., T.I. Kostina, V.P. Medvedchikov and Yu.A. Kuskova, 1979, Magnetic Properties of

- Cr-Ni and Cr-V Alloys, *Fiz. Magn. Mater.* **48**, 1158.
- Kopaev, Yu.V., 1975, Concerning the Theory of Interrelation Between Electronic and Structural Transformations and Superconductivity, *Tr. Fiz. Inst. Akad. Nauk SSSR* **86**, 3.
- Kopaev, Yu.V., and V.G. Mokerov, 1982, The Mechanism of Phase Transitions in Vanadium and Titanium Oxides, *Dokl. Akad. Nauk SSSR* **264**, 1370.
- Kopaev, Yu.V., and A.I. Rusinov, 1969, The Theory of Impurity States in an Excitonic Insulator, *Fiz. Tverd. Tela* **11**, 1306.
- Kopaev, Yu.V., and R.Kh. Timerov, 1971, The Effect of Impurity States on the Semiconductor-Semimetal Phase Transition, *Fiz. Tverd. Tela* **13**, 122.
- Korenman, V., J. Murray and R. Prauge, 1977, Local-Band Theory of Itinerant Ferromagnetism, *Phys. Rev. B* **16**, 4032.
- Korenman, V., J. Murray and R. Prauge, 1979, Local-Band Theory of Itinerant Ferromagnetism, *Phys. Rev. B* **19**, 4691.
- Kostina, T.I., V.N. Menshov and V.V. Tugushev, 1985, The Formation of Local Magnetic Moments on Nonmagnetic Impurities in Dilute Chromium Alloys Above the Néel Temperature, *Fiz. Magn. Mater.* **59**(3), 430.
- Kostina, T.I., V.N. Menshov, V.V. Tugushev, K. Tselikyan, L.N. Ekonomova and V.Yu. Galkin, 1986, Impurity states in antiferromagnetic chromium alloys, in: Abstracts of 24th USSR Conference on Low-Temperature Physics, Tbilisi, 1986, part III, p. 51.
- Kotani, A., 1975, Theory of the Incommensurate Sinusoidal Spin-Density-Wave in Chromium and Its Alloys, *J. Phys. Soc. Jpn.* **38**, 974.
- Kotani, A., 1975, Spin-Density-Wave, Charge-Density-Wave and Strain-Wave in Chromium, *J. Phys. Soc. Jpn.* **39**, 851.
- Kotani, A., 1978, Effect of Harmonics in Nearly Commensurate Spin-Density-Wave, *J. Phys. Soc. Jpn.* **45**, 766.
- Kotani, A., 1978, Spin-Density-Wave, Charge-Density-Wave and Strain-Wave in Chromium, *J. Phys. Soc. Jpn.* **44**, 1455.
- Kozlov, A.N., and L.A. Maksimov, 1965, Concerning the Metal-Dielectric Transition. A Divalent Crystal, *Zh. Eksp. & Teor. Fiz.* **48**, 1184.
- Kulatov, E.T., N.I. Kulikov and V.V. Tugushev, 1986, Localized magnetic moments in metals and alloys with spin-density wave instability, in: *Magnetic and Electron Structures of Transition Metals and Alloys*, eds V.G. Veselago and L.I. Vinokurova (Nova Science Publishers, New York).
- Kulikov, N.I., 1985, Theory of Antiferromagnetic Ordering in Pt₃Fe Alloys, *J. Phys. F* **15**, 1139.
- Kulikov, N.I., and V.V. Tugushev, 1981, The Influence of Electron-Phonon Coupling on the Transition Temperature into the SDW and CDW States, *J. Phys. C* **14**, L809.
- Kulikov, N.I., and V.V. Tugushev, 1984, Spin-Density Waves and Itinerant Antiferromagnetism in metals, *Usp. Fiz. Nauk.* **144**, 964.
- Kulikov, N.I., E.T. Kulatov, L.I. Vinokurova and M. Pardavi-Horvath, 1982, Electronic Band Structure and Magnetic Order in FeRh, *J. Phys. F* **12**, L91.
- Landau, L.D., and E.M. Lifshitz, 1974, *Quantum Mechanics. Nonrelativistic Theory* (Nauka, Moscow) [English translation: Pergamon Press, London, 1977].
- Levanyuk, A.P., V.V. Osipov, A.A. Sigov and A.A. Sobyanin, 1979, Variation of the Defect Structure and the Attendant Anomalies of the Properties of Compounds Near the Phase Transitions Points, *Zh. Eksp. & Teor. Fiz.* **76**, 345.
- Liu, S., L. Kopp, W. England and H.W. Myron, 1975, Energy Bands, Electronic Properties and Magnetic Ordering of CrB₂, *Phys. Rev. B* **11**, 3463.
- Lomer, W., 1962, Electronic Structure of Chromium Group Metals, *Proc. Phys. Soc. II*, **80**, 489.
- Machida, K., and M. Fujita, 1984, Soliton Lattice Structure of Incommensurate Spin-Density-Waves: Application to Cr and Cr-rich Cr-Mn and Cr-V Alloys, *Phys. Rev. B* **30**, 5284.
- Machida, K., and H. Nakanishi, 1984, Superconductivity under a Ferromagnetic Molecular Field, *Phys. Rev. B* **30**, 122.
- Machida, K., M. Lind and J. Stanford, 1984, Temperature Dependence of Infrared Reflectivity of

- Chromium – Relization of Soliton Lattice Structure of Spin-Density-Wave, *J. Phys. Soc. Jpn.* **53**, 4020.
- Maki, K., and M. Sakurai, 1972, Spin Susceptibility of Excitonic States, *Prog. Theor. Phys.* **47**, 1110.
- Malaspinas, A., and T. Rice, 1971, On the Order of Itinerant Antiferromagnetic Phase Transitions and Superconducting Phase Transitions in an Exchange Field, *Phys. Kondens. Mater.* **13**, 193.
- Mertsching, J., and H. Fischbeck, 1981, The Incommensurate Peierls Phase of the Quasi-One-Dimensional Fröhlich Model With a Nearly Half-Filled Band, *Phys. Status Solidi B* **103**, 783.
- Moriya, T., 1985, Spin Fluctuations in Itinerant Electron Magnetism (Springer, Berlin).
- Moriya, T., and A. Kawabata, 1973a, Effect of Spin Fluctuations on Itinerant Electron Ferromagnetism, *J. Phys. Soc. Jpn.* **34**, 639.
- Moriya, T., and A. Kawabata, 1973b, Effect of Spin Fluctuations on Itinerant Electron Ferromagnetism, *J. Phys. Soc. Jpn.* **35**, 669.
- Nakai, Y., and S. Iida, 1981, Empirical Relation Between Amplitude and Period of SDW for Cr(V) and Cr(Mn) Alloys, *J. Phys. Soc. Jpn.* **50**, 3637.
- Nakanishi, K., and K. Maki, 1972, First-Order Phase Transition in Itinerant Antiferromagnetism, *Prog. Theor. Phys.* **48**, 1059.
- Overhauser, A., 1962, Spin-Density Waves in an Electron Gas, *Phys. Rev. B* **128**, 1437.
- Rice, T.M., 1970, Band-Structure Effects in Itinerant Antiferromagnetism, *Phys. Rev. B* **2**, 3619.
- Ruesink, D., J. Perz and I. Templeton, 1980, Pressure-Induced “Hardening” of Q-Vector Locking in Chromium, *Phys. Rev. Lett.* **45**, 734.
- Sato, H., and K. Maki, 1973, Ultrasonic Attenuation of Itinerant Antiferromagnetism Above the Néel Temperature, *Int. J. Magn.* **4**, 163.
- Schluter, M., 1988, The Electronic Structure and Superconductivity of the High- T_c Copper Oxides, *Int. J. Mod. Phys.* **2**, 167.
- Shibatani, A., K. Motizuki and T. Nagamiya, 1969, Spin-Density-Wave in Chromium and Its Alloys, *Phys. Rev. B* **177**, 984.
- Shirane, G., Y. Endoh, R.J. Birgeneau, M.A. Kastner, Y. Shidaka, M. Oda, M. Suzuki and T. Murokami, 1987, Two-Dimensional Antiferromagnetic Spin-Fluid State in La_2CuO_4 , *Phys. Rev. Lett.* **59**, 1613.
- Shraishi, K., A. Oshiyama, N. Shima, T. Nakayama and H. Kamimura, 1988, Spin-Polarized Electronic Structures of La_2CuO_4 , *Solid State Commun.* **66**, 629.
- Takayama, H., Y.R. Lin-Liu and K. Maki, 1980, Continuum Model for Solitons in Polyacetylene, *Phys. Rev. B* **21**, 2388.
- Tsunoda, Y., M. Mori, N. Kunitomi, Y. Teraoka and J. Kanamori, 1974, Strain Wave in Pure Chromium, *Solid State Commun.* **14**, 287.
- Umebayashi, H., G. Shirane, B.C. Frazer and W. Daniels, 1968, Neutron Diffraction Study of Cr Under High Pressure, *J. Phys. Soc. Jpn.* **24**, 368.
- Vinokurova, L.I., A.G. Gapatchenko, E.S. Itskevich, E.T. Kulatov and N.I. Kulikov, 1979, The Effect of Pressure on the Fermi Surface of Antiferromagnetic Chromium, *Pis'ma Zh. Eksp. & Teor. Fiz.* **30**, 265.
- Volkov, B.A., and M.S. Nunuparov, 1980, On the Nature of Local Magnetic Moments in Itinerant Antiferromagnets, *Zh. Eksp. & Teor. Fiz.* **78**, 632.
- Volkov, B.A., and V.V. Tugushev, 1979, Inhomogeneous Structures in an Excitonic Ferromagnet, *Zh. Eksp. & Teor. Fiz.* **77**, 2104.
- Volkov, B.A., and V.V. Tugushev, 1984, The Formation of Local Magnetic Moments and Resonance Scattering in Dilute Chromium Alloys with Nonmagnetic Impurities, *Fiz. Tverd. Tela* **26**(8), 2428.
- Volkov, B.A., V.G. Kantser and Yu.V. Kopaev, 1978a, Spin–Orbital Interaction in an Excitonic Insulator, *Zh. Eksp. & Teor. Fiz.* **75**, 1402.
- Volkov, B.A., Yu.V. Kopaev and V.V. Tugushev, 1978b, The Inhomogeneous State of an Excitonic Ferromagnet, *Zh. Eksp. & Teor. Fiz.* **75**, 735.
- Volkov, B.A., V.G. Kantser and Yu.V. Kopaev, 1979a, Ferromagnetism of Filled-Band Electrons, *Pis'ma Zh. Eksp. & Teor. Fiz.* **76**, 1856.

- Volkov, B.A., Yu.V. Kopaev and M.S. Nunuparov, 1979b, Impurity Scattering in an Excitonic Insulator with Spontaneous Currents, *Fiz. Tverd. Tela* **21**, 2733.
- Volkov, B.A., Yu.V. Kopaev, M.S. Nunuparov and V.V. Tugushev, 1979c, On the Structure of the Supermagnetic State, *Pis'ma Zh. Eksp. & Teor. Fiz.* **30**, 317.
- Whittaker, E.T., and G.N. Watson, 1927, *A Course of Modern Analysis* (Cambridge University Press, Cambridge).
- Yang, B., J. Tranquada and G. Shirane, 1988, Neutron Scattering Studies of the Magnetic Structure of Cupric Oxide, *Phys. Rev. B* **38**, 174.
- Young, W., and N. Cade, 1977, Spin Susceptibilities and the Theory of Itinerant-Electron Antiferromagnetism, *Adv. Phys.* **26**, 393.
- Zawadowski, A., and I. Tütto, 1985, Quantum Theory of Local Perturbation of the CDW by an Impurity: Friedel Oscillations, *Phys. Rev. B* **32**, 2449.

This page intentionally left blank

AUTHOR INDEX

- Abrahams, E., 3–5, 29–31, 40, 41, 43–45, 47–49, 51
Abrahams, E., *see* Anderson, P.W., 51
Abrahams, E., *see* Shapiro, B., 42, 48
Abrikosov, A.A., 4, 19–21, 39, 40, 72, 242, 249, 264, 271, 297
Abrikosov, N.Kh., 147, 148
Abrikosov, N.Kh., *see* Novikova, S.I., 148, 149
Abrikosov, N.Kh., *see* Shelimova, L.E., 147, 148
Aharony, A., 167
Aharony, A., *see* Berker, A.N., 172
Aharony, A., *see* Blankschtein, D., 170
Aiyer, R.N., 60, 61
Akinci, G., *see* Bak, P., 172
Akkermans, E., 56
Albrecht, H., 122
Alder, B.J., *see* Ceperley, D.M., 139, 148
Allan, G., 280
Altshuler, B.L., 6, 8, 13, 17, 38, 53, 293, 295
Amit, D.J., 92, 129, 130, 144, 163
Anderson, P.W., 3, 8, 9, 15, 50, 51, 55, 57, 59, 81, 154
Anderson, P.W., *see* Abrahams, E., 3–5, 29–31, 40, 41, 43–45, 47
Anderson, P.W., *see* Edwards, S.F., 82, 90, 91, 93
Anderson, P.W., *see* Fu, Y., 85, 88, 123, 125, 126
Apel, W., 54
Arajs, S., 292, 293
Aronov, A.G., *see* Altshuler, B.L., 6, 8, 13, 17, 38, 53, 293, 295
Arp, V., *see* Owen, J., 81
Arya, K., 56
Asano, S., 287
Athanasius, G.G., 105
Avilov, E.S., *see* Novikova, S.I., 148

Baberschke, K., *see* Fert, A., 122
Bachas, C.P., *see* Athanasius, G.G., 105
Bachelet, G.B., 139, 148

Bak, P., 172
Balakrishnan, G., *see* Paul, D.McK., 172
Banavar, J.R., 85, 88, 123
Bar-Yam, Y., *see* Kaxiras, E., 171
Barma, M., 198
Baroni, S., *see* Sorella, S., 207, 213, 226
Barrett, C.S., *see* Goldak, J., 151
Bartelt, N.C., *see* Bak, P., 172
Beattie, A.G., 150
Beckman, O., *see* Bierly, J.N., 148
Behnke, G., 143
Belitz, D., 50
Belitz, D., *see* Kirkpatrick, T.R., 7
Belson, H.S., *see* Houston, B., 150
Bender, G., 155
Benedict, K.A., 52
Benedict, K.A., *see* Carra, P., 52
Benedict, K.A., *see* Chalker, J.T., 49, 52
Benettin, G., 213
Berezinskii, V.L., 4, 39, 40, 51, 56, 72
Bergman, D., *see* Imry, Y., 42, 48
Bergmann, G., 5, 7, 13, 29, 53
Berker, A.N., 172
Bernhoeft, N.R., *see* Paul, D.McK., 172
Bhatt, R.N., 38, 107, 111–115, 121, 142
Bhatt, R.N., *see* Milovanovic, M., 7
Bhatt, R.N., *see* Wölfle, P., 35, 36
Bickers, N.E., *see* White, S.R., 219, 220
Bierly, J.N., 148
Bigava, A.D., 147, 148
Bilz, H., *see* Behnke, G., 143
Bilz, H., *see* Bussmann-Holder, A., 154
Binder, K., 81, 111, 193
Binder, K., *see* Morgenstern, I., 110
Birgeneau, R.J., *see* Shirane, G., 297
Birman, J.L., *see* Arya, K., 56
Blankenbecler, R., 194, 202
Blankenbecler, R., *see* Hirsch, J.E., 191
Blankschtein, D., 170

- Booth, J., 293
 Booth, R., *see* Borg, R.J., 81
 Borg, R.J., 81
 Borland, R.E., 4
 Bouchiat, H., *see* Monod, P., 96
 Bowman, D.R., 126
 Boyer, L.L., 146, 171
 Boyer, L.L., *see* Katkanant, V., 143
 Bray, A.J., 90, 98, 103, 107, 110, 111, 113, 115
 Bray, A.J., *see* Roberts, S.A., 122
 Bray, A.J., *see* Viana, L., 126
 Brazovskii, S.A., 256, 257, 263, 280, 298
 Brout, R., 90
 Browne, M.E., *see* Owen, J., 81
 Bruss, F., *see* Fert, A., 122
 Buendia, G.M., 185, 225
 Baker, D., 242, 246, 247
 Bulka, B., 58, 62, 68–70
 Bunker, B.A., *see* Islam, Q.T., 143
 Bussmann-Holder, A., 154
 Buttner, H., *see* Behnke, G., 143
 Butz, T., 241
 Buzdin, A.I., 255, 263, 277, 280, 283
 Bychkov, Yu.A., 242
- Cade, N., *see* Young, W., 244, 245
 Cafisch, R.G., *see* Berker, A.N., 172
 Calogero, F., 285, 300
 Campbell, I.A., *see* Hamzic, A., 119
 Canella, V., 82, 97
 Capellmann, H., 296
 Car, R., *see* Sorella, S., 207, 213, 226
 Caracciolo, S., 113
 Carrà, P., 52
 Carrà, P., *see* Chalker, J.T., 49, 52
 Castellani, C., 7
 Celli, V., 55
 Celli, V., *see* McGurn, A.R., 55
 Ceperley, D.M., 139, 148
 Chakrabarti, A., 121
 Chakravarty, S., 5, 8
 Chalker, J.T., 5, 49, 52, 53
 Chalker, J.T., *see* Benedict, K.A., 52
 Chalker, J.T., *see* Carrà, P., 52
 Chaplot, S.L., *see* Choudhury, N., 143
 Chen, J.H., 96
 Chen, Y., *see* Ye, Y.-Y., 146
 Cheng, Z., 56
 Chiang, C., *see* Hamann, D.R., 139
 Choudhury, N., 143
 Chui, S., 241
 Cochran, W., 142, 154
- Cohen, A., 6
 Cohen, M.L., 140
 Cohen, M.L., *see* Ihm, J., 143
 Cohen, M.L., *see* Louie, S.G., 141
 Cohen, S.M., 56
 Cohen, S.M., *see* Condat, C.A., 56
 Coleman, R., 241
 Coles, B.R., 81
 Condat, C.A., 56
 Condat, C.A., *see* Cohen, S.M., 56
 Convert, P., *see* Maletta, H., 95
 Coqueblin, B., 240
 Cragg, D.M., 119, 122
 Creutz, M., 182
 Cristofides, N., 123
- Dagotto, E., *see* Scalettar, R.T., 218, 220–222
 Daniell, G.J., *see* Chalker, J.T., 53
 Daniels, W., *see* Umebayashi, H., 290
 Dasgupta, C., *see* Chakrabarti, A., 121
 David, W.I.F., *see* Paul, D.McK., 172
 Davis, E.A., *see* Mott, N.F., 4
 de Almeida, J.R., 98, 127
 De Cloiseaux, J., 241
 De Dominicis, C., 105, 110, 127
 De Dominicis, C., *see* de Almeida, J.R., 127
 De Dominicis, C., *see* Mottishaw, P., 127
 De Dominicis, C., *see* Wong, K.Y.M., 127
 Dechter, S., *see* Arajs, S., 292
 Degasperis, A., *see* Calogero, F., 285, 300
 Demenskii, G.K., *see* Abrikosov, N.Kh., 148
 Demenskii, G.K., *see* Korzhuev, M.A., 169
 DeRaedt, H., 225
 Derrida, B., 116
 Derrida, B., *see* Neumann, A.U., 117
 Dersch, U., 68
 Dewar, R., *see* Wong, K.Y.M., 127
 DiCastro, C., *see* Castellani, C., 7
 Domb, C., 169
 Dorokhov, O.N., 54
 Dunlop, M.W., 120, 121
 Dunmyre, G., *see* Arajs, S., 292
 Dzyaloshinskii, I.E., 247
 Dzyaloshinskii, I.E., *see* Abrikosov, A.A., 19–21, 242, 249, 264, 271, 297
 Dzyaloshinskii, I.E., *see* Brazovskii, S.A., 263, 280, 298
 Dzyaloshinskii, I.E., *see* Gor'kov, L.P., 247
- Ebeling, K., *see* Butz, T., 241
 Economou, E.N., 58, 68
 Economou, E.N., *see* Soukoulis, C.M., 58

- Economou, E.N., *see* Zdetsis, A.D., 58, 68
 Edwards, S.F., 9, 10, 82, 90, 91, 93
 Edwards, S.F., *see* Tanaka, F., 90
 Edwardson, P.J., *see* Katkanant, V., 143
 Efetov, K.B., 5, 43, 45
 Egorushkin, V.E., 241
 Einstein, T.L., *see* Bak, P., 172
 Eiserman, G., *see* Coleman, R., 241
 Ekonomova, L.N., *see* Kostina, T.I., 272
 Elderfield, D., 119, 120, 122
 Elesin, V.F., 241
 Elliott, R.J., *see* Aiyer, R.N., 60, 61
 Emery, V.J., 223
 Endoh, Y., *see* Shirane, G., 297
 England, W., *see* Liu, S., 241
 Erdős, P., 4
 Esterling, D.M., *see* Hassing, R.F., 184
 Evenson, W.E., 184
 Everson, M., *see* Coleman, R., 241
 Evertz, H., 271
 Evseev, B.A., *see* Novikova, S.I., 148, 149
 Eyert, V., 241
- Falicov, L., *see* Coleman, R., 241
 Fang, J.X., *see* Cheng, Z., 56
 Fawcett, E., 240
 Fedders, P., 240
 Fert, A., 122
 Fetter, A.L., 195
 Feynman, R.P., 182, 183
 Finkelstein, A.M., 7
 Firsov, Yu.A., 54
 Firsov, Yu.A., *see* Prigodin, V.N., 54, 55
 Fisch, R., 96
 Fischbeck, H., *see* Mertsching, J., 257
 Fischer, D.S., 113
 Fischer, K.H., 81
 Flannery, B.P., *see* Press, W.H., 203
 Fontanari, J.F., 171
 Foster, D., 18
 Frazer, B.C., 143
 Frazer, B.C., *see* Umebayashi, H., 290
 Freedman, B., *see* Creutz, M., 182
 Fricke, H., *see* Schubert, K., 148
 Froyen, S., *see* Louie, S.G., 141
 Fu, Y., 85, 88, 123, 125, 126
 Fujita, M., *see* Machida, K., 288–290
 Fukuyama, H., *see* Sasō, T., 72
 Fukuyama, H., *see* Yoshioka, D., 51
 Fye, R.M., 209
 Fye, R.M., *see* Hirsch, J.E., 225
- Gaba, M., *see* De Dominicis, C., 105
 Gabay, M., 118
 Gabay, M., *see* Cragg, D.M., 119
 Gabedava, A.A., *see* Bigava, A.D., 147, 148
 Galgani, L., *see* Benettin, G., 213
 Galkin, V.Yu., 275, 293, 294
 Galkin, V.Yu., *see* Kostina, T.I., 272
 Galyutin, V.I., *see* Novikova, S.I., 148, 149
 Gapatchenko, A.G., *see* Vinokurova, L.I., 290
 Gardner, E., 130
 Garey, M.R., 123
 Gebhart, W., *see* Kett, H., 120
 Gefen, Y., *see* Imry, Y., 42, 48
 Gelatt, C.D., *see* Kirkpatrick, S., 85, 88, 92, 123, 125
 Gelatt, C.D., *see* von Barth, U., 141
 Geldart, D.J.W., 141
 Ghazali, A., 141
 Glass, A.M., *see* Lines, M.E., 142–144, 169
 Godby, R.W., 141
 Gogolin, A.A., 55
 Gold, A., 50
 Gold, A., *see* Belitz, D., 50
 Goldak, J., 151
 Goldschmidt, Y.Y., 88
 Goldschmidt, Y.Y., *see* De Dominicis, C., 127
 Gordyunin, S.A., *see* Brazovskii, S.A., 256, 257
 Gor'kov, L.P., 5, 29, 30, 48, 49, 240, 247
 Gor'kov, L.P., *see* Abrikosov, A.A., 19–21, 242, 249, 264, 271, 297
 Götze, P., *see* Wölfe, P., 49
 Götze, W., 32, 38, 42, 49, 50
 Götze, W., *see* Belitz, D., 50
 Graebner, J., 289
 Grest, G.S., *see* Soukoulis, C.M., 58
 Grest, G.S., *see* Zdetsis, A.D., 58, 68
 Gu, S.W., *see* Cheng, Z., 56
 Gubernatis, J.E., 225
 Gubernatis, J.E., *see* Loh Jr, E.Y., 180, 181, 210, 213
 Gubernatis, J.E., *see* Scalettar, R.T., 218, 220–222
 Gubernatis, J.E., *see* White, S.R., 218–220, 225
 Gunnarsson, O., 141
 Gupta, S.C., *see* Seddon, T., 151
 Gutfreund, H., *see* Amit, D.J., 92, 129, 130
- Hagh, E., *see* Butz, T., 241
 Halawa, M., *see* Kurzynski, M., 143
 Halperin, B.I., 241
 Hamaguchi, Y., *see* Iizumi, M., 148
 Hamann, D.R., 139, 184

- Hamann, D.R., *see* Bachelet, G.B., 139, 148
 Hamzic, A., 119
 Harada, I., 247
 Hardy, J.R., *see* Boyer, L.L., 146, 171
 Hardy, J.R., *see* Katkanant, V., 143
 Harmon, B.N., *see* Ye, Y.-Y., 146
 Harris, A.B., *see* Fisch, R., 96
 Harrison, H.R., *see* Nagata, S., 83
 Harrison, W.A., *see* Shaw, R.W., 140, 141
 Harrison, W.T.A., *see* Paul, D.McK., 172
 Hasegawa, H., 296
 Hassing, R.F., 184
 Hedgecock, F.T., *see* Albrecht, H., 122
 Held, G.A., *see* Horn, P.M., 172
 Henrichs, J., 6
 Herman, F., *see* Kasowski, R., 241
 Herndon, R.C., *see* Erdős, P., 4
 Herring, C., 239
 Hertz, J., 118
 Hibbs, A.R., *see* Feynman, R.P., 182, 183
 Hidaka, M., 172
 Hikami, S., 5, 17, 42, 43, 45, 48, 50, 52, 53
 Hippert, F., *see* Fert, A., 122
 Hirsch, E., *see* Tang, S., 225
 Hirsch, J.E., 185, 191, 195, 207, 210, 219, 220, 225
 Hirsch, J.E., *see* Lin, H.Q., 225
 Ho, K.M., *see* Ye, Y.-Y., 146
 Hohenberg, P., 138
 Holtzberg, F., *see* Horn, P.M., 172
 Hopfield, J.J., 127
 Hopfield, J.J., *see* Topp, W.C., 140, 141
 Horn, P.M., 172
 Horovitz, B., 256
 Houston, B., 150
 Hsu, W., *see* Chui, S., 241
 Hsu, W., *see* Kasowski, R., 241
 Hubbard, J., 181–183
 Huse, D.A., *see* Fischer, D.S., 113
 Idlis, B.G., 241
 Igarashi, J., 57
 Ihm, J., 143, 146, 171
 Iida, S., 288–290
 Iida, S., *see* Nakai, Y., 289
 Izumi, M., 148
 Imry, Y., 18, 42, 48
 Innes, D., *see* Goldak, J., 151
 Ioffe, A.F., 4
 Iordanskii, S.V., *see* Bychkov, Yu.A., 242
 Islam, Q.T., 143
 Itskevich, E.S., *see* Vinokurova, L.I., 290
 Izymov, Yu.A., 252, 280
 Joannopoulos, J.D., 140
 Joannopoulos, J.D., *see* Ihm, J., 146, 171
 Joannopoulos, J.D., *see* Kaxiras, E., 171
 Joannopoulos, J.D., *see* Needels, M., 171
 Joannopoulos, J.D., *see* Rabe, K.M., 147, 148, 150, 154
 Joannopoulos, J.D., *see* Starkloff, T., 139
 John, S., 55, 56
 Johnson, A., *see* Coleman, R., 241
 Johnson, D.S., *see* Garey, M.R., 123
 Jordan-Sweet, J.L., *see* Horn, P.M., 172
 Josephson, B., 49
 Jüngling, K., 49
 Jüngling, K., *see* Oppermann, R., 53
 Kachi, S., *see* Kitaoka, Y., 241
 Kaiser, D.L., *see* Horn, P.M., 172
 Kamimura, H., *see* Shraishi, K., 241
 Kanamori, J., *see* Tsunoda, Y., 289
 Kanter, I., 126
 Kantser, V.G., *see* Volkov, B.A., 241, 245
 Karpinskii, O.G., *see* Abrikosov, N.Kh., 147, 148
 Karpinskii, O.G., *see* Novikova, S.I., 148
 Kasowski, R., 241
 Kasowski, R., *see* Chui, S., 241
 Kastner, M.A., *see* Shirane, G., 297
 Katkanant, V., 143
 Kato, Y., *see* Izumi, M., 148
 Katsura, S., 127
 Katz, E., *see* Dzyaloshinskii, I.E., 247
 Katzenmeyer, W., *see* Arajs, S., 293
 Kaveh, M., 56
 Kaveh, M., *see* Schmeltzer, D., 56
 Kawabata, A., 50
 Kawabata, A., *see* Moriya, T., 296
 Kaxiras, E., 171
 Keane, D.T., *see* Horn, P.M., 172
 Keesom, P.H., *see* Nagata, S., 83
 Keldysh, L.V., 240, 241
 Kett, H., 120
 Keune, W., *see* Lauer, J., 119
 Khaikin, M.S., 280
 Khlyustikov, I.N., *see* Khaikin, M.S., 280
 Khmelnitskii, D.E., 13
 Khmelnitskii, D.E., *see* Altshuler, B.L., 13
 Khmelnitskii, D.E., *see* Efetov, K.B., 5, 43, 45
 Khmelnitskii, D.E., *see* Gor'kov, L.P., 5, 29, 30, 48, 49
 Kinzel, W., 117

- Kip, A.F., *see* Owen, J., 81
Kirkpatrick, S., 85, 88, 92, 94, 105, 106, 123,
125, 127
Kirkpatrick, S., *see* Sherrington, D., 92, 94–98,
106
Kirkpatrick, T.R., 7, 51, 56
Kirkpatrick, T.R., *see* Cohen, S.M., 56
Kirkpatrick, T.R., *see* Condat, C.A., 56
Kirova, N.N., *see* Brazovskii, S.A., 256, 257,
263, 280, 298
Kitaoaka, Y., 241
Kleban, P., *see* Bak, P., 172
Kochler, W., 287
Kogut, J., *see* Wilson, K.G., 156
Kohn, W., 138, 139
Kohn, W., *see* Hohenberg, P., 138
Kohno, M., *see* Iida, S., 288, 289
Komatsubara, K.F., *see* Iizumi, M., 148
Kondor, I., *see* De Dominicis, C., 110
Kondorskii, E.I., 295
Koonin, S.E., *see* Sugiyama, G., 213
Kopaev, Yu.V., 241, 243, 271
Kopaev, Yu.V., *see* Elesin, V.F., 241
Kopaev, Yu.V., *see* Idlis, B.G., 241
Kopaev, Yu.V., *see* Keldysh, L.V., 240, 241
Kopaev, Yu.V., *see* Volkov, B.A., 169, 241, 245,
247, 292
Kopp, L., *see* Liu, S., 241
Kopp, T., 59, 63–65, 71
Kopp, T., *see* Kroha, H., 6, 59
Korenman, V., 296
Korzhuev, M.A., 169
Korzhuev, M.A., *see* Abrikosov, N.Kh., 147, 148
Korzhuev, M.A., *see* Novikova, S.I., 148
Kostina, T.I., 272, 280, 281, 295
Kostina, T.I., *see* Kondorskii, E.I., 295
Kosuge, K., *see* Kitaoka, Y., 241
Kotani, A., 244, 247, 255
Kotani, A., *see* Harada, I., 247
Kotliar, G., *see* Castellani, C., 7
Kotov, E.A., 50, 68
Kozlov, A.N., 241
Kramer, B., *see* Bulka, B., 58, 62, 68–70
Kramer, B., *see* MacKinnon, A., 57, 213
Kramer, B., *see* Sak, J., 57
Kravtsov, V.E., *see* Altshuler, B.L., 6
Krey, U., *see* Kett, H., 120
Kroha, H., 6, 59, 67–71
Krumhansl, J.A., *see* Aiyer, R.N., 60, 61
Kübler, J., *see* Eyert, V., 241
Kulatov, E.T., 241, 296
Kulatov, E.T., *see* Kulikov, N.I., 240
- Kulatov, E.T., *see* Vinokurova, L.I., 290
Kulich, M.L., *see* Buzdin, A.I., 263, 280
Kulikov, N.I., 240, 241, 245, 263, 270, 271
Kulikov, N.I., *see* Kulatov, E.T., 241, 296
Kulikov, N.I., *see* Vinokurova, L.I., 290
Kulkov, S.N., *see* Egorushkin, V.E., 241
Kulkova, S.E., *see* Egorushkin, V.E., 241
Kunchuliya, E.D., *see* Bigava, A.D., 147, 148
Kunitomi, N., *see* Iida, S., 288–290
Kunitomi, N., *see* Tsunoda, Y., 289
Kunz, H., 5
Kurkijärvi, J., *see* Wölfle, P., 49
Kurzynski, M., 143
Kuskova, Yu.A., *see* Kondorskii, E.I., 295
- Lagendijk, A., *see* DeRaedt, H., 225
Lagendijk, A., *see* Van Albada, M.P., 15, 56
Lai, P.-Y., *see* Goldschmidt, Y.Y., 88
Landau, L.D., 282
Landauer, R., 4
Langer, J.S., 29
Langreth, D.C., 140
Larkin, A.I., *see* Altshuler, B.L., 13
Larkin, A.I., *see* Efetov, K.B., 5, 43, 45
Larkin, A.I., *see* Gor'kov, L.P., 5, 29, 30, 48, 49
Larkin, A.I., *see* Hikami, S., 17, 53
Lauer, J., 119
Lawler, E.L., 127
Leath, P.L., 61
Leath, P.L., *see* Aiyer, R.N., 60, 61
Lee, D.H., *see* Ihm, J., 146, 171
Lee, P.A., 7, 8
Lee, P.A., *see* Abrahams, E., 45, 48, 49, 51
Lee, P.A., *see* Castellani, C., 7
Lekner, J., *see* Josephson, B., 49
Lenstra, J.K., *see* Lawler, E.L., 127
Lerf, A., *see* Butz, T., 241
Lerner, I.V., *see* Altshuler, B.L., 6
Leroux Hugon, P., *see* Ghazali, A., 141
Levanyuk, A.P., 280, 281
Levin, K., *see* Bowman, D.R., 126
Levine, H., 53
Libby, S.B., *see* Levine, H., 53
Licciardello, D.C., *see* Abrahams, E., 3–5,
29–31, 40, 41, 43–45, 47
Lifshitz, E.M., *see* Landau, L.D., 282
Lin, H.Q., 225
Lin-Liu, Y.R., *see* Takayama, H., 257
Lind, M., *see* Machida, K., 288
Lindgård, P.A., *see* Ye, Y.-Y., 146
Lines, M.E., 142–144, 154, 169
Little, W.A., *see* Parks, R.D., 18

- Littlewood, P.B., 144, 154
 Liu, S., 241
 Loh Jr, E.Y., 180, 181, 186, 210, 213
 Loh Jr, E.Y., *see* Scalettar, R.T., 218, 220–222
 Loh Jr, E.Y., *see* White, S.R., 218–220, 225
 Lomer, W., 240
 Louie, S.G., 141
 Löwdin, P.O., 149
 Lubensky, T.C., *see* Chen, J.H., 96
 Lundqvist, B.I., *see* Gunnarsson, O., 141
 Lutes, O.S., 81
- Ma, M., *see* Castellani, C., 7
 Ma, S.-K., 144
 Machida, K., 262, 288–290
 Machta, J., *see* Cohen, S.M., 56
 MacKinnon, A., 57, 213
 Mackintosh, A., *see* Kochler, W., 287
 Maki, K., 244, 245
 Maki, K., *see* Nakanishi, K., 246
 Maki, K., *see* Sato, H., 245
 Maki, K., *see* Takayama, H., 257
 Maksimov, L.A., *see* Kozlov, A.N., 241
 Malaspinas, A., 246
 Maleev, S.V., 20
 Maletta, H., 95
 Maradudin, A.A., *see* Celli, V., 55
 Maradudin, A.A., *see* McGurn, A.R., 54, 55
 Marcus, J., *see* Graebner, J., 289
 Mardix, S., 143
 Maret, G., *see* Wolf, P.E., 15, 56
 Martin, P., *see* Fedders, P., 240
 Martins, J.L., 144
 Marvin, A.M., *see* Celli, V., 55
 Matsubara, T., 60
 Maynard, R., *see* Akkermans, E., 56
 McCulloch, W.S., 127
 McGurn, A.R., 54, 55
 McGurn, A.R., *see* Celli, V., 55
 McKane, A.J., 45
 McLenaghan, I.R., 88
 McMillan, W.L., 142
 McMillan, W.L., *see* Bhatt, R.N., 142
 Medvedchikov, V.P., *see* Kondorskii, E.I., 295
 Menshov, V.N., *see* Buzdin, A.I., 277, 283
 Menshov, V.N., *see* Kostina, T.I., 272, 280, 281, 295
 Mermin, N.D., 141
 Mertsching, J., 257
 Metropolis, N., 111, 193
 Metzner, W., 5
 Mézard, M., 81, 103, 105, 126, 127
- Miedema, A.R., *see* Domb, C., 169
 Mihill, K., *see* Sherrington, D., 118
 Millis, A.J., 172
 Milovanovic, M., 7
 Miyako, Y., *see* Murayama, S., 122
 Moiseenko, S.S., *see* Bigava, A.D., 147, 148
 Mokerov, V.G., *see* Kopaev, Yu.V., 241
 Monhorst, H.J., 149, 157
 Monod, P., 96
 Monod, P., *see* Albrecht, H., 122
 Moon, R., *see* Kochler, W., 287
 Moore, M.A., *see* Bray, A.J., 90, 98, 103, 107, 110, 111, 113, 115
 Moreo, A., *see* Scalettar, R.T., 218, 220–222
 Morgenstern, I., 110
 Morgenstern, I., *see* Ogielski, A.T., 111
 Mori, M., *see* Tsunoda, Y., 289
 Moriya, T., 241, 296
 Motizuki, K., *see* Shibatani, A., 244, 247
 Mott, N.F., 4, 40, 55, 71
 Mottishaw, P., 127
 Mottishaw, P., *see* Wong, K.Y.M., 127
 Muldawer, L., *see* Bierly, J.N., 148
 Murakami, T., *see* Shirane, G., 297
 Murata, K.K., 155
 Murayama, S., 122
 Murray, J., *see* Korenman, V., 296
 Muttalib, K.A., 6
 Mydosh, J.A., *see* Canella, V., 82, 97
 Myron, H.W., *see* Liu, S., 241
- Nagamiya, T., *see* Shibatani, A., 244, 247
 Nagaoka, Y., *see* Hikami, S., 17, 53
 Nagashima, T., *see* Shimada, I., 213
 Nagata, S., 83
 Nahm, I.H., *see* Chalker, J.T., 49
 Nakai, Y., 289
 Nakai, Y., *see* Iida, S., 289, 290
 Nakanishi, H., *see* Machida, K., 262
 Nakanishi, K., 246
 Nakayama, T., *see* Shraishi, K., 241
 Natterman, T., 145, 155, 168
 Neal, T., *see* Langer, J.S., 29
 Needels, M., 171
 Negele, J.W., 227
 Nelson, D.R., *see* Rudnick, J., 145, 168
 Neumann, A.U., 117
 Nobre, F.D., 118
 Novikova, S.I., 148, 149
 Nunuparov, M.S., *see* Volkov, B.A., 245, 273, 292

- Ochab, J., *see* Bak, P., 172
 Oda, M., *see* Shirane, G., 297
 Ogielski, A.T., 111, 116
 Ohama, N., *see* Hidaka, M., 172
 Oka, Y., *see* Kitaoka, Y., 241
 Okazaki, A., *see* Hidaka, M., 172
 Olive, J.A., 121, 122
 Ono, Y., 52
 Ono, Y., *see* Yoshioka, D., 51
 Oppermann, R., 43, 45, 49, 52, 53
 Oppermann, R., *see* Jüngling, K., 49
 Orland, H., *see* De Dominicis, C., 105
 Orlando, H., *see* Negele, J.W., 227
 Oshiyama, A., *see* Shraishi, K., 241
 Osipov, V.V., *see* Levanyuk, A.P., 280, 281
 Overhauser, A., 239
 Owen, J., 81
 Pack, J.D., *see* Monkhorst, H.J., 149, 157
 Pandey, K.C., *see* Kaxiras, E., 171
 Papadimitriou, C.H., 123
 Pardavi-Horvath, M., *see* Kulikov, N.I., 240
 Parga, N., 107
 Parisi, G., 98, 100
 Parisi, G., *see* Caracciolo, S., 113
 Parisi, G., *see* Mézard, M., 81, 103, 105, 126, 127
 Parisi, G., *see* Parga, N., 107
 Parks, R.D., 18
 Parrinello, M., *see* Sorella, S., 207, 213, 226
 Patarnello, S., *see* Caracciolo, S., 113
 Paul, D.McK., 172
 Payne, M.C., *see* Needels, M., 171
 Perdew, J.P., 139, 148
 Perdew, J.P., *see* Langreth, D.C., 140
 Perz, J., *see* Ruesink, D., 289, 290
 Petrov, L.A., *see* Abrikosov, N.Kh., 148
 Petrova, L.I., *see* Korzhuev, M.A., 169
 Pfeuty, P., 144
 Pichard, J.L., 57, 58
 Pichard, J.L., *see* Muttalib, K.A., 6
 Pitts, W., *see* McCulloch, W.S., 127
 Polonskii, S.A., *see* Buzdin, A.I., 263
 Prauge, R., *see* Korenman, V., 296
 Prelovsek, P., 50, 68
 Prelovsek, P., *see* Götze, W., 50
 Press, W.H., 203
 Prigodin, V.N., 51, 54, 55
 Prigodin, V.N., *see* Firsov, Yu.A., 54
 Pruisken, A.M.M., 53
 Pruisken, A.M.M., *see* Levine, H., 53
 Pureur, P., *see* Fert, A., 122
 Pytte, E., 98
 Rabe, K.M., 147, 148, 150, 154
 Rabe, K.M., *see* Millis, A.J., 172
 Ramakrishnan, T.V., *see* Abrahams, E., 3–5,
 29–31, 40, 41, 43–45, 47
 Ramakrishnan, T.V., *see* Anderson, P.W., 51
 Ramakrishnan, T.V., *see* Bhatt, R.N., 38
 Ramakrishnan, T.V., *see* Lee, P.A., 7, 8
 Rammal, R., 103
 Rao, K.R., *see* Choudhury, N., 143
 Rasolt, M., *see* Geldart, D.J.W., 141
 Regel, A.R., *see* Ioffe, A.F., 4
 Rice, J.R., 203
 Rice, T.M., 244, 246
 Rice, T.M., *see* Apel, W., 54
 Rice, T.M., *see* Halperin, B.I., 241
 Rice, T.M., *see* Horn, P.M., 172
 Rice, T.M., *see* Malaspina, A., 246
 Rickayzen, G., 19, 27
 Rinnov Kan, A.H.G., *see* Lawler, E.L., 127
 Roberts, S.A., 122
 Rosenbluth, A.W., *see* Metropolis, N., 111, 193
 Rosenbluth, M.N., *see* Metropolis, N., 111, 193
 Roth, Y., *see* Cohen, A., 6
 Rudnick, J., 145, 168
 Rudnick, J., *see* Pytte, E., 98
 Ruesink, D., 289, 290
 Rusinov, A.I., *see* Kopaev, Yu.V., 271
 Ryshkin, I.A., *see* Abrikosov, A.A., 4, 39, 40, 72
 Sachdev, S., *see* Milovanovic, M., 7
 Sadovskii, M.V., 7, 8, 53
 Sadovskii, M.V., *see* Kotov, E.A., 50, 68
 Sahu, D., 144
 Saibene, S., *see* Butz, T., 241
 Sak, J., 57
 Sakashita, H., *see* Hidaka, M., 172
 Sakurai, M., *see* Maki, K., 244, 245
 Sarma, G., *see* Pichard, J.L., 57, 58
 Saso, T., 72
 Sato, H., 245
 Saunders, G.A., *see* Seddon, T., 151
 Scalapino, D.J., 194, 195, 202
 Scalapino, D.J., *see* Blankenbecler, R., 194, 202
 Scalapino, D.J., *see* Hirsch, J.E., 191
 Scalapino, D.J., *see* Scalettar, R.T., 194, 218,
 220–224
 Scalapino, D.J., *see* White, S.R., 218–220, 225
 Scalettar, R.T., 194, 218, 220–224
 Scalettar, R.T., *see* Fye, R.M., 209
 Scalettar, R.T., *see* Loh Jr, E.Y., 180, 181, 210,
 213

- Scalettar, R.T., *see* White, S.R., 210, 218–220, 225
 Schäfer, L., 5
 Schluter, M., 241
 Schluter, M., *see* Bachelet, G.B., 139, 148
 Schluter, M., *see* Godby, R.W., 141
 Schluter, M., *see* Hamann, D.R., 139
 Schmeltzer, D., 56
 Schmid, A., *see* Chakravarty, S., 5, 8
 Schmit, J.L., *see* Lutes, O.S., 81
 Schmoys, D.M., *see* Lawler, E.L., 127
 Schreiber, M., *see* Bulka, B., 58, 62, 68–70
 Schrieffer, J.R., *see* Evenson, W.E., 184
 Schubert, K., 148
 Schwalm, W.A., *see* Soonpaa, H.H., 47
 Seddon, T., 151
 Sham, L.J., *see* Godby, R.W., 141
 Sham, L.J., *see* Kohn, W., 138, 139
 Shapiro, B., 5, 6, 41, 42, 48
 Shapiro, B., *see* Cohen, A., 6
 Sharvin, D.Yu., 18
 Sharvin, Yu.V., *see* Sharvin, D.Yu., 18
 Shastry, B.S., *see* Barma, M., 198
 Shaw, R.W., 140, 141
 Shelimova, L.E., 147, 148
 Shelimova, L.E., *see* Abrikosov, N.Kh., 147, 148
 Shelimova, L.E., *see* Novikova, S.I., 148, 149
 Sheng, P., 56
 Sherrington, D., 88, 92, 94–98, 106, 118–120, 124, 126
 Sherrington, D., *see* Banavar, J.R., 85, 88, 123
 Sherrington, D., *see* Cragg, D.M., 119, 122
 Sherrington, D., *see* Dunlop, M.W., 120, 121
 Sherrington, D., *see* Elderfield, D., 119, 120, 122
 Sherrington, D., *see* Kirkpatrick, S., 94, 105, 106
 Sherrington, D., *see* McLenaghan, I.R., 88
 Sherrington, D., *see* Nobre, F.D., 118
 Sherrington, D., *see* Olive, J.A., 121, 122
 Sherrington, D., *see* Wiethge, W., 127
 Sherrington, D., *see* Wong, K.Y.M., 127, 130
 Shibatani, A., 244, 247
 Shidaka, Y., *see* Shirane, G., 297
 Shima, N., *see* Shraishi, K., 241
 Shimada, I., 213
 Shirane, G., 297
 Shirane, G., *see* Umebayashi, H., 290
 Shirane, G., *see* Yang, B., 297
 Shraishi, K., 241
 Shvngiradze, R.R., *see* Bigava, A.D., 147, 148
 Siak, S., *see* Chalker, J.T., 5
 Sigov, A.A., *see* Levanyuk, A.P., 280, 281
 Sinha, S.K., 143
 Smith, H., *see* Wölfle, P., 49
 Sobyanin, A.A., *see* Levanyuk, A.P., 280, 281
 Sommers, H.-J., 108
 Sompolsky, H., 105
 Sompolsky, H., *see* Amit, D.J., 92, 129, 130
 Sompolsky, H., *see* John, S., 55, 56
 Sompolsky, H., *see* Kanter, I., 126
 Soonpaa, H.H., 47
 Sorella, S., 207, 213, 226
 Sorella, S., *see* Castellani, C., 7
 Souillard, B., *see* Kunz, H., 5
 Soukoulis, C.M., 58
 Soukoulis, C.M., *see* Economou, E.N., 58, 68
 Soukoulis, C.M., *see* Zdetsis, A.D., 58, 68
 Souletie, J., 86
 Sourlas, N., 113
 Sourlas, N., *see* Banavar, J.R., 85, 88, 123
 Sourlas, N., *see* Caracciolo, S., 113
 Sourlas, N., *see* Mézard, M., 103, 105
 Southern, B.W., *see* Sherrington, D., 94
 Soven, P., 58
 Spivak, B.Z., *see* Altshuler, B.L., 17, 38
 Stanford, J., *see* Machida, K., 288
 Starkloff, T., 139
 Steglitz, K., *see* Papadimitriou, C.H., 123
 Stephen, M.J., *see* John, S., 55, 56
 Sticht, J., *see* Eyert, V., 241
 Stone, A., *see* Muttalib, K.A., 6
 Stone, M., *see* McKane, A.J., 45
 Strakna, R.E., *see* Houston, B., 150
 Su, Z.B., *see* Arya, K., 56
 Sugar, R.L., *see* Blankenbecler, R., 194, 202
 Sugar, R.L., *see* Hirsch, J.E., 191
 Sugar, R.L., *see* Loh Jr, E.Y., 180, 181, 210, 213
 Sugar, R.L., *see* Scalapino, D.J., 194, 195, 202
 Sugar, R.L., *see* Scalettar, R.T., 194, 218, 220–224
 Sugar, R.L., *see* White, S.R., 210, 218–220, 225
 Sugiyama, G., 213
 Suslov, I.M., 5
 Suzuki, M., 182, 183, 209
 Suzuki, M., *see* Shirane, G., 297
 Suzumura, Y., *see* Sasō, T., 72
 Tabet, E., *see* Castellani, C., 7
 Takayama, H., 257
 Tanaka, F., 90
 Tang, S., 225
 Taylor, R., *see* Geldart, D.J.W., 141
 Teller, A.H., *see* Metropolis, N., 111, 193
 Teller, E., *see* Metropolis, N., 111, 193

- Templeton, I., *see* Ruesink, D., 289, 290
 Teplov, O.A., *see* Abrikosov, N.Kh., 148
 Teplov, O.A., *see* Korzhuev, M.A., 169
 Teraoka, Y., *see* Tsunoda, Y., 289
 Teukolsky, S.A., *see* Press, W.H., 203
 Theumann, W.K., *see* Fontanari, J.F., 171
 Tholence, J.L., 83, 84
 Thomas, P., *see* Dersch, U., 68
 Thouless, D.J., 4, 43, 44, 126
 Thouless, D.J., *see* de Almeida, J.R., 98
 Timerov, R.Kh., *see* Kopaev, Yu.V., 271
 Ting, C.S., 51
 Tong, S.Y., *see* Van Hove, M.A., 143
 Toperberg, B.P., *see* Maleev, S.V., 20
 Topp, W.C., 140, 141
 Tosatti, E., 143
 Tosatti, E., *see* Sorella, S., 207
 Toulouse, G., 109
 Toulouse, G., *see* Gabay, M., 118
 Toulouse, G., *see* Kirkpatrick, S., 127
 Toulouse, G., *see* Mézard, M., 103, 105
 Toulouse, G., *see* Pfeuty, P., 144
 Toulouse, G., *see* Rammal, R., 103
 Tournier, R., *see* Souletie, J., 86
 Tournier, R., *see* Tholence, J.L., 83, 84
 Toussaint, D., *see* Scalettar, R.T., 194
 Toyozawa, Y., *see* Matsubara, T., 60
 Tranquada, J., *see* Yang, B., 297
 Tregó, A., *see* Kochler, W., 287
 Trotter, H.F., 182, 183
 Tselikyan, K., *see* Kostina, T.I., 272
 Tsunoda, Y., 289
 Tsunoda, Y., *see* Iida, S., 288–290
 Tugushev, V.V., *see* Buzdin, A.I., 255, 263, 277, 280, 283
 Tugushev, V.V., *see* Galkin, V.Yu., 275
 Tugushev, V.V., *see* Kostina, T.I., 272, 280, 281, 295
 Tugushev, V.V., *see* Kulatov, E.T., 241, 296
 Tugushev, V.V., *see* Kulikov, N.I., 240, 245, 263, 270, 271
 Tugushev, V.V., *see* Volkov, B.A., 247, 271, 292
 Tugusheva, T.E., *see* Galkin, V.Yu., 275, 293, 294
 Tütto, I., *see* Zawadowski, A., 271
 Twose, W.D., *see* Mott, N.F., 4
 Umebayashi, H., 290
 Unertl, W.N., *see* Bak, P., 172
 Van Albada, M.P., 15, 56
 Van Dongen, P., 5
 Van Hove, M.A., 143
 Vecchi, M.P., *see* Kirkpatrick, S., 85, 88, 92, 123, 125
 Verlet, L., 193
 Vetterling, W.T., *see* Press, W.H., 203
 Viana, L., 126
 Vieira, V., *see* Capellmann, H., 296
 Villain, J., 88
 Vinokurova, L.I., 290
 Vinokurova, L.I., *see* Kulikov, N.I., 240
 Violet, C.E., *see* Borg, R.J., 81
 Virasoro, M.A., *see* Mézard, M., 81, 103, 105
 Virasoro, M.A., *see* Parga, N., 107
 Virasoro, M.A., *see* Rammal, R., 103
 Vogl, P., *see* Bussmann-Holder, A., 154
 Volkov, B.A., 169, 241, 245, 247, 271, 273, 292
 Vollhardt, D., 6, 15, 18, 20, 24, 27, 28, 32, 39, 40, 42, 47, 48, 50
 Vollhardt, D., *see* Metzner, W., 5
 Vollhardt, D., *see* Van Dongen, P., 5
 Vollhardt, D., *see* Wölfle, P., 20, 32, 42
 von Barth, U., 141
 von Barth, U., *see* Williams, A.R., 138
 Walecka, J.D., *see* Fetter, A.L., 195
 Wang, S.Q., *see* Evenson, W.E., 184
 Washburn, S., 5
 Wassermann, E.F., *see* Albrecht, H., 122
 Wassermann, E.F., *see* Murayama, S., 122
 Watson, G.N., *see* Whittaker, E.T., 257, 267
 Webb, R.B., *see* Washburn, S., 5
 Webman, I., *see* Soukoulis, C.M., 58
 Wegner, F., 4, 5, 25, 31, 32, 41–43, 45, 48, 50, 51, 53
 Wegner, F., *see* Oppermann, R., 43, 45, 49
 Wegner, F., *see* Schäfer, L., 5
 Weisbuch, G., *see* Derrida, B., 116
 Weller, W., *see* Prigodin, V.N., 54, 55
 White, S.R., 210, 218–220, 225
 White, S.R., *see* Loh Jr, E.Y., 180, 181, 210, 213
 White, S.R., *see* Scalettar, R.T., 218, 220–224
 Whittaker, E.T., 257, 267
 Wiethge, W., 127
 Wilkinson, J.H., 213
 Williams, A.R., 138
 Wilson, K.G., 156
 Wolf, P.E., 15, 56
 Wolf, P.E., *see* Akkermans, E., 56
 Wolff, W.F., *see* Athanasiu, G.G., 105
 Wölfle, P., 20, 32, 35, 36, 42, 49
 Wölfle, P., *see* Bhatt, R.N., 38
 Wölfle, P., *see* Götz, W., 50
 Wölfle, P., *see* Kroha, H., 6, 59

- Wölfle, P., *see* Vollhardt, D., 6, 20, 24, 27, 28, 32, 39, 40, 42, 47, 48, 50
Wong, K.Y.M., 127, 130
Wong, K.Y.M., *see* Sherrington, D., 126
Xiong, J.J., *see* Ihm, J., 146, 171
Yamakawa, S., *see* Hidaka, M., 172
Yamashita, J., *see* Asano, S., 287
Yang, B., 297
Yasuoka, H., *see* Kitaoka, Y., 241
Ye, Y.-Y., 146
Ying, S.C., 172
Yokosawa, K., *see* Murayama, S., 122
Yoshioka, D., 51
Youdelis, W., *see* Goldak, J., 151
Young, A.P., 107, 109
Young, A.P., *see* Bhatt, R.N., 107, 111–115, 121
Young, A.P., *see* Binder, K., 81
Young, A.P., *see* Bray, A.J., 103, 107
Young, A.P., *see* Nobre, F.D., 118
Young, A.P., *see* Olive, J.A., 121, 122
Young, W., 244, 245
Zaslavskii, A.I., *see* Zhukova, T.B., 148, 151
Zavaritskaya, E.I., 47
Zawadowski, A., 271
Zdetsis, A.D., 58, 68
Zdetsis, A.D., *see* Economou, E.N., 58
Zdetsis, S., *see* Soukoulis, C.M., 58
Zech, E., *see* Butz, T., 241
Zhang, Z.Q., *see* Sheng, P., 56
Zhdanova, V.V., *see* Shelimova, L.E., 147, 148
Zhukova, T.B., 148, 151
Zimanyi, G.T., *see* Gogolin, A.A., 55
Zippelius, A., *see* Sompolinsky, H., 105
Zirnbauer, M., 5
Zittartz, I., *see* Evertz, H., 271
Zunger, A., *see* Martins, J.L., 144
Zunger, A., *see* Perdew, J.P., 139, 148
Zvyagin, I.P., *see* Zavaritskaya, E.I., 47

SUBJECT INDEX

- A-15, 142, 144
ab initio statistical mechanics, 145, 171
– GeTe, 146
Anderson Hamiltonian, 180, 225
Anderson lattice, 209
Anderson localization of spin waves in Heisenberg antiferromagnets, 57
Anderson models of disorder, 8
Anderson transition, 31, 40
anharmonicity, 142, 143, 146, 154, 155, 166, 169
anisotropic systems, 35
anomalous magnetoresistance, 17
anti-localization, 53
antiferroelectrics, 144
antiferromagnetic structure factor, 206, 219
Ashkin–Teller, 172
atomic relaxation at defects, 140
- Bäcklund transformation, 285
backscattering, 15
– effects, 14, 16
band structure, 140, 148, 150
 β -function, 46
 β -NaN₃, 144
Bethe–Salpeter equation, 23
bipartitioning, 123
Boltzmann theory, 14
Boltzmann transport theory, 12, 16
bonding, 140, 148, 171
Born–Oppenheimer approximation, 138, 141, 154
broken time-reversal invariance, 51, 52
bulk modulus, 140, 149
- C–I transition, 244
capacity of the reservoir, 244
charge density wave, 142, 172
– structure, 222
charge transfer, 150
- checkerboard breakup, 197
chemisorbed surface layers, 143, 172
classical diffusion, 14
cohesive energy, 140
collision time, 11
commensurate SDW structure, 244
conductance, 43
– dimensionless, 44
– length dependence, 42
conjugate-gradient, 190
– methods, 226
convergence, 149
Cooperon, 29
copper oxide, 223
correction to Boltzmann conductivity, 16, 18
CPA equation, 61
critical behaviour, 165
critical disorder, 40
critical exponent s of the conductivity, 40
critical exponents, 144, 145, 172
critical region, 144, 154
critical temperature, 145
crossover, 145
cubic-anisotropy model, 167, 168
current relaxation, 26
– function, 24
- DC conductivity, 69
de Almeida–Thouless (AT) surface, 98
deformation wave, 289
density functional, 142
density functional theory (DFT), 138, 139, 141
density of states, 62
density relaxation function, 24, 38, 49
density response function, 19
density–density correlation function, 18
determinantal methods, 224
determinantal simulations, 191

- diffusion, 12, 28
 - coefficient, 19
 - pole, 18
- dilute chromium alloys, 287
- dimerization reconstruction, 171
- discrete Hubbard–Stratonovich, 196
- disorder parameter, 11
- displacive and order-disorder structural transitions, 169
- displacive transitions, 143, 154
- Drude or Boltzmann theory, 11
- dynamical conductivity, 26, 66, 70
- Edwards model of disorder, 9
- Einstein relation, 10
- elastic constants, 140, 143, 151, 170
- elastic neutron scattering, 143, 147
- electrical polarizability, 26
- electrical resistivity, 148
- electron-electron interaction effects, 53
- electron-hole coupling, 241
- electron-impurity scattering, 263
- electron-phonon coupling, 150
- Emery model, 223
- entropy, 141, 142, 172
- EXAFS, 143
- extended Hubbard model, 226
- ferroelastics, 144
- ferroelectrics, 142, 143
- Feynman paths, 13
- field cooling (FC), 83
- finite-size scaling, 112
- first-order behaviour, 170
- first-order transitions, 145, 148, 168
- fixed points, 145, 165–168, 171
- flow diagrams, 145, 165
- flows, 166, 168
- fluctuations, 144, 165, 168, 170
- fluctuations-driven first-order transitions, 168–170
- free energy, 164, 172
- frequency-dependent diffusion coefficient, 42
- frozen core, 139, 141
- frustration, 86
- full renormalization group treatment of $D(q,\omega)$, 51
- functional integral, 144, 164
- gap, 141, 142
- gauge symmetry in the locator expansion, 64
- Gell-Mann low function, 50, 52, 53
- GeTe, 147, 149, 153, 154, 156, 164, 165, 168, 169
- Ginzburg–Landau expansion, 246
- Gordon–Kim, 146
- gradient expansion, 140
- Gram–Schmidt, 211
- graph bipartitioning, 85
- graph partitioning, 123
- graphite, 143
- Green’s function, 194
- H on W (100) and Mo (100), 143
- hard optimization, 85
- hardening of the SDW wave vector, 289
- Hartree–Fock, 184
- heat bath, 193
- heterostructures, 144
- Hubbard Hamiltonian, 179, 180
- Hubbard models, 209, 218
 - attractive, 220
- Hubbard–Stratonovich transformation, 146, 163, 182
- “hybrid” combination, 194
- hydrodynamic model, 27
- ice, 143
- imaginary time, 182
- importance sampling, 182, 192
- impurity algorithm, 225
- incommensurate phases, 143
- incommensurate SDW structure, 244
- incommensurate structure, 172
- inelastic neutron scattering, 143
- inelastic processes, 13
- infrared absorption, 288
- infrared divergence, 27, 31
- infrared spectroscopy, 143
- interference of the paths, 14
- ionic and covalent bonding, 150
- irreducible vertex function, 21, 64
- Ising Hamiltonian, 171
- Ising model, 169
- isothermal remanent magnetization (IRM), 83
- isotropic model, 167
- itinerant antiferromagnetism, 241
- itinerant magnetism, 239
- kinetic equation, 24
- KMnF₃, 172
- Kohn–Sham equations, 138, 141
- ladder approximation, 62
- Landau level, 52

- Landau theory, 144
- Landau–Ginzburg–Wilson, 164
 - Hamiltonian, 144
- Langevin method, 194
- lattice constants, 140, 149, 151
- $\text{La}_{2-x}\text{Sr}_x\text{CuO}_4-\delta$, 172
- LEED, 143
- length-dependent correction to σ_0 , 31
- Lifshitz point, 246
- LiKSO_4 , 143
- local-density approximation (LDA), 139–141, 151
- local mode, 157, 158, 161, 162
- local-mode variables, 154, 156, 157, 169
- local transition, 284
- localization
 - acoustic, 56
 - of a surface plasmon polariton, 56
 - of classical waves, 55
 - of electromagnetic waves, 55
 - of sound waves, 56
 - optical, 56
- localization length, 38, 41, 52, 69
 - critical exponent v , 41
- localization transition on a Bethe lattice, 5
- localized impurity states, 271
- localized spin density waves, 279
- locator expansion, 59
- low dimensions ($d \leq 2$), 39
- magnetic alloys, 81
- Markov chain, 192
- martensitic transitions, 142, 144
- maximally crossed diagrams, 29
- mean-field, 165
- mean-field theory (MFT), 147, 168, 171
- mean free path, 11
- metastable, 83
- Metropolis algorithm, 193, 200
- Migdal–Kadanoff renormalization group, 5
- minimum metallic conductivity, 4
- minus-sign problem, 209, 226
- Miura transformation, 285
- Mo (001), 143, 172
- mobility edge, 4
- modified Korteweg–de Vries (MKdV)
 - equation, 260
- molecular crystals, 143
- molecular dynamics, 193
- Monte Carlo simulations, 111, 172
- multicritical points, 171
- multiple occupancy corrections, 61
- Nb_3Sn , 142, 144
- negative low-temperature magnetoresistance, 295
- negative low-temperature variation of $\rho(T)$, 293
- nesting, 240
- neural networks, 81, 127
- neutron scattering cross section, 288
- nodal barriers, 225
- nodal surfaces, 192
- nonlinear σ -model, 5
- nonlocal density response, 44
- norm conservation, 141
- numerical diagonalization, 57
- numerical stabilization, 209
- O and Se on Ni (111), 143
- off-diagonal disorder, 50
- one-parameter scaling theory, 31, 40
 - of localization, 5
 - validity, 6
- one-particle Green function, 19
- optimization, 81
- order parameter, 142–144, 147, 157, 163, 170, 171
- order–disorder transitions, 142, 143
- overlap, 100
- P–I transition, 244
- Parisi Ansatz, 98
- particle–hole ladder, 28
- partition function, 145, 163, 164
- path integrals, 182
- PbTe, 147, 150
- perovskite, 171
- perturbation theory
 - breakdown, 31
 - renormalized, 21
- phase diagram, 68, 94, 142, 145, 165, 168, 171, 172
- phonon frequencies, 140
- phonon mobility edge, 55
- photon mobility edge, 55
- physisorbed layers, 172
- physisorbed surface layers, 143
- polymorphic, 143
- polytypic, 143
- Potts model, 171
- preparation-dependence effects of spin glass
 - alloys, 82
- principle of nonlinear superposition, 285
- pseudopotentials, 139, 141, 148, 153, 170, 171
- pseudospin, 120

- quantum diffusion, 14
- quantum oscillations in the magnetoresistance, 18
- quasi-one-dimensional systems, 55
- weakly disordered, 54
- quenched disorder, 86
- Raman scattering, 143
- random-bond Ising model, 88
- random field, 9
- random-phase approximations, 184
- RbCaF₃, 146, 171
- Rb₂ZnCl₄, 143
- recursion relations, 145, 165, 166, 168, 170
- relevant variables, 145
- renormalization, 172
- renormalization group (RG), 144–147, 164, 168–171
 - treatment, 48
- replica mean-field theory, 91
- replica-symmetric Ansatz, 93
- replica theory, 90
- resonance contribution to the resistivity, 291
- resonance impurity levels, 270
- resonance tunnelling, 71
- response function, 66
- roton, 223
- s–p hybridization, 148
- scaling, 110
- scaling behaviour of the dynamical conductivity, 38
- scaling function $g(L)$, 45
- scaling theory of the interacting disordered system, 7
- scattering parameter, 245
- Se on Ni (100), 172
- second-order region, 165
- second-order transitions, 144, 145, 148, 168
- self-consistency, 32
- self-consistency equation, 250
- self-consistent equation, 32, 50
 - for $D(\omega)$, 31
 - for dynamical conductivity $\sigma(\omega)$, 35
 - for the diffusion coefficient, 67
 - generalization to anisotropic systems, 38
 - numerical evaluation, 68
- self-consistent phonon, 154
- self-consistent theory of Anderson localization, 6
 - alternative derivations, 49
 - application, 54
- extensions, 49
- shear, 147, 151
- short-range order, 246
- Si, 141
- Si (100), 143
- Si (111), 143
- Si and Ge (100), 146, 171
- sign problem, 190, 220
- silica, 143
- singular-value decomposition, 211
- Slater determinant, 190
- SnTe, 147, 148, 150
- soft mode, 142, 154
- soliton lattice model, 247
- specific heat, 143, 144
- spin density wave (SDW), 240
 - commensurate and incommensurate structures, 244
 - hardening of the SDW wave vector, 289
 - localized, 279
- spin glass, 81
 - susceptibility, 96
- spin–orbit scattering, 53
- spin–orbit splitting, 148
- SrTiO₃, 171
- staggered magnetization, 207
- stationary-phase approximation, 144, 164
- statistical mechanics, 163
- Stoner–Hubbard criterion, 239
- strain, 142, 144, 156–158, 161, 162, 164–166, 168–170
- structural phase transitions, 142, 143, 154, 171
- structural transitions, 146
- superconductivity, 172
- surface reconstructions, 140, 143
- surfaces, 143
- susceptibility, 144
- systematic calculation of corrections $\delta\sigma$ and δD , 18
- temperature-dependent correction, 31
- thermal expansion, 148, 149
 - coefficient, 170
- thermoremanent magnetization (TRM), 83
- tight-binding, 146, 150, 171
- tight-binding model with site-diagonal disorder, 57
- time-reversal invariance, 22
- time-reversal symmetry, 16
- time-reversed paths, 14
- tin, 143

- total-energy calculations, 139, 145, 146, 155, 170, 171
transition temperature, 148, 163, 165, 167, 168, 171
travelling salesman, 85
triplet order parameter, 242
Trotter approximation, 182, 196
- ultrametricity, 103
universal correction, 30
universality, 144, 145, 169
- variational principle, 138, 141
vector spin glasses, 118
vertex function, 21
- V₃Si, 142, 144
W (001), 143, 172
Ward identity, 24, 65
weak localization, 3, 11, 15
Wick's theorem, 195, 206
world-line methods, 191, 225
- X-ray diffraction, 143, 148
 ξ -expansion, 165
YBa₂Cu₃O_{7- δ} , 172
- zero field cooling (ZFC), 83
ZnS, 143
Zr, 146

This page intentionally left blank

CUMULATIVE INDEX, VOLUMES 1–32*

Monographs

Agranovich, V.M., and M.D. Galanin, Electronic excitation energy transfer in condensed matter	3
Brandt, N.B., S.M. Chudinov and Ya.G. Ponomarev, Semimetals – 1. Graphite and its compounds	20.1
Chudinov, S.M., <i>see</i> Brandt, N.B.	20.1
Galanin, M.D., <i>see</i> Agranovich, V.M.	3
Gantmakher, V.F., and Y.B. Levinson, Carrier scattering in metals and semiconductors	19
Gurevich, V.L., Transport in phonon systems	18
Levinson, Y.B., <i>see</i> Gantmakher, V.F.	19
Mashkova, E.S., and V.A. Molchanov, Medium-energy ion scattering by solid surfaces	11
Molchanov, V.A., <i>see</i> Mashkova, E.S.	11
Ponomarev, Ya.G., <i>see</i> Brandt, N.B.	20.1
Wagner, M., Unitary transformations in solid state physics	15

Contributed Volumes

Abelés, F., and T. Lopez-Rios, Surface polaritons at metal surfaces and interfaces	1, 239
Agranovich, V.M., Effects of the transition layer and spatial dispersion in the spectra of surface polaritons	1, 187
Agranovich, V.M., V.E. Kravtsov and T.A. Leskova, Scattering of surface polaritons by order parameter fluctuations near phase transition points	1, 511
Agranovich, V.M., Biphonons and Fermi resonance in vibrational spectra of crystals	4, 83
Agranovich, V.M., Surface excitons	9, 513
Agranovich, V.M., and V.V. Kirsanov, Production of radiation defects by collision cascades in metals	13, 117
Agranovich, V.M., and O.A. Dubovsky, Phonon multimode spectra: biphonons and triphonons in crystals with defects	23, 297
Akhmediev, N.N., The problem of stability and excitation of nonlinear surface waves	29, 289

The chapters of volume 31, which is still in production, have not been included.

Alekseevskii, N.E., M.I. Kaganov and V.I. Nizhankovskii, Oscillatory effects and the local geometry of Fermi-surfaces	27.1 , 1357
Alexandrova, I.P., Nuclear quadrupole resonance of the incommensurate phase in Rb_2ZnCl_4 and Rb_2ZnBr_4	14.1 , 277
Altshuler, B.L., and A.G. Aronov, Electron-electron interaction in disordered conductors	10 , 1
Altshuler, B.L., V.E. Kravtsov and I.V. Lerner, Distribution of mesoscopic fluctuations and relaxation processes in disordered conductors	30 , 449
Al'tshuler, S.A., A.Kh. Khasanov and B.I. Kochelaev, Studies of spin systems by means of light scattering in paramagnetic crystals	21 , 607
Ambrazevičiene, V., R. Brazis and A. Kunigėlis, Nonlinear surface magnetoplasma polaritons in semiconductors	29 , 417
Aoyagi, K., <i>see</i> Tanabe, Y.	2 , 603
Aronov, A.G., and A.S. Ioselevich, Exciton electrooptics	2 , 267
Aronov, A.G., <i>see</i> Altshuler, B.L.	10 , 1
Aronov, A.G., and G.E. Pikus, Magneto-optical phenomena in electric and magnetic fields	27.1 , 513
Aronov, A.G., Yu.M. Gal'perin, V.L. Gurevich and V.I. Kozub, Nonequilibrium properties of superconductors (transport equation approach)	12 , 325
Artemenko, S.N., and A.F. Volkov, Transport phenomena in CDW conductors, microscopic approach	25 , 365
Aslamazov, L.G., and A.F. Volkov, Nonequilibrium phenomena in superconducting weak links	12 , 65
Averin, D.V., and K.K. Likharev, Single electronics: A correlated transfer of single electrons and Cooper pairs in systems of small tunnel junctions	30 , 173
Avrutsky, I.A., <i>see</i> Prokhorov, A.M.	29 , 525
Axe, J.D., M. Iizumi and G. Shirane, Phase transformations in K_2SeO_4 and structurally related insulators	14.2 , 1
Bageev, V.S., T.I. Galkina and N.N. Sibeldin, Interaction of EHD with deformation field, ultrasound and non-equilibrium phonons	6 , 267
Bak, P., <i>see</i> Pokrovsky, V.L.	17 , 71
Barash, Yu.S., and V.L. Ginzburg, Electromagnetic fluctuations and molecular (Van der Waals) forces in condensed matter	24 , 389
Bar'yakhtar, V.G., and E.A. Turov, Magnetoelastic excitations	22.2 , 333
Basiev, T.T., V.A. Malyshev and A.K. Przhevuskii, Spectral migration of excitations in rare-earth activated glasses	21 , 275
Basun, S.A., <i>see</i> Kaplyanskii, A.A.	16 , 373
Bauer, G., Magnetoplasma effects in IV-VI compounds	27.1 , 277
Bazakutsa, P.V., <i>see</i> Prokhorov, A.M.	29 , 525
Beasley, M.R., <i>see</i> De Lozanne, A.L.	12 , 111
Belousov, M.V., Vibrational Frenkel excitons	2 , 771
Belyakov, V.A., and E.I. Kats, Light scattering and phase transitions in liquid crystals	5 , 227
Benoit à la Guillaume, C., <i>see</i> Planel, R.	8 , 353
Bereznyak, P.A., <i>see</i> Slyozov, V.V.	13 , 575
Berkovits, V.L., <i>see</i> Paget, D.	8 , 381
Bernard, L., <i>see</i> Currat, R.	14.2 , 161
Bersuker, I.B., and V.Z. Polinger, Theoretical background of the Jahn-Teller effect	7 , 21
Beyer, J., C.J. Pethick, J. Rammer and H. Smith, Pair breaking in nonequilibrium superconductors	12 , 129
Bhatt, R.N., <i>see</i> Milligan, R.F.	10 , 231
Bill, H., Observation of the Jahn-Teller effect with electron paramagnetic resonance	7 , 709

Birman, J.L., Electrodynamic and non-local optical effects mediated by exciton polaritons	2, 27
Bishop, A.R., <i>see</i> Steiner, M.	17, 783
Blinc, R., P. Prelovšek, V. Rutar, J. Seliger and S. Žumer, Experimental observations of incommensurate phases	14.1, 143
Boardman, A.D., P. Egan, F. Lederer, U. Langbein and D. Mihalache, Third-order nonlinear electromagnetic TE and TM guided waves	29, 73
Bonch-Bruevich, A.M., and M.N. Libenson, Laser-induced surface polaritons and optical breakdown	29, 561
Bonfait, G., L. Puech and A. Schuhl, Experiments on spin-polarized liquid ^3He -A	26, 881
Borovik-Romanov, A.S., and N.M. Kreines, Light scattering from spin waves	22.1, 81
Borovik-Romanov, A.S., and S.K. Sinha, Introduction	22, xi
Borstel, G., <i>see</i> Wöhlecke, M.	8, 423
Bozler, H.M., Textures in flowing superfluid ^3He -A	26, 695
Brazis, R., <i>see</i> Ambrazevičiene, V.	29, 417
Brazovskii, S., Solitons in crystals of charge density waves	25, 425
Bron, W.E., Phonon generation, transport and detection through electronic states in solids	16, 227
Brown, S.E., and A. Zettl, Charge density wave current oscillations and interference effects	25, 223
Bullough, R., and M.H. Wood, Theory of microstructural evolution	13, 189
Burns, M.J., W.K. Liu and A.H. Zewail, Nonlinear laser spectroscopy and dephasing of molecules: An experimental and theoretical overview	4, 301
Burstein, E., <i>see</i> Chen, Y.J.	1, 587
Büttner, H., <i>see</i> Mertens, F.G.	17, 723
Cailleau, H., Incommensurate phases in an aromatic molecular crystal: biphenyl	14.2, 71
Castner, T.G., Hopping conduction in the critical regime approaching the metal-insulator transition	28, 1
Celotta, R.J., <i>see</i> Pierce, D.T.	8, 259
Challis, L.J., and A.M. de Goërs, Phonon spectroscopy of Jahn-Teller ions	7, 533
Challis, L.J., Crossing effects in phonon scattering	16, 145
Chang, Jhy-Jiun, Kinetic equations in superconducting thin films	12, 453
Chen, Y.J., and E. Burstein, Three wave nonlinear interactions involving surface polaritons; Raman scattering, light diffraction and parametric mixing	1, 587
Chubukov, A.V., <i>see</i> Kaganov, M.I.	22.1, 1
Chubukov, A.V., <i>see</i> Kaganov, M.I.	29, 497
Clarke, J., Experiments on charge imbalance in superconductors	12, 1
Clinard Jr, F.W., and L.W. Hobbs, Radiation effects in non-metals	13, 387
Comes, R., <i>see</i> Pouget, J.P.	25, 85
Cone, R.L., and R.S. Meltzer, Ion-ion interactions and exciton effects in rare earth insulators	21, 481
Cottam, M.G., and A.A. Maradudin, Surface linear response functions	9, 1
Cummins, H.Z., Brillouin scattering studies of phase transitions in crystals	5, 359
Currat, R., <i>see</i> Durand, D.	14.2, 101
Currat, R., <i>see</i> Dénoyer, F.	14.2, 129
Currat, R., L. Bernard and P. Delamoye, Incommensurate phase in β -ThBr ₄	14.2, 161
Davydov, A.S., Solitons in biology	17, 1
de Goërs, A.M., <i>see</i> Challis, L.J.	7, 533
De Lozanne, A.L., and M.R. Beasley, Time-dependent superconductivity in SNS bridges: an example of TDGL theory	12, 111

de Wolff, P.M., and F. Tuinstra, The incommensurate phase of Na ₂ CO ₃	14.2, 253
Delamoye, P., <i>see</i> Currat, R.	14.2, 161
deMartini, F., <i>see</i> Shen, Y.R.	1, 629
Dénoyer, F., <i>see</i> Durand, D.	14.2, 101
Dénoyer, F., and R. Currat, Modulated phases in thiourea	14.2, 129
Dmitriev, V.M., V.N. Gubankov and F.Ya. Nad', Experimental study of enhanced superconductivity	12, 163
Dolgopolov, V.T., and I.L. Landau, Resistive states in type-I superconductors	12, 641
Dolgov, O.V., and E.G. Maksimov, The dielectric function of crystalline systems	24, 221
Dolino, G., The incommensurate phase of quartz	14.2, 205
Dubovsky, O.A., <i>see</i> Agranovich, V.M.	23, 297
Durand, D., F. Dénoyer, R. Currat and M. Lambert, Incommensurate phase in NaNO ₂	14.2, 101
Dyakonov, M.I., and V.I. Perel', Theory of optical spin orientation of electrons and nuclei in semiconductors	8, 11
Echegut, P., <i>see</i> Gervais, F.	14.1, 337
Efros, A.L., and B.I. Shklovskii, Coulomb interaction in disordered systems with localized electronic states	10, 483
Efros, A.L., and M.E. Raikh, Effect of composition disorder on the electronic properties of semiconducting mixed crystals	23, 133
Egan, P., <i>see</i> Boardman, A.D.	29, 73
Ehrhart, P., K.H. Robrock and H.R. Schober, Basic defects in metals	13, 3
Elesin, V.F., <i>see</i> Galitskii, V.M.	12, 377
Eliashberg, G.M., and B.I. Ivlev, Theory of superconductivity stimulation	12, 211
Elliott, R.J., Introduction	23, xi
Entin-Wohlman, O., <i>see</i> Jagannathan, A.	28, 125
Eremenko, V.V., Yu.G. Litvinenko and E.V. Matyushkin, Optical magnetic excitations	22.1, 175
Eremenko, V.V., and V.M. Naumenko, Magnetic impuritons in antiferromagnetic dielectric crystals	22.2, 259
Errandonéa, G., <i>see</i> Tolédano, J.C.	14.2, 233
Fayer, M.D., Exciton coherence	4, 185
Feigel'man, M.V., <i>see</i> Pokrovsky, V.L.	22.2, 67
Feigel'man, M.V., and V.M. Vinokur, Theory of CDW pinning by weak impurities	25, 293
Feng, S., Conductance fluctuations and 1/f noise magnitudes in small disordered structures: Theory	30, 107
Firsov, Yu.A., V.L. Gurevich, R.V. Parfeniev and I.M. Tsidil'kovskii, Magnetophonon resonance	27.2, 1181
Fischer, B., <i>see</i> Lagois, J.	1, 69
Fleisher, V.G., and I.A. Merkulov, Optical orientation of the coupled electron–nuclear spin system of a semiconductor	8, 173
Fleury, P.A., and K.B. Lyons, Central peaks near structural phase transitions	5, 449
Flores, F., and F. Garcia-Molinier, Electronic surface excitations	9, 441
Fomin, I.A., Pulsed NMR and the spatially nonuniform precession of spin in the superfluid phases of ³ He	26, 609
Fowler, A.B., J.J. Wainer and R.A. Webb, Hopping in mesoscopic samples	28, 233
Frait, Z., and D. Frajtová, Spin-wave resonance in metals	22.2, 1
Frajtová, D., <i>see</i> Frait, Z.	22.2, 1
Fukuyama, H., Interaction effects in the weakly localized regime of two- and three-dimensional disordered systems	10, 155
Fulde, P., and M. Loewenhaft, 4f Moments and their interaction with conduction electrons	22.1, 367

Furrer, R., Electron paramagnetic resonance in the excited states of rare earth ions in crystals	21 , 641
Galaiko, V.P., and N.B. Kopnin, Theory of the resistive state in narrow superconducting channels	12 , 543
Galitskii, V.M., V.F. Elesin and Yu.V. Kopaev, The kinetic theory of superconductors with excess quasiparticles	12 , 377
Galkina, T.I., <i>see</i> Bagaev, V.S.	6 , 267
Gal'perin, Yu.M., <i>see</i> Aronov, A.G.	12 , 325
Galperin, Yu.M., V.L. Gurevich and D.A. Parshin, Non-Ohmic microwave hopping conductivity	28 , 81
Gantmakher, V.F., and V.N. Zverev, Magnetoimpurity resonances in semiconductor transport	27.2 , 1135
Garcia-Moliner, F., <i>see</i> Flores, F.	9 , 441
Gershenson, E.M., A.P. Mel'nikov and R.I. Rabinovich, H^- -like impurity centers, molecular complexes and electron delocalization in semiconductors	10 , 483
Gervais, F., and P. Echegut, Infrared studies of incommensurate systems	14.1 , 337
Ginzburg, V.L., A.A. Sobyanin and A.P. Levanyuk, General theory of light scattering near phase transitions in ideal crystals	5 , 3
Ginzburg, V.L., <i>see</i> Barash, Yu.S.	24 , 389
Giordano, N., Conductance fluctuations and low-frequency noise in small disordered systems: Experiment	30 , 131
Gladkii, V.V., Macroscopic electric quadrupole moment in the incommensurate phase in ferroelectrics	14.1 , 309
Glinchuck, M.D., Paraelectric resonance of off-center ions	7 , 819
Goldburg, W.I., Light scattering investigations of the critical region in fluids	5 , 531
Goldman, A.M., <i>see</i> Kadin, A.M.	12 , 253
Golo, V.L., and A.A. Leman, Spin relaxation in superfluid ^3He in turned-off and weak magnetic fields	26 , 727
Golovko, V.A., and A.P. Levanyuk, Light scattering from incommensurate phases	5 , 169
Gor'kov, L.P., Disorder and interactions in the system of quasi one-dimensional electrons	10 , 619
Gor'kov, L.P., and G. Grüner, Introduction	25 , 1
Gor'kov, L.P., Phase slipping processes and the generation of narrow-band oscillations by charge density waves	25 , 403
Gornik, E., Landau emission	27.2 , 911
Gorobchenko, V.D., V.N. Kohn and E.G. Maksimov, The dielectric function of the homogeneous electron gas	24 , 87
Grun, J.B., B. Hönerlage and R. Lévy, Biexcitons in CuCl and related systems	2 , 459
Grüner, G., <i>see</i> Gor'kov, L.P.	25 , 1
Grüner, G., and P. Monceau, Dynamical properties of charge density waves	25 , 137
Gubankov, V.N., <i>see</i> Dmitriev, V.M.	12 , 163
Gubernatis, J.E., <i>see</i> Loh Jr, E.Y.	32 , 177
Guénault, A.M., and G.R. Pickett, Dynamic and thermal behaviour of quasi-particles in superfluid $^3\text{He-B}$	26 , 659
Gurevich, V.L., <i>see</i> Aronov, A.G.	12 , 325
Gurevich, V.L., <i>see</i> Firsov, Yu.A.	27.2 , 1181
Gurevich, V.L., <i>see</i> Galperin, Yu.M.	28 , 81
Guseva, M.I., and Yu.V. Martynenko, Blistering	13 , 621
Haarer, D., and M.R. Philpott, Excitons and polarons in organic weak charge transfer crystals	4 , 27

Häfele, H.G., Spin-flip Raman scattering	27.1, 207
Hajdu, J., The Shubnikov-de Haas effect: an introduction to the theory	27.2, 997
Halperin, W.P., and E. Varoquaux, Order-parameter collective modes in superfluid ^3He	26, 353
Hamano, K., Thermal hysteresis phenomena in incommensurate systems	14.1, 365
Hanson, D.M., J.S. Patel, I.C. Winkler and A. Morrobel-Sosa, Effects of electric fields on the spectroscopic properties of molecular solids	4, 621
Harley, R.T., Spectroscopic studies of Jahn-Teller phase transitions in rare-earth crystals	21, 557
Hayes, W., and M.C.K. Wiltshire, Infrared and Raman studies of disordered magnetic insulators	23, 177
Heinz, T.F., Second-order nonlinear optical effects at surfaces and interfaces	29, 353
Hermann, C., and C. Weisbuch, Optical detection of conduction electron spin resonance in semiconductors and its application to $k \cdot p$ perturbation theory	8, 463
Hesselink, W.H., and D.A. Wiersma, Theory and experimental aspects of photon echoes in molecular solids	4, 249
Hizhnyakov, V.V., and N.N. Kristoffel, Jahn-Teller mercury-like impurities in ionic crystals	7, 383
Hobbs, L.W., <i>see</i> Clinard Jr, F.W.	13, 387
Hönerlage, B., <i>see</i> Grun, J.B.	2, 459
Hook, J.R., Texture and anisotropic properties of a slab of $^3\text{He-A}$ in a magnetic field	26, 135
Horovitz, B., Solitons in charge and spin density wave systems	17, 691
Huber, D.L., Energy transfer in crystals	21, 251
Hunt, A., <i>see</i> Pollak, M.	28, 175
Iizumi, M., <i>see</i> Axe, J.D.	14.2, 1
Ionov, A.N., and I.S. Shlimak, Hopping conduction in heavily doped semiconductors	28, 397
Ioselevich, A.S., <i>see</i> Aronov, A.G.	2, 267
Ipatova, I.P., Universal parameters in mixed crystals	23, 1
Ishibashi, Y., Phenomenology of incommensurate phases in the A_2BX_4 family	14.2, 49
Ivchenko, E.L., Spatial dispersion effects in the exciton resonance region	2, 141
Ivchenko, E.L., <i>see</i> Pikus, G.E.	2, 205
Ivlev, B.I., <i>see</i> Eliashberg, G.M.	12, 211
Jagannathan, A., R. Orbach and O. Entin-Wohlman, Thermal conduction due to hopping processes in amorphous solids	28, 125
Janssen, T., Microscopic theories of incommensurate crystal phases	14.1, 67
Jeffries, C.D., <i>see</i> Wolfe, J.P.	6, 431
Joannopoulos, J.D., <i>see</i> Rabe, K.M.	32, 135
Judd, B.R., Group theoretical approaches	7, 87
Kadin, A.M., and A.M. Goldman, Dynamical effects in nonequilibrium superconductors: some experimental perspectives	12, 253
Kaganov, M.I., and A.V. Chubukov, Spin waves in magnetic dielectrics. Current status of the theory	22.1, 1
Kaganov, M.I., <i>see</i> Alekseevskii, N.E.	27.1, 1357
Kaganov, M.I., A.P. Levanyuk, S.A. Minyukov and A.V. Chubukov, Surface magnetic and structural phase transitions	29, 497
Kalia, R.K., <i>see</i> Vashishta, P.	6, 1
Kamimura, H., Electron-electron interactions in the Anderson-localised regime near the metal-insulator transition	10, 555
Kaplan, A.E., P.W. Smith and W.J. Tomlinson, Nonlinear waves and switching effects at nonlinear interfaces	29, 323

Kaplyanskii, A.A., and S.A. Basun, Multiple resonant scattering of the 29 cm^{-1} acoustic phonons in optically excited ruby	16 , 373
Kaplyanskii, A.A., and A.I. Ryskin, P.P. Feofilov and the spectroscopy of activated crystals	21 , 1
Kats, E.I., <i>see</i> Belyakov, V.A.	5 , 227
Keldysh, L.V., and N.N. Sibeldin, Phonon wind in highly excited semiconductors	16 , 455
Keldysh, L.V., Introduction	24 , 1
Keßler, F.R., and J. Metzdorf, Landau level spectroscopy: interband effects and Faraday rotation	27.1 , 579
Kharađze, G.A., The properties of the rotating superfluid phases of liquid ^3He	26 , 167
Khasanov, A.Kh., <i>see</i> Al'tshuler, S.A.	21 , 607
Kholodar, G.A., <i>see</i> Vinetskii, V.L.	13 , 283
Kind, R., and P. Murali, Unique incommensurate–commensurate phase transitions in a layer-structure perovskite	14.2 , 301
Kirzhnitz, D.A., General properties of electromagnetic response functions	24 , 41
Kivelson, S., Soliton model of polyacetylene	17 , 301
Klein, M.V., Light scattering studies of incommensurate transitions	5 , 503
Klyuchnik, A.V., <i>see</i> Lozovik, Yu.E.	24 , 299
Kochelaev, B.I., <i>see</i> Al'tshuler, S.A.	21 , 607
Kohn, V.N., <i>see</i> Gorobchenko, V.D.	24 , 87
Kolb, D.M., The study of solid–liquid interfaces by surface plasmon polariton excitation	1 , 299
Kopaev, Yu.V., <i>see</i> Galitskii, V.M.	12 , 377
Kopelman, R., Energy transport in mixed molecular crystals	4 , 139
Kopnin, N.B., <i>see</i> Galaiko, V.P.	12 , 543
Korenblit, I.Ya., and E.F. Shender, Theory of magnetic excitations in disordered systems	22.2 , 109
Kosevich, A.M., Dynamical and topological solitons in ferromagnets and antiferromagnets	17 , 555
Koteles, E.S., Investigation of exciton-polariton dispersion using laser techniques	2 , 83
Kozub, V.I., <i>see</i> Aronov, A.G.	12 , 325
Kravtsov, V.E., <i>see</i> Agranovich, V.M.	1 , 511
Kravtsov, V.E., <i>see</i> Altshuler, B.L.	30 , 449
Kreines, N.M., <i>see</i> Borovik-Romanov, A.S.	22.1 , 81
Kristoffel, N.N., <i>see</i> Hizhnyakov, V.V.	7 , 383
Kulakovskii, V.D., and V.B. Timofeev, Thermodynamics of electron–hole liquid in semiconductors	6 , 95
Kunigēlis, A., <i>see</i> Ambrasheviciene, V.	29 , 417
Kurkijärvi, J., and D. Rainer, Andreev scattering in superfluid ^3He	26 , 313
Kurkin, M.I., and E.A. Turov, Nuclear spin excitations	22.2 , 381
Kuznetsov, E.A., <i>see</i> Zakharov, V.E.	17 , 503
Lagois, J., and B. Fischer, Surface exciton polaritons from an experimental viewpoint	1 , 69
Lambert, M., <i>see</i> Durand, D.	14.2 , 101
Landau, I.L., <i>see</i> Dolgopolov, V.T.	12 , 641
Landwehr, X.X., and E.I. Rashba, Introduction	27.1 , xi
Langbein, U., <i>see</i> Boardman, A.D.	29 , 73
Larkin, A.I., and Yu.N. Ovchinnikov, Vortex motion in superconductors	12 , 493
Larsen, D.M., Polaron effects in cyclotron resonance	27.1 , 109
Lederer, F., <i>see</i> Boardman, A.D.	29 , 73
Leggett, A.J., and S.K. Yip, Nucleation and growth of $^3\text{He-B}$ in the supercooled A-phase	26 , 523

Lemaistre, J., <i>see</i> Zewail, A.H.	2, 665
Leman, A.A., <i>see</i> Golo, V.L.	26, 727
Lerner, I.V., <i>see</i> Altshuler, B.L.	30, 449
Leskova, T.A., <i>see</i> Agranovich, V.M.	1, 511
Levanyuk, A.P., <i>see</i> Ginzburg, V.L.	5, 3
Levanyuk, A.P., A.S. Sigov and A.A. Sobyanin, Light scattering anomalies due to defects	5, 129
Levanyuk, A.P., <i>see</i> Golovko, V.A.	5, 169
Levanyuk, A.P., General ideas about incommensurate phases	14.1, 1
Levanyuk, A.P., <i>see</i> Kaganov, M.I.	29, 497
Levinson, Y.B., Phonon assisted cyclotron resonance	27.1, 79
Levinson, Y.B., Phonon propagation with frequency down-conversion	16, 91
Lévy, R., <i>see</i> Grun, J.B.	2, 459
Libenson, M.N., <i>see</i> Bonch-Bruevich, A.M.	29, 561
Likharev, K.K., <i>see</i> Averin, D.V.	30, 173
Lindgård, P.-A., Theory of spin excitations in the rare earth systems	22.1, 287
Litster, J.D., Scattering spectroscopy of liquid crystals	5, 583
Littlewood, P.B., Computer simulations of CDW dynamics	25, 321
Litvinenko, Yu.G., <i>see</i> Eremenko, V.V.	22.1, 175
Liu, W.K., <i>see</i> Burns, M.J.	4, 301
Loewenhaupt, M., <i>see</i> Fulde, P.	22.1, 367
Loh Jr, E.Y., and J.E. Gubernatis, Stable numerical simulations of models of interacting electrons in condensed-matter physics	32, 177
Long, A.R., Hopping conductivity in the intermediate frequency regime	28, 207
Lopez-Rios, T., <i>see</i> Abelés, F.	1, 239
Loudon, R., <i>see</i> Ushioda, S.	1, 535
Loudon, R., Ripples on liquid interfaces	9, 589
Lozovik, Yu.E., and A.V. Klyuchnik, The dielectric function and collective oscillations in inhomogeneous matter	24, 299
Luhman, T., <i>see</i> Snead Jr, C.L.	13, 345
Lushchik, Ch.B., Free and self-trapped excitons in alkali halides: spectra and dynamics	2, 505
Lushchik, Ch.B., Creation of Frenkel defect pairs by excitons in alkali halides	13, 473
L'vov, V.S., and L.A. Prozorova, Spin waves above the threshold of parametric excitations	22.1, 233
L'vov, V.S., Solitons and nonlinear phenomena in parametrically excited spin waves	17, 241
Lynn, J.W., and J.J. Rhyne, Spin dynamics of amorphous magnets	22.2, 177
Lyons, K.B., <i>see</i> Fleury, P.A.	5, 449
Lyuksyutov, I.F., A.G. Naumovets and Yu.S. Vedula, Solitons and surface diffusion	17, 605
Macfarlane, R.M., and R.M. Shelby, Coherent transient and holeburning spectroscopy of rare earth ions in solids	21, 51
Maki, K., Solitons in superfluid ^3He	17, 435
Maksimov, E.G., <i>see</i> Gorobchenko, V.D.	24, 87
Maksimov, E.G., <i>see</i> Dolgov, O.V.	24, 221
Malkin, B.Z., Crystal field and electron–phonon interaction in rare-earth ionic paramagnets	21, 13
Malyshev, V.A., <i>see</i> Basiev, T.T.	21, 275
Mansfield, R., Hopping conduction in III–V compounds	28, 349
Maradudin, A.A., Interaction of surface polaritons and plasmons with surface roughness	1, 405
Maradudin, A.A., <i>see</i> Cottam, M.G.	9, 1
Maris, H.J., Phonon focusing	16, 51

Markiewicz, R.S., and T. Timusk, Interaction of electromagnetic radiation with electron-hole droplets	6, 543
Martynenko, Yu.V., <i>see</i> Guseva, M.I.	13, 621
Matyushkin, E.V., <i>see</i> Eremenko, V.V.	22.1, 175
McCombe, B.D., <i>see</i> Petrou, A.	27.2, 679
McKenzie, R.H., and J.A. Sauls, Collective modes and nonlinear acoustics in superfluid $^3\text{He-B}$	26, 255
Meier, F., and D. Pescia, Spin-polarized photoemission by optical orientation	8, 295
Mello, P.A., <i>see</i> Stone, A.D.	30, 369
Mel'nikov, A.P., <i>see</i> Gershenzon, E.M.	10, 483
Meltzer, R.S., <i>see</i> Cone, R.L.	21, 481
Merkulov, I.A., <i>see</i> Fleisher, V.G.	8, 173
Mertens, F.G., and H. Büttner, Solitons on the Toda lattice: thermodynamical and quantum-mechanical aspects	17, 723
Metzdorf, J., <i>see</i> Keßler, F.R.	27.1, 579
Meyerovich, A.E., Spin-polarized phases of $^3\text{He-B}$	26, 757
Mihalache, D., <i>see</i> Boardman, A.D.	29, 73
Mikhailov, A.V., Integrable magnetic models	17, 623
Mikhailov, S.A., <i>see</i> Volkov, V.A.	27.2, 855
Milligan, R.F., T.F. Rosenbaum, R.N. Bhatt and G.A. Thomas, A review of the metal-insulator transition in doped semiconductors	10, 231
Mills, D.L., Surface spin waves on magnetic crystals	9, 379
Mills, D.L., <i>see</i> Nizzoli, F.	29, 445
Min'yukov, S.A., <i>see</i> Kaganov, M.I.	29, 497
Mirlin, D.N., Surface phonon polaritons in dielectrics and semiconductors	1, 3
Mirlin, D.N., Optical alignment of electron momenta in GaAs-type semiconductors	8, 133
Monceau, P., <i>see</i> Grüner, G.	25, 137
Monroe, D., Hopping in band tails, far from equilibrium	28, 49
Mook, H.A., Neutron scattering studies of magnetic excitations in itinerant magnets	22.1, 425
Morrobel-Sosa, A., <i>see</i> Hanson, D.M.	4, 621
Moskalova, M.A., <i>see</i> Zhizhin, G.N.	1, 93
Muralt, P., <i>see</i> Kind, R.	14.2, 301
Muttalib, K.A., <i>see</i> Stone, A.D.	30, 369
Nad', F.Ya., <i>see</i> Dmitriev, V.M.	12, 163
Nad', F.Ya., Deformation and phase-slip in charge density waves in quasi-one-dimensional conductors	25, 191
Natadze, A.L., A.I. Ryskin and B.G. Vekhter, Jahn-Teller effects in optical spectra of II-VI and III-V impurity crystals	7, 347
Naumenko, V.M., <i>see</i> Eremenko, V.V.	22.2, 259
Naumovets, A.G., <i>see</i> Lyuksyutov, I.F.	17, 605
Nelson, R.J., Excitons in semiconductor alloys	2, 319
Nicholas, R.J., The magnetophonon effect in two dimensions	27.2, 777
Nizhankovskii, V.I., <i>see</i> Alekseevskii, N.E.	27.1, 1357
Nizzoli, F., <i>see</i> Stegeman, G.I.	9, 195
Nizzoli, F., and D.L. Mills, Light scattering from phonons and spin waves on surfaces	29, 445
Orbach, R., <i>see</i> Jagannathan, A.	28, 125
Ortuño, M., <i>see</i> Pollak, M.	10, 287
Osad'ko, I.S., Theory of light absorption and emission by organic impurity centers	4, 437
Otsuka, E., Cyclotron resonance	27.1, 1
Ovchinnikov, Yu.N., <i>see</i> Larkin, A.I.	12, 493

Ovsyankin, V.V., Spectroscopy of collective states and cooperative transitions in disordered rare-earth activated solids	21 , 343
Paget, D., and V.L. Berkovits, Optical investigation of hyperfine coupling between electronic and nuclear spins	8 , 381
Pankratov, O.A., and B.A. Volkov, The energy spectrum and magneto-optics in band-inverting heterojunctions	27.2 , 817
Parfeniev, R.V., <i>see</i> Firsov, Yu.A.	27.2 , 1181
Parshin, D.A., <i>see</i> Galperin, Yu.M.	28 , 81
Patel, J.S., <i>see</i> Hanson, D.M.	4 , 621
Pearlstein, R.M., Excitons in photosynthetic and other biological systems	2 , 735
Pedersen, N.F., Solitons in Josephson transmission lines	17 , 469
Perel', V.I., and B.P. Zakharchenya, Major physical phenomena in the optical orientation and alignment in semiconductors	8 , 1
Perel', V.I., <i>see</i> Dyakonov, M.I.	8 , 11
Perlin, Yu.E., and M. Wagner, Introduction	7 , 1
Perlin, Yu.E., and B.S. Tsukerblat, Optical bands and polarization dichroism of Jahn-Teller centers	7 , 251
Permogorov, S., Optical emission due to exciton scattering by LO phonons in semiconductors	2 , 177
Personov, R.I., Site selection spectroscopy of complex molecules in solutions and its applications	4 , 555
Pescia, D., <i>see</i> Meier, F.	8 , 295
Pethick, C.J., <i>see</i> Beyer, J.	12 , 129
Petrou, A., and B.D. McCombe, Magnetospectroscopy of confined semiconductor systems	27.2 , 679
Philpott, M.R., <i>see</i> Haarer, D.	4 , 27
Pichard, J.-L., <i>see</i> Stone, A.D.	30 , 369
Pick, R.M., <i>see</i> Poulet, H.	14.1 , 315
Pickett, G.R., <i>see</i> Guénault, A.M.	26 , 659
Pidgeon, C.R., Interband magneto-optics in narrow-gap semiconductors	27.1 , 445
Pierce, D.T., and R.J. Celotta, Applications of polarized electron sources utilizing optical orientation in solids	8 , 259
Pikin, S.A., Incommensurate structures in liquid crystals	14.2 , 319
Pikus, G.E., and E.L. Ivchenko, Optical orientation and polarized luminescence of excitons in semiconductors	2 , 205
Pikus, G.E., and A.N. Titkov, Spin relaxation under optical orientation in semiconductors	8 , 73
Pikus, G.E., <i>see</i> Aronov, A.G.	27.1 , 513
Pitaevskii, L.P., Superfluid ^3He , a short introduction into the theory	26 , 1
Planell, R., and C. Benoit à la Guillaume, Optical orientation of excitons	8 , 353
Pokrovskii, Ya.E., Transport phenomena in electron-hole liquid	6 , 509
Pokrovsky, V.L., A.L. Talapov and P. Bak, Thermodynamics of two-dimensional soliton systems	17 , 71
Pokrovsky, V.L., M.V. Feigel'man and A.M. Tsvelick, Excitations in low-dimensional magnetic systems	22.2 , 67
Polinger, V.Z., <i>see</i> Bersuker, I.B.	7 , 21
Pollak, M., and M. Ortúñoz, The effect of Coulomb interactions on electronic states and transport in disordered insulators	10 , 287
Pollak, M., and A. Hunt, Slow processes in disordered solids	28 , 175
Pooler, D.R., Numerical diagonalization techniques in the Jahn-Teller effect	7 , 199
Pouget, J.P., and R. Comes, The CDW transition, structural studies	25 , 85

Poulet, H., and R.M. Pick, Light scattering in incommensurate systems	14.1, 315
Prelovšek, P., <i>see</i> Blinc, R.	14.1, 143
Prokhorov, A.M., I.A. Avrutsky, P.V. Bazakutsa, V.A. Sychugov and A.V. Tischenko, Laser-induced surface gratings	29, 525
Prozorova, L.A., <i>see</i> Lvov, V.S.	22.1, 233
Przhevuskii, A.K., <i>see</i> Basiev, T.T.	21, 275
Puech, L., <i>see</i> Bonfait, G.	26, 881
Rabe, K.M., and J.D. Joannopoulos, Ab initio statistical mechanics of structural phase transitions	32, 135
Rabinovich, R.I., <i>see</i> Gershenzon, E.M.	10, 483
Raether, H., Surface plasmons and roughness	1, 331
Raikh, M.E., <i>see</i> Efros, A.L.	23, 133
Raikh, M.E., and I.M. Ruzin, Transmittancy fluctuations in randomly non-uniform barriers and incoherent mesoscopics	30, 315
Rainer, D., <i>see</i> Kurkijärvi, J.	26, 313
Raj, N., and D. Tilley, The electrodynamics of superlattices	24, 459
Rammer, J., <i>see</i> Beyer, J.	12, 129
Rashba, E.I., Self-trapping of excitons	2, 543
Rashba, E.I., <i>see</i> Landwehr, X.X.	27.1, xi
Rashba, E.I., and V.I. Sheka, Electric-dipole spin resonances	27.1, 131
Rashba, E.I., Spectroscopy of excitons in disordered molecular crystals	23, 215
Reik, H.G., Non-adiabatic systems: analytical approach and exact results	7, 117
Renk, K.F., Detection of high-frequency phonons by phonon-induced fluorescence	16, 277
Renk, K.F., Optical generation and detection of 29 cm^{-1} phonons in ruby	16, 317
Reznichenko, E.A., <i>see</i> Zelensky, V.F.	13, 527
Rhyne, J.J., <i>see</i> Lynn, J.W.	22.2, 177
Robrock, K.H., <i>see</i> Ehrhart, P.	13, 3
Rosenbaum, T.F., <i>see</i> Milligan, R.F.	10, 231
Roth, S., Hopping conduction in electrically conducting polymers	28, 377
Rouxel, J., and C. Schlenker, Structural, electronic properties and design of quasi-one-dimensional inorganic conductors	25, 15
Rubenchik, A.M., <i>see</i> Zakharov, V.E.	17, 503
Rutar, V., <i>see</i> Blinc, R.	14.1, 143
Ruzin, I.M., <i>see</i> Raikh, M.E.	30, 315
Ryskin, A.I., <i>see</i> Natadze, A.L.	7, 347
Ryskin, A.I., <i>see</i> Kaplyanskii, A.A.	21, 1
Sannikov, D.G., Phenomenological theory of the incommensurate-commensurate phase transition	14.1, 43
Sauls, J.A., <i>see</i> McKenzie, R.H.	26, 255
Schlenker, C., <i>see</i> Rouxel, J.	25, 15
Schnecke, J., <i>see</i> Tolédano, J.C.	14.2, 233
Schneider, T., and E. Stoll, Spin dynamics of Heisenberg chains	17, 129
Schneider, T., Classical statistical mechanics of lattice dynamic model systems	17, 389
Schober, H.R., <i>see</i> Ehrhart, P.	13, 3
Schön, G., Collective modes in superconductors	12, 589
Schuhl, A., <i>see</i> Bonfait, G.	26, 881
Scott, A.C., Experimental observation of a Davydov-like soliton	17, 53
Scott, J.F., Raman spectroscopy of structural phase transitions	5, 291
Scott, J.F., Statics and dynamics of incommensurate BaMnF_4	14.2, 283

- Seiler, D.G., and A.E. Stephens, The Shubnikov-de Haas effect in semiconductors: a comprehensive review of experimental aspects **27.2**, 1031
- Seisyan, R.P., and B.P. Zakharchenya, Interband magneto-optics of semiconductors as diamagnetic exciton spectroscopy **27.1**, 345
- Seliger, J., *see* Blinc, R. **14.1**, 143
- Shapiro, S.M., Magnetic excitations in spin glasses **22.2**, 219
- Sheka, V.I., *see* Rashba, E.I. **27.1**, 131
- Shelby, R.M., *see* Macfarlane, R.M. **21**, 51
- Sheleg, A.U., and V.V. Zaretskii, List of incommensurate crystals **14.2**, 367
- Shen, Y.R., and F. deMartini, Nonlinear wave interaction involving surface polaritons **22.2**, 109
- Shender, E.F., *see* Korenblit, I.Ya. **32**, 79
- Sherrington, D., Spin glasses **14.2**, 1
- Shirane, G., *see* Axe, J.D. **10**, 483
- Shklovskii, B.I., *see* Efros, A.L. **28**, 271
- Shklovskii, B.I., and B.Z. Spivak, Scattering and interference effects in variable range hopping conduction **28**, 397
- Shlimak, I.S., *see* Ionov, A.N. **1**, 93
- Shomina, E.V., *see* Zhizhin, G.N. **5**, 605
- Shustin, O.A., *see* Yakovlev, I.A. **6**, 267
- Sibeldin, N.N., *see* Bagaev, V.S. **16**, 455
- Sibeldin, N.N., *see* Keldysh, L.V. **7**, 495
- Sigmund, E., Phonon scattering at Jahn-Teller defects in semiconductors **5**, 129
- Sigov, A.S., *see* Levanyuk, A.P. **4**, 1
- Silbey, R., Theories of energy transport **6**, 619
- Silin, A.P., Electron-hole liquid in a magnetic field **6**, 1
- Singwi, K.S., *see* Vashishta, P. **22**, xi
- Sinha, S.K., *see* Borovik-Romanov, A.S. **1**, 661
- Sipe, J.E., and G.I. Stegeman, Nonlinear optical response of metal surfaces **13**, 575
- Slyozov, V.V., and P.A. Bereznyak, Irradiation creep in metals **Small, G.J.**, Persistent nonphotochemical hole burning and the dephasing of impurity electronic transitions in organic glasses **4**, 515
- Smith, D.D., *see* Zewail, A.H. **2**, 665
- Smith, H., *see* Beyer, J. **12**, 129
- Smith, P.W., *see* Kaplan, A.E. **29**, 323
- Snead Jr, C.L., and T. Luhman, Radiation damage and stress effects in superconductors: Materials for high-field applications **13**, 345
- Sobyanin, A.A., *see* Ginzburg, V.L. **5**, 3
- Sobyanin, A.A., *see* Levanyuk, A.P. **5**, 129
- Sohler, W., Second-order nonlinear guided wave interactions **29**, 1
- Spivak, B.Z., *see* Shklovskii, B.I. **28**, 271
- Spivak, B.Z., and A.Yu. Zyuzin, Mesoscopic fluctuations of current density in disordered conductors **30**, 37
- Stegeman, G.I., *see* Sipe, J.E. **1**, 661
- Stegeman, G.I., and F. Nizzoli, Surface vibrations **9**, 195
- Steiner, M., and A.R. Bishop, Nonlinear effects in low-dimensional magnets **17**, 783
- Stephen, M.J., Interference, fluctuations and correlations in the diffusive scattering of light from a disordered medium **30**, 81
- Stephens, A.E., *see* Seiler, D.G. **27.2**, 1031
- Stoll, E., *see* Schneider, T. **17**, 129
- Stone, A.D., P.A. Mello, K.A. Muttalib and J.-L. Pichard, Random matrix theory and maximum entropy models for disordered conductors **30**, 369
- Sturge, M.D., Introduction **2**, 1

Sugakov, V.I., Excitons in strained molecular crystals	2, 709
Sychugov, V.A., <i>see</i> Prokhorov, A.M.	29, 525
Talapov, A.L., <i>see</i> Pokrovsky, V.L.	17, 71
Tanabe, Y., and K. Aoyagi, Excitons in magnetic insulators	2, 603
Taylor, D.W., Phonon response theory and the infrared and Raman experiments	23, 35
Thewalt, M.L.W., Bound multiexciton complexes	2, 393
Thomas, G.A., <i>see</i> Milligan, R.F.	10, 231
Tilley, D., <i>see</i> Raj, N.	24, 459
Timofeev, V.B., Free many particle electron-hole complexes in an indirect gap semiconductor	2, 349
Timofeev, V.B., <i>see</i> Kulakovskii, V.D.	6, 95
Timp, G., Ballistic transport in one dimension	30, 273
Timusk, T., <i>see</i> Markiewicz, R.S.	6, 543
Tischenko, A.V., <i>see</i> Prokhorov, A.M.	29, 525
Titkov, A.N., <i>see</i> Pikus, G.E.	8, 73
Tolédano, J.C., J. Schneck and G. Errandonéa, Incommensurate phase of barium sodium niobate	14.2, 233
Tomlinson, W.J., <i>see</i> Kaplan, A.E.	29, 323
Tsidil'kovskii, I.M., <i>see</i> Firsov, Yu.A.	27.2, 1181
Tsukerblat, B.S., <i>see</i> Perlin, Yu.E.	7, 251
Tsvetlik, A.M., <i>see</i> Pokrovsky, V.L.	22.2, 67
Tugushev, V.V., Modulated and localized structures of spin density waves in itinerant antiferromagnets	32, 237
Tuinstra, F., <i>see</i> de Wolff, P.M.	14.2, 253
Turov, E.A., <i>see</i> Bar'yakhtar, V.G.	22.2, 333
Turov, E.A., <i>see</i> Kurkin, M.I.	22.2, 381
Ulrici, W., Manifestations of the Jahn-Teller effect in the optical spectra of transition metal impurities in crystals	7, 439
Ushioda, S., and R. Loudon, Raman scattering by surface polaritons	1, 535
Varoquaux, E., <i>see</i> Halperin, W.P.	26, 353
Vashishta, P., R.K. Kalia and K.S. Singwi, Electron-hole liquid: theory	6, 1
Vedula, Yu.S., <i>see</i> Lyuksyutov, I.F.	17, 605
Vekhter, B.G., <i>see</i> Natadze, A.L.	7, 347
Vinetzkii, V.L., and G.A. Kholodar, Quasichemical reactions involving point defects in irradiated semiconductors	13, 283
Vinogradov, E.A., G.N. Zhizhin and V.I. Yudson, Thermally stimulated emission of surface polaritons	1, 145
Vinokur, V.M., <i>see</i> Feigel'man, M.V.	25, 293
Volkov, A.F., <i>see</i> Aslamazov, L.G.	12, 65
Volkov, A.F., <i>see</i> Artemenko, S.N.	25, 365
Volkov, B.A., <i>see</i> Pankratov, O.A.	27.2, 817
Volkov, V.A., and S.A. Mikhailov, Electrodynamics of two-dimensional electron systems in high magnetic fields	27.2, 855
Vollhardt, D., and P. Wölfle, Self-consistent theory of Anderson localization	32, 1
Volovik, G.E., Symmetry in superfluid ^3He	26, 27
Wagner, M., <i>see</i> Perlin, Yu.E.	7, 1
Wagner, M., Unitary transformation methods in vibronic problems	7, 155
Wainer, J.J., <i>see</i> Fowler, A.B.	28, 233

Washburn, S., Aharonov–Bohm effects in loops of gold	30, 1
Webb, R.A., <i>see</i> Fowler, A.B.	28, 233
Weis, O., Phonon radiation across solid/solid interfaces within the acoustic mismatch model	16, 1
Weisbuch, C., <i>see</i> Hermann, C.	8, 463
Westervelt, R.M., Kinetics of electron–hole drop formation and decay	6, 187
Wiedersich, H., Phase stability and solute segregation during irradiation	13, 225
Wiersma, D.A., <i>see</i> Hesselink, W.H.	4, 249
Wiltshire, M.C.K., <i>see</i> Hayes, W.	23, 177
Winkler, I.C., <i>see</i> Hanson, D.M.	4, 621
Wöhlecke, M., and G. Borstel, Spin-polarized photoelectrons and crystal symmetry	8, 423
Wolfe, J.P., and C.D. Jeffries, Strain-confined excitons and electron–hole liquid	6, 431
Wölfle, P., <i>see</i> Vollhardt, D.	32, 1
Wood, M.H., <i>see</i> Bullough, R.	13, 189
Yakovlev, I.A., and O.A. Shustin, Light scattering in quartz and ammonium chloride and its peculiarities in the vicinity of phase transition of crystals. A retrospective view and recent results	5, 605
Yakovlev, V.A., <i>see</i> Zhizhin, G.N.	1, 93
Yakovlev, V.A., <i>see</i> Zhizhin, G.N.	1, 275
Yen, W.M., Experimental studies of energy transfer in rare earth ions in crystals	21, 185
Yip, S.K., <i>see</i> Leggett, A.J.	26, 523
Yudson, V.I., <i>see</i> Vinogradov, E.A.	1, 145
Zakharchenya, B.P., <i>see</i> Perel', V.I.	8, 1
Zakharchenya, B.P., <i>see</i> Seisyan, R.P.	27.1, 345
Zakharov, V.E., E.A. Kuznetsov and A.M. Rubenchik, Soliton stability	17, 503
Zapasskii, V.S., Optical detection of spin-system magnetization in rare-earth-activated crystals and glasses	21, 673
Zaretskii, V.V., <i>see</i> Sheleg, A.U.	14.2, 367
Zawadzki, W., Intraband and interband magneto-optical transitions in semiconductors	27.1, 483
Zawadzki, W., Shallow magneto-impurities in semiconductors	27.2, 1305
Zelensky, V.F., and E.A. Reznichenko, Irradiation growth of metals and alloys	13, 527
Zettl, A., <i>see</i> Brown, S.E.	25, 223
Zewail, A.H., D.D. Smith and J. Lemaistre, Dynamics of molecular excitons: disorder, coherence and dephasing	2, 665
Zewail, A.H., <i>see</i> Burns, M.J.	4, 301
Zhizhin, G.N., M.A. Moskalova, E.V. Shomina and V.A. Yakovlev, Surface electromagnetic wave propagation on metal surfaces	1, 93
Zhizhin, G.N., <i>see</i> Vinogradov, E.A.	1, 145
Zhizhin, G.N., and V.A. Yakovlev, Resonance of transition layer excitations with surface polaritons	1, 275
Žumer, S., <i>see</i> Blinc, R.	14.1, 143
Zverev, V.N., <i>see</i> Gantmakher, V.F.	27.2, 1135
Zvyagin, I.P., The hopping thermopower	28, 143
Zyuzin, A.Yu., <i>see</i> Spivak, B.Z.	30, 37